

Distribution Agreement

In presenting this thesis or dissertation as a partial fulfillment of the requirements for an advanced degree from Emory University, I hereby grant to Emory University and its agents the non-exclusive license to archive, make accessible, and display my thesis or dissertation in whole or in part in all forms of media, now or hereafter known, including display on the world wide web. I understand that I may select some access restrictions as part of the online submission of this thesis or dissertation. I retain all ownership rights to the copyright of the thesis or dissertation. I also retain the right to use in future works (such as articles or books) all or part of this thesis or dissertation.

Signature:

Amy E. Solinski

Date

Carolacton and Honokiol: using natural product inspiration to target the oral microbiome

By

Amy E. Solinski
Doctor of Philosophy

Chemistry

William M. Wuest, Ph.D.
Advisor

Jennifer M. Heemstra, Ph.D.
Committee Member

Nathan T. Jui, Ph.D.
Committee Member

Accepted:

Lisa A. Tedesco, Ph.D.
Dean of the James T. Laney School of Graduate Studies

Date

Carolacton and Honokiol: using natural product inspiration to target the oral microbiome

By

Amy E. Solinski
B.S., The College of New Jersey, 2015

Advisor: William M. Wuest, Ph.D.

An abstract of
A dissertation submitted to the Faculty of the
James T. Laney School of Graduate Studies of Emory University
in partial fulfillment of the requirements for the degree of
Doctor of Philosophy in Chemistry
2020

Abstract

Carolacton and Honokiol: using natural product inspiration to target the oral microbiome

By Amy E. Solinski

Streptococcus mutans, one of the cariogenic species within the oral microbiome, has become a model organism for the formation of bacterial biofilm. In contrast to free floating, planktonic cells, biofilm cells use various methods to attach to environmental surfaces. Investigating biofilm has become more prevalent as it has been connected to antibiotic resistance. Scientists are searching for new compounds that can inhibit, or eradicate the formation of these disease causing biofilms. Carolacton and honokiol are natural products that have been found to target *S. mutans* biofilm. Carolacton demonstrates lethal effects towards cells in *S. mutans* biofilm but a full understanding of the biological target and mechanism of action have remained elusive for the past decade. Herein we present two generations of novel carolacton analogs that were developed into tool compounds and used to probe the target and mechanism of action. From these molecules we have gained a better understanding of the antibiofilm mechanism of carolacton. In contrast, we have proven that honokiol lacks potent biofilm activity in physiologically relevant conditions. We were able to develop a library of approximately 80 compounds that led to the identification of a new, potent antimicrobial bisphenolic scaffold, C2. Furthermore, from our structure-activity relationship study, we have identified a secondary modification that appears to change the mechanism of the inhibition against *S. mutans*. The investigation of these two natural products has led to multiple discoveries that are impactful for the field of antibiotic development. The data provided in this dissertation will influence the future of antibiofilm research.

Carolacton and Honokiol: using natural product inspiration to target the oral microbiome

By

Amy E. Solinski
B.S., The College of New Jersey, 2015

Advisor: William M. Wuest, Ph.D.

A dissertation submitted to the Faculty of the
James T. Laney School of Graduate Studies of Emory University
in partial fulfillment of the requirements for the degree of
Doctor of Philosophy in Chemistry
2020

Acknowledgements:

My graduate experience would not be the same if I did not have my supportive family, friends and mentors by my side for the past five years. To these people, I owe my past, present and future successes. I need to thank my advisor Bill Wuest for giving me access to all of the opportunities that I have experienced both at Temple University and Emory University. I always dreamt of a career in academia but was too scared to pursue that dream. Bill not only encouraged me to seriously consider this career, but has also helped me carve out my own path towards this goal. Thank you for being a helpful and considerate mentor, but also for not being afraid to push me to #dobetter.

Thank you to my family for always reminding me to take a break from work and catch up with the real world. To my mother Christine, I am indebted to you for your unyielding support. To my father Robert, thank you for teaching me to take life less seriously. To my siblings, Emily and Patrick, your love and support has been a constant our whole lives. I have also been supported by my extended family members and my future family members. To the Freedners, thank you for supporting Jordan and I while we tackled long-distance between Philadelphia and Atlanta.

My science was supported by researchers around the globe. The members of Prof. Robert Quivey laboratory at University of Rochester have been consistent advisors on all things *S. mutans*. Specifically, researcher Roberta Faustoferri facilitated the transfer of genetic knockout strains that were integral for the successes of the carolacton project. The laboratory of Prof. Stephan Sieber at the Technical University of Munich has been essential to the proteomic work shown in Chapter 3. Graduate student Ines Hübner, not only was a wonderful mentor, but also a great friend during my time in Munich.

Since joining the Wuest Group in 2015, I have been acquainted with wonderful colleagues that have helped me grow as a scientist. It would be hard to list every single member, but I thank all of you for making this experience as memorable as it has been. Specifically, I need to thank my first lab mentor, Dr. Alex Koval, for practicing extreme patience while I was learning in my first year. Once moving to Emory University, Amber Scharnow joined team carolacton and I am thankful that she fully incorporated herself into the project. I thank her for being a good teammate, confidant, mentee and mentor depending on the day, and a good friend. Working alongside her has taught me how to be unabashedly be myself (i.e. high energy) and get things done.

At the start of this process I was gifted with a wonderful cohort of friends: Andrew Mellinger, Dr. Kelly Morrison, Lauren (Martin) Rossiter, and Sean Rossiter. They have helped me succeed through graduate school and our friendships have withstood many of life's challenges. Thank you guys for always being there!

One of my favorite years of my life was when I moved into "Casa LaVista" with Erika Csatory, Dr. Colleen Keohane, Sean Rossiter, and Dr. Andrew Steele. We turned from roommates to family and I will forever be grateful for that. Soon after, Raven Shah and Sam Druzak also joined the family by moving into the house. I am thankful for all of our good times!

Finally, I need to thank Jordan Freedner for loving and supporting me through every up and down of graduate school. We were naïve when I started, thinking that Manayunk to New Jersey was far, but I am beyond thankful that our relationship has continued to grow and develop into what it is today. I cannot wait to see what our future holds.

Table of Contents

Chapter 1	Introduction	1
1.1	Oral Microbiome	1
1.1.1	Introduction	1
1.1.2	Commensal vs pathogenic bacteria: dysbiosis in the oral microbiome	2
1.1.3	Dental cavities	3
1.2	Biofilm Formation	4
1.2.1	Global impact	4
1.2.2	Mechanism of biofilm formation	5
1.2.3	A model organism – <i>Streptococcus mutans</i>	7
1.3	Anti-biofilm small molecules against <i>S. mutans</i>	8
1.3.1	Introduction – Prevention vs Treatment	8
1.3.2	Sucrose-dependent mechanisms	9
1.3.3	Sucrose-independent mechanisms	10
1.3.4	Cellular signaling interference	11
1.3.5	Next generation anti-biofilm compounds	12
1.4	References	13
Chapter 2	Natural Product Carolacton	18
2.1	Background	18
2.1.1	Carolacton's isolation and biofilm specific activity	18
2.2	Total syntheses	19
2.2.1	Kirschning Group	19
2.2.2	Wuest/Phillips Group	21
2.2.3	Goswami Group	22
2.2.4	Carolacton derivatives	22
2.3	Progress towards target identification	24
2.3.1	Carolacton: a decade of biological investigation	24
2.3.2	Target or targets?	28
2.3.3	Rationale and design for simplified analogs	29
2.4	Generation 1: Carylacton Analogs	30
2.4.1	Synthesis of carylacton analogs	30
2.4.2	Discovery of new phenotypes	32
2.4.3	Computational modeling	36
2.4.4	Generation 1 conclusions	37
2.5	Generation 2: Simplified Sidechain Analogs	38
2.5.1	Analog development	38
2.5.2	Synthesis of simplified analogs	39
2.5.3	Biofilm-specific inhibition	41
2.5.4	LIVE/DEAD® Staining with Confocal Imaging	42

2.5.5	Colony Forming Unit Assay	44
2.5.6	Acid tolerance based activity	44
2.5.7	Genetic Screen with Analog 2.....	45
2.5.8	Conclusions.....	48
2.6	References	50
Chapter 3 Analog 2 Target Elucidation.....		52
3.1	Affinity-based proteomic probe	52
3.1.1	Affinity-based Protein Profiling.....	52
3.1.2	Synthesis of analog 2 probe.....	53
3.1.3	Developing the biofilm workflow	54
3.1.4	Identified protein targets	57
3.1.5	Competition assay	58
3.1.6	Proteomic pulldown results.....	60
3.2	Proteomic result validation	61
3.2.1	Resistance assay development	61
3.2.2	Δ ftsA, Δ ftsX, Δ brpA, and Δ folD screen	62
3.2.3	Δ folD.....	64
3.2.4	GbpB: the main biofilm target?.....	66
3.3	Future directions	68
3.4	Conclusions	69
3.5	References	72
Chapter 4 Honokiol		74
4.1	Background	74
4.1.1	Isolation	74
4.1.2	Anti-bacterial activity	75
4.2	Generation 1	76
4.2.1	Synthesis of Generation 1	76
4.2.2	Micro-aerophilic vs aerophilic growth conditions	79
4.2.3	Structure-activity relationships of Generation 1.....	80
4.2.4	Lead compound C2 and Generation 2 design	83
4.3	Generation 2.....	83
4.3.1	Structure-activity relationships of generation 2	83
4.3.2	Hemolysis results	85
4.3.3	Mechanism of action – C2	86
4.4	Mechanism of action – C2-propyl	90
4.5	Future Directions	96
4.5.1	Sortase A Hypothesis	97
4.6	Conclusions	97
4.7	References	99
Chapter 5 Experimental Details		101

5.1	Supplemental Figures.....	101
5.2	Biofilm Replicates Generation 1 (Aryl).....	106
5.2.1	Concentrations 500 μ M or 250 μ M.....	106
5.2.2	Concentrations 125 μ M to 0.5 μ M	137
5.3	Biofilm Replicates Generation 2 (Simplified).....	150
5.4	Carolacton Generation 2 IC₅₀ Curves	155
5.5	Analog 2 Mutant Screen.....	163
5.6	Honokiol Master Compound List.....	167
5.7	Membrane Assay Data	170
5.8	Biological Procedures.....	180
5.9	Chemistry General Notes	189
5.10	Procedures and Characterization	190

List of Figures:

Figure 1.1	The oral microbiome	1
Figure 1.2	Dysbiosis in the oral microbiome	3
Figure 1.3	Mechanism of oral biofilm formation.....	5
Figure 1.4	S. mutans colonies taken from a Wuest Lab member's oral microbiome.	7
Figure 1.5	Mechanism of sucrose-dependent adhesion inhibition.	9
Figure 1.6	Small molecule examples of Gtfs inhibitors.	10
Figure 1.7	Mechanism of sucrose-independent adhesion inhibition.	10
Figure 1.8	Small molecule examples of SrtA inhibitors.	11
Figure 1.9	Mechanisms of bacterial signaling.....	11
Figure 1.10	Small molecule examples of cellular signaling inhibitors.	12
Figure 2.1	Natural product carolacton	18
Figure 2.2	Carolacton derivatives.....	23
Figure 2.3	Biofilm phenotype of CD1	24
Figure 2.4	Timeline for carolacton's biological discoveries	25
Figure 2.5	Connections between carolacton's biological activities	27
Figure 2.6	Carolacton analog design - Generation 1	28
Figure 2.7	Synthetic approach for carolacton analogs	29
Figure 2.8	Analog C3 biofilm inhibition	32
Figure 2.9	Analog D2 and C1 microcolony biofilm phenotype.....	34
Figure 2.10	Carolacton and D4 cause biofilm defects at low concentrations	35
Figure 2.11	Molecular modeling of C3 , C4 , and D4	36
Figure 2.12	Molecular modeling of D4 and carolacton.....	37
Figure 2.13	Analog design for Generation 2	38
Figure 2.14	Planktonic and biofilm inhibition.....	41
Figure 2.15	Biofilm inhibition during confocal imaging	42
Figure 2.16	Analog 2 kills cells in biofilm.....	43
Figure 2.17	Low concentration biofilm effects of carolacton and analog 2.....	43
Figure 2.18	CFU/mL calculation for cell death in biofilm after treatment with analog 2.....	44

Figure 2.19 Analog 2 's acid mechanism	45
Figure 2.20 Analog 2 genetic mutant screen.....	47
Figure 2.21 CcpA gene regulation map.....	48
Figure 2.22 Carolacton and analog 2 comparison	49
Figure 3.1 Affinity-based protein profiling workflow.....	52
Figure 3.2 Comparison of 5 μ M of analog 2 and analog 2-probe on <i>S. mutans</i> biofilm	54
Figure 3.3 Biofilm methods for AfBPP experiment.....	55
Figure 3.5 LC-MS/MS results for analog 2-probe	56
Figure 3.4 Analytical AfBPP results.	56
Figure 3.6 LC-MS/MS results for dose dependent response of analog 2-probe	57
Figure 3.7 AfBPP competition analytical gel.....	58
Figure 3.8 Competition experiment with analog 2	59
Figure 3.9 Competition experiment with carolacton.....	60
Figure 3.10 Potential target overlap of analog 2 and carolacton	61
Figure 3.11 Inhibition mutant screen.....	63
Figure 3.12 Analog 2 biofilm mutant screen	63
Figure 3.13 Folate dehydrogenase activity.....	65
Figure 3.14 FoLD biofilm screen.....	65
Figure 3.15 Two potential targets for analog 2	66
Figure 3.16 <i>S. mutans</i> regulation of GbpB.....	67
Figure 3.17 <i>S. pneumoniae</i> cell division model	68
Figure 4.1 Natural products isolated from <i>Magnolia officinalis</i>	74
Figure 4.2 Growth differences for <i>S. mutans</i> in aerobic and CO ₂ supplemented environments	79
Figure 4.3 Generation 1 honokiol analog scaffolds.....	81
Figure 4.4 Most active compounds from Generation 1 and honokiol	82
Figure 4.5 SAR goals for Generation 2	83
Figure 4.6 SAR results from Generation 1	84
Figure 4.7 Oral antiseptic CPC.....	86
Figure 4.8 TEM images of C2 treated cells.....	87
Figure 4.9 DiBAC ₄ (3) assay	88
Figure 4.10 PI assay.....	89
Figure 4.11 SYTOX assay.....	89
Figure 4.12 Discovery of C2-propyl	90
Figure 4.13 Control compounds for membrane assays	91
Figure 4.14 DiBAC ₄ (3) full results	92
Figure 4.15 PI full results	93
Figure 4.16 SYTOX full results	94
Figure 4.17 Membrane protein assay	95
Figure 4.18 Illustration of Sortase A hypothesis	97
Figure 5.1 Biofilm crystal violet measurement replicates of carolacton generation 2.	101
Figure 5.2 Relative biofilm mass after compound dosing relative to negative control (top). Average biofilm mass after compound dosing (bottom).....	102
Figure 5.3 MIC and MBIC results from honokiol generation 1.	103
Figure 5.4 MBC results for honokiol generation 1.....	104

List of Tables:

Table 2.1 Other carolacton total synthesis attempts	20
---	----

Table 2.2 Conditions for hydrogenation.....	40
Table 2.3 <i>S. mutans</i> mutants from the Quivey Group library	46
Table 3.1 Genetic mutations from contaminated resistance development assay	62
Table 4.1 Timeline of honokiol antibacterial activity against <i>S. mutans</i>	75
Table 4.2 Generation 1 biological activities.....	80
Table 4.3 Generation 2 biological activities and toxicities	85
Table 5.1 MIC and MBC results for honokiol generation 2.....	105

List of Schemes:

Scheme 2.1 Kirschning total synthesis	19
Scheme 2.2 Wuest/Phillips total synthesis of carolacton	21
Scheme 2.3 Goswami total synthesis of carolacton	22
Scheme 2.4 Generation 1 carolacton analog synthesis.....	30
Scheme 2.5 Synthesis of Generation 2	39
Scheme 3.1 Synthesis of analog 2-probe	53
Scheme 3.2 Synthesis of analog 2-biotin	69
Scheme 4.1 Prior syntheses to honokiol.....	77
Scheme 4.2 Kozlowski synthesis of honokiol	78

Abbreviations:

(COCl)₂ – oxalyl chloride
 9-BBN – 9-borabicyclo(3.3.1)nonane
A.a – *Aggregatibacter actinomycetemcomitans*
 Ack – acetate kinase
 AcOH – acetic acid
 ADP – adenosine diphosphate
 AgDS – agmatine deiminase; two-component system
 AgI/II – antigen I/II surface proteins
 ATP – adenosine triphosphate
 ATR – acid tolerance response
 BCA – bicinchoninic acid protein assay
 BrpA – biofilm regulatory protein A
 BzCl – benzoyl chloride
 CcpA – carbon catabolite protein A
 CF – Cystic Fibrosis
 CFU/mL – colony forming unit per milliliter
 CH₂Cl₂ – dichloromethane or DCM
 CidAB – putative membrane proteins
 CodY – global regulator
 ComDE – two-component system; recognizes CSP
 CSA – camphorsulfonic acid
 CsP – competence stimulating peptide
 ddH₂O – double-distilled water
 DDQ – 2,3-Dichloro-5,6-Dicyanobenzoquinone
 DexA – dextranase A

DFT – Discrete Fourier Transform
DIBAL-H – diisobutylaluminum hydride
DivIVa – cell division proteins
DMA – dimethylacetamide
DMAP – 4-dimethylaminopyridine
DMP – Dess-Martin periodane
DMSO – dimethyl sulfoxide
DNA – deoxyribonucleic acid
dppf – 1,1'-Bis(diphenylphosphino)ferrocene
DTS – diverted total synthesis
DTT – dithiothreitol
EDC – coupling reagent; 1-ethyl-3-(3-dimethylaminopropyl)carbodiimide
EPS – extracellular polymeric substances
ETPPI – ethyltriphenylphosphonium iodide
EzrA – cell shape regulator
FA – formic acid
FOLD – folate dehydrogenase
FruA – fructanase
Ftf – fructosyltransferase
FtsA – cell division protein
FtsX – cell division protein
G – glycine
GbpB – glucan binding protein B
GbpC – glucan binding protein C
GFP – green fluorescent protein
GlnA – glutamine synthase
GlnR – controls nitrogen assimilation into cell
Gtfs – Glucosyltransferases
HEPES – (4-(2-hydroxyethyl)-1-piperazineethanesulfonic acid
HF•pyr – hydrogen fluoride pyridine
*i*PrOH – isopropyl alcohol
 K_D – binding affinity; dissociation constant
L – leucine
 $LiAlH_4$ – lithium aluminum hydride
 $LiHMDS$ – lithium hexamethyldisilazide,
 $LiOH$ – lithium hydroxide
LrgAB – putative membrane proteins; pyruvate uptake
MBC – minimum bactericidal concentration
MBIC – minimum biofilm inhibition concentration
mbrABCD – genes associated with bacitracin resistance
MeCN – acetonitrile
MeOH – methanol
MIC – minimum inhibition concentration
MNBA – 2-methyl-6-nitrobenzoic anhydride
MS – mass spectrometry
 $NaClO_2$ – sodium chlorite

NaIO₄ – sodium periodate
NaOCl – sodium hypochlorite
NEt₃ – triethylamine
P – proline
PBS – phosphate buffer saline solution
PcsB – peptidoglycan hydrolase
Pd/C – palladium on carbon, loading 10 wt. %
PknB – serine/threonine-protein kinase B
PMB – *p*-methoxybenzyl
PPTS – pyridinium *p*-toluenesulfonic acid.
Pta – phosphotransacetylase
*p*TSA – *p*-Toluenesulfonic acid
PyrR – regulates transcription of pyrimidine nucleotide
QS – quorum sensing
RCM – ring closing metathesis
RhN₃ – rhodium azide
RT – room temperature
SAR – structure-activity relationship
SDS – sodium dodecyl sulfate
SrtA – sortase A
T – threonine
TBAF – tetra-*n*-butylammonium fluoride
TBAI – tetrabutylammonium iodide
TBS – *tert*-Butyldimethylsilyl
TBSCl – *tert*-Butyldimethylsilyl chloride
TBTA – tris[(1-benzyl-1H-1,2,3-triazol-4-yl)methyl]amine
*t*BuOH – *tert*-Butyl alcohol
TCBC – 2,4,6-trichlorobenzoyl chloride
TCEP – (tris(2-carboxyethyl)phosphine
TCS – two-component system
TEAB – triethylammonium bicarbonate
TEMPO – 2,2,6,6-tetramethylpiperidin-1-yl)oxyl or (2,2,6,6-tetramethylpiperidin-1-yl)oxidanyl
TESOTf – triethylsilyl trifluoromethanesulfonate
TFA – trifluoroacetic acid
THB – Todd Hewitt Broth
THB-S – Todd Hewitt Broth with 0.1% sucrose
THF – tetrahydrofuran
TolC – outer membrane protein; efflux
VicKRX – two component system
WapA – cell-wall associated protein
WapE – cell-wall associated protein
X – any amino a

Chapter 1 Introduction

Section 1.3 has been adapted with permission from (Scharnow, A. M.; Solinski, A. E.; Wuest, W. M. Targeting: *S. mutans* Biofilms: A Perspective on Preventing Dental Caries. *MedChemComm*. 2019. <https://doi.org/10.1039/c9md00015a>). Copyright © 2019 Royal Society of Chemistry.

1.1 Oral Microbiome

1.1.1 Introduction

The oral microbiome contains a broad representation of bacterial species, in a relatively small physiological space. So far, 700 bacterial species have been identified in the oral cavity (Figure 1.1).^{1,2} These species share unique evolutionary relationships between themselves and the host. The oral cavity offers niche growing environments including the tongue, gums, cheek, hard and soft palette, tonsils and more recently work has shown bacterial influence from the nostrils.^{2,3} Researchers have been interested in characterizing this aspect of the human microbiome and the ease of sample collection has advanced research techniques at this interface. In the 1670's, Anthony van Leeuwenhoek was the first researcher to examine oral bacteria and he swabbed his own mouth to examine these species.^{4,5} We continue to study the oral microbiome today in an

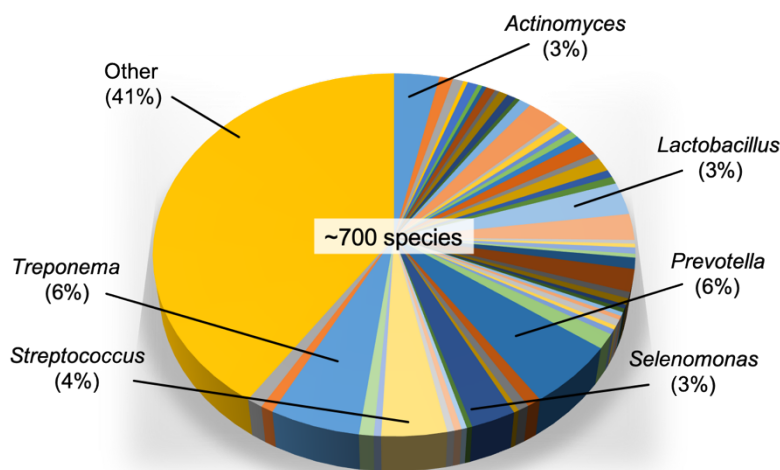


Figure 1.1 The oral microbiome

attempt to gain insight for developing next generation antibiotics and to improve the chemical tools we have to study the complex ecosystem that exists in the human mouth. This text will focus on small molecules that target the pathogenicity of *Streptococcus mutans*, a cariogenic species in the oral cavity. As a preface to that, the larger picture of interactions between commensal and pathogenic species is needed to fully appreciate the complex system that researchers are attempting to understand.

1.1.2 Commensal vs pathogenic bacteria: dysbiosis in the oral microbiome

A common misconception is that bacteria are bad for human health, but in reality there are both good and bad bacteria that populate the world.⁶ There are beneficial bacteria that help with digestion and prevent harmful bacteria from causing infections. These beneficial species are called commensal bacteria and they exist on your skin,⁷ in your gut,⁸ in the soil,⁹ and even on the food you eat.¹⁰ In contrast to commensal bacteria, there are disease-causing, pathogenic bacteria.⁶ Pathogenesis, the formation of disease, can occur through various mechanisms, such as tissue invasion that promotes bacterial adhesion and inflammation, or through toxin production that causes cytotoxicity.¹¹

Within the mouth there are a multitude of commensal and pathogenic bacteria that are constantly competing for dominance in the oral microbiome.¹² For example, *Streptococcus sanguinis* and *Streptococcus gordonii* are related to *S. mutans* but are not pathogenic.¹³ These species will attach to surfaces in the mouth but will not directly cause disease. Intriguingly, *S. sanguinis* and *S. gordonii* have been shown to produce hydrogen peroxide in an effort to neutralize the acid producing, pathogenic bacteria that cause disease in the mouth.¹³

Well-known, pathogenic species *S. mutans* (dental cavities),¹⁴ *Porphyromonas gingivalis* (gingivitis),¹⁵ and *Aggregatibacter actinomycetemcomitans* (A.a) (periodontitis)¹⁶ reside in the oral

cavity. Other pathogenic species, such as the anaerobe *Treponema pallidum*, exist in the mouth but are harder to culture outside of the mouth due to its requirement to grow in a low oxygen environment.¹⁷ *T. pallidum* is the causative agent of syphilis and has been identified to be pervasive in the oral microbiome even in seemingly health patients. Furthermore, pathogenic oral bacteria have been connected to systemic diseases (i.e. infective endocarditis and diabetes) thus highlighting the importance of understanding the connections within the oral microbiome.¹⁸⁻²⁰

The commensal and pathogenic bacteria described above are a few examples of the over 700 species that are competing for the same nutrients and growth territory in the oral cavity. This competitive environment leads to a struggle for survival between species. Normally, there is an equilibrium, or symbiosis.^{8, 20} When external stresses cause a shift in this balance, pathogenic species have the ability to take over and cause disease (Figure 1.2).²¹ Some bacteria can even demonstrate both commensal and pathogenic behaviors. For example, *P. gingivalis* is benign in most circumstances, but under the right conditions it can infect the gums and cause gingivitis, a common gum disease condition that inflicts 46% of American adults.¹⁵

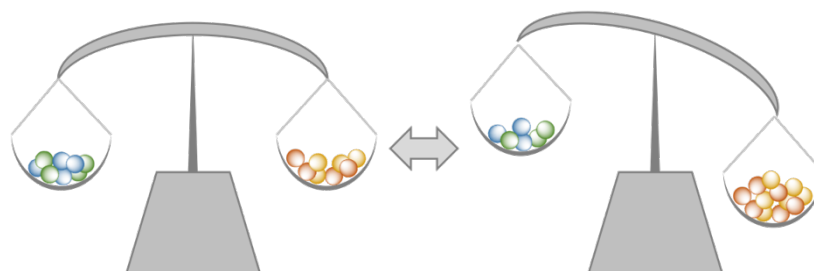


Figure 1.2 Dysbiosis in the oral microbiome

1.1.3 Dental cavities

Dental cavities (caries) is the most common childhood disease and a worldwide burden. In 2016 alone it affected 3.58 billion people.²² In the United States roughly 46% of children (ages 2-19) have cavities in their primary/permanent teeth.²³ In comparison, over 92% of adults (ages 20-64) in the United States have cavities in their permanent teeth, showing the enormous, wide-spread

impact of the disease.²⁴ In 2010, it was calculated that \$298 billion was paid world-wide for direct treatment of dental cavities.¹⁸ The same report also stated that an additional \$144 billion was lost due to indirect costs. These indirect costs were calculated from the decrease in productivity due to parents taking off work to care for their children's cavities.¹⁸ The health and financial burdens of this disease have led to societal concern, attention from large pharmaceutical companies and also the development of research programs with the focus of understanding how to limit and prevent the formation of dental cavities. Acid producing bacteria create dental cavities by forming dental plaque. The plaque, or dental biofilm, causes an environmental acidification that leads to tooth decay.¹⁴ The mechanism of biofilm formation will be discussed further in the subsequent sections.

1.2 Biofilm Formation

1.2.1 Global impact

For a long time, bacterial cells were viewed as free floating, or planktonic cells.²⁵ Bacteria can also adhere to surfaces, where they form conglomerates of cells on these surfaces, and thrive as a connected bacterial community.²⁵ These clusters of cells are called biofilms and are protected by an extracellular polymeric substance (EPS) matrix.²⁶ The adhered cells and the EPS matrix have the ability to evade external stresses via a cooperative effort.²⁷ It has been found that 80% of chronic bacterial infections are biofilm in nature, thus biofilm processes have become prevalent targets in the search for the next generation of antibiotics.²⁸ Biofilm has been classified as a virulence factor due to its connection to severe bacterial infections.²⁹ In particular, biofilm mechanisms dominant the bacterial landscape in the cystic fibrosis (CF) lung.^{30, 31} Additionally, patients receiving implants (joint replacement, heart valve replacement, etc.), catheter insertions or other medical devices, are at risk for infection.^{32, 33} Approximately 25% of these procedures will have complications form due to biofilm infections.³⁴ Even in the shipping industry biofilms adhere

on the hull of ships, which leads to the attachment of larger organisms, such as barnacles. This process is called biofouling and it has been calculated to cause a 35-40% increase in fuel usage per year due to increased drag for naval ships.³⁵ Due to the prevalence of biofilm growth in multiple industries, researchers have been highly interested in 1) understanding the mechanism of biofilm formation and 2) developing ways to impede the formation and permanence of biofilm.

1.2.2 Mechanism of biofilm formation

Biofilm can form in a large array of locations. For the purpose of simplicity, the mechanism of biofilm formation will be described from the perspective of the oral microbiome and an illustration of a general biofilm lifecycle can be seen in Figure 1.3. Early bacterial colonizers have the ability to make the first attachment to surfaces in the oral cavity (teeth, gums, tonsils cheeks, hard and soft palates, and tongue).³⁶ This process begins with sucrose-dependent and sucrose-independent attachment (details: *vide infra*).³⁷ If left undisturbed, these small colonies will progress to mature biofilm. In other situations, invading species, sometimes pathogenic, can invade the primary colonies, proliferate, and take over the growth of that colony. Microcolonies, or small clusters of biofilm, form first.³⁸ At this stage, the cells are able to upregulate the use of

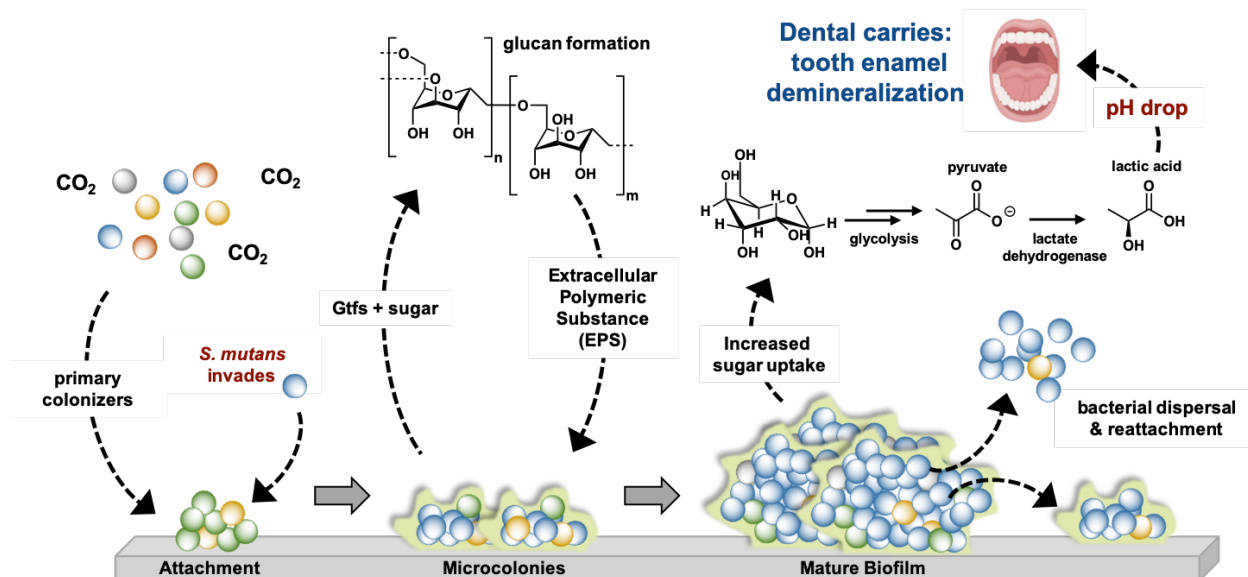


Figure 1.3 Mechanism of oral biofilm formation

their glucosyltransferases (Gtfs) to form glucan polymers that contribute to the building of the EPS matrix and the attachment of more cells.

While biofilm matures, sugar uptake increases.³⁹ As previously mentioned, the sugar can be converted to glucan polymers by the various Gtfs, but it will also be used in glycolysis.⁴⁰ All bacteria will produce energy from external nutrients, but in the oral cavity there are aciduric bacteria that use their nutrients to create organic acids.⁴¹ The accumulation of the acids is used to outcompete other species that do not thrive at low pH.¹³ Lactic acid is commonly produced, and will cause a decrease in the environmental pH. In the oral cavity, the pH can drop as low as four when the production is uninterrupted and there is a lack of alkaline producing species to compete against the acid production.⁴² The lactic acid can build up and erode the tooth enamel to form a dental cavity.⁴³ Bacterial species that can withstand this drop of pH are called acidogenic and have mechanisms that allow the cells to stay viable at a low pH.⁴⁴

After formation of the biofilm, the cells share a level of protection from outside stresses.^{28, 45, 46} For example, it has been shown that cells are in a dormant stage and are able to withstand antibiotics since the normal metabolic pathways have been decreased.⁴⁷ Additionally, the EPS matrix offers protection from physical stresses. The mature biofilm has the ability to disperse at a later time to reattach and infect a new area within the host.⁴⁸ Bacteria have systems to coordinate attachment and dispersal depending on what stresses are present.⁴⁹ These signaling systems will be discussed in later sections as potential targets for developing anti-biofilm molecules. It is evident that understanding the mechanisms of biofilm would be beneficial for multiple industries and that targeting the biofilm lifecycle could be prudent in the search for new potent antibiotics.⁵⁰ For these reasons, we have focused our efforts at studying this issue with the use of a model organism for biofilm formation: *S. mutans*.¹⁴

1.2.3 A model organism – *Streptococcus mutans*



Figure 1.4 *S. mutans* colonies taken from a Wuest Lab member's oral microbiome.

S. mutans is a Gram-positive facultative anaerobe that can be found mainly in the oral cavity.^{2, 14} “Coccus” refers to its spherical shape shown in Figure 1.4. It was first described by J. Killan Clarke in 1924 and since then has been one of the main focuses of oral research due to its connection with the formation of dental cavities.⁵¹ Other acid producing species are undoubtedly connected to the pathology of tooth decay and cavity formation, but *S. mutans* has been a staple in this field due to its easy genetic trackability and manipulation.^{52, 53} *S. mutans* was first identified to have biofilm formation in the 1960's.⁵⁴ Moreover, *S. mutans* has been a model species for studying the formation of biofilm due to the simple conditions needed to replicate biofilm growth in a laboratory setting.¹⁴ Professor Robert J. Quivey, an expert in *S. mutans* biofilm from University of Rochester, has even described *S. mutans* as the “new Gram-positive paradigm”. For these reasons we have chosen *S. mutans* for our model biofilm organism for the formation of dental cavities.

1.2.3.1 *Streptococcus mutans* acid tolerance mechanisms

S. mutans has the ability to evade the stress of a lower pH environments via multiple mechanisms which collectively are referred to as the acid tolerance response (ATR).⁴⁴ This

bacterium upregulates the production and proportion of unsaturated fatty acid that exist in the cellular membrane and also increases the glucan production (one proponent of the EPS) to allow a higher tolerance of low pH environments.⁴² It actively regulates the cytoplasm to keep a neutral pH by overexpressing ATPases that actively pump protons into the extracellular space.⁴² *S. mutans* also has the ability to counteract the presence of lactic acid by increasing the function of the agmatine deaminase system (AgDS).⁵⁵ This system catabolizes agmatine, a form of arginine that has been decarboxylated, to putrescine, CO₂ and ammonia, which help neutralize the cytoplasm directly.⁵⁵ *S. mutans* has also adapted to turn on malolactic fermentation, increase branched-chain amino acid synthesis and also down regulate the influx of sucrose by decreasing the abundance of phosphotransferase (PTS) systems.⁵⁵ Finally, if the above systems fail, *S. mutans* has a special acid inducible base excision repair system that can repair any DNA damage that occurs when the cells are experiencing low pH environments.⁴² Together, these processes allow *S. mutans* to survive the low pH environment that it creates to outcompete other bacterial species that exist in the oral microbiome.¹³ For an oral therapeutic standpoint, targeting the acid tolerance mechanisms would be a plausible method to specifically target the pathogenic bacteria that contribute to dental cavities in the oral cavity.

1.3 Anti-biofilm small molecules against *S. mutans*

1.3.1 Introduction – Prevention vs Treatment

There have been many approaches to combat the growth of dental biofilm (plaque). It would be prudent to have a diet low in sugar, brush and floss teeth regularly to prevent the formation of this cavity-inducing biofilm.⁵⁶ During routine cleanings, dentists will often use fluoride to reinforce your teeth in an attempt to prevent the plaque acidification from eroding the enamel and repair existing damage to the enamel.⁵⁷ Moreover, oral health professionals have also

produced data showing that nonfermentable sugars (i.e. xylitol) could be used in food products to decrease the occurrence of cavities.⁵⁸ However, this idea has not gained widespread acceptance. Despite these prevention techniques, people struggle with severe dental/oral issues. Research has shown that differences in oral microbiome make-up can contribute to prevalence of dental cavities and also other oral diseases.⁵⁹ Some data has even shown parent oral health is connected to their children's oral health.⁶⁰ In these incidences, prevention techniques might not suffice and treatment techniques are needed. Currently, mouthwashes and toothpastes contain antimicrobial agents to kill bacteria residing in the mouth. These agents, such as chlorhexidine and cetylpyridinium chloride, are used to kill bacteria but are not as useful against the cavity-causing biofilms that grow on the tooth enamel.⁶¹⁻⁶³ Researchers are interested in discovering compounds that will affect *S. mutans* biofilms specifically and have found success by targeting three many methods: sucrose-dependent mechanisms, sucrose-independent mechanisms and cellular signaling.³⁷

1.3.2 Sucrose-dependent mechanisms

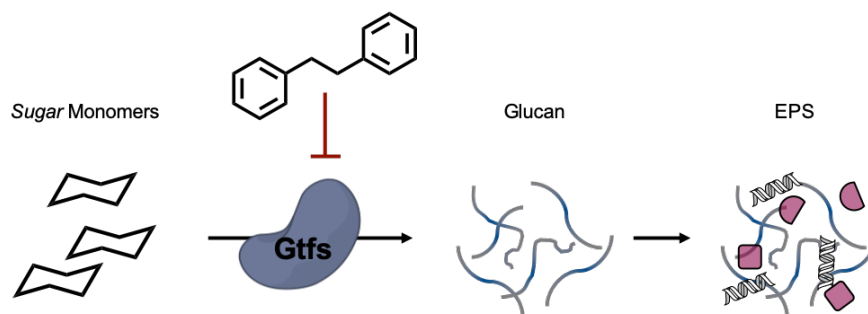


Figure 1.5 Mechanism of sucrose-dependent adhesion inhibition.

S. mutans has evolved multiple methods of cellular attachment. Sucrose-dependent mechanisms rely on the uptake and usage of sugar monomers from its environment (Figure 1.5).⁴⁰ It was previously mentioned that glucosyltransferases (Gtfs) have the ability to form glucan polymers and it is known that this process happens inside and outside the cells. Three different Gtfs contribute to *S. mutans* glucan production, and they are coded for in the *gtfBCD* operon.⁶⁴

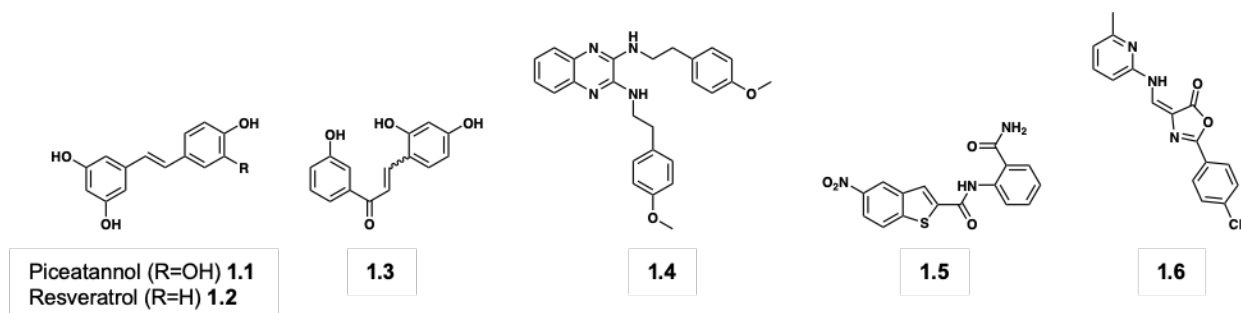


Figure 1.6 Small molecule examples of Gtfs inhibitors.

Examples have shown that GtfC can bind to enamel, where their sole purpose is to produce the glucans that contribute to dental plaque. GtfD makes glucan primers that can be used by the other Gtfs. Finally, GtfB binds to bacteria stimulating cell clustering within the biofilm. Together these enzymes contribute greatly to the EPS formation and for that reason have been targeted by chemists to inhibit biofilm formation. Nijampatnam and coworkers have been very proliferative in this field identifying many resveratrol-like compounds, 1.1 and 1.3, as effective inhibitors against *S. mutans* Gtfs (Figure 1.6).⁶⁵⁻⁶⁷

1.3.3 Sucrose-independent mechanisms

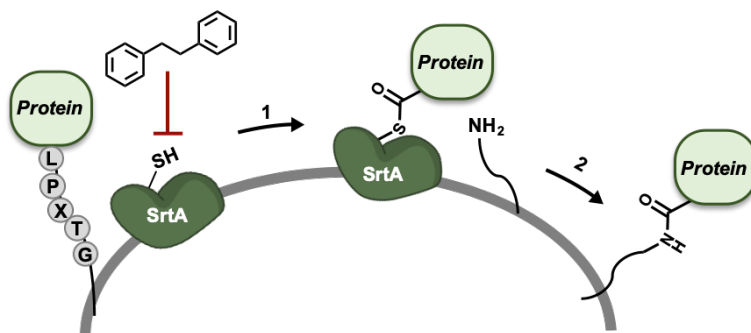


Figure 1.7 Mechanism of sucrose-independent adhesion inhibition.

S. mutans uses sucrose-independent mechanisms that help create “sticky” contacts on the outside of the cells to help cell-cell and cell-surface adhesion.⁶⁸ This process is aided by Sortase A (SrtA), an enzyme that covalently attaches proteins to the surface of the cell (Figure 1.7).⁶⁹ SrtA recognizes the LPXTG motif in the substrate protein, cleaves between the threonine (T) and the glycine (G), and then transfers the protein to the cell wall via amide bond formation.⁷⁰ A small

group of proteins have the correct motif to be identified and adhered to the outside of the cell (AgI/II, FruA, WapA, WapE, GbpC, and DexA).⁷¹ AgI/II, or antigen I/II is a great example of the impact that these sucrose-independent mechanisms have on adhesion. After attachment to the outside of the cell, AgI/II are able to create adherence interactions with the tooth enamel via recognition of salivary glycoproteins.⁷² Without these interactions, adhesion is greatly depleted. A diversity of chemical scaffolds has been identified to inhibit SrtA activity. A sample of these structures are shown in Figure 1.8.³⁷

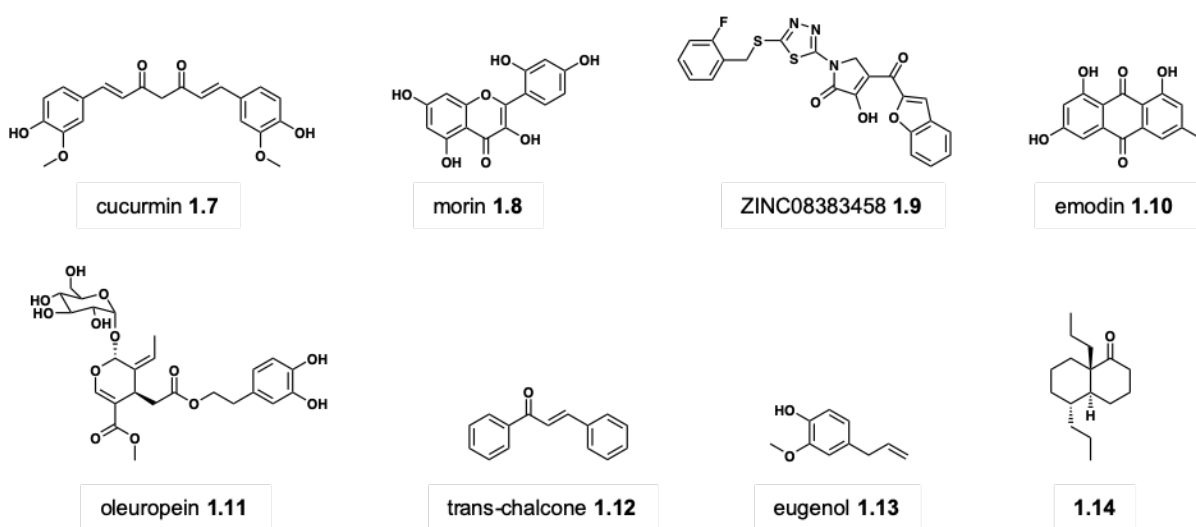


Figure 1.8 Small molecule examples of SrtA inhibitors.

1.3.4 Cellular signaling interference

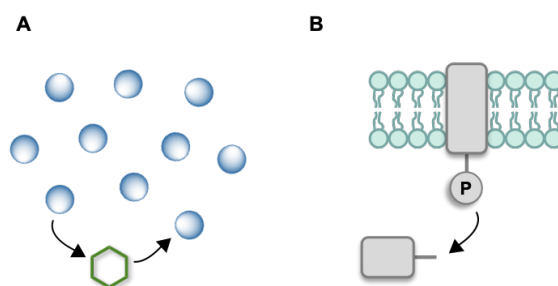


Figure 1.9 Mechanisms of bacterial signaling.

The last method that has been used to target cellular adhesion during biofilm formation is interruption of the cellular signaling pathways that direct the biofilm behavior. This indirect

method of halting adherence mechanisms has gained popularity as the quorum sensing (QS) field has gained momentum.⁷³ QS is the collective behavior that is controlled by small molecule signals (Figure 1.9 A).⁷⁴ When the bacterial cells are present in a large population density, or a quorum, chemical signals are used to direct group behaviors.⁷⁵ Two-component systems (TCS) are also used to disseminate cellular signals.⁷⁶ TCSs start signal transduction within the cell via phosphorylation cascade (Figure 1.9 B).⁷⁷ The TCS contains two proteins, a histidine kinase, that works as a sensor, and a response regulator, that receives the signal and translates it to an action within the cell. A diversity of chemical scaffolds has been identified to inhibit signaling activity. A sample of these structures are shown in Figure 1.10.³⁷

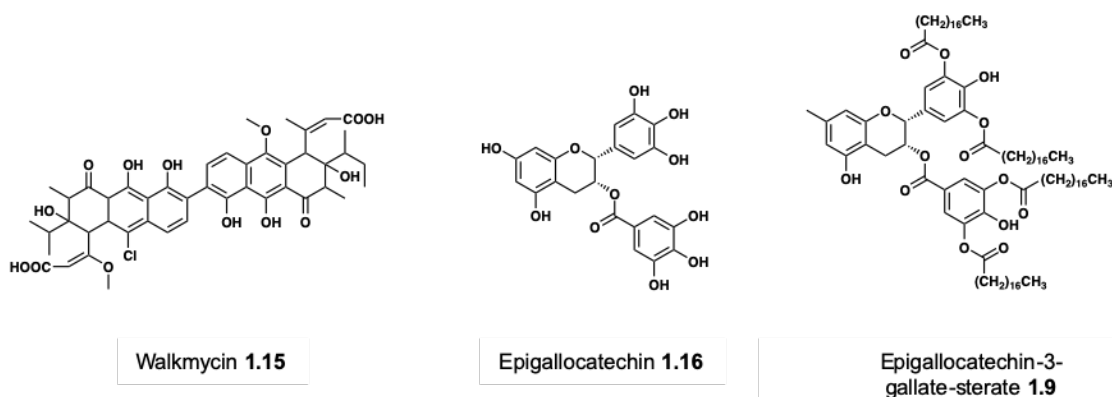


Figure 1.10 Small molecule examples of cellular signaling inhibitors.

1.3.5 Next generation anti-biofilm compounds

The sections above have outlined the small molecules that have been shown to inhibit various mechanisms of biofilm formation in *S. mutans*. These themes are consistently explored throughout the biofilm literature. Development of anti-biofilm compounds has been limited by our general knowledge of biofilm formation and development. Discovering new anti-biofilm compounds could lead to 1) a better understanding of biofilm mechanics and 2) would offer alternate routes for development novel antibiotics. The ATR would be an interesting target due to its direct connection to the pathogenicity of *S. mutans*, but finding a selective ATR target is not

facile due to the complexity of the ATR response. Nonetheless, it is worth investigating these systems due to the impact they would have on global health and industry. Additionally, multiple fields of fundamental science would also benefit from having novel tool compounds that perturb biofilm mechanisms. In the following chapters, these themes will be addressed with the scientific stories regarding investigation of the natural products **carolacton** and **honokiol**.

1.4 References

1. Aas, J. A.; Paster, B. J.; Stokes, L. N.; Olsen, I.; Dewhirst, F. E., Defining the normal bacterial flora of the oral cavity. *J Clin Microbiol* **2005**, *43* (11), 5721-32.
2. Dewhirst, F. E.; Chen, T.; Izard, J.; Paster, B. J.; Tanner, A. C. R.; Yu, W.-H.; Lakshmanan, A.; Wade, W. G., The Human Oral Microbiome. *Journal of Bacteriology* **2010**, *192* (19), 5002.
3. Escapa, I. F.; Chen, T.; Huang, Y.; Gajare, P.; Dewhirst, F. E.; Lemon, K. P., New Insights into Human Nostril Microbiome from the Expanded Human Oral Microbiome Database (eHOMD): a Resource for the Microbiome of the Human Aerodigestive Tract. *mSystems* **2018**, *3* (6), e00187-18.
4. Deo, P. N.; Deshmukh, R., Oral microbiome: Unveiling the fundamentals. *J Oral Maxillofac Pathol* **2019**, *23* (1), 122-128.
5. Yamashita, Y.; Takeshita, T., The oral microbiome and human health. *Journal of Oral Science* **2017**, *59* (2), 201-206.
6. Hornef, M., Pathogens, Commensal Symbionts, and Pathobionts: Discovery and Functional Effects on the Host. *ILAR Journal* **2015**, *56* (2), 159-162.
7. Christensen, G.; Brüggemann, H., Bacterial skin commensals and their role as host guardians. *Beneficial microbes* **2013**, *5*, 1-15.
8. Thursby, E.; Juge, N., Introduction to the human gut microbiota. *Biochem J* **2017**, *474* (11), 1823-1836.
9. Finkel, O. M.; Castrillo, G.; Herrera Paredes, S.; Salas González, I.; Dangl, J. L., Understanding and exploiting plant beneficial microbes. *Curr Opin Plant Biol* **2017**, *38*, 155-163.
10. Wang, H.; Yabes-Manuzon, M.; Lehman, M.; Wan, K.; Luo, H.; Wittum, T.; Yousef, A.; Bakaletz, L., Food commensal microbes as a potentially important avenue in transmitting antibiotic resistance genes. *FEMS microbiology letters* **2006**, *254*, 226-31.
11. Wilson, J. W.; Schurr, M. J.; LeBlanc, C. L.; Ramamurthy, R.; Buchanan, K. L.; Nickerson, C. A., Mechanisms of bacterial pathogenicity. *Postgrad Med J* **2002**, *78* (918), 216-224.
12. Dewhirst, F. E.; Chen, T.; Izard, J.; Paster, B. J.; Tanner, A. C.; Yu, W. H.; Lakshmanan, A.; Wade, W. G., The human oral microbiome. *J Bacteriol* **2010**, *192* (19), 5002-17.

13. Kreth, J.; Zhang, Y.; Herzberg, M. C., Streptococcal antagonism in oral biofilms: Streptococcus sanguinis and Streptococcus gordonii interference with Streptococcus mutans. *Journal of bacteriology* **2008**, *190* (13), 4632-4640.
14. Lemos, J. A.; Quivey, R. G.; Koo, H.; Abranches, J., Streptococcus mutans: a new Gram-positive paradigm? *Microbiology (Reading, England)* **2013**, *159* (Pt 3), 436-445.
15. How, K. Y.; Song, K. P.; Chan, K. G., Porphyromonas gingivalis: An Overview of Periodontopathic Pathogen below the Gum Line. *Frontiers in microbiology* **2016**, *7*, 53-53.
16. Raja, M.; Ummer, F.; Dhivakar, C. P., Aggregatibacter actinomycetemcomitans - a tooth killer? *J Clin Diagn Res* **2014**, *8* (8), ZE13-ZE16.
17. Radolf, J. D.; Deka, R. K.; Anand, A.; Šmajš, D.; Norgard, M. V.; Yang, X. F., Treponema pallidum, the syphilis spirochete: making a living as a stealth pathogen. *Nature reviews. Microbiology* **2016**, *14* (12), 744-759.
18. Listl, S.; Galloway, J.; Mossey, P. A.; Marcenes, W., Global Economic Impact of Dental Diseases. *J Dent Res* **2015**, *94* (10), 1355-61.
19. Petersen, P. E.; Bourgeois, D.; Ogawa, H.; Estupinan-Day, S.; Ndiaye, C., The global burden of oral diseases and risks to oral health. *Bull World Health Organ* **2005**, *83* (9), 661-669.
20. Sudhakara, P.; Gupta, A.; Bhardwaj, A.; Wilson, A., Oral Dysbiotic Communities and Their Implications in Systemic Diseases. *Dent J (Basel)* **2018**, *6* (2), 10.
21. Lamont, R. J.; Koo, H.; Hajishengallis, G., The oral microbiota: dynamic communities and host interactions. *Nature reviews. Microbiology* **2018**, *16* (12), 745-759.
22. Disease, G. B. D.; Injury, I.; Prevalence, C., Global, regional, and national incidence, prevalence, and years lived with disability for 328 diseases and injuries for 195 countries, 1990-2016: a systematic analysis for the Global Burden of Disease Study 2016. *Lancet* **2017**, *390* (10100), 1211-1259.
23. Flemming, E.; Afful, J., Prevalence of total and untreated dental caries among youth: United States 2015-2016. *NCHHS Data Brief* **2018**, *307*.
24. Dental Caries (Tooth Decay) in Adults (Age 20 to 64). *National Institute of Dental and Craniofacial Research* **2018**.
25. Costerton, J. W.; Geesey, G. G.; Cheng, K. J., How Bacteria Stick. *Scientific American* **1978**, *238*, 86-95.
26. Flemming, H.-C.; Neu, T. R.; Wozniak, D. J., The EPS matrix: the "house of biofilm cells". *Journal of bacteriology* **2007**, *189* (22), 7945-7947.
27. Sharma, D.; Misba, L.; Khan, A. U., Antibiotics versus biofilm: an emerging battleground in microbial communities. *Antimicrobial Resistance & Infection Control* **2019**, *8* (1), 76.
28. Davies, D., Understanding biofilm resistance to antibacterial agents. *Nature Reviews Drug Discovery* **2003**, *2* (2), 114-122.
29. Koo, H.; Allan, R. N.; Howlin, R. P.; Stoodley, P.; Hall-Stoodley, L., Targeting microbial biofilms: current and prospective therapeutic strategies. *Nature reviews. Microbiology* **2017**, *15* (12), 740-755.
30. Høiby, N.; Ciofu, O.; Bjarnsholt, T., Pseudomonas aeruginosa biofilms in cystic fibrosis. *Future Microbiology* **2010**, *5* (11), 1663-1674.
31. Moreau-Marquis, S.; Stanton, B. A.; O'Toole, G. A., Pseudomonas aeruginosa biofilm formation in the cystic fibrosis airway. *Pulm Pharmacol Ther* **2008**, *21* (4), 595-599.
32. Hazan, Z.; Zumeris, J.; Jacob, H.; Raskin, H.; Kratysh, G.; Vishnia, M.; Dror, N.; Barliya, T.; Mandel, M.; Lavie, G., Effective prevention of microbial biofilm formation on

- medical devices by low-energy surface acoustic waves. *Antimicrobial agents and chemotherapy* **2006**, *50* (12), 4144-4152.
33. Trautner, B. W.; Darouiche, R. O., Role of biofilm in catheter-associated urinary tract infection. *Am J Infect Control* **2004**, *32* (3), 177-183.
 34. Khatoon, Z.; McTiernan, C. D.; Suuronen, E. J.; Mah, T.-F.; Alarcon, E. I., Bacterial biofilm formation on implantable devices and approaches to its treatment and prevention. *Heliyon* **2018**, *4* (12), e01067-e01067.
 35. Munk, T.; Kane, D.; Yebra, D. M., 7 - The effects of corrosion and fouling on the performance of ocean-going vessels: a naval architectural perspective. In *Advances in Marine Antifouling Coatings and Technologies*, Hellio, C.; Yebra, D., Eds. Woodhead Publishing: 2009; pp 148-176.
 36. Avila, M.; Ojcius, D. M.; Yilmaz, O., The oral microbiota: living with a permanent guest. *DNA Cell Biol* **2009**, *28* (8), 405-411.
 37. Scharnow, A. M.; Solinski, A. E.; Wuest, W. M., Targeting *S. mutans* biofilms: a perspective on preventing dental caries. *MedChemComm* **2019**, *10* (7), 1057-1067.
 38. Xiao, J.; Koo, H., Structural organization and dynamics of exopolysaccharide matrix and microcolonies formation by *Streptococcus mutans* in biofilms. *Journal of Applied Microbiology* **2010**, *108* (6), 2103-2113.
 39. Jacobson, G. R.; Lodge, J.; Poy, F., Carbohydrate uptake in the oral pathogen *Streptococcus mutans*: mechanisms and regulation by protein phosphorylation. *Biochimie* **1989**, *71* (9), 997-1004.
 40. Ooshima, T.; Matsumura, M.; Hoshino, T.; Kawabata, S.; Sobue, S.; Fujiwara, T., Contributions of Three Glucosyltransferases to Sucrose-dependent Adherence of *Streptococcus mutans*. *Journal of Dental Research* **2001**, *80* (7), 1672-1677.
 41. Guo, L.; Hu, W.; He, X.; Lux, R.; McLean, J.; Shi, W., investigating acid production by *Streptococcus mutans* with a surface-displayed pH-sensitive green fluorescent protein. *PLoS one* **2013**, *8* (2), e57182-e57182.
 42. Matsui, R.; Cvitkovitch, D., Acid tolerance mechanisms utilized by *Streptococcus mutans*. *Future microbiology* **2010**, *5* (3), 403-417.
 43. Forssten, S. D.; Björklund, M.; Ouweland, A. C., *Streptococcus mutans*, caries and simulation models. *Nutrients* **2010**, *2* (3), 290-298.
 44. Georgios, A.; Vassiliki, T.; Sotirios, K., Acidogenicity and acidurance of dental plaque and saliva sediment from adults in relation to caries activity and chlorhexidine exposure. *Journal of oral microbiology* **2015**, *7*, 26197-26197.
 45. Donlan, R. M., Biofilms: microbial life on surfaces. *Emerg Infect Dis* **2002**, *8* (9), 881-890.
 46. Kolenbrander, P. E., Oral Microbial Communities: Biofilms, Interactions, and Genetic Systems. *Annual Review of Microbiology* **2000**, *54* (1), 413-437.
 47. Stewart, P. S., Mechanisms of antibiotic resistance in bacterial biofilms. *International Journal of Medical Microbiology* **2002**, *292* (2), 107-113.
 48. Kaplan, J. B., Biofilm dispersal: mechanisms, clinical implications, and potential therapeutic uses. *Journal of dental research* **2010**, *89* (3), 205-218.
 49. Guillen, C.; Forestier, C.; Balestrino, D., Biofilm dispersal: multiple elaborate strategies for dissemination of bacteria with unique properties. *Molecular Microbiology* **2017**, *105* (2), 188-210.

50. Gebreyohannes, G.; Nyerere, A.; Bii, C.; Sbhatu, D. B., Challenges of intervention, treatment, and antibiotic resistance of biofilm-forming microorganisms. *Heliyon* **2019**, *5* (8), e02192-e02192.
51. Clarke, J. K., On the Bacterial Factor in the Ætiology of Dental Caries. *Br J Exp Pathol* **1924**, *5* (3), 141-147.
52. Banas, J. A.; Drake, D. R., Are the mutans streptococci still considered relevant to understanding the microbial etiology of dental caries? *BMC Oral Health* **2018**, *18* (1), 129.
53. Nishikawara, F.; Nomura, Y.; Imai, S.; Senda, A.; Hanada, N., Evaluation of cariogenic bacteria. *Eur J Dent* **2007**, *1* (1), 31-39.
54. Macdonald, J. B.; Gibbons, R. J.; Socransky, S. S., BACTERIAL MECHANISMS IN PERIODONTAL DISEASE*. *Annals of the New York Academy of Sciences* **1960**, *85* (1), 467-478.
55. Baker, J. L.; Faustoferri, R. C.; Quivey, R. G., Jr., Acid-adaptive mechanisms of Streptococcus mutans-the more we know, the more we don't. *Molecular oral microbiology* **2017**, *32* (2), 107-117.
56. Zero, D. T.; Fontana, M.; Martínez-Mier, E. A.; Ferreira-Zandoná, A.; Ando, M.; González-Cabezas, C.; Bayne, S., The Biology, Prevention, Diagnosis and Treatment of Dental Caries: Scientific Advances in the United States. *The Journal of the American Dental Association* **2009**, *140*, 25S-34S.
57. Petersen, P., Prevention of dental caries through the effective use of fluoride – the public health approach. *STOMATOLOGY EDU JOURNAL* **2016**, *3*, 130-140.
58. Milgrom, P.; Rothen, M.; Milgrom, L., Developing Public Health Interventions with Xylitol for the US and US-Associated Territories and States. *Suom Hammaslaakarilehti* **2006**, *13* (10-11), 2-11.
59. Gao, L.; Xu, T.; Huang, G.; Jiang, S.; Gu, Y.; Chen, F., Oral microbiomes: more and more importance in oral cavity and whole body. *Protein Cell* **2018**, *9* (5), 488-500.
60. Sampaio-Maia, B.; Monteiro-Silva, F., Acquisition and maturation of oral microbiome throughout childhood: An update. *Dent Res J (Isfahan)* **2014**, *11* (3), 291-301.
61. Asadoorian, P. J.; Williams, K. B., Efficacy of sodium chloride plus zinc gluconate on volatile sulfur compound halitosis. *Canadian Journal of Dental Hygiene* *82*, 1-5.
62. Masadeh, M. M.; Gharaibeh, S. F.; Alzoubi, K. H.; Al-Azzam, S. I.; Obeidat, W. M., Antimicrobial activity of common mouthwash solutions on multidrug-resistance bacterial biofilms. *J Clin Med Res* **2013**, *5* (5), 389-394.
63. Walsh, T.; Oliveira-Neto, J. M.; Moore, D., Chlorhexidine treatment for the prevention of dental caries in children and adolescents. *Cochrane Database Syst Rev* **2015**, (4), CD008457.
64. Senadheera, M. D.; Guggenheim, B.; Spatafora, G. A.; Huang, Y.-C. C.; Choi, J.; Hung, D. C. I.; Treglown, J. S.; Goodman, S. D.; Ellen, R. P.; Cvitkovitch, D. G., A VicRK signal transduction system in Streptococcus mutans affects gtfBCD, gbpB, and ftf expression, biofilm formation, and genetic competence development. *Journal of bacteriology* **2005**, *187* (12), 4064-4076.
65. Nijampatnam, B.; Casals, L.; Zheng, R.; Wu, H.; Velu, S. E., Hydroxychalcone inhibitors of Streptococcus mutans glucosyl transferases and biofilms as potential anticaries agents. *Bioorganic & medicinal chemistry letters* **2016**, *26* (15), 3508-3513.
66. Nijampatnam, B.; Zhang, H.; Cai, X.; Michalek, S. M.; Wu, H.; Velu, S. E., Inhibition of Streptococcus mutans Biofilms by the Natural Stilbene Piceatannol Through the Inhibition of Glucosyltransferases. *ACS Omega* **2018**, *3* (7), 8378-8385.

67. Zhang, Q.; Nijampatnam, B.; Hua, Z.; Nguyen, T.; Zou, J.; Cai, X.; Michalek, S. M.; Velu, S. E.; Wu, H., Structure-Based Discovery of Small Molecule Inhibitors of Cariogenic Virulence. *Scientific Reports* **2017**, *7* (1), 5974.
68. Matsumoto-Nakano, M., Role of Streptococcus mutans surface proteins for biofilm formation. *Japanese Dental Science Review* **2018**, *54* (1), 22-29.
69. Lee, S. F.; Boran, T. L., Roles of Sortase in Surface Expression of the Major Protein Adhesin P1, Saliva-Induced Aggregation and Adherence, and Cariogenicity of Streptococcus mutans. *Infection and Immunity* **2003**, *71* (2), 676.
70. Siegel, S. D.; Reardon, M. E.; Ton-That, H., Anchoring of LPXTG-Like Proteins to the Gram-Positive Cell Wall Envelope. In *Protein and Sugar Export and Assembly in Gram-positive Bacteria*, Bagnoli, F.; Rappuoli, R., Eds. Springer International Publishing: Cham, 2017; pp 159-175.
71. Lévesque, C. M.; Voronejskaia, E.; Huang, Y.-C. C.; Mair, R. W.; Ellen, R. P.; Cvitkovitch, D. G., Involvement of sortase anchoring of cell wall proteins in biofilm formation by Streptococcus mutans. *Infection and immunity* **2005**, *73* (6), 3773-3777.
72. Brady, L. J.; Maddocks, S. E.; Larson, M. R.; Forsgren, N.; Persson, K.; Deivanayagam, C. C.; Jenkinson, H. F., The changing faces of Streptococcus antigen I/II polypeptide family adhesins. *Molecular microbiology* **2010**, *77* (2), 276-286.
73. Szafranski, S. P.; Deng, Z.-L.; Tomasch, J.; Jarek, M.; Bhujju, S.; Rohde, M.; Sztajer, H.; Wagner-Döbler, I., Quorum sensing of Streptococcus mutans is activated by Aggregatibacter actinomycetemcomitans and by the periodontal microbiome. *BMC Genomics* **2017**, *18* (1), 238-238.
74. Whiteley, M.; Diggle, S. P.; Greenberg, E. P., Progress in and promise of bacterial quorum sensing research. *Nature* **2017**, *551* (7680), 313-320.
75. Kaur, G.; Rajesh, S.; Princy, S. A., Plausible Drug Targets in the Streptococcus mutans Quorum Sensing Pathways to Combat Dental Biofilms and Associated Risks. *Indian journal of microbiology* **2015**, *55* (4), 349-356.
76. Liu, Y.; Burne, R. A., Multiple two-component systems of Streptococcus mutans regulate agmatine deiminase gene expression and stress tolerance. *J Bacteriol* **2009**, *191* (23), 7363-6.
77. Zschiedrich, C. P.; Keidel, V.; Szurmant, H., Molecular Mechanisms of Two-Component Signal Transduction. *J Mol Biol* **2016**, *428* (19), 3752-3775.

Chapter 2 Natural Product Carolacton

Section 2.4 has been adapted with permission from (Solinski, A. E.; Koval, A. B.; Brzozowski, R. S.; Morrison, K. R.; Fraboni, A. J.; Carson, C. E.; Eshraghi, A. R.; Zhou, G.; Quivey, R. G.; Voelz, V. A.; Wuest, W. M. Diverted Total Synthesis of Carolacton-Inspired Analogs Yields Three Distinct Phenotypes in *Streptococcus mutans* Biofilms. *J. Am. Chem. Soc.* **2017**, *139* (21), 7188–7191. <https://doi.org/10.1021/jacs.7b03879>). Copyright © American Chemical Society.

Section 2.5 has been adapted with permission from (Solinski, A. E.; Scharnow, A. M.; Fraboni, A. J.; Wuest, W. M. Synthetic Simplification of Carolacton Enables Chemical Genetic Studies in *Streptococcus mutans*. *ACS Infect. Dis.* **2019**. <https://doi.org/10.1021/acsinfectdis.9b00213>). Copyright © 2020 American Chemical Society.

Chapter 2 was completed with the help of Prof. Bettina Buttaro (Lewis Katz School of Medicine, Temple University), Prof. Vincent Voelz (Temple University) and Prof. Robert Quivey (University of Rochester).

2.1 Background

2.1.1 Carolacton's isolation and biofilm specific activity

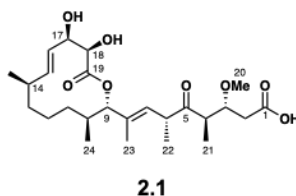


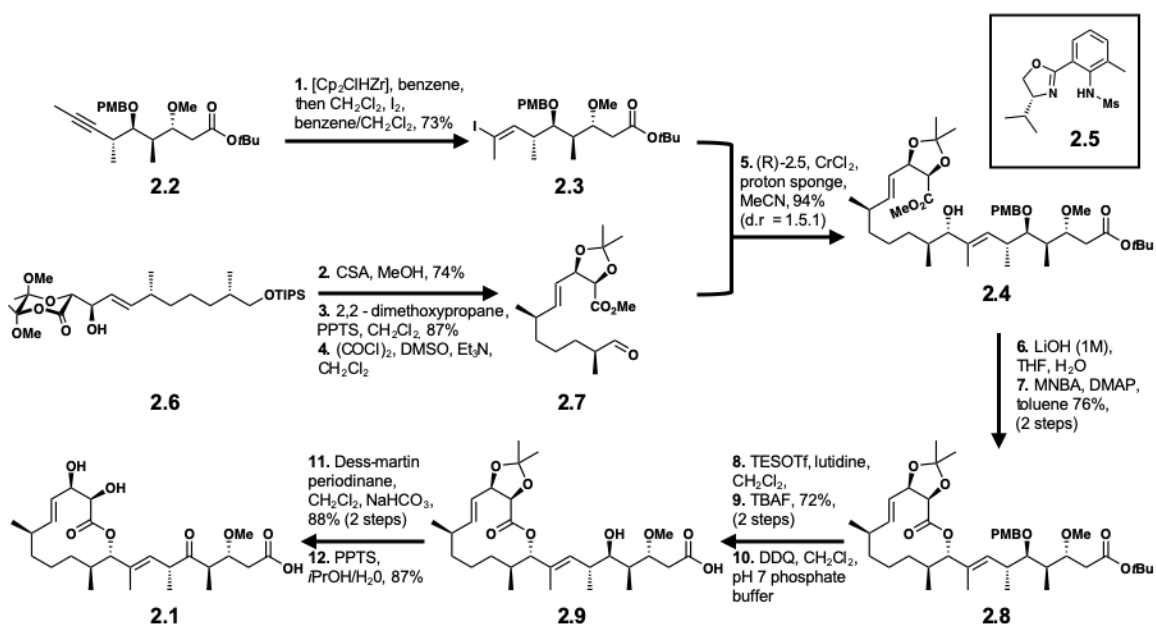
Figure 2.1 Natural product carolacton

Sorangium cellulosum is a highly studied myxobacterium due to its prolific production of biologically active natural products.⁷⁸ Müller and Kirschning were isolating potent compounds from *S. cellulosum*, strain So ce960, and discovered a macrolide natural product, carolacton **2.1** (Figure 2.1).⁷⁹ Carolacton was determined to specifically target *S. mutans* biofilm and not cause harm to planktonic cultures. Using LIVE/DEAD[®] stain, a fluorescent stain used to distinguish between viable and non-viable cells, researchers were able to show that 0.005 µg/mL and 0.025 µg/mL of carolacton caused 35% and 66% biofilm cell death, respectively.⁸⁰ As described in Section 1.1, compounds that can prevent, or eradicate biofilm growth are of great interest. Toward

this end, the total synthesis of carolacton and derivatives (Section 2.2), and investigations of carolacton's mechanism of action (Section 2.3) have been the subject of several publications.

2.2 Total syntheses

2.2.1 Kirschning Group



Scheme 2.1 Kirschning total synthesis

The first total synthesis of carolacton was completed in 2012 by the Kirschning group (Scheme 2.1).⁸¹ They approached the synthesis by building a linear chain that would then undergo a macrolactonization step to access the carbon scaffold of carolacton (**2.8**). After producing alkyne **2.2**, a hydrozirconation step followed by electrophilic trapping with iodine produced vinyl iodide **2.3**. The vinyl iodide **2.3** was coupled to compound **2.7** with a Nozaki-Hiyama-Kishi coupling to give the linear precursor to the macrolactonization **2.4**. From **2.4**, chemoselective hydrolysis of the methyl ester and then macrolactonization with Shiina's protocol was accomplished. Macrocycle **2.8** was pushed toward the natural product via a 2-step transesterification and TBAF sequence to

access the unprotected carboxylic acid. Then with a PMB deprotection, the acid-alcohol **2.9** was isolated. Finally, with a Dess-Martin periodinane oxidation and subsequent acetonide deprotection, carolacton **2.1** was realized.

This brief account demonstrates the synthetic prowess that was exhibited by the Kirschning group to reach carolacton. Others did emulate this approach in practice, using other methods to

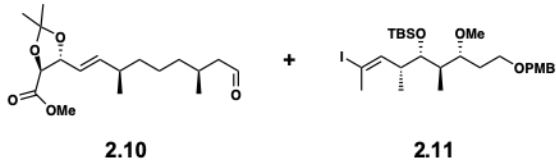
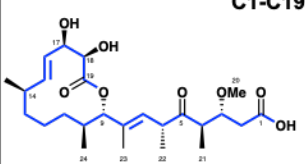
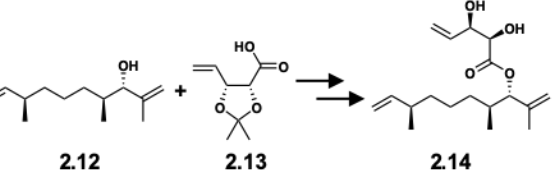
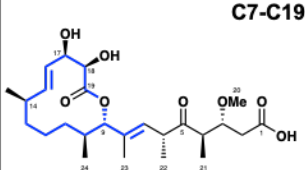
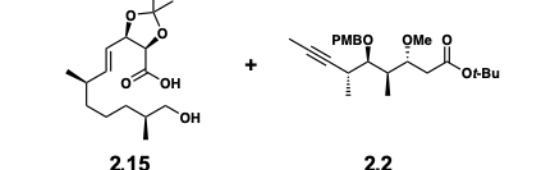
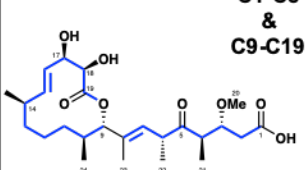
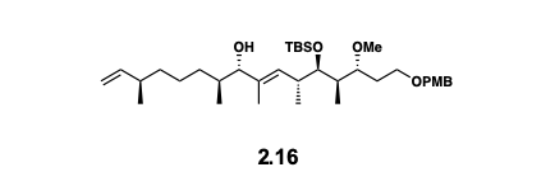
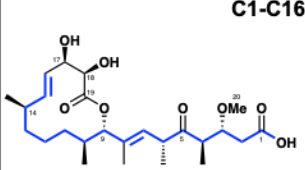
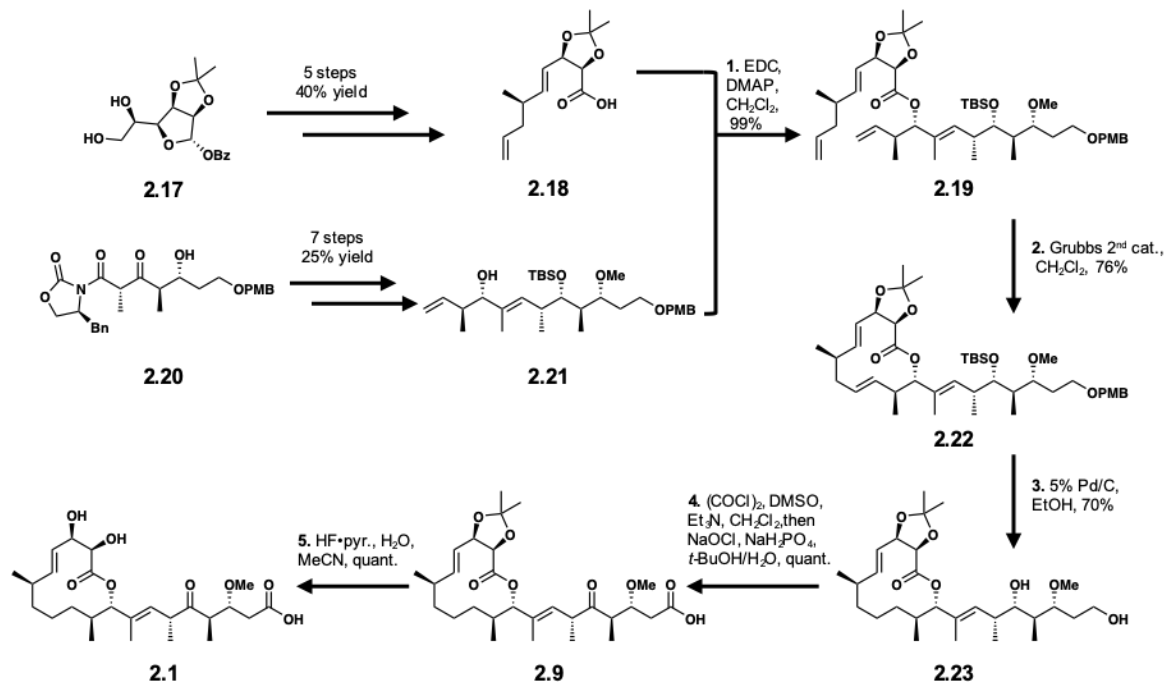
Year	Authors	Precursors	Carbon Skeleton
2012	Sabitha, G.; Shankaraiah, K.; Prasad, M. N.; Yadav, J. S.		
2013	Sharma, G. V. M.; Reddy, S. V.		
2013	Rao, K. S.; Ghosh, S.		
2015	Reddy, S. V.; Kumar, K. P.; Ramakrishna, K. V. S.; Sharma, G. V. M.		

Table 2.1 Other carolacton total synthesis attempts

access carolacton and carolacton precursors. A similar vinyl iodide approach was attempted by Yadav and coworkers.⁸² Shown in Table 2.1, their attempted vinyl iodide approach only lead to the C1-C19 fragment of the macrocycle, highlighted in blue. A year after, Reddy and coworkers were able to access a truncated macrocycle (C7-C19) by utilizing a RCM strategy.⁸³ Rao and

Ghosh developed a strategy similar to Yadav, which lead to the completion of fragments C1-C8 and C9-C19 but could not find a method to connect these two pieces.⁸⁴ Lastly, in 2015 Reddy and coworkers expanded on their work from 2013.⁸⁵ Instead of making the truncated C7-C19 piece, they present a formal synthesis of carolacton, by accessing C1-C16 fragment.

2.2.2 Wuest/Phillips Group



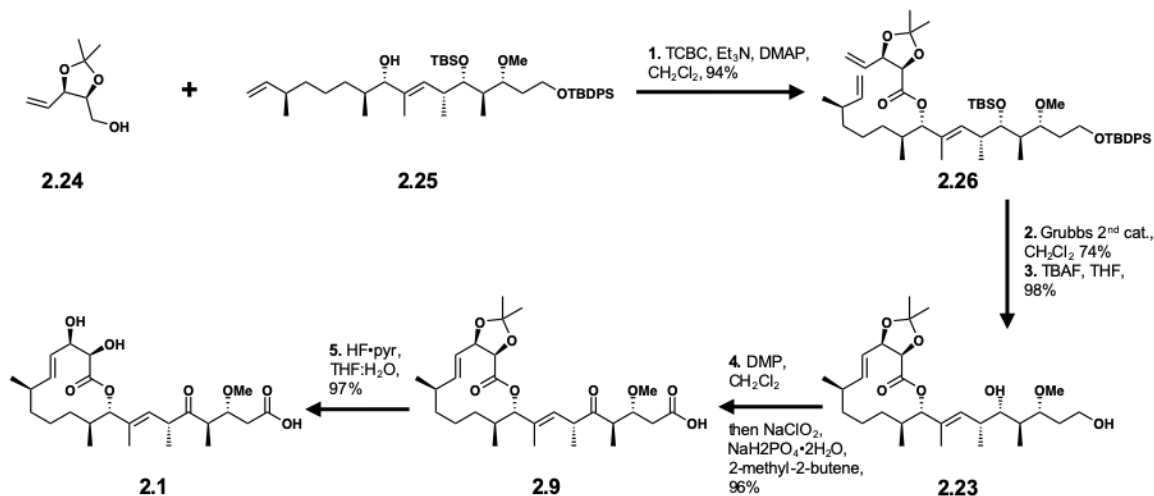
Scheme 2.2 Wuest/Phillips total synthesis of carolacton

In 2014, our lab collaborated with the Phillips group and developed a new method of accessing carolacton.⁸⁶ We decided to separate the macrocycle core into two separate pieces and envisioned connecting the precursors with a 2-step esterification and RCM. With this method they hoped to evaluate the structure-activity relationship with carolacton derivatives that could be accessed throughout the total synthesis. A convergent synthesis was prepared that could be easily modified to access different derivatives of carolacton (Scheme 2.2). Precursors **2.18** and **2.21** were connected via esterification using EDC in the presence of DMAP to achieve **2.19**. With two terminal alkenes, **2.19** then underwent a RCM to reach the full carbon skeleton of carolacton, **2.22**.

Using selective hydrogenation conditions, **2.22** was saturated at the C11-C12 position to yield **2.23**. Since the PMB protecting group was removed in the prior step, the terminal alcohol was prepared for a two-step oxidation. First Swern conditions accessed the aldehyde and subsequent Pinnick conditions achieved the carboxylic acid **2.9**. Finally, carolacton **2.1** was completed via an acetonide removal with acidic conditions. This synthetic route has been successfully utilized to access a multitude of carolacton-inspired derivatives (Sections 2.24, 2.3, 2.4).

2.2.3 Goswami Group

More recently a total synthesis for carolacton was published by the Goswami group.⁸⁷ Using a modified approach from the Phillip and Wuest report from 2014, they used precursor **2.24** and **2.25** to reach **2.26** via a Yamaguchi esterification. From **2.26** they performed a RCM to access to **2.23**. The Goswami group was able to finish the synthesis of carolacton **2.1** with an oxidation and acetonide sequence similar to the aforementioned routes.



Scheme 2.3 Goswami total synthesis of carolacton

2.2.4 Carolacton derivatives

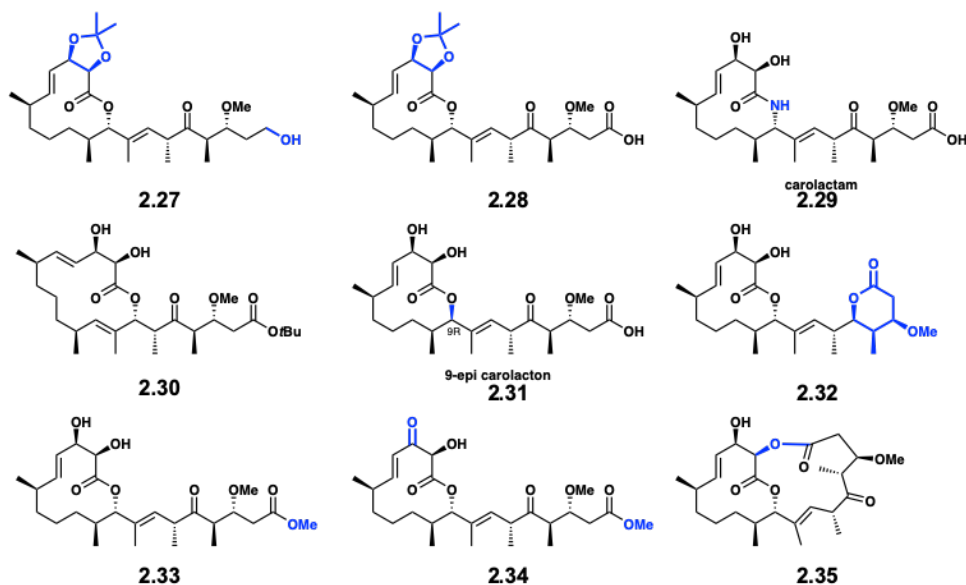


Figure 2.2 Carolacton derivatives

Ultimately understanding the mode of action of carolacton was a goal of these synthetic efforts. Multiple groups approached this problem by derivatizing the natural product with key structural changes that would help elucidate the chemical motifs necessary for activity. The first two derivatives that were published by our group, **2.27** and **2.28**, demonstrated the importance of the terminal carboxylic acid and the macrocyclic diol.⁸⁶ These findings were emphasized further when Kirschning and coworkers published compounds **2.29-2.35**.^{81, 88, 89} By masking the carboxylic acid with a methyl ester (**2.33**) and expanding the secondary macrocyclic structure (**2.35**) they discovered that the ester would hydrolyze in cell culture conditions. These analogs demonstrated biofilm activity but only because the resulting active metabolite was the natural product carolacton. Additionally, compound **2.32** successfully abolished activity by masking the side chain as the hydrolytically stable δ -lactone. Other modifications such as introducing a highly stable lactam (**2.29**), repositioning of the ester bond to form a larger macrocycle (**2.30**), epimerizing the ester (**2.31**), and oxidation of the macrocyclic diol (**2.34**) eliminated the biological activity from the natural product scaffold. These results suggested a specific biological target and

mechanism of action, as most modifications produced inactive compounds. Our group then tested a structure coined CD1 (**2.36**), and a dramatic change to the growth of *S. mutans* biofilm was observed (Figure 2.3). This result prompted our lab to further investigate simplified carolacton analogs to efficiently access derivatives as tool compounds to study this novel mechanism of action (*vide infra*).

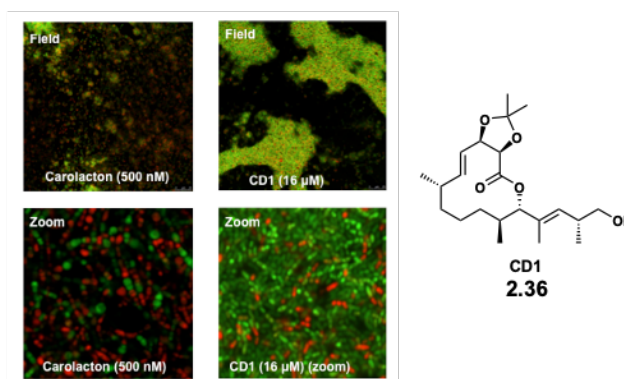


Figure 2.3 Biofilm phenotype of CD1

2.3 Progress towards target identification

2.3.1 Carolacton: a decade of biological investigation

Concurrently with the synthetic progress detailed in Section 2.2, there has been a decade of discoveries toward understanding carolacton's mode of action since the initial isolation report in 2010. These events are placed chronologically in Figure 2.4. Soon after the isolation, a report came out by Kunze et al. that described the effects of carolacton in greater detail.⁸⁰ Through their investigation they determined that 35% of biofilm cells were non-viable after treatment with 10 nM of carolacton. With fluorescence microscopy and LIVE/DEAD[®] staining they observed that carolacton-treated cells were elongated and had altered cell morphology. After a quorum sensing

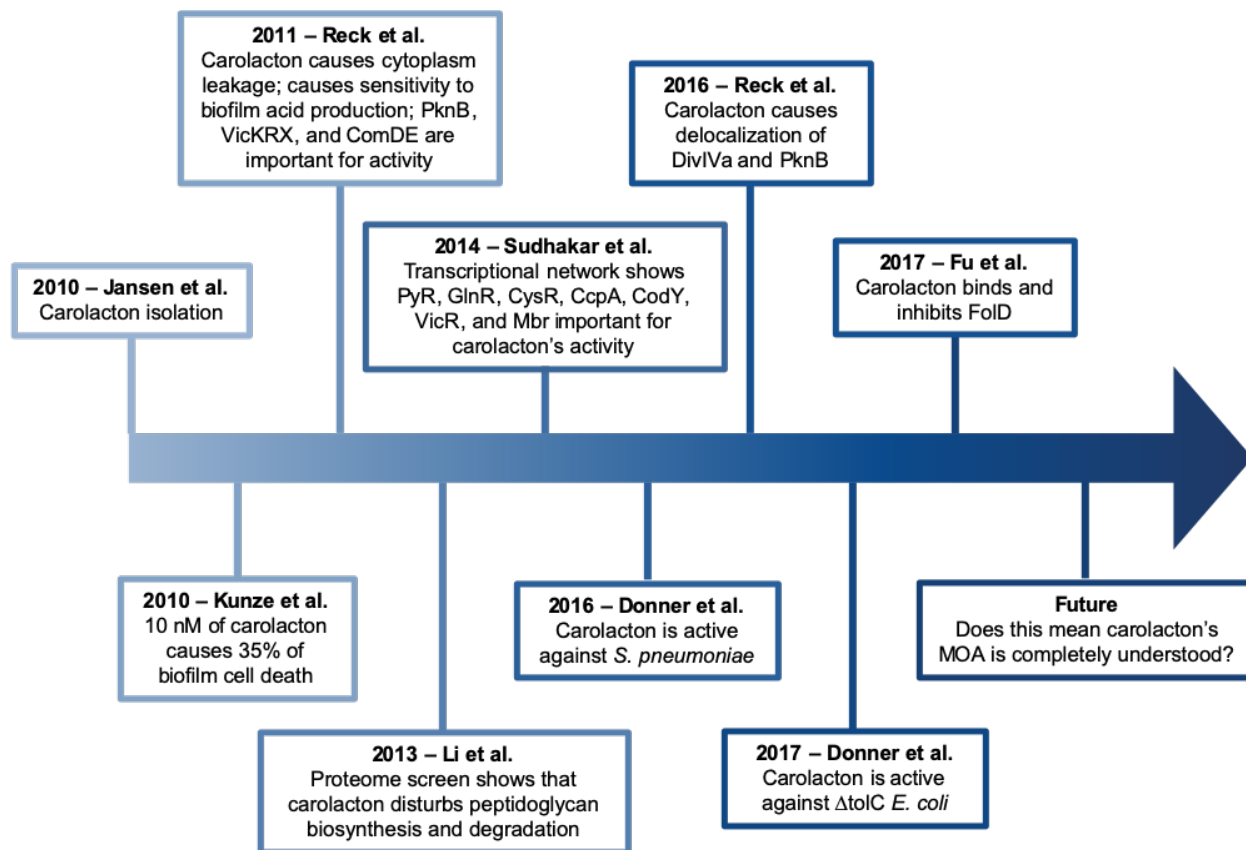


Figure 2.4 Timeline for carolacton's biological discoveries

genetic mutant screen, they identified ComD as being important for carolacton's activity. ComD is a response regulator of a TCS that detects the competence stimulating peptide (CSP) for *S. mutans*. Soon after, Reck et al. confirmed the previously reported biofilm activity and determined that cytoplasmic content would leak from cells when grown in the presence of carolacton.⁹⁰ The leakage was caused by a carolacton directed cell membrane damage. During biofilm formation, the effect of the cell membrane damage is multiplied because of the drop in environmental pH. They demonstrated that VicRK (TCS) and ComDE (TCS) were essential for carolacton to cause the biofilm effect via microarray analysis. Through this work they also found that Δ PknB, a knockout of protein kinase B and master regulator in *S. mutans*, was highly similar to carolacton treated cells in a transcriptome comparison. In 2016, work from Sudhakar et al. identified which response regulators in *S. mutans* were influenced by carolacton treatment.⁹¹ Due to the identified

connection to bacterial signaling, they analyzed the transcriptional regulatory response network with and without carolacton. They were able to show that response regulators PyR, GlnR, CysR, CcpA, CodY, VicR, and Mbr were all highly affected, and coordinated when carolacton applied stress to the cell. Compiled, it seemed that carolacton was affecting a part of the bacterial signaling that occurred in *S. mutans* but a direct target remained elusive.

In 2013, data was published by Li and coworkers that suggested an alternate mechanism unrelated to bacterial signaling and *S. mutans* regulation like the previous research had shown. Instead, they found that carolacton disturbed peptidoglycan biosynthesis and degradation, which could explain why it was discovered to cause cell membrane damage.⁹² Specifically, they performed a proteome screen that showed that GlmS, MurC, DapB, GlnA, GbpB, all important enzymes for peptidoglycan maintenance, were upregulated after treatment of carolacton. In 2016 Reck and coworkers published data that seemed to support that carolacton was affecting the cellular membrane. Using a GFP fusion to monitor the localization of certain proteins after treatment with carolacton, they found that both DivIVA, a cell division protein, and PknB were delocalized after treatment.⁹⁰ From these experiments, they also observed that there was an increased septum formation, as well as defects during daughter cell separation. These findings pointed toward cell division defects as the primary mode of action of carolacton. Although not fully contradictory, the contrast between the cell membrane data, and the bacterial signaling data, left the target elusive.

Over time, researchers started investigating carolacton's effect on other biological systems. In 2016, it was shown that carolacton could inhibit planktonic *Streptococcus pneumoniae* (TIGR4) and even the multidrug resistant serotype, 19A.⁹³ Carolacton was also found to be potent against Gram-negative *Escherichia coli* when the efflux pump TolC was inactive, either by genetic

knockout or by small molecule inhibition.⁹⁴ Additionally, Fu et al. screened cancer cell lines and found that carolacton had moderate potency; inhibiting HCT-116 (colon cancer) with an IC_{50} of 25 μ M, KB-3.1 (endocervical adenocarcinoma) with an IC_{50} of 11 μ M, and KB-V.1 1 (endocervical adenocarcinoma) with an IC_{50} of 42 μ M.⁹⁵ These findings warrant further investigation to carolacton's effect outside of *S. mutans* biofilm.

In 2017 carolacton was found to target folate dehydrogenase (FolD). Fu et al.⁹⁵ used the aforementioned *E. coli* Δ TolC to select for a resistance mutant of carolacton. They identified FolD to be the target of carolacton via resistant mutant sequencing, showed high binding affinity to purified FolD from *E. coli* ($K_D=10$ nM), and also determined the crystal structure of the FolD-

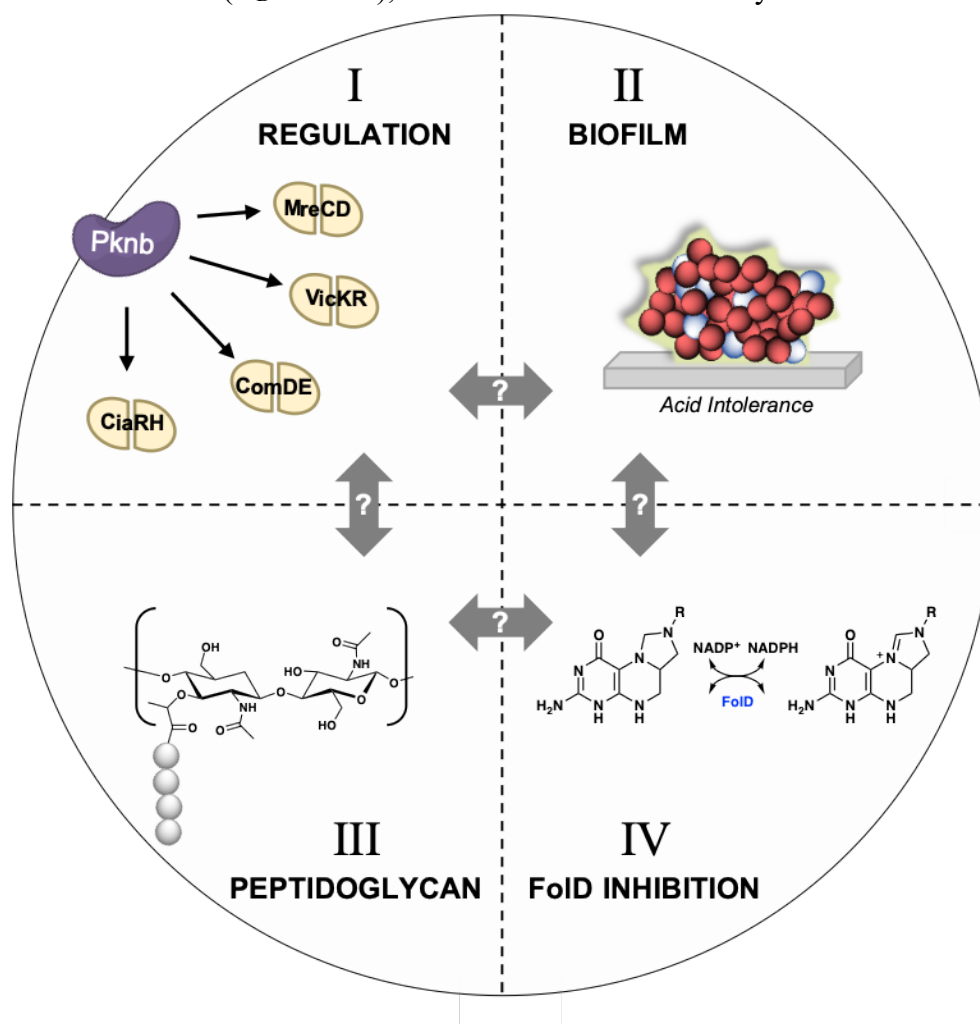


Figure 2.5 Connections between carolacton's biological activities

carolacton complex. Since the work was initially performed in *E. coli*, they also used FOLD from *S. pneumoniae* to determine binding affinity ($K_D = 27$ nM) in a streptococcal species. They did not report an attempt to isolate FOLD from *S. mutans* to calculate the binding affinity or show *S. mutans* Δ FOLD biofilm data. These scientific gaps leave some unanswered questions in regards to the mechanism of biofilm inhibition by the natural product carolacton.

2.3.2 Target or targets?

In Section 2.3.1, an all-encompassing outline of carolacton's mechanism of action studies was presented to highlight the varied findings that came from studying its biological activity. As illustrated in Figure 2.5, there have been four major discoveries that have been made for the mechanism of action: I) regulation via cellular signaling, II) decrease in biofilm acidification tolerance, III) peptidoglycan maintenance, and IV) FOLD Inhibition. Most recently, Fu et al. has published that carolacton targets FOLD but there are still unanswered questions. For one, how does FOLD connect to the other three discoveries (I-III)? Does FOLD interact with these other systems or does carolacton exhibit polypharmacology? Does targeting FOLD lead to biofilm specificity in *S. mutans*? The work presented in this dissertation demonstrates that there is more to understand about carolacton's biological effect against biofilm and bacteria in general.

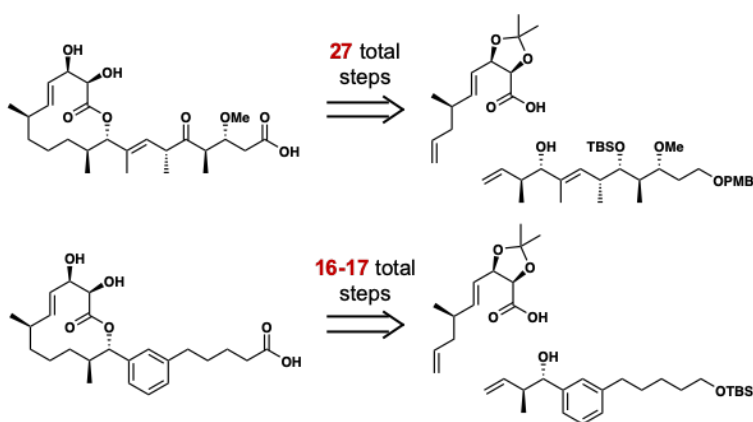


Figure 2.6 Carolacton analog design - Generation 1

2.3.3 Rationale and design for simplified analogs

In 2012, the Wuest Group decided to make carolacton inspired analogs to investigate the SAR of the natural product in an attempt to increase the potency against biofilm. In Section 2.2.4, analogs previously published are presented. These findings informed which modifications would not be tolerated. Modifications to the macrocycle and the terminal carboxylic acid of the sidechain had been shown to cause decreases in activity. Therefore, the lead of the project at that time, Dr. Rich Brzozowski, proposed modifying and simplifying the sidechain. I would join the project to help complete the synthesis of the proposed analogs and complete the biofilm investigation. He proposed a technique used for the derivatives of pladienolide, in which a tri-substituted alkene was replaced with an aryl moiety in order to synthesize simplified, truncated analogs. He envisioned that simplifying the sidechain would not cause a decrease in potency and would be synthetically beneficial, leading to an overall 10 step decrease (Figure 2.6). In order to access a wide arrange of derivatives, both a convergent and diverted total synthesis (DTS) strategy would be used (Figure 2.7). Through a convergent strategy, modifications could be made to starting materials and incorporated into the final compounds. The DTS strategy would allow for late stage modifications, to quickly diversify the structures and allow us to develop a large library of carolacton derivatives. As we progressed through multiple generations of analog design and testing, we became aware of

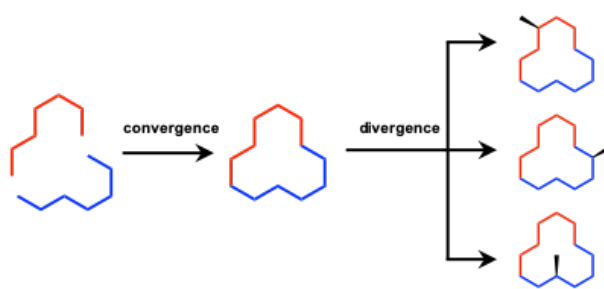
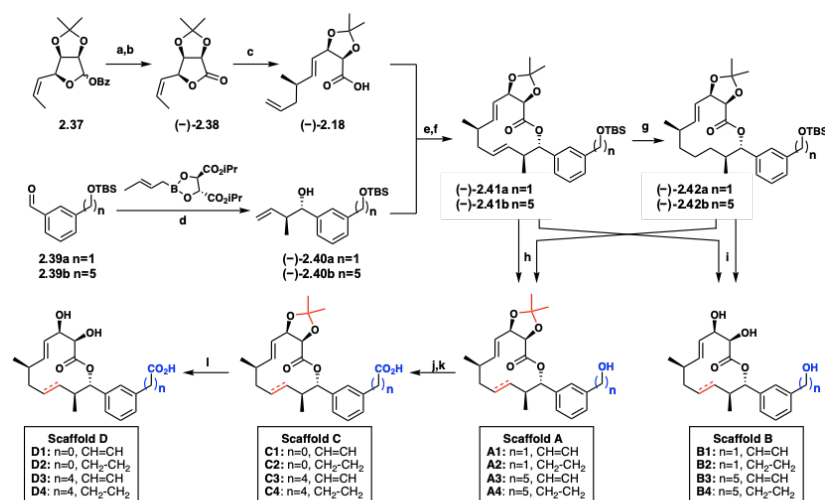


Figure 2.7 Synthetic approach for carolacton analogs

the possibility of using these molecules as chemical probes to further understand the biological interactions that carolacton undergoes. The application of the tool compounds will be discussed in Section 2.5 and in Chapter 3.

2.4 Generation 1: Carylacton Analogs

2.4.1 Synthesis of carylacton analogs



(a) K_2CO_3 , MeOH/THF, >99% (b) DMSO, $(COCl)_2$, CH_2Cl_2 , 94% (c) CuCN, Allyl-MgBr, THF, 90% (d) 4 Å MS, NaOH, PhMe, 83–85% (e) EDCI, DMAP, CH_2Cl_2 , 89–96% (f) Grubbs 2nd generation catalyst, CH_2Cl_2 , 78–99% (g) Pd/C, H_2 , 55–69% (h) TBAF, 64–94% (i) HCl, THF/MeOH, 50–82% (j) DMSO, $SO_3 \cdot pyr$, CH_2Cl_2 , 63–89% (k) *t*-BuOH, 2-methyl-2-butene, NaH_2PO_4 , $NaClO_2$, MeCN, H_2O , 65–96% (l) TFA/ H_2O , 59–79%.

Scheme 2.4 Generation 1 carylacton analog synthesis

Our first generation DTS library focused on conserving the connectivity of the twelve-membered macrolactone, and significantly simplifying the carolacton side chain. Along with replacing the tri-substituted alkene with an aryl motif, we chose to vary both the length ($n=1$, $n=5$) and oxidation state of the side chain (-OH, COOH). $n=1$ was chosen to mimic the chain length of CD1 (**2.36**) and $n=5$ was used to mimic the natural product carolacton ((-)-**2.1**). The isosteric aryl substitution would maintain the structural integrity of the compound, most importantly the integrity of the macrocycle. We leveraged a key intermediate (compound (-)-**2.18**) from our total synthesis, which served to help construct the sixteen-member analog library (Scheme 2.4).

Although the synthesis of (–)-**2.18** was previously published, the yield of the synthetic sequence was increased by 50% over the completion of Generation 1 analogs. Starting from intermediate **2.36**, we performed a benzoyl deprotection using potassium carbonate, and then a subsequent Swern oxidation to access (–)-**2.38**. The lactone is then primed for a S_N2' nucleophilic ring opening utilizing allyl magnesium bromide and copper cyanide to access the carboxylic acid (–)-**2.18**.

With a reliable and scalable route to (–)-**2.18**, we turned our attention to the synthesis of the simplified side chains. We chose two aryl diols to use as side chain precursors: a pentyl moiety (n=5; carolacton) and a methyl-derivative (n=1; CD1) to interrogate the importance of chain length. Toward this end, monoprotection followed by oxidation of the corresponding 1,3-disubstituted benzene diols provided the known compounds **2.39a/2.39b** (Scheme 2.4). Roush crotylation converts the benzylic aldehydes to the desired alcohols, furnishing structures (–)-**2.40a/**(–)-**2.40b**. Leveraging our previous endgame strategy from the total synthesis, an esterification combined the side chain alcohols with acid (–)-**2.18**. Finally, a RCM reaction using Grubbs 2nd generation catalyst resulted in the selective formation of the (*E*)-olefin embedded within the macrocycle, providing the fully protected analog precursors (–)-**2.41a/**(–)-**2.41b**. Diversity can be introduced into the library of analogs by selectively hydrogenating the more sterically accessible olefin providing (–)-**2.42a/**(–)-**2.42b**. These four intermediates, bearing the fully protected analog scaffold, represent the two main branching points from which we would synthesize our analog library. Based on these prior derivative reports discussed in Section 2.2.4, we sought to fully evaluate all desilylated compounds en route to “carylacton” to better understand the SAR of perturbations to both the side chain and the macrocycle of the natural product. We envisioned three logical branching points that would produce four distinct scaffolds (A-D), where we could evaluate the role that the acetonide, olefin, and oxidation state play in bioactivity. Within each scaffold we

produced four separate analogs, leading to the final count of 16 total structures. To access these analogs we first performed a TBS deprotection of silyl-ethers (-)-**2.41a**/(-)-**2.41b** and (-)-**2.42a**/(-)-**2.42b** with TBAF to generate **Scaffold A** (Scheme 2.4). Full deprotection, with HCl, of silyl-ethers (-)-**2.41a**/(-)-**2.41b** and (-)-**2.42a**/(-)-**2.42b** was used to generate **Scaffold B**. **Scaffold A**, bearing the primary alcohol, can then undergo a two-step oxidation, providing the corresponding carboxylic acid found in **Scaffold C**. Finally, the acetone was treated with trifluoroacetic acid in water to access **Scaffold D** (Scheme 2.4). In total, milligram quantities of sixteen analogs were synthesized and evaluated for their biological activity in *S. mutans* (UA159) assays described in the next section.

2.4.2 Discovery of new phenotypes

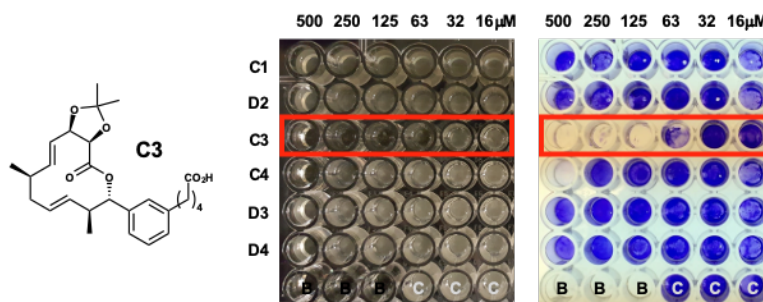


Figure 2.8 Analog C3 biofilm inhibition

As carolacton specifically targets transitioning *S. mutans* biofilm cells and does not inhibit planktonic cells, we first wanted to test the carolacton analogs biofilm specificity. We performed Minimum Inhibitory Concentration (MIC) assays against planktonic bacteria and found that all of the carolacton analogs were ineffective at inhibiting planktonic growth. We next tested the analogs in the presence of 0.1% sucrose, which initiates biofilm formation. Through this process we discovered a few interesting phenotypes that seemed related to carolacton's biofilm activity. In the presence of 0.1% sucrose, compound **C3** inhibits biofilm adherence (Figure 2.8). This result was quantified using crystal violet staining and we observed 50% inhibition of biofilm formation

(MBIC₅₀) at 63 μ M. Additionally, hemolysis assays were performed to gather initial data on potential toxicity. **A4**, **B3**, and **C4** were the only analogs that displayed any appreciable lytic activity with modest Lysis₂₀ values of 250 μ M. The discovery of **C3**, a greatly simplified analog of carolacton, that inhibits biofilm formation was an unexpected result. Carolacton does not inhibit biofilm growth. Instead it causes lethal defects to the cells in biofilm causing them to be non-viable. The inhibition of C3 was presumed to be connected to carolacton due to its biofilm specific nature, but carolacton had not demonstrated biofilm inhibition previously, therefore showcasing the novelty of this discovery.

As discussed previously, LIVE/DEAD[®] stain and fluorescence imaging was originally used to calculate the percent of viable and non-viable cells for carolacton treated cultures. Therefore, we investigated the cellular viability of analog treated biofilm samples and used confocal imaging to screen for phenotypic biofilm responses. We rationalized that the structural diversity could offer us insight to the important functionality on the natural product.

We inoculated *S. mutans* UA159 cells in THB with 0.1% sucrose and serial diluted compound, starting at 500 μM , in 96-well glass flat bottom plates. After 20 hours the biofilms were washed to remove planktonic cells, stained with LIVE/DEAD[®], and imaged via confocal microscopy. To our surprise, analogs displayed unique phenotypic responses that had not previously been seen through our studies of carolacton. A few analogs appeared to arrest growth at the stage of microcolony formation, which can be seen by their rosette-like pattern, appearing to halt biofilm maturation (Figure 2.9). Specifically, **C1** and **D2** were the leading examples of this

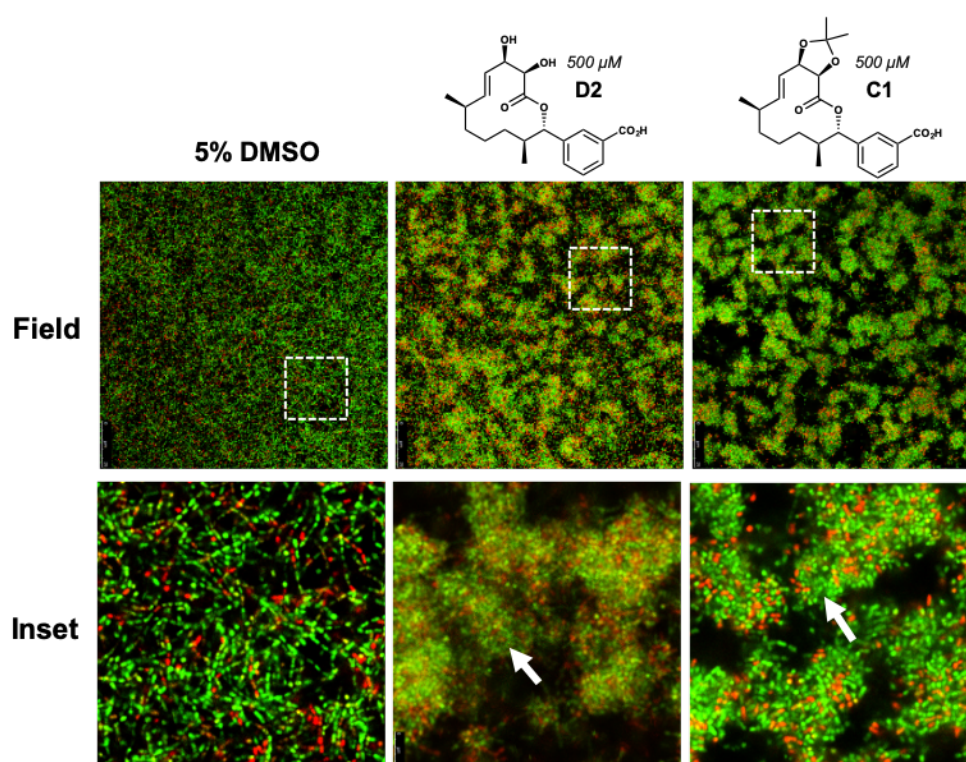


Figure 2.9 Analog **D2** and **C1** microcolony biofilm phenotype

phenotype (Figure 2.9; see Section 6.3 for full set of images). At 4x zoom, a haze (marked by the white arrow) is apparent surrounding the microcolonies indicating possible increased staining of extracellular DNA (eDNA) in the EPS. This biofilm phenotype is distinctly different to that of carolacton-treated cells. Based on these findings we postulated that this subset of analogs could be affecting *S. mutans* biofilm growth via a separate mechanism of action compared to carolacton.

With that said, all members of this subset need a carboxylic acid to demonstrate this phenotype. Thus **C1**, **D2**, and carolacton all need the carboxylic acid to be active, demonstrating that there may be a connection between the modes of action.

“Carylacton”, or **D4**, named for its semblance to carolacton, displays a similar biofilm phenotype to the natural product. During the course of our initial phenotypic screen of the analog library we discovered that compound **D4** visually perturbed growth, biofilm phenotype and cell morphology at a high concentration of 500 μM . It has been shown previously that carolacton maintains its activity at low, nanomolar concentrations. Therefore, we sought to investigate the range of activity for **D4** into the nanomolar range (Figure 2.10). We found that the phenotype

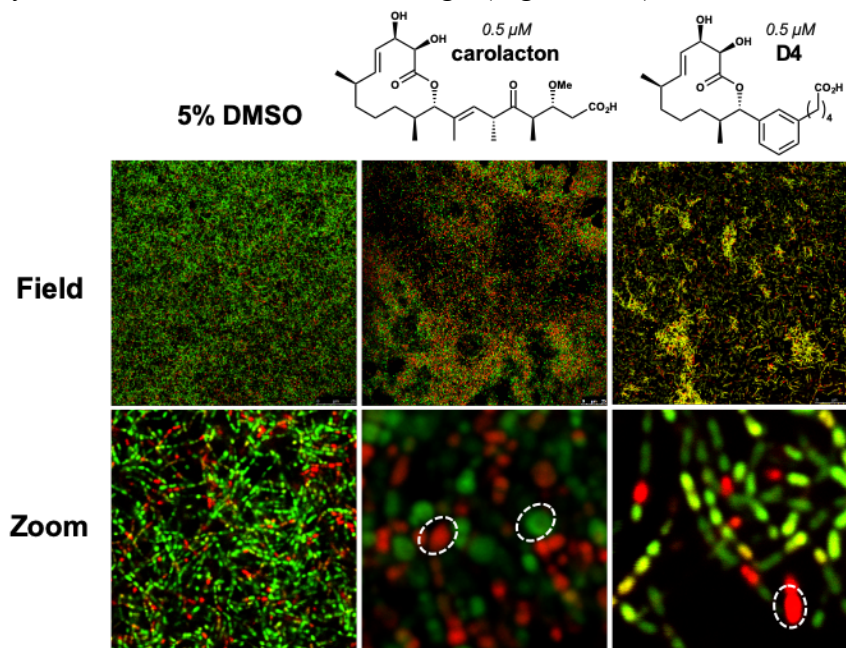


Figure 2.10 Carolacton and **D4** cause biofilm defects at low concentrations

persisted at concentrations as low as 500 nM, equivalent to values previously recorded for carolacton (highlighted by white circles in Figure 2.10). This observation supports our earlier hypothesis that the rationally designed isosteric structure would maintain biological activity similar to carolacton. This work reveals that significant side chain modifications are tolerated without the loss of significant biological activity. This opens up future directions for analog design.

It also serves as an example that meta-substituted aryl rings can serve as isosteres of trisubstituted olefins, which are present in a number of structurally diverse natural products.

2.4.3 Computational modeling

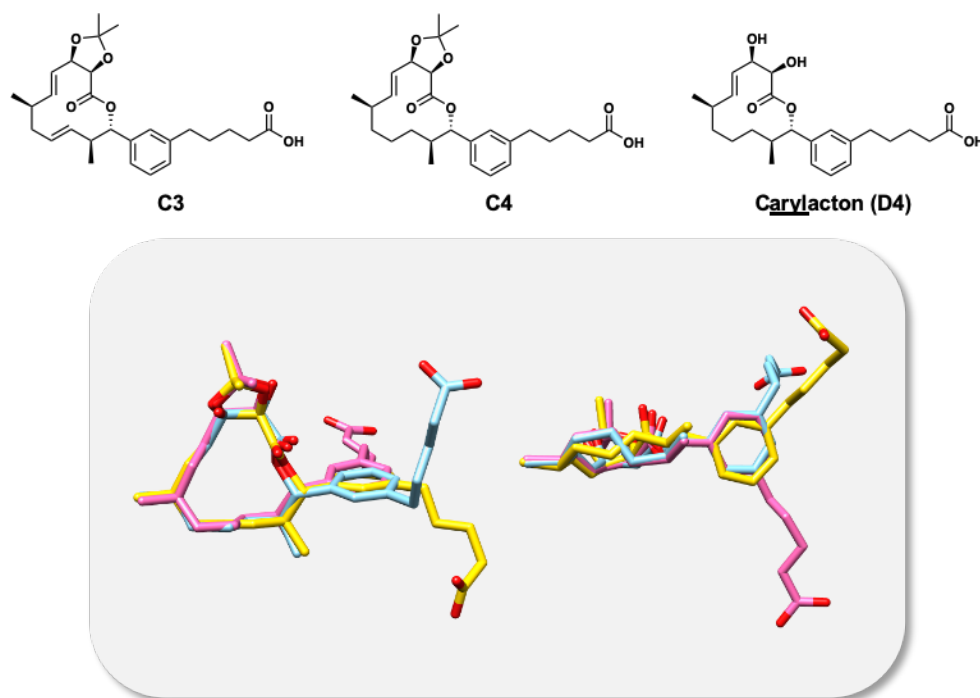


Figure 2.11 Molecular modeling of **C3**, **C4**, and **D4**

With the results from the previous section, we were interested in understanding if the analogs maintained a similar structural and/or macrocyclic confirmation, therefore we collaborated with the Voelz Lab (Temple University). They performed molecular modeling of analogs **C3** (yellow), **C4** (pink), **D4** (blue) using a two-step approach of replica-exchange molecular dynamics simulations followed by QM refinement using DFT to determine what role the structural changes played in the three-dimensional structure (Figure 2.11). The modeling reveals subtle differences between the lowest-energy structures of each analog that are not readily apparent when viewed perpendicular to the chemical plane. We rationalized that differences in the selectivity of our aryl analogs may result from these structural modifications of the macrolactone ring confirmation. When the overlay is rotated 90 degrees, key differences are observed. The alkene present in **C3**,

that is absent for **C4** and **D4**, torques the macrocycle in a different confirmation. Additionally, steric contributions of the acetonide have a significant effect on the confirmation. Together these modifications have caused significant disruptions to the biological outcome. Lastly, modeling of carolacton ((-)-**2.1**; grey) and carylacton (**D4**; blue) was also completed and showed that they have almost identical macrocyclic confirmations (Figure 2.12). The aryl motif did maintain the sidechain rigidity of the natural product, but the simplification did provide more rotational flexibility for the terminus of the sidechain. From this model we can see how the simplified analog **D4** can maintain the potent biofilm activity that carolacton demonstrates.

2.4.4 Generation 1 conclusions

Using a DTS strategy we were able to reveal carolacton inspired structures, not available via nature, that maintained biological activity or demonstrated new phenotypic responses against cariogenic biofilm. Our results have demonstrated that rigidity, oxidation, and chain length determine the overall efficacy of the compounds against *S. mutans* biofilms. Additionally, we have

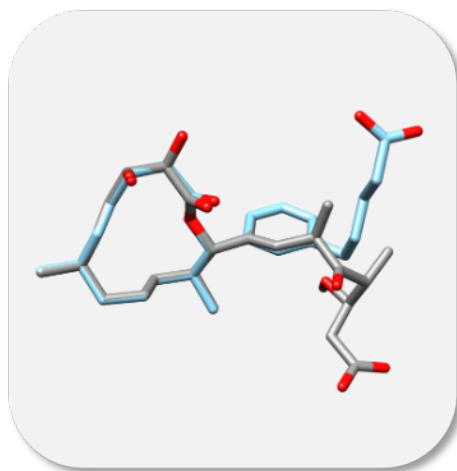
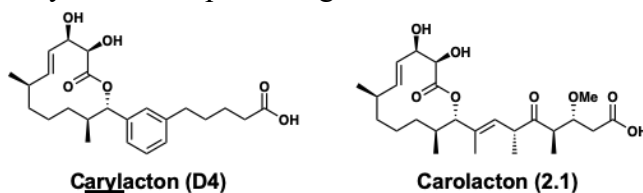


Figure 2.12 Molecular modeling of **D4** and carolacton

further validated the use of meta-substituted benzene rings as isosteres of trisubstituted olefins. We will use these discoveries in the future to devise next generation carolacton analogs (Section 2.5) and also perform target identification studies (Chapter 3). The findings presented above demonstrate that our analogs have the potential to control the growth of *S. mutans* biofilm at discrete points in biofilm maturation (i.e. microcolony formation). It would be interesting to use our compounds to investigate the proteome, transcriptome, metabolome, etc. during discrete points of biofilm growth.

2.5 Generation 2: Simplified Sidechain Analogs

2.5.1 Analog development

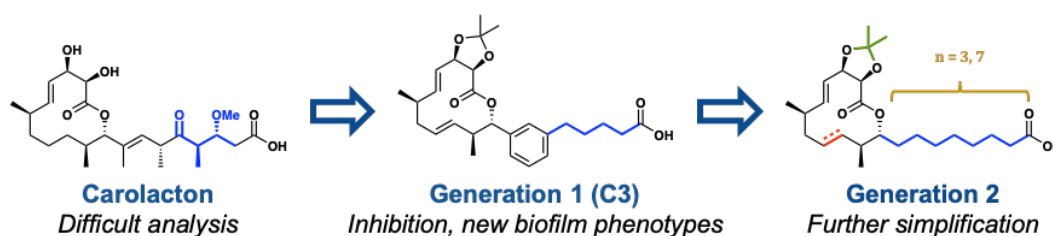
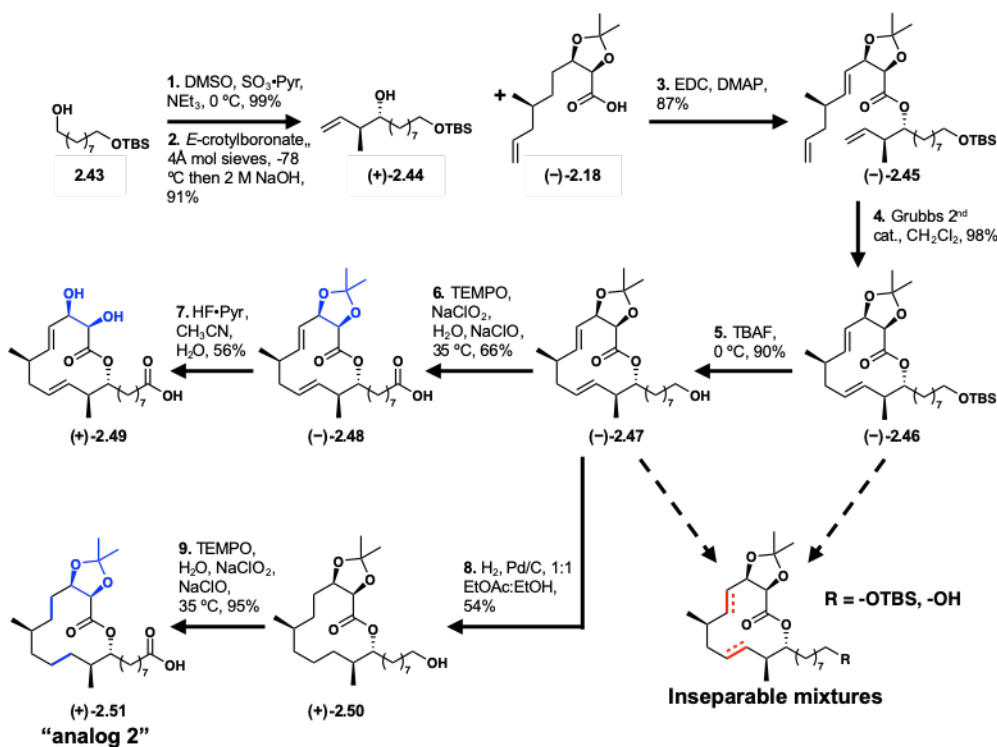


Figure 2.13 Analog design for Generation 2

In our first DTS effort (Section 2.4), we found that replacing the tri-substituted alkene with an aryl bioisostere provided analogs with unique biofilm phenotypes when observed with confocal microscopy (Figure 2.8-2.10). Most importantly, we identified a simplified structure, **C3**, that inhibited 50% of biofilm formation at 63 μM . The discovery of this compound demonstrated the importance of the side chain length and reinforced the importance of the terminal carboxylic acid in the bioactivity of carolacton. Therefore, we sought to design a second generation of analogs that would incorporate these factors and simplify the synthesis further (Figure 2.13). Generation 1 showed sidechain modifications were tolerated, and we aimed to determine if sidechain functionally was necessary, besides the carboxylic acid. It should be noted that we synthesized both long and short chain varieties of the simplified carolacton analogs. The short analogs did have

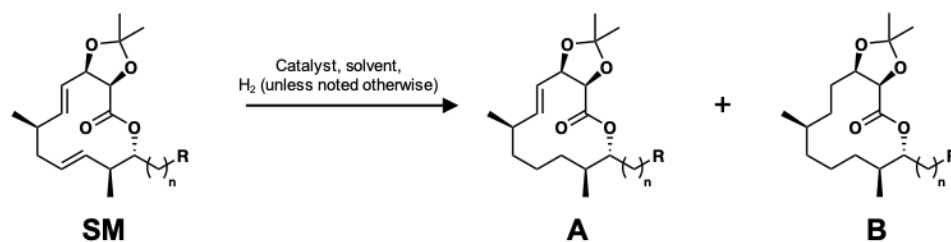
some microcolony affect, but less pronounced than Generation 1 (images in Section 5.4). These analogs were not included in our publication.

2.5.2 Synthesis of simplified analogs



Scheme 2.5 Synthesis of Generation 2

To access the long chain, simplified analogs, we employed our previous synthetic route (Scheme 2.5). Starting from the commercially available nonanediol, a TBS-mono protection followed by a Parikh-Doering oxidation, and a Roush crotylation with (*E*)-crotylboronate furnishes the alcohol side chain (+)-2.44. Esterification with the previously published carboxylic acid precursor ((-)-2.18) followed by ring-closing metathesis provides macrocycle (-)-2.46. Deprotection of the TBS-silyl ether and subsequent oxidation affords (-)-2.47 and analog (-)-2.48, respectively. Finally, analog (+)-2.49 was accessed by removing the acetonide protecting group with HF·pyridine.



R	Catalyst	Catalyst Load	Solvent	Reaction Time	Conversion (SM:A:B)
-CO ₂ Bn	Pd/C (10%)	7 mol %	EtOAc	20 hrs	NR
	Pd/C (10%)	20 mol %	EtOH	45 min	0:54:46
	Pd/C (10%)	7 mol %	EtOH	10 min	NR
	Pd/C (10%)	10 mol %	EtOAc:MeOH (1:1)	45 min	0:67:33
	Pd/C (10%)	26 mol %	EtOAc:MeOH (1:1)	30 min	0:75:25
	Pd/C (10%)	20 mol %	MeOH:EtOH (1:1)	60 min	NR
	Pd/C (10%)	10 mol %	EtOAc:EtOH (1:1)	10 min	0:90:10
	Pd/C (10%)	20 mol %	EtOAc:EtOH (3:1)	30 min	0:90:10
-CO ₂ H	Pd/C (10%)	10 mol %	EtOAc:EtOH (1:1)	20 min	90:2.5:2.5
-CH ₂ OTBS	Pd/C (10%)	7 mol %	EtOAc	60 min	NR
	Pd/C (10%)	7 mol %	EtOH	90 min	0:0:100
	Pd/C (10%)	7 mol %	EtOH	90 min	NR
	Pd/C (10%)	7 mol %	EtOAc:EtOH (1:1)	60 min	0:70:30
	Pd/C (10%)	13 mol %	EtOAc:EtOH (1:1)	60 min	0:84:16
-CH ₂ OH	Pd/C (10%)	13 mol %	EtOAc:EtOH (1:1)	30 min	0:0:100
	Pd/C (10%)	13 mol %	EtOAc:EtOH (1:1)	20 min	0:77:33
	Pd/C (10%) w/ HCO ₂ NH ₄	8 mol %	EtOAc:MeOH (1:1)	48 hrs	91:9:0
	Wilkinson Cat.	10 mol %	EtOAc	10 min	NR
	Wilkinson Cat.	10 mol %	EtOAc	24 hrs	NR
	Wilkinson Cat.	20 mol %	EtOH:THF (2:1)	24 hrs	84:16:0
	Wilkinson Cat.	20 mol %	EtOH:THF (2:1)	48 hrs	43:25:7
	Wilkinson Cat.	20 mol %	PhH	24 hrs	67:21:12
	Pt/C (10%)	10 mol %	MeOH	30 min	NR
Pt/C (10%)	10 mol %	MeOH:EtOAc (1:1)	30 min	81:14:5	
-CH ₂ OPMB	Pd/C (10%)	7 mol %	EtOH	1.5 hrs	0:71:29

Table 2.2 Conditions for hydrogenation

To mimic the macrocyclic structure of carolacton, we sought the mono-hydrogenated versions of (–)-**2.48** and (+)-**2.49**, analogous to our previous synthetic efforts. Unfortunately, all attempts to perform the selective hydrogenation on (–)-**2.46**, (–)-**2.47** and analog (–)-**2.48** were unsuccessful and led to inseparable mixtures (Table 2.2). We rationalized that the increased flexibility of the sidechain significantly affected the selectivity of the hydrogenation. We postulated that the

increased number of rotatable bonds brings the side chain into closer proximity to the macrocycle and accordingly reduces the selectivity of the palladium loading during the hydrogenation. With this knowledge and the oversaturated macrocycle material in hand, we questioned if maximal macrocycle flexibility would also correlate to improved bioactivity. For this reason, (+)-**2.51** (“**analog 2**”) was accessed via a TEMPO oxidation from (+)-**2.50** (Scheme 2.5) to yield the corresponding carboxylic acid.

2.5.3 Biofilm-specific inhibition

Analog	<i>S. mutans</i> MIC (μM)
carolacton	>500
analog 2	250
(-)-2.48	>500
(+)-2.49	>500
C3	>500

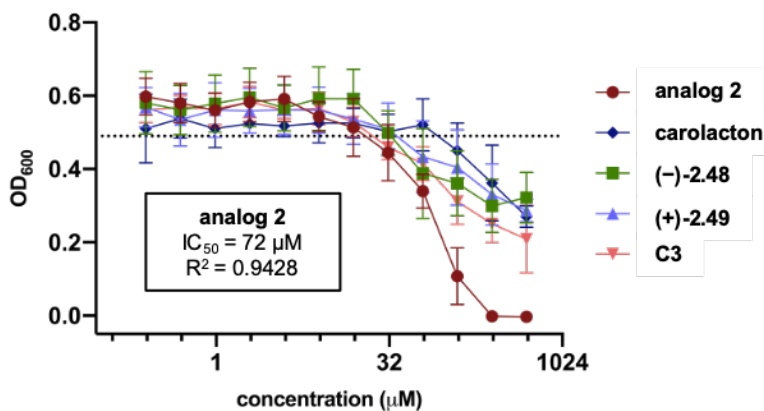


Figure 2.14 Planktonic and biofilm inhibition

Similar to the first generation of carolacton analogs, we tested the biological activity of analogs (-)-**2.48**, (+)-**2.49**, and **analog 2** against *S. mutans* to explore the effect of our structural changes. First, compound-treated *S. mutans* was grown in planktonic conditions and compared to carolacton and **C3**, the generation 1 analog that has previously demonstrated biofilm inhibition. Interestingly, the fully saturated **analog 2** inhibited *S. mutans* with a MIC of 250 μM (Figure 2.14). It should be noted that this was the first observation of an MIC value, in *S. mutans*, for any compound structurally related to carolacton, including the natural product. When promoting biofilm formation with 0.1% sucrose supplement to the media, (-)-**2.48**, (+)-**2.49**, carolacton, and **C3** all performed similarly (Figure 2.15). In contrast, **analog 2** exhibited more potent inhibitory activity against biofilm growth, demonstrating an inhibition effect (Biofilm IC_{50} = 72 μM) on *S.*

mutans. The difference between the biofilm and planktonic response suggests that the activity of **analog 2** trends with increased biofilm character.

2.5.4 LIVE/DEAD® Staining with Confocal Imaging

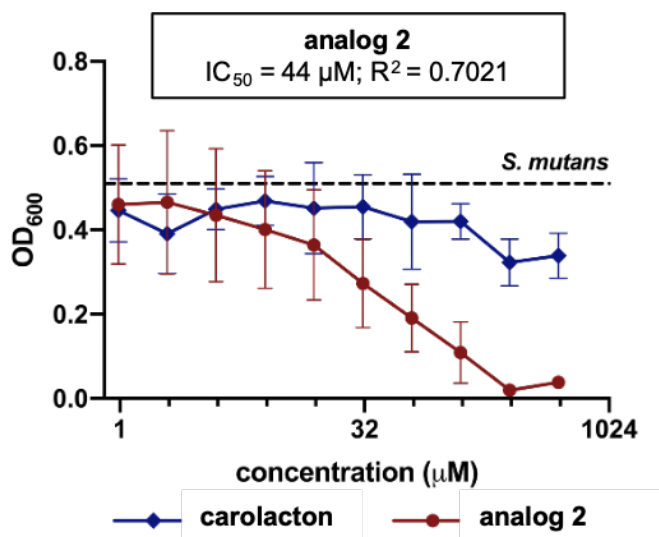


Figure 2.15 Biofilm inhibition during confocal imaging

To probe this hypothesis further, we used LIVE/DEAD® stain and confocal imaging to visualize the effect of **analog 2** on biofilm formation and determine the viability of the cells in the biofilm, like previous accounts. Compound-treated *S. mutans* biofilm was grown in glass bottom plates to further promote biofilm formation and to allow for direct visualization of biofilm phenotypes. In our confocal conditions (THB media, sucrose, and glass bottom plate), the biofilm growth inhibition was improved with a biofilm IC₅₀ of 44 µM, further demonstrating its preference for biofilm mechanisms (Figure 2.15). It should be noted that carolacton does not have an IC₅₀ under these conditions. Visualized with LIVE/DEAD® stain, high densities of non-viable cells (red) were observed at 125 µM and 63 µM and percent viabilities were calculated from the fluorescence measurements (Figure 2.16). According to these calculations, **analog 2** caused 76%

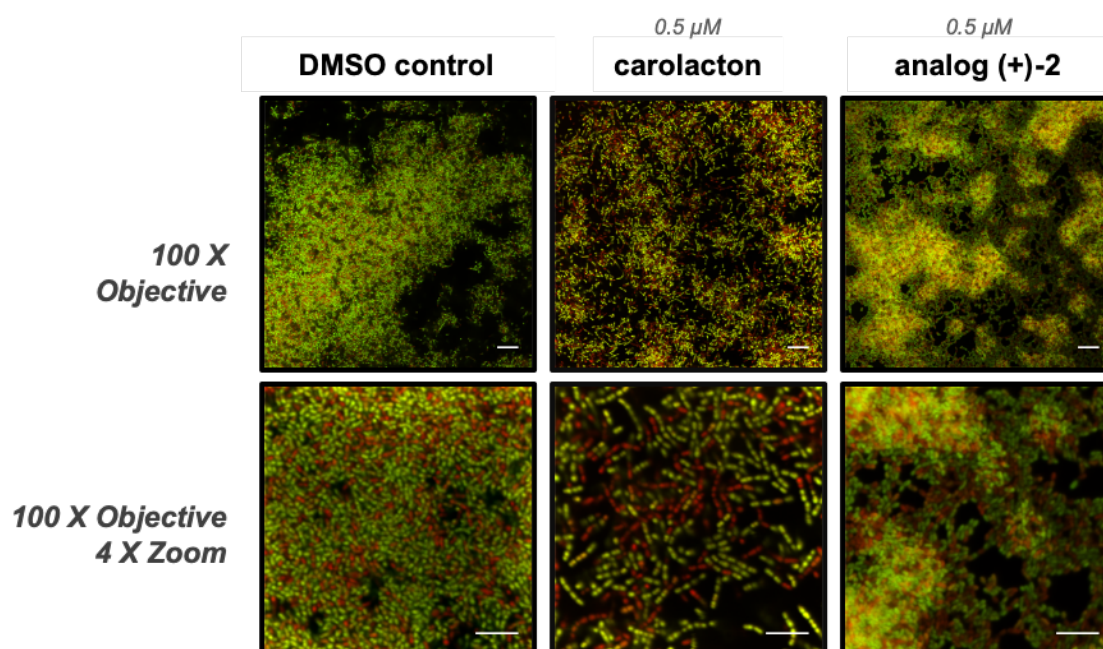


Figure 2.17 Low concentration biofilm effects of carolacton and analog 2

of non-viable biofilm cells at 125 μM , and 59% at 63 μM . We also observed a spike in biofilm mass, calculated with crystal violet staining, at higher concentrations (Figure 2.16). These results show that the observed increase in biofilm mass corresponded to accumulation of cells with cell membrane defects (shown in red). Carolacton was shown to kill biofilm cells at lower

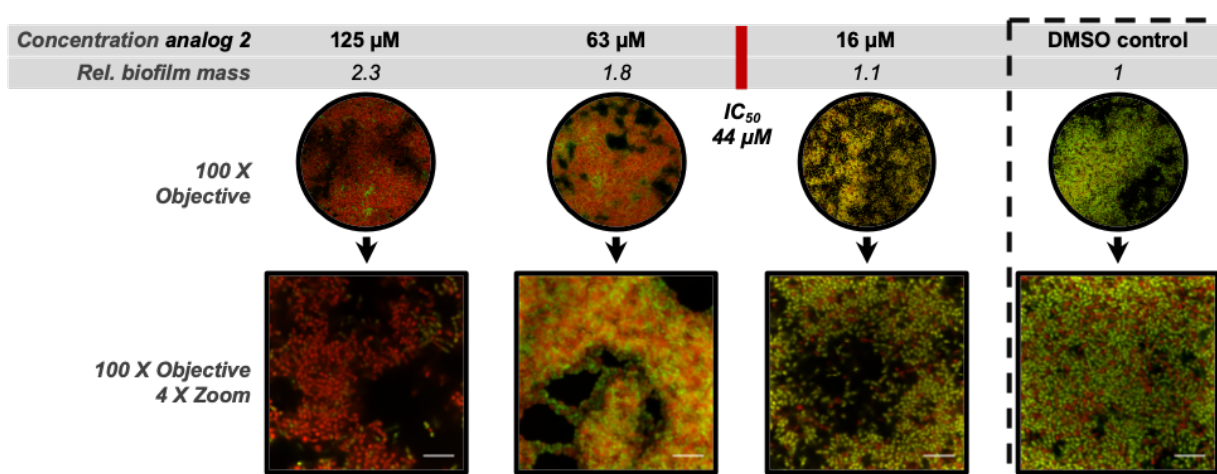


Figure 2.16 Analog 2 kills cells in biofilm

concentrations too. We therefore compared **analog 2** and carolacton at 0.5 μM and observed similar biofilm defect effects (Figure 2.17).

2.5.5 Colony Forming Unit Assay

To validate that our compound was causing viability issues to *S. mutans* cells, we conducted

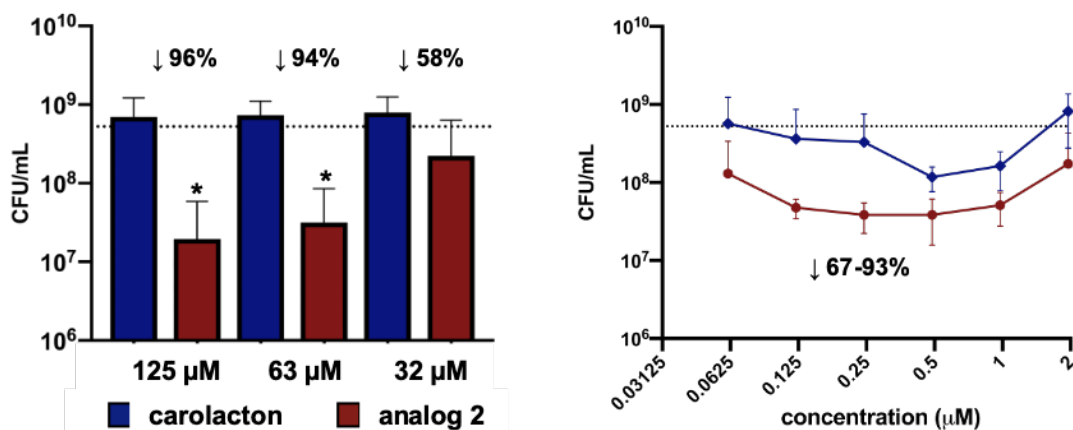


Figure 2.18 CFU/mL calculation for cell death in biofilm after treatment with analog 2

CFU/mL counts to validate the LIVE/DEAD[®] images in Figures 2.16 and 2.17. From the CFU/mL calculations. It was found that **analog 2** decreased biofilm cell viability by 96% at 125 μM , 94% at 63 μM , and 58% at 32 μM compared to the DMSO control (Figure 2.18). More interestingly, it was discovered that **analog 2** also decreased biofilm cell viability at low concentrations (between 62.5 nM and 2 μM), demonstrating decreases between 75% and 93% (Figure 2.18). At the same concentrations, carolacton decreased biofilm cell viability between 30% and 78%. Therefore, our simplified analog has a more potent effect on *S. mutans* biofilm.

2.5.6 Acid tolerance based activity

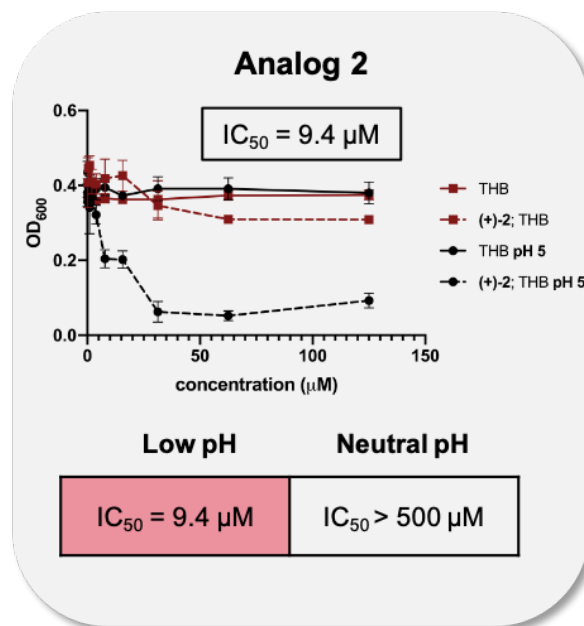


Figure 2.19 **Analog 2**'s acid mechanism

After confirmation that **analog 2**'s activity was biofilm specific, we sought to investigate the mechanism of **analog 2**. Carolacton's activity is dependent on the drastic drop in pH that is observed during biofilm formation.⁸⁰ With structural and biological similarities between **analog 2** and carolacton, we deemed it appropriate to investigate if **analog 2** acted via a similar mechanism. To test this, we measured the susceptibility of pre-acidified planktonic cultures to **analog 2**. This experiment had been previously used to connect the activity of carolacton to decreases in environmental pH. We found that **analog 2** was able to inhibit planktonic cells with an IC₅₀ of approximately 10 µM when the media was pre-acidified (Figure 2.19, black dotted line). This data supports our hypothesis that **analog 2** acts, at least in part, via an acid-mediated mechanism.

2.5.7 Genetic Screen with Analog 2

We were next prompted to further characterize the mechanism by which **analog 2** targets the ATR of *S. mutans*. Taking advantage of the inhibitory activity of our compound, we utilized a

Oragen ID	Gene Locus	Gene Name	Description
UA159 0022	SMU.026	plsX ylpD	putative fatty acid/phospholipid synthesis protein
UA159 0023	SMU.027	ACP acpP	putative acyl carrier protein
UA159 0209	SMU.231	als ilvB	acetolactate synthase, large subunit (AHAS)
UA159 0210	SMU.232	ilvH	acetolactate synthase, small subunit
UA159 0223	SMU.246	rgpG	cell wall division; glycosyl transferase
UA159 0328	SMU.363	glnR	transcriptional regulator glutamine synthetase repressor; DNA interactions
UA159 0371	SMU.410	-	putative transcriptional regulator
UA159 0371	SMU.410	brpA	biofilm regulatory protein precursor A
UA159 0438	SMU.484	pknB	putative serine/threonine protein kinase
UA159 0454	SMU.0501	-	hypothetical protein
UA159 0491	SMU.540	dpr	peroxide resistance protein
UA159 0501	SMU.551	ftsA	cell division
UA159 0501	SMU.551	ftsA	cell division protein FtsA
UA159 0521	SMU.572	folD	folate dehydrogenase
UA159 0555	SMU.609	bsp	putative 50K cell wall protein precursor; murein=peptidoglycane
UA159 0556	SMU.610	pac pags-5 spaP sr	cell surface antigen
UA159 0801	SMU.878	msmE	multiple sugar-binding ABC transporter, sugar binding protein precursor
UA159 0802	SMU.879	msmF	multiple sugar-binding ABC transporter, permease protein MsmF
UA159 0836	SMU.922	-	putative ABC transporter, ATP-binding protein
UA159 0846	SMU.933	atmA	putative amino acid ABC transporter; periplasmic amino acid
UA159 0847	SMU.934	-	putative amino acid ABC transporter; permease protein
UA159 0914	SMU.1004	gtfb	glucosyltransferase-I
UA159 0918	SMU.1008	llrG	putative response regulator; two component system
UA159 0947	SMU.1038c	vicR ycbL	putative response regulator; two component system
UA159 0952	SMU.1043c	pta	putative phosphotransacetylase
UA159 1092	SMU.1193	yhcF	putative transcriptional regulator; DNA interactions
UA159 1099	SMU.1203	bcat ilvE	putative branched-chain amino acid aminotransferase IlvE
UA159 1123	SMU.1280c	gat	possible amidotransferase
UA159 1158	SMU.1266	hisH	putative glutamine amido transferase
UA159 1166	SMU.1276c	ezrA	septation ring formation regulator
UA159 1209	SMU.1324	ftsX	putative cell-division protein
UA159 1267	SMU.1390	-	conserved hypothetical protein
UA159 1446	SMU.1591	ccpA regM	catabolite control protein A, CcpA; DNA interactions
UA159 1591	SMU.1745c	-	putative transcriptional regulator
UA159 1662	SMU.1824c	codY	putative transcriptional regulator
UA159 1707	SMU.1877	manL ptnAB	putative PTS system, mannose-specific component IIAB
UA159 1708	SMU.1878	manM ptnC	putative PTS system, mannose-specific component IIAC
UA159 1779	SMU.1960c	levE	putative PTS system mannose specific IIB component
UA159 1796	SMU.1978	ackA comYI	putative acetate kinase
UA159 1823	SMU.2007	rI15 rplO	50S ribosomal protein LI5
UA159 1854	SMU.2042	dexT	dextranase precursor

Table 2.3 *S. mutans* mutants from the Quivey Group library

forward chemical genetic approach in which we screened genetic mutants for decreases in susceptibility. This approach would help us identify which genes are involved in or are related to the mode of action of **analog 2**. Recently, our collaborators from the Quivey Lab reported an extensive library of *S. mutans* mutants with complete phenotypic profiles.⁹⁶ After comparison of these biofilm phenotypes with the previous reports highlighted in Section 2.3.1, we selected 17 mutants that we hypothesized to be associated with carolacton's, and presumably **analog 2**'s, activity. This group contained genes responsible for *S. mutans* acid tolerance mechanisms, two

component systems, cell division, cellular regulation and glucan synthesis (full list of mutants Table 2.3).

As mentioned above, a significant benefit of **analog 2** is that it elicits an inhibitory effect that allowed for the expedited screen of this library with the goal of identifying a non-susceptible mutant strain. Each mutant was dosed with 125 μM of **analog 2** and viability was measured (Figure 2.20). Fourteen of the mutant strains were as susceptible as the WT strain, UA159, but two mutants, SMU_484 (Protein kinase B; ΔpknB) and SMU_1276c (cell shape regulator; ΔezrA), were found to be more susceptible. It is interesting that the master regulator PknB, which has been previously implicated as part of the mode of action of carolacton, is a slightly more susceptible mutant to our tool compound **analog 2** ($p=0.131$). Most strikingly, the activity of **analog 2** was significantly reduced against the SMU_1591 mutant when compared to the parent UA159 strain, signifying that

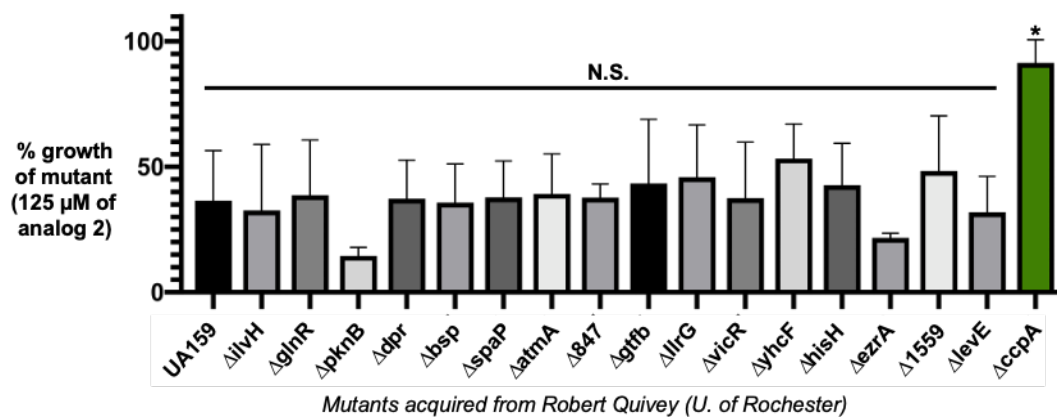


Figure 2.20 **Analog 2** genetic mutant screen

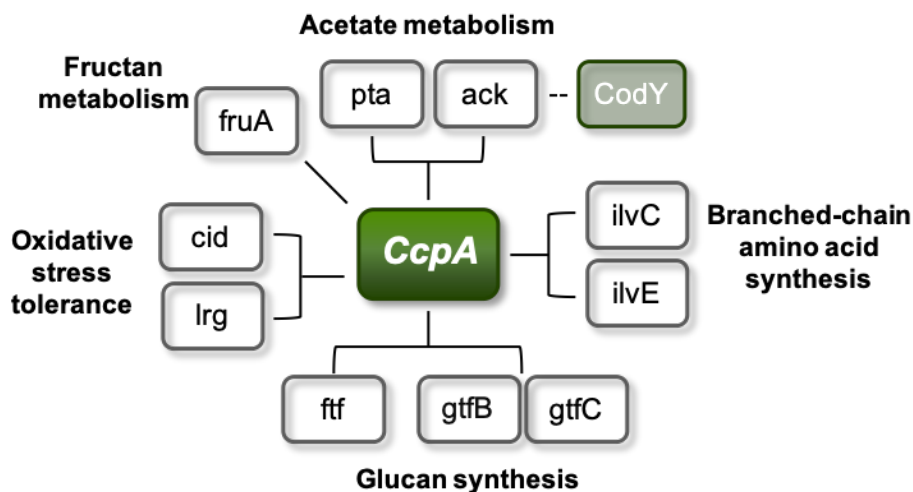


Figure 2.21 CcpA gene regulation map

this gene is partially responsible, or related, to the inhibition patterns described above for **analog 2**. SMU_1591 is deficient in the gene that codes for carbon catabolite protein A (CcpA). This transcriptional regulator is responsible for controlling carbon usage within the cell and regulates a handful of downstream pathways associated with the ATR mechanism of *S. mutans* (Figure 2.21). Specifically, CcpA has been shown to regulate EPS formation (ftf, gtfBC), cell attachment (fruA), acetate metabolism (pta, ack), branched-chain amino acid synthesis (ilvCE), oxidative stress tolerance (cid, lrg), and other virulence mechanisms. These mechanisms have large implications in the maintenance of *S. mutans* ATR system.

2.5.8 Conclusions

This work details the successful implementation of DTS to develop a tool compound, **analog 2**, that demonstrates biofilm specificity. **Analog 2** exhibits three distinct advantages over the natural product: 1) the synthesis is greatly expedited due to the structural simplification, 2) its activity enabled a preliminary screen of *S. mutans* mutants that resulted in identification of CcpA signaling as a putative pathway, and 3) it is more potent than the natural product eliciting both an IC_{50} and causing higher levels of cell death at low concentrations in biofilm samples (Figure 2.22).

Further characterization of the activity of **analog 2** and its connection to its parent structure, carolacton, will be addressed in Chapter 3.

Taken together, our proof of concept chemical genetic screen has identified the CcpA signaling pathway as the one that harbors the target of **analog 2**. It should be noted that CcpA regulates a large number of pathways in *S. mutans* and was also implicated in the activity of carolacton via transcriptomic studies by Sudhakar. Intriguingly, that study did not show a connection between CcpA and Folds, the proposed target of carolacton. Intriguingly, previous studies have postulated that CcpA is an ideal target for the oral microbiome as multispecies communities devoid of CcpA allowed for commensal bacteria to outcompete *S. mutans*. We plan to utilize **analog 2** as a chemical probe to better understand carolacton's biofilm mechanisms (Chapter 3) and apply them to multispecies communities (Future work; Section 3.3).

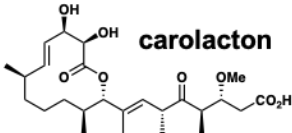
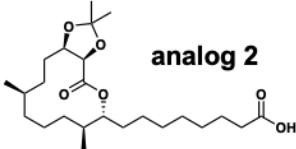
	 carolacton	 analog 2
Synthesis: sidechain steps	8	2
Synthesis: total steps	27	16
Biofilm specific activity	✓	✓
Acid tolerance mechanism	✓	✓
Nanomolar biofilm phenotype	✓	✓
Quantitative inhibition activity	✗	✓
Mutant screening capabilities	✗	✓

Figure 2.22 Carolacton and analog 2 comparison

Through two generations of DTS analog design, we have discovered a toolbox of carolacton-inspired analogs that cause interesting, and sometimes unique, biological outcomes. We will continue to study these effects until we understand the slight differences between the structure activity relationships of the analogs. For example, is the microcolony response related to carolacton or **analog 2** or is it a completely new target? Does carolacton have more than one target? Do these new analogs have better or worse selectivity between the multiple targets causing the variation in biofilm growth? Chapter 3 will outline the first step we have taken to answer these questions.

2.6 References

78. Schneiker, S.; Perlova, O.; Kaiser, O.; Gerth, K.; Alici, A.; Altmeyer, M. O.; Bartels, D.; Bekel, T.; Beyer, S.; Bode, E.; Bode, H. B.; Bolten, C. J.; Choudhuri, J. V.; Doss, S.; Elnakady, Y. A.; Frank, B.; Gaigalat, L.; Goesmann, A.; Groeger, C.; Gross, F.; Jelsbak, L.; Jelsbak, L.; Kalinowski, J.; Kegler, C.; Knauber, T.; Konietzny, S.; Kopp, M.; Krause, L.; Krug, D.; Linke, B.; Mahmud, T.; Martinez-Arias, R.; McHardy, A. C.; Merai, M.; Meyer, F.; Mormann, S.; Muñoz-Dorado, J.; Perez, J.; Pradella, S.; Rachid, S.; Raddatz, G.; Rosenau, F.; Rückert, C.; Sasse, F.; Scharfe, M.; Schuster, S. C.; Suen, G.; Treuner-Lange, A.; Velicer, G. J.; Vorhölter, F.-J.; Weissman, K. J.; Welch, R. D.; Wenzel, S. C.; Whitworth, D. E.; Wilhelm, S.; Wittmann, C.; Blöcker, H.; Pühler, A.; Müller, R., Complete genome sequence of the myxobacterium *Sorangium cellulosum*. *Nature Biotechnology* **2007**, *25* (11), 1281-1289.
79. Jansen, R.; Irschik, H.; Huch, V.; Schummer, D.; Steinmetz, H.; Bock, M.; Schmidt, T.; Kirschning, A.; Müller, R., Carolacton - A Macrolide Ketocarboxylic Acid that Reduces Biofilm Formation by the Caries- and Endocarditis-Associated Bacterium *Streptococcus mutans*. *European Journal of Organic Chemistry* **2010**, *2010* (7), 1284-1289.
80. Kunze, B.; Reck, M.; Dotsch, A.; Lemme, A.; Schummer, D.; Irschik, H.; Steinmetz, H.; Wagner-Dobler, I., Damage of *Streptococcus mutans* biofilms by carolacton, a secondary metabolite from the myxobacterium *Sorangium cellulosum*. *BMC Microbiol* **2010**, *10*, 199.
81. Schmidt, T.; Kirschning, A., Total synthesis of carolacton, a highly potent biofilm inhibitor. *Angew Chem Int Ed Engl* **2012**, *51* (4), 1063-6.
82. Sabitha, G.; Shankaraiah, K.; Prasad, M.; S. Yadav, J., Studies toward the Total Synthesis of Carolacton. *Synthesis* **2012**, *45* (02), 251-259.
83. Sharma, G. V. M.; Reddy, S. V., Stereoselective synthesis of the macrocyclic core (C7–C19) of carolacton. *RSC Advances* **2013**, *3* (44).
84. Ghosh, S.; Rao, K., Synthetic Studies of Carolacton: Enantioselective Total Synthesis of C1-C8 and C9-C19 Fragments of the Molecule. *Synthesis* **2013**, *45* (19), 2745-2751.

85. Reddy, S. V.; Prasanna Kumar, K.; Ramakrishna, K. V. S.; Sharma, G. V. M., Approaches towards the total synthesis of carolacton: synthesis of C1–C16 fragment. *Tetrahedron Letters* **2015**, *56* (15), 2018-2022.
86. Hallside, M. S.; Brzozowski, R. S.; Wuest, W. M.; Phillips, A. J., A concise synthesis of carolacton. *Org Lett* **2014**, *16* (4), 1148-51.
87. Kuilya, T. K.; Goswami, R. K., Stereoselective Total Synthesis of Carolacton. *Org Lett* **2017**, *19* (9), 2366-2369.
88. Ammermann, J.; Schmidt, T.; Donner, J.; Reck, M.; Dalton, M.; Stumpp, N.; Stiesch, M.; Wagner-Dobler, I.; Kirschning, A., The carolactam strategy is ineffective: synthesis and biological evaluation of carolactam. *Org Biomol Chem* **2017**, *15* (40), 8553-8558.
89. Stumpp, N.; Premnath, P.; Schmidt, T.; Ammermann, J.; Dräger, G.; Reck, M.; Jansen, R.; Stiesch, M.; Wagner-Döbler, I.; Kirschning, A., Synthesis of new carolacton derivatives and their activity against biofilms of oral bacteria. *Organic & Biomolecular Chemistry* **2015**, *13* (20), 5765-5774.
90. Reck, M.; Rutz, K.; Kunze, B.; Tomasch, J.; Surapaneni, S. K.; Schulz, S.; Wagner-Dobler, I., The biofilm inhibitor carolacton disturbs membrane integrity and cell division of *Streptococcus mutans* through the serine/threonine protein kinase PknB. *J Bacteriol* **2011**, *193* (20), 5692-706.
91. Sudhakar, P.; Reck, M.; Wang, W.; He, F. Q.; Wagner-Döbler, I.; Zeng, A.-P., Construction and verification of the transcriptional regulatory response network of *Streptococcus mutans* upon treatment with the biofilm inhibitor carolacton. *BMC Genomics* **2014**, *15*, 362-362.
92. Li, J.; Wang, W.; Wang, Y.; Zeng, A.-P., Two-dimensional gel-based proteomic of the caries causative bacterium *Streptococcus mutans* UA159 and insight into the inhibitory effect of carolacton. *PROTEOMICS* **2013**, *13* (23-24), 3470-3477.
93. Donner, J.; Bunk, B.; Schober, I.; Sproer, C.; Bergmann, S.; Jarek, M.; Overmann, J.; Wagner-Dobler, I., Complete Genome Sequences of Three Multidrug-Resistant Clinical Isolates of *Streptococcus pneumoniae* Serotype 19A with Different Susceptibilities to the Myxobacterial Metabolite Carolacton. *Genome Announc* **2017**, *5* (7).
94. Donner, J.; Reck, M.; Bunk, B.; Jarek, M.; App, C. B.; Meier-Kolthoff, J. P.; Overmann, J.; Müller, R.; Kirschning, A.; Wagner-Dobler, I., The Biofilm Inhibitor Carolacton Enters Gram-Negative Cells: Studies Using a TolC-Deficient Strain of *Escherichia coli*. *mSphere* **2017**, *2* (5).
95. Fu, C.; Sikandar, A.; Donner, J.; Zaburannyi, N.; Herrmann, J.; Reck, M.; Wagner-Döbler, I.; Koehnke, J.; Müller, R., The natural product carolacton inhibits folate-dependent C1 metabolism by targeting FOLD/MTHFD. *Nature Communications* **2017**, *8* (1), 1529.
96. Quivey, R. G., Jr.; Grayhack, E. J.; Faustoferri, R. C.; Hubbard, C. J.; Baldeck, J. D.; Wolf, A. S.; MacGilvray, M. E.; Rosalen, P. L.; Scott-Anne, K.; Santiago, B.; Gopal, S.; Payne, J.; Marquis, R. E., Functional profiling in *Streptococcus mutans*: construction and examination of a genomic collection of gene deletion mutants. *Molecular oral microbiology* **2015**, *30* (6), 474-495.

Chapter 3 Analog 2 Target Elucidation

Chapter 3 contains unpublished data completed in collaboration with the Sieber Lab (Technical University of Munich). Section 3.2 was completed with Amber Scharnow (Wuest) and she will lead the completion of this work.

3.1 Affinity-based proteomic probe

In Chapter 2, work was presented to describe the discovery of **analog 2**, a more potent and accessible carolacton mimic. It was proven useful in a genetic screen, where it identified CcpA as a putative pathway for the activity of these molecules. Prompted with these successes we desired to fully elucidate the biological target(s) of **analog 2** and further prove the connection between carolacton and **analog 2**. With this goal in mind, a probe version of **analog 2** was synthesized and used in proteomic experiments to discover compound-protein binding interactions that could lead to the identification of the target(s) of **analog 2**.

3.1.1 Affinity-based Protein Profiling

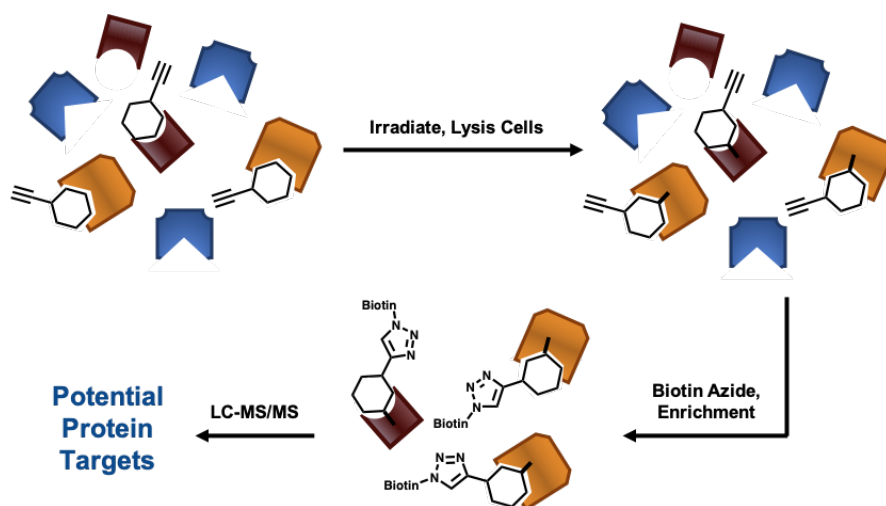


Figure 3.1 Affinity-based protein profiling workflow

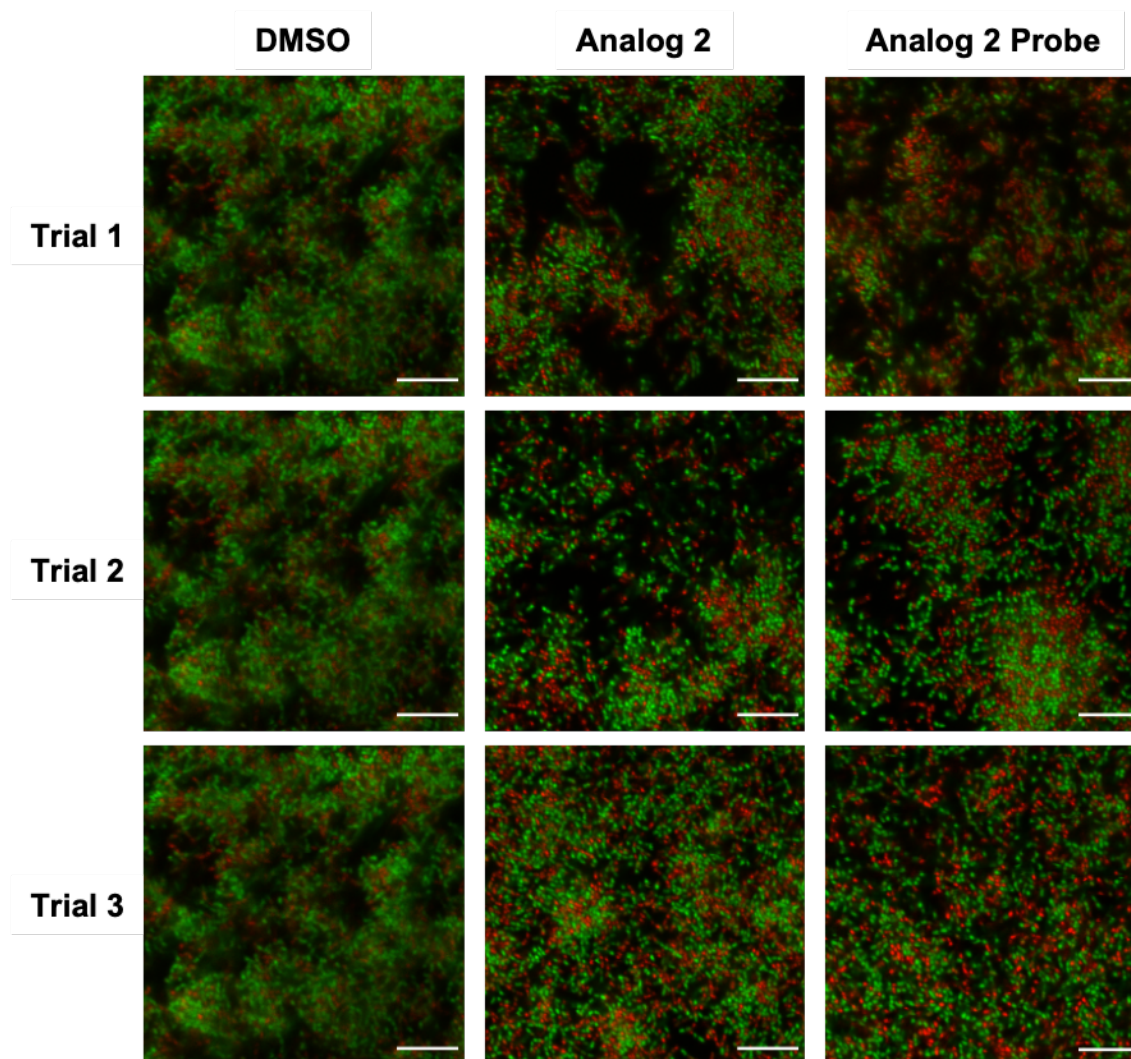


Figure 3.2 Comparison of 5 μM of **analog 2** and **analog 2-probe** on *S. mutans* biofilm

Other optimized minimalist probes have been published but are not yet commercially available.¹⁰¹

We chose to use the amine version of the Yao minimalist probe (**3.1**) to introduce the required functionality to **analog 2**. The amine (**3.1**) was coupled to **analog 2** to form **analog 2-probe** (**3.2**) in 61% yield (Scheme 3.1). Retention of biofilm biological activity was confirmed with LIVE/DEAD[®] staining and confocal imaging (Figure 3.2).

3.1.3 Developing the biofilm workflow

The workflow for the AfBPP experiment, described above, is more commonly used for planktonic bacteria. Therefore, optimization was needed in order to execute the experiment with

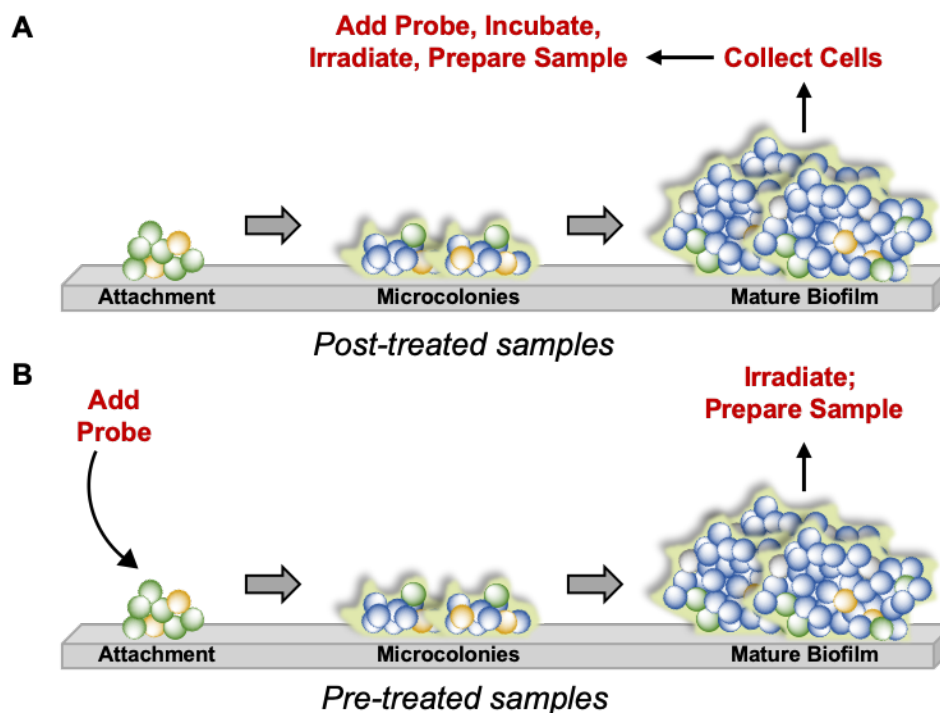


Figure 3.3 Biofilm methods for AfBPP experiment

biofilm samples. Optimization and execution of the AfBPP experiments were completed in the laboratory of Prof. Stephan Sieber. His graduate student Ines Hübner mentored me while I learned the method. The Sieber Group had previously published a procedure in which they performed AfBPP on biofilm samples according to Figure 3.3A.¹⁰² We have termed this method “Post-treated samples”. In this method the biofilm cells were grown to maturity, collected and then incubated with compound. This was successful for other modes of action but I believed that **analog 2** needed to be present while the cells were growing to have its biological effect and interact with its target(s). I therefore modified the procedure in which the probe was added at the start of growth, and cells were irradiated immediately following the biofilm growth cycle (Figure 3.2B “Pre-treated samples”). In order to compare the methods, I ran an analytical AfBPP experiment where instead of performing the “click” reaction with biotin azide I used rhodium azide. I was then able to analyze the crude protein samples with gel electrophoresis (Figure 3.4). We knew **analog 2** caused decreases in biofilm viability at concentrations as low as 60 nM, but we tested the probe starting

at 10 μM to ensure we could visualize protein cross-linking. From this experiment, I determined that the pre-treated method was more successful in cross-linking to protein (Figure 3.4). Notably, the probe showed a gradient effect, signifying that the probe was interacting with biological targets in a dose-dependent manner. With the help of the expertise from the Sieber Group, I chose 5 and 1 μM as the optimal concentrations of probe to use for sample preparation.

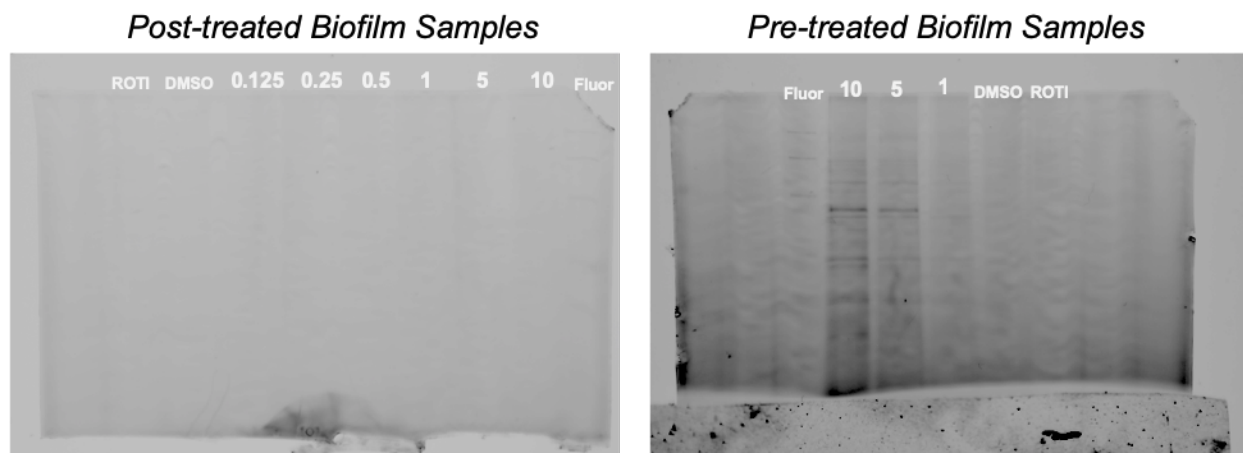


Figure 3.5 Analytical AfBPP results.

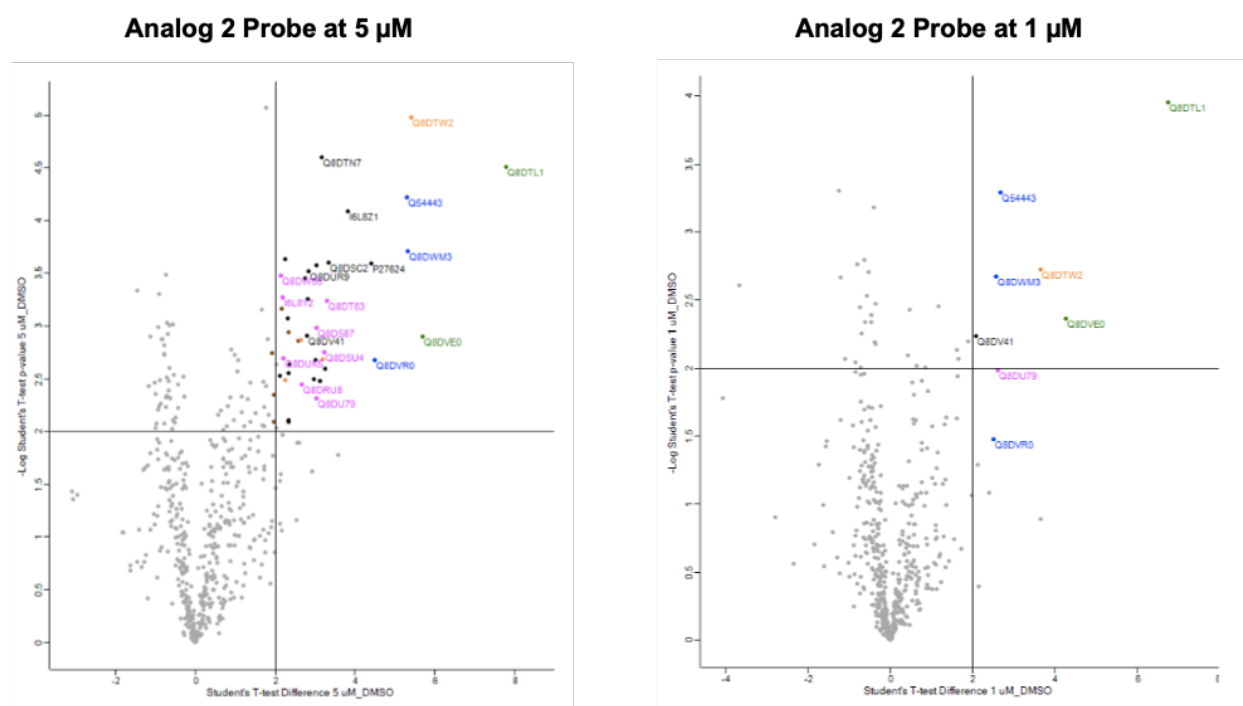


Figure 3.4 LC-MS/MS results for **analog 2-probe**

3.1.4 Identified protein targets

After preparation of the AfBPP samples, the Sieber Group performed LC-MS/MS analysis. From this data we gathered clear trends for the binding interactions of the **analog 2-probe**. We identified more protein interactions at 5 μM than at 1 μM . This suggests that **analog 2-probe** works in a dose-dependent manner (Figure 3.5). We observed peripheral protein interactions at 5 μM which is not uncommon. The probe will cross link with any protein in proximity even if the compound is not specifically bound to or causing a biological change to those proteins. There are two methods we used to further decipher which protein targets are the most significant: dose-dependency analysis and AfBPP competition assay. The first method identifies which proteins have the strongest dose-dependent response by comparing the protein enrichment from 5 μM and 1 μM (Figure 3.6). This comparison allowed us to narrow down the protein interactions and

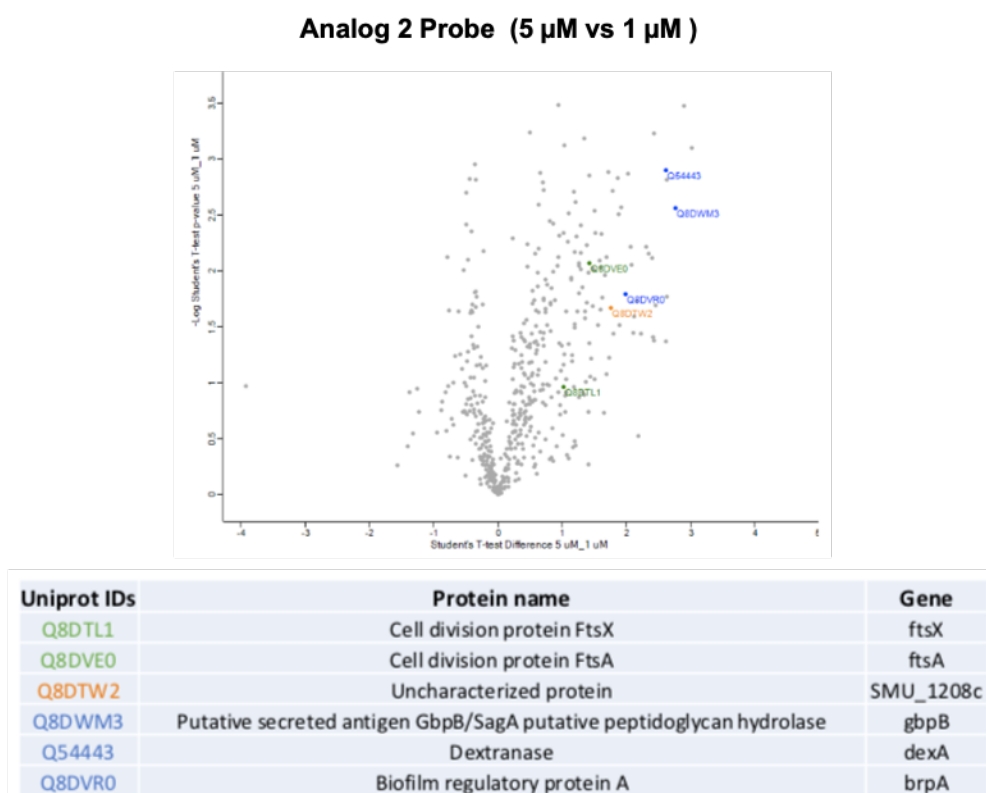


Figure 3.6 LC-MS/MS results for dose dependent response of **analog 2-probe**

distinguish the most promising biological target(s). When this data was cross referenced with Figure 3.4, we identified six proteins that were 1) highly enriched and 2) dose-dependent responses. DexA (dextranase), BrpA (biofilm regulatory protein A), FtsA/FtsX (cell division proteins), GbpB (glucan binding protein B) and an uncharacterized protein (SMU_1208c) were identified. These results will be described in more detail and validated in Section 3.1.6.

3.1.5 Competition assay

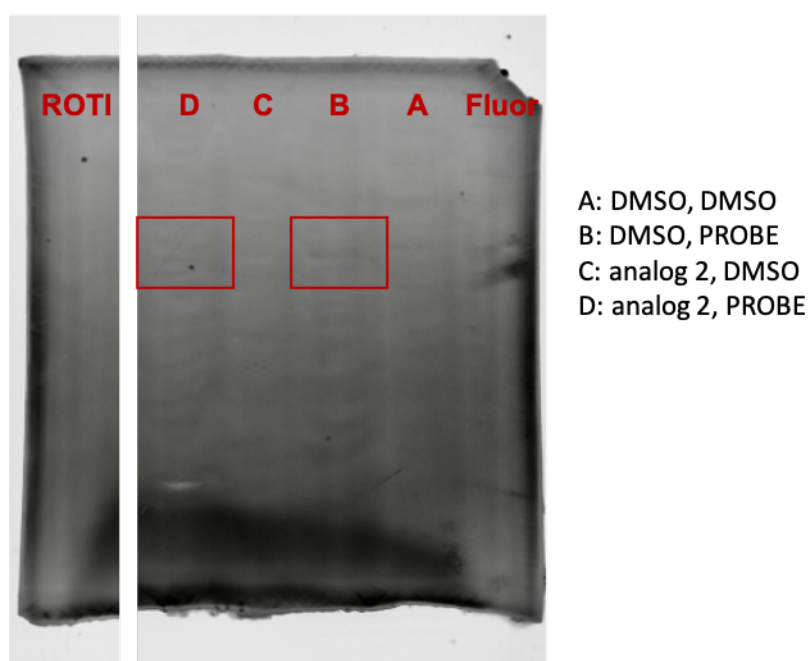


Figure 3.7 AfBPP competition analytical gel

The second method of discovering the most promising protein targets is a competition assay. Adding the minimalist probe onto **analog 2** could increase our chance of isolating non-specific binding interactions that were not relevant to the biological activity to **analog 2**. Therefore, the competition assay is an important control to run for AfBPP experiments. This assay requires pretreating with excess of the active compound before dosing the probe version. The active compound will fill all possible binding pockets and leave the probe to interact with its non-specific binding partners. It is possible to identify false positives with this method and is useful to further clarify your proteomic data.

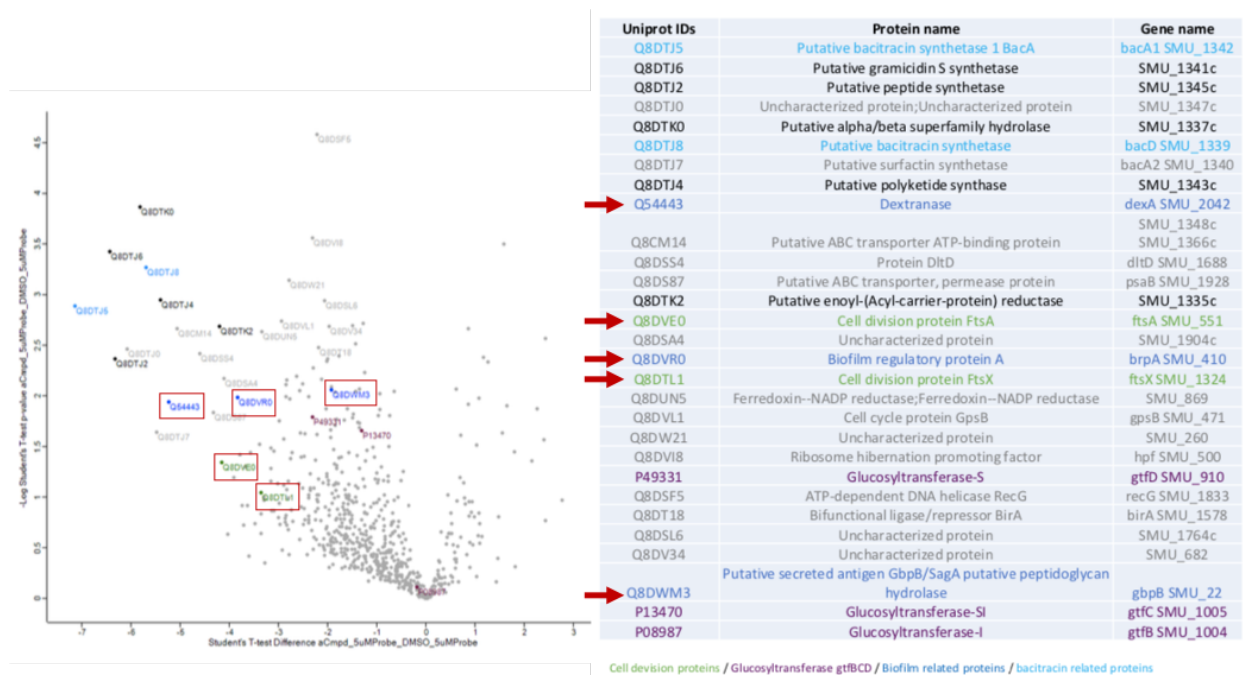


Figure 3.8 Competition experiment with **analog 2**

I performed the competition experiment by dosing 50 μM of **analog 2** to *S. mutans* biofilm culture. After 1 hour of incubation, I then added 5 μM of **analog 2-probe**. Similar to section 3.1.4, I first optimized conditions analytically (Figure 3.7). Comparison of the red boxes shows upon incubation with **analog 2** prior to the probe (Lane D) removes the faint protein band that is identified with just the probe (Lane B). With these conditions I then prepared MS samples (Figure 3.8). We found that a handful of binding interactions were outcompeted by pre-dosing **analog 2**. Unfortunately, we also found that our conditions resulted in low protein levels for the LC-MS/MS analysis. The low protein level could be a result of the cells being compromised at such a high concentration. We have decided to use the competition data for reference, but the results may be distorted due to the drastic change in protein level. We see that five of the six identified targets from Figure 3.6 were outcompeted, further verifying the accuracy of our probe (Figure 3.8; red arrows). The uncharacterized protein (SMU_1208c) was not outcompeted potentially signaling that it was a false positive. Further validation will be needed to solidify these findings.

Concurrently, I performed a competition assay using the natural product carolacton. I added 50 μM of carolacton to *S. mutans* cells and then after 1 hour of incubation, added 5 μM of **analog 2-probe**. Once again we observed low protein levels, but did find that some proteins were outcompeted by the natural product (Figure 3.9). We found that DexA and GbpB were both downregulated when carolacton was present, signifying that carolacton competes against **analog 2-probe** for binding these substrates (Figure 3.9; red arrows). The remaining protein hits were not outcompeted (Figure 3.9; black arrows). These results show promise that **analog 2** induces anti-biofilm activity by interacting with the similar biological target(s) as carolacton. Details of how this connection will be fully confirmed will be outlined in Section 3.3.

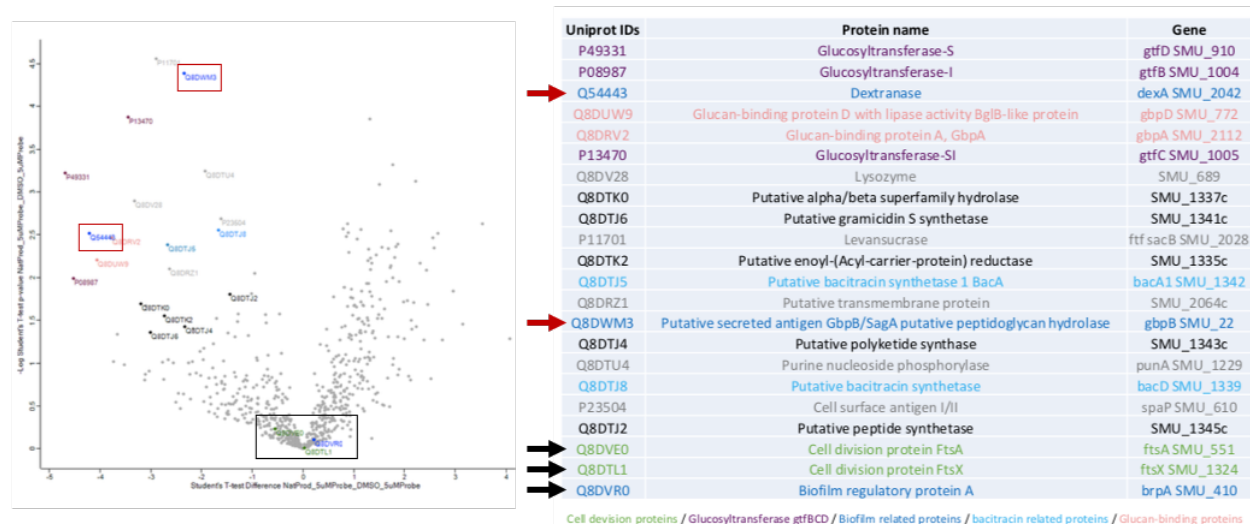


Figure 3.9 Competition experiment with carolacton

3.1.6 Proteomic pulldown results

Using **analog 2-probe** as a tool compound to understand carolacton's biofilm activity we have identified five lead protein targets: DexA (dextranase), BrpA (biofilm regulatory protein A), FtsA/FtsX (cell division proteins) and GbpB (glucan binding protein B). As discussed before, **analog 2-probe** was outcompeted by **analog 2**, validating the binding interactions. The same experiment with carolacton only showed competition with GbpB and DexA. Figure 3.10 shows an illustration of this relationship, in which there is an overlap of binding interactions for carolacton

and **analog 2** (GbpB and DexA). Also included in this diagram is folate dehydrogenase (FolD); the protein identified as carolacton's target in 2017.⁹⁵ **Analog 2** was not found to interact with FolD in our AfBPP experiments. One possible explanation for this could be a result of the chemical simplification of carolacton observed with **analog 2**. The structural simplicity of **analog 2** could lead to an increase in binding promiscuity, and decrease in affinity to FolD. Validation of these ideas and protein targets is currently underway in the Wuest Group and is displayed in Section 3.2.

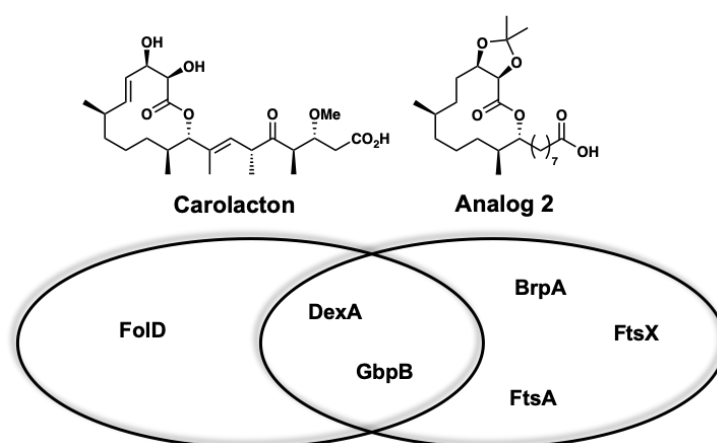


Figure 3.10 Potential target overlap of **analog 2** and carolacton

3.2 Proteomic result validation

3.2.1 Resistance assay development

Our efforts to confirm the AfBPP results began with attempts at evolving a strain of *S. mutans* that was resistant to **analog 2**. A resistance strain harboring a genetic mutation could validate the proteins identified with AfBPP. First we plated 10^{10} cells on THB agar with 1X, 2X and 4X the MIC of **analog 2**, but the formation of resistant colonies was not observed. This could be due to the biofilm-specific mechanism of action, but it is also notoriously hard to generate mutated strains with this method. We then attempted to perform a biofilm serial passage assay for 24 days in the presence of increasing concentration of **analog 2**. Unfortunately, the samples were

contaminated with *Candida* yeast but still showed that *S. mutans* acquired a few mutations. Of note, a fibronectin/fibrinogen-binding protein (SMU.1449) and a tagatose utilization transcriptional regulator (SMU.112c) were mutated (Table 3.1). Replications of this experiment are underway to confirm the initial findings and remove uncertainty from the contaminated data.

Mapping	Reference Position	Type	Length	Reference	Allele	Linkage	Zygoty	Count	Coverage	Frequency	Forward/reverse balance	Average quality	Overlapping annotations
DVT874_S14_R1_001_(paired)_contig_3 mapping	89837	SNV	1	T	A		Homozygous	12	12	100	0.454545	34.16667	
DVT874_S14_R1_001_(paired)_contig_3 mapping	89851	SNV	1	T	A		Homozygous	11	11	100	0.45	35.27273	
DVT874_S14_R1_001_(paired)_contig_7 mapping	121342	SNV	1	C	G		Homozygous	15	15	100	0.318182	34	CDS: Mobile element protein CDS: Tagatose utilization transcriptional regulator, RpiR family
DVT874_S14_R1_001_(paired)_contig_10 mapping	3670	SNV	1	T	G		Homozygous	43	49	87.7551	0.493671	33.81395	
DVT874_S14_R1_001_(paired)_contig_12 mapping	5255	SNV	1	A	T		Homozygous	44	44	100	0.45679	34.63636	RNA: RNA
DVT874_S14_R1_001_(paired)_contig_12 mapping	5279	SNV	1	C	G		Homozygous	23	23	100	0.452381	34.47826	
DVT874_S14_R1_001_(paired)_contig_13 mapping	209682	SNV	1	G	A		Homozygous	15	15	100	0.454545	29.6	CDS: Fibronectin/fibrinogen-binding protein
DVT874_S14_R1_001_(paired)_contig_14 mapping	15071	Insertion	6	-	CAAAAT		Homozygous	11	11	100	0.384615	32.27273	
DVT874_S14_R1_001_(paired)_contig_14 mapping	109554	SNV	1	A	T		Homozygous	21	21	100	0.432432	31.57143	
DVT874_S14_R1_001_(paired)_contig_14 mapping	109557	SNV	1	C	G		Homozygous	21	21	100	0.432432	34.19048	
DVT874_S14_R1_001_(paired)_contig_14 mapping	109592	SNV	1	A	T		Homozygous	19	19	100	0.387097	32.84211	
DVT874_S14_R1_001_(paired)_contig_20 mapping	84623	SNV	1	A	C		Homozygous	35	35	100	0.396552	35	tRNA: tRNA-Met-CAT
DVT874_S14_R1_001_(paired)_contig_22 mapping	23391	SNV	1	T	G		Homozygous	13	13	100	0.458333	30.76923	

Mapping	UA159 location	Coding region change	Amino acid change
DVT874_S14_R1_001_(paired)_contig_3 mapping	SMU_1894c, SMU_1895c		
DVT874_S14_R1_001_(paired)_contig_3 mapping	SMU_1894c, SMU_1895c		
DVT874_S14_R1_001_(paired)_contig_7 mapping	SMU_437c	Mobile element protein:c.23C>G	Mobile element protein:p.Thr8Arg
DVT874_S14_R1_001_(paired)_contig_10 mapping	SMU_112c	Tagatose utilization transcriptional regulator, RpiR family:c.678A>C	Tagatose utilization transcriptional regulator, RpiR family:p.Glu226Asp
DVT874_S14_R1_001_(paired)_contig_12 mapping	5S rRNA		
DVT874_S14_R1_001_(paired)_contig_12 mapping	5S rRNA		
DVT874_S14_R1_001_(paired)_contig_13 mapping	SMU_1449	Fibronectin/fibrinogen-binding protein:c.28C>T	Fibronectin/fibrinogen-binding protein:p.His10Tyr
DVT874_S14_R1_001_(paired)_contig_14 mapping	SMU_860, SMU_862		
DVT874_S14_R1_001_(paired)_contig_14 mapping	SMU_767, SMU_768c		
DVT874_S14_R1_001_(paired)_contig_14 mapping	SMU_767, SMU_768c		
DVT874_S14_R1_001_(paired)_contig_14 mapping	SMU_767, SMU_768c		
DVT874_S14_R1_001_(paired)_contig_20 mapping	tRNA-Met		
DVT874_S14_R1_001_(paired)_contig_22 mapping	tRNA-Tyr, tRNA-Phe		

Table 3.1 Genetic mutations from contaminated resistance development assay

3.2.2 Δ ftsA, Δ ftsX, Δ brpA, and Δ fold screen

Simultaneously, we approached validation of targets by utilizing the Quivey mutant library mentioned previously in Chapter 2. Essential genes, DexA and GbpB, do not have viable genetic knockouts and could not be included in these assays. Additionally, we had previously connected Analog 2's activity to the drop in environmental pH that occurs during biofilm growth and calculated its IC₅₀ to be 9 μ M in THB media at pH 5. For this reason, we decided to screen the

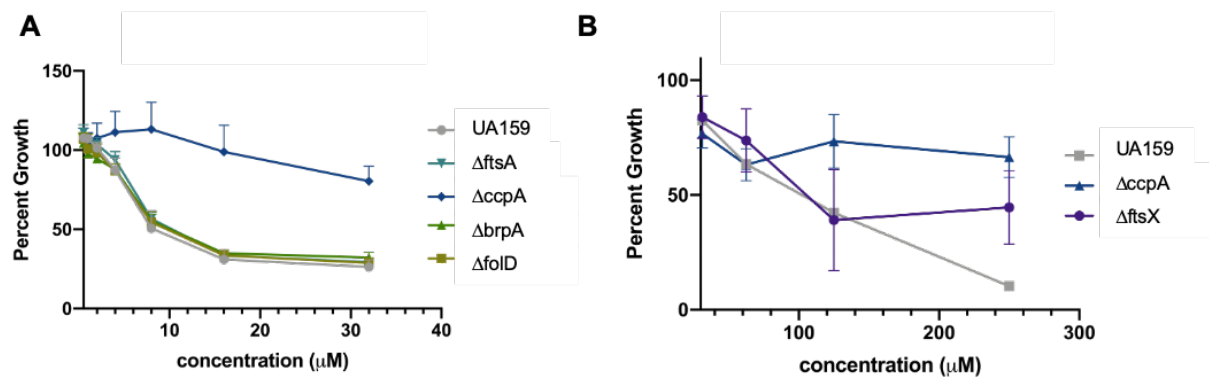
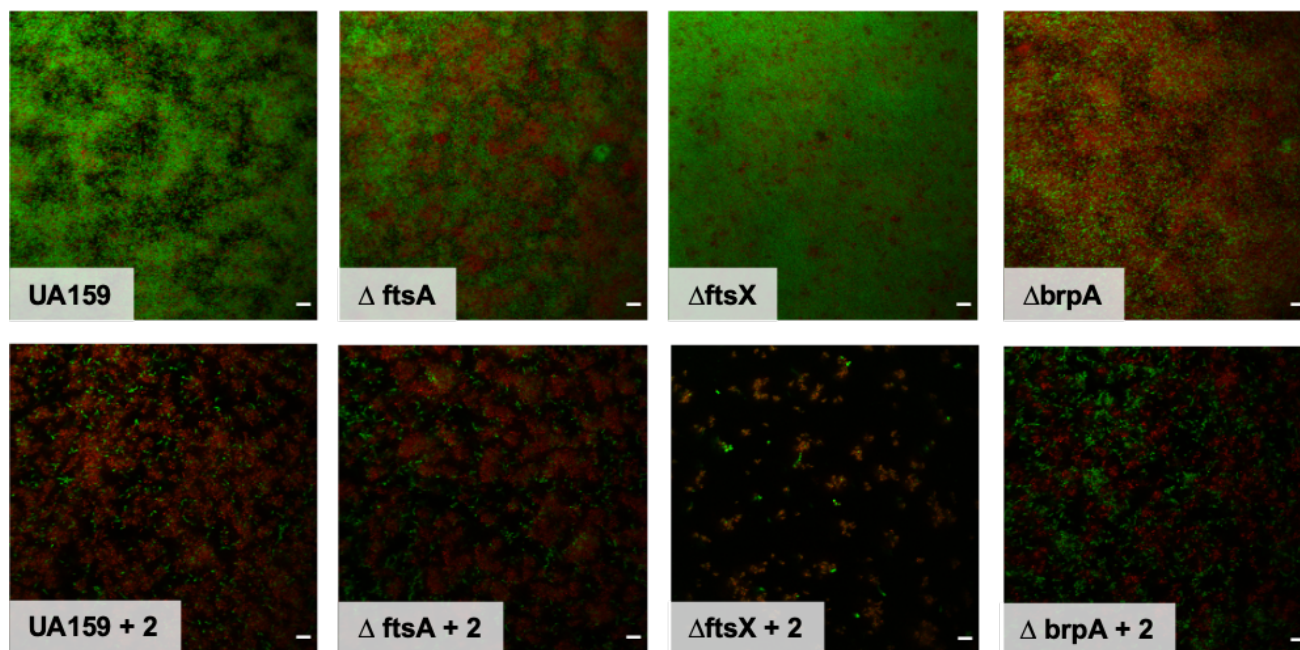


Figure 3.11 Inhibition mutant screen

mutants in this condition to conserve our stock of **analog 2** and to avoid the high error that we normally observed with measuring inhibition in the biofilm assay. We used ΔaccpA and UA159 as controls (Figure 3.11). We found that the mutants of FtsA, and BrpA, were susceptible to **analog 2** leading to the conclusion that they were false positives identified during the AfBPP experiment (Figure 3.11 A). FoliD was also susceptible, further confirming that it is not targeted by **analog 2**. ΔftsX is an acid sensitive strain, therefore it was screened in biofilm conditions (Figure 3.11 B). Interestingly, we found that ΔftsX was still susceptible to **analog 2**, but it was not inhibited to the

Figure 3.12 **Analog 2** biofilm mutant screen

same extent as UA159. This data shows that FtsX might be connected to the biological activity of **analog 2**.

To support the collected inhibition data, we used LIVE/DEAD[®] and confocal imaging to visualize the effect of **analog 2** on the mutants in comparison to UA159 (Figure 3.12). We used 63 μM to ensure a pronounced effect against the *S. mutans* biofilm. As expected, we observed a drastic change from green to red cells when grown in the presence of **analog 2** for UA159. The ΔftsA control demonstrated levels of red cells without compound added. This demonstrates the importance of FtsA for the growth of healthy biofilm. Once compound was added there was an increase of red cells, demonstrating that **analog 2** was still able to hit its biological target. The ΔftsX control showed a hazy green biofilm, but then when compound was added the biofilm only grew sparsely and the cells were non-viable. Finally, the ΔbrpA control showed mostly red cells in the biofilm. The biofilm was still affected when the strain was grown in the presence of **analog 2** demonstrating the uninterrupted effect of **analog 2**. The data presented proves that FtsA and BrpA are not targets of **analog 2**. FtsX does not appear to be the main target of **analog 2** but may have unknown implications in its biological activity.

3.2.3 Δfold

We sought to thoroughly examine whether **analog 2** was active against, and/or binding to FOLD since it has been shown to be a target of the natural product carolacton. The data in Figure 3.11 A shows that Δfold is still susceptible but we aimed to rule out any possibility of false negative results. Thus, we utilized a FOLD enzymatic assay and examined the viability of the biofilms with confocal imaging.

3.2.3.1 Enzymatic assay

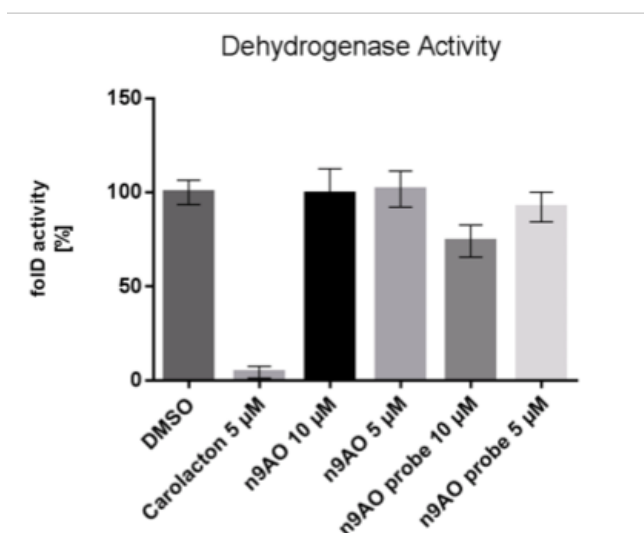


Figure 3.13 Folate dehydrogenase activity

Our collaborators in the Sieber Group ran an enzymatic assay to compare FOLD inhibition of carolacton, **analog 2**, and **analog 2-probe** (Figure 3.13). They confirmed that carolacton inhibited FOLD (Figure 3.13). They did not observe any change of dehydrogenase activity with **analog 2**, and only a slight response with **analog 2-probe**.

3.2.3.2 Biofilm assay

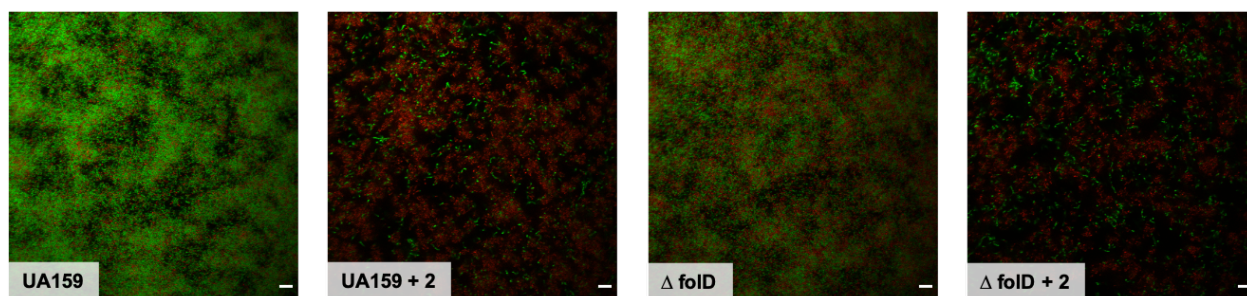
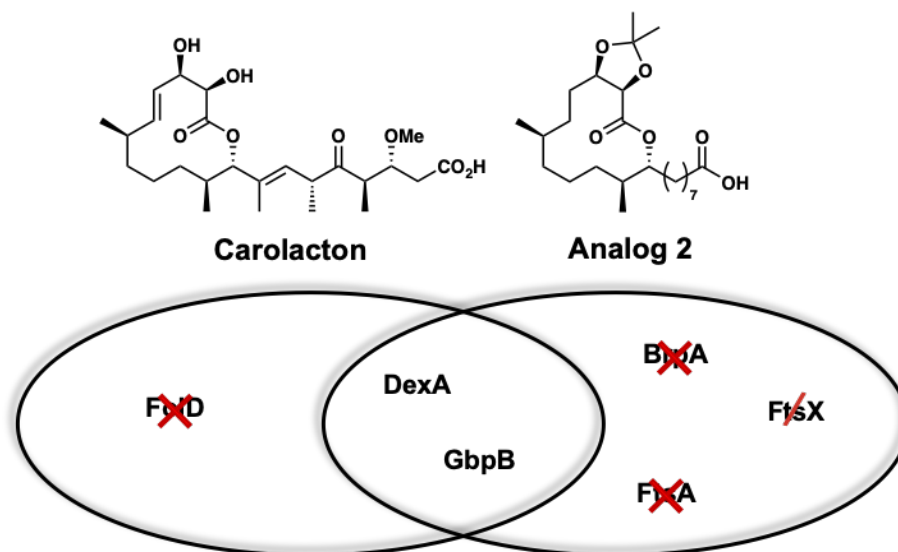


Figure 3.14 FOLD biofilm screen

Concurrently, we were able to show that Δ fold was susceptible to **analog 2** when visualized with LIVE/DEAD[®] and confocal imaging (Figure 3.12). The Δ fold control shows normal growth, albeit with a higher concentration of non-viable (red) cells. When dosed with 63 μ M the biofilm was visibly depleted and an increase of non-viable cells was noted.

3.2.4 GbpB: the main biofilm target?

Figure 3.15 Two potential targets for **analog 2**

With the data presented, we have been able to remove four potential targets for **analog 2**, three of which were identified with the AfBPP experiment (Figure 3.15). DexA and GbpB were unable to be tested due to the lack of a viable genetic mutant. A significant observation is that the two targets that remain, were the two targets that connected **analog 2** and carolacton during the proteomic competition assay. We hypothesize that one of these targets could be a common biofilm target that is shared between **analog 2** and carolacton. If this is true, it would give reason to why these compounds demonstrated biofilm specificity, an issue that has not been fully addressed in the literature as describe in the introduction to Chapter 2. For this reason, further elucidating the roles of DexA and GbpB in **analog 2**'s biological activity is of utmost importance for understanding carolacton's mode of action. Being synthetically more accessible and more amenable towards probe design will allow **analog 2** to continue to be an important natural product inspired tool compound.

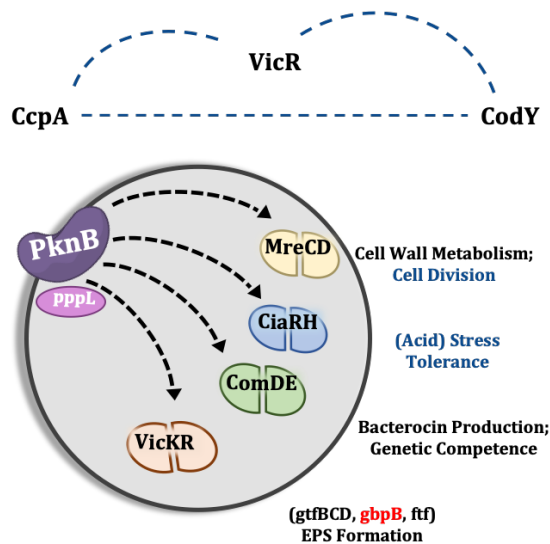


Figure 3.16 *S. mutans* regulation of GbpB

With all of the information available about both DexA and GbpB we believe that GbpB is the main biological target of **analog 2**. In 2013, data showed that important enzymes for peptidoglycan maintenance were upregulated after treatment of carolacton, GbpB being one of those enzymes.⁹² Further, it has been shown that CcpA, VicRK and CodY regulation cross talk is increased after treatment with carolacton (Figure 3.16).⁹¹ Remarkably, these regulators have also been connected to the regulation of peptidoglycan maintenance, including GbpB. PknB was initially found to be necessary for carolacton's activity and it is known to regulate VicRK which coordinates GbpB's activity (Figure 3.16).⁹⁰ In contrast, DexA has less known about its actual role. If **analog 2** were to target DexA, we could use that relationship to characterize DexA's role in *S. mutans*.

We found in the literature that there are cell division proteins in *Streptococcus pneumoniae* that share a high level of homology with proteins in *S. mutans*, including GbpB.¹⁰³ The peptidoglycan hydrolase PcsB, is homologous to GbpB in *S. mutans*, and has been shown to work in the cell division model shown in Figure 3.17. This model is informative for the future directions

of the carolacton project. For example, FtsA and FtsX, are found adjacent to the peptidoglycan hydrolase in this model. We believe that this cell division model exists in *S. mutans* and is the reason why FtsA and FtsX were identified in the AfBPP experiment. Intriguingly, our data showed that FtsX plays a role in **analog 2**'s activity and in this model directly interacts with the peptidoglycan hydrolase PcsB. This protein-protein interaction could be where **analog 2** binds. Reports have shown that carolacton is affecting the cell division of *S. mutans*^{80, 91, 92} which leads us to believe that targeting GbpB was conserved during the synthetic simplification process to access **analog 2**. Future work, which will be outlined in the next section, will highlight the broader impacts of the discoveries we have made in this chapter.

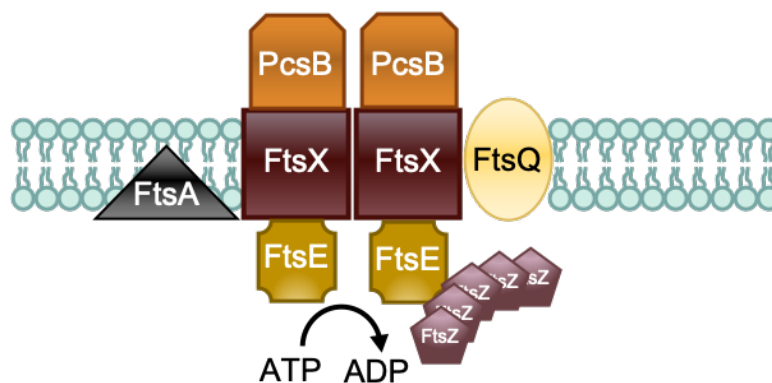


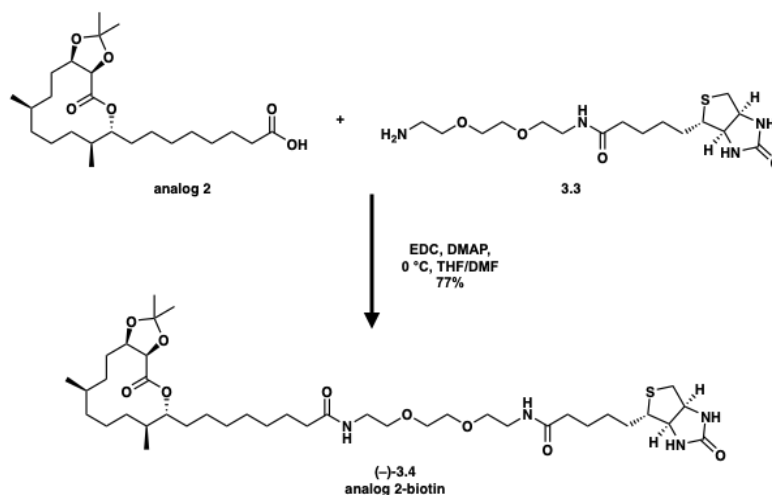
Figure 3.17 *S. pneumoniae* cell division model

3.3 Future directions

The work presented above has shown the utility of developing chemical tools from natural products for target identification. We are continuing our efforts to select for a resistant mutant by optimizing a serial dilution biofilm assay. Additionally, we are exploring a method to monitor levels of dextran in *S. mutans* biofilm. By using a fluorescent sugar that incorporates into the dextran, we can measure the levels of dextran in our biofilm samples either with the plate reader or with confocal imaging. The downside to this method is that it is not an exact measure of DexA

activity. Chapter 3 contains unpublished data that we will submit after confirming **analog 2** binds to GbpB. Fortunately, the Wu lab at The University of Alabama at Birmingham has offered to collaborate and help us obtain that data by measuring the binding affinity of **analog 2** and GbpB. In order to do so, we need to convert **analog 2** into a second probe that utilizes biotin as a handle. As shown in Scheme 3.2, we have synthesized this second probe by coupling the biotin-PEG (**3.3**) to **analog 2** using EDC coupling conditions. The resultant compound, **analog 2-biotin** (**3.4**), will be tested for retention of biological activity and then subjected to the binding assay in the laboratory of Dr. Wu.

Once this work has been completed, Amber Scharnow plans to compare carolacton, and the active carolacton analogs in a transcriptome screen to determine structure-activity relationships on a genetic level. This data will also contribute to the validation of the proteomic findings presented in Chapter 3. Due to the homology of the cell division model in *S. pneumoniae*, we will also investigate the activity of carolacton and **analog 2** on strains of *S. pneumoniae* and Group B



Scheme 3.2 Synthesis of **analog 2-biotin**

Streptococcus. With this work and identification of the target of **analog 2**, we also could look into using our tool compound to help characterize the GbpB cell division model in *S. mutans*.

3.4 Conclusions

Through both Chapter 2 and Chapter 3, I have presented the data collected on the carolacton-inspired analogs that have been developed in the Wuest Group. We have found that chemical manipulations can be tolerated on the carolacton scaffold and that biofilm-specificity can be retained through those modifications. Our work has led to the discovery of a more potent compound, **analog 2**, which has been successfully used as a chemical tool to better understand the biological activity of these biofilm targeting compounds. From **analog 2**, we have designed **analog 2-probe**. This compound was then used to identify protein targets and help discover the biofilm specific mechanism in which these compounds are acting. Future work will be completed to further elucidate the connection between these two molecules and fully understand how the chemical changes affected the binding interactions. The findings presented herein can be rationalized in one of three ways: 1) carolacton and **analog 2** have two distinct targets, 2) the target of carolacton in *S. mutans* biofilm is separate from FOLD or 3) carolacton has undiscovered polypharmacology.

The search for carolacton's target has been a decade long search. Both chemists and microbiologists have contributed to understanding the chemical importance of the natural product, and have created an almost complete picture of the biological activity of carolacton. As of 2017, FOLD was considered to be the biological target.⁹⁵ We deemed this work unsatisfactory due to the incomplete connection between FOLD to the breadth of work that had been previously demonstrated for carolacton (Figure 2.5). Carolacton was confirmed to bind to FOLD, but the information presented in Chapter 3 and 4 give evidence that multiple biological targets are a great possibility. Through synthetic modification, analog design, proteomic probe development, and biochemical analysis we have identified two plausible targets for the natural product: GbpB and DexA. Due to the work previously published on carolacton, we believe that GbpB is the main biofilm target of carolacton and is the reason why biofilm specificity is observed against *S. mutans*. In review, the

peptidoglycan hydrolase GbpB is associated to carolacton's biological affect via multiple connections. It is regulated by CcpA,⁹¹ PknB,⁹¹ and VicKRX,^{104, 105} peptidoglycan maintenance proteins are upregulated after treatment of carolacton treatment,⁹² and the proteomic hits FtsA and FtsX are both in proximity to GbpB in the *S. pneumoniae* cell division model.¹⁰³ There are still more details to uncover about the mechanism, but the contributions listed have proven that truly understanding the biological target of carolacton is not simple. These compounds have indirectly targeted the ATR of *S. mutans* by targeting GbpB and causing the cells to have decreased abilities of withstanding the acidification that occurs during biofilm growth. The data presented here will help researchers decide the next steps to take in understanding the structural motifs and the biological mechanisms of carolacton.

3.5 References

80. Kunze, B.; Reck, M.; Dotsch, A.; Lemme, A.; Schummer, D.; Irschik, H.; Steinmetz, H.; Wagner-Dobler, I., Damage of *Streptococcus mutans* biofilms by carolacton, a secondary metabolite from the myxobacterium *Sorangium cellulosum*. *BMC Microbiol* **2010**, *10*, 199.
90. Reck, M.; Rutz, K.; Kunze, B.; Tomasch, J.; Surapaneni, S. K.; Schulz, S.; Wagner-Dobler, I., The biofilm inhibitor carolacton disturbs membrane integrity and cell division of *Streptococcus mutans* through the serine/threonine protein kinase PknB. *J Bacteriol* **2011**, *193* (20), 5692-706.
91. Sudhakar, P.; Reck, M.; Wang, W.; He, F. Q.; Wagner-Döbler, I.; Zeng, A.-P., Construction and verification of the transcriptional regulatory response network of *Streptococcus mutans* upon treatment with the biofilm inhibitor carolacton. *BMC Genomics* **2014**, *15*, 362-362.
92. Li, J.; Wang, W.; Wang, Y.; Zeng, A.-P., Two-dimensional gel-based proteomic of the caries causative bacterium *Streptococcus mutans* UA159 and insight into the inhibitory effect of carolacton. *PROTEOMICS* **2013**, *13* (23-24), 3470-3477.
95. Fu, C.; Sikandar, A.; Donner, J.; Zaburannyi, N.; Herrmann, J.; Reck, M.; Wagner-Döbler, I.; Koehnke, J.; Müller, R., The natural product carolacton inhibits folate-dependent C1 metabolism by targeting FOLD/MTHFD. *Nature Communications* **2017**, *8* (1), 1529.
97. Medvedev, A.; Kopylov, A.; Buneeva, O.; Zgoda, V.; Archakov, A., Affinity-based proteomic profiling: Problems and achievements. *PROTEOMICS* **2012**, *12* (4-5), 621-637.
98. Li, Z.; Hao, P.; Li, L.; Tan, C. Y. J.; Cheng, X.; Chen, G. Y. J.; Sze, S. K.; Shen, H.-M.; Yao, S. Q., Design and Synthesis of Minimalist Terminal Alkyne-Containing Diazirine Photo-Crosslinkers and Their Incorporation into Kinase Inhibitors for Cell- and Tissue-Based Proteome Profiling. *Angewandte Chemie International Edition* **2013**, *52* (33), 8551-8556.
99. Keohane, C. E.; Steele, A. D.; Fetzer, C.; Khowsathit, J.; Van Tyne, D.; Moynié, L.; Gilmore, M. S.; Karanicolas, J.; Sieber, S. A.; Wuest, W. M., Promysalin Elicits Species-Selective Inhibition of *Pseudomonas aeruginosa* by Targeting Succinate Dehydrogenase. *Journal of the American Chemical Society* **2018**, *140* (5), 1774-1782.
100. Zhang, Y.; Kao, D.-S.; Gu, B.; Bomjan, R.; Srivastava, M.; Lu, H.; Zhou, D.; Tao, W. A., Tracking Pathogen Infections by Time-Resolved Chemical Proteomics. *Angewandte Chemie International Edition* **2020**, *59* (6), 2235-2240.
101. Chang, C.-F.; Mfuh, A.; Gao, J.; Wu, H.-Y.; Woo, C. M., Synthesis of an electronically-tuned minimally interfering alkynyl photo-affinity label to measure small molecule-protein interactions. *Tetrahedron* **2018**, *74* (26), 3273-3277.
102. Hofbauer, B.; Vomacka, J.; Stahl, M.; Korotkov, V. S.; Jennings, M. C.; Wuest, W. M.; Sieber, S. A., Dual Inhibitor of *Staphylococcus aureus* Virulence and Biofilm Attenuates Expression of Major Toxins and Adhesins. *Biochemistry* **2018**, *57* (11), 1814-1820.
103. Bajaj, R.; Bruce, K. E.; Davidson, A. L.; Rued, B. E.; Stauffacher, C. V.; Winkler, Malcolm E., Biochemical characterization of essential cell division proteins FtsX and FtsE that mediate peptidoglycan hydrolysis by PcsB in *Streptococcus pneumoniae*. *MicrobiologyOpen* **2016**, *5* (5), 738-752.
104. Senadheera, M. D.; Guggenheim, B.; Spatafora, G. A.; Huang, Y.-C. C.; Choi, J.; Hung, D. C. I.; Treglown, J. S.; Goodman, S. D.; Ellen, R. P.; Cvitkovitch, D. G., A VicRK Signal Transduction System in *Streptococcus mutans* Affects

gt;gtfBCD, gt;gbpB, and gt;ftf; Expression, Biofilm Formation, and Genetic Competence Development. *Journal of Bacteriology* **2005**, *187* (12), 4064.

105. Duque, C.; Stipp, R. N.; Wang, B.; Smith, D. J.; Höfling, J. F.; Kuramitsu, H. K.; Duncan, M. J.; Mattos-Graner, R. O., Downregulation of GbpB, a Component of the VicRK Regulon, Affects Biofilm Formation and Cell Surface Characteristics of gt;Streptococcus mutans. *Infection and Immunity* **2011**, *79* (2), 786.

Chapter 4 Honokiol

Section 4.2 has been adapted with permission from (Solinski, A. E.; Ochoa, C.; Lee, Y. E.; Paniak, T.; Kozlowski, M. C.; Wuest, W. M. Honokiol-Inspired Analogs as Inhibitors of Oral Bacteria. *ACS Infect. Dis.* **2018**, *4* (2), 118–122. <https://doi.org/10.1021/acsinfecdis.7b00178>). Copyright © 2020 American Chemical Society.

Section 4.3 has been adapted with permission from (Ochoa, C.; Solinski, A. E.; Nowlan, M.; Dekarske, M. M.; Wuest, W. M.; Kozlowski, M. C. A Bisphenolic Honokiol Analog Outcompetes Oral Antimicrobial Agent Cetylpyridinium Chloride via a Membrane-Associated Mechanism. *ACS Infect. Dis.* **2019**. <https://doi.org/10.1021/acsinfecdis.9b00190>). Copyright © 2020 American Chemical Society.

Chapter 4 was completed in collaboration with the Kozlowski Group at the University of Pennsylvania. Synthesis was finished in the Kozlowski lab and the biological activity was completed in the Wuest Group. Section 4.4 contains unpublished data and Madeline Dekarske (Wuest) will take the lead on completing this work for publication. The Kozlowski Group has additional structures that they are interested in investigating and Madeline will coordinate to perform those assays.

4.1 Background

4.1.1 Isolation

For centuries, people have turned to traditional Chinese and Japanese medicines for cures of various illnesses.¹⁰⁶ Using plants, roots, or even bark to make teas with healing powers sounds

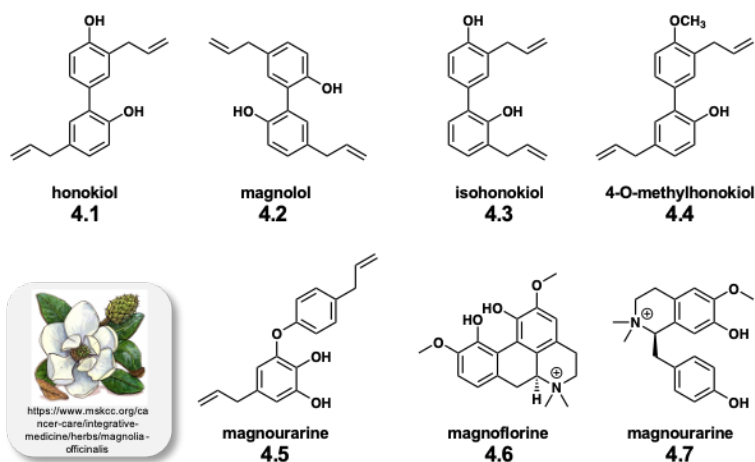


Figure 4.1 Natural products isolated from *Magnolia officinalis*

Year	Discovery
1972	Isolation from <i>Magnolia officinalis</i> and <i>Magnolia obovata</i>
2008	Honokiol: 16 µg/mL MIC against <i>S. mutans</i>
2016	Honokiol “improves breath freshness”
2016	Antibiofilm effects of honokiol 50% biofilm inhibition at 10 µg/mL

Table 4.1 Timeline of honokiol antibacterial activity against *S. mutans*

like witchcraft, but in its essence, it is simply a laboratory extraction experiment from Organic I. Today, researchers are trying to uncover the active entities, or small molecules from these mixtures. One such example is that of prolific *Magnolia* genus.¹⁰⁷ These species are productive producers of various active natural products. Shown in Figure 4.1 are bisphenolic and alkaloid natural products that have been isolated from the various parts (stem, bark, root, leaf, flower, etc.) that have been studied for their biological activities. Honokiol (**4.1**), a biologically active metabolite, was isolated in 1972 from the bark of *M. obovata* and was named after the Japanese term for the magnolia tree, “hōnki”.¹⁰⁸ Other similar metabolites, such as magnolol (**4.2**), isohonokiol (**4.3**), and 4-O-methylhonokiol (**4.4**), make the isolation of honokiol tedious due to their isomeric nature.¹⁰⁹ Other diverse compounds have also been isolated alongside honokiol, such as magnourarine (**4.5**), and alkaloids magnoflorine (**4.6**) and magnourarine (**4.7**).¹⁰⁶ Throughout the last half century, a large focus has been on honokiol due to its potent effects across areas of medicine, specifically its promise as an anti-cancer agent.¹¹⁰⁻¹¹³ More recently, it has been found to inhibit *Vibrio harveyi* virulence and also reduces virulence of the grape vine pathogen, *Botrytis cinerea*.^{114, 115}

4.1.2 Anti-bacterial activity

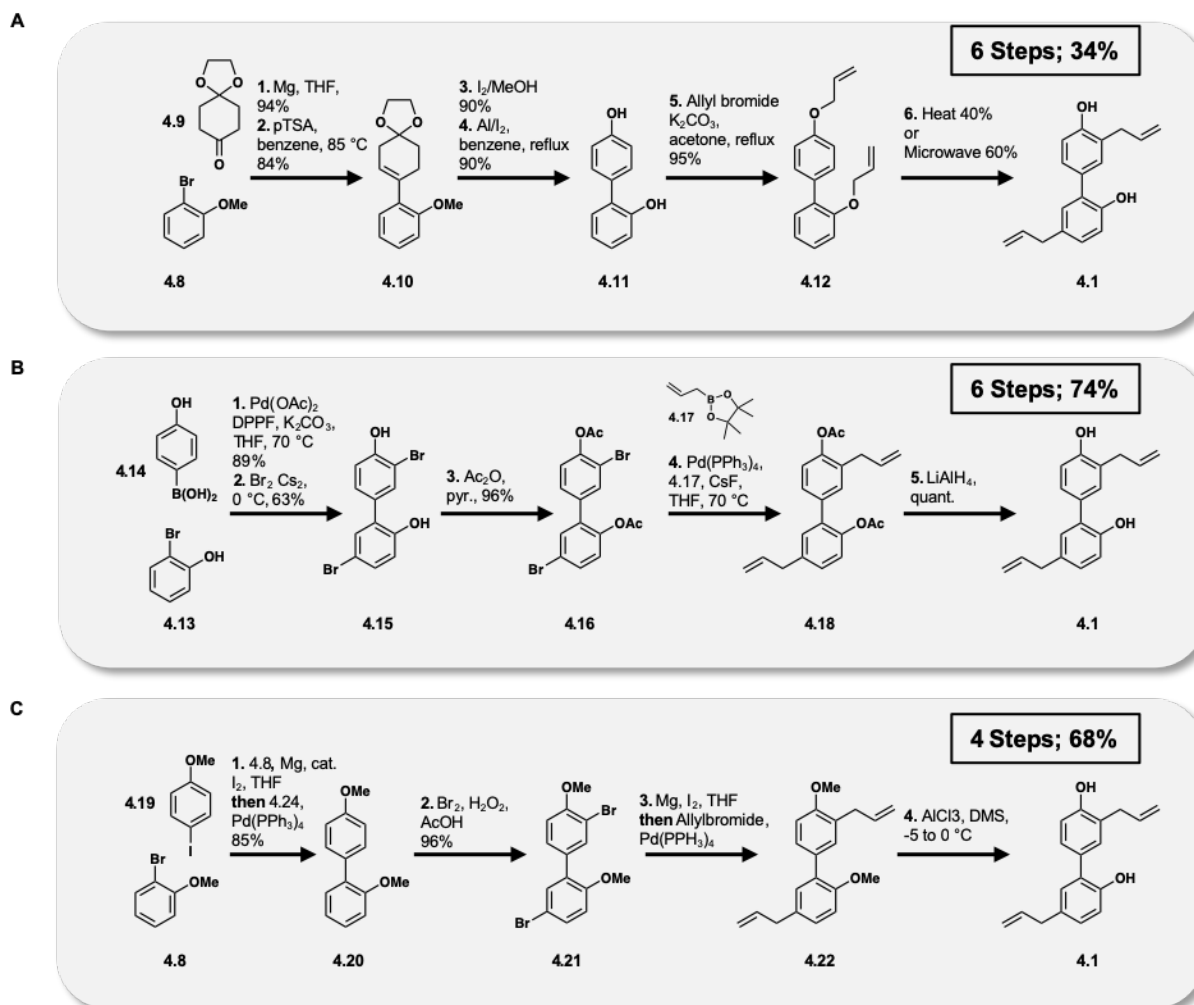
Honokiol (**4.1**) was isolated in 1972 but was not tested against oral bacteria until 2008, when it was found to be active against *S. mutans* with an MIC of 16 µg/mL (Table 4.1).¹¹⁶ Then in 2016 a report studied the effect of honokiol (**4.1**) on breath freshness, which correlates to the presence of oral bacteria.¹¹⁷ They found that compared to the control, there was a longer lasting

period of “breath freshness” after exposure to honokiol (**4.1**). Although this data point does not lend much detail to how this natural compound exhibits this activity, it does support that it is active against oral bacteria. In the same year, Sakaue et al. published that honokiol (**4.1**) and magnolol (**4.2**) demonstrated anti-biofilm and bactericidal effects against *S. mutans*.¹¹⁸ Interest in honokiol (**4.1**) has even spread from academia to pharmaceutical companies due to the desire to use natural products in their products. The next section will highlight our groups contribution to understanding honokiol’s activity but also our development of more potent *S. mutans* inhibitors with interesting modes of action profiles.

4.2 Generation 1

4.2.1 Synthesis of Generation 1

Originally, isolation of the natural product was being attempted to study the biological activity. After tediously purifying honokiol (**4.1**) from the various isomers that coexist, many researchers turned to synthesis to access the compound, hopefully in a more facile way. Shown in Scheme 4.1, are three examples taken from the handful of syntheses that have been published for honokiol to demonstrate some of the limitations of making this natural product for pharmaceutical purposes (**4.1**). Reddy et al. presented a synthesis in 2014 that utilized a Claisen rearrangement to access the natural product (Scheme 4.1 A). Starting from 1,4-cyclohexadione-monoethylene-acetal (**4.9**) and they performed a Grignard reaction with *ortho*-bromoanisole (**4.8**). Using *p*TSA dehydration of the tertiary alcohol was completed (**4.10**). The following two steps used stoichiometric amounts of iodine to remove the acetal and then used aluminum powder and iodine to demethylate and generate the bis-phenolic intermediate **4.11**. *O*-allylation was completed in the presence of allylbromide and potassium carbonate to reach the Claisen precursor **4.12**, which was subsequently subjected to heat or microwave to furnish honokiol (**4.1**).



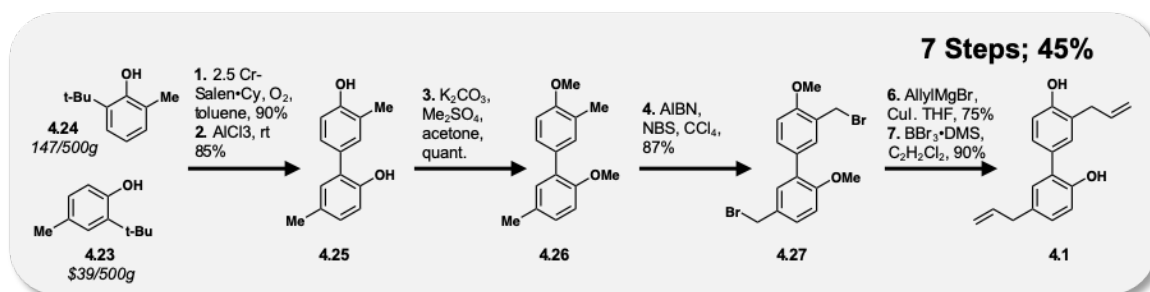
Scheme 4.1 Prior syntheses to honokiol

In contrast to Reddy, Harada et al. chose to utilize a sequence of Suzuki-Miyaura reactions to access the natural product (Scheme 4.1 B). Starting with 2-bromophenol (**4.13**) and 4-hydroxyphenylboronic acid (**4.14**), the first Suzuki-Miyaura coupling was completed with subsequent bromination to access **4.15**. Then, the hydroxy groups were acetylated (**4.16**) to prepare for the second Suzuki-Miyaura reaction that produced protected honokiol (**4.18**). To finish the synthesis LiAlH_4 was used to fully deprotect honokiol (**4.1**). In the same year, a similar procedure was published by Srinivas et al. that used a Kumada coupling strategy instead of Suzuki-Miyura conditions (Scheme 4.1 C). Starting from *ortho*-bromoanisole (**4.8**) coupling with *para*-

iodoanisole (**4.19**), the team was able to access the honokiol backbone **4.20**. From here a four step sequence of bromination (**4.21**), organomagnesium preparation, a second Kumada reaction (**4.22**), and demethylation, led to the synthesis of honokiol (**4.1**) in 68% yield.

The syntheses outlined above were successful at accessing honokiol (**4.1**) with high yields, but demonstrated limitations when considering the translation to pharmaceutical preparations. First, the starting materials are more expensive than the traditional pharmaceutical starting materials. Second, utilizing metal catalysts towards the end of the synthesis is undesirable due to contamination concerns. With isolation leading to undesirable isomers of honokiol, it would be useful to investigate processes that fit the pharmaceutical profile.

4.2.1.1 Kozlowski coupling technique and development of analog library



Scheme 4.2 Kozlowski synthesis of honokiol

In 2014, the Kozlowski group at the University of Pennsylvania published a vanadium-catalyzed phenol homocoupling methodology that would eventually be utilized in producing honokiol in a pharmaceutically relevant method. Their method produced a lower yield, but the inexpensive starting materials and the lack of metals in the final steps made the route desirable and was patented in 2017.¹⁰⁹ Using their chromium catalyst in step 1, they gain access to the full bisphenolic backbone (**4.25**). From there, they methylated the hydroxys (**4.26**), performed a benzylic bromination (**4.27**), which was used as a handle for addition of the allyl group, and achieved honokiol (**4.1**) after demethylation.

The Kozlowski group acquired a large library of honokiol analogs that were produced during their method optimization and substrate screen. The Wuest group began a collaboration with the Kozlowski group to determine if any of these molecules had improved activity compared to the natural product.

4.2.2 Micro-aerophilic vs aerophilic growth conditions

At the beginning of our investigation we were interested in comparing the inhibitory activity of honokiol (**4.1**) to that of our newly synthesized analogs. MIC assays, MBIC assays, and minimum bactericidal concentration (MBC) assays were undertaken. We initially performed the MIC assay in a 5% CO₂-supplemented environment to promote growth of *S. mutans* in an environment that mimics a normal oral cavity. The MIC of honokiol was determined to be 250 μM (66.6 μg/mL), which was in stark contrast to the literature value of 10 μg/mL (Table 4.1). After revisiting the original procedures, we recognized that the original assays were completed in an aerobic environment, which prohibits the growth of *S. mutans*. Aerobic conditions were employed in the assay, and the potency of honokiol increased to 125 μM (33.3 μg/mL). Additionally, we

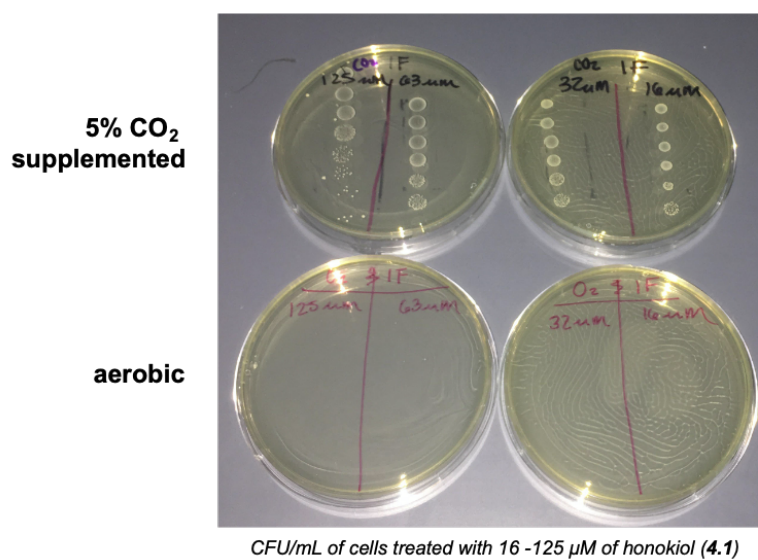


Figure 4.2 Growth differences for *S. mutans* in aerobic and CO₂ supplemented environments

tested the ability of *S. mutans* to regrow after treatment of honokiol (Figure 4.2). The top plates were grown with 5% CO₂ and saw full growth. The bottom plates were grown in aerobic conditions and the bacteria were unable to grow. These results demonstrate that although *S. mutans* growth is inhibited by honokiol, the overall efficacy of the compound will be less under physiological conditions. Our studies show that honokiol is unable to inhibit planktonic or biofilm growth, and was not bactericidal at concentrations as high as 250 μM.

4.2.3 Structure-activity relationships of Generation 1

Analogue	MIC <i>S. mutans</i>	MIC <i>S. sanguinis</i>	MIC <i>S. gordonii</i>	MBC <i>S. mutans</i>	
A	1	250	125	125	-
	2	32	32	32	63
	3	>250	>250	>250	-
	4	>250	>250	>250	-
	5	>250	>250	>250	-
	6	>250	>250	>250	-
	7	32	32	16	32
	8	>250	125	125	-
	9	>250	>250	>250	-
	10	>250	250	250	-
	11	>250	>250	>250	-
B	1	>250	>250	>250	-
	2	>250	>250	>250	-
	3	63	63	63	-
	4	125	125	125	-
	5	8	4	16	125
	6	>250	>250	>250	-
	7	125	63	125	-
	8	16	8	16	32
	9	32	32	32	32
	10	32	8	8	32
	11	16	8	16	63
	12	>250	250	250	-
	13	>250	>250	>250	-
	14	63	16	32	-
C	1	>250	125	125	-
	2	2	2.5	1.25	4

Table 4.2 Generation 1 biological activities

Undeterred by these findings, we sought to evaluate the bioactivity of our honokiol-inspired analogs against a panel of representative oral bacteria via MIC, MBIC, and MBC assays (Table 4.2). Our initial interest in the natural product honokiol was two-fold: 1) to probe the bioactivity profile of the compound and 2) as a means to showcase the newly developed synthetic method to access biaryl scaffolds. Out of the 26 honokiol analogs, emerged three structural trends. We have arranged these trends into three scaffolds (Figure 4.3; A-C). Scaffold A represents the

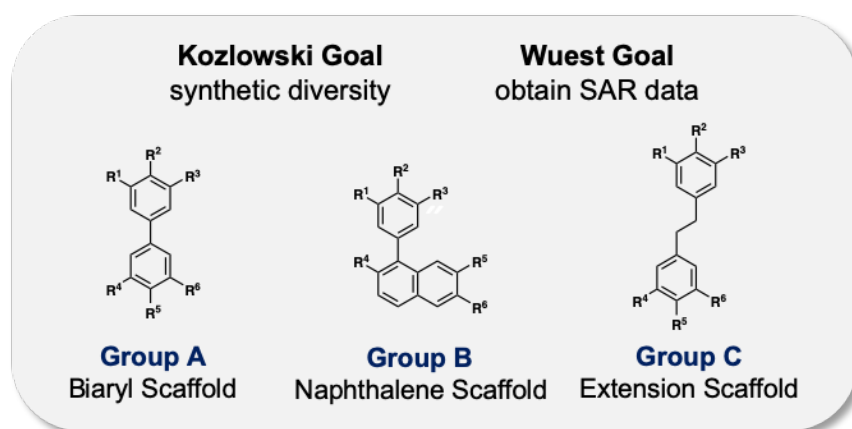


Figure 4.3 Generation 1 honokiol analog scaffolds

bisphenolic backbone that mimics honokiol. Modifications to Scaffold A would investigate the importance of the substitutions on the aryl groups. Scaffold B is a derivative in which one of the aryls is changed to a naphthalene to probe larger aryl substituents. Scaffold C extends the linker to two carbons for the aryl connection, which would help determine the optimal distance needed between the two phenol groups.

Out of the 26 honokiol analogs (see Section 5.6 for master analog list) four compounds showed significant inhibition at low concentrations ($\leq 16 \mu\text{M}$). Analogs **C2**, **B5**, **B8**, and **B11** were the most impressive with MIC values of $2 \mu\text{M}$, $8 \mu\text{M}$, $16 \mu\text{M}$, and $16 \mu\text{M}$, respectively, against planktonic *S. mutans* (Table 4.2). The analogs were also tested against two commensal strains that are early colonizers in the oral microbiome: *S. gordonii* and *S. sanguinis*. Generally, the MICs for

these commensal strains mirrored the values for the pathogenic *S. mutans* hinting at general Gram-positive activity.

Initial reports identified honokiol as a biofilm inhibitor.¹¹⁸ Honokiol and the analogs tested herein all potently deterred the formation of biofilms when the cells were grown in the presence of sucrose, albeit at the previously determined MIC values (Table 4.2). It is likely that biofilm inhibition is an effect of the inherent toxicity of the compounds to the planktonic bacteria and not by a biofilm-specific mechanism. This indicates that the compounds are targeting the bacteria in a general fashion and do not show any preferential killing to biofilms.

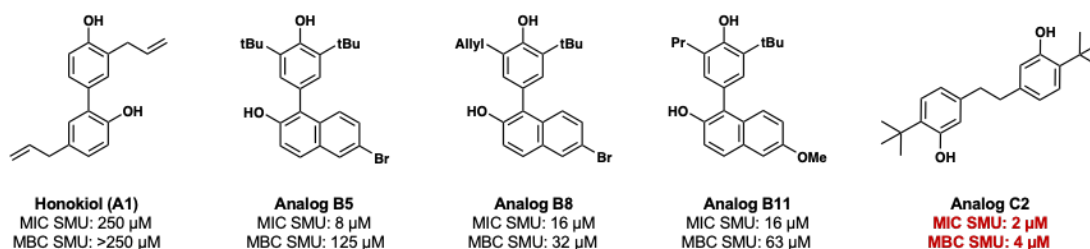


Figure 4.4 Most active compounds from Generation 1 and honokiol

To better understand the mode of action of these compounds, we sought to determine if the compounds were working in a bacteriostatic or bactericidal manner. Toward this end, a regrowth analysis was completed to determine the MBC values of the active analogs against *S. mutans*. The MBC values reported refer to the concentration at which there is a three-Log reduction in CFU/mL count corresponding to 99.9% bacterial cell death (Table 4.2; Figure 4.4). Analog **C2** had the lowest MBC value at 4 μ M confirming that the molecule is bactericidal. Analogs **B8** and **B11** were also shown to be bactericidal; however, the MIC and MBC of analog **B5** differs by four dilutions hinting at a bacteriostatic mechanism (Figure 4.4). These findings suggest that compounds **C2** and **B5** may be inhibiting the growth of *S. mutans* by different mechanisms. By extending the aryl connectivity with a two-carbon linker, the potency of the lead compound increased from 250 μ M to 2 μ M. There were only two analogs, **C1** and **C2**, that contained an extended scaffold. This new

scaffold greatly improved upon the natural product, but it was unclear what structural features were causing this potent activity and what biological mechanism led to the potent effect. Therefore, we sought to expand the SAR knowledge in regard to our new lead compound **C2** and investigate the mode of action with more detail. Results of this work are found in Section 4.3.

4.2.4 Lead compound **C2** and Generation 2 design

Synthesis of 44 analogs to probe the role of linker length, the phenolic interactions, ring substitution patterns, and steric interactions were completed (Figure 4.5). Synthesized structures were supplemented with commercially available bibenzyl compounds (**3AG-3AR**) (for structures, see Section 5.6). Together the 66 new analogs of **C2** were designed to assess the SAR of the lead compound.

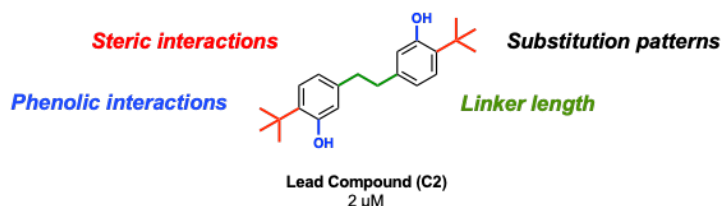


Figure 4.5 SAR goals for Generation 2

4.3 Generation 2

4.3.1 Structure-activity relationships of generation 2

We tested our second Generation analogs against *S. mutans* growth and determined the MIC values. From this data we were able to make conclusions on the structural importance of lead compound **C2**. Importantly, the corresponding monomer of **C2** (**4M**) did not exhibit bioactivity, illustrating the importance of the biaryl motif for the observed inhibition. Analogs **3A-3M** and **3O-3AD** (Section 5.6), which did not possess alkyl groups on the aromatic rings, were inactive proving the importance of the tert-butyl groups in compound **C2**. Additionally, we observed a

“Goldilocks” response in terms of the steric functionality (Figure 4.6). Derivatives that contained smaller substituents ortho to the phenol (**4B**, **4C**, **4D**) also led to a decrease in efficacy, establishing that one tert-butyl substituent on each aromatic ring is optimal (Figure 4.6). In previous work, the bis-hydroxyl functionality of **C2** was found to be a significant feature of the active structure. Here, we discover that potency can be maintained if one hydroxyl group is alkylated with a small group such as a methyl (**3AE**). If both hydroxyls are alkylated, as is the case with **4K**, there is a more drastic drop in activity, leading to the conclusion that the hydroxyl groups are creating important binding contacts, most likely through hydrogen bonds. Larger alkylating groups, as found in **4O**, also cause large decreases in potency, possibly due to a lack of hydrogen donors as well as changes in overall solubility. Also, altering the substituents on the aryl rings can alter the projection of the key functional groups, and these changes can result in drastic changes in inhibition. Analogs **4H** and **4G** show that slight modification in the substitution around the aryl ring allows potency to be retained. However, larger changes, such as in **4R**, cause slightly decreased inhibition due to hydroxyl proximity to the linker. We postulate that **4R** is not able to bind as well as **C2** to the

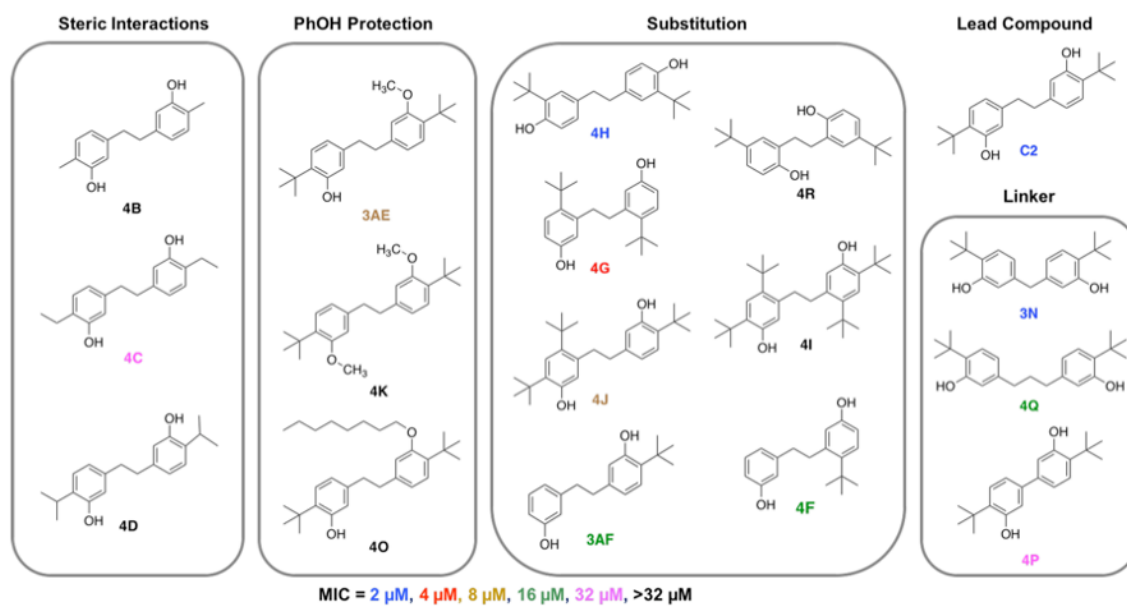


Figure 4.6 SAR results from Generation 1

target due to misalignment of the hydrogen bonding. Steric interactions were already proven to be important, with analogs **4B**, **4C**, and **4D**, but the amount of steric substitution was not yet probed. We found that the optimal number of tert-butyl groups was found to be two (**C2**, **4G**), as analogs with additional (**4J**, **4I**) or fewer (**3AF**, **4F**) tert-butyl substituents have decreased bioactivity. Finally, the testing of analogs with differing linker lengths (**4Q**, **4P**) showed that the ideal length is one (**3N**) or two carbons (**C2**), alluding to a specific binding interaction that will not tolerate a longer connection between the two aryl rings.

4.3.2 Hemolysis results

Compound	<i>S. mutans</i>	<i>S. gordonii</i>	<i>S. sanguinis</i>	<i>S. sobrinus</i>	<i>S. Mutans</i> MBC	Lysis ₂₀	Therapeutic Index (TI)
3N	2 μ M	2 μ M	2 μ M	4 μ M	2 μ M	63 μ M	32
4B	>250 μ M	250 μ M	250 μ M	>250 μ M	-	-	-
4G	4 μ M	1 μ M	1 μ M	2 μ M	4 μ M	32 μ M	8
4H	2 μ M	4 μ M	8 μ M	8 μ M	2 μ M	63 μ M	32
4I	>250 μ M	>250 μ M	63 μ M	250 μ M	-	-	-
4K	>250 μ M	>250 μ M	>250 μ M	>250 μ M	-	-	-
4P	32 μ M	32 μ M	32 μ M	32 μ M	-	-	-
4R	8 μ M	8 μ M	8 μ M	8 μ M	8 μ M	-	-
CPC	2 μ M	1 μ M	0.5 μ M	0.5 μ M	8 μ M	16 μ M	8
C2	2 μ M	1 μ M	1 μ M	1 μ M	4 μ M	63 μ M	32
Honokiol	250 μ M	-	-	-	-	>500 μ M	N/A

Table 4.3 Generation 2 biological activities and toxicities

With the SAR knowledge in hand, and believing that the lead **C2** was as optimized as it could be, we turned our attention to the mechanism of action of this bisphenolic, honokiol-inspired compound. We hypothesized that these antimicrobials were working via a membrane-specific mechanism due to similar SAR trends seen in our group's previous work.¹¹⁹ Furthermore, attempts at selecting for a resistant mutant of *S. mutans*, after treatment of **C2**, were unsuccessful. Todd

Hewitt Broth (THB) agar plates with a range of concentrations of **C2** (MIC 2X MIC, 4X MIC, and 8X MIC) were plated with *S. mutans* cells. Three colonies were isolated and tested, but resistance to the activity of **C2** was not observed. Failure to select for resistant colonies is a hallmark of membrane-targeting mechanisms. We then calculated MBC values to determine if **C2** was acting via bacteriostatic or bactericidal cell inhibition. CFU/mL counts were used to determine viability with the MBC referring to a 3-Log reduction in growth, corresponding to 99.9% bacterial death (Table 4.3). In accordance with our previous work, **C2** demonstrated bactericidal mechanisms, since the MBCs were within 4X of the MIC.

Due to the bactericidal effect, the toxicity of **C2** relative to cetylpyridinium chloride (**CPC**; Figure 4.7) was explored. **CPC** is a notable compound used in toothpastes, mouthwashes, throat sprays, and breath sprays, because **CPC** has been found to reduce the amount of plaque due to its high affinity for Gram-positive bacterial cell membranes, such as those of *S. mutans*. However, **CPC** has also been shown to have toxic effects at higher concentrations. For this reason, hemolysis values were determined using defibrinated sheep blood (Table 4.3). Interestingly, **CPC** exhibits significant hemolytic activity with a Lysis₂₀ of 16 μ M. Based on these results, **CPC** has a therapeutic index (TI) of 8, which is expressed as the ratio Lysis₂₀/MIC. Conversely, equally potent analog **C2** has a Lysis₂₀ of 63 μ M, yielding a higher TI of 32 again hinting at a mechanism of action that is disparate from that of **CPC**. This finding establishes the potential of compound **C2** for use in dental health agents based on its superior TI. We next sought to further characterize its mode of action, presumably on the cellular membrane of *S. mutans* cells.

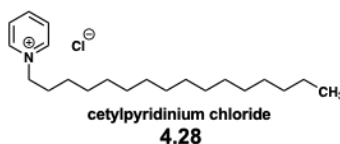


Figure 4.7 Oral antiseptic CPC

4.3.3 Mechanism of action – **C2**

4.3.3.1 TEM Images of C2 treated cells

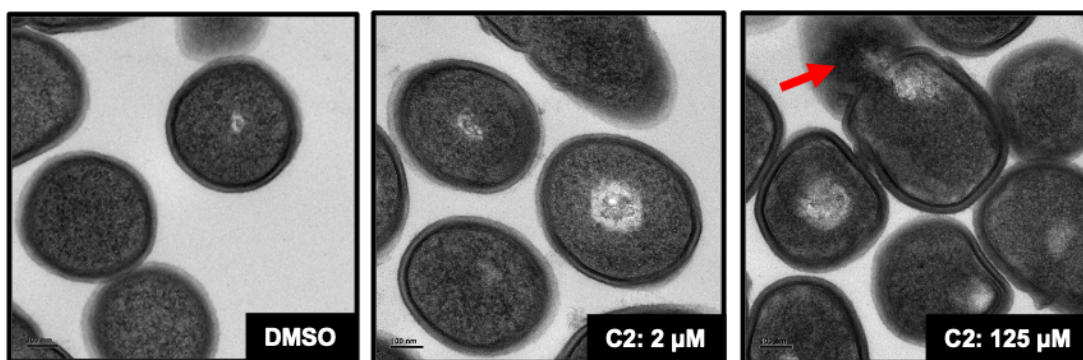
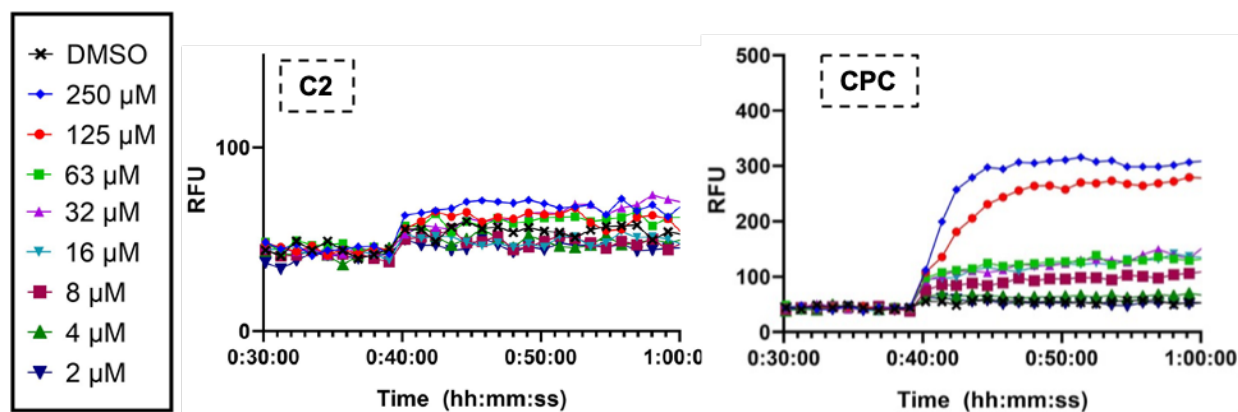


Figure 4.8 TEM images of C2 treated cells

To visualize if C2 was causing an effect on *S. mutans* cell membranes we prepared samples of compound treated cells that were then imaged at the Robert P. Apkarian Integrated Electron Microscopy Core at Emory University. In Figure 4.8, three transmission electron microscopy images taken of cells treated with DMSO (negative control), cells treated with 2 μM of C2, and cells treated with 125 μM of C2 are shown. The DMSO control shows the spherical shape of the *S. mutans* cell. When dosed with 2 μM , the MIC, the cells begin to lose shape, becoming slightly elongated. When higher concentrations are used, cells are fully lysed and the burst cells are visible (red arrow). We were curious as to why we did not see lysis at the MIC (2 μM) and decided to further investigate what C2 was doing to the cellular membrane. For that reason, the effect of our compound on bacterial membrane integrity was investigated.

4.3.3.2 Membrane assays

Figure 4.9 DiBAC₄(3) assay

We decided to use DiBAC₄(3) to measure depolarization effects of our lead compound **C2**. Depolarization occurs when there is a change in the electrical charge across the membrane such that less negative charge is inside the bacterial cell and although can be related to lytic mechanisms, is not the same as a lysis event. We used **CPC** as a positive control to show a depolarization response (Figure 4.10). DMSO was used a negative control (Shown in Figure 4.10; black line). We analyzed the affects between 2 and 250 μM of both compounds. **C2** did not have a significant depolarization response when compared to the DMSO vehicle control. **CPC**, known to act via a lytic mechanism, showed higher levels of membrane depolarization, causing a response as low as 8 μM (Figure 4.9).

We also investigated the lytic potential of both **C2** and **CPC** with Propidium Iodide (PI). We observed that both **C2** and **CPC** demonstrated a lytic response, denoted by an increase in PI fluorescence. Interestingly, **C2** did not show lytic responses below 32 μM , whereas **CPC** showed lytic responses as low as 8 μM (Figure 4.10). This difference alludes to differences in mechanism of these two structures.

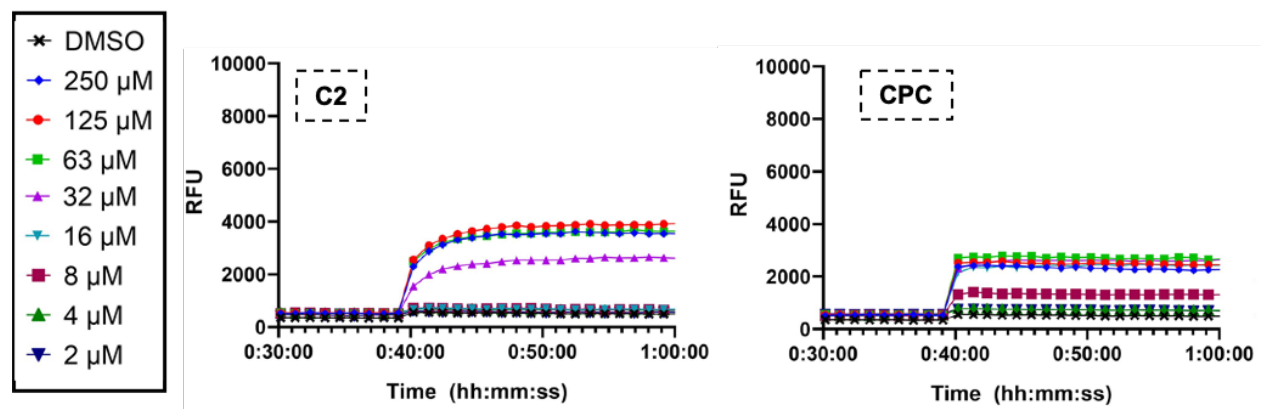


Figure 4.10 PI assay

To hopefully uncover the differences between **C2** and **CPC**, we utilized SYTOX Green Nucleic Acid Stain to measure membrane permeabilization. Membrane permeabilization is the process of making a membrane permeable, but does not denote full lysis. The bacterial membrane was permeabilized by **C2** from 32 μM to 250 μM (Figure 4.11). **C2** has a more striking effect, responding with a higher maximum fluorescence, when compared to **CPC**, although **CPC** once again is active as low as 8 μM (Figure 4.11). With these data points in consideration, it appears

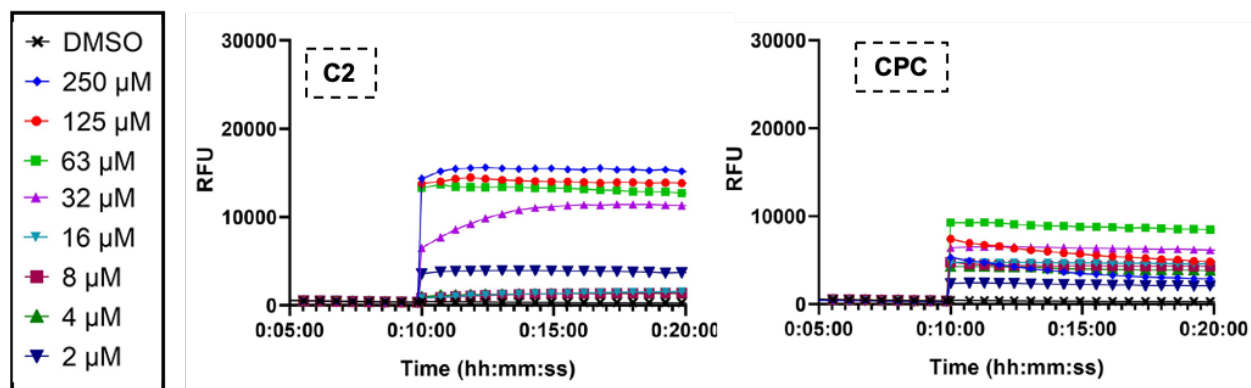


Figure 4.11 SYTOX assay

that **C2** affects the membrane stability and fluidity, which is evidenced in both the lytic (Figure 4.10) and permeabilization activity (Figure 4.11). The lack of depolarization events leads to the conclusion that **C2** does not interfere with the membrane potential. Thus, the inhibitory activity must stem from a more physical mode of action, akin to the mechanism demonstrated by bithionol and nTZDpa.^{119, 120} However, it seems that there is a window of biological activity from 2 μM to 8 μM where **C2**'s bactericidal activity has not yet been explained. Due to its connection to membrane mechanisms at higher concentrations, we hypothesize that **C2** is interfering with a cellular membrane process. Work is ongoing to uncover these details (Section 4.5). Other active analogs were tested and demonstrate similar membrane effects (Section 5.7). One analog, **C2-propyl** has demonstrated a whole new activity profile and will be discussed in the next section.

4.4 Mechanism of action – **C2-propyl**

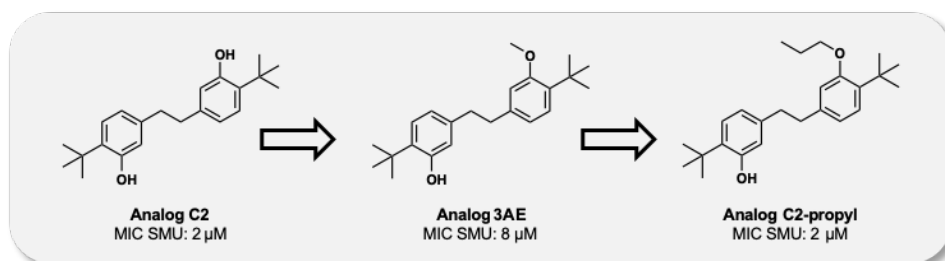


Figure 4.12 Discovery of **C2-propyl**

While determining the SAR trends for **C2**, we probed the necessity of the hydroxy groups on the active structure. We found masking the hydroxy group with a methyl, **3AE**, led to the decrease of activity from 2 μM to 8 μM . Larger groups, such as the 8-carbon alkyl group on **40**, removed all activity. Curiously, the additional of a propyl group, **C2-propyl**, did not abolish activity (Figure 4.12). We also observed stark differences between the mechanisms **C2** and the

C2-propyl analogs in the context of cellular membranes. Similar to the mechanism investigation of **C2** (Section 4.3), we first approached understanding **C2-propyl** by screening it against DiBAC₄(3) to measure cellular depolarization. We used **CPC** as a positive lytic control, PBS and DMSO as negative controls, analogs **C2**, **3N**, **4G**, and **4H** as reference to the aforementioned membrane mechanism (Section 4.3). Inactive compounds were also used as a negative control. Additionally, we introduced two new control compounds (Figure 4.13). First, we used quaternary ammonium compound 12(3)2(3)12, **QAC**, as a secondary positive control that demonstrates lytic affects.¹²¹ Second, we introduced chlorogenic acid **CGC** as a positive control for hyperpolarization. Hyperpolarization occurs when the natural polarization that exists across the cellular membrane increases, therefore the opposite of depolarization. Accordingly, the positive controls (**CPC**, **QAC**) showed increase fluorescence in the DiBAC₄(3) assay (Figure 4.14). **CGA**, along with negative controls PBS and DMSO did not show a fluorescent response. Similar to **C2**, **C2-propyl** did not demonstrate a depolarization response. We therefore continued to test its physical effects on the membrane.

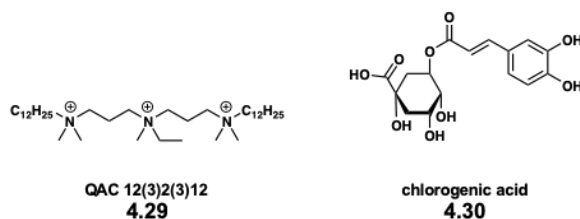


Figure 4.13 Control compounds for membrane assays

While testing effect on the PI assay we observed that **C2-propyl** did not cause cells to lyse at high concentrations similar to **C2** (Figure 4.15). The controls responded as expected. We previously had used SYTOX Green to determine if the membrane was being permeabilized and therefore investigated this mechanism for **C2-propyl** (Figure 4.16). Once again, we did not see a

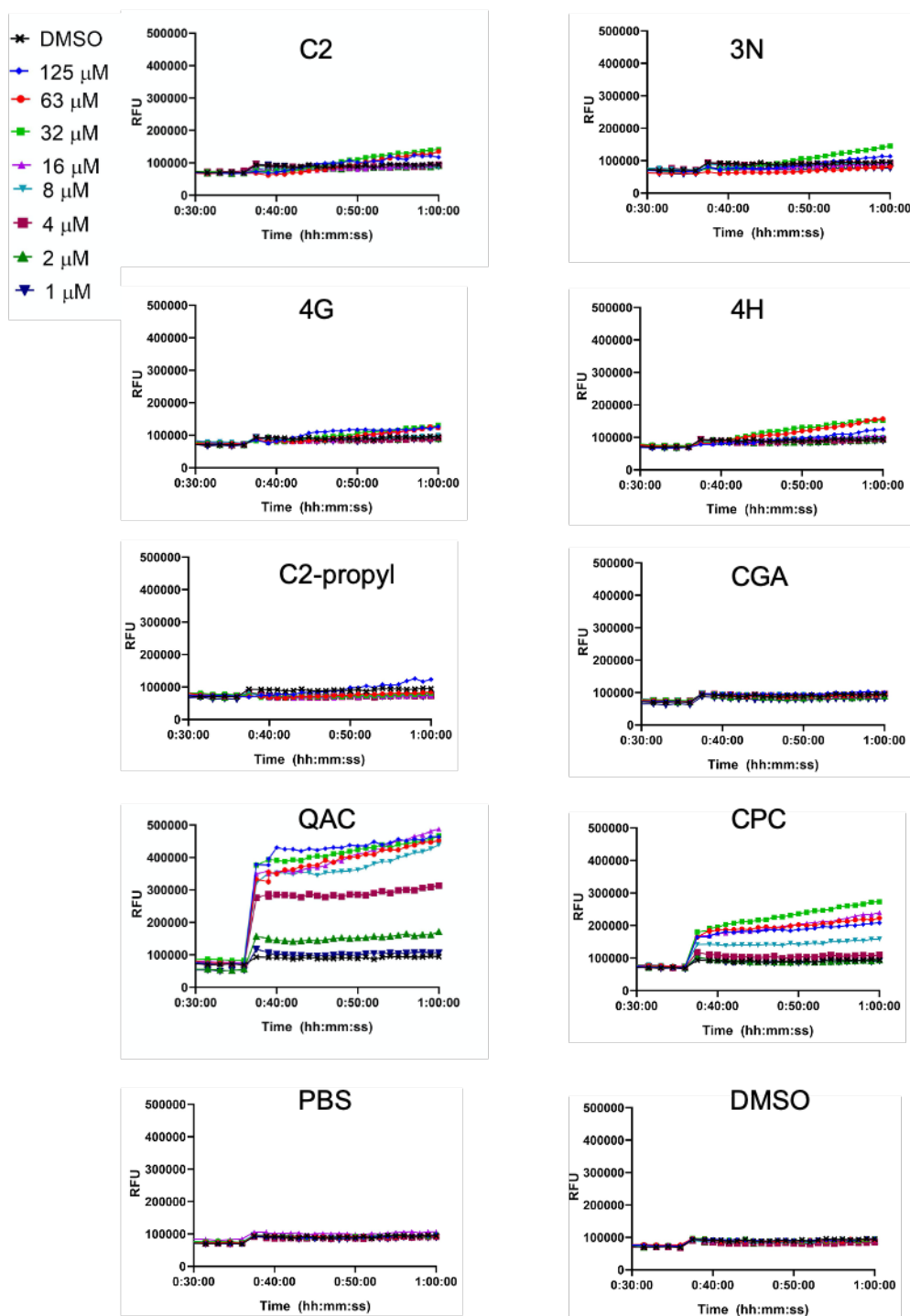


Figure 4.14 DiBAC4(3) full results

positive response for **C2-propyl** while the other controls responded accordingly. Combined these results were confounding. First, the structural difference seems to be very minor to cause such a

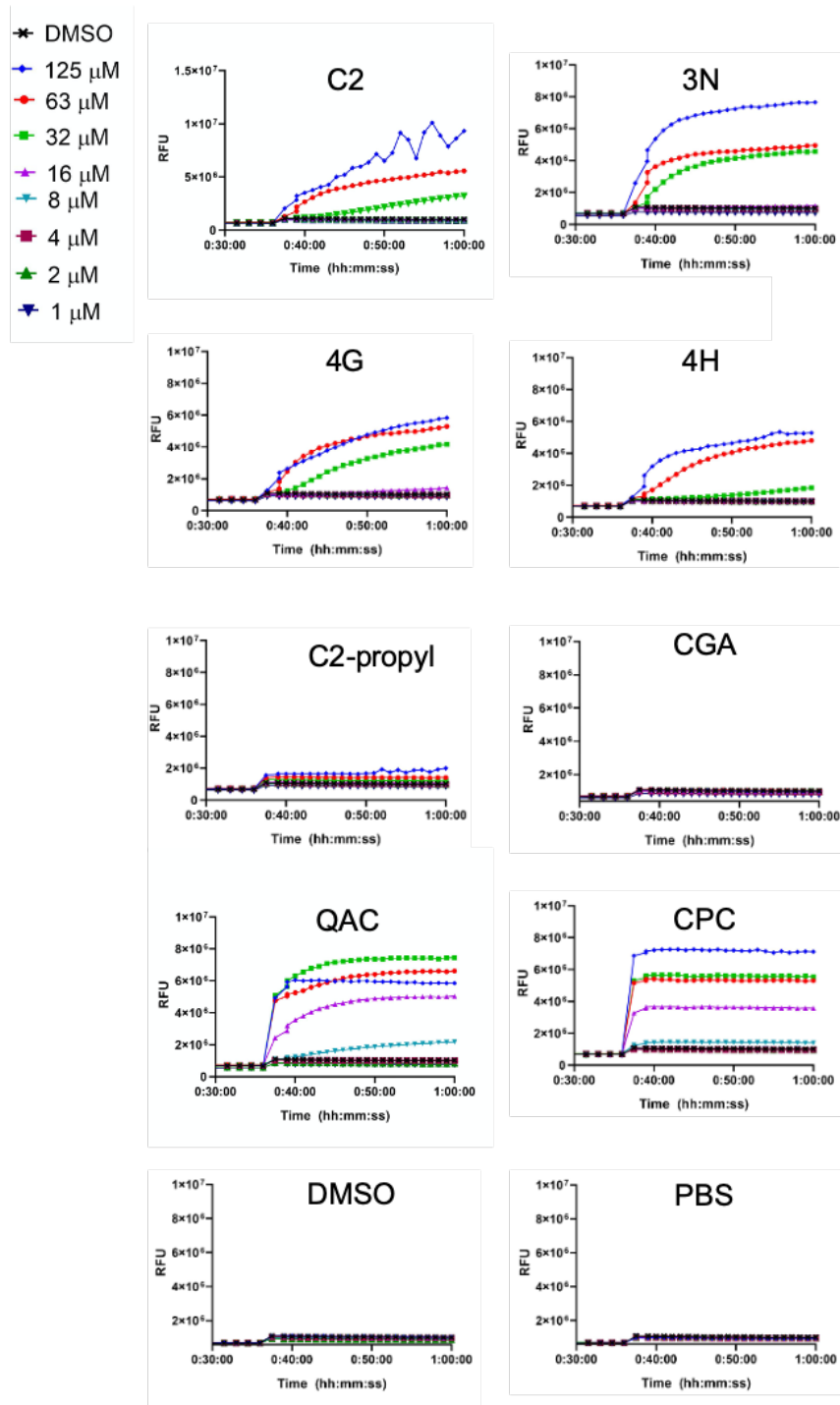


Figure 4.15 PI full results

drastic difference in biological response. Second, similar masked **C2** analogs did not maintain activity like **C2-propyl**. There were high structural similarities and we deemed it probable that the mechanism of **C2-propyl** was still membrane related, but the propyl mask led to a unique

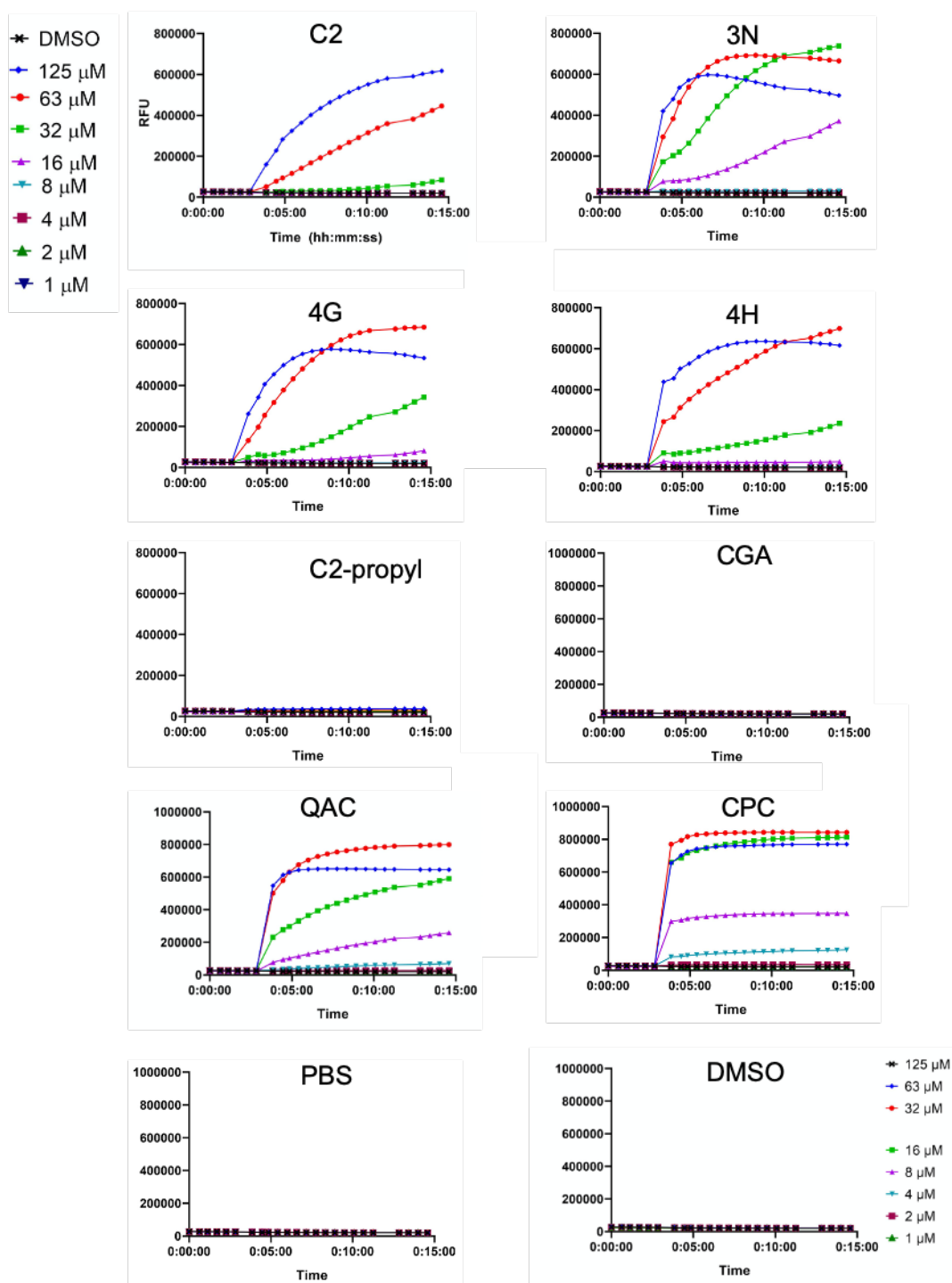


Figure 4.16 SYTOX full results

interaction that decreased the lytic/permeabilization effects at high concentrations. Discovering this interaction and unearthing its mechanism would be impactful for the antibiotic field since it could help researchers decrease toxicity for membrane-targeting antibiotics.

We attempted to select for a **C2-propyl** resistant mutant of *S. mutans* to aide in target identification of a protein target but were unsuccessful similar to attempts made for **C2** in Section 4.3. We therefore turned to investigating other aspects of cellular membranes. Membrane proteins

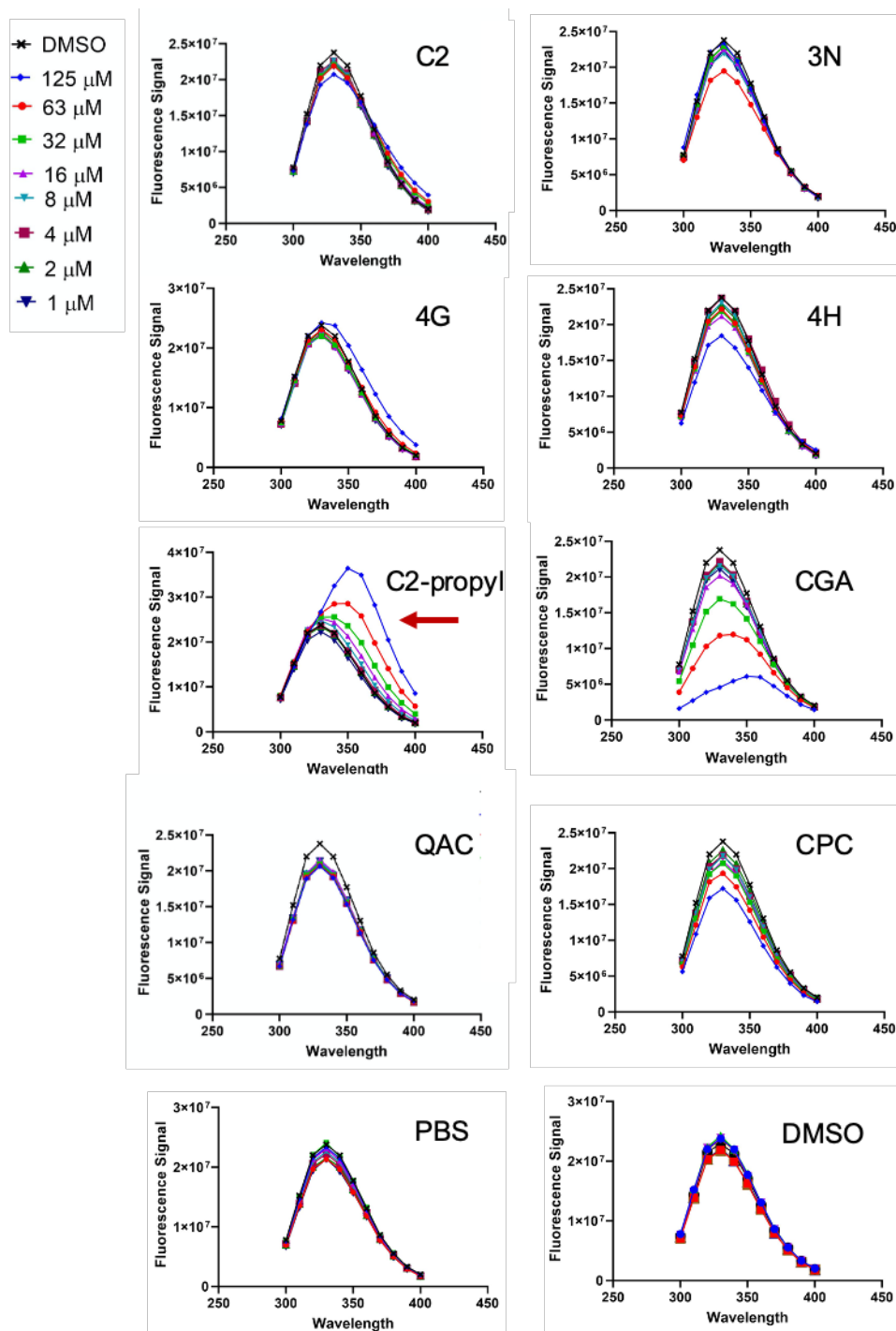


Figure 4.17 Membrane protein assay

are important for a whole host of processes for bacteria. By examining the confirmation and composition of bacterial membrane proteins, we can gain more evidence to prove that **C2-propyl** is still interacting with the bacterial membrane, even when DiBAC₄(3), PI, and SYTOX Green assays showed no affect for **C2-propyl**. Therefore, we measured the emission spectra of compound treated cells to observe the compound-induced changes in fluorescence. The fluorescence signal is caused by the aromatic amino acids that are present in the proteins in the cell membrane and/or external proteins. Shifts in fluorescence maxima would signal that the composition of the cellular membrane is being disturbed. Decreases in fluorescence intensity would signal that these signals are masked. We found that **C2**, **3N**, **4G**, **4H**, **QAC** and **CPC** did not change the composition or intensity of the membrane protein intensity. In contrast, **C2-propyl** caused an increase and shift fluorescence maxima, signifying that it disturbs the membrane. **CGA**, the hyperpolarization control, showed decreases in intensity, ruling out hyperpolarization as a mechanism of action. We are excited to move forward with investigating the mechanism of **C2-propyl** with this new data in hand. The next section will outline our main hypothesis and also identify which experiments will be used for further investigation.

4.5 Future Directions

Upon completion of membrane protein assay, we have organized a list of experiments that we will perform to gather more information about the effect of **C2-propyl** on the cellular membrane. First, we are curious as to the changes that occur to ion channels, such as Ca²⁺, Mg²⁺ and K⁺. The regulation of these channels is important for cellular homeostasis and could be the reason we see such potent antimicrobial effects. Concurrently, we are also designing analogs that we propose will have activity against Gram-negative bacteria, by incorporating amine functionality into the bisphenol structure. Taking inspiration from Hergenrother's group, we hope

to transform our potent Gram-positive activity to a broad spectrum antimicrobial that be beneficial for other diseases outside of the oral cavity.

4.5.1 Sortase A Hypothesis

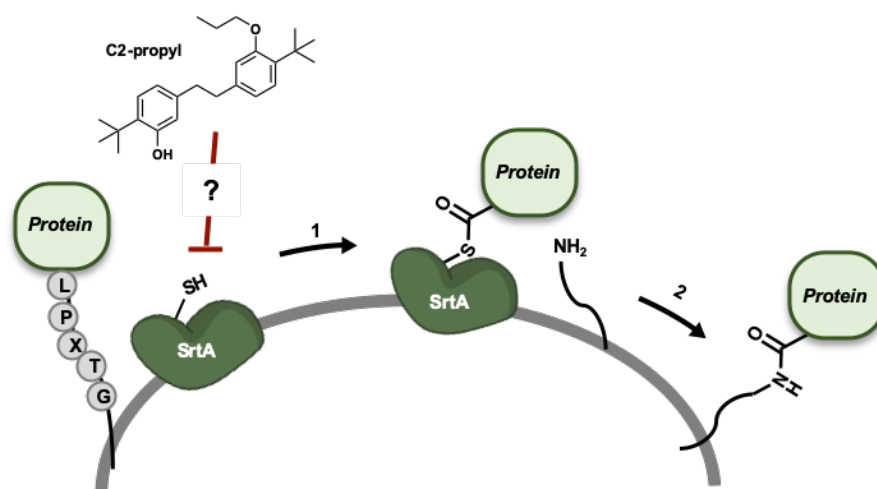


Figure 4.18 Illustration of Sortase A hypothesis

We hypothesize that **C2-propyl** is interfering with Sortase A (SrtA) protein attachment (Figure 4.18). As discussed in Section 1.3.3., SrtA is responsible for the covalent attachment of antigens to the outside of the cell. These antigens are responsible for a host of processes, including signaling and bacterial attachment. There are compounds that have been found to target SrtA (Section 1.3.3) and is likely that this chemical scaffold is in this group. We see a shift in protein composition and this might be because of changes in SrtA activity (Figure 4.17). Future work will examine the effect of **C2-propyl** on SrtA mechanisms both in vitro and in vivo (bacterial cell).

4.6 Conclusions

The work presented herein highlights the importance of 1) performing biological testing at physiologically relevant conditions, 2) investigating antimicrobial mechanisms and 3) using chemical synthesis to create diversity that does not exist in nature. Our results have demonstrated

that the bioactivity of honokiol may be overstated. However, our curiosity surrounding the natural product led to the serendipitous discovery of a highly potent, bactericidal analog, **C2**, with an MIC value of 2 μM (66 ng/mL). From this project we have also gained insight to the current toxicity profiles of an oral antimicrobial agent (**CPC**). Furthermore, we have identified new scaffolds that are promising leads towards new mechanisms against *S. mutans*. In Section 4.3, **C2** was identified as the lead molecule, but **B5** also demonstrated bacteriostatic properties which means it most likely is acting with a different mechanism, warranting further study. In Section 4.4, **C2** was shown to be active against the cellular membrane but surprisingly the **C2-propyl** analog did not follow the same trend. These compounds serve as exciting starting points for future translational studies which may be of particular interest to the oral care industry based on its simple structural architecture and potent bioactivity.

This dissertation has highlighted two stories that were initiated because of interest in a natural product. From carolacton and honokiol, we have developed a handful of compounds that are being investigated further to uncover novel mechanisms of action. These compounds have potential to be developed into next generation antibiotics or chemical tools which will elucidate biological targets for *S. mutans*, the chronic oral pathogen. *S. mutans*' pathogenicity is still a prevalent topic. Researchers have recently discovered that *S. mutans* produces its own antibiotics that target commensal species, which leads to further tooth decay.¹²² As we learn more about this disease causing bacteria and the compounds that can eliminate its pathogenicity, such as carolacton and honokiol, we will see progress on this antimicrobial front.

4.7 References

106. Poivre, M.; Duez, P., Biological activity and toxicity of the Chinese herb *Magnolia officinalis* Rehder & E. Wilson (Houpo) and its constituents. *Journal of Zhejiang University Science. B* **2017**, *18* (3), 194-214.
107. Choi, N. H.; Choi, G. J.; Min, B. S.; Jang, K. S.; Choi, Y. H.; Kang, M. S.; Park, M. S.; Choi, J. E.; Bae, B. K.; Kim, J. C., Effects of neolignans from the stem bark of *Magnolia obovata* on plant pathogenic fungi. *Journal of Applied Microbiology* **2009**, *106* (6), 2057-2063.
108. Fujita, M.; Itokawa, H.; Sashida, Y., Honokiol, a New Phenolic Compound isolated from the Bark of *Magnolia obovata*. *Chemical and Pharmaceutical Bulletin* **1972**, 212-213.
109. Jaracz, S.; Kozłowski, M. C.; Lee, Y. E.; Kim, S. M., Improved Synthesis of Honokiol. **2017**.
110. Nagalingam, A.; Arbiser, J. L.; Bonner, M. Y.; Saxena, N. K.; Sharma, D., Honokiol activates AMP-activated protein kinase in breast cancer cells via an LKB1-dependent pathway and inhibits breast carcinogenesis. *Breast Cancer Res* **2012**, *14* (1), R35.
111. Chen, P. J.; Wang, Y. L.; Kuo, L. M.; Lin, C. F.; Chen, C. Y.; Tsai, Y. F.; Shen, J. J.; Hwang, T. L., Honokiol suppresses TNF-alpha-induced neutrophil adhesion on cerebral endothelial cells by disrupting polyubiquitination and degradation of IkappaBalpha. *Sci Rep* **2016**, *6*, 26554.
112. Pan, J.; Lee, Y.; Zhang, Q.; Xiong, D.; Wan, T. C.; Wang, Y.; You, M., Honokiol Decreases Lung Cancer Metastasis through Inhibition of the STAT3 Signaling Pathway. *Cancer Prev Res (Phila)* **2017**, *10* (2), 133-141.
113. Yuan, Y.; Subedi, L.; Lim, D.; Jung, J. K.; Kim, S. Y.; Seo, S. Y., Synthesis and anti-neuroinflammatory activity of N-heterocyclic analogs based on natural biphenyl-neolignan honokiol. *Bioorg Med Chem Lett* **2019**, *29* (2), 329-333.
114. Guo, L.; McLean, J. S.; Yang, Y.; Eckert, R.; Kaplan, C. W.; Kyme, P.; Sheikh, O.; Varnum, B.; Lux, R.; Shi, W.; He, X., Precision-guided antimicrobial peptide as a targeted modulator of human microbial ecology. *Proc Natl Acad Sci U S A* **2015**, *112* (24), 7569-74.
115. Ma, D.; Cui, X.; Zhang, Z.; Li, B.; Xu, Y.; Tian, S.; Chen, T., Honokiol suppresses mycelial growth and reduces virulence of *Botrytis cinerea* by inducing autophagic activities and apoptosis. *Food Microbiology* **2019**, 103411.
116. Greenberg, M.; Dodds, M.; Tian, M., Naturally Occurring Phenolic Antibacterial Compounds Show Effectiveness against Oral Bacteria by a Quantitative Structure–Activity Relationship Study. *Journal of Agricultural and Food Chemistry* **2008**, *56* (23), 11151-11156.
117. Wessel, S. W.; van der Mei, H. C.; Slomp, A. M.; van de Belt-Gritter, B.; Maitra, A.; Dodds, M. W. J.; Busscher, H. J., *Magnolia* bark extract increases oral bacterial cell surface hydrophobicity and improves self-perceived breath freshness when added to chewing gum. *Journal of Functional Foods* **2016**, *25*, 367-374.
118. Sakaue, Y.; Domon, H.; Oda, M.; Takenaka, S.; Kubo, M.; Fukuyama, Y.; Okiji, T.; Terao, Y., Anti-biofilm and bactericidal effects of magnolia bark-derived magnolol and honokiol on *Streptococcus mutans*. *Microbiol Immunol* **2016**, *60* (1), 10-6.
119. Kim, W.; Zou, G.; Hari, T. P. A.; Wilt, I. K.; Zhu, W.; Galle, N.; Faizi, H. A.; Hendricks, G. L.; Tori, K.; Pan, W.; Huang, X.; Steele, A. D.; Csatory, E. E.; Dekarske, M. M.; Rosen, J. L.; Ribeiro, N. d. Q.; Lee, K.; Port, J.; Fuchs, B. B.; Vlahovska, P. M.; Wuest, W. M.; Gao, H.; Ausubel, F. M.; Mylonakis, E., A selective membrane-targeting repurposed

antibiotic with activity against persistent methicillin-resistant Staphylococcus aureus. *Proceedings of the National Academy of Sciences* **2019**, *116* (33), 16529.

120. Kim, W.; Steele, A. D.; Zhu, W.; Csatory, E. E.; Fricke, N.; Dekarske, M. M.; Jayamani, E.; Pan, W.; Kwon, B.; Sinitsa, I. F.; Rosen, J. L.; Conery, A. L.; Fuchs, B. B.; Vlahovska, P. M.; Ausubel, F. M.; Gao, H.; Wuest, W. M.; Mylonakis, E., Discovery and Optimization of nTZDpa as an Antibiotic Effective Against Bacterial Persisters. *ACS Infectious Diseases* **2018**, *4* (11), 1540-1545.

121. Jennings, M. C.; Buttaro, B. A.; Minbiole, K. P. C.; Wuest, W. M., Bioorganic Investigation of Multicationic Antimicrobials to Combat QAC-Resistant *Staphylococcus aureus*. *ACS Infectious Diseases* **2015**, *1* (7), 304-309.

122. Tang, X.; Kudo, Y.; Baker, J. L.; LaBonte, S.; Jordan, P. A.; McKinnie, S. M. K.; Guo, J.; Huan, T.; Moore, B. S.; Edlund, A., Cariogenic *Streptococcus mutans* Produces Tetramic Acid Strain-Specific Antibiotics That Impair Commensal Colonization. *ACS Infectious Diseases* **2020**.

Chapter 5 Experimental Details

5.1 Supplemental Figures

Trial 1	500.00	250.00	125.00	63.00	32.00	16.00	8.00	4.00	2.00	1.00	0.50	0.25
(-)-2.48	11.21	11.25	10.63	8.80	7.11	6.12	5.76	5.75	6.11	5.91	5.76	5.80
(+)-2.49	11.61	9.87	9.90	9.19	6.83	6.33	5.91	5.71	5.64	6.73	7.26	6.36
analog 2	1.03	1.77	11.96	12.07	10.56	7.43	6.29	5.99	6.52	6.43	6.12	5.79
carolacton	11.05	12.25	7.67	7.57	7.54	6.73	6.58	6.83	6.61	6.87	6.96	7.90
DMSO	7.63	7.13	6.91	7.04	7.16	7.39	6.94	7.45	7.04	7.28	6.89	6.70
Trial 2	500.00	250.00	125.00	63.00	32.00	16.00	8.00	4.00	2.00	1.00	0.50	0.25
(-)-2.48	3.90	8.55	7.55	5.84	5.84	4.69	4.65	6.08	4.31	4.90	5.33	3.51
(+)-2.49	11.19	7.49	5.93	6.81	5.53	4.76	5.23	4.67	5.03	4.75	4.56	5.42
analog 2	2.94	2.32	10.45	8.79	6.35	7.26	6.11	4.66	5.41	6.49	4.66	5.05
carolacton	10.00	7.37	8.28	6.27	6.40	5.65	5.89	6.09	6.45	5.63	5.48	5.68
DMSO	7.25	5.64	7.28	5.92	6.72	6.75	8.14	6.53	6.26	6.14	5.76	5.18
Trial 3	500.00	250.00	125.00	63.00	32.00	16.00	8.00	4.00	2.00	1.00	0.50	0.25
(-)-2.48	4.63	7.02	7.50	7.44	6.98	5.00	4.97	5.52	4.82	6.86	6.17	6.70
(+)-2.49	10.42	12.18	7.39	5.94	6.30	5.38	5.23	5.27	5.32	5.41	6.84	5.14
analog 2	1.78	1.16	7.89	8.74	6.54	5.98	6.75	5.46	5.58	5.77	5.04	5.70
carolacton	10.35	8.35	6.29	5.12	6.31	6.64	6.99	6.53	6.28	6.55	5.33	5.64
DMSO	6.96	4.99	5.20	6.32	8.24	7.39	7.68	6.96	6.65	6.82	6.78	5.91
Trial 4	500.00	250.00	125.00	63.00	32.00	16.00	8.00	4.00	2.00	1.00	0.50	0.25
(-)-2.48	4.39	6.33	4.39	4.08	4.06	3.34	3.65	2.08	2.02	2.32	2.16	1.53
(+)-2.49	6.10	5.26	6.05	4.60	4.12	3.40	3.44	2.39	2.36	2.65	2.14	1.87
analog 2	1.12	1.57	6.81	4.51	3.64	2.35	2.06	1.79	2.07	2.45	2.21	2.08
carolacton	-----	-----	-----	-----	-----	-----	-----	-----	-----	-----	-----	-----
DMSO	2.65	2.68	2.67	2.66	1.91	2.40	1.85	1.94	2.27	2.42	1.81	1.79
Trial 5	500.00	250.00	125.00	63.00	32.00	16.00	8.00	4.00	2.00	1.00	0.50	0.25
(-)-2.48	5.70	7.83	8.95	8.76	5.54	5.27	4.89	3.33	3.73	3.78	2.87	2.96
(+)-2.49	5.81	11.83	10.26	8.13	6.93	6.25	4.03	2.91	4.27	3.92	3.24	1.83
analog 2	1.17	1.93	10.88	6.70	5.01	5.22	4.30	2.80	3.35	3.64	2.53	2.24
carolacton	-----	-----	-----	-----	-----	-----	-----	-----	-----	-----	-----	-----
DMSO	2.79	3.26	3.50	2.82	2.89	3.86	3.42	3.30	2.73	3.20	2.68	2.43
Trial 6	500.00	250.00	125.00	63.00	32.00	16.00	8.00	4.00	2.00	1.00	0.50	0.25
(-)-2.48	7.05	10.23	6.01	5.83	3.79	2.57	3.32	2.97	2.30	2.58	1.94	1.92
(+)-2.49	5.12	6.06	5.14	5.17	2.89	4.55	3.36	2.49	2.53	2.12	2.24	2.16
analog 2	2.98	1.58	19.35	5.11	3.79	3.64	3.39	2.73	2.20	3.30	2.29	1.79
carolacton	-----	-----	-----	-----	-----	-----	-----	-----	-----	-----	-----	-----
DMSO	2.87	2.80	2.50	2.44	2.39	2.94	3.59	2.51	2.28	2.68	2.03	2.01
Trial 7	500.00	250.00	125.00	63.00	32.00	16.00	8.00	4.00	2.00	1.00	0.50	0.25
(-)-2.48	4.35	6.30	6.94	5.69	4.98	4.02	3.19	2.68	2.62	2.70	3.04	2.52
(+)-2.49	4.31	5.28	6.66	5.16	4.46	3.78	3.47	2.83	2.85	2.65	2.95	2.46
analog 2	1.13	1.18	8.66	5.83	4.45	3.46	3.22	3.16	2.58	2.47	2.90	2.48
carolacton	-----	-----	-----	-----	-----	-----	-----	-----	-----	-----	-----	-----
DMSO	4.04	3.60	3.62	3.33	3.49	3.51	3.03	2.88	2.78	2.53	2.89	2.72
Trial 8	500.00	250.00	125.00	63.00	32.00	16.00	8.00	4.00	2.00	1.00	0.50	0.25
(-)-2.48	3.97	5.81	6.41	11.51	5.86	5.15	5.18	4.93	4.44	3.91	4.48	3.80
(+)-2.49	4.95	5.43	8.13	7.27	6.07	4.88	4.82	4.18	4.20	3.82	4.99	2.98
analog 2	1.95	1.09	6.51	5.80	4.56	4.39	4.10	3.98	3.65	4.52	3.97	3.72
carolacton	-----	-----	-----	-----	-----	-----	-----	-----	-----	-----	-----	-----
DMSO	3.74	3.18	3.16	2.63	3.21	2.72	3.29	2.55	5.24	2.70	2.86	2.53
Trial 9	500.00	250.00	125.00	63.00	32.00	16.00	8.00	4.00	2.00	1.00	0.50	0.25
(-)-2.48	3.40	6.01	6.73	5.22	3.05	2.78	2.38	2.44	2.12	2.24	2.04	1.69
(+)-2.49	4.72	5.35	5.46	5.38	2.99	3.30	2.88	2.70	2.42	2.27	2.04	1.76
analog 2	1.19	1.33	4.68	5.77	3.63	2.75	3.00	2.22	2.25	2.07	1.91	2.42
carolacton	-----	-----	-----	-----	-----	-----	-----	-----	-----	-----	-----	-----
DMSO	4.27	2.83	2.71	2.47	2.22	2.45	2.28	2.80	2.33	1.99	2.54	2.22

Figure 5.1 Biofilm crystal violet measurement replicates of carolacton generation 2.

Values shown are the result of $(CV \text{ OD}_{595} / \text{growth } O_{D600})$ to demonstrate biofilm formation relative to bacterial growth.

	Relative Biomass Compared to DMSO control											
conc (μM)	500.00	250.00	125.00	63.00	32.00	16.00	8.00	4.00	2.00	1.00	0.50	0.25
(-)-2.48	1.00	1.82	1.63	1.72	1.18	0.94	0.90	0.92	0.79	0.92	0.92	0.88
(+)-2.49	1.40	1.85	1.65	1.53	1.16	1.04	0.91	0.84	0.87	0.87	0.95	0.84
analog 2	0.36	0.39	2.32	1.78	1.27	1.08	0.97	0.89	0.89	1.04	0.92	0.99
carolacton	1.44	1.58	1.15	0.98	0.91	0.88	0.86	0.93	0.97	0.94	0.91	1.08

	Average Biomass Trials 1-9											
DMSO	4.69	3.99	4.17	3.96	4.25	4.38	4.47	4.10	4.18	3.97	3.80	3.50
(-)-2.48	4.67	7.26	6.81	6.79	5.01	4.10	4.03	3.75	3.29	3.66	3.50	3.08
(+)-2.49	6.58	7.36	6.88	6.06	4.91	4.54	4.06	3.43	3.62	3.45	3.62	2.95
analog 2	1.70	1.55	9.69	7.04	5.39	4.72	4.36	3.65	3.73	4.13	3.51	3.47
	Average Biomass Trials 1-3											
DMSO	7.28	5.92	6.46	6.43	7.38	7.18	7.59	6.98	6.65	6.75	6.48	5.93
carolacton	10.47	9.32	7.41	6.32	6.75	6.34	6.49	6.48	6.45	6.35	5.92	6.41

Figure 5.2 Relative biofilm mass after compound dosing relative to negative control (top). Average biofilm mass after compound dosing (bottom).

		Concentration (μM)											
		250	125	63	32	16	8	4	2	1	0.5	0.25	0.125
A1		0.00	0.00	3.14	1.47	1.55	1.15	1.55	1.78	1.34	1.58	1.50	2.20
A2		0.00	0.00	0.00	0.00	4.65	2.34	2.92	2.28	1.71	1.76	2.02	1.67
A3		7.00	3.30	1.27	1.64	2.09	3.08	1.15	1.76	1.33	1.44	1.05	1.65
A4		5.08	3.51	2.75	2.39	1.12	1.23	2.58	1.75	2.14	1.44	1.02	2.61
A5		5.22	4.65	2.23	2.54	2.36	1.60	1.88	1.44	1.28	1.75	1.70	2.17
A6		4.99	1.47	1.79	1.58	1.31	0.95	1.53	1.07	3.38	1.21	1.28	2.30
A7		0.00	0.00	0.00	0.00	4.92	1.54	1.19	1.25	1.39	1.00	0.95	2.14
A8		6.35	4.23	3.49	1.53	1.60	1.56	1.65	1.35	1.95	1.74	1.12	1.78
A9		5.56	3.63	2.73	1.47	1.76	2.40	1.91	1.76	1.32	1.53	1.96	2.81
A10		3.22	2.16	1.96	2.05	1.57	2.05	1.79	2.08	1.85	1.99	1.93	2.76
B1		3.19	1.89	1.70	1.34	2.10	2.28	1.79	1.76	2.60	1.63	1.62	1.52
B2		6.59	2.16	0.94	1.45	1.83	1.10	1.54	1.65	3.89	1.01	1.11	1.80
B3		0.00	0.00	0.00	5.92	2.78	1.73	1.63	1.63	2.05	1.23	1.26	2.64
B4		0.00	0.00	5.68	2.38	1.80	1.24	2.93	1.35	1.28	1.49	1.68	1.62
B5		0.000	0.000	0.000	0.000	0.000	0.000	4.990	2.094	1.227	1.775	1.543	2.940
B6		4.372	5.921	5.253	5.279	4.465	4.431	4.898	4.430	1.270	1.622	1.551	1.637
B7		0.000	0.000	3.999	1.438	1.320	2.261	1.719	2.323	1.428	1.784	1.592	2.151
B8		0.000	0.000	0.000	0.000	0.000	6.854	1.939	1.675	1.370	1.220	2.127	2.025
B9		0.000	0.000	0.000	0.000	3.092	2.452	2.564	2.272	1.893	2.306	2.808	2.269
B10		0.000	0.000	0.000	0.000	0.000	6.168	3.285	2.019	1.765	1.812	2.135	2.544
B11		0.000	0.000	0.000	0.000	0.000	4.323	1.864	2.175	1.862	2.552	1.911	2.674
B12		6.183	4.391	3.460	2.380	2.353	1.955	2.069	3.302	2.141	2.015	1.945	2.219
B13		4.539	5.392	6.320	6.827	5.635	3.391	2.104	2.287	2.309	2.163	2.089	2.262
B14		0.000	0.000	0.000	11.091	5.716	2.755	3.090	1.952	2.007	1.628	1.594	2.180
C1		4.756	4.254	3.177	3.095	2.205	2.614	1.449	2.905	2.021	2.281	1.240	1.183
C2		0.000	0.000	0.000	0.000	0.000	0.000	0.000	8.131	2.151	2.066	1.606	1.952

Below: Representative plate from crystal violet MBIC assay.

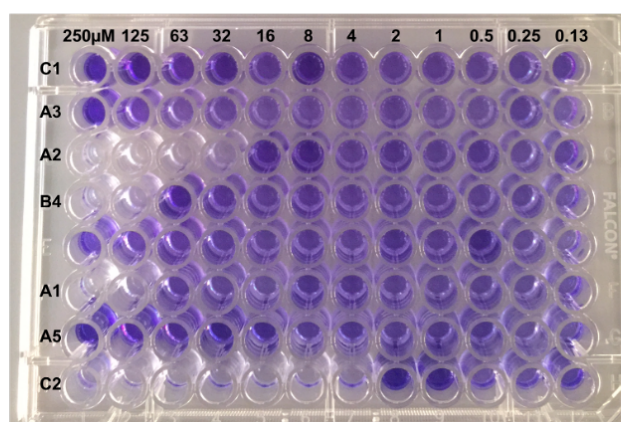


Figure 5.3 MIC and MBIC results from honokiol generation 1.

$$(\text{Colony Count}/5\mu\text{L}) * 1000\mu\text{L}/\text{mL} * 10^X$$

X=dilution factor

	125 μM	63 μM	16 μM	8 μM	4 μM
A1	7.1 \pm 1.0	9.8 \pm 0.7	10.3 \pm 0.2		
A2	0.0 \pm 0.0	5.9 \pm 0.8	9.9 \pm 0.7		
A7	3.9 \pm 0.1	3.8 \pm 0.3	8.8 \pm 0.7		
B5	4.0 \pm 0.5	7.6 \pm 0.7	7.0 \pm 0.3		
B8	5.8 \pm 0.9	6.4 \pm 0.5	7.5 \pm 0.8		
B11	8.2 \pm 1.4	6.25 \pm 0.1	8.3 \pm 1.1		
C2	0.0 \pm 0.0	0.0 \pm 0.0	0.0 \pm 0.0	0.0 \pm 0.0	5.9 \pm 1.1
Cells	9.9 \pm 0.5				

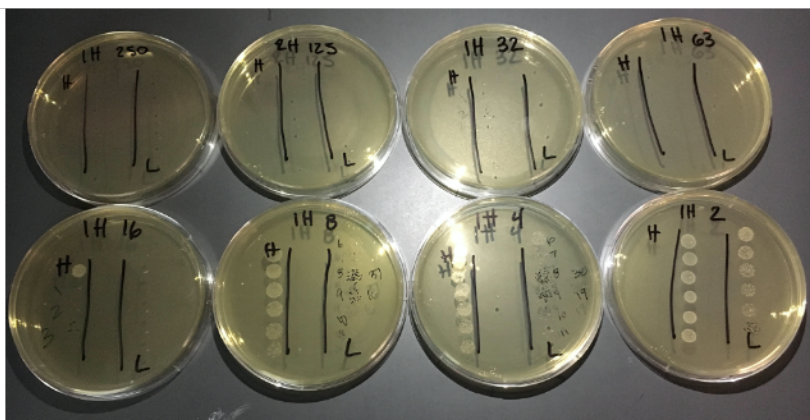


Figure 5.4 MBC results for honokiol generation 1

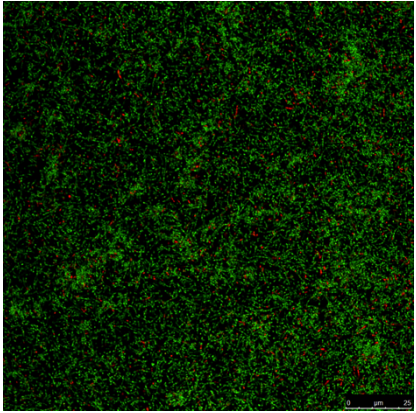
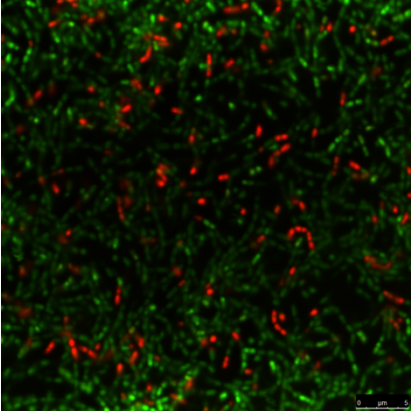
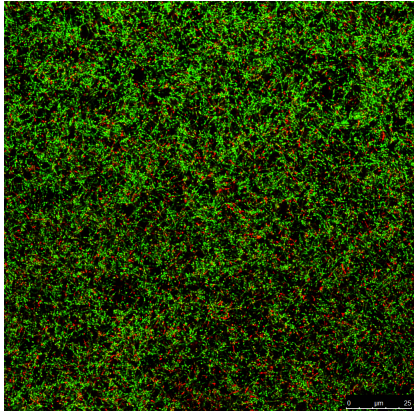
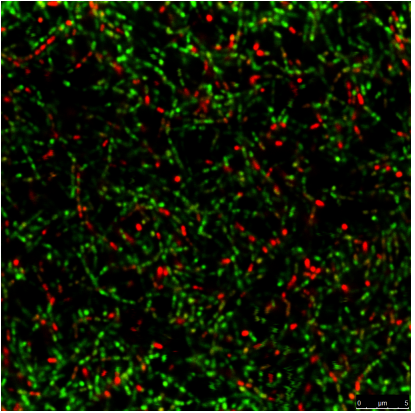
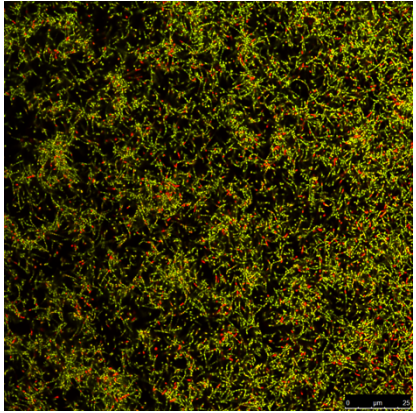
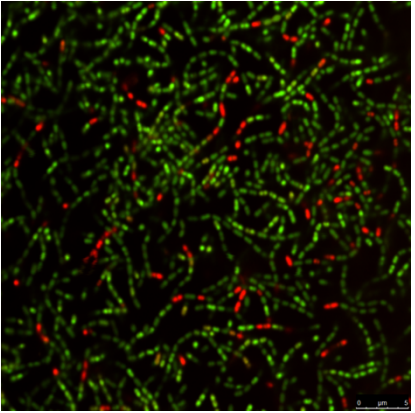
Compound	<i>S. mutans</i>	<i>S. gordonii</i>	<i>S. sanguinis</i>	<i>S. sobrinus</i>	<i>S. Mutans</i> MBC	Lysis ₂₀	Therapeutic Index (TI)
3A-3M; 3O-3Z	>250 µM	-	-	-	-	-	-
3N	2 µM	2 µM	2 µM	4 µM	2 µM	63 µM	32
3AA-3AD	>250 µM	-	-	-	-	-	-
3AE	8 µM	-	-	-	-	-	-
3AF	16 µM	-	-	-	-	-	-
3AG-3AR	>250 µM	-	-	-	-	-	-
4A	>250 µM	-	-	-	-	-	-
4B	>250 µM	250 µM	250 µM	>250 µM	-	-	-
4C	32 µM	-	-	-	-	-	-
4D-4E	>250 µM	-	-	-	-	-	-
4F	16 µM	-	-	-	-	-	-
4G	4 µM	1 µM	1 µM	2 µM	4 µM	32 µM	8
4H	2 µM	4 µM	8 µM	8 µM	2 µM	63 µM	32
4I	>250 µM	>250 µM	63 µM	250 µM	-	-	-
4J	8 µM	-	-	-	-	-	-
4K	>250 µM	>250 µM	>250 µM	>250 µM	-	-	-
4L-4M	>250 µM	-	-	-	-	-	-
4N	16 µM	-	-	-	-	-	-
4O	>250 µM	-	-	-	-	-	-
4P	32 µM	32 µM	32 µM	32 µM	-	-	-
4Q	16 µM	-	-	-	-	-	-
4R	8 µM	8 µM	8 µM	8 µM	8 µM	-	-
4S	>250 µM	-	-	-	-	-	-
CPC	2 µM	1 µM	0.5 µM	0.5 µM	8 µM	16 µM	8
C2	2 µM	1 µM	1 µM	1 µM	4 µM	63 µM	32
Honokiol	250 µM	-	-	-	-	-	N/A

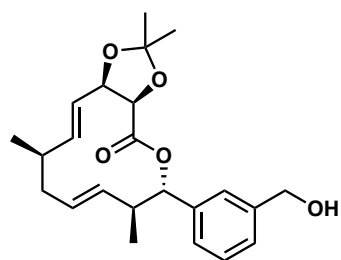
Table 5.1 MIC and MBC results for honokiol generation 2

5.2 Biofilm Replicates Generation 1 (Aryl)

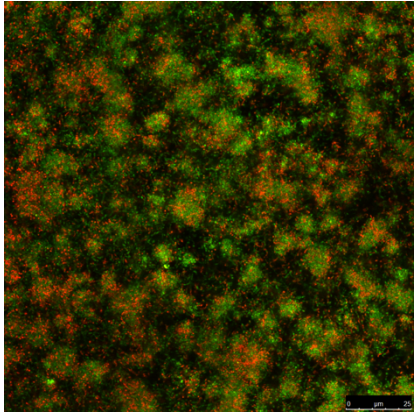
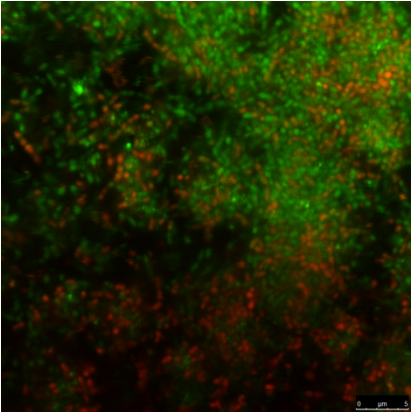
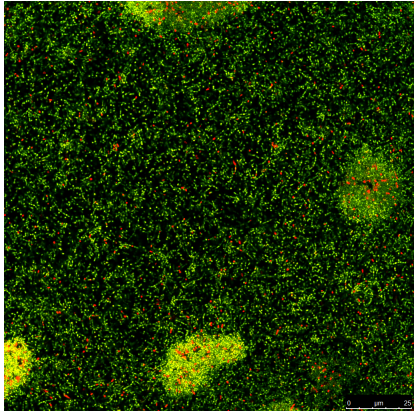
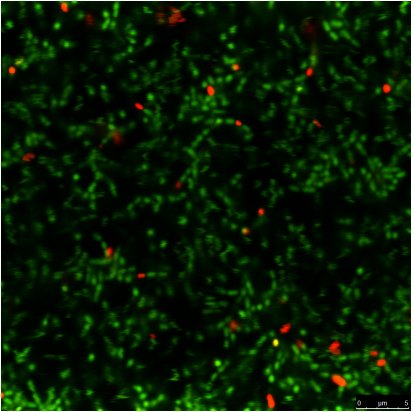
5.2.1 Concentrations 500 μ M or 250 μ M

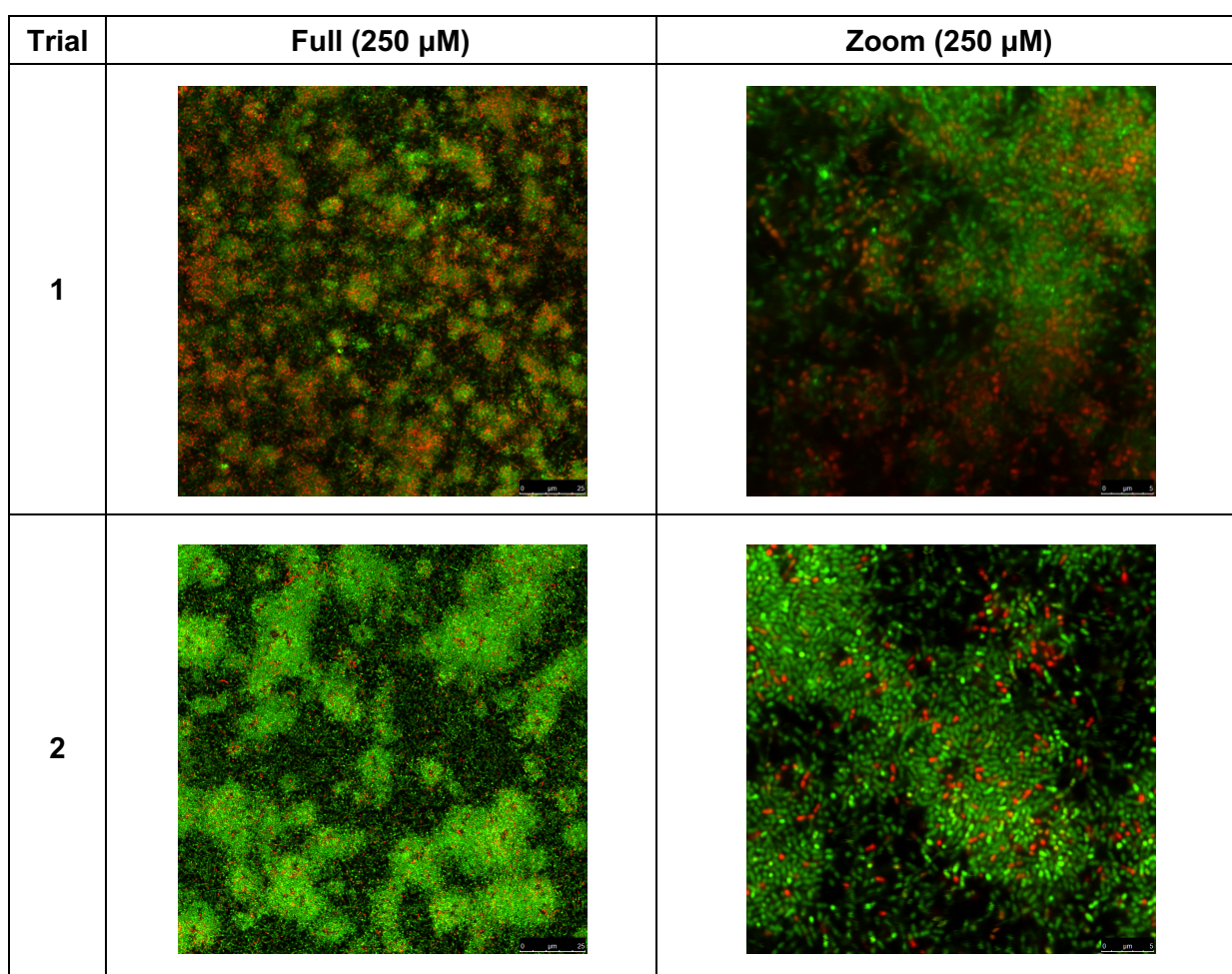
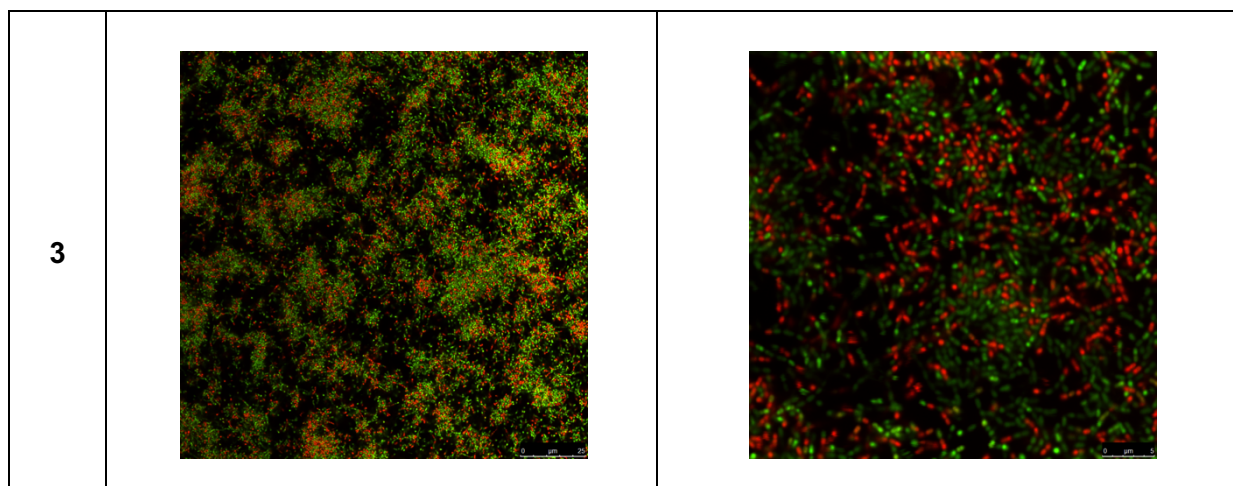
DMSO Control

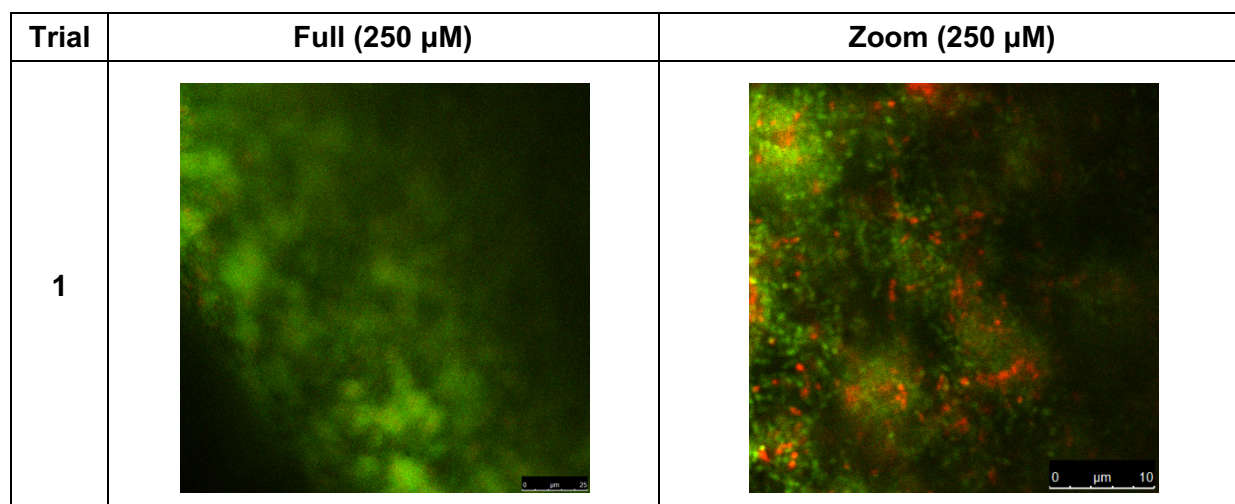
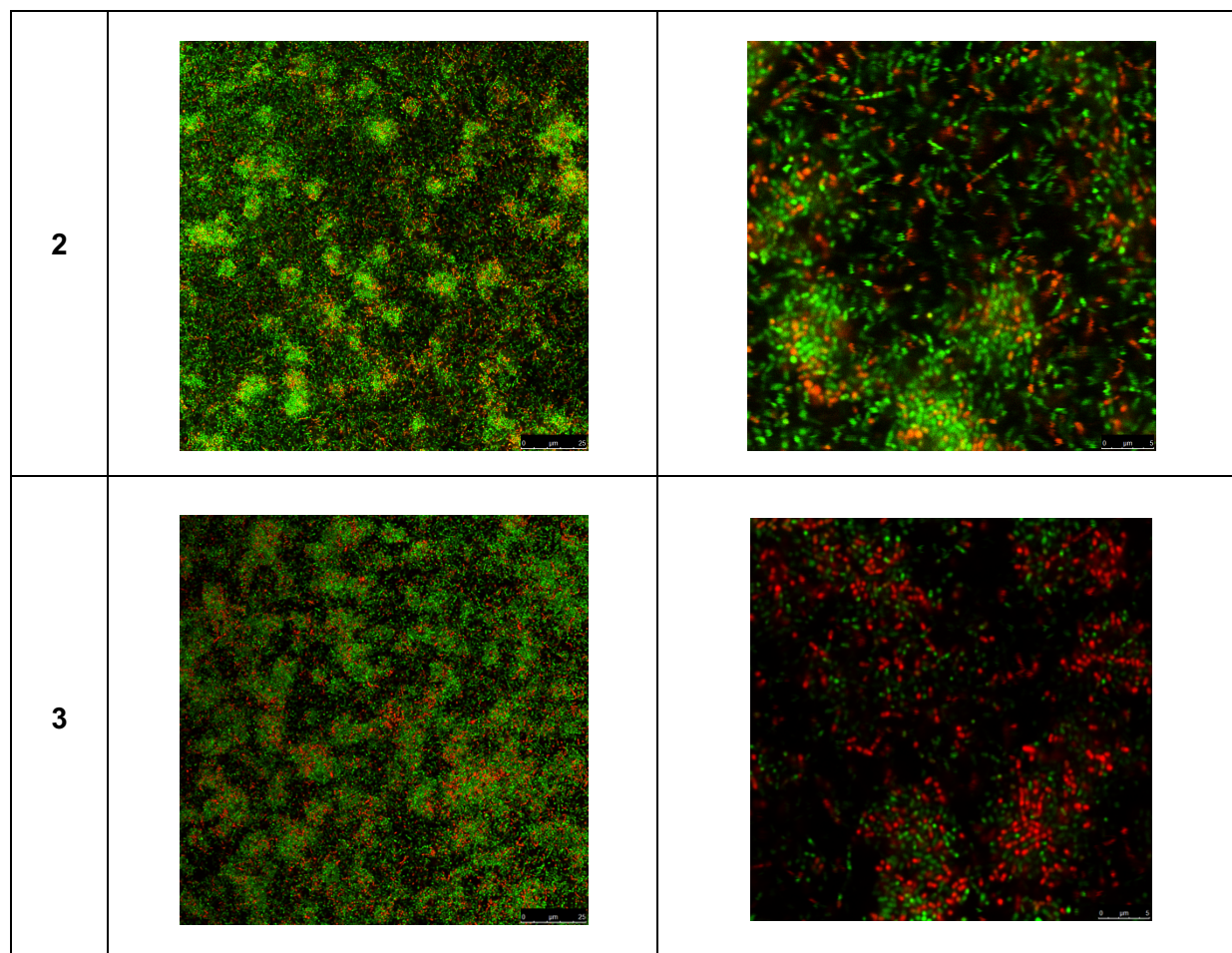
Trial	Full	Zoom
1		
2		
3		

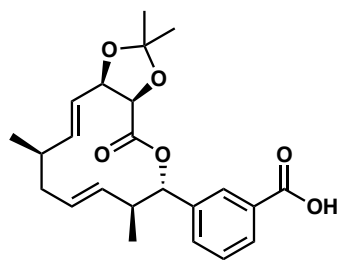
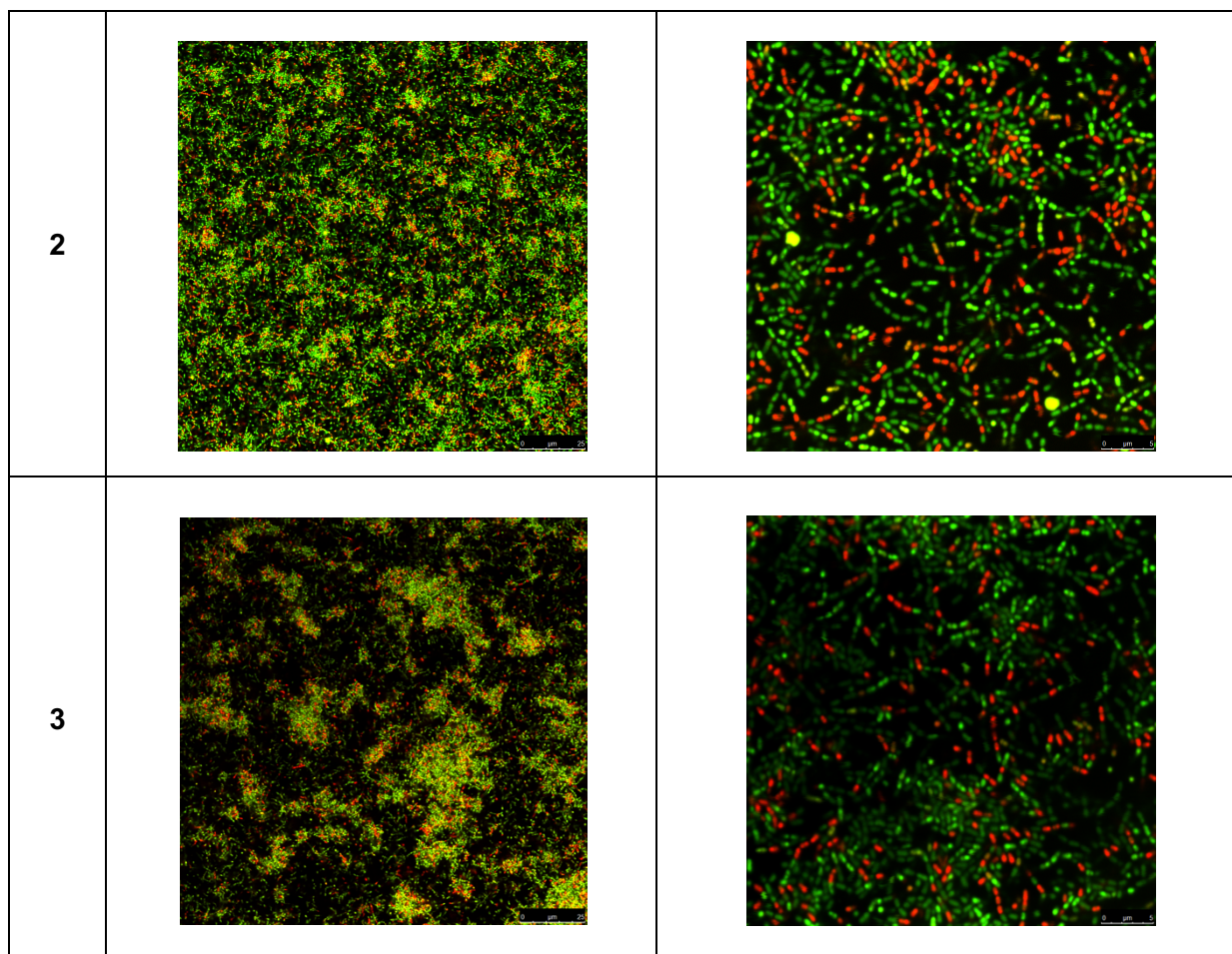


(-)-A1

Trial	Full (500 μ M)	Zoom (500 μ M)
1		
2		

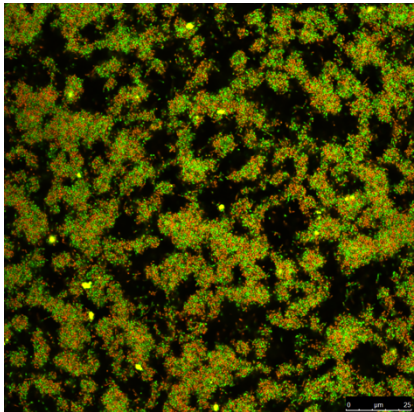
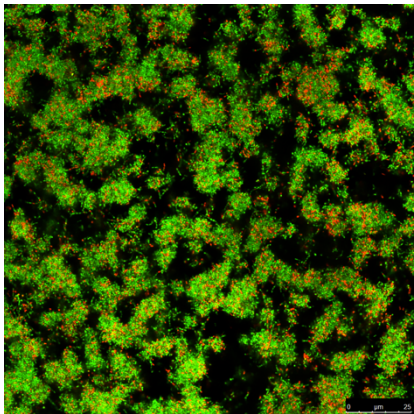
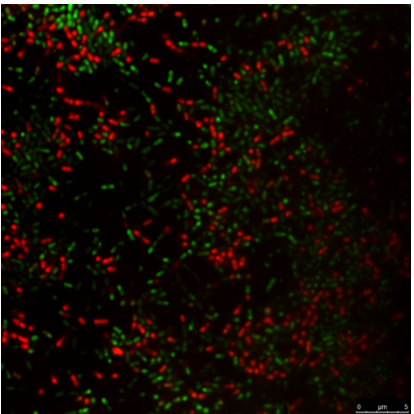


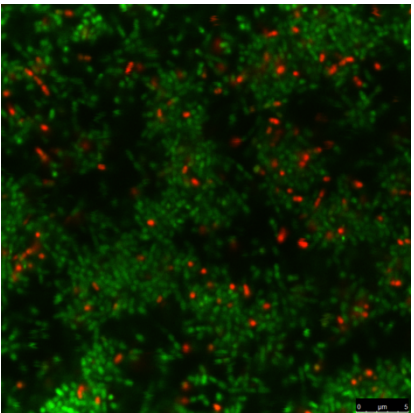


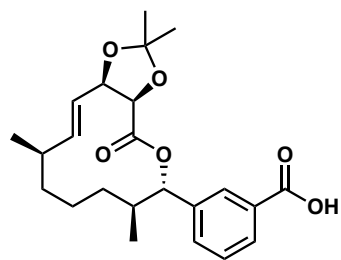
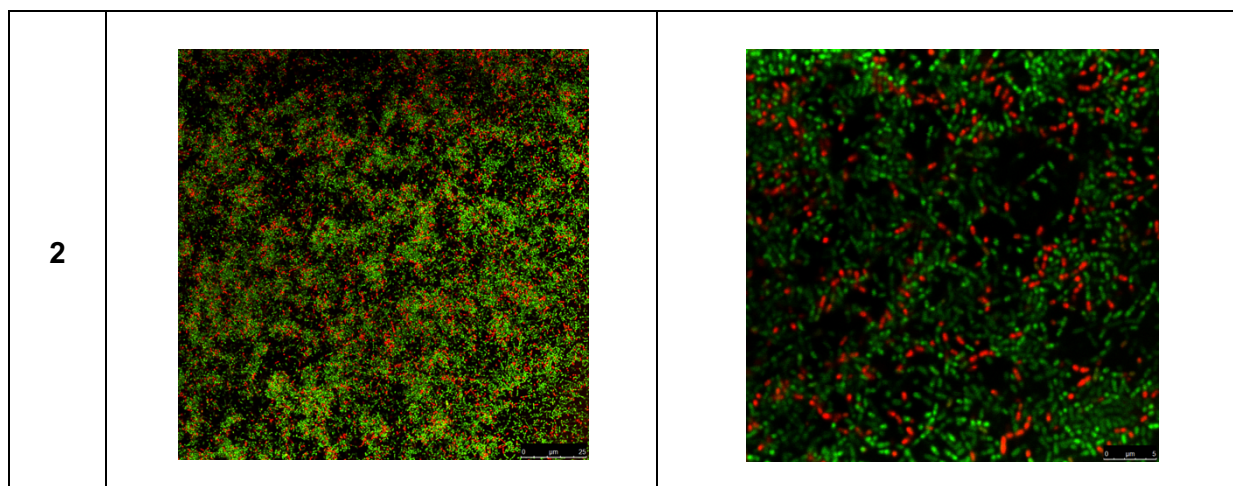


(-)-C1

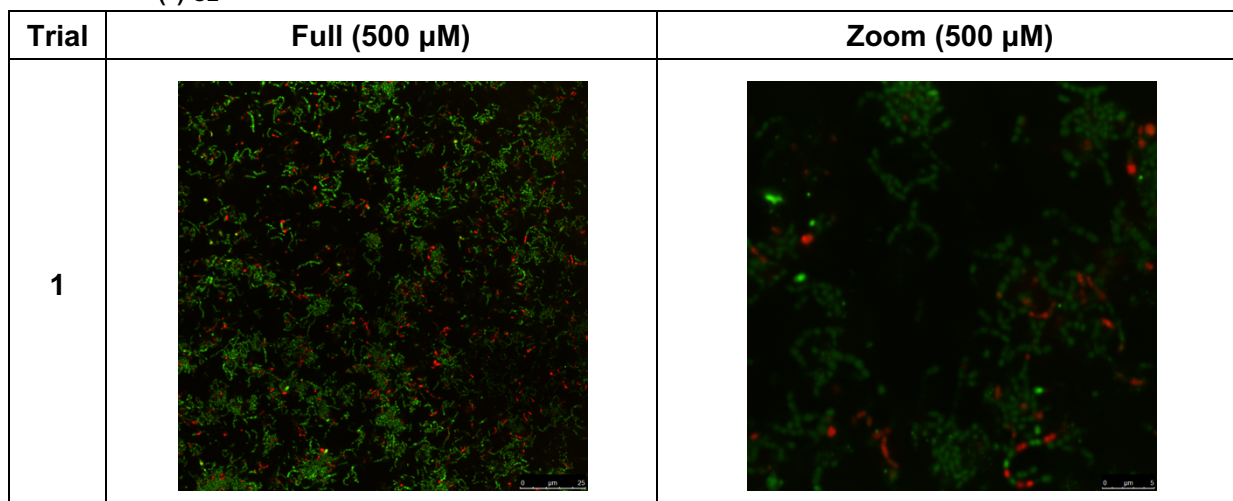
Trial	Full (500 μ M)	Zoom (500 μ M)
-------	--------------------	--------------------

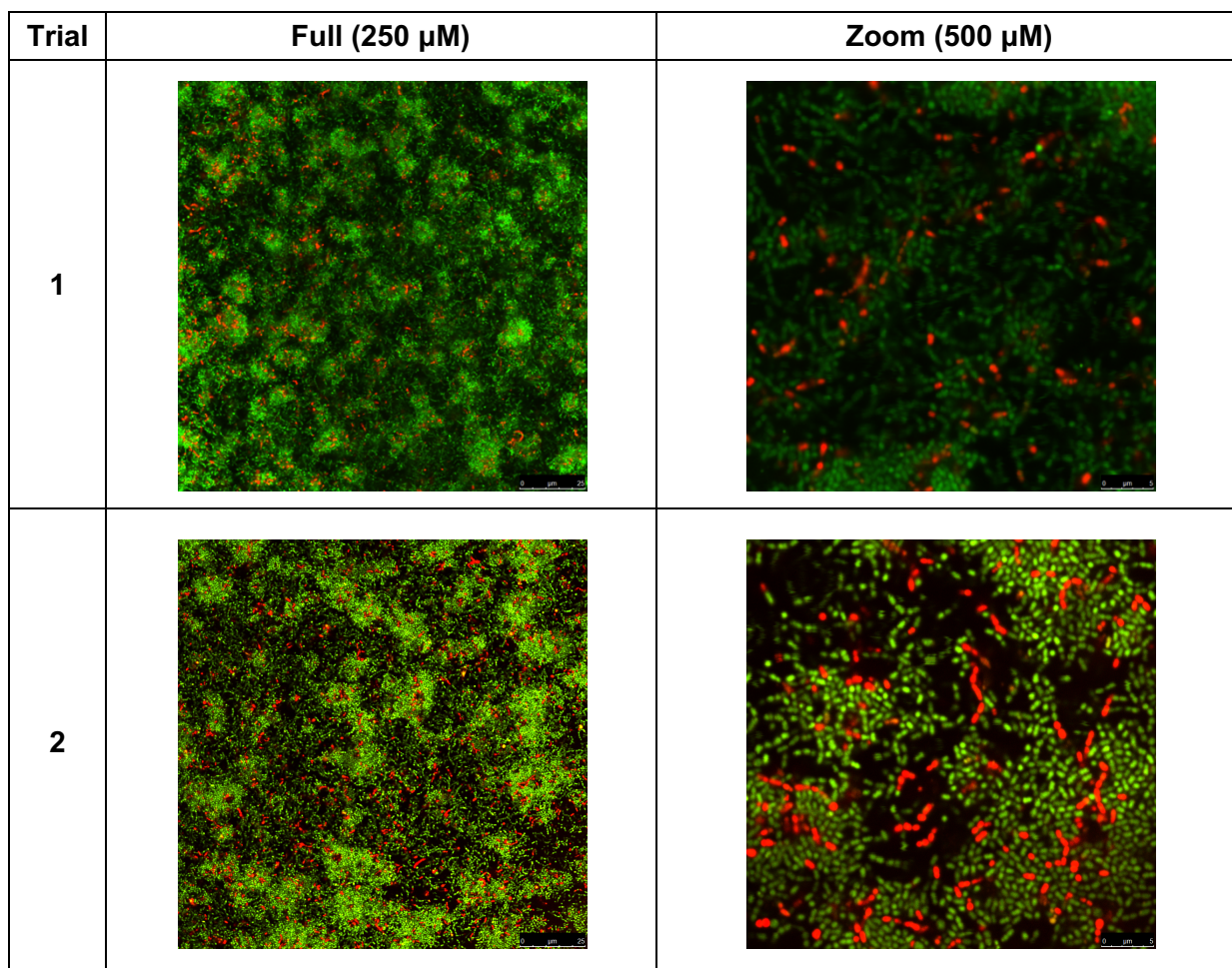
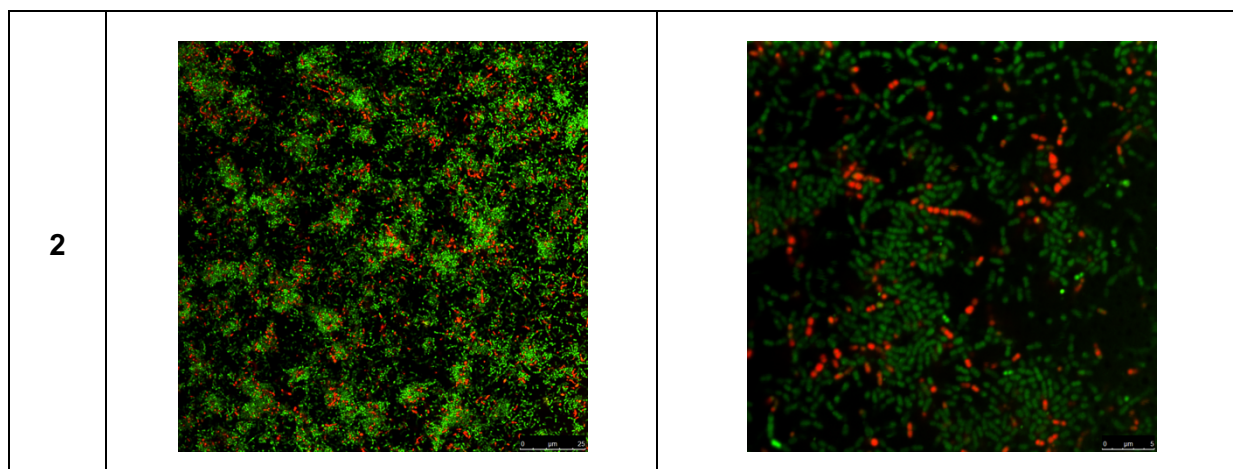
1		
2		

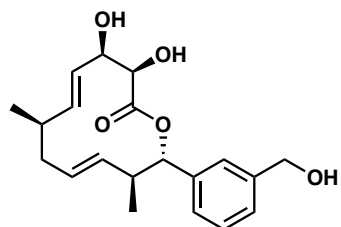
Trial	Full (250 μ M)	Zoom (250 μ M)
1		



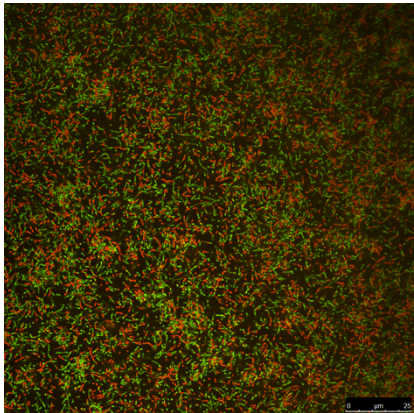
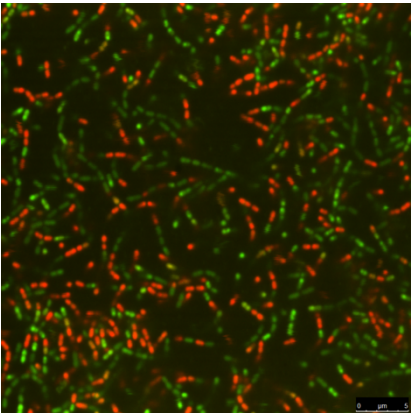
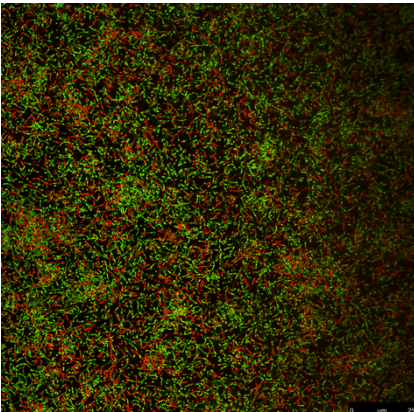
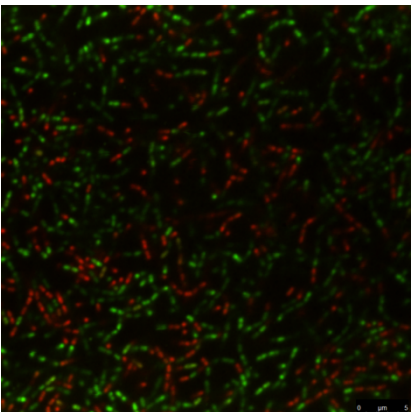
(-)-C2



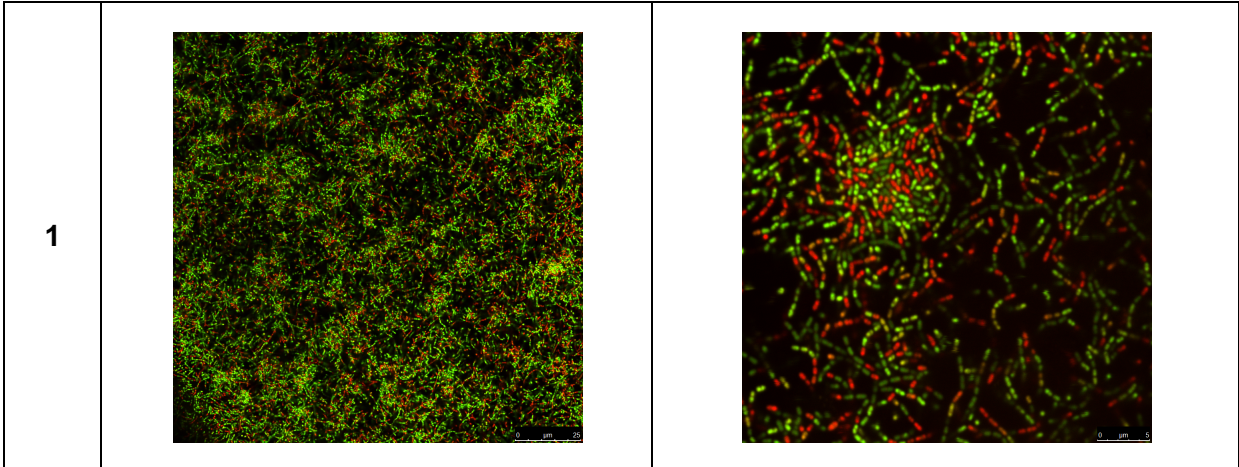


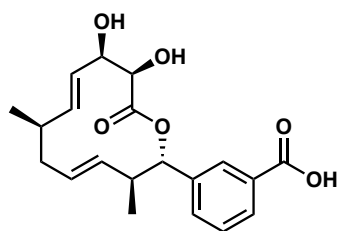
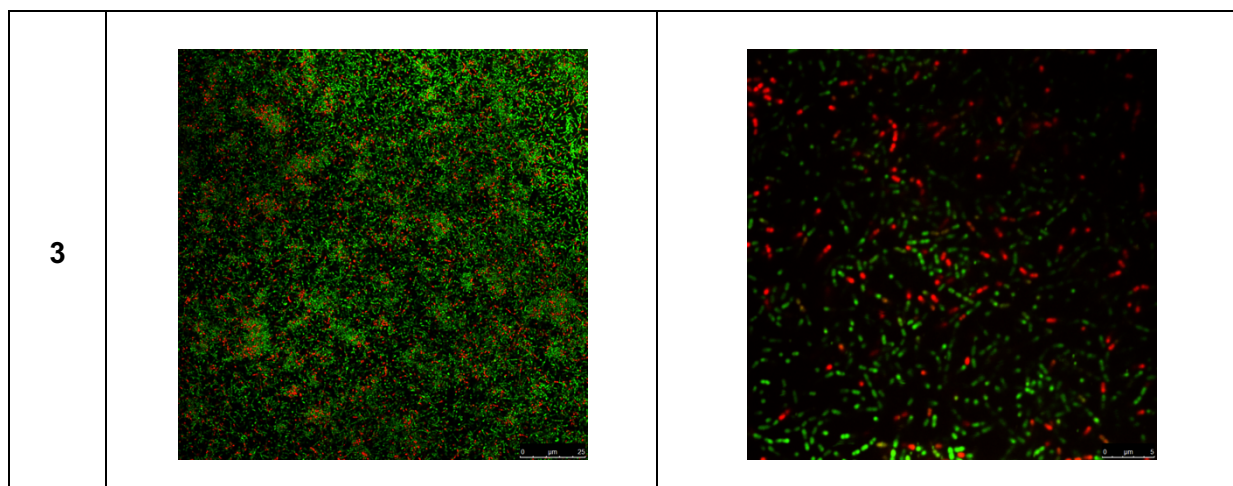


(-)-B1

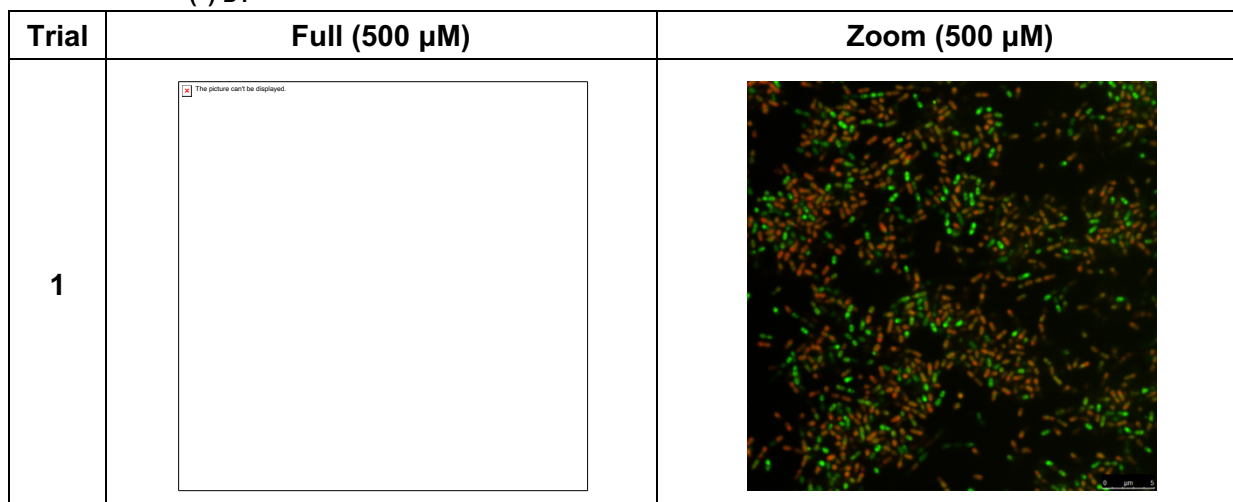
Trial	Full (500 μ M)	Zoom (500 μ M)
1		
2		

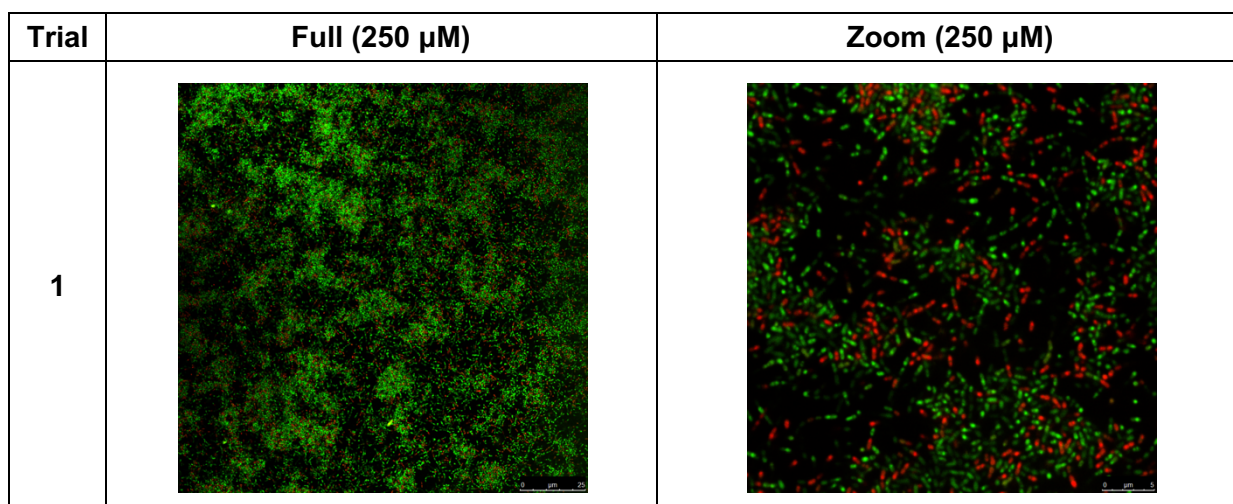
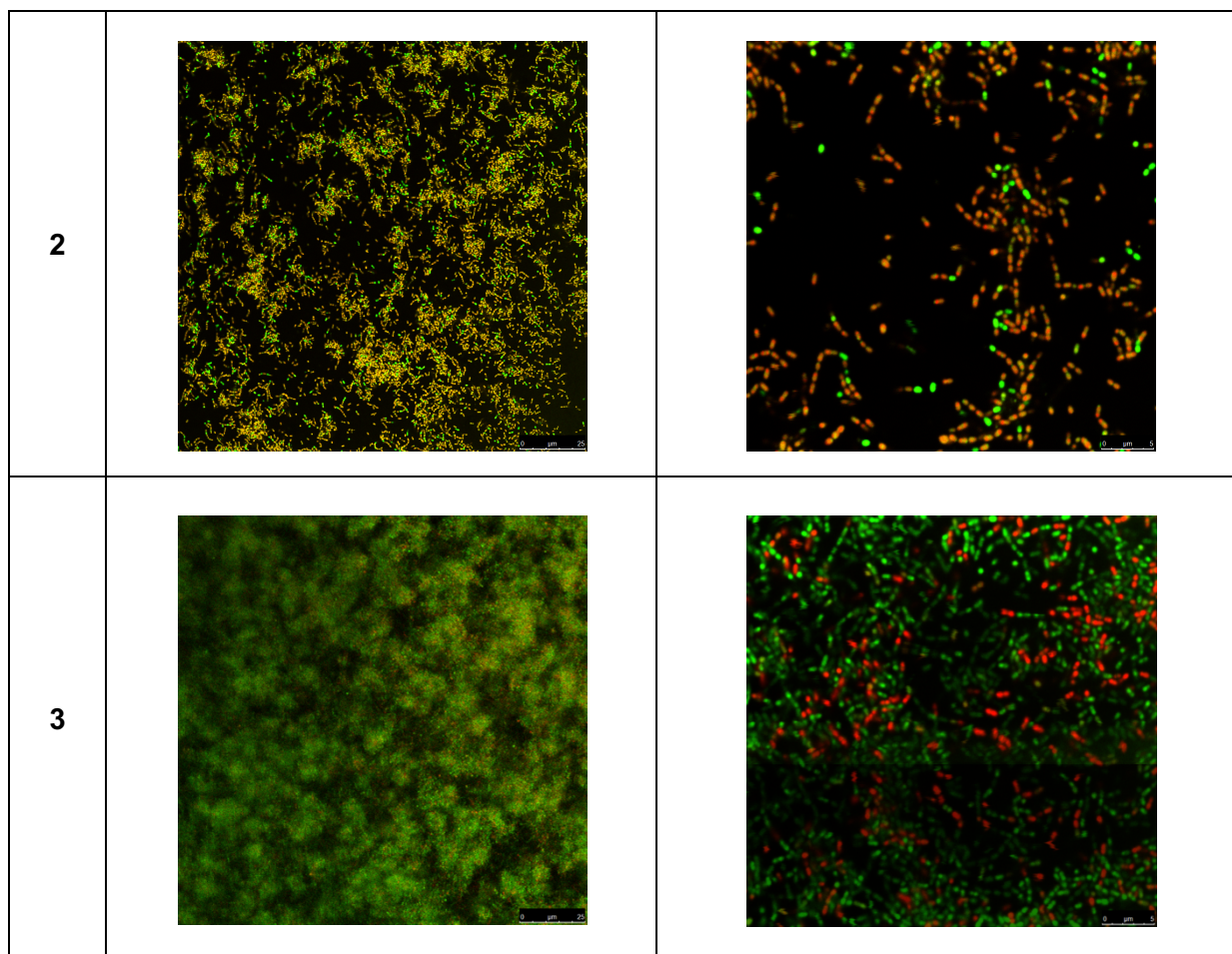
Trial	Full (250 μ M)	Zoom (250 μ M)
-------	--------------------	--------------------

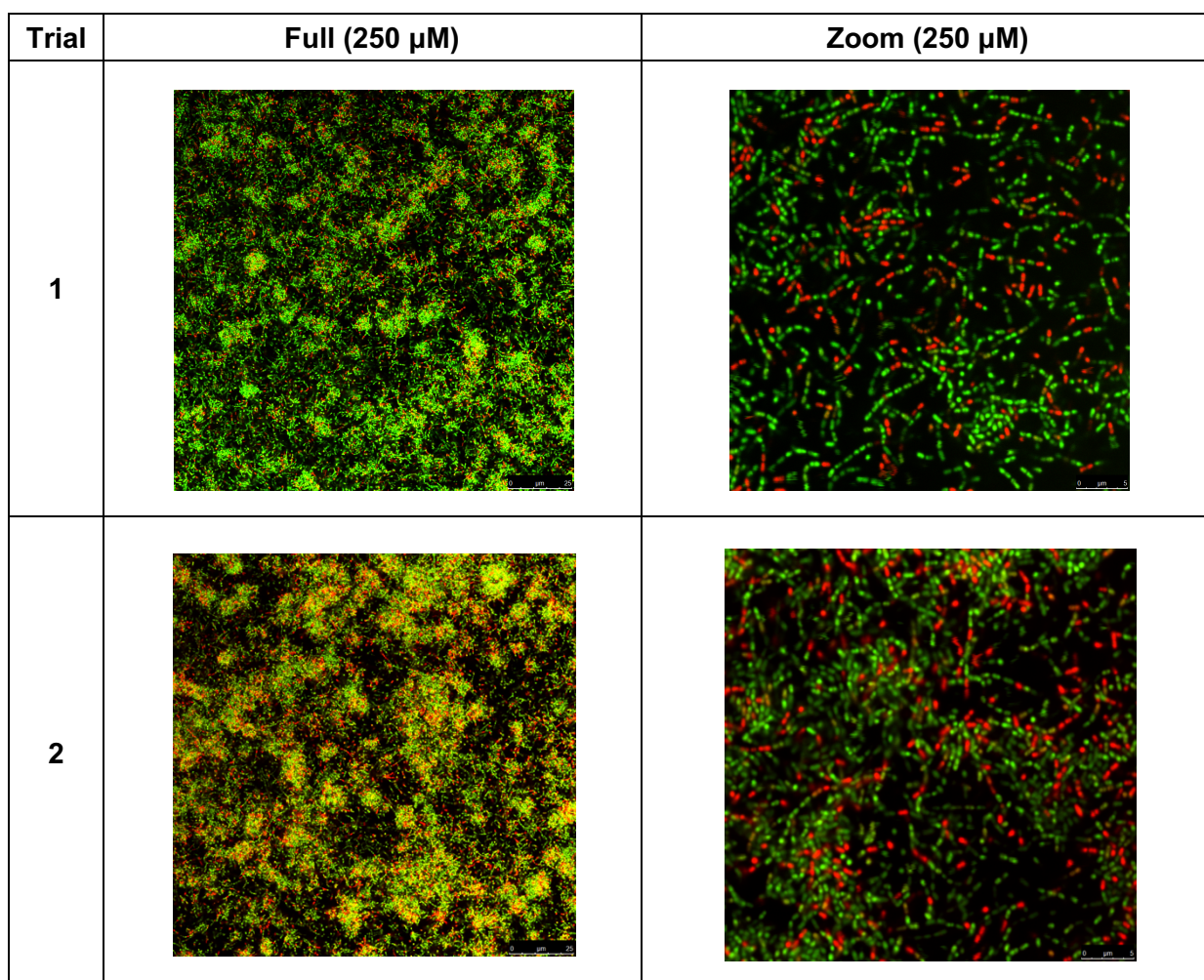
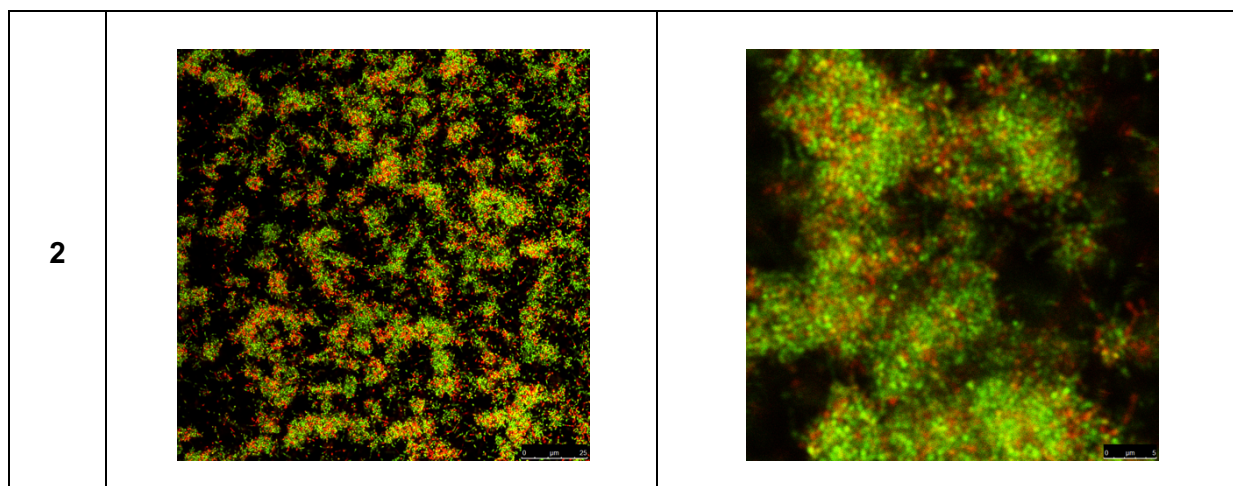


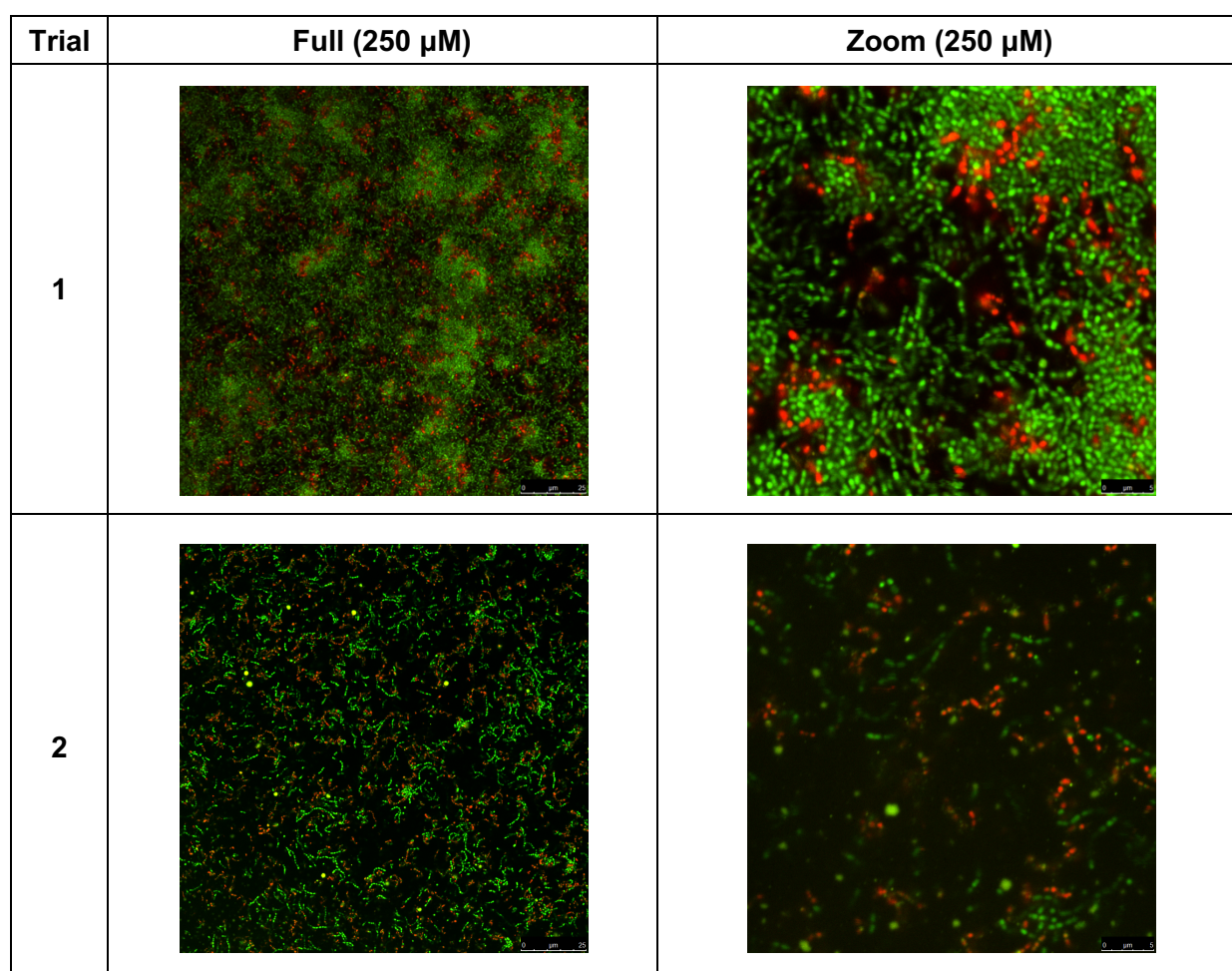
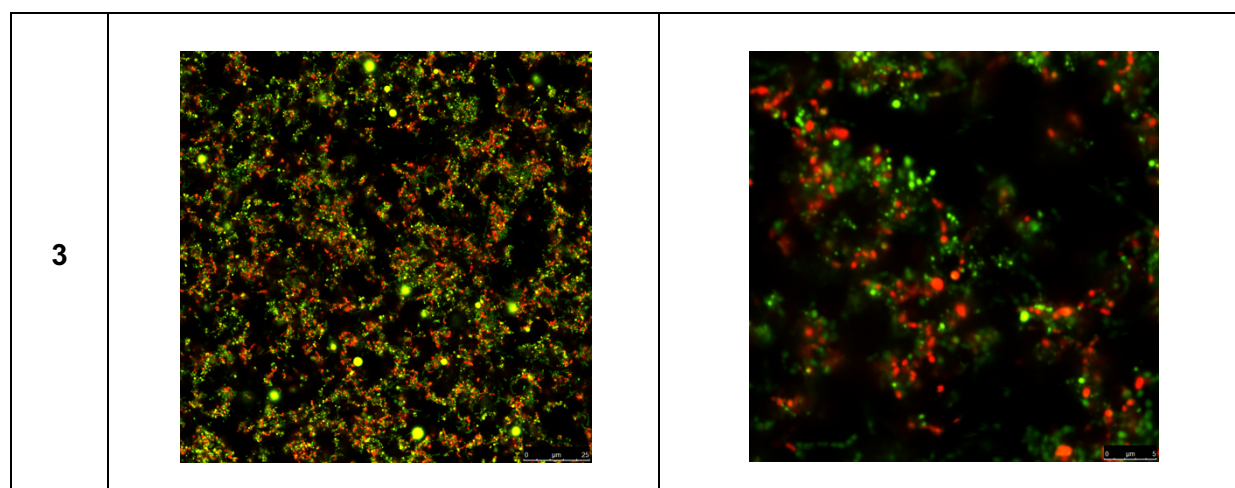


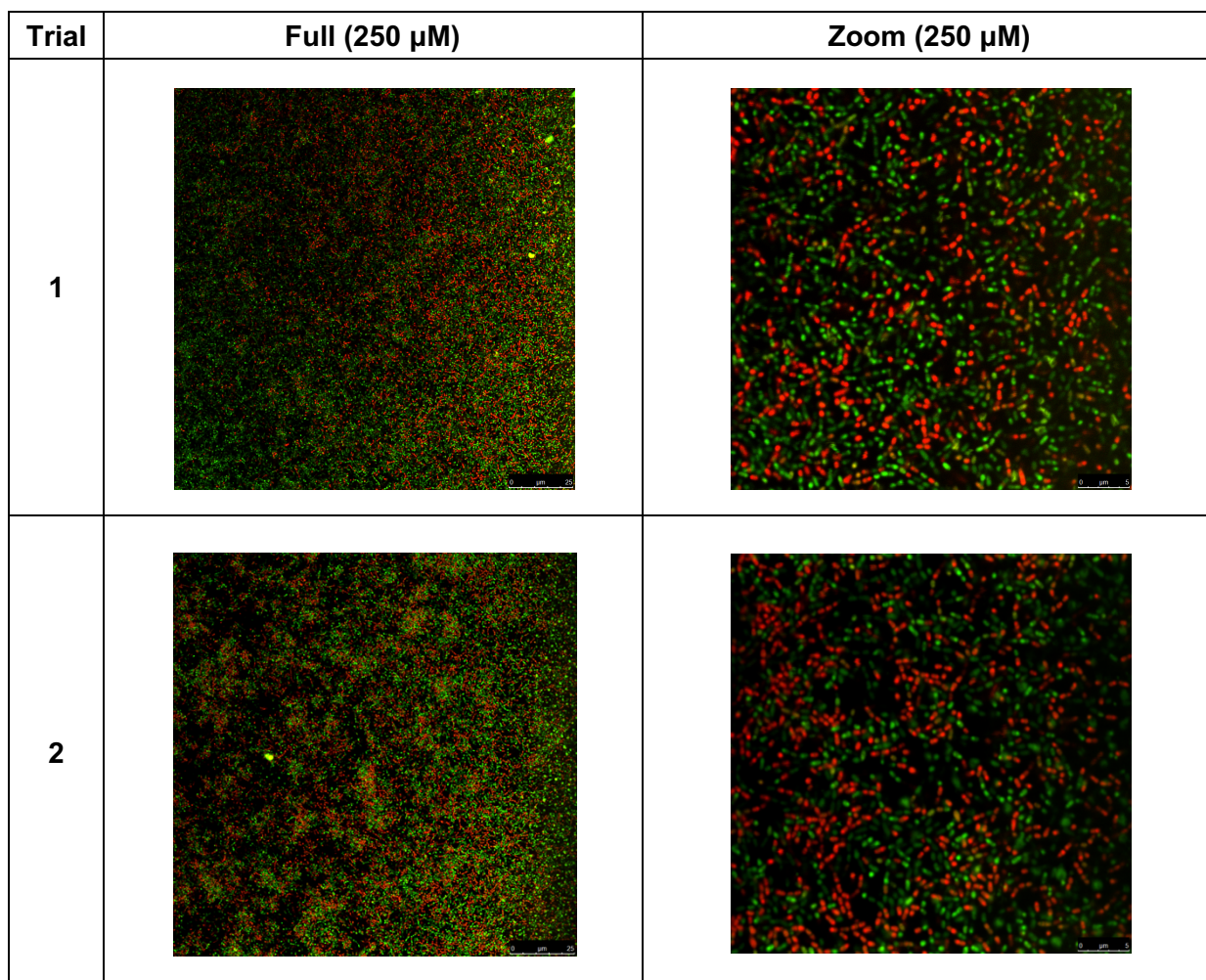
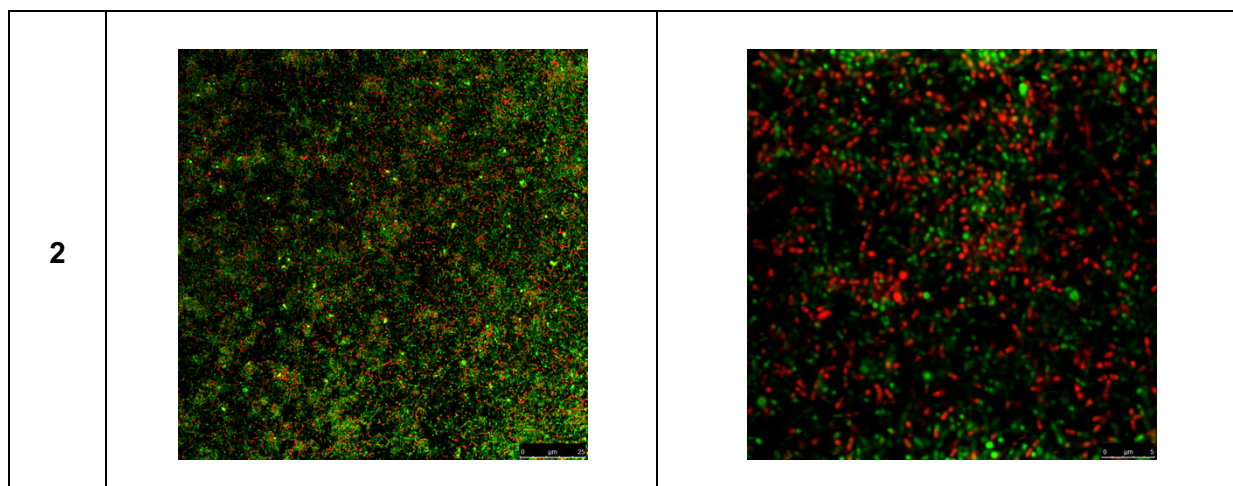
(-)-D1

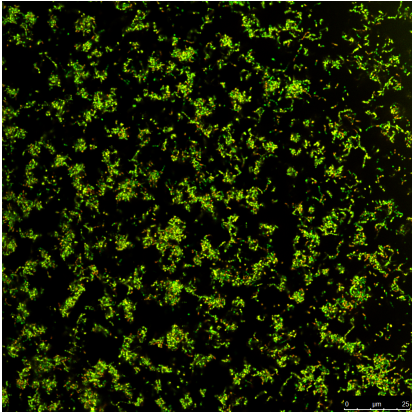
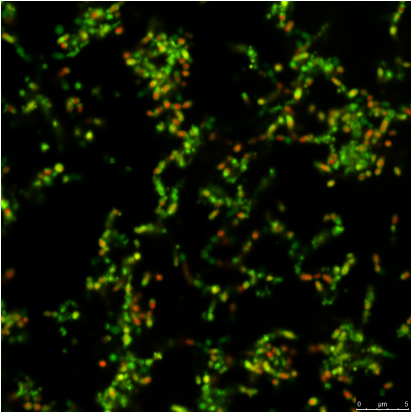
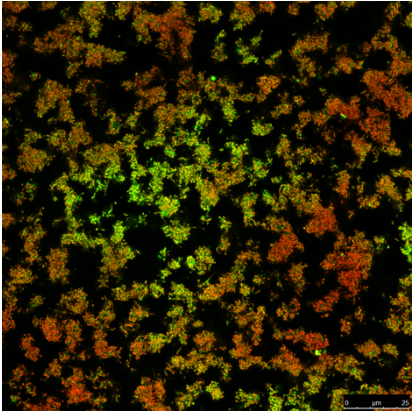
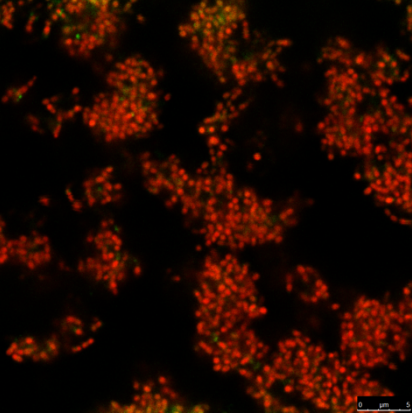
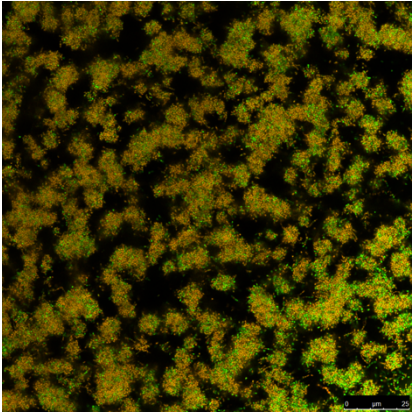
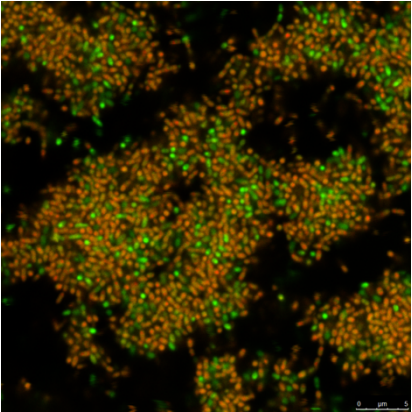


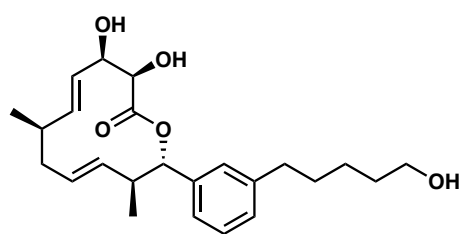
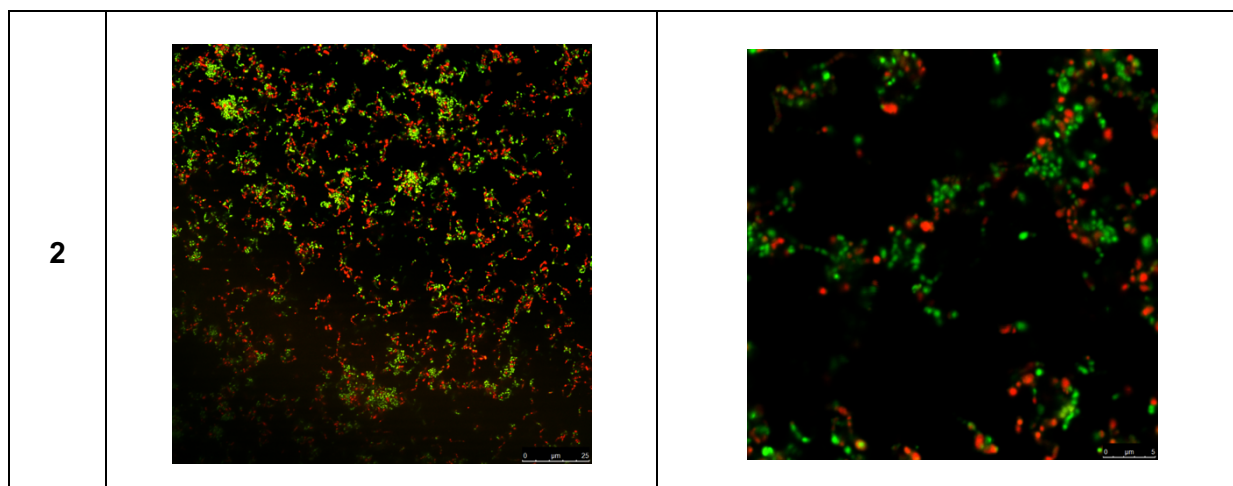




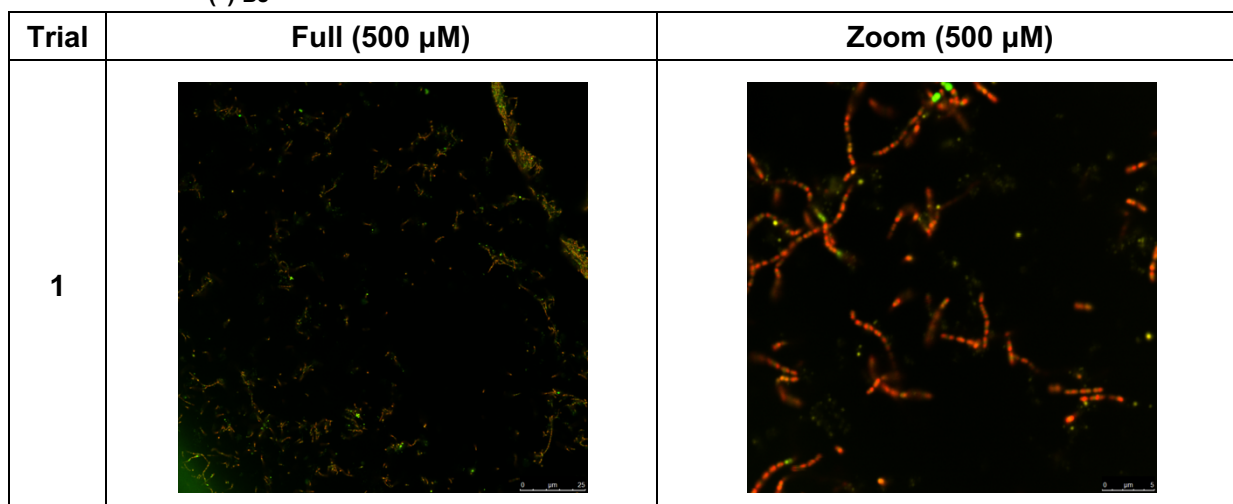


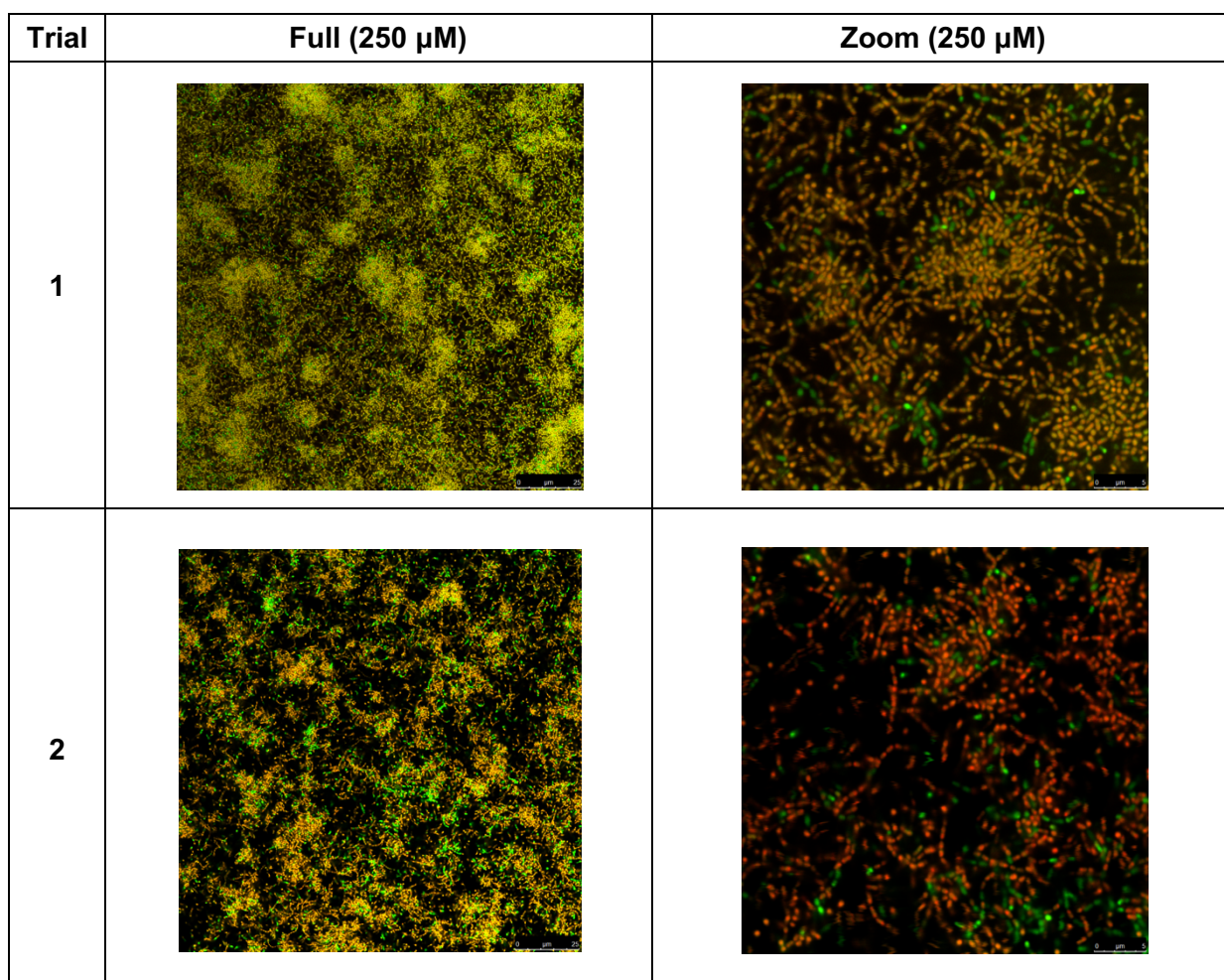
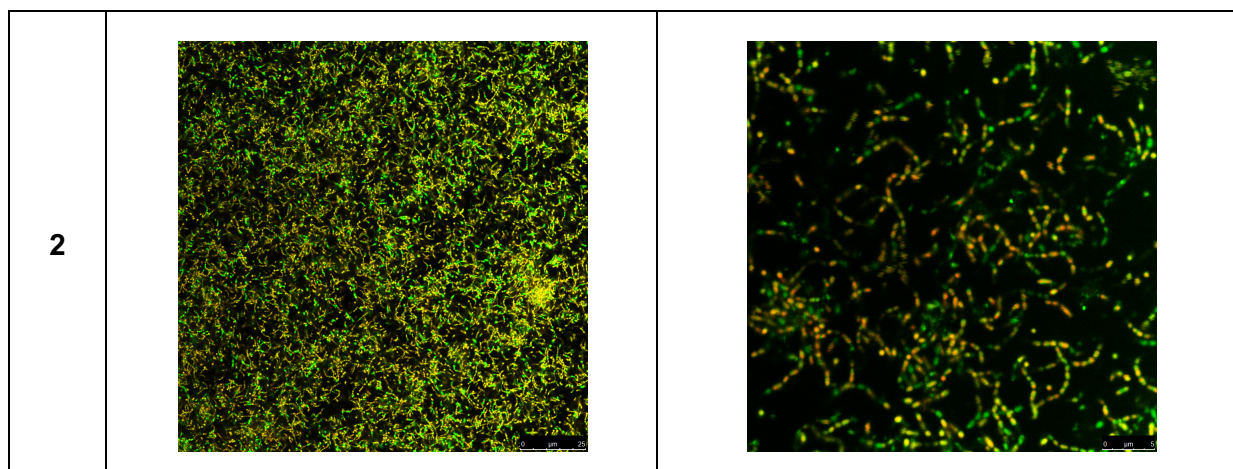


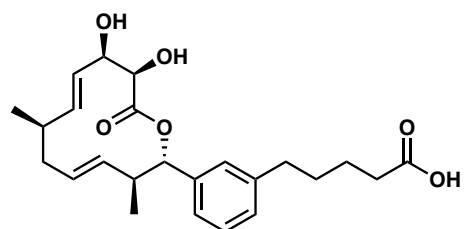
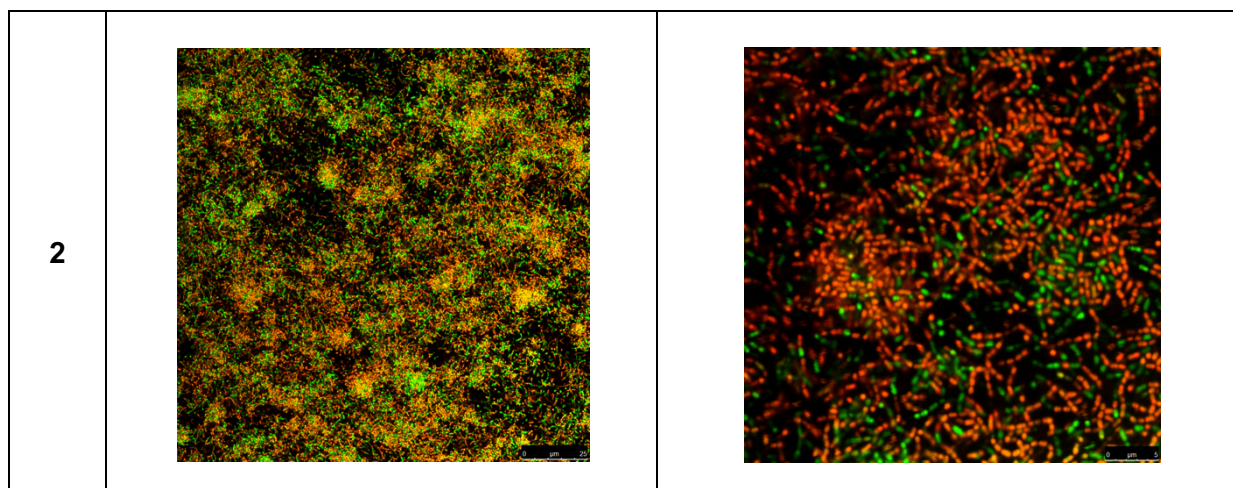
2		
3		
Trial	Full (250 μ M)	Zoom (250 μ M)
1		



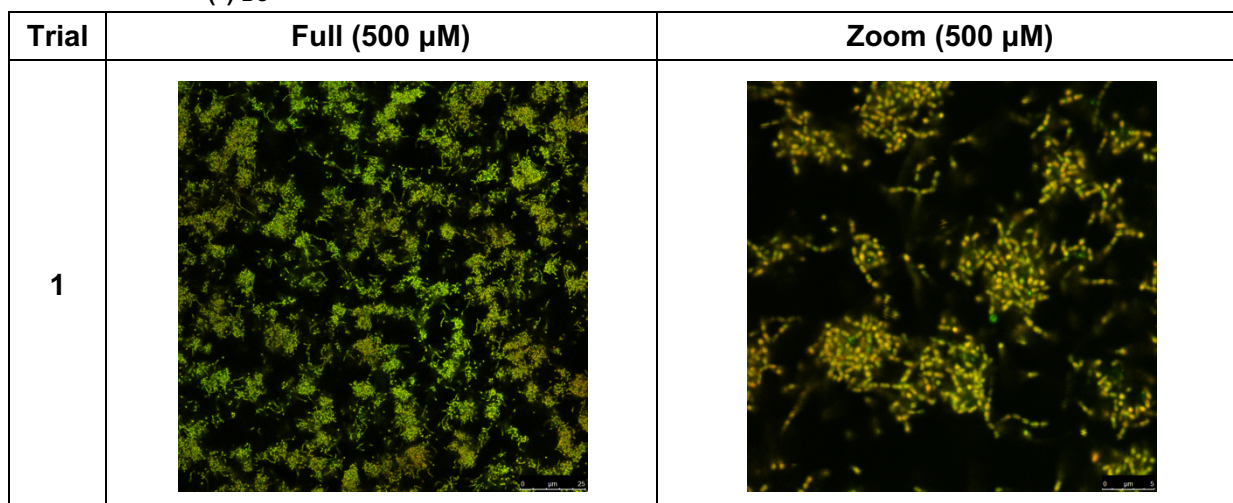
(-)-B3

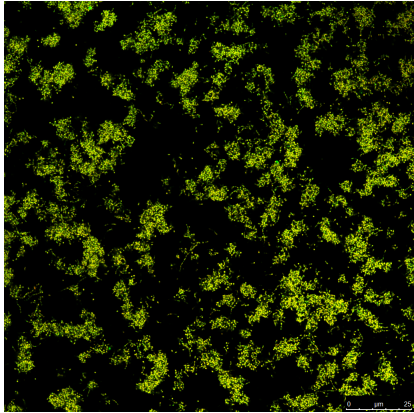
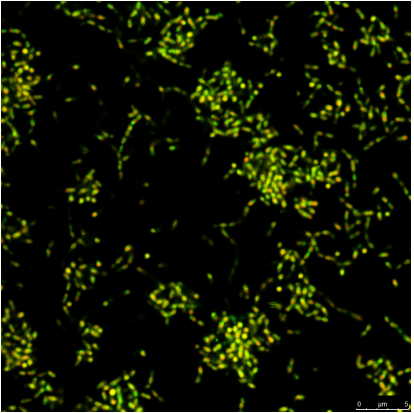
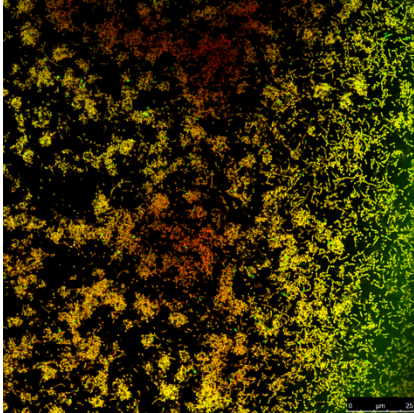
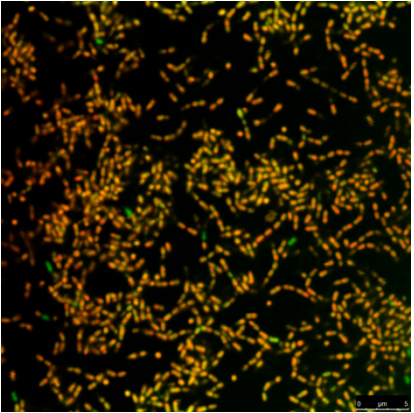


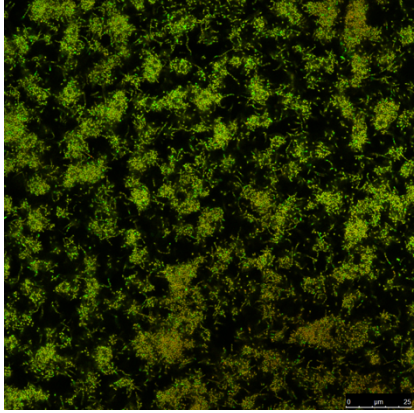
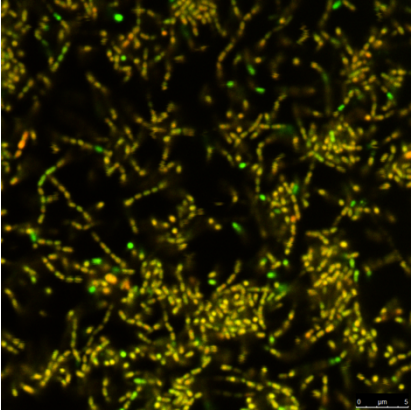


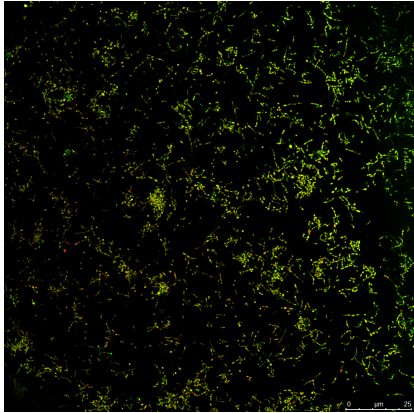
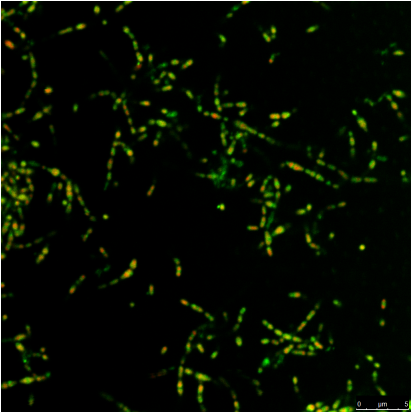
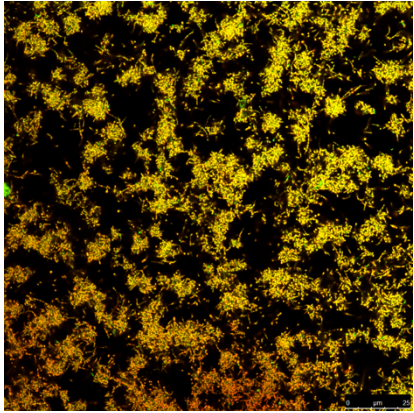
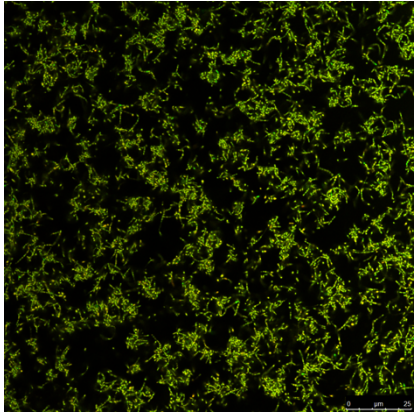
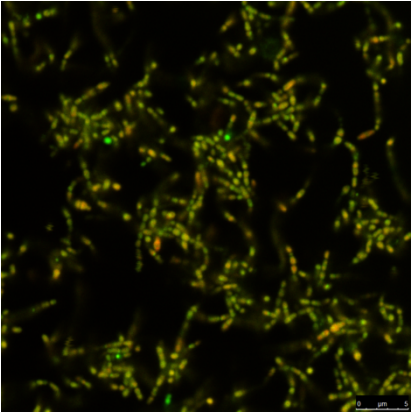


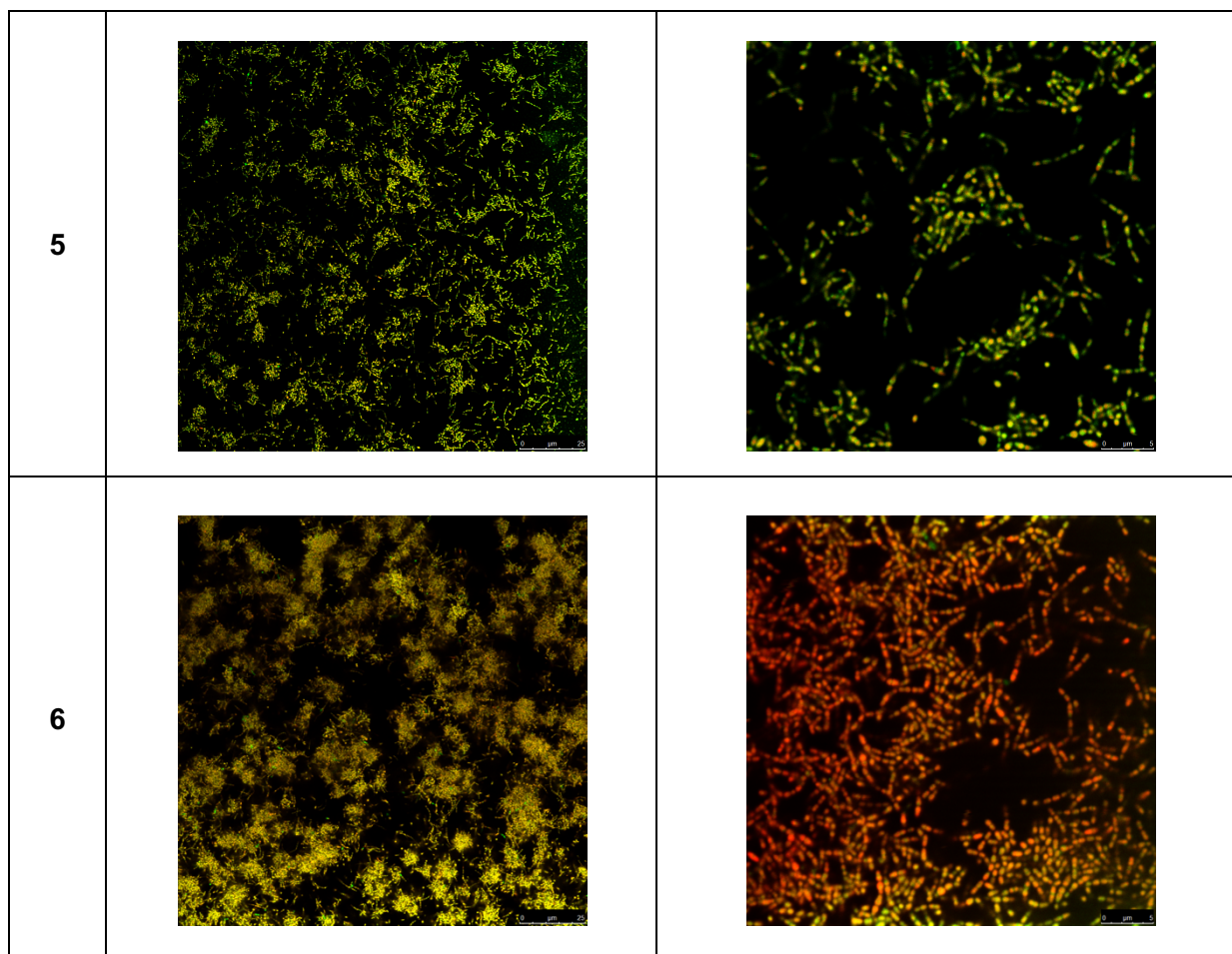
(-)-D3



2		
3		

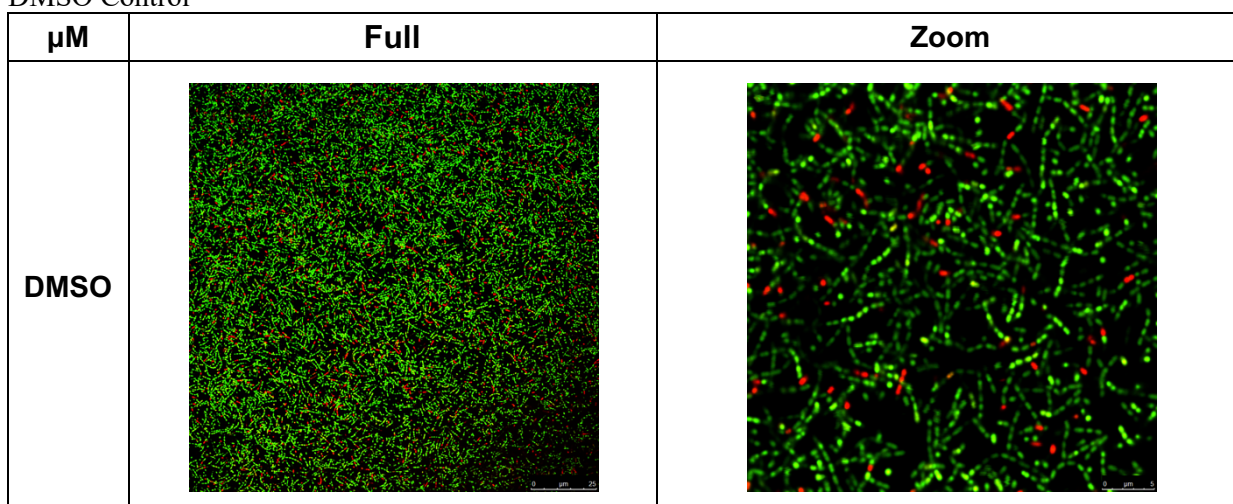
Trial	Full (250 μ M)	Zoom (250 μ M)
1		

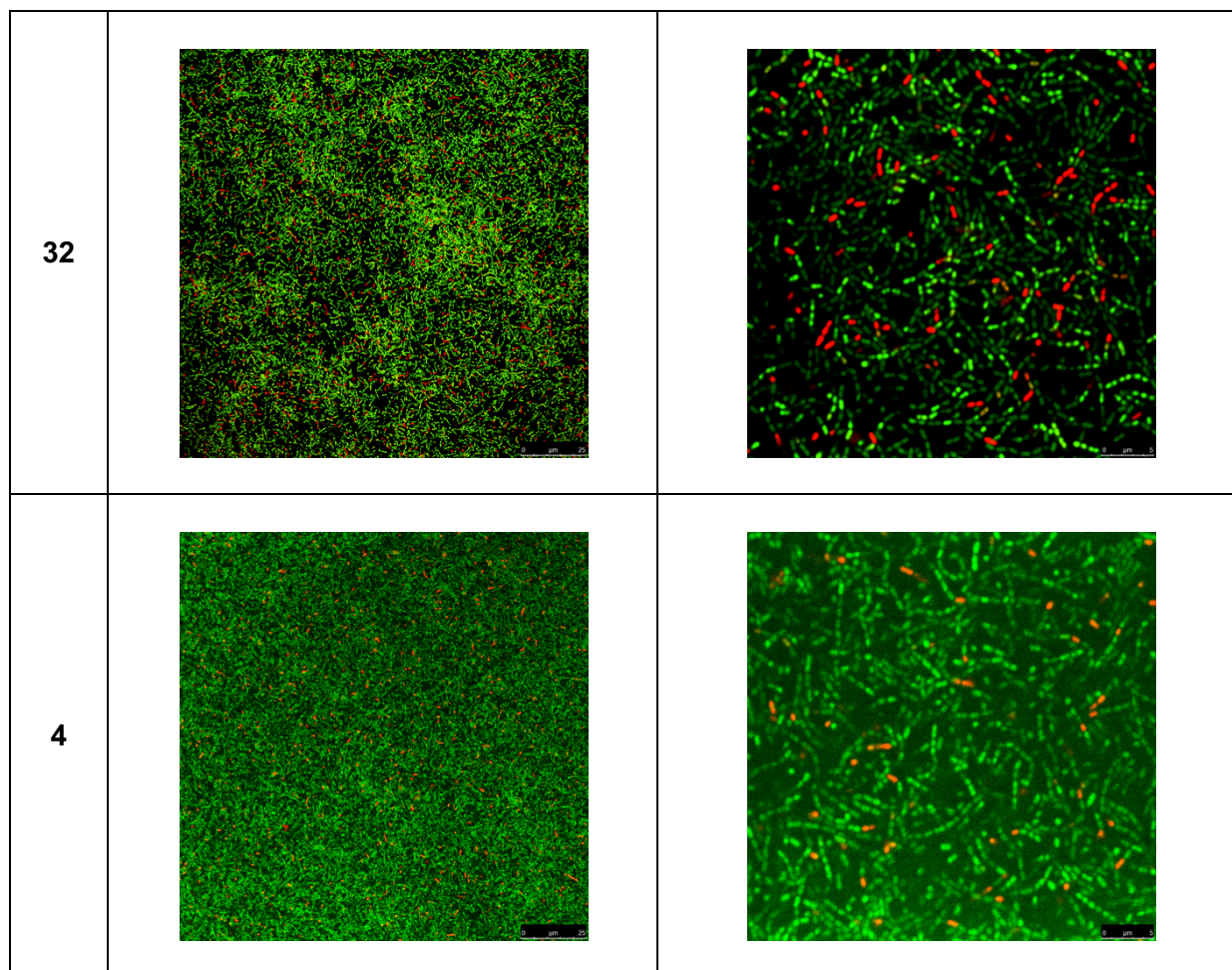
2		
3		
Trial	Full (250 μ M)	Zoom (250 μ M)
4		

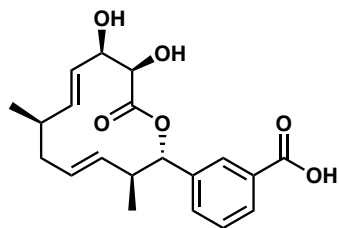


5.2.2 Concentrations 125 μ M to 0.5 μ M

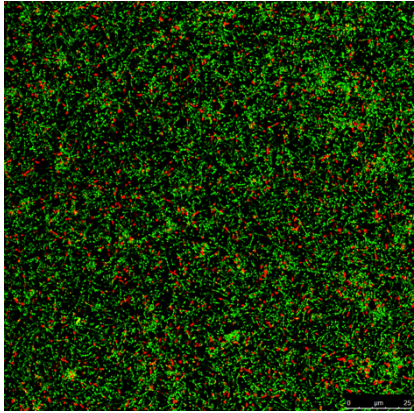
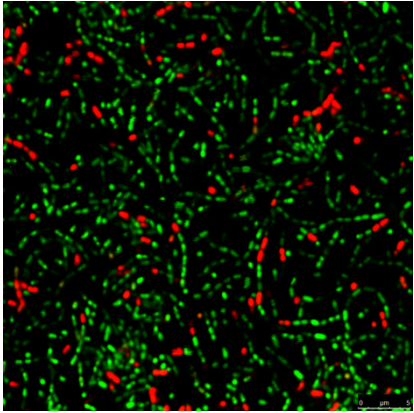
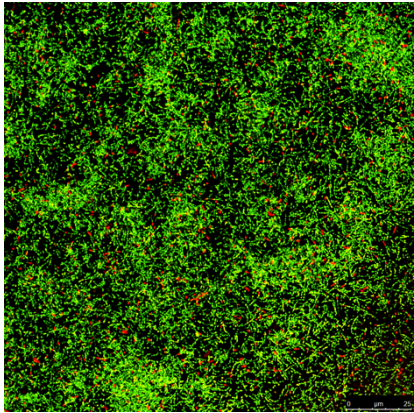
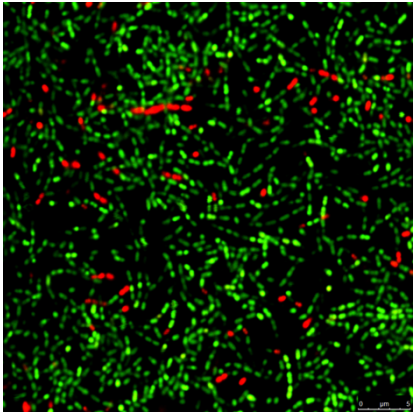
DMSO Control

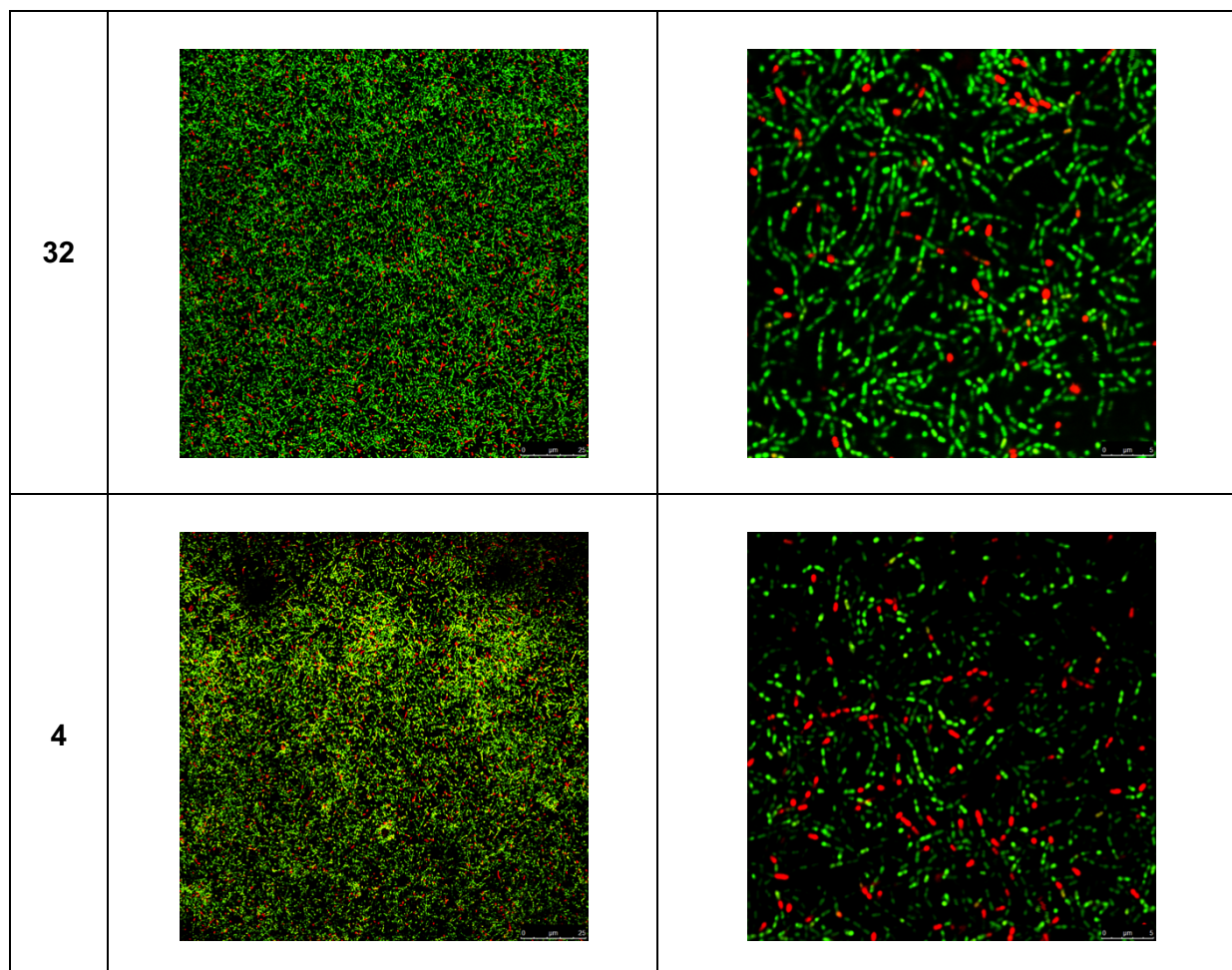


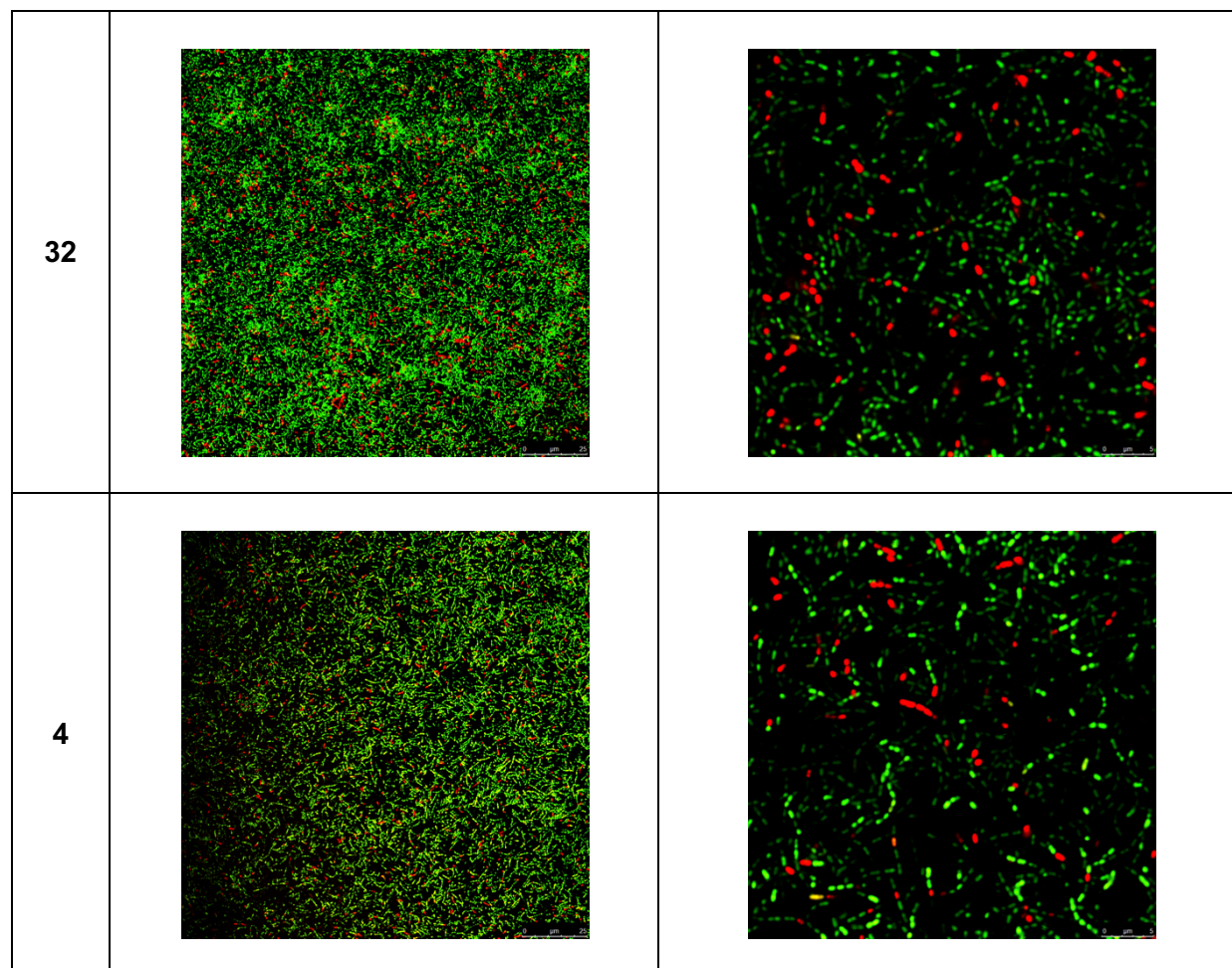


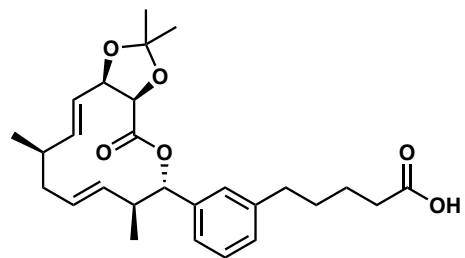


(-)-D1

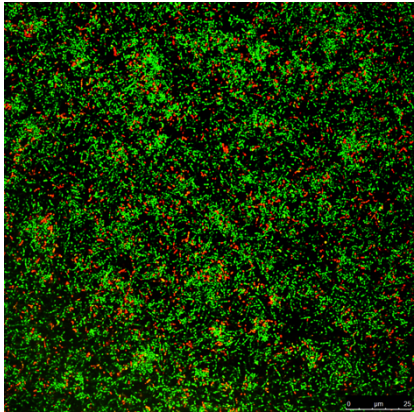
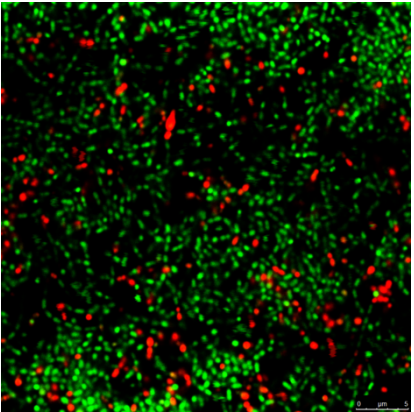
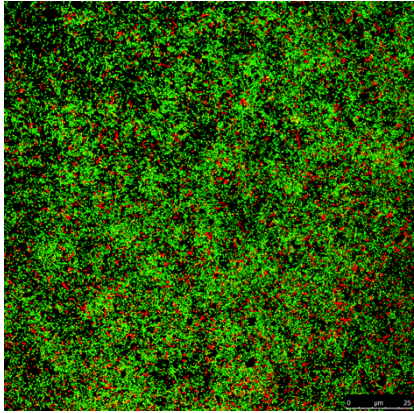
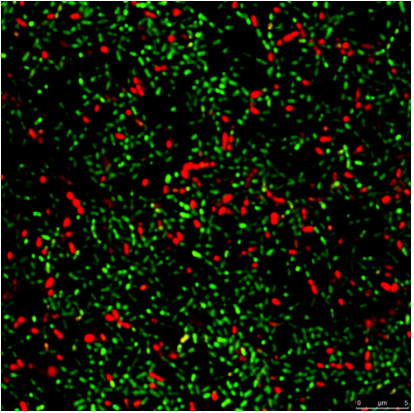
μM	Full	Zoom
125		
63		

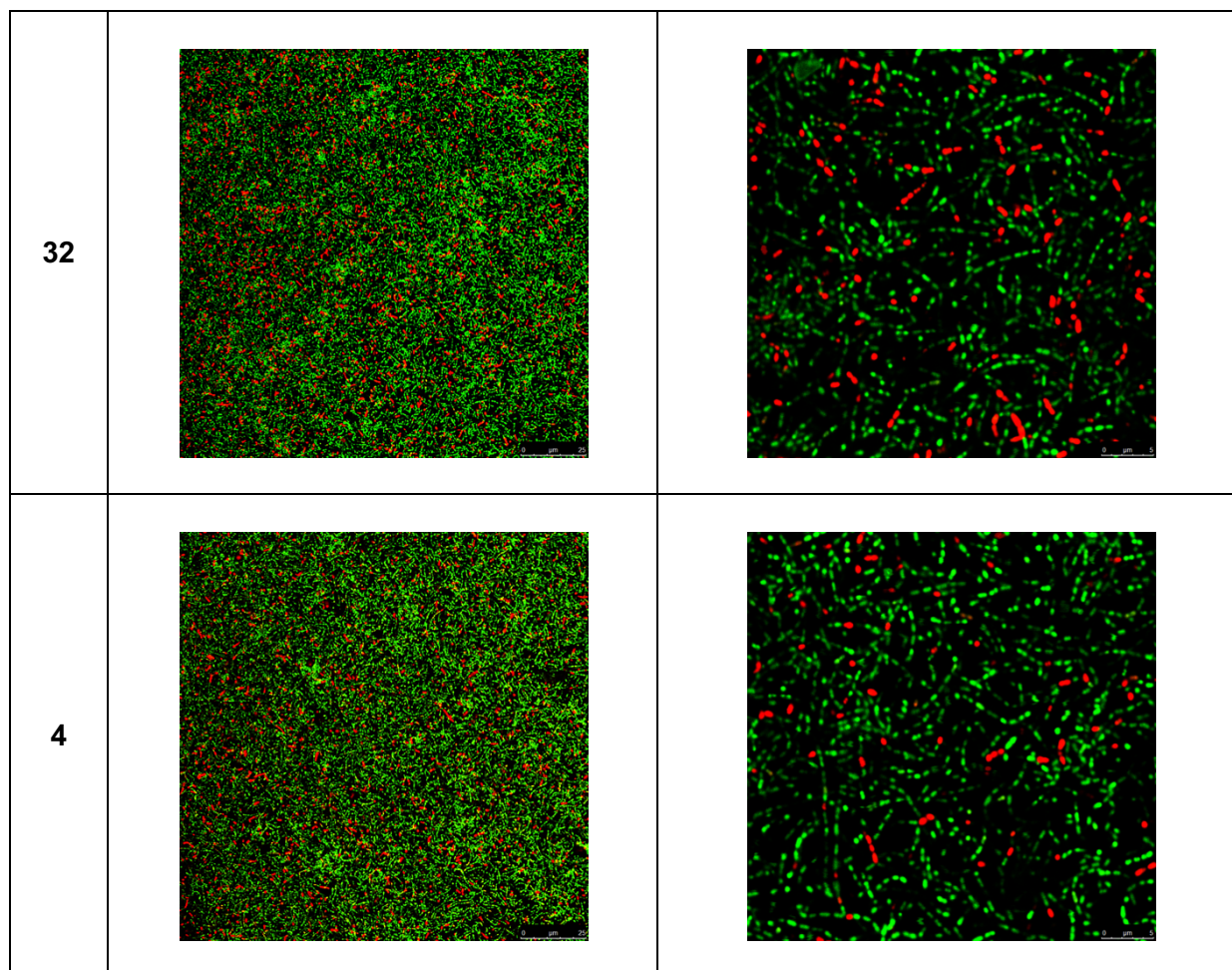


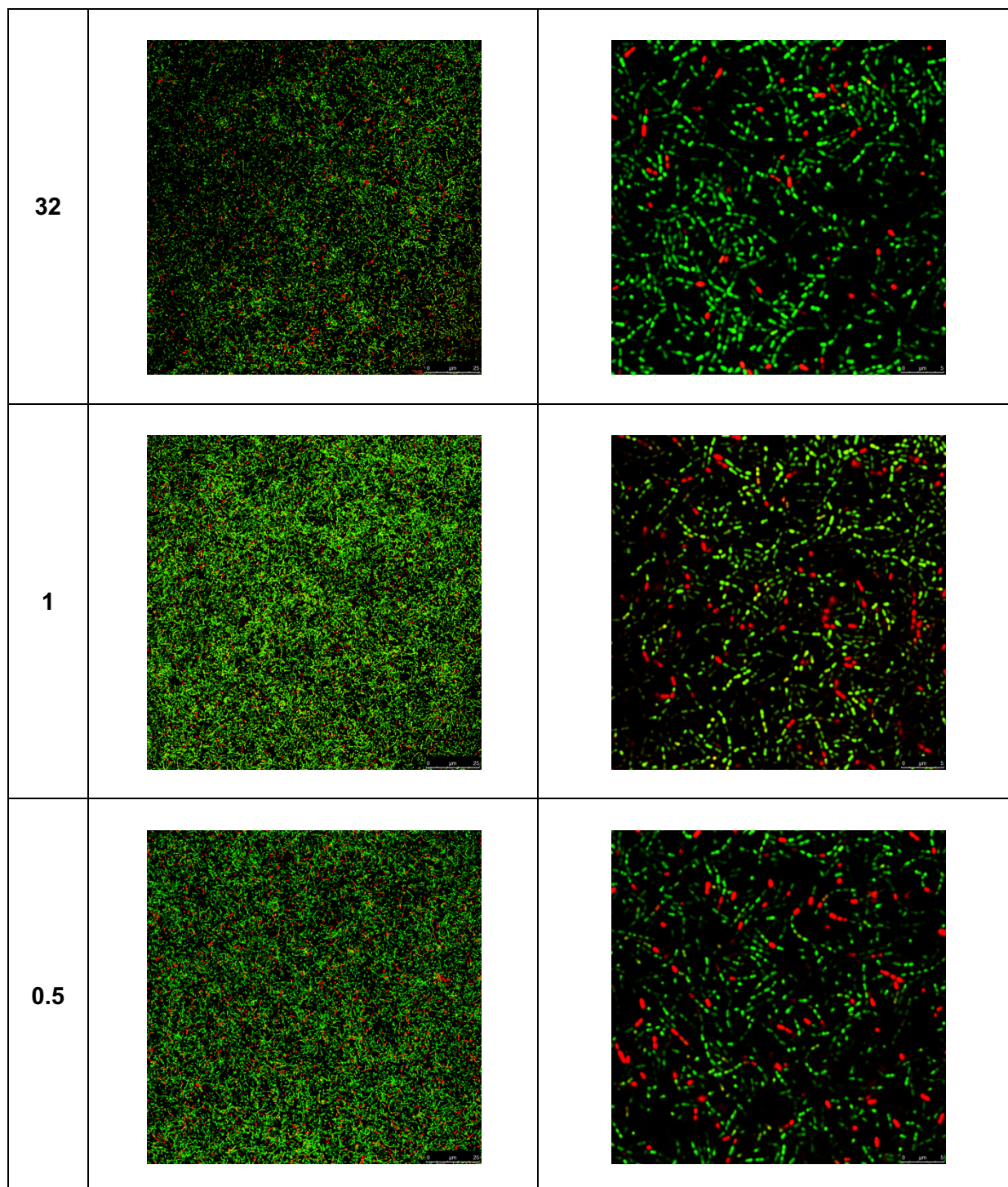


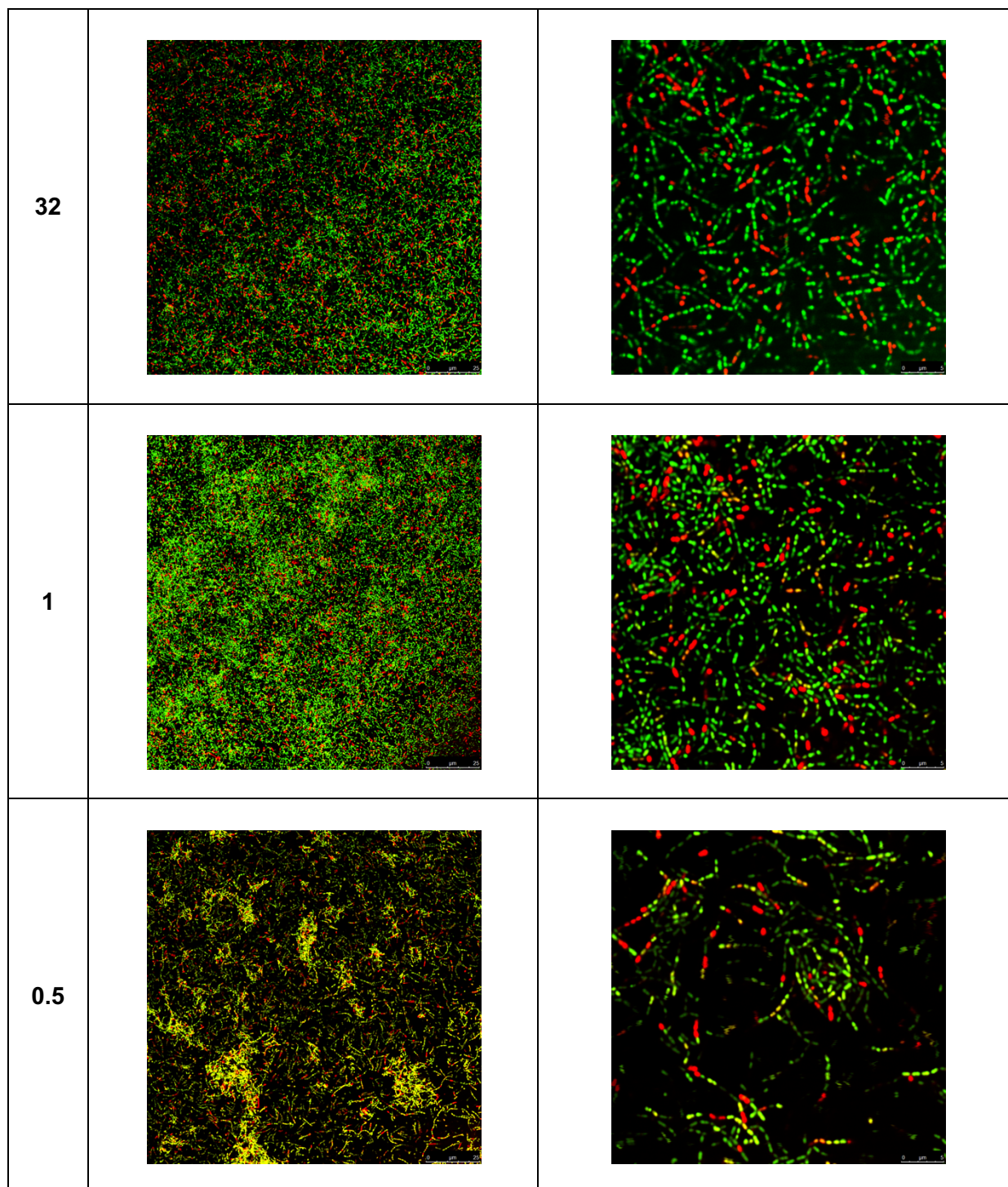


(-)-C3

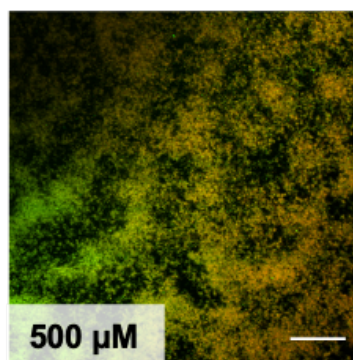
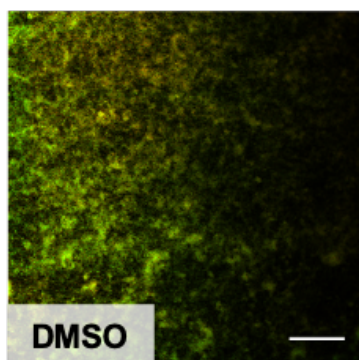
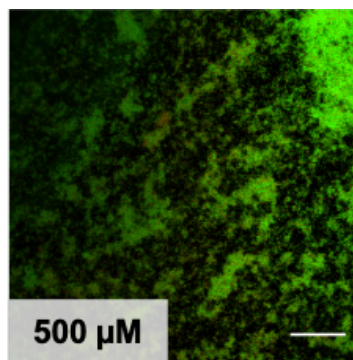
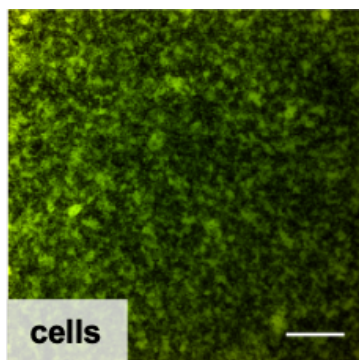
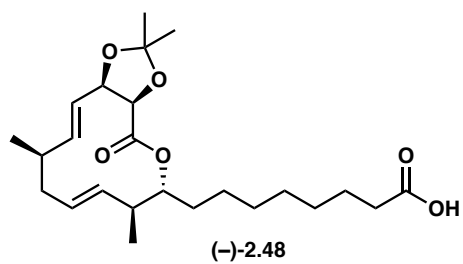
μM	Full	Zoom
125		
63		



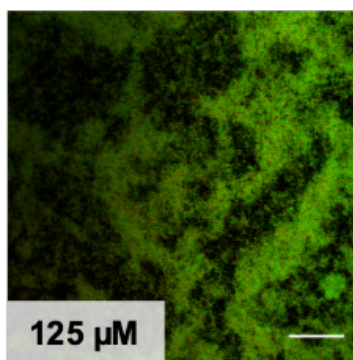


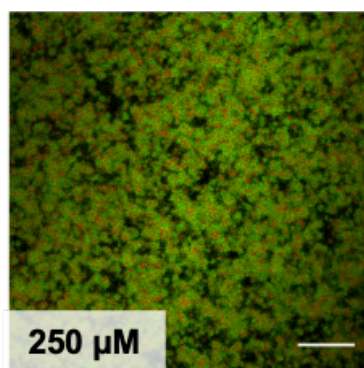
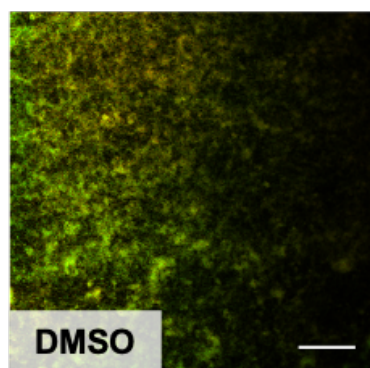
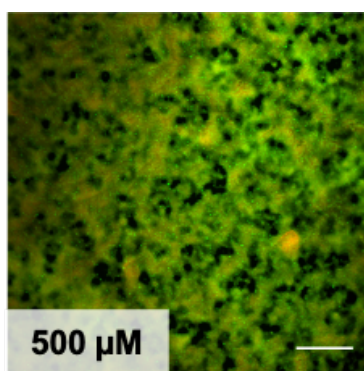
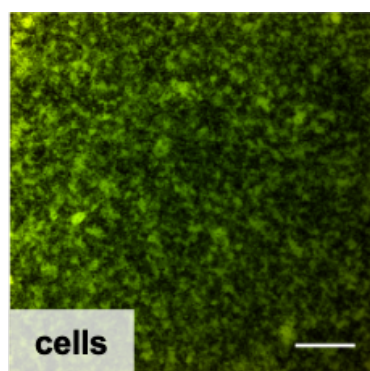
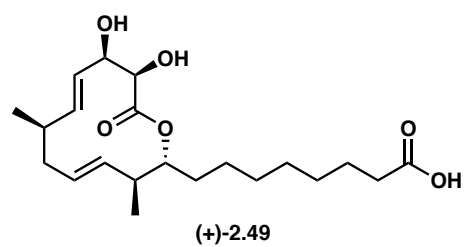


5.3 Biofilm Replicates Generation 2 (Simplified)

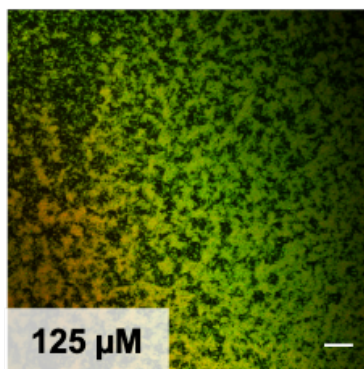


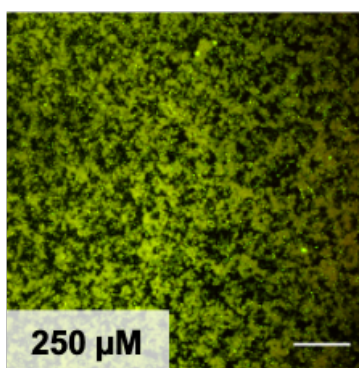
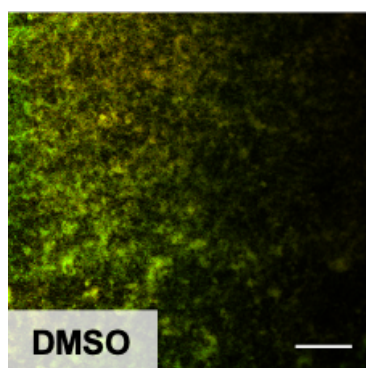
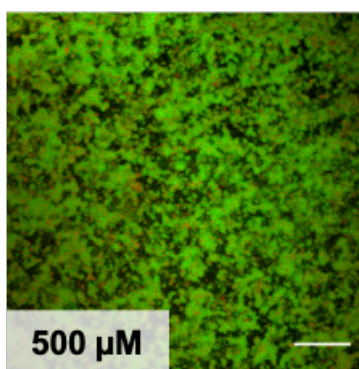
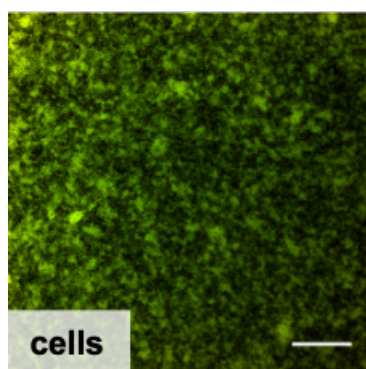
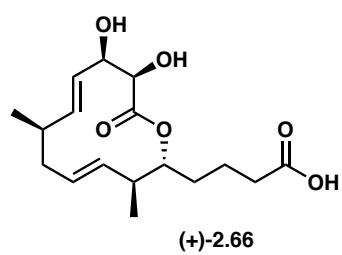
(-)-2.48
20 X optical lens.
Scale bar is 100 μ m.



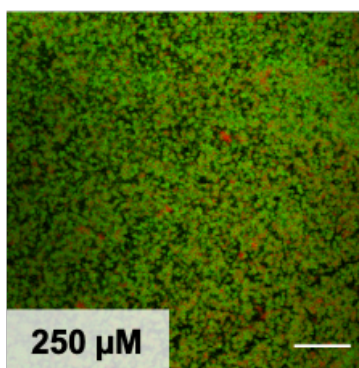


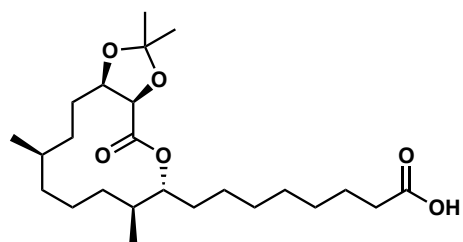
(+)-2.49
20 X optical lens.
Scale bar is 100 μm.



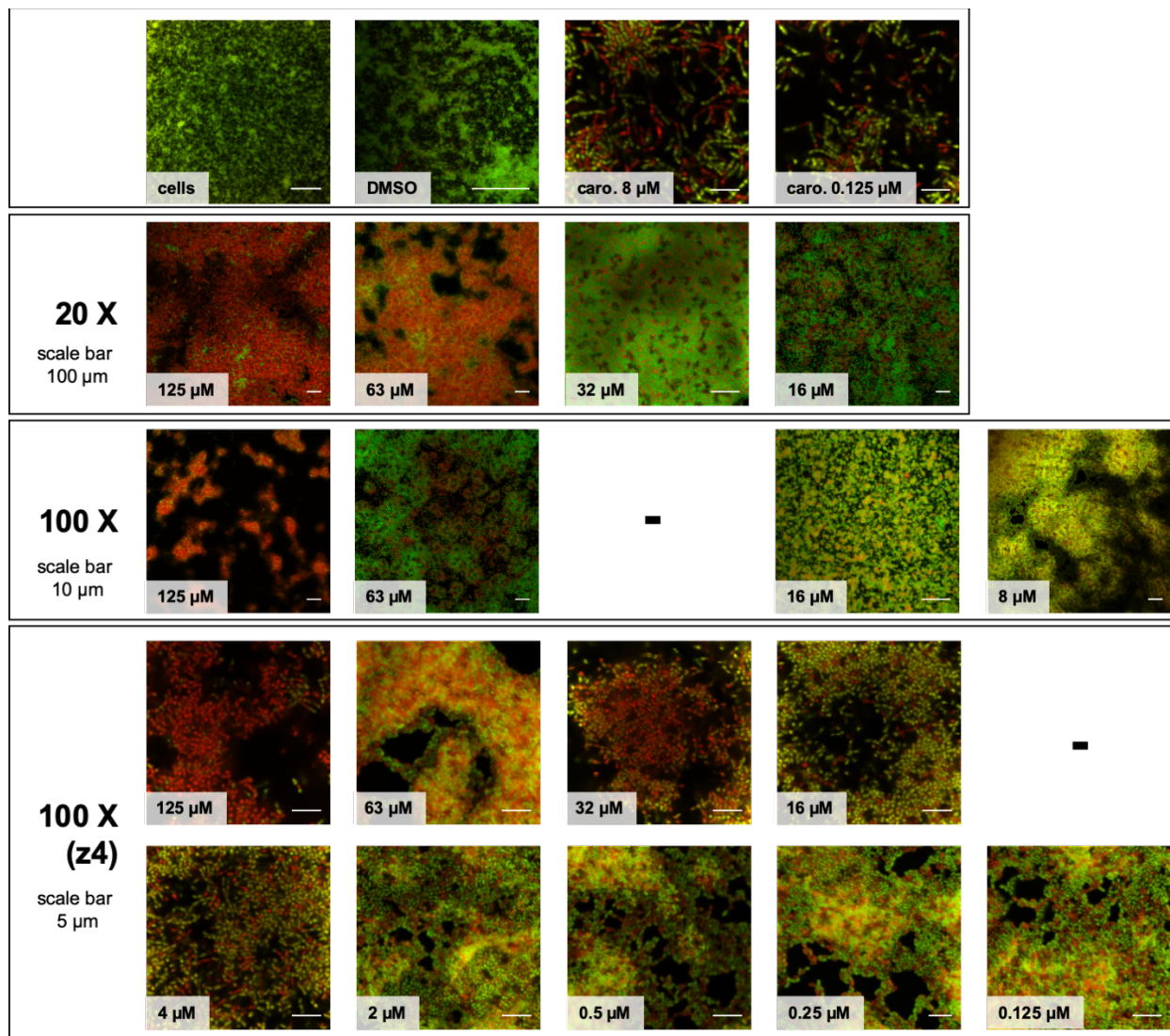


(+)-2.66
20 X optical lens.
Scale bar is 100 μ m.



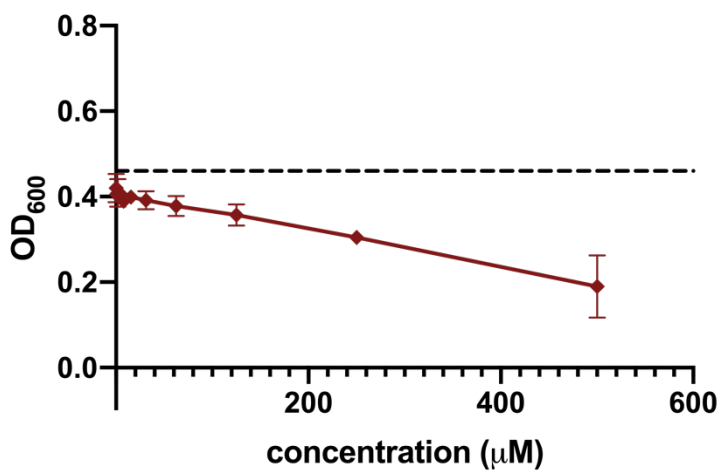


(+)-2.51
"analog 2"

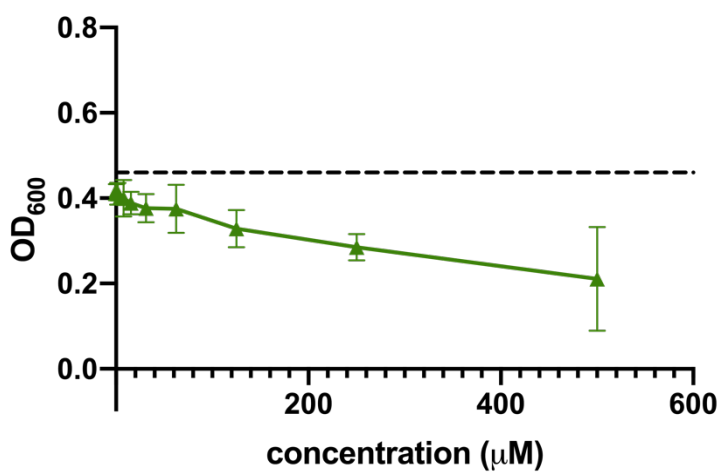


5.4 Carolacton Generation 2 IC₅₀ Curves

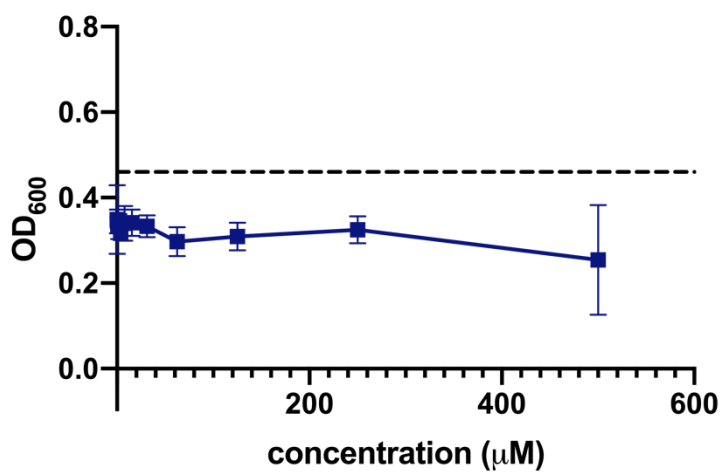
Bacteria: *S. mutans* **Growth Conditions:** THB Media **Compound:** carolacton



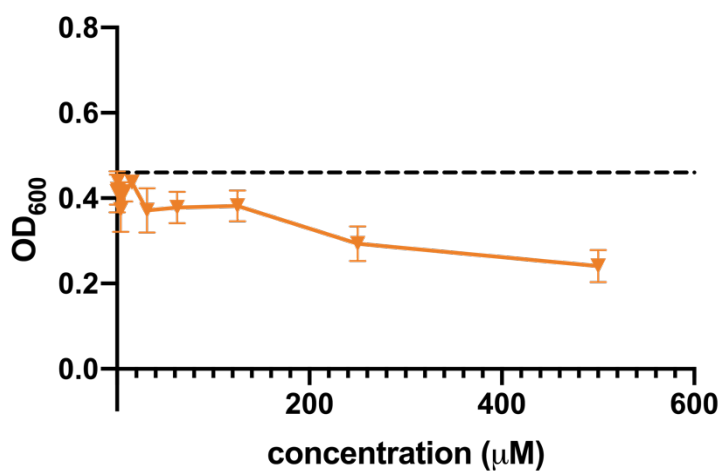
Bacteria: *S. mutans* **Growth Conditions:** THB Media **Compound:** C3



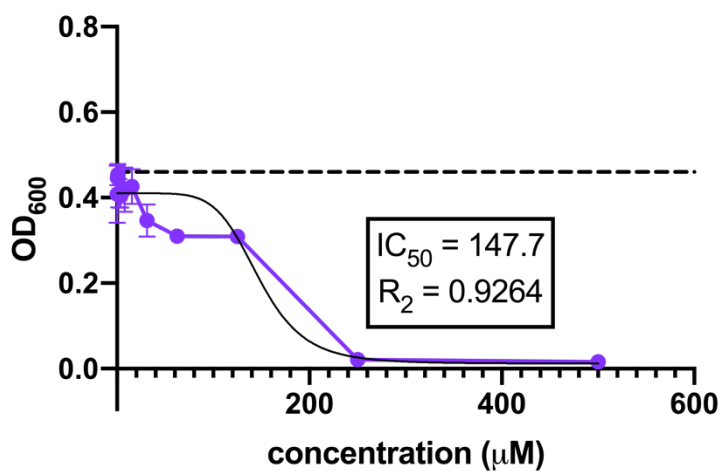
Bacteria: *S. mutans* **Growth Conditions:** THB Media **Compound:** (-)-2.48



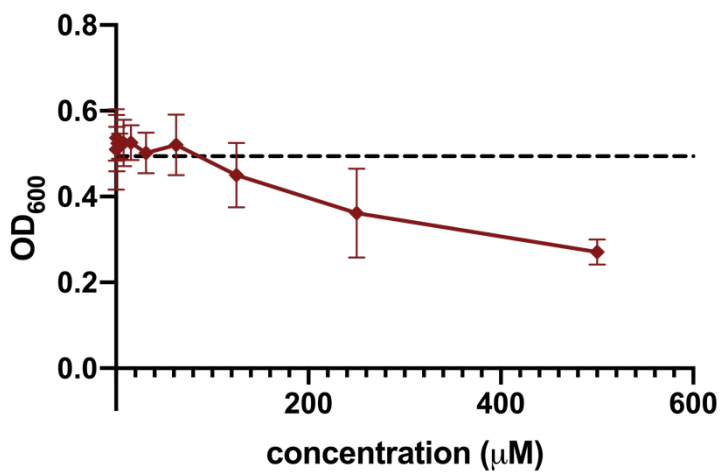
Bacteria: *S. mutans* **Growth Conditions:** THB Media **Compound:** (+)-2.49



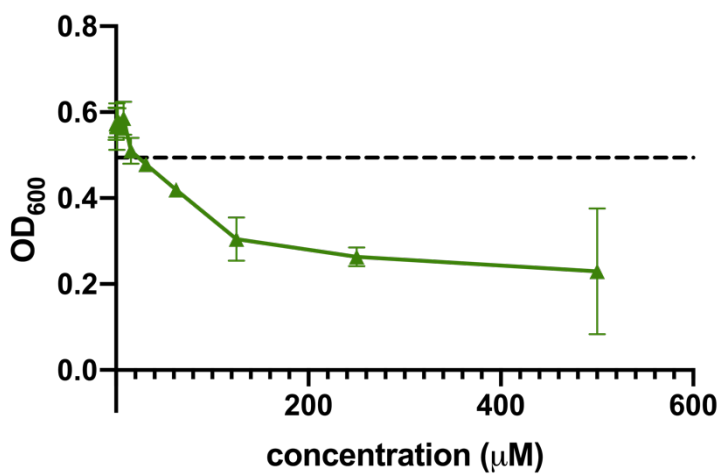
Bacteria: *S. mutans* **Growth Conditions:** THB Media **Compound:** analog 2



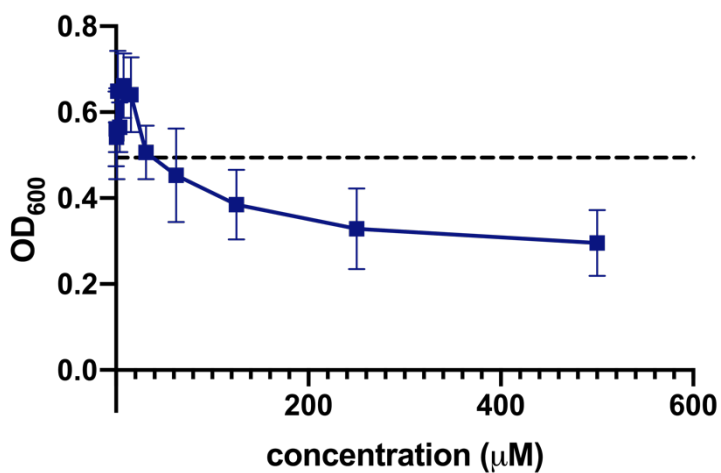
Bacteria: *S. mutans* **Growth Conditions:** THB Media + 0.1% sucrose **Compound:** carolacton



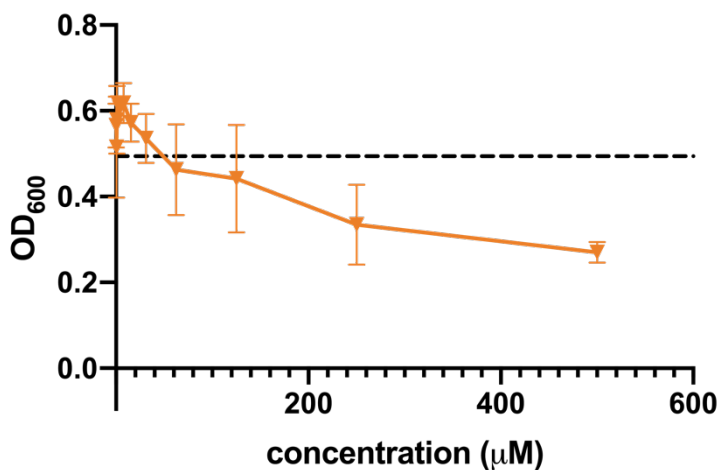
Bacteria: *S. mutans* **Growth Conditions:** THB Media + 0.1% sucrose **Compound:** C3



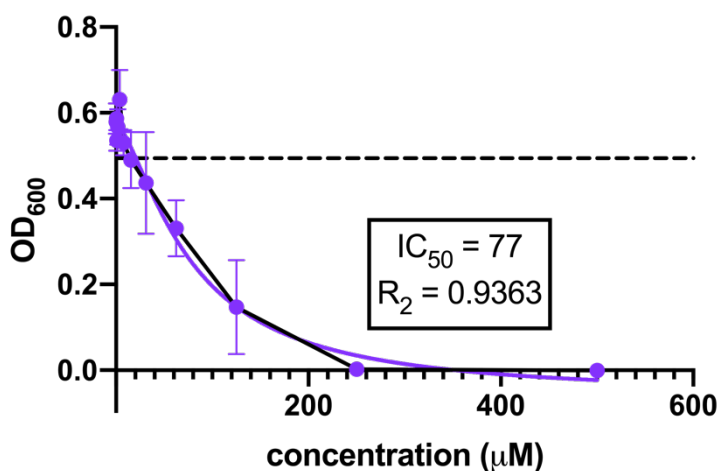
Bacteria: *S. mutans* **Growth Conditions:** THB Media + 0.1% sucrose **Compound:** (-)-2.48



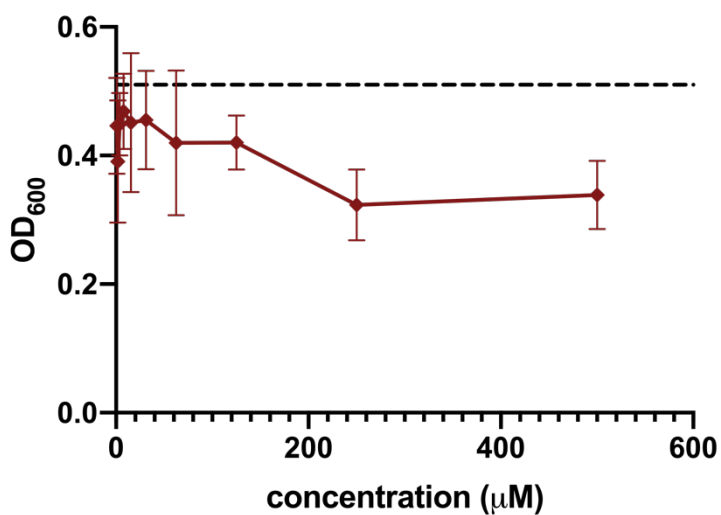
Bacteria: *S. mutans* **Growth Conditions:** THB Media + 0.1% sucrose **Compound:** (+)-2.49



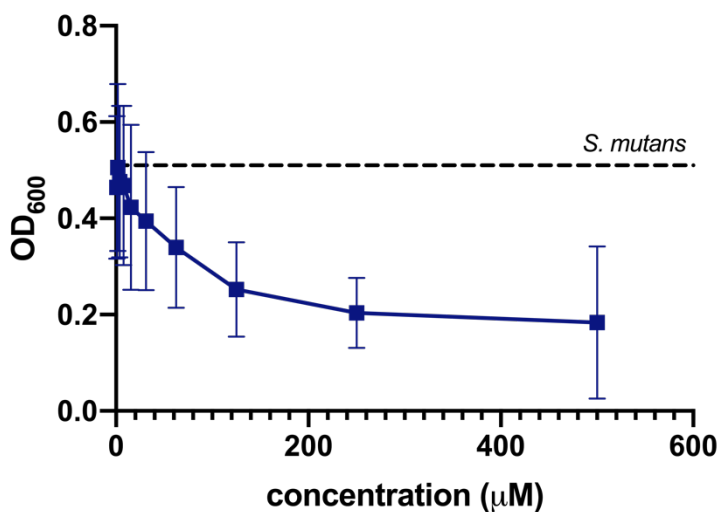
Bacteria: *S. mutans* **Growth Conditions:** THB Media + 0.1% sucrose **Compound:** analog 2



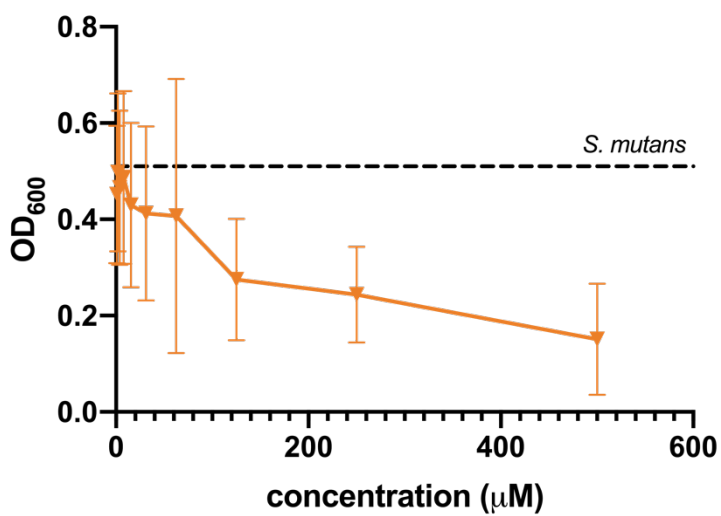
Bacteria: *S. mutans* **Growth Conditions:** THB + 0.1% sucrose + glass bottom 96-well plate
Compound: carolacton



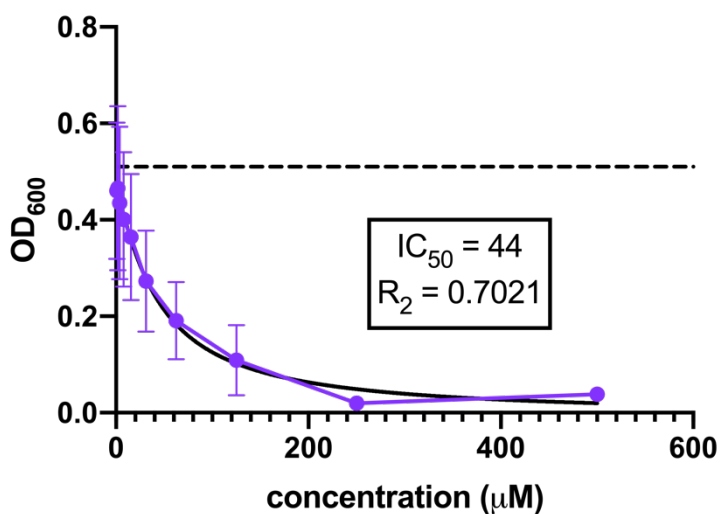
Bacteria: *S. mutans* **Growth Conditions:** THB + 0.1% sucrose + glass bottom 96-well plate
Compound: (-)-2.48



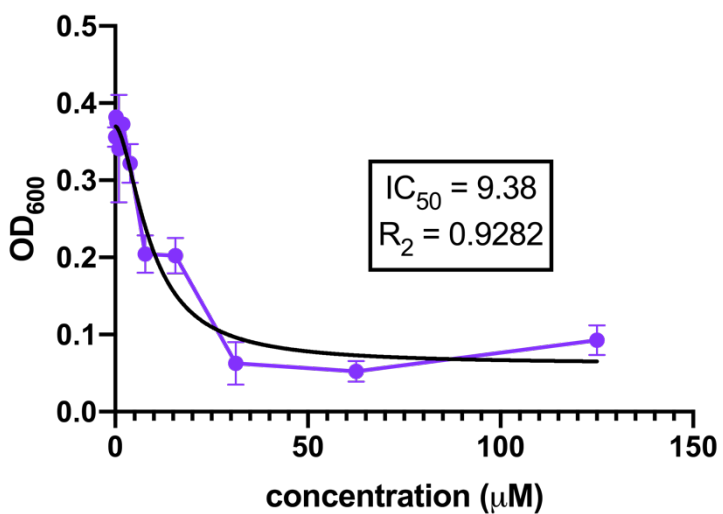
Bacteria: *S. mutans* **Growth Conditions:** THB + 0.1% sucrose + glass bottom 96-well plate
Compound: (+)-2.49



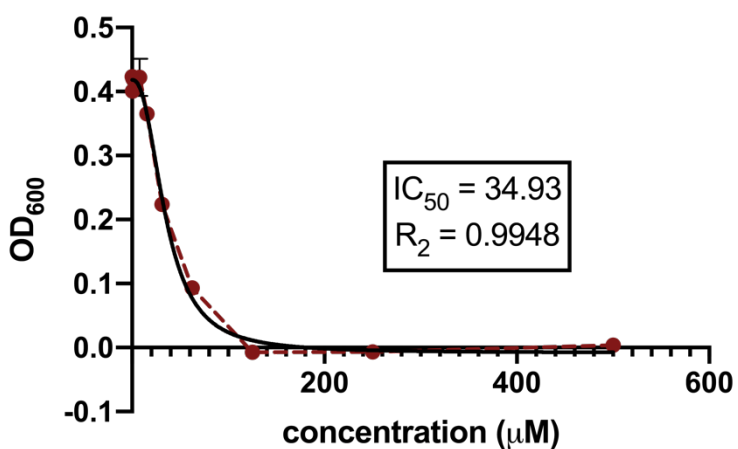
Bacteria: *S. mutans* **Growth Conditions:** THB + 0.1% sucrose + glass bottom 96-well plate
Compound: analog 2



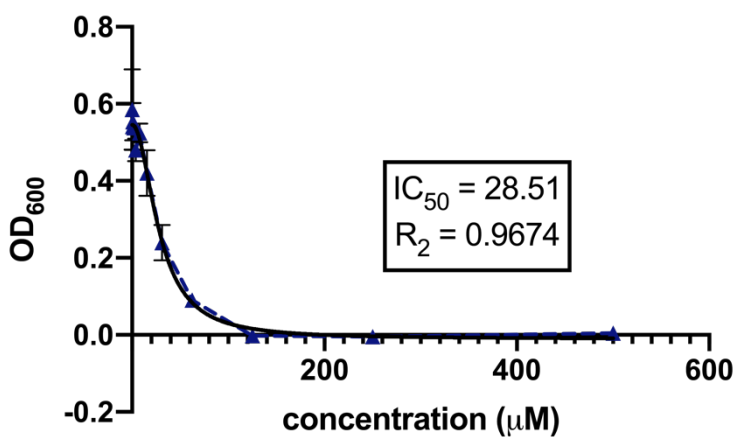
Bacteria: *S. mutans* **Growth Conditions:** THB; pH 5 **Compound:** analog 2



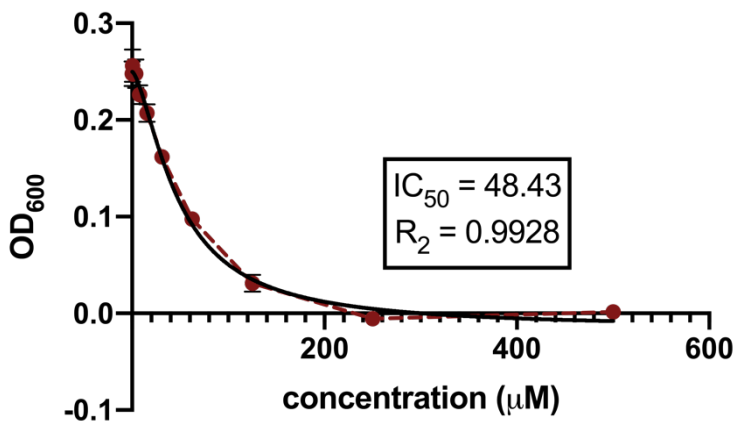
Bacteria: *S. gordonii* **Growth Conditions:** THB **Compound:** analog 2



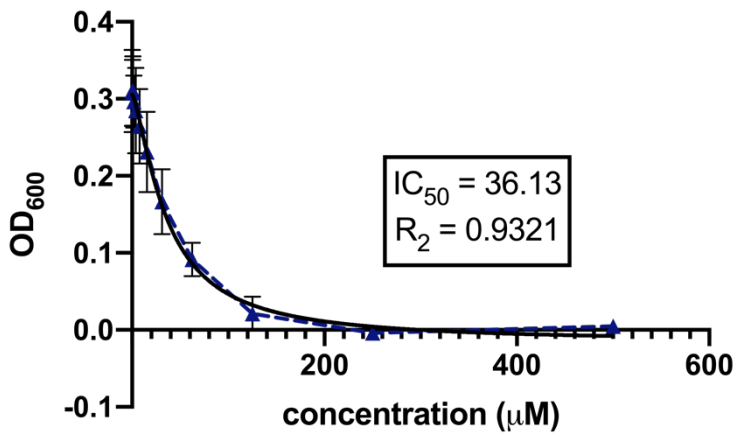
Bacteria: *S. gordonii* **Growth Conditions:** THB + 0.1% sucrose **Compound:** analog 2



Bacteria: *S. sanguinis* **Growth Conditions:** THB **Compound:** analog 2

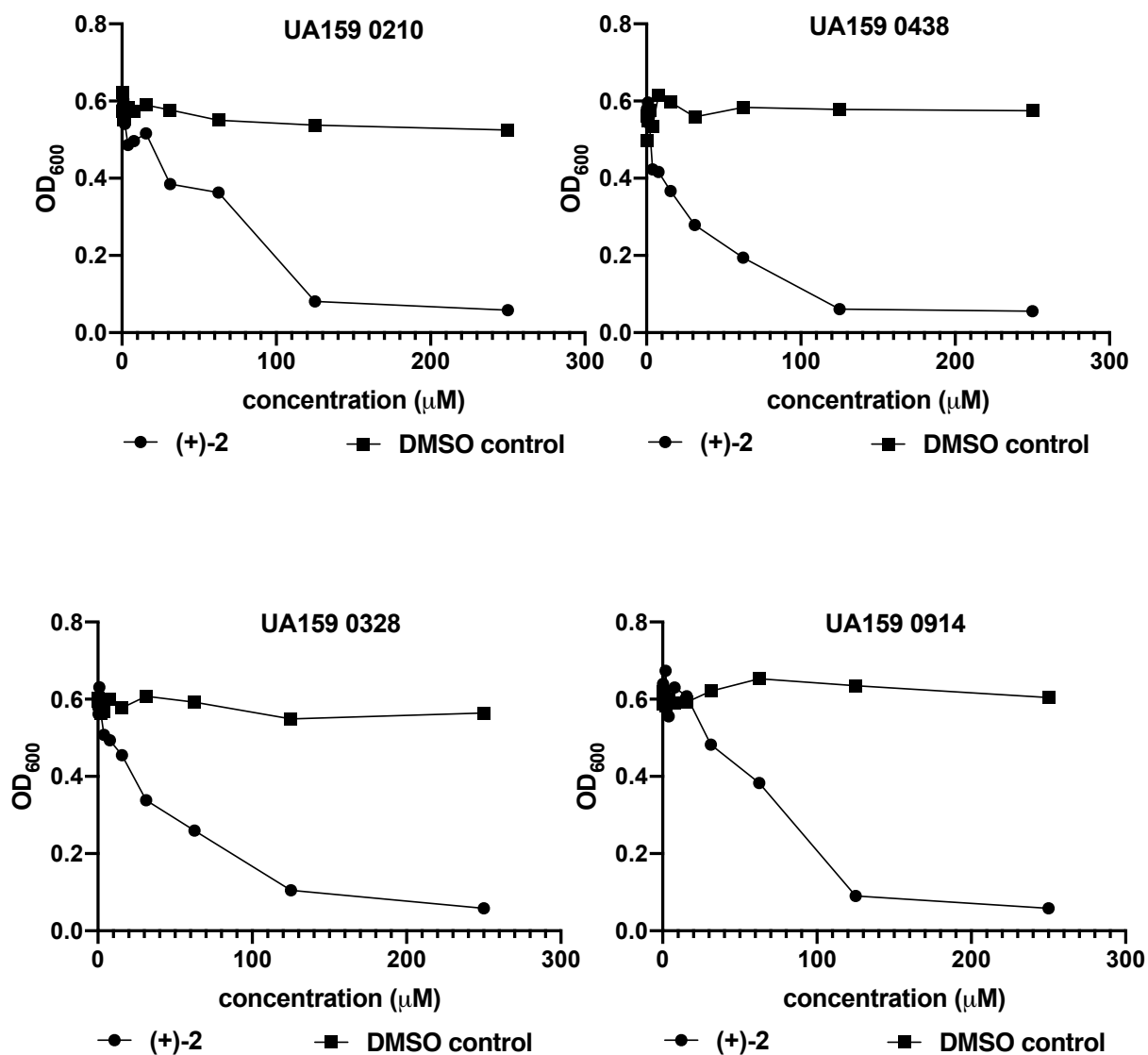


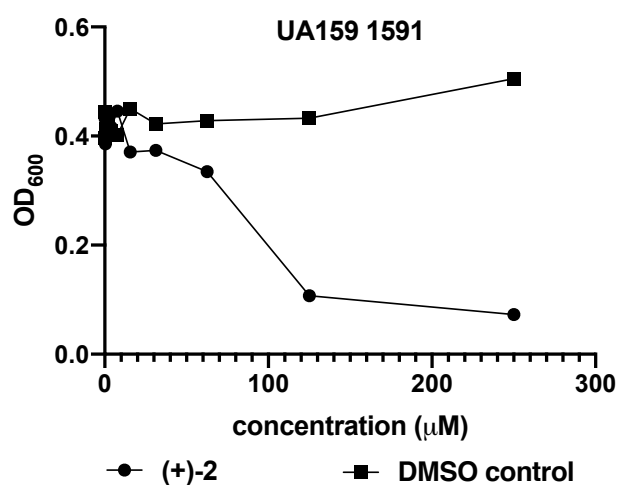
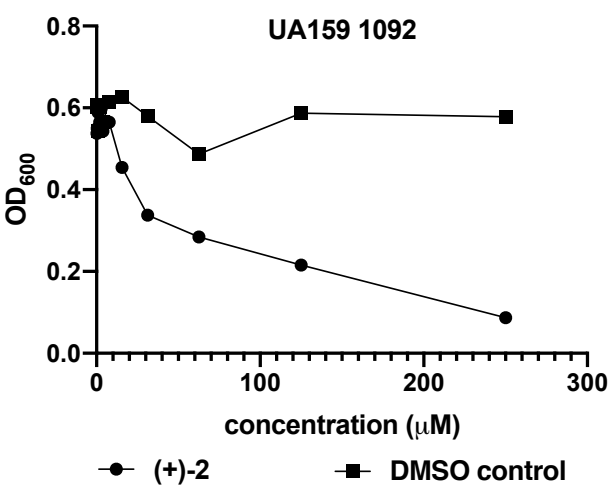
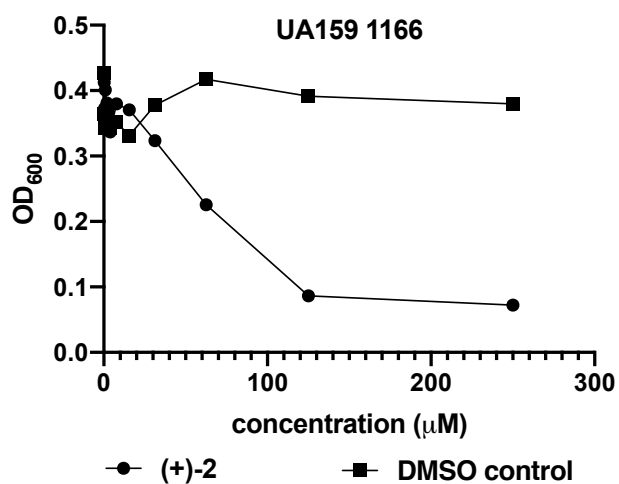
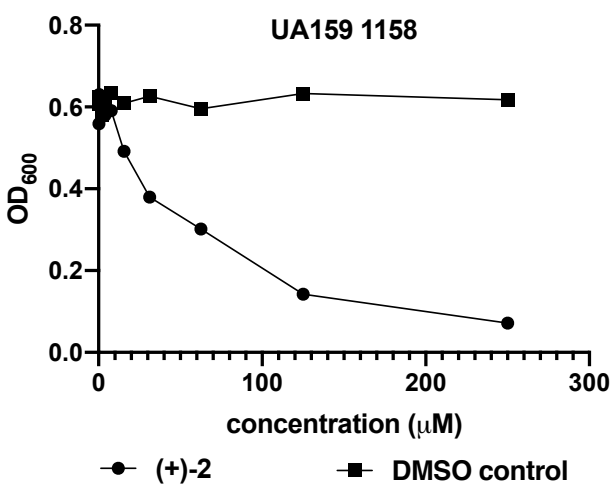
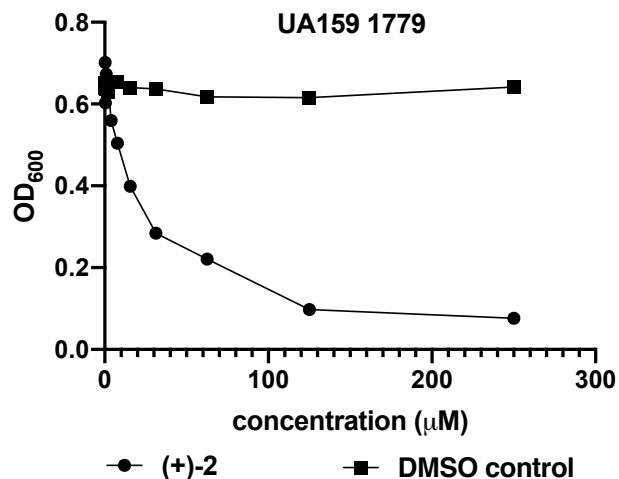
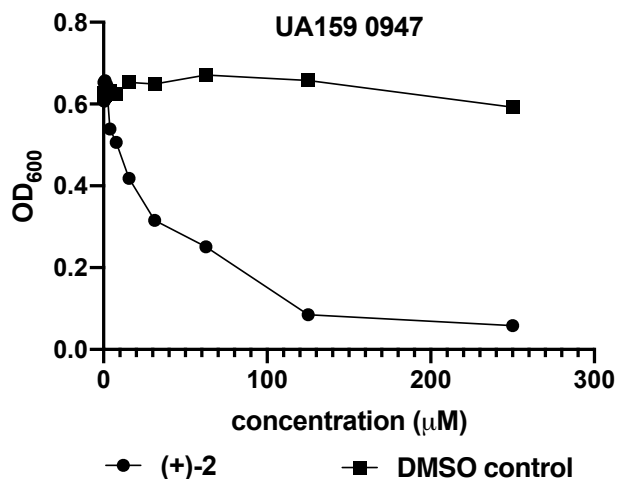
Bacteria: *S. sanguinis* **Growth Conditions:** THB + 0.1% sucrose **Compound:** analog 2

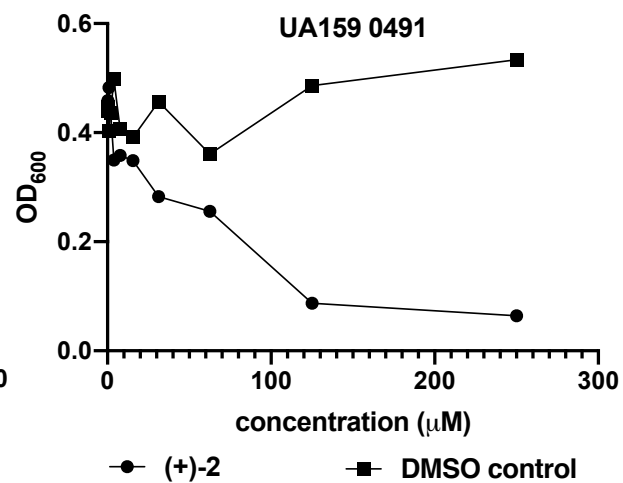
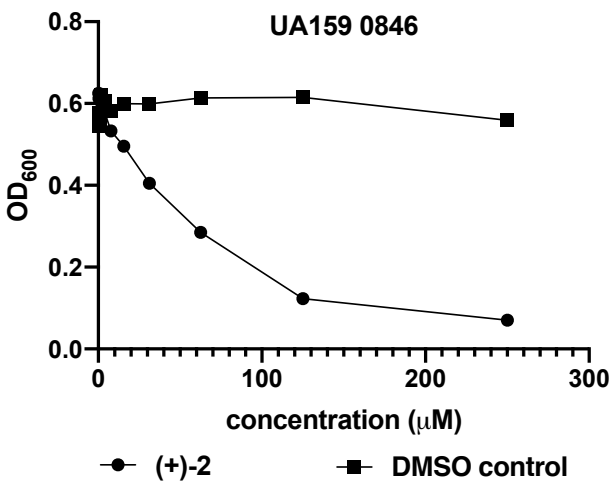
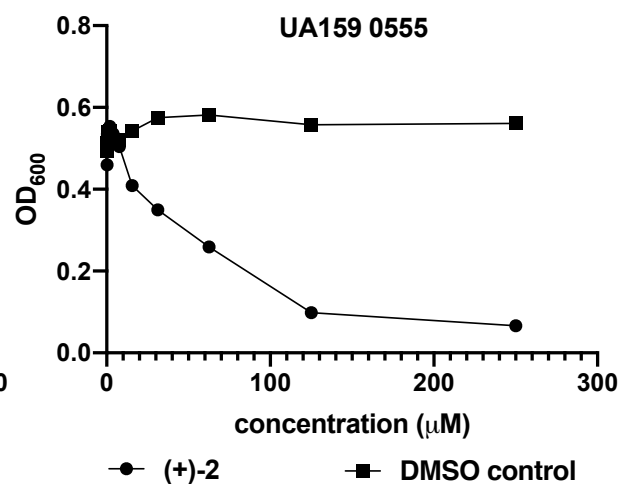
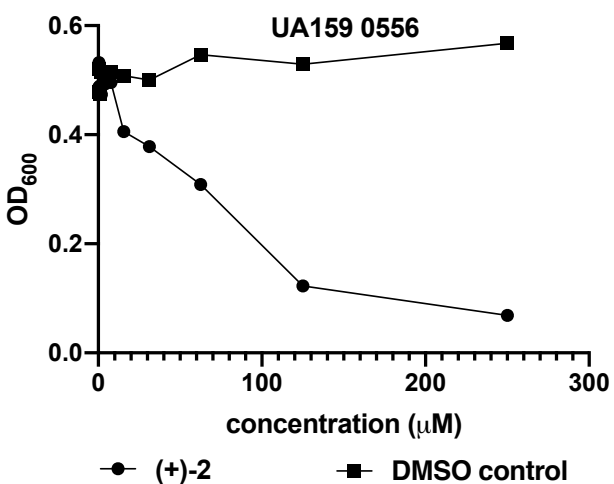
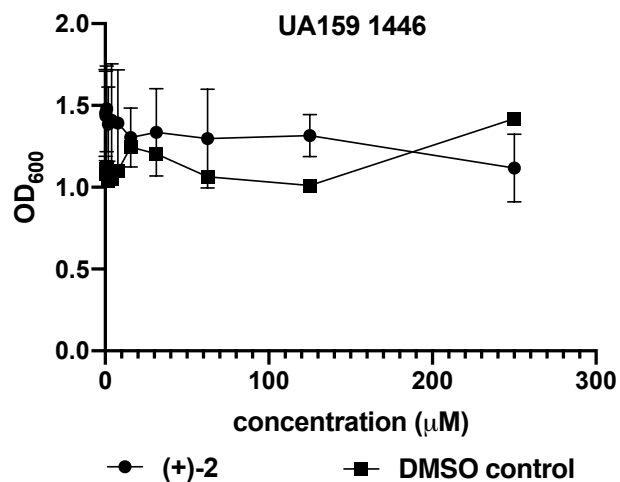
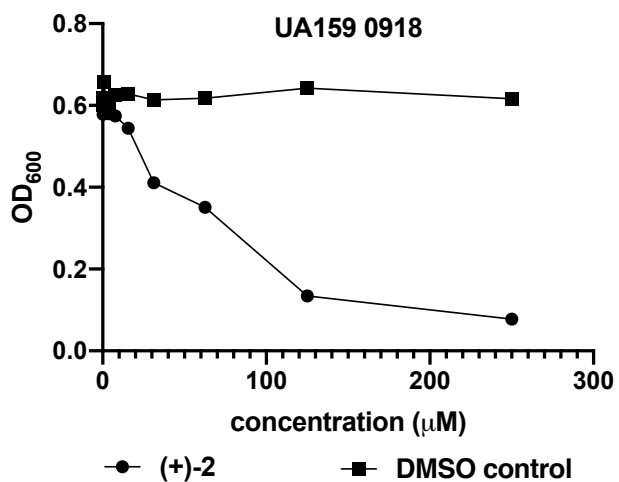


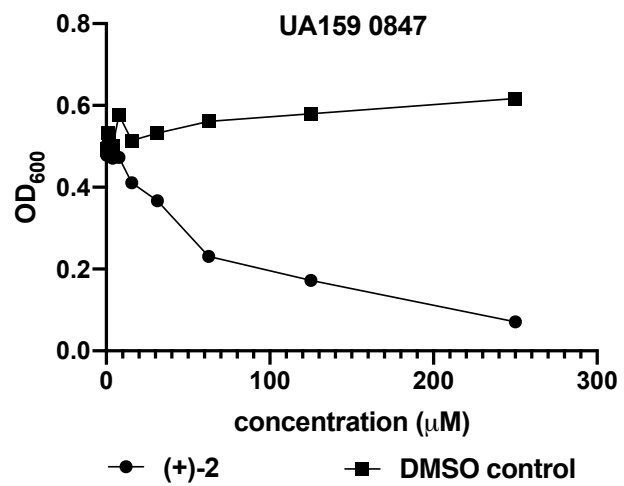
5.5 Analog 2 Mutant Screen

S. mutans mutants were screened against analog (+)-2. Strains were screened in biological triplicate with compound and with the DMSO vehicle (top). The % growth at 125 mL for all 17 mutants is shown (middle). “% growth” refers to (growth with compound/growth with vehicle*100).

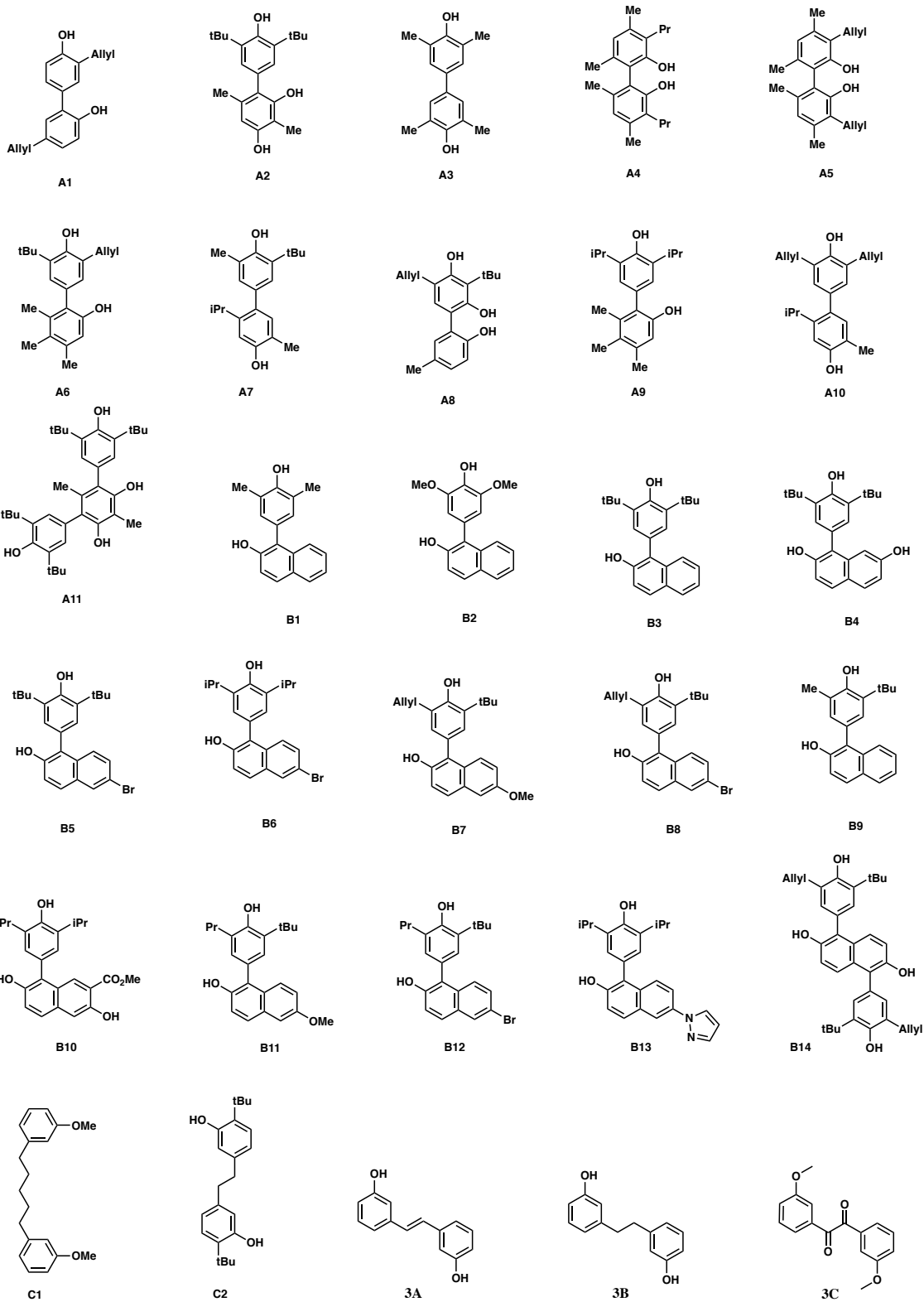


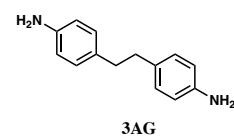
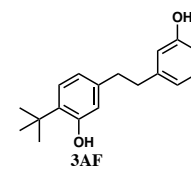
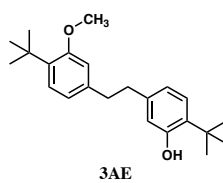
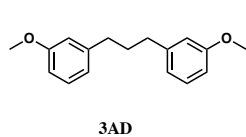
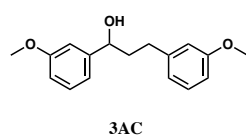
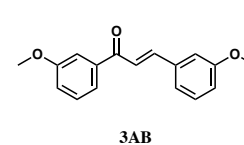
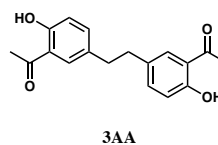
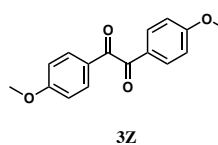
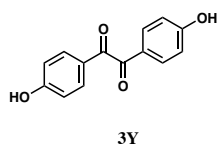
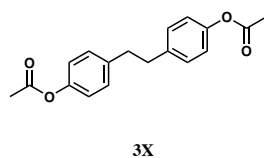
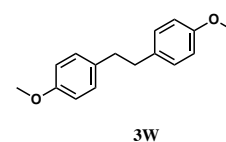
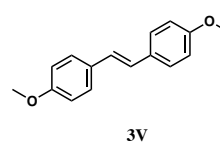
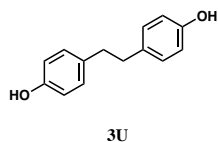
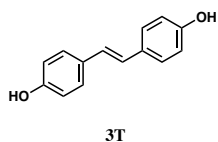
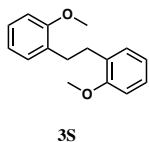
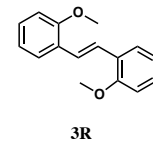
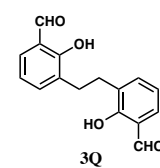
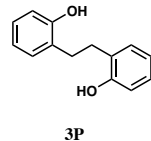
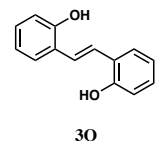
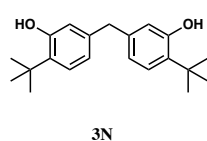
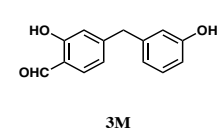
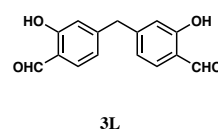
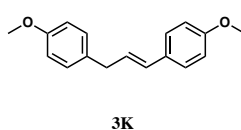
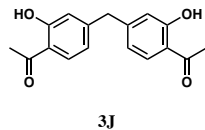
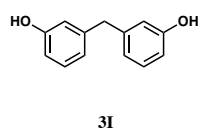
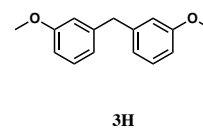
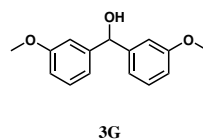
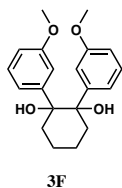
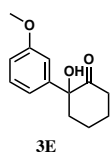
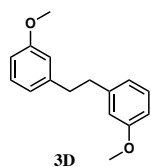


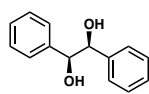




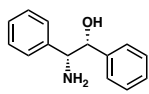
5.6 Honokiol Master Compound List



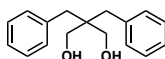




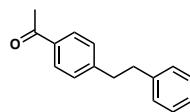
3AH



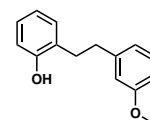
3AI



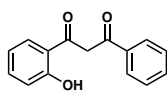
3AJ



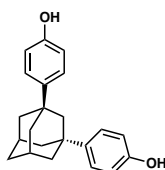
3AK



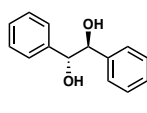
3AL



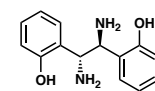
3AM



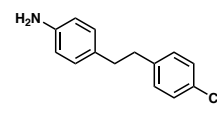
3AN



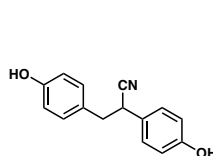
3AO



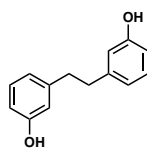
3AP



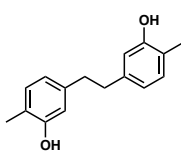
3AQ



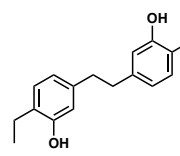
3AR



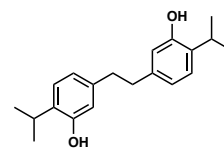
4A



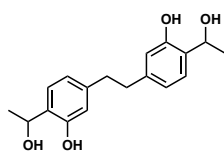
4B



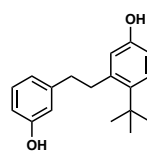
4C



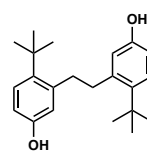
4D



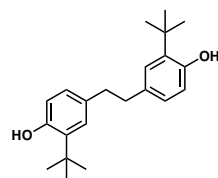
4E



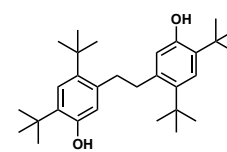
4F



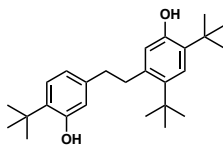
4G



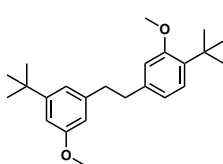
4H



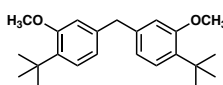
4I



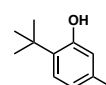
4J



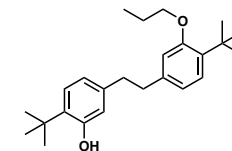
4K



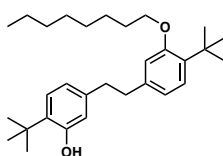
4L



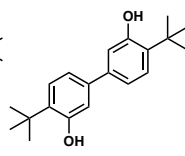
4M



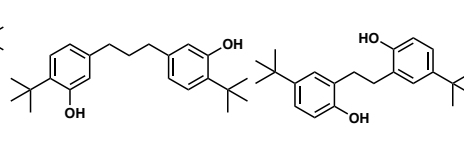
C2-propyl



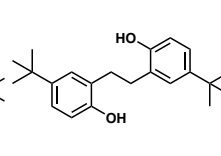
4O



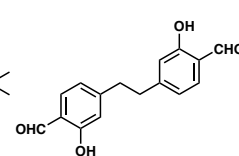
4P



4Q

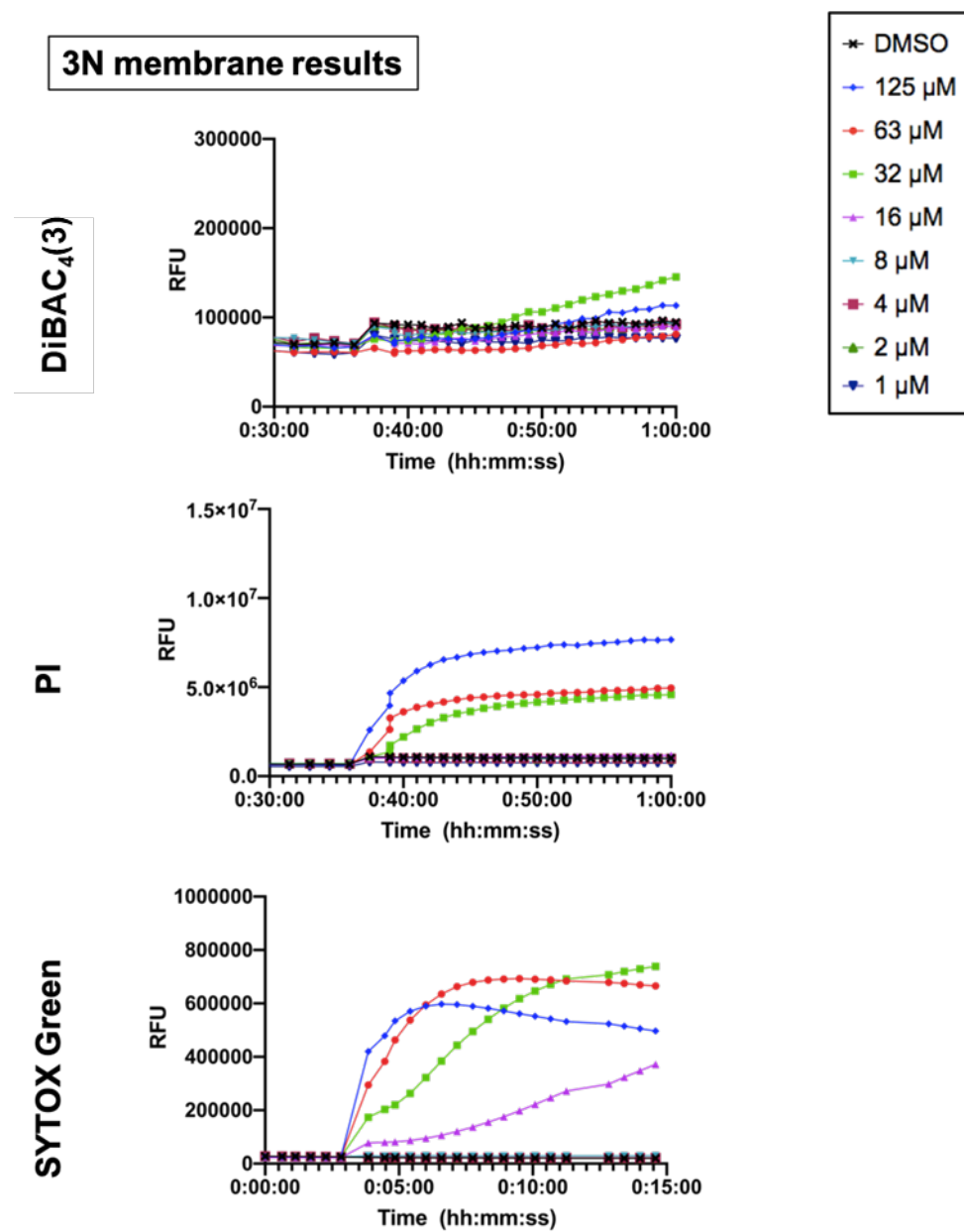


4R

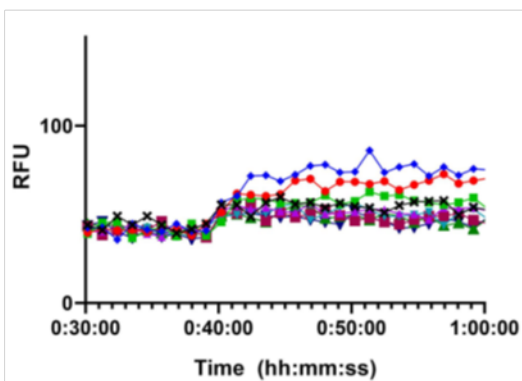


4N

5.7 Membrane Assay Data

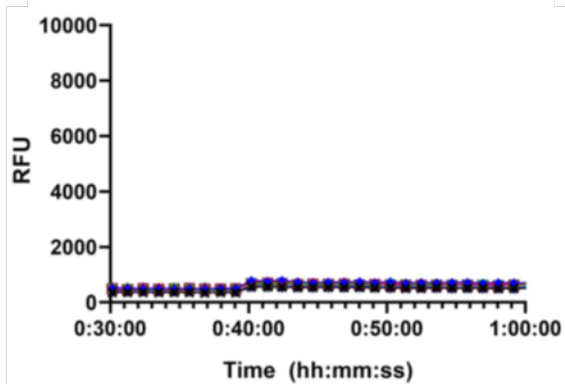


4B membrane results

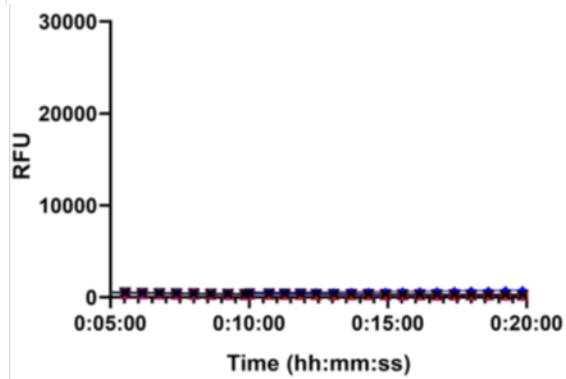
DiBAC₄(3)

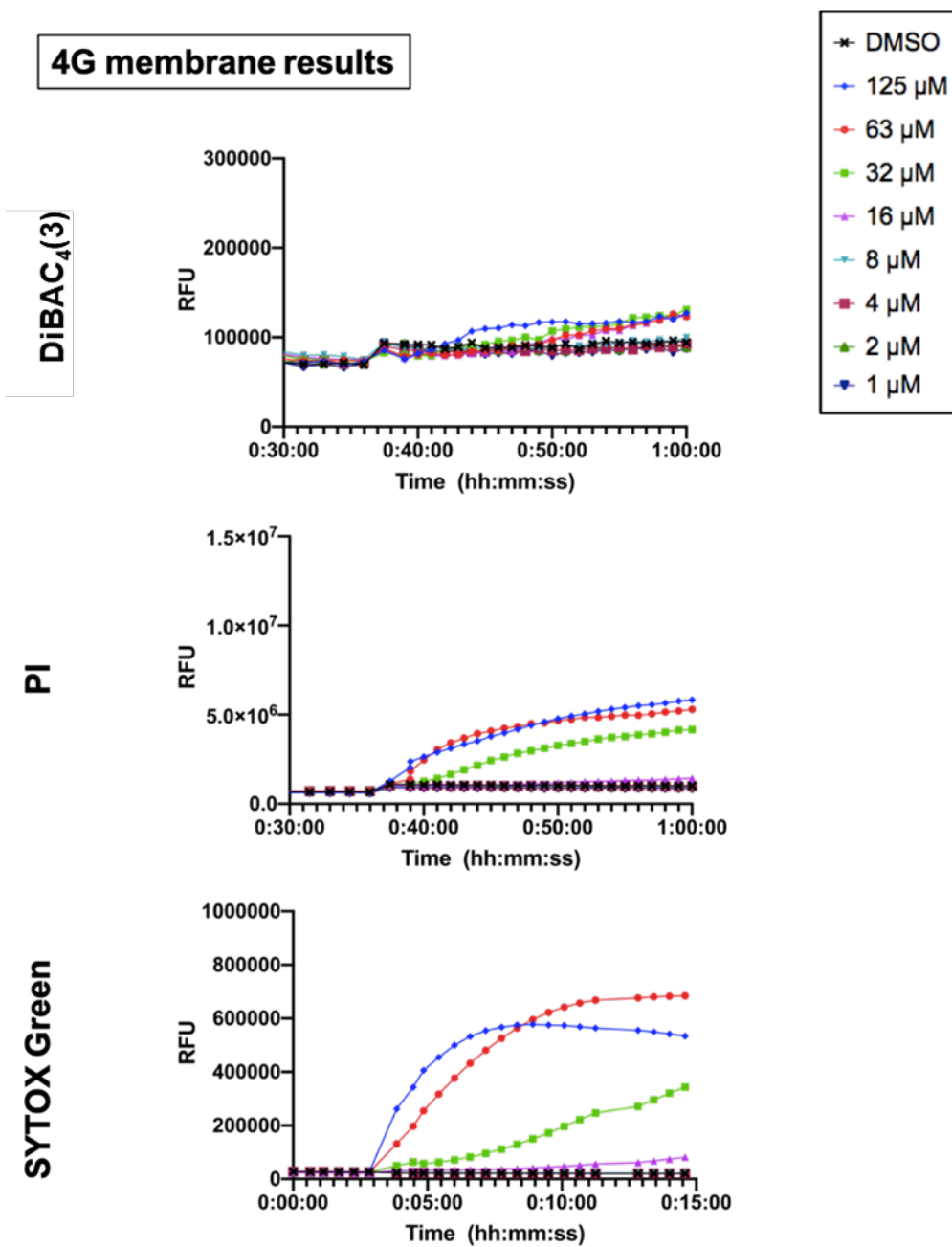
- * DMSO
- ◆ 250 μM
- 125 μM
- 63 μM
- ▲ 32 μM
- ▼ 16 μM
- 8 μM
- ▲ 4 μM
- ▼ 2 μM

PI

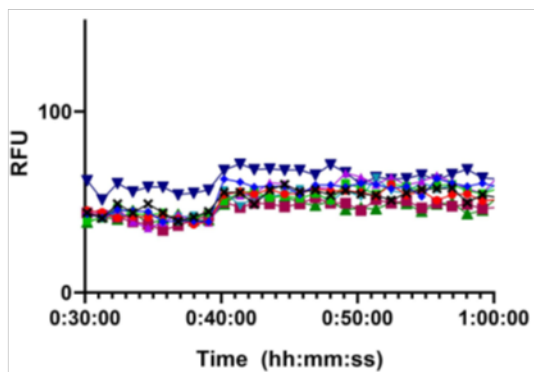


SYTOX Green

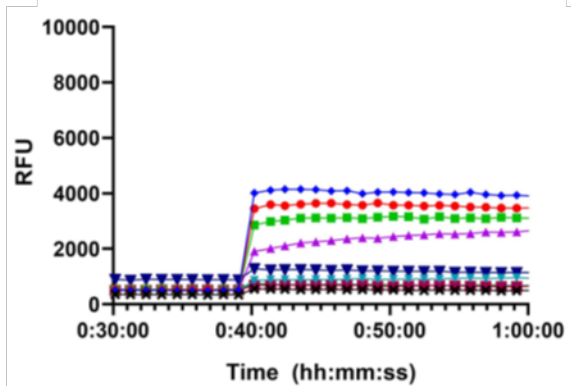


4G membrane results

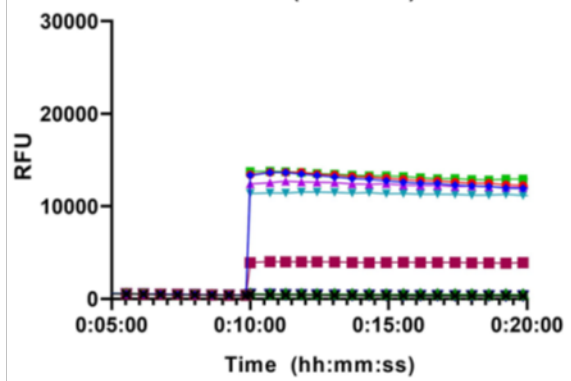
4H membrane results

DiBAC₄(3)

PI

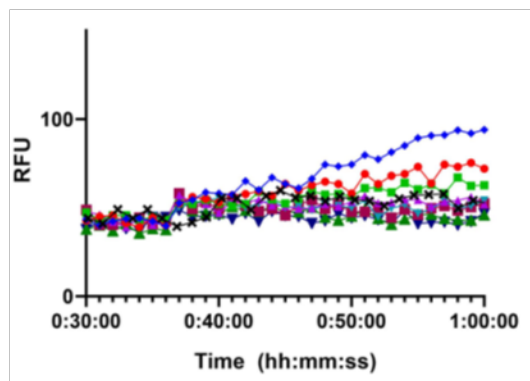


SYTOX Green



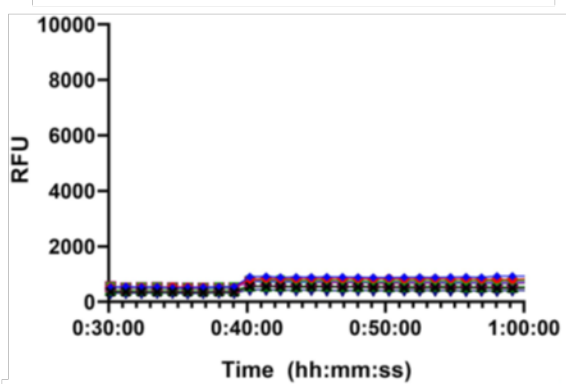
- * DMSO
- + 250 μ M
- 125 μ M
- 63 μ M
- ▲ 32 μ M
- ▼ 16 μ M
- 8 μ M
- ▲ 4 μ M
- ▼ 2 μ M

4I membrane results

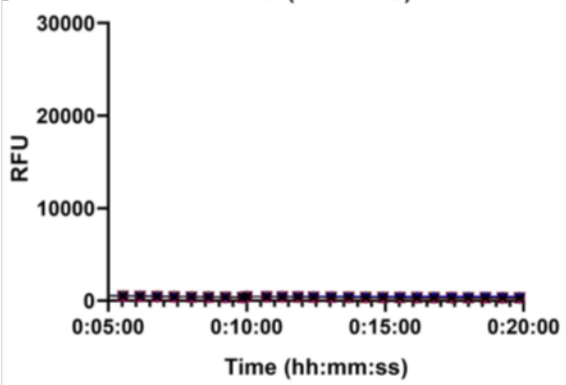
DiBAC₄(3)

- * DMSO
- ◆ 250 μM
- 125 μM
- 63 μM
- ▲ 32 μM
- ▼ 16 μM
- 8 μM
- ▲ 4 μM
- ▼ 2 μM

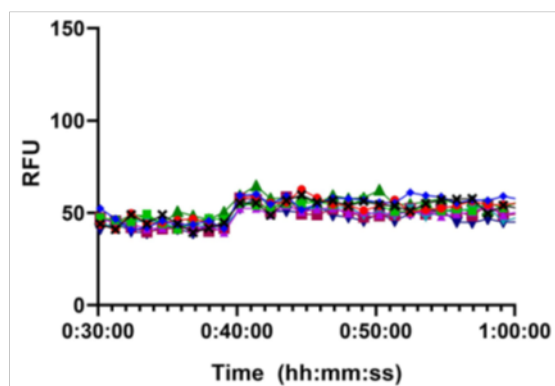
PI



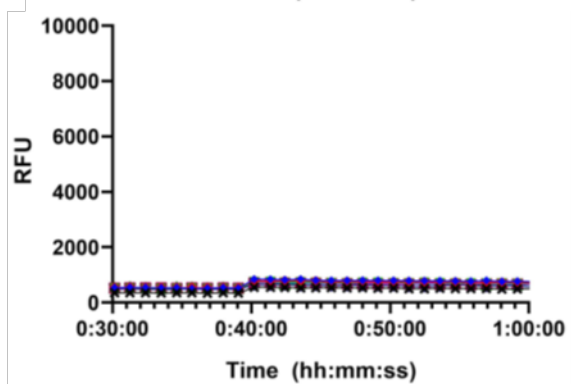
SYTOX Green



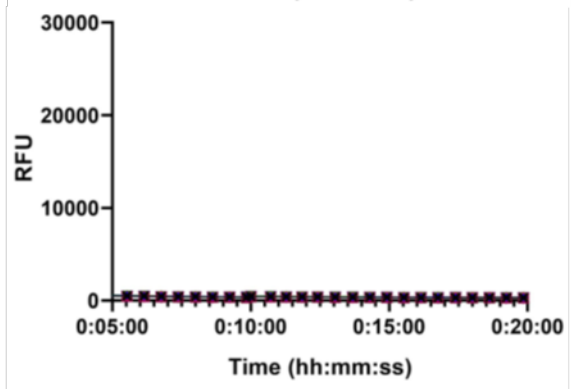
4K membrane results

DiBAC₄(3)

PI

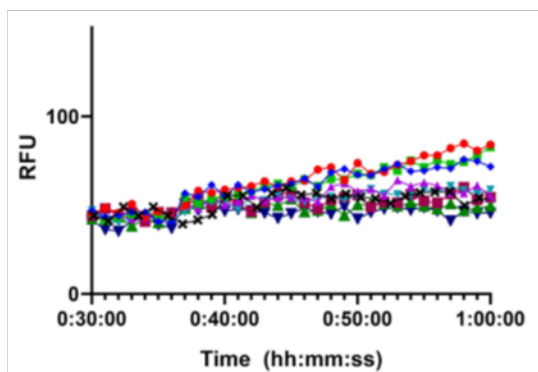


SYTOX Green



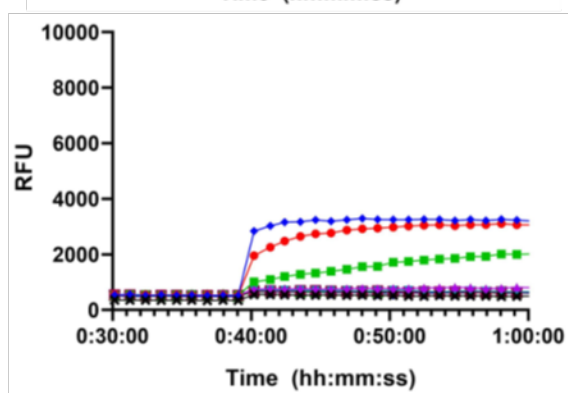
- * DMSO
- ◆ 250 μM
- 125 μM
- 63 μM
- ▲ 32 μM
- ▼ 16 μM
- 8 μM
- ▲ 4 μM
- ▼ 2 μM

4P membrane results

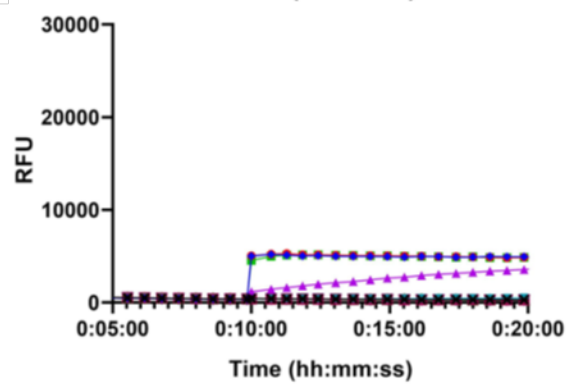
DiBAC₄(3)

- * DMSO
- + 250 μ M
- 125 μ M
- 63 μ M
- ▲ 32 μ M
- ▼ 16 μ M
- 8 μ M
- ▲ 4 μ M
- ▼ 2 μ M

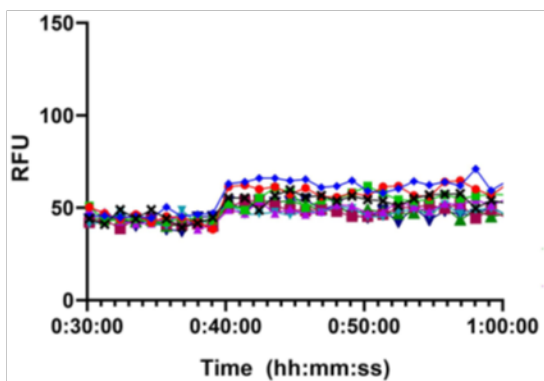
PI



SYTOX Green

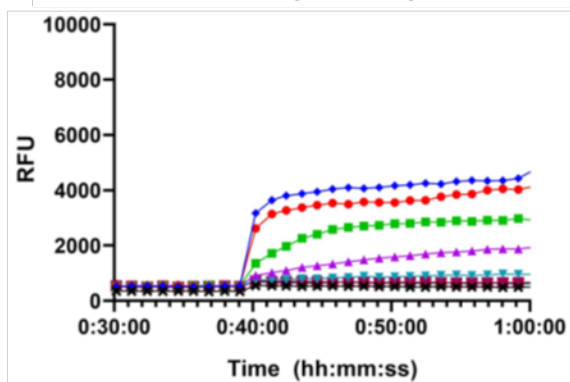


4R membrane results

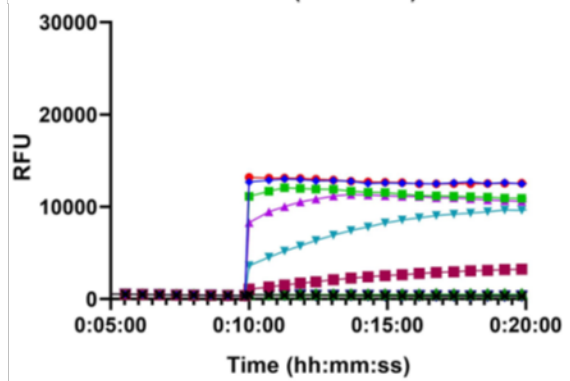
DiBAC₄(3)

- * DMSO
- ◆ 250 μM
- 125 μM
- 63 μM
- ▲ 32 μM
- ▼ 16 μM
- 8 μM
- ▲ 4 μM
- ▼ 2 μM

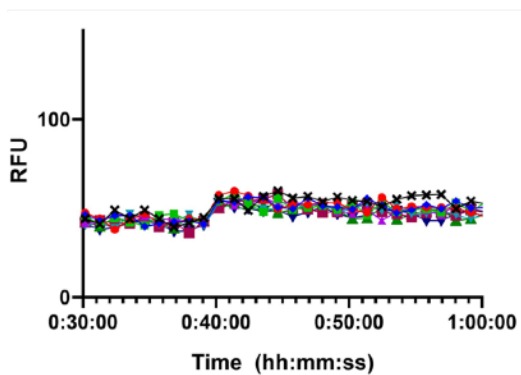
PI



SYTOX Green

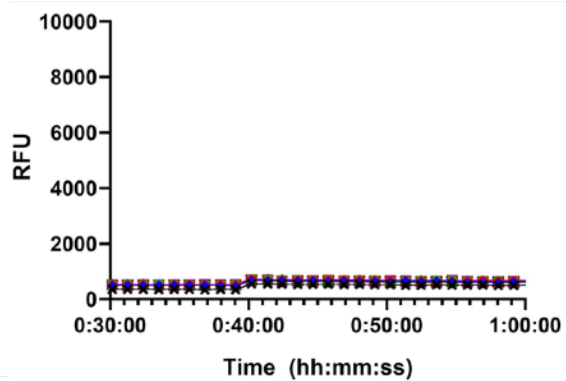


PBS membrane results

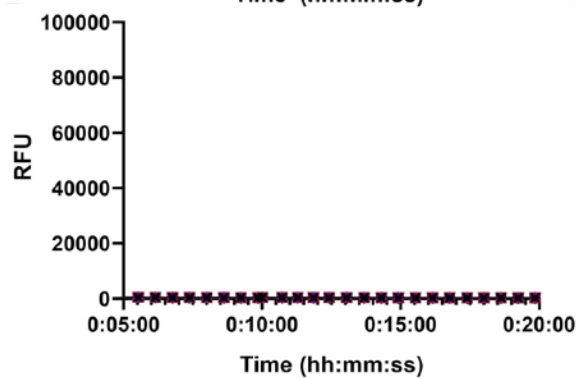
DiBAC₄(3)

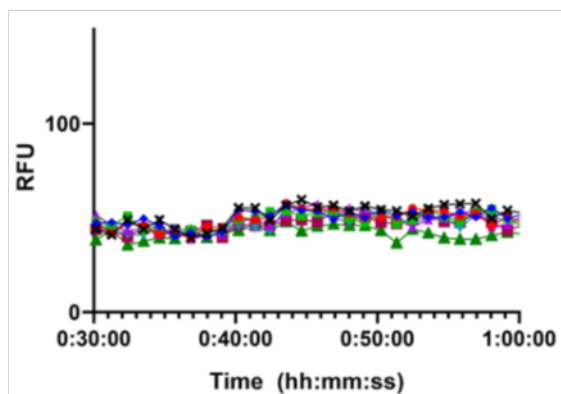
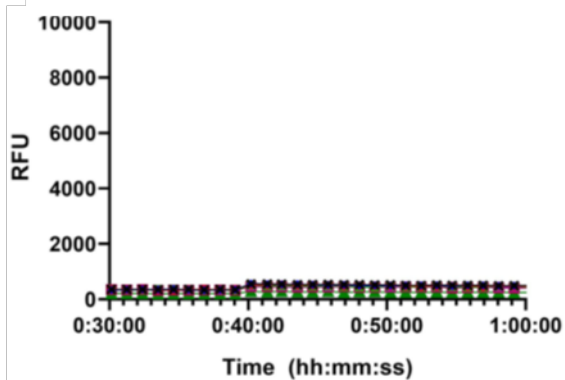
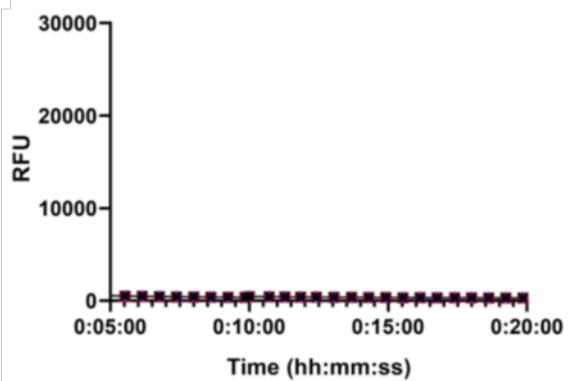
- DMSO
- 125 μM
- 63 μM
- 32 μM
- 16 μM
- 8 μM
- 4 μM
- 2 μM
- 1 μM

PI



SYTOX Green



DMSO membrane results**DiBAC₄(3)****PI****SYTOX Green**

- * DMSO
- ◆ 250 μM
- 125 μM
- 63 μM
- ▲ 32 μM
- ▼ 16 μM
- 8 μM
- ▲ 4 μM
- ▼ 2 μM

5.8 Biological Procedures

Materials. *Streptococcus mutans* wild-type strain UA159 was provided by Dr. Bettina Buttaro from Temple University Medical School, Philadelphia, PA. Bacteria were routinely maintained in Bacto™ Todd-Hewitt agar plates and liquid cultures were grown in in Bacto™ Todd-Hewitt broth (THB). For growth of biofilms, THB was supplemented with 0.1% sucrose. Incubation was stagnant at 37 °C with 5% CO₂. *S. mutans* mutants were provided by Dr. Robert G. Quivey from the Department of Microbiology and Immunology of University of Rochester. Bacterial mutants were maintained in Bacto™ Todd-Hewitt broth with erythromycin. The bacterial strain *Streptococcus Sobrinus* SL1 [CCM 6070, CNCTC 9/89], was purchased from the American Type Culture Collection. *Streptococcus gordonii* strain DL1 and *Streptococcus sanguinis* strain 10904 were provided by Dr. Robert G. Quivey from University of Rochester Medical School. All optical density (OD) measurements were performed on a Molecular Devices SpectraMax iD3 plate reader.

S. mutans MIC assay. Stock solution of carolacton analogs, 10,000 μM in DMSO, were serially diluted in THB media in flat-bottom 96-well microtiter plates. Mid-exponential phase cell culture was diluted to an OD₆₀₀ of 0.004 and added to the serially diluted compound to reach a final volume of 200 μL. Plates are incubated at 37 °C in 5% CO₂ for 20-24 hours upon which time wells are evaluated visually for bacterial growth and the OD₆₀₀ was recorded with the plate reader. The MIC is determined as the lowest concentration of compound resulting in no bacterial growth visible to the naked eye. The IC₅₀ is the concentration of compound needed for 50% growth inhibition. Biological triplicates were performed.

Compound treated S. mutans biofilm preparation model. Stock solution of carolacton analogs, 10,000 μM, were serially diluted in THB media with 0.1% sucrose (w/v) in glass flat-bottom 96-well microtiter plates. Mid-exponential phase cell culture was diluted to an OD₆₀₀ of 0.004 and

added to the serial diluted compound to reach final volume of 200 μL . Plates were incubated at 37 $^{\circ}\text{C}$ in 5% CO_2 for 24 hours at which time wells were evaluated visually for bacterial growth. OD_{600} measurements of growth was performed after visual inspection. Biological triplicates were performed.

Colony-Forming Units Assay Compound treated *S. mutans* biofilms were prepared as described above. Plates were incubated at 37 $^{\circ}\text{C}$ in 5% CO_2 for 24 hours at which time wells were evaluated visually for bacterial growth. OD_{600} measurements of growth was performed after visual inspection, and then emptied by inverting carefully, as to not disturb the biofilm. Wells were washed three times with 200 μL of phosphate buffer solution (PBS) or THB media to remove planktonic cells. Following the washes, 200 μL of PBS or THB were added, and the biofilm cells were resuspended. Then, the biofilm suspensions were diluted in PBS or THB, in log fashion, and plated on THB agar plates. Plates were incubated for 24-48 hours and colonies were counted.

***S. mutans* mutant screen** Stock solution of **analog 2**, 10,000 μM , were serial diluted in THB media with 0.1% sucrose (w/v) in glass flat-bottom 96-well microtiter plates. Each mutant was grown with compound, and separately with the DMSO vehicle. Mid-exponential phase cell culture was diluted to an OD_{600} of 0.004 and added to the serial diluted compound or DMSO control to reach final volume of 200 μL . Plates were incubated at 37 $^{\circ}\text{C}$ in 5% CO_2 for 24 hours at which time wells were evaluated visually for bacterial growth. OD_{600} measurements of growth was performed after visual inspection.

***S. mutans* MBIC₅₀ assay.** Biofilms were prepared with above procedure, evaluated visually, OD_{600} of bacterial growth was recorded, and then wells were emptied by inverting carefully, as to not disturb the biofilm. Wells were washed with 200 μL of phosphate buffer solution (PBS) and

dried overnight at 37°C. Once dry, plates were incubated for 10 min at room temperature with 200 μ L of 1% w/v crystal violet in DI H₂O. Excess crystal violet was removed by aspirating off the liquid and performing DI H₂O rinses until the run off was colorless. Plates were then inverted and dried overnight at 37°C. Crystal violet stained biofilm was dissolved with 200 μ L of 10% acetic acid in DI H₂O. The crystal violet plate with acetic acid solution was allowed to incubate at room temperature for 10-30 minutes to allow for full dissolution. Then 100 μ L was transferred to a fresh flat-bottom 96-well plate for absorbance measurements at 595 nm. DMSO controls corresponding to each test concentration were performed. Crystal violet reading was set relative to bacterial growth (OD₅₉₅/OD₆₀₀) to allow for appropriate comparison of biofilm mass formation. MBIC₅₀ refers to the concentration at which biofilm growth is inhibited by 50% compared to the control. Biological triplicates were performed.

Confocal Imaging. Biofilms were prepared with above procedure. In order to perform direct imaging, uncoated 96-Well Plates with 5 mm Glass Diameter from MatTek (Part No: P96G-0-5-F) were used for confocal imaging experiments. After incubation, media was removed, and each well was carefully rinsed three times with PBS to remove planktonic cells. Subsequently, 20 μ L of BacLight LIVE/DEAD™ stain was added to each well. Excess dye was rinsed off biofilm with PBS. Images of biofilms were then obtained using the Olympus FV1000 inverted microscope in the Integrated Cellular Imaging Core at Emory University (Sections 2.5 and Chapter 3) and the Lewis Katz School of Medicine Confocal Microscope at Temple University (Section 2.4).

Hemolysis Assay (Lysis₂₀) Hemolysis assays were performed on mechanically defibrinated sheep blood (Hemostat Labs: DSB030). 1.5 mL of blood was placed into a microcentrifuge tube and centrifuged at 10,000 rpm for ten minutes. The supernatant was removed and then cells were resuspended with 1 mL of phosphate-buffered saline (PBS). The suspension was centrifuged as

previously, the supernatant was removed, and cells were resuspended two more times. The final cell suspension was diluted twentyfold with PBS. The twentyfold suspension dilution was then aliquoted into microcentrifuge tubes containing compound serially diluted in PBS. TritonX (1% by volume) served as a positive control (100% lysis marker) and sterile PBS served as a negative control (0% lysis marker). Samples were then placed in an incubator at 37 °C and shaken at 200 rpm. After 1 hour, the samples were centrifuged at 10,000 rpm for ten minutes. The absorbance of the supernatant was measured with a UV spectrometer at a 540 nm wavelength.

SYTOX Assay. Bacterial overnight cultures were regrown to mid-log phase in THB media and the culture was centrifuged, and washed with PBS three times. Cells were then suspended in the same volume of PBS corresponding to the original regrow volume, and SYTOX green solution (5 mM in DMSO) was added to reach a final concentration of 5 μ M. Cells were incubated at room temperature and in the dark for 30 minutes. 150 μ L of cells were then added to a black, clear bottom 96-well plate. Fluorescence was recorded for 10 minutes in plate reader to allow equilibration (excitation wavelength 485 nm and emission wavelength 525 nm). In a new 96-well plate, test compounds (10 mM DMSO stock solutions) were serially diluted in PBS. 50 μ L of serially diluted compound was added to the SYTOX prepared cells in the plate reader and fluorescence was recorded overtime (excitation wavelength 485 nm, emission wavelength 525 nm). Biological triplicates were completed.

Detecting Membrane Depolarization and Rupture. Bacterial overnight cultures were regrown to mid-log phase in THB media and the culture was centrifuged, and washed with PBS three times. Cells were then suspended in the same volume of PBS corresponding to the original regrow

volume. To 20 mLs of cell suspension, 500 μ L of 1 M sterile filter glucose solution was added (Final glucose concentration = 24.4 mM). Cells were incubated for 15 minutes at 37°C. Then 100 μ L of 50 μ M solution of DiBAC₄(3) was added (Final concentration = 243 nM). Next, 400 μ L of 2 mg/ml solution of PI was added (Final concentration 19 μ g/ml). The sample was mixed thoroughly and 150 μ L of sample was added into the wells of a black, clear bottom 96-well plate. The plate was then placed in a pre-warmed (37°C) fluorescence detection plate reader. The measurements were recorded until readings stabilized (~40 mins). In a new 96-well plate, test compounds (10 mM DMSO stock solutions) were serially diluted in PBS. The fluorescence plate was ejected, 50 μ L of test compound was added and then quickly returned to the plate reader. Fluorescence was recorded overtime. Biological triplicates were completed.

Measurements

1. DiBAC₄(3) measures changes in polarity. (490 nm excitation and 516 nm emission) detection
2. PI measures cell rupture. (535 nm excitation and 617 nm emission) detection

TEM Imaging. Cells were grown to mid-log phase in THB media, centrifuged, and washed with PBS three times. Cells were then suspended to the original volume with PBS. The cells were then incubated with test compound for 30 minutes at 37°C. Following treatment, cells were collected, washed, and prepared for transmission electron microscopy by fixing the cells in 2.5% glutaraldehyde in 0.1 M cacodylate buffer. Images were recorded on a JEOL JEM-1400 Transmission electron microscope at the Integrated Cellular Imaging Core at Emory University.

Label-free ABPP in bacterial biofilm. 5 mL of THB media was inoculated with *S. mutans* (UA159) from freezer stock and grown overnight. The overnight culture was diluted (1:100) and regrown to $OD_{600} = 0.4$ (exponential phase). To a petri dish, 200 μ l of 100X stock solution was added to 19.8 mL of THB sucrose 0.1% sucrose (w/v). Petri dishes were incubated at 37 °C in 5% CO_2 for 24 hours. Petri dishes were then immediately irradiated with UV light (280-315 nm). Irradiation cycle was repeated three times (6 minutes irradiation, 6 minutes on cold pack). Then the biofilm supernatant was removed and the biofilm were carefully rinsed with PBS three times. Biofilm cells were resuspended with 10 mL of PBS and transferred to 25 mL falcon tubes. Samples were centrifuged for 10 minutes (6000 x g), supernatant discarded, and pellet was transferred to Eppendorf tube with 800 μ L of PBS. The samples were then again centrifuged for 10 minutes (8000 rpm), supernatant was disposed and pellet was resuspended in PBS with 0.4% SDS (4 °C). Bacterial cell lysis was completed with 3 cycles of 30 second sonification at 80% intensity. Samples were then centrifuged at max speed for 10 minutes (4 °C) thus separating the cytosolic fraction (supernatant) and the membrane fraction (pellet). We only performed the experiment on the cytosolic fraction.

Analytical method:

With the cytosolic fraction, we performed click chemistry with rhodium azide using a freshly prepared “master mix”. Master mix included (per sample) 2 μ l of RhN_3 (10 mM in DMSO), 2 μ l TCEP (52 mM, 15 mg/mL in dd H_2O), and 6 μ l TBTA ligand (1.677 M 1 x ligand; 800 μ L *t*-BuOH, 180 μ L DMSO, 20 μ L 50 x ligand) (50 x ligand = 8.85 mg in 200 μ L DMSO). 88 μ L of the cytosolic fraction and 10 μ L of the master mix were combined in an Eppendorf and vortexed. Then, 2 μ L of 50 mM $CuSO_4$ were added to each sample and vortexed. Samples were incubated for 1 hour at RT. 100 μ l of 2 X SDS loading buffer were added to the samples, vortexed and stored

at – 80 °C. Samples were run on a SDS-gel to compare **analog 2-probe**'s ability at cross linking protein.

Preparative method:

Protein concentration was measured with the BCA Assay and samples were adjusted to 0.63 mg/mL using SDS buffer (500 µL of each sample). Click chemistry was performed with biotin azide using a freshly prepared “master mix”. Master mix included (per 500 µL sample) 3 µL of biotin azide (10 mM in DMSO), 10 µL TCEP (52 mM, 15 mg/mL in dd H₂O), and 30 µL TBTA ligand (1.677 M 1 x ligand; 800 uL *t*-BuOH, 180 µl DMSO, 20 µL 50 x ligand) (50 x ligand = 8.85 mg in 200 uL DMSO), and 10 µl of CuSO₄ (50 mM stock in dd H₂O). 500 µL of the cytosolic fraction and 53 µL of the master mix were combined in a 15 mL falcon tube, vortexed and incubated for 1 hour at RT.

Proteins were precipitated by adding 4x volume (2 mL) cold acetone (-80 °C) using a glass pipette. Samples were then stored in the -20 °C freezer for 1 hour (up to overnight). Precipitated proteins were pelletized for 15 minutes at 16900 x g at 4 °C and the supernatants were discarded. Protein pellets were washed twice with 500 uL of cold methanol (-80 °C) and resuspension with sonication (10 seconds, lowest intensity). Pelletize protein for 15 minutes at 16900 x g at 4 °C, discard supernatant and resuspend protein pellet in 500 uL 0.2-0.4% SDS in PBS (at RT) by sonication (10 seconds, lowest intensity).

Protein enrichment was then started by transferring 50 uL of Avidin bead suspension into Protein LoBind Eppendorf tubes with a cropped pipette tip. Beads were washed with 0.2-0.4% SDS (MS grade) in PBS three times (3 minutes, 400 x g). Incompletely solubilized aggregates were removed with centrifugation, and then 0.5 mL of protein sample was transferred to the LoBind Eppendorf tubes containing the Avidin beads. Samples were incubated at RT with

continuous mixing for 1 hour. Beads were then washed three times with 1 mL 0.2 – 0.4% SDS in PBS (MS grade), two times with 1 mL 6 M urea in ddH₂O (MS grade) and three times with 1 mL PBS (MS grade).

On bead digestion was completed by first resuspending pellets in 200 μ L of X buffer (7 M urea, 2 M thiourea in 20 mM HEPES buffer pH 7.5). 2 μ L of 500 mM TCEP was added, vortexed and the samples were incubated for 1 hour at 37 °C. Then 4 μ L 500 mM of iodoacetamide was added, vortexed and incubated at RT for 30 minutes in the dark. Reagents were quenched with the addition of 4 μ L 500 mM DTT. Samples were vortexed and incubated at RT for 30 minutes.

The protein samples were digested with LysC (1 μ L per sample) for 2-4 hours at RT. Then 600 μ L of 50 mM of TEAB was added and samples were checked to make sure a pH of 8 was maintained. 1.5 μ L of 0.5 μ g/ μ L trypsin in acetic acid was added and the samples were incubated overnight at 37 °C. Digestion reagents were quenched by adding 10 μ L of FA to the samples. The pH was checked (3 or below). Samples were centrifuged to prepare for the desalting steps.

Samples were desalted by using SepPak cartridges. Columns were washed with 1 mL of MeCN (80% MeCN, 0.5% FA), two times. Columns were equilibrated with 1 mL of 0.1% TFA, three times. Samples were loaded. The beads were rinsed with 500 μ L of 0.1% TFA, vortexed and centrifuged again. The rinses were then also loaded on the columns. Loaded columns were washed with 1 mL 0.1% TFA, three times, and then 500 μ L 0.5% FA, once. Finally, the peptide samples were then eluted off the column with 250 μ L 80% MeCN/0.5% FA, three times. Vacuum was used to remove all of the liquid from the column. Samples were then evaporated in the speedvac.

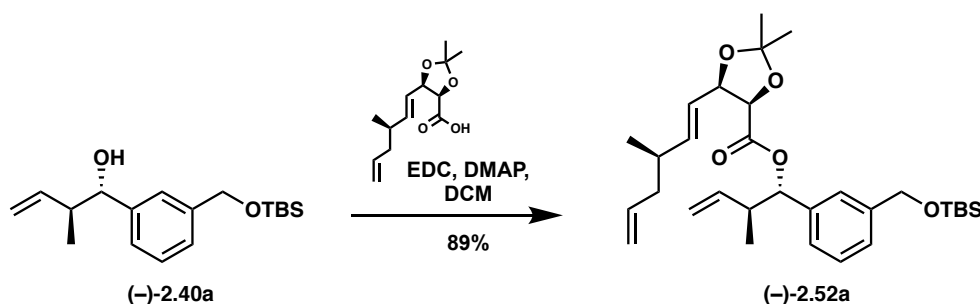
The last step in preparing the MS samples is to filter the samples. In order to do so, the samples were dissolved in 25-40 μ L 1% FA, vortexed and sonicated. With the help of centrifugation, 0.2 μ m Millipore filters were washed with 300 μ L of 1% FA. Samples were then

applied to the center of the filter and spun down. The samples were then carefully transferred to a MS vial to avoid bubble formation. Samples were then analyzed using LC-MS/MS.

5.9 Chemistry General Notes

General. NMR spectra were recorded using the following spectrometers: Varian INOVA 600, INOVA 500, INOVA 400, VNMR 400, Mercury 300, Bruker AVANCE III HD 600, Bruker NANO HD III 400, Bruker AVANCE 600 WB SSNMR and Bruker AVANCE III 300 WB SSNMR. Chemical shifts are quoted in ppm relative to tetramethylsilane and with the indicated solvent as an internal reference. The following abbreviations are used to describe signal multiplicities: s (singlet), d (doublet), t (triplet), q (quartet), m (multiplet), br (broad), dd (doublet of doublets), dt (doublet of triplets), etc. Accurate mass spectra were recorded on a Thermo LTQ FTMS, infrared spectra were obtained using a Thermo Scientific Nicolet is10 Smart Orbit FT-IR spectrophotometer and specific rotation measurements were made with a 1 dm path length using a Perkin Elmer 341 Polarimeter. Non-aqueous reactions were performed under an atmosphere of argon, in flame-dried glassware, with HPLC-grade solvents dried by passage through activated alumina. Amine bases were freshly distilled from CaH_2 prior to use. Brine refers to a saturated aqueous solution of sodium chloride. Products purified via flash chromatography using Biotage Isolera One Automated column. Reactions monitored via thin-layer chromatography (TLC) using EMD Millipore® TLC silica gel glass plates with KMnO_4 stain.

5.10 Procedures and Characterization

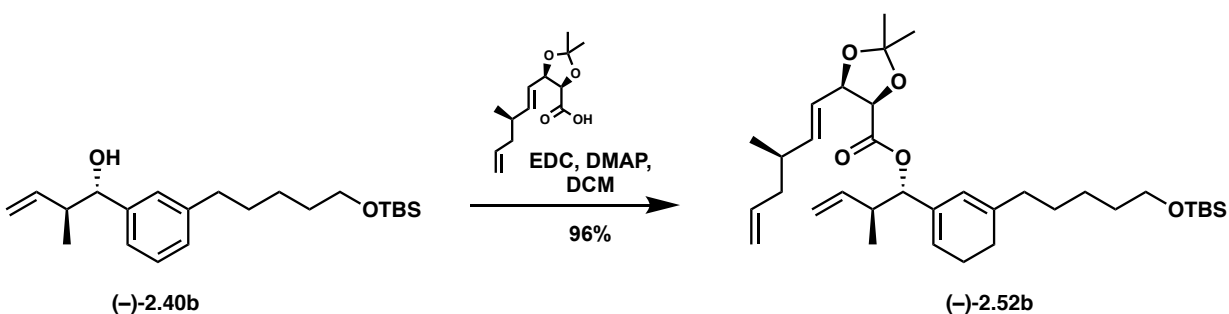
**Representative Procedure A: Esterification**

(4*R*,5*R*)-(1*S*,2*S*)-1-(3-(((*tert*-Butyldimethylsilyl)oxy)methyl)phenyl)-2-methylbut-3-en-1-yl-2,2-dimethyl-5-((*R,E*)-3-methylhexa-1,5-dien-1-yl)-1,3-dioxolane-4-carboxylate ((-)-2.52a) A flame dried flask was charged with argon and (-)-2.40a (100 mg, 0.416 mmol) and DCM (4.2 mL) and subsequently cooled to 0 °C. Once cool, DMAP (34 mg, 0.027 mmol) and EDCI (106 mg, 0.555 mmol) were added consecutively followed by a solution of (-)-5a (85 mg, 0.277 mmol) in DCM (2.8 mL) added via syringe pump. The reaction was stirred 18 hours whereupon it was added to a separatory funnel containing H₂O (15 mL). The organic layer was separated and the aqueous layer was extracted with DCM (3 x 15 mL). The combined organic layers were washed with brine, dried over magnesium sulfate, filtered, and concentrated. Purification by flash column chromatography (0 to 20% EtOAc in hexanes) afforded the product as a clear oil (130 mg, 89%).

¹H NMR (500 MHz, CDCl₃) δ 7.32 – 7.24 (m, 3H), 7.22 – 7.17 (m, 1H), 5.85 – 5.64 (m, 3H), 5.61 (d, *J* = 7.5 Hz, 1H), 5.19 – 5.10 (m, 1H), 5.10 – 5.03 (m, 2H), 5.01 – 4.92 (m, 2H), 4.79 – 4.71 (m, 3H), 4.61 (d, *J* = 7.0 Hz, 1H), 2.74 – 2.64 (m, 1H), 2.08 – 1.95 (m, 2H), 1.89 – 1.83 (m, 1H), 1.66 (s, 3H), 1.40 (s, 3H), 0.95 (s, 9H), 0.90 (d, *J* = 6.9 Hz, 3H), 0.82 (d, *J* = 6.6 Hz, 3H), 0.10 (s, 6H);

¹³C NMR (126 MHz, CDCl₃) δ 169.12, 142.70, 141.55, 139.54, 138.49, 136.78, 128.24, 126.06, 125.80, 125.13, 122.13, 116.19, 115.96, 110.95, 80.33, 79.37, 78.34, 64.93, 43.04, 40.72, 35.93,

27.18, 26.08, 25.81, 19.16, 18.53, 16.06, -5.09; **IR** (neat): 3076, 2956, 2928, 2856, 1758, 1733, 1641, 1471, 1462, 1379, 1253, 1217, 1183, 1162, 1082, 1042, 1004, 973, 913, 880, 836, 815, 776, 703, 668, 567, 561 cm⁻¹; **[α]²⁵_D** -61.6 (c = 0.92 in CHCl₃); **HRMS** (ES⁺): Found 551.3152 (-1.1 ppm), C₃₁H₄₈O₅SiNa (M+Na⁺) requires 551.3163

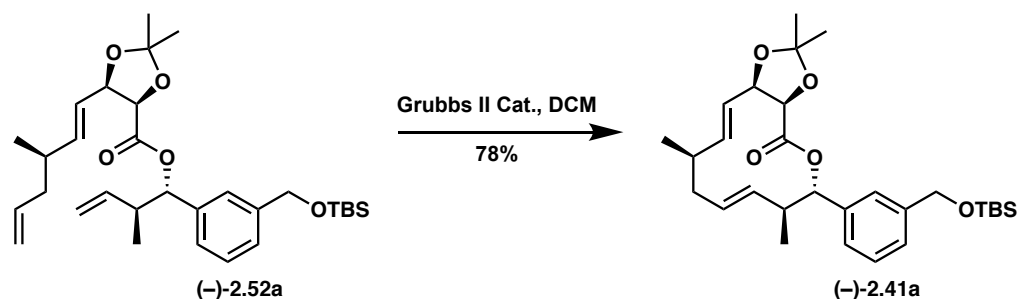


(4*R*,5*R*)-(1*S*,2*S*)-1-(3-(5-((*tert*-Butyldimethylsilyl)oxy)pentyl)phenyl)-2-methyl but-3-en-1-yl-2,2-dimethyl-5-((*R,E*)-3-methylhexa-1,5-dien-1-yl)-1,3-dioxolane-4-carboxylate ((-)-2.52b)

Prepared according to Representative Procedure A: (-)-**2.18** (650 mg, 2.71 mmol), in DCM (27 mL), DMAP (826 mg, 6.76 mmol), EDCI (778 mg, 4.06 mmol), and (-)-**2.40b** (490 mg, 1.35 mmol) in DCM (14 mL) yielded 759 mg (96%) of the ester. Purified by column chromatography (0 to 20% EtOAc in hexanes).

¹H NMR (500 MHz, CDCl₃) δ 7.24 – 7.18 (m, 1H), 7.14 – 7.03 (m, 3H), 5.82 – 5.61 (m, 3H), 5.58 (d, *J* = 7.6 Hz, 1H), 5.13 – 5.06 (m, 1H), 5.06 – 5.00 (m, 2H), 4.99 – 4.91 (m, 2H), 4.77 – 4.70 (m, 1H), 4.59 (d, *J* = 7.0 Hz, 1H), 3.60 (t, *J* = 6.6 Hz, 2H), 2.70 – 2.66 (m, 1H), 2.61 – 2.56 (m, 2H), 2.02 – 1.93 (m, 2H), 1.87 – 1.81 (m, 1H), 1.65 (s, 3H), 1.63 – 1.52 (m, 4H), 1.40 – 1.34 (m, 5H), 0.91 – 0.86 (m, 12H), 0.79 (d, *J* = 6.6 Hz, 3H), 0.04 (s, 6H); **¹³C NMR** (126 MHz, CDCl₃) δ 169.17, 142.73, 142.69, 139.65, 138.52, 136.80, 128.20, 127.65, 124.78, 122.10, 116.18, 115.90, 110.96, 80.35, 79.40, 78.40, 63.35, 43.12, 40.73, 36.06, 35.91, 32.87, 31.41, 27.18, 26.14, 25.83,

25.72, 19.15, 18.53, 16.16, -5.11; **IR** (neat): 2929, 2857, 1735, 1641, 1608, 1461, 1372, 1234, 1163, 1091, 1022, 997, 974, 913, 880, 834, 774, 706, 661 cm⁻¹; [α]²⁵_D -47.3 (c = 0.30 in CHCl₃); **HRMS** (ES⁺): Found 602.4218 (-2.3 ppm), C₃₅H₆₀O₅SiN (M+NH₄⁺) requires 602.4241



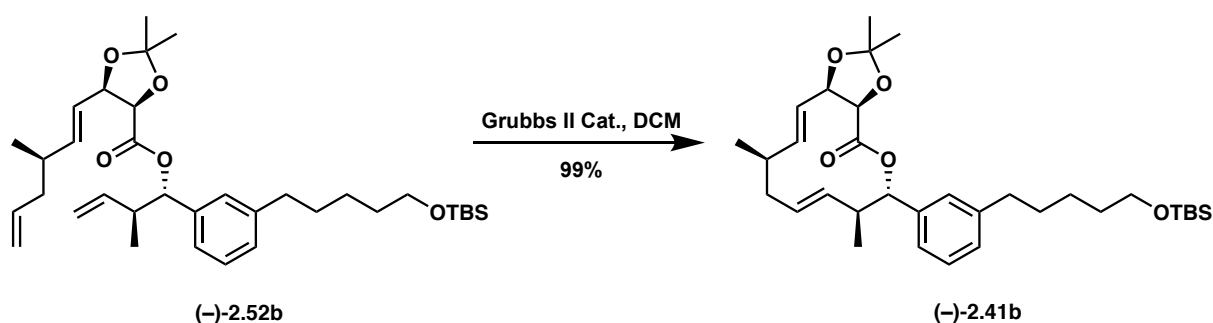
Representative Procedure B: Ring-Closing Metathesis

(3aR,6S,7S,8E,11R,12E,13aR)-6-(3-(((tert-Butyldimethylsilyl)oxy)methyl)phenyl)-2,2,7,11-tetramethyl-6,7,10,11-tetrahydro-3aH-[1,3]dioxolo[4,5-c][1]oxacyclododecin-4(13aH)-one

(-)-2.41a A flask was charged with **(-)-2.52a** (80 mg, 0.150 mmol) and DCM (30 mL). Grubbs 2nd generation catalyst (6.0 mg, 0.0076 mmol, 5 mol%) was added and the reaction was stirred at room temperature for 20 hours. The solvent was removed and the crude residue was purified by flash column chromatography (0 to 3% EtOAc in hexanes) to afford the product as a yellowish oil (59 mg, 78%). *NOTE: In our experience, degassing solvent prior to use had no noticeable effect on the outcome of the reaction.*

¹H NMR (400 MHz, CDCl₃) δ 7.28 – 7.25 (m, 3H), 7.21 – 7.17 (m, 1H), 5.87 – 5.75 (m, 1H), 5.58 (d, *J* = 10.8 Hz, 1H), 5.38 – 5.22 (m, 3H), 4.77 – 4.69 (m, 3H), 4.45 (d, *J* = 6.6 Hz, 1H), 2.66 – 2.49 (m, 1H), 2.39 – 2.19 (m, 2H), 2.16 – 1.98 (m, 1H), 1.66 (s, 3H), 1.37 (s, 3H), 1.08 (d, *J* = 6.7 Hz, 3H), 0.93 (s, 9H), 0.75 (d, *J* = 6.8 Hz, 3H), 0.08 (s, 6H); **¹³C NMR** (101 MHz, CDCl₃) δ 169.85, 141.81, 139.29, 138.85, 134.70, 130.68, 128.43, 126.56, 126.12, 125.54, 123.65, 111.03, 80.72, 79.11, 78.43, 64.91, 43.29, 38.54, 35.90, 26.90, 26.07, 25.99, 20.99, 17.61, -5.07; **IR** (neat):

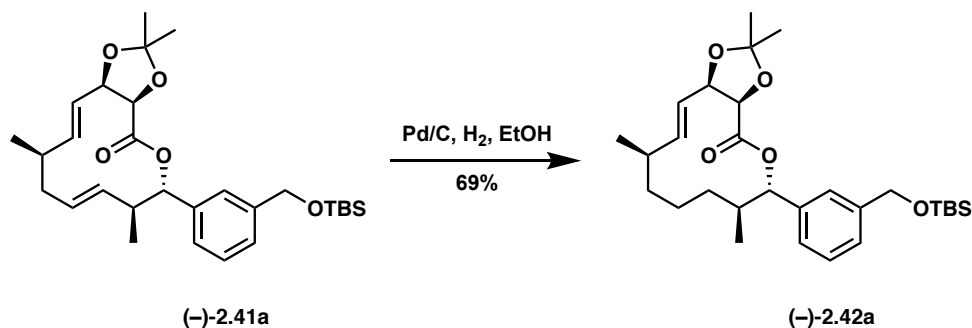
2955, 2928, 2856, 1796, 1750, 1472, 1461, 1379, 1252, 1222, 1180, 1161, 1081, 1001, 968, 879, 814, 776, 735, 703, 670 cm^{-1} ; $[\alpha]_{\text{D}}^{25}$ -34.4 ($c = 1.00$ in CHCl_3); **HRMS** (ES^+): Found 523.2869 (+1.3 ppm), $\text{C}_{29}\text{H}_{44}\text{O}_5\text{SiNa}$ ($\text{M}+\text{Na}^+$) requires 523.2856



(3a*R*,6*S*,7*S*,8*E*,11*R*,12*E*,13a*R*)-6-(3-(5-((*tert*-Butyldimethylsilyl)oxy) penty)phenyl)-2,2,7,11-tetramethyl-6,7,10,11-tetrahydro-3a*H*-[1,3]dioxolo[4,5-*c*][1]oxacyclo dodecin-4(13a*H*)-one
((-)-2.41.b) Prepared according to Representative Procedure B: **(-)-2.52b** (750 mg, 1.28 mmol), Grubbs 2nd Generation catalyst (54 mg, 0.064 mmol, 5 mol%), and DCM (128 mL) yielded 710 mg (99%) of the product as a clear oil. Purified by column chromatography (0 to 3% EtOAc in hexanes).

¹H NMR (500 MHz, CDCl_3) δ 7.23 – 7.17 (m, 1H), 7.15 – 7.06 (m, 3H), 5.85 – 5.78 (m, 1H), 5.57 (d, $J = 10.8$ Hz, 1H), 5.35 – 5.29 (m, 1H), 5.29 – 5.23 (m, 2H), 4.77 – 4.70 (m, 1H), 4.47 (d, $J = 6.7$ Hz, 1H), 3.60 (t, $J = 6.6$ Hz, 2H), 2.62 – 2.55 (m, 3H), 2.34 – 2.21 (m, 2H), 2.09 – 1.99 (m, 1H), 1.67 (s, 3H), 1.63 – 1.57 (m, 2H), 1.57 – 1.51 (m, 2H), 1.39 – 1.33 (m, 5H), 1.09 (d, $J = 6.8$ Hz, 3H), 0.89 (s, 9H), 0.75 (d, $J = 6.8$ Hz, 3H), 0.04 (s, 6H); **¹³C NMR** (126 MHz, CDCl_3) δ 169.81, 142.99, 139.25, 138.84, 134.79, 130.59, 128.44, 127.93, 125.20, 123.69, 111.00, 80.76, 79.11, 78.42, 63.28, 43.30, 38.53, 35.98, 35.88, 32.79, 31.40, 26.88, 26.10, 25.96, 25.68, 21.00, 18.47, 17.65, -5.15; **IR** (neat): 2954, 2928, 2856, 1751, 1608, 1586, 1459, 1379, 1251, 1222, 1180,

1085, 1002, 968, 880, 834, 813, 775, 705, 662 cm^{-1} ; $[\alpha]_{\text{D}}^{25}$ -69.4 ($c = 1.90$ in CHCl_3); **HRMS** (ES^+): Found 557.3639 (-1.8 ppm), $\text{C}_{33}\text{H}_{52}\text{O}_5\text{Si}$ ($\text{M}+\text{H}^+$) requires 557.3657



Representative Procedure C: Hydrogenation

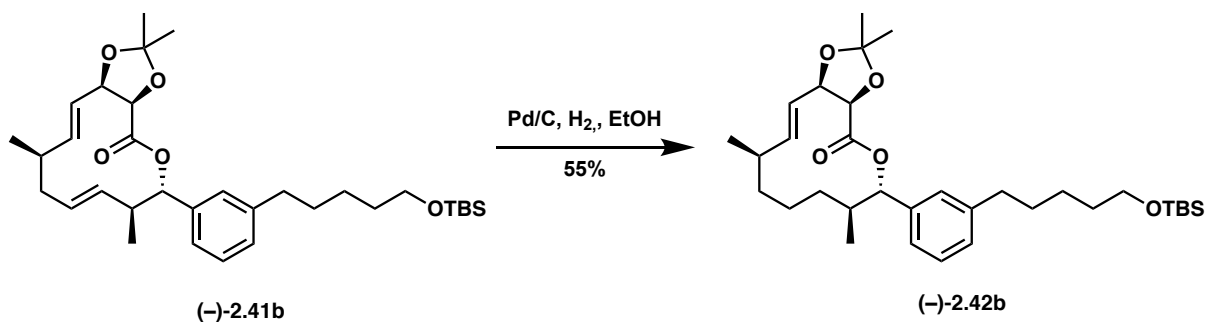
(3aR,6S,7S,11R,13aR,E)-6-(3-(((tert-Butyldimethylsilyl)oxy)methyl)phenyl)-2,2,7,11-

tetramethyl-6,7,8,9,10,11-hexahydro-3aH-[1,3]dioxolo[4,5-c][1]oxacyclododecin-4(13aH)-

one ((-)-2.42a) To a solution of **(-)-2.41a** (36 mg, 0.072 mmol) in ethanol (7.2 mL) was added palladium on carbon (10% w/w, 6 mg). The reaction was sparged with hydrogen gas 5 times from a balloon and stirred for 1.5 hours. The reaction was passed through a pad of celite with EtOAc (100 mL) and the solvent was removed. The residue was purified by preparative TLC (3% EtOAc in hexanes, eluted twice, to remove a more non-polar impurity) to afford the product as a clear oil (25 mg, 69%).

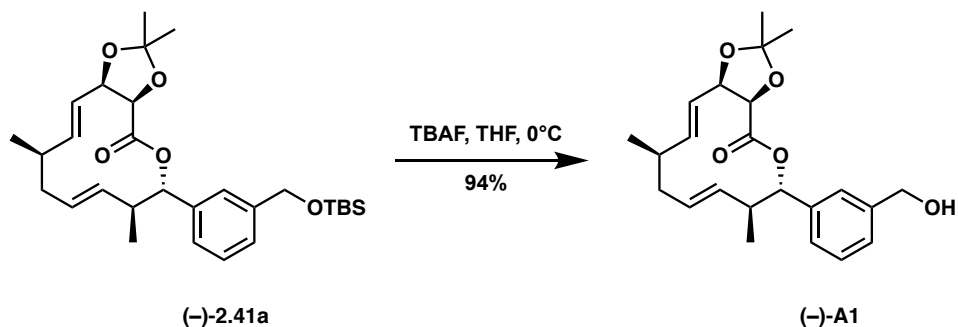
$^1\text{H NMR}$ (400 MHz, CDCl_3) δ 7.26 – 7.20 (m, 3H), 7.19 – 7.14 (m, 1H), 5.72 – 5.59 (m, 2H), 5.51 (d, $J = 11.3$ Hz, 1H), 4.87 – 4.82 (m, 1H), 4.70 (s, 2H), 4.52 (d, $J = 6.6$ Hz, 1H), 2.44 – 2.33 (m, 1H), 2.28 – 2.17 (m, 1H), 2.03 – 1.92 (m, 1H), 1.68 (s, 3H), 1.41 – 1.36 (m, 6H), 1.02 (d, $J = 6.6$ Hz, 2H), 0.93 (s, 9H), 0.68 (d, $J = 7.0$ Hz, 3H), 0.08 (s, 6H); **$^{13}\text{C NMR}$** (126 MHz, CDCl_3) δ 169.49, 141.63, 139.92, 135.89, 128.32, 126.56, 125.95, 125.46, 122.37, 110.98, 79.40, 78.66, 65.00, 36.26, 35.81, 33.87, 29.44, 26.95, 26.09, 26.03, 21.06, 18.54, 17.99, 15.91, -5.06; **IR** (neat):

2956, 2928, 2856, 2904, 1752, 1462, 1379, 1250, 1224, 1176, 1123, 1081, 1006, 976, 815, 776, 719, 702, 668, 617 cm^{-1} ; $[\alpha]^{25}_{\text{D}} -106$ ($c = 1.88$ in CHCl_3); **HRMS** (ES^+): Found 525.3036 (+2.4 ppm), $\text{C}_{29}\text{H}_{46}\text{O}_5\text{SiNa}$ ($\text{M}+\text{Na}^+$) requires 525.3012



(3a*R*,6*S*,7*S*,11*R*,13a*R*,*E*)-6-(3-(5-((*tert*-Butyldimethylsilyl)oxy)pentyl)phenyl)-2,2,7,11-tetramethyl-6,7,8,9,10,11-hexahydro-3a*H*-[1,3]dioxolo[4,5-*c*][1]oxacyclododecin-4(13a*H*)-one ((-)-3.42b**)** Prepared according to Representative Procedure C: **(-)-2.41b** (20 mg, 0.036 mmol), Pd/C (10% w/w, 2 mg), and EtOH (3.6 mL) yielded 11 mg (55%) of the product as a clear oil. Purified by preparative TLC (3% EtOAc in hexanes, eluted twice).

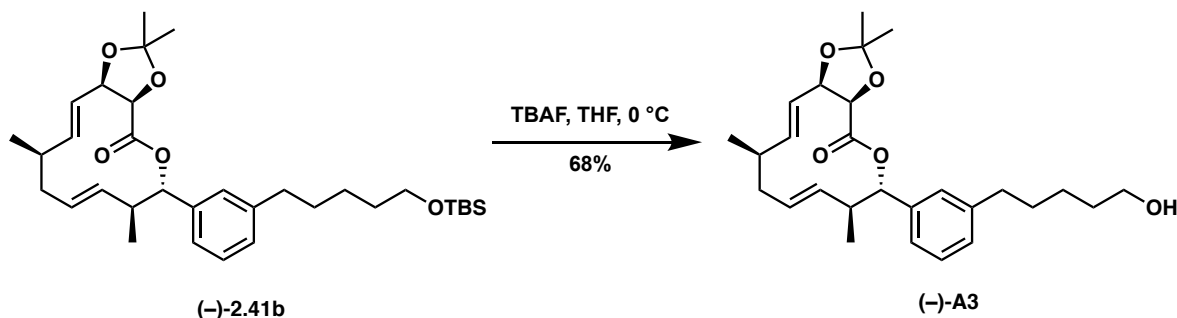
^1H NMR (500 MHz, CDCl_3) δ 7.20 – 7.15 (m, 1H), 7.11 – 7.08 (m, 2H), 7.07 – 7.03 (m, 1H), 5.71 – 5.60 (m, 2H), 5.49 (d, $J = 11.5$ Hz, 1H), 4.87 – 4.80 (m, 1H), 4.54 (d, $J = 6.6$ Hz, 1H), 3.59 (t, $J = 6.6$ Hz, 1H), 2.58 – 2.54 (m, 2H), 2.42 – 2.36 (m, 1H), 2.28 – 2.17 (m, 1H), 2.01 – 1.94 (m, 1H), 1.68 (s, 3H), 1.63 – 1.50 (m, 6H), 1.39 – 1.37 (m, 3H), 1.37 – 1.32 (m, 3H), 1.08 – 1.04 (m, 2H), 1.02 (d, $J = 6.5$ Hz, 3H), 0.89 (s, 9H), 0.68 (d, $J = 7.0$ Hz, 3H), 0.04 (s, 6H); **^{13}C NMR** (126 MHz, CDCl_3) δ 169.49, 142.84, 139.98, 135.91, 128.29, 128.24, 127.83, 125.18, 122.37, 110.99, 79.50, 78.69, 63.37, 36.36, 36.02, 35.82, 33.90, 32.85, 31.41, 29.44, 26.96, 26.14, 26.04, 25.73, 21.07, 18.53, 17.97, 15.95, -5.10; **IR** (neat): 2928, 2856, 2360, 1753, 1608, 1460, 1379, 1250, 1223, 1176, 1085, 1005, 977, 874, 834, 775, 705, 667 cm^{-1} ; $[\alpha]^{25}_{\text{D}} -63.9$ ($c = 0.43$ in CHCl_3); **HRMS** (ES^+): Found 581.3630 (-0.8 ppm), $\text{C}_{33}\text{H}_{54}\text{O}_5\text{SiNa}$ ($\text{M}+\text{Na}^+$) requires 581.3638



Representative Procedure D: TBS removal

(3aR,6S,7S,8E,11R,12E,13aR)-6-(3-(Hydroxymethyl)phenyl)-2,2,7,11-tetramethyl-6,7,10,11-tetrahydro-3aH-[1,3]dioxolo[4,5-c][1]oxacyclododecin-4(13aH)-one ((-)-A1) To a solution of (-)-2.41a (21 mg, 0.0420 mmol) in THF (0.42 mL) was added *tetra*-butylammonium fluoride (1M in THF, 0.13 mL), and the reaction was stirred for 1 hour. The reaction was quenched with saturated aqueous ammonium chloride and diluted in diethyl ether. The organic layer was separated and the aqueous layer was extracted 4 times with diethyl ether. The combined organic layers were washed with water and brine, dried over sodium sulfate, filtered, and concentrated. The crude product was purified by preparative TLC (3:2 hexanes/EtOAc) to afford the product alcohol as a clear oil (15 mg, 94%).

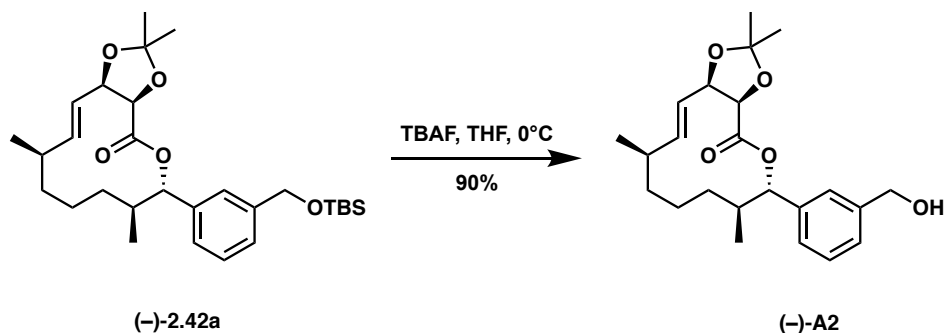
¹H NMR (400 MHz, CDCl₃) δ 7.36 – 7.31 (m, 1H), 7.32 – 7.26 (m, 1H), 7.28 – 7.22 (m, 1H), 5.82 (dd, *J* = 15.7, 6.6 Hz, 1H), 5.58 (d, *J* = 10.8 Hz, 1H), 5.36 – 5.23 (m, 3H), 4.76 – 4.70 (m, 1H), 4.67 (s, 2H), 4.46 (d, *J* = 6.7 Hz, 1H), 2.69 – 2.52 (m, 1H), 2.36 – 2.20 (m, 2H), 2.11 – 1.99 (m, 1H), 1.65 (s, 3H), 1.37 (s, 3H), 1.08 (d, *J* = 6.5 Hz, 3H), 0.76 (d, *J* = 6.8 Hz, 3H); ¹³C NMR (126 MHz, CDCl₃) δ 169.89, 141.29, 139.45, 139.38, 134.63, 130.77, 128.78, 127.33, 127.02, 126.40, 123.67, 111.10, 80.69, 79.22, 78.43, 65.31, 43.15, 38.49, 35.87, 26.91, 25.99, 20.95, 17.61; IR (neat): 3467, 2959, 2929, 2872, 1746, 1455, 1378, 1293, 1251, 1221, 1183, 1161, 1082, 1039, 1000, 969, 910, 880, 785, 729, 705, 673, 647 cm⁻¹; [α]²⁵_D -76.4 (c = 1.40 in CHCl₃); HRMS (ES⁺): Found 387.2169 (+0.3 ppm), C₂₃H₃₀O₅ (M+H⁺) requires 387.2166



(3aR,6S,7S,8E,11R,12E,13aR)-6-(3-(5-Hydroxypentyl)phenyl)-2,2,7,11-tetramethyl-6,7,10,11-tetrahydro-3aH-[1,3]dioxolo[4,5-c][1]oxacyclododecin-4(13aH)-one((-)-A3)

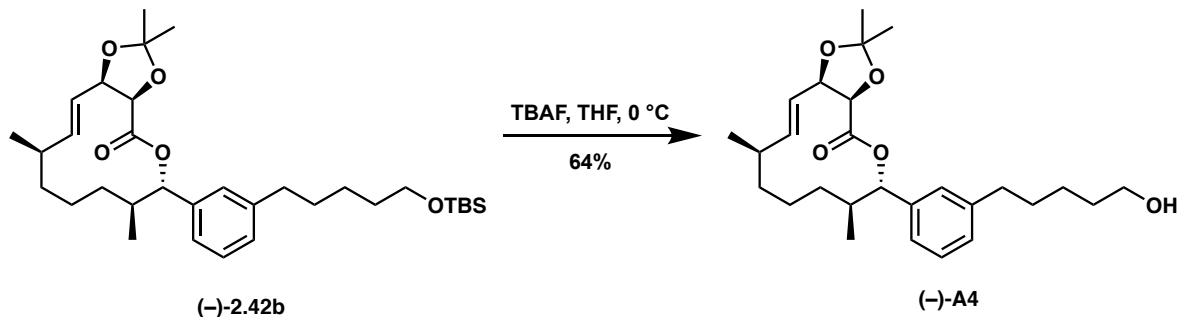
Prepared according to Representative Procedure D: (-)-2.41b (35 mg, 0.063 mmol), TBAF (1M in THF, 0.63 mL), and THF (0.63 mL) yielded 19 mg (68%) of the product as a clear oil. Purified by preparative TLC (1:1 EtOAc/hexanes).

$^1\text{H NMR}$ (400 MHz, CDCl_3) δ 7.25 – 7.20 (m, 1H), 7.16 – 7.08 (m, 3H), 5.82 (dd, $J = 15.6, 6.6$ Hz, 1H), 5.56 (d, $J = 10.8$ Hz, 1H), 5.37 – 5.22 (m, 3H), 4.73 (t, $J = 7.1$ Hz, 1H), 4.47 (d, $J = 6.6$ Hz, 1H), 3.63 (t, $J = 6.6$ Hz, 2H), 2.64 – 2.56 (m, 3H), 2.37 – 2.23 (m, 2H), 2.12 – 2.02 (m, 1H), 1.66 (s, 3H), 1.64 – 1.53 (m, 4H), 1.43 – 1.33 (m, 5H), 1.09 (d, $J = 6.7$ Hz, 3H), 0.76 (d, $J = 6.8$ Hz, 3H); $^{13}\text{C NMR}$ (126 MHz, CDCl_3) δ 169.88, 142.83, 139.44, 138.90, 134.81, 130.65, 128.50, 128.12, 125.24, 123.70, 111.09, 80.88, 79.21, 78.44, 63.05, 43.20, 38.52, 35.91, 32.73, 31.28, 26.92, 25.99, 25.51, 20.99, 17.65; **IR** (neat): 3313, 2927, 2855, 1748, 1608, 1456, 1379, 1221, 1182, 1083, 969, 880, 786, 753, 705, 667 cm^{-1} ; $[\alpha]_D^{25}$ -46.2 ($c = 0.58$ in CHCl_3); **HRMS** (ES^+): Found 443.2788 (-0.4 ppm), $\text{C}_{27}\text{H}_{38}\text{O}_5$ (M^+H^+) requires 443.2792



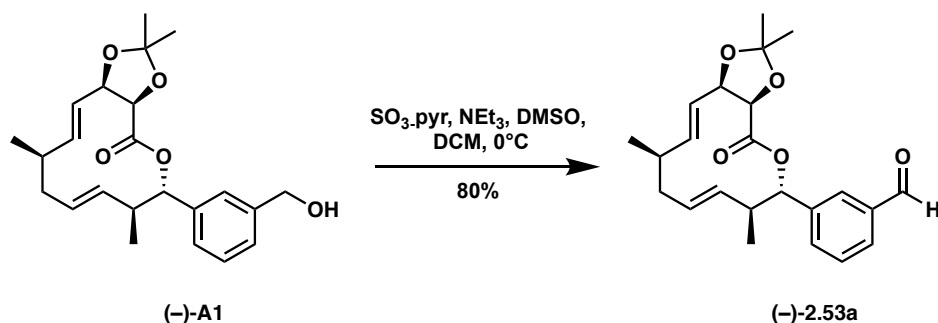
(3a*R*,6*S*,7*S*,11*R*,13a*R*,*E*)-6-(3-(Hydroxymethyl)phenyl)-2,2,7,11-tetramethyl-6,7,8,9,10,11-hexahydro-3a*H*-[1,3]dioxolo[4,5-*c*][1]oxacyclododecin-4(13a*H*)-one ((-)-A2) Prepared according to Representative Procedure D: (-)-2.42a (28 mg, 0.058 mmol), TBAF (1M in THF, 0.17 mL), and THF (0.56 mL) yielded 19.5 mg (90%) of the product as a clear oil. Purified by preparative TLC (3:2 hexanes/EtOAc).

¹H NMR (500 MHz, CDCl₃) δ 7.31 – 7.24 (m, 3H), 7.24 – 7.21 (m, 1H), 5.70 – 5.59 (m, 2H), 5.52 (d, *J* = 11.5 Hz, 1H), 4.87 – 4.82 (m, 1H), 4.66 (s, 2H), 4.54 (d, *J* = 6.6 Hz, 1H), 2.44 – 2.34 (m, 1H), 2.28 – 2.20 (m, 1H), 2.02 – 1.94 (m, 1H), 1.67 (s, 3H), 1.44 – 1.33 (m, 7H), 1.11 – 1.05 (m, 2H), 1.02 (d, *J* = 6.6 Hz, 3H), 0.69 (d, *J* = 7.0 Hz, 3H); **¹³C NMR** (101 MHz, CDCl₃) δ 169.60, 141.08, 140.42, 135.87, 128.70, 127.19, 126.84, 126.42, 122.32, 111.03, 79.32, 78.63, 65.38, 36.23, 35.81, 33.83, 29.34, 26.94, 26.01, 21.07, 17.91, 15.91; **IR** (neat): 3500, 2931, 2360, 2342, 1748, 1455, 1379, 1223, 1182, 1162, 1123, 1083, 974, 909, 873, 837, 738, 729, 704, 648 cm⁻¹; **[α]_D²⁵** -100 (c = 0.50 in CHCl₃); **HRMS** (ES⁺): Found 411.2125 (-1.7 ppm), C₂₃H₃₂O₅Na (M+Na⁺) requires 411.2142



(3aR,6S,7S,11R,13aR,E)-6-(3-(5-Hydroxypentyl)phenyl)-2,2,7,11-tetramethyl-6,7,8,9,10,11-hexahydro-3aH-[1,3]dioxolo[4,5-c][1]oxacyclododecin-4(13aH)-one ((-)-A4) Prepared according to representative Procedure D: (-)-2.42b (21 mg, 0.038 mmol), TBAF (1M in THF, 0.11 mL), and THF (0.38 mL) yielded 10.7 mg (64%) of the product as a clear oil. Purified by preparative TLC (3:2 hexanes/EtOAc).

¹H NMR (400 MHz, CDCl₃) δ 7.21 – 7.15 (m, 1H), 7.12 – 7.08 (m, 2H), 7.07 – 7.03 (m, 1H), 5.71 – 5.57 (m, 2H), 5.48 (d, *J* = 11.5 Hz, 1H), 4.85 (dd, *J* = 6.5, 3.2 Hz, 1H), 4.54 (d, *J* = 6.6 Hz, 1H), 3.62 (t, *J* = 6.6 Hz, 2H), 2.58 (t, *J* = 7.6 Hz, 2H), 2.43 – 2.35 (m, 1H), 2.28 – 2.18 (m, 1H), 2.04 – 1.93 (m, 1H), 1.68 (s, 3H), 1.65 – 1.52 (m, 6H), 1.42 – 1.32 (m, 7H), 1.13 – 1.05 (m, 2H), 1.02 (d, *J* = 6.6 Hz, 3H), 0.68 (d, *J* = 7.0 Hz, 3H); **¹³C NMR** (101 MHz, CDCl₃) δ 169.53, 142.59, 139.95, 135.88, 128.36, 128.27, 128.07, 125.11, 122.34, 111.02, 79.53, 78.64, 63.04, 36.23, 35.88, 35.81, 33.87, 32.73, 31.20, 29.39, 26.94, 26.01, 25.45, 21.07, 17.93, 15.94; **IR** (neat): 3392, 2932, 2859, 2360, 2341, 1748, 1608, 1456, 1380, 1184, 1123, 1083, 976, 874, 836, 785, 752, 705, 667 cm⁻¹; **[α]_D²⁵** -100.6 (c = 0.72 in CHCl₃); **HRMS** (ES⁺): Found 445.2935 (-1.4 ppm), C₂₇H₄₀O₅ (M+H⁺) requires 445.2949

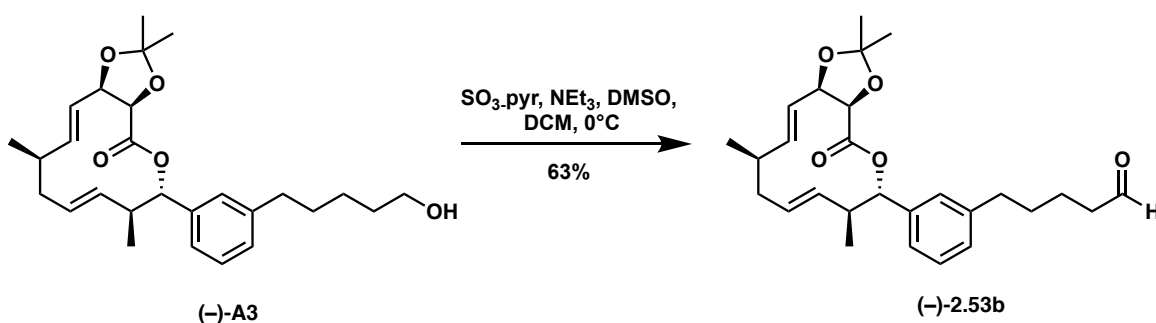


Representative Procedure E: Parikh-Döering Oxidation

3-((3a*R*,6*S*,7*S*,8*E*,11*R*,12*E*,13a*R*)-2,2,7,11-Tetramethyl-4-oxo-4,6,7,10,11,13a-hexahydro-3a*H*-[1,3]dioxolo[4,5-*c*][1]oxacyclododecin-6-yl)benzaldehyde ((-)-2.53a) To a solution of (-)-A1 (10 mg, 0.026 mmol) in DCM (0.26 mL) was added DMSO (0.04 mL, 0.52 mmol) and triethylamine (0.04 mL, 0.26 mmol). The solution was cooled to 0 °C and SO₃-Pyr (33 mg, 0.21 mmol) was added in a single portion. The reaction mixture was removed from the cooling bath and allowed to stir at room temperature for 45 minutes. The reaction was then quenched with saturated aqueous ammonium chloride, diluted in DCM, and poured into a separatory funnel. The organic layer was removed and the aqueous layer was extracted 5x DCM (5 mL). The combined organic layers were washed with brine, dried over sodium sulfate, filtered, and reduced. The residue was purified by preparative TLC (4:1 hexanes/EtOAc) to afford the product as a clear oil (8 mg, 80%).

¹H NMR (500 MHz, CDCl₃) δ 10.01 (s, 1H), 7.88 (s, 1H), 7.85 – 7.78 (m, 1H), 7.64 – 7.55 (m, 1H), 7.50 (t, *J* = 7.6 Hz, 1H), 5.83 (dd, *J* = 15.7, 6.7 Hz, 1H), 5.65 (d, *J* = 10.8 Hz, 1H), 5.36 – 5.21 (m, 3H), 4.78 – 4.72 (m, 1H), 4.48 (d, *J* = 6.6 Hz, 1H), 2.66 – 2.57 (m, 1H), 2.37 – 2.31 (m, 1H), 2.30 – 2.24 (m, 1H), 2.12 – 2.05 (m, 1H), 1.66 (s, 3H), 1.37 (s, 3H), 1.09 (d, *J* = 6.8 Hz, 3H), 0.77 (d, *J* = 6.8 Hz, 3H); ¹³C NMR (101 MHz, CDCl₃) δ 192.15, 169.90, 140.35, 139.60, 136.78, 134.20, 134.07, 131.21, 130.07, 129.32, 128.66, 123.52, 111.19, 79.99, 79.23, 78.34, 43.20, 38.41, 35.84, 26.88, 25.96, 20.90, 17.45; IR (neat): 2958, 2927, 2876, 2851, 2726, 2257, 1821, 1748,

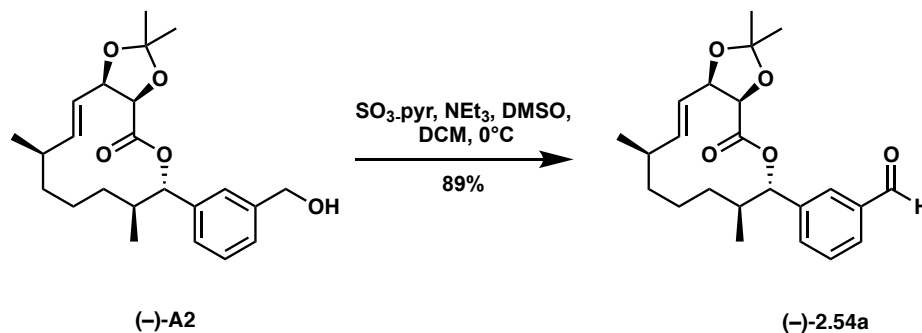
1699, 1604, 1535, 1455, 1379, 1290, 1250, 1220, 1180, 1161, 1040, 1000, 969, 911, 880, 785, 731, 696, 675, 650 cm^{-1} ; $[\alpha]^{25}_{\text{D}} -65.3$ ($c = 0.30$ in CHCl_3); **HRMS** (ES^+): Found 407.1825 (-0.9 ppm), $\text{C}_{23}\text{H}_{28}\text{O}_5\text{Na}$ ($\text{M}+\text{Na}^+$) requires 407.1834



5-(3-((3aR,6S,7S,8E,11R,12E,13aR)-2,2,7,11-Tetramethyl-4-oxo-4,6,7,10,11,13a-hexahydro-3aH-[1,3]dioxolo[4,5-c][1]oxacyclododecin-6-yl)phenyl)pentanal **(-)-2.53** Prepared according to Representative Procedure E: **(-)-A3** (10 mg, 0.026 mmol), DMSO (0.03 mL, 0.45 mmol), triethylamine (0.03 mL, 0.23 mmol), $\text{SO}_3\text{-Pyr}$ (29 mg, 0.18 mmol), and DCM (0.23 mL) yielded 6.2 mg (63%) of the product as a clear oil. Purified by preparative TLC (4:1 hexanes/EtOAc).

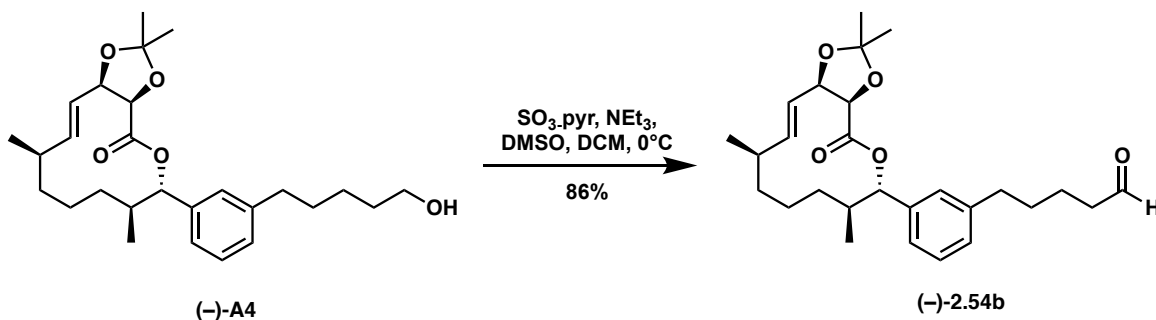
$^1\text{H NMR}$ (400 MHz, CDCl_3) δ 9.76 (t, $J = 3.6$ Hz, 1H), 7.22 (t, $J = 7.4$ Hz, 1H), 7.16 – 7.07 (m, 3H), 5.82 (dd, $J = 15.6, 6.6$ Hz, 1H), 5.56 (d, $J = 10.9$ Hz, 1H), 5.36 – 5.23 (m, 3H), 4.76 – 4.70 (m, 1H), 4.47 (d, $J = 6.6$ Hz, 1H), 2.64 – 2.52 (m, 3H), 2.49 – 2.42 (m, 2H), 2.36 – 2.21 (m, 2H), 2.11 – 2.01 (m, 1H), 1.70 – 1.62 (m, 7H), 1.37 (s, 3H), 1.08 (d, $J = 6.7$ Hz, 3H), 0.75 (d, $J = 6.8$ Hz, 3H); **$^{13}\text{C NMR}$** (126 MHz, CDCl_3) δ 202.69, 169.89, 142.25, 139.42, 139.06, 134.77, 130.70, 128.56, 128.47, 125.49, 123.69, 111.08, 80.79, 79.20, 78.46, 43.87, 43.29, 38.54, 35.90, 35.71, 30.97, 26.92, 26.00, 21.86, 21.01, 17.66; **IR** (neat): 3031, 2959, 2024, 2873, 2854, 2720, 2360, 2343, 1748, 1724, 1608, 1559, 1488, 1457, 1379, 1252, 1222, 1183, 1084, 1041, 1000, 970, 880,

786, 706, 667 cm^{-1} ; $[\alpha]_{\text{D}}^{25}$ -84 ($c = 0.22$ in CHCl_3); **HRMS** (ES^+): Found 463.2487 (+2.7 ppm), $\text{C}_{27}\text{H}_{36}\text{O}_5\text{Na}$ ($\text{M}+\text{Na}^+$) requires 463.2460



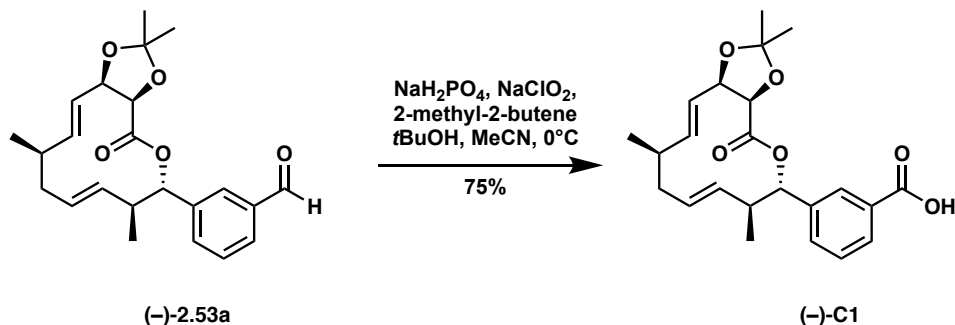
3-((3aR,6S,7S,11R,13aR,E)-2,2,7,11-Tetramethyl-4-oxo-4,6,7,8,9,10,11,13a-octahydro-3aH-[1,3]dioxolo[4,5-c][1]oxacyclododecin-6-yl)benzaldehyde ((-)-2.54a) Prepared according to Representative Procedure E: (-)-A2 (14 mg, 0.036 mmol), DMSO (0.05 mL, 0.72 mmol), triethylamine (0.05 mL, 0.36 mL) $\text{SO}_3\text{-Pyr}$ (46 mg, 0.29 mmol), and DCM (0.36 mL) yielded 12.5 mg (89%) of the product as a clear oil. Purified by preparative TLC (4:1 hexanes/EtOAc).

$^1\text{H NMR}$ (400 MHz, CDCl_3) δ 9.99 (s, 1H), 7.84 – 7.83 (m, 1H), 7.80 – 7.77 (m, 1H), 7.60 – 7.55 (m, 1H), 7.47 (t, $J = 7.6$ Hz, 1H), 5.74 – 5.63 (m, 2H), 5.59 (d, $J = 11.5$ Hz, 1H), 4.86 (dd, $J = 6.5, 3.3$ Hz, 1H), 4.55 (d, $J = 6.6$ Hz, 1H), 2.46 – 2.35 (m, 1H), 2.33 – 2.23 (m, 1H), 2.06 – 1.97 (m, 1H), 1.67 (s, 3H), 1.46 – 1.35 (m, 6H), 1.13 – 1.06 (m, 2H), 1.02 (d, $J = 6.6$ Hz, 3H), 0.69 (d, $J = 7.0$ Hz, 3H); $^{13}\text{C NMR}$ (126 MHz, CDCl_3) δ 192.19, 169.65, 141.40, 136.72, 135.92, 134.18, 129.80, 129.23, 128.77, 122.31, 111.13, 78.64, 78.58, 36.33, 35.81, 33.77, 29.27, 26.92, 25.99, 21.05, 17.90, 15.79; **IR** (neat): 2959, 2926, 2852, 2729, 2160, 2031, 1974, 1790, 1749, 1698, 1604, 1455, 1379, 1288, 1224, 1178, 1160, 1124, 1082, 977, 908, 873, 837, 789, 728, 696, 650 cm^{-1} ; $[\alpha]_{\text{D}}^{25}$ -84.4 ($c = 0.50$ in CHCl_3); **HRMS** (ES^+): Found 409.1999 (+0.8 ppm), $\text{C}_{23}\text{H}_{30}\text{O}_5\text{Na}$ ($\text{M}+\text{Na}^+$) requires 409.1991



5-(3-((3a*R*,6*S*,7*S*,11*R*,13a*R*,*E*)-2,2,7,11-Tetramethyl-4-oxo-4,6,7,8,9,10,11,13a-octahydro-3a*H*-[1,3]dioxolo[4,5-*c*][1]oxacyclododecin-6-yl)phenyl)pentanal ((-)-2.54b) Prepared according to Representative Procedure E: (-)-A4 (7.0 mg, 0.016 mmol), DMSO (0.02 mL, 0.315 mmol), triethylamine (0.02 mL, 0.157 mmol) SO₃-Pyr (20 mg, 0.126 mmol), and DCM (0.16 mL) yielded 6 mg (86 %) of the product as a clear oil. Purified by preparative TLC (4:1 hexanes/EtOAc).

¹H NMR (500 MHz, CDCl₃) δ 9.75 (s, 1H), 7.19 (t, *J* = 7.5 Hz, 1H), 7.13 – 7.04 (m, 3H), 5.71 – 5.60 (m, 2H), 5.49 (d, *J* = 11.5 Hz, 1H), 4.86 – 4.84 (m, 1H), 4.54 (d, *J* = 6.6 Hz, 1H), 2.59 (t, *J* = 7.1 Hz, 2H), 2.46 – 2.43 (m, 2H), 2.40 – 2.35 (m, 1H), 2.25 – 2.18 (m, 1H), 2.02 – 1.95 (m, 1H), 1.68 (s, 3H), 1.66 – 1.61 (m, 4H), 1.42 – 1.34 (m, 6H), 1.09 – 1.05 (m, 2H), 1.02 (d, *J* = 6.6 Hz, 3H), 0.68 (d, *J* = 7.0 Hz, 3H); **¹³C NMR** (126 MHz, CDCl₃) δ 202.74, 169.52, 142.02, 140.15, 135.91, 128.44, 128.22, 127.87, 125.40, 122.36, 111.01, 79.45, 78.67, 43.87, 36.33, 35.82, 35.68, 33.88, 30.92, 29.41, 26.96, 26.03, 21.85, 21.07, 17.95, 15.94; **IR** (neat): 2926, 2855, 1749, 1724, 1608, 1488, 1456, 1379, 1223, 1180, 1124, 1084, 977, 911, 874, 836, 785, 731, 706, 648 cm⁻¹; **[α]_D²⁵** -76.6 (c = 0.60 in CHCl₃); **HRMS** (ES⁺): Found 443.2757 (-4.0 ppm), C₂₇H₃₉O₅ (M+H⁺) requires 443.2797

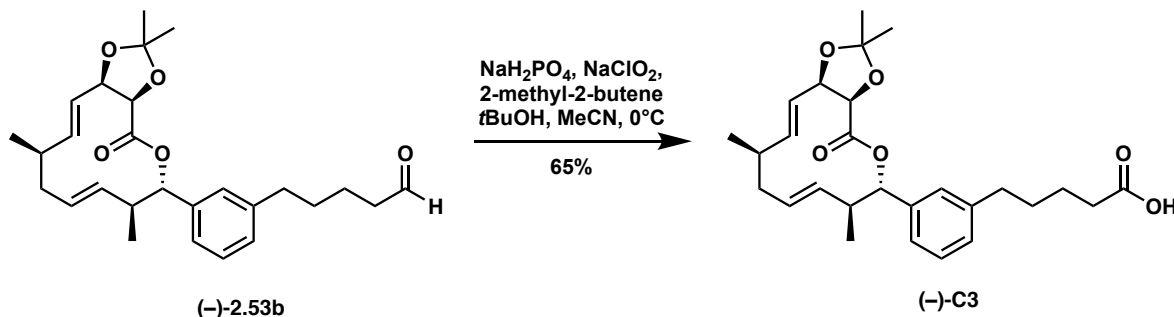


Representative Procedure F: Pinnick Oxidation

3-((3a*R*,6*S*,7*S*,8*E*,11*R*,12*E*,13a*R*)-2,2,7,11-Tetramethyl-4-oxo-4,6,7,10,11,13a-hexahydro-3a*H*-[1,3]dioxolo[4,5-*c*][1]oxacyclododecin-6-yl)benzoic acid ((-)-C1) To a rapidly stirring solution of (-)-2.53a (8.0 mg, 0.021 mmol) in *tert*-butyl alcohol (0.42 mL) and acetonitrile (0.21 mL) was added 2-methyl-2-butene (neat, 0.11 mL), and the reaction vessel was sparged with argon. The solution was cooled to 0 °C, and a freshly prepared solution of NaH₂PO₄ (12 mg, 0.10 mmol) and NaClO₂ (10 mg, 0.11 mmol) in water (0.62 mL) was added dropwise. The reaction was slowly warmed to room temperature and stirred overnight. The reaction was quenched by addition of a saturated aqueous solution of sodium thiosulfate (1 mL) and diluted in EtOAc. The aqueous layer was separated and acidified to pH 3 with 1N HCl. The acidified aqueous layer was extracted 5x EtOAc (5x 5 mL). The combined organic extracts were washed with brine, dried over sodium sulfate, filtered, and concentrated. The residue was purified by preparative TLC (1% AcOH, 49% hexanes, 50% EtOAc) to afford the product (6 mg, 75%) as an off white residue.

¹H NMR (500 MHz, CDCl₃) δ 8.10 (s, 1H), 8.06 – 8.02 (m, 1H), 7.60 – 7.55 (m, 1H), 7.44 (t, *J* = 7.7 Hz, 1H), 5.87 – 5.79 (m, 1H), 5.65 (d, *J* = 10.8 Hz, 1H), 5.36 – 5.21 (m, 3H), 4.78 – 4.71 (m, 1H), 4.50 (d, *J* = 6.6 Hz, 1H), 2.70 – 2.57 (m, 1H), 2.35 – 2.24 (m, 2H), 2.11 – 2.02 (m, 1H), 1.66 (s, 3H), 1.38 (s, 3H), 1.09 (d, *J* = 6.8 Hz, 3H), 0.77 (d, *J* = 6.8 Hz, 3H); **¹³C NMR** (101 MHz, CDCl₃) δ 170.96, 169.90, 139.76, 139.54, 134.21, 133.65, 131.14, 130.31, 129.67, 129.40, 128.81,

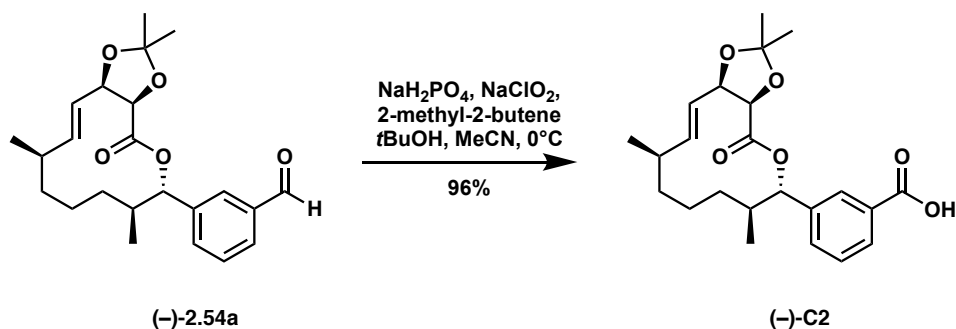
123.56, 111.17, 80.09, 79.21, 78.36, 43.28, 38.46, 35.87, 26.89, 25.97, 20.94, 17.50; **IR** (neat): 2957, 2925, 2853, 2360, 1749, 1727, 1693, 1554, 1486, 1455, 1379, 1252, 1222, 1177, 1083, 1039, 970, 913, 880, 814, 784, 758, 696, 668 cm^{-1} ; $[\alpha]^{25}_{\text{D}} -169$ ($c = 0.40$ in CHCl_3); **HRMS** (ES^+): Found 423.1777 (-0.1 ppm), $\text{C}_{23}\text{H}_{28}\text{O}_6\text{Na}$ ($\text{M}+\text{Na}^+$) requires 423.1778



5-(3-((3a*R*,6*S*,7*S*,8*E*,11*R*,12*E*,13a*R*)-2,2,7,11-Tetramethyl-4-oxo-4,6,7,10,11,13a-hexahydro-3a*H*-[1,3]dioxolo[4,5-*c*][1]oxacyclododecin-6-yl)phenyl)pentanoic acid ((-)-C3) Prepared according to Representative Procedure F: **(-)-2.53b** (5.0 mg, 0.011 mmol), *tert*-butyl alcohol (0.23 mL), 2-methyl-2 butene (0.06 mL), acetonitrile (0.11 mL), NaH_2PO_4 (7.0 mg, 0.057 mmol), NaClO_2 (6.0 mg, 0.062 mmol), and H_2O (0.34 mL) yielded 3.3 mg (65%) of the product as an off-white residue. Purified by preparative TLC (1% AcOH, 49% hexanes, 50% EtOAc).

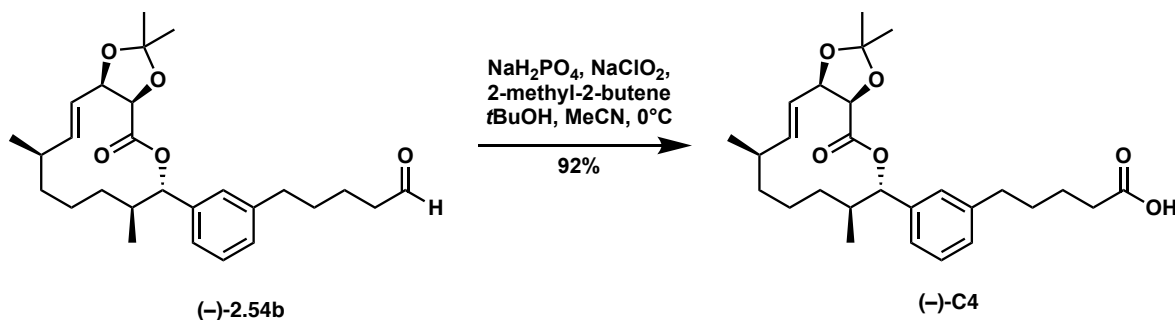
$^1\text{H NMR}$ (500 MHz, CDCl_3) δ 7.22 (t, $J = 7.5$ Hz, 1H), 7.16 – 7.12 (m, 2H), 7.10 – 7.08 (m, 1H), 5.85 – 5.79 (m, 1H), 5.56 (d, $J = 10.8$ Hz, 1H), 5.35 – 5.24 (m, 3H), 4.76 – 4.72 (m, 1H), 4.48 (d, $J = 6.7$ Hz, 1H), 2.65 – 2.55 (m, 3H), 2.39 – 2.34 (m, 2H), 2.34 – 2.30 (m, 1H), 2.28 – 2.24 (m, 1H), 2.10 – 2.02 (m, 1H), 1.69 – 1.63 (m, 7H), 1.38 (s, 3H), 1.09 (d, $J = 6.8$ Hz, 3H), 0.76 (d, $J = 6.8$ Hz, 3H); **$^{13}\text{C NMR}$** (101 MHz, CDCl_3) δ 177.74, 169.87, 142.32, 139.48, 138.99, 134.78, 130.68, 128.55, 128.52, 125.43, 123.65, 111.12, 80.82, 79.21, 78.40, 43.16, 38.51, 35.88, 35.54, 33.63, 30.76, 26.91, 26.00, 24.37, 21.01, 17.65; **IR** (neat): 2925, 2854, 1747, 1707, 1608, 1488, 1455, 1412, 1378, 1221, 1182, 1162, 1084, 1042, 1000, 969, 880, 786, 755, 705, 667 cm^{-1} ; $[\alpha]^{25}_{\text{D}}$

-67.2 (c = 0.33 in CHCl₃); **HRMS** (ES⁺): Found 457.2576 (-0.9 ppm), C₂₇H₃₆O₆ (M+H⁺) requires 457.2585



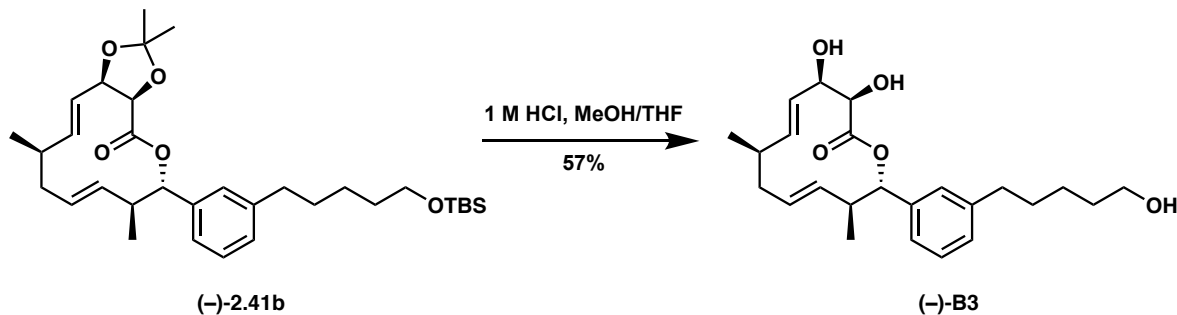
3-((3aR,6S,7S,11R,13aR,E)-2,2,7,11-Tetramethyl-4-oxo-4,6,7,8,9,10,11,13a-octahydro-3aH-[1,3]dioxolo[4,5-c][1]oxacyclododecin-6-yl)benzoic acid ((-)-C2) Prepared according to Representative Procedure F: (-)-**2.54a** (5.0 mg, 0.013 mmol), *tert*-butyl alcohol (0.26 mL), 2-methyl-2 butene (0.07 mL), acetonitrile (0.13 mL), NaH₂PO₄ (8.0 mg, 0.065 mmol), NaClO₂ (6.0 mg, 0.071 mmol), and H₂O (0.39 mL) yielded 5 mg (96%) of the product as an off-white residue. Purified by preparative TLC (1% AcOH, 49% hexanes, 50% EtOAc).

¹H NMR (500 MHz, CDCl₃) δ 8.06 (s, 1H), 8.02 – 7.98 (m, 1H), 7.57 – 7.53 (m, 1H), 7.40 (t, *J* = 7.7 Hz, 1H), 5.72 – 5.62 (m, 2H), 5.58 (d, *J* = 11.5 Hz, 1H), 4.87 (dd, *J* = 6.6, 3.6 Hz, 1H), 4.57 (d, *J* = 6.5 Hz, 1H), 2.46 – 2.35 (m, 1H), 2.31 – 2.23 (m, 1H), 2.05 – 1.98 (m, 1H), 1.68 (s, 3H), 1.42 – 1.36 (m, 6H), 1.11 – 1.07 (m, 2H), 1.03 (d, *J* = 6.6 Hz, 3H), 0.70 (d, *J* = 7.0 Hz, 3H); **¹³C NMR** (126 MHz, CDCl₃) δ 170.82, 169.60, 140.81, 135.91, 133.64, 130.10, 129.55, 129.30, 128.68, 122.34, 111.09, 78.75, 78.59, 36.38, 35.81, 33.80, 29.31, 26.94, 26.00, 21.06, 17.92, 15.81; **IR** (neat): 2927, 2853, 2553, 1781, 1749, 1681, 1608, 1589, 1454, 1413, 1380, 1283, 1228, 1175, 1123, 1084, 979, 940, 893, 873, 825, 782, 758, 723, 695, 677 cm⁻¹; **[α]_D²⁵** -130.5 (c = 0.36 in CHCl₃); **HRMS** (ES⁺): Found 369.1669 (-0.3 ppm), C₂₀H₂₆O₅Na (M+Na⁺) requires 369.1672



5-(3-((3a*R*,6*S*,7*S*,11*R*,13a*R*,*E*)-2,2,7,11-Tetramethyl-4-oxo-4,6,7,8,9,10,11,13a-octahydro-3a*H*-[1,3]dioxolo[4,5-*c*][1]oxacyclododecin-6-yl)phenyl)pentanoic acid ((-)-C4) Prepared according to Representative Procedure F: (-)-2.54b (6.0 mg, 0.014 mmol), *tert*-butyl alcohol (0.27 mL), 2-methyl-2 butene (0.07 mL), acetonitrile (0.14 mL), NaH₂PO₄ (8.1 mg, 0.068 mmol), NaClO₂ (6.7 mg, 0.075 mmol), and H₂O (0.41 mL) yielded 5.7 mg (92%) of the product as an off-white residue. Purified by preparative TLC (1% AcOH, 49% hexanes, 50% EtOAc).

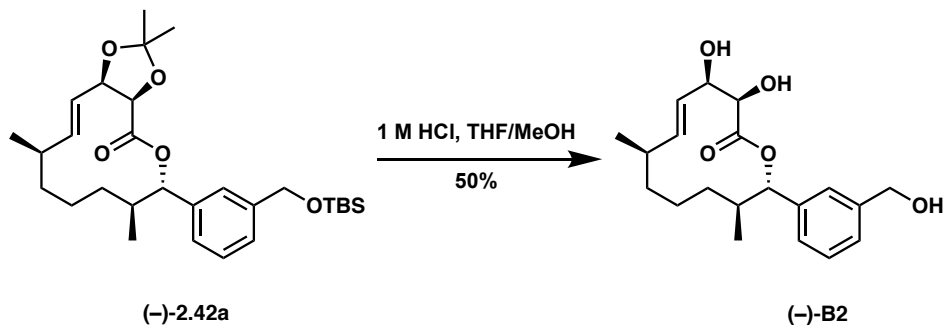
¹H NMR (500 MHz, CDCl₃) δ 7.21 – 7.16 (m, 1H), 7.13 – 7.09 (m, 2H), 7.07 – 7.03 (m, 1H), 5.70 – 5.59 (m, 2H), 5.49 (d, *J* = 11.5 Hz, 1H), 4.85 (ddd, *J* = 6.5, 3.9, 0.9 Hz, 1H), 4.55 (d, *J* = 6.5 Hz, 1H), 2.64 – 2.57 (m, 2H), 2.41 – 2.32 (m, 3H), 2.26 – 2.19 (m, 1H), 2.02 – 1.94 (m, 1H), 1.68 (s, 3H), 1.66 – 1.60 (m, 4H), 1.41 – 1.36 (m, 6H), 1.09 – 1.05 (m, 2H), 1.02 (d, *J* = 6.6 Hz, 3H), 0.68 (d, *J* = 7.0 Hz, 3H); **¹³C NMR** (126 MHz, CDCl₃) δ 169.51, 142.11, 140.09, 135.91, 128.38, 127.90, 125.33, 122.32, 111.08, 79.50, 78.62, 76.91, 36.22, 35.83, 35.51, 33.89, 33.62, 32.08, 30.68, 29.40, 26.94, 26.03, 24.36, 22.85, 21.09, 17.95, 15.94, 14.28; **IR** (neat): 2921, 2852, 1750, 1708, 1607, 1554, 1456, 1377, 1284, 1224, 1178, 1124, 1085, 977, 874, 836, 787, 720, 706 cm⁻¹; **[α]_D²⁵** -48.1 (*c* = 0.54 in CHCl₃); **HRMS** (ES⁺): Found 481.2583, C₂₇H₃₈O₆Na (M+Na⁺) requires 481.2566



(3*R*,4*R*,5*E*,7*R*,9*E*,11*S*,12*S*)-3,4-Dihydroxy-12-(3-(5-hydroxypentyl)phenyl)-7,11-

dimethyloxacyclododeca-5,9-dien-2-one ((-)-B3) Prepared according to Representative Procedure G: (-)-2.41b (19 mg, 0.034 mmol), MeOH (1.7 mL), THF (0.37 mL), and 1N HCl (1.7 mL) yielded 8 mg (57 %) of the product as an off-white residue. Purified by preparative TLC (5% MeOH in DCM).

¹H NMR (500 MHz, CDCl₃) δ 7.26 – 7.22 (m, 1H), 7.15 – 7.09 (m, 3H), 5.41 – 5.35 (m, 2H), 5.35 – 5.29 (m, 2H), 5.07 – 4.97 (m, 1H), 4.45 (d, *J* = 2.8 Hz, 1H), 4.09 (d, *J* = 2.8 Hz, 1H), 3.61 (t, *J* = 6.5 Hz, 2H), 2.67 – 2.54 (m, 4H), 2.25 – 2.18 (m, 2H), 1.80 – 1.70 (m, 1H), 1.69 – 1.52 (m, 6H), 1.41 – 1.32 (m, 2H), 1.08 (d, *J* = 6.5 Hz, 3H), 0.72 (d, *J* = 6.8 Hz, 3H); **¹³C NMR** (126 MHz, CDCl₃) δ 171.96, 142.83, 138.81, 135.22, 134.31, 131.26, 128.62, 128.53, 128.05, 126.56, 125.17, 81.67, 74.11, 73.80, 62.99, 43.42, 40.93, 38.36, 35.82, 32.62, 31.10, 25.29, 21.42, 17.69; **IR** (neat): 3409, 2925, 2854, 1729, 1608, 1589, 1488, 1453, 1373, 1235, 1192, 1111, 1080, 1018, 965, 887, 839, 794, 706, 647 cm⁻¹; **[α]_D²⁵** -36.2 (c = 0.64 in CHCl₃); **HRMS** (ES⁺): Found 403.2481 (+0.2 ppm), C₂₄H₃₄O₅ (M+H⁺) requires 403.2479

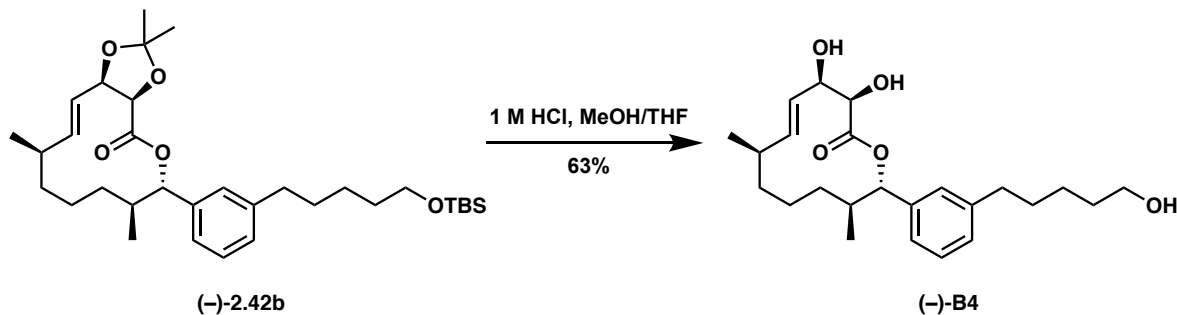


(3*R*,4*R*,7*R*,11*S*,12*S*,*E*)-3,4-Dihydroxy-12-(3-(hydroxymethyl)phenyl)-7,11-

dimethyloxacyclododec-5-en-2-one ((-)-B2) Prepared according to Representative Procedure G:

(-)-2.42a (14 mg, 0.028 mmol), MeOH (1.4 mL), THF (0.30 mL), and 1N HCl (1.4 mL) yielded 5 mg (50 %) of the product as an off-white residue. Purified by preparative TLC (5% MeOH in DCM).

¹H NMR (500 MHz, CDCl₃) δ 7.34 – 7.26 (m, 3H), 7.24 – 7.21 (m, 1H), 5.61 (dd, *J* = 15.4, 2.3 Hz, 1H), 5.55 – 5.45 (m, 1H), 5.29 (d, *J* = 11.4 Hz, 1H), 4.68 (s, 2H), 4.53 – 4.46 (m, 1H), 4.19 (dd, *J* = 8.8, 3.7 Hz, 1H), 3.25 (d, *J* = 8.8 Hz, 1H), 2.47 – 2.35 (m, 2H), 2.29 – 2.19 (m, 1H), 2.02 – 1.94 (m, 1H), 1.79 (s, 1H), 1.48 – 1.28 (m, 3H), 1.13 – 1.07 (m, 2H), 1.01 (d, *J* = 6.5 Hz, 3H), 0.67 (d, *J* = 7.0 Hz, 3H); ¹³C NMR (126 MHz, CDCl₃) δ 171.98, 141.23, 140.28, 134.54, 128.73, 127.08, 126.93, 126.00, 125.57, 80.86, 73.78, 73.02, 65.32, 36.77, 35.84, 34.60, 28.76, 21.86, 18.96, 15.66; IR (neat): 3441, 3413, 3240, 2965, 2936, 2857, 2360, 2342, 1727, 1451, 1373, 1353, 1307, 1247, 1203, 1125, 1096, 1051, 1016, 982, 908, 890, 864, 837, 799, 784, 718, 668, 654 cm⁻¹; [α]_D²⁵ -49.8 (c = 0.90 in CHCl₃); HRMS (ES⁺): Found 371.1874 (+4.0 ppm), C₂₀H₂₈O₅Na (M+Na⁺) requires 371.1834

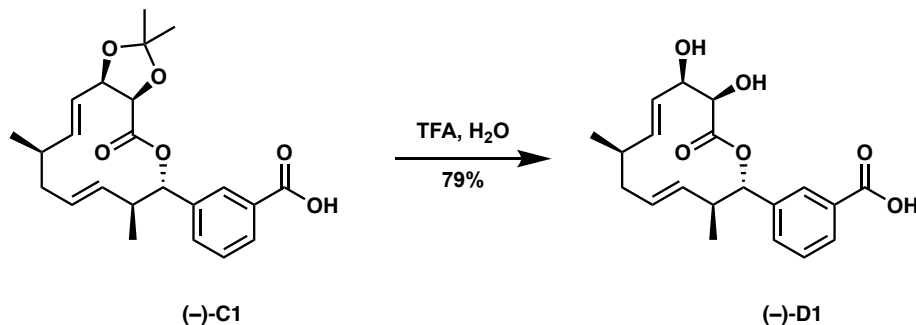


(3*R*,4*R*,7*R*,11*S*,12*S*,*E*)-3,4-Dihydroxy-12-(3-(5-hydroxypentyl)phenyl)-7,11-

dimethyloxacyclododec-5-en-2-one ((-)-B4) Prepared according to Representative Procedure G:

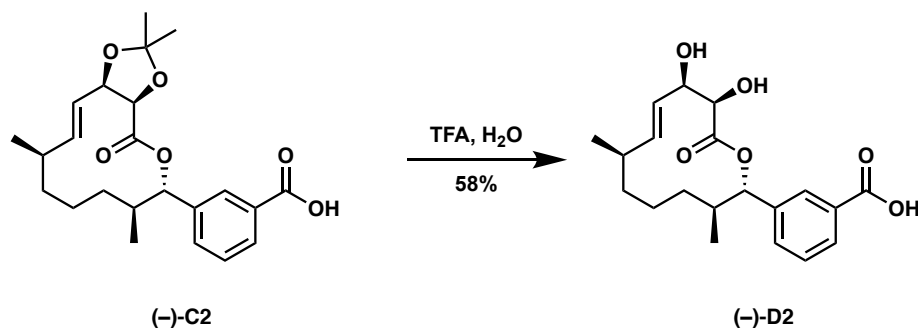
(-)-2.42b (11 mg, 0.020 mmol), MeOH (1.0 mL), THF (0.22 mL), and 1N HCl (1.0 mL) yielded 5 mg (63 %) of the product as an off-white residue. Purified by preparative TLC (5% MeOH in DCM).

¹H NMR (400 MHz, CDCl₃) δ 7.25 – 7.17 (m, 1H), 7.14 – 7.04 (m, 3H), 5.66 – 5.44 (m, 2H), 5.26 (d, *J* = 11.4 Hz, 1H), 4.50 (s, 1H), 4.19 (d, *J* = 3.6 Hz, 1H), 3.60 (t, *J* = 6.5 Hz, 2H), 2.61 (t, *J* = 7.4 Hz, 2H), 2.54 – 2.46 (m, 1H), 2.42 – 2.33 (m, 1H), 2.27 – 2.17 (m, 1H), 2.01 – 1.93 (m, 1H), 1.67 – 1.51 (m, 7H), 1.38 – 1.31 (m, 4H), 1.11 – 1.04 (m, 2H), 1.01 (d, *J* = 6.5 Hz, 3H), 0.68 (d, *J* = 7.0 Hz, 3H); ¹³C NMR (126 MHz, CDCl₃) δ 171.94, 142.63, 139.77, 134.50, 128.45, 127.97, 125.59, 124.99, 81.00, 73.81, 73.01, 63.02, 36.65, 35.78, 34.63, 32.62, 30.98, 28.77, 25.18, 21.87, 18.92, 15.66, 1.17; IR (neat): 3423, 2930, 1732, 1553, 1450, 1373, 1201, 1125, 1055, 1013, 979, 844, 780, 710 cm⁻¹; [α]_D²⁵ -52.9 (c = 0.17 in CHCl₃); HRMS (ES⁺): Found 427.2445 (-1.0 ppm), C₂₄H₃₆O₅Na (M+Na⁺) requires 427.2455



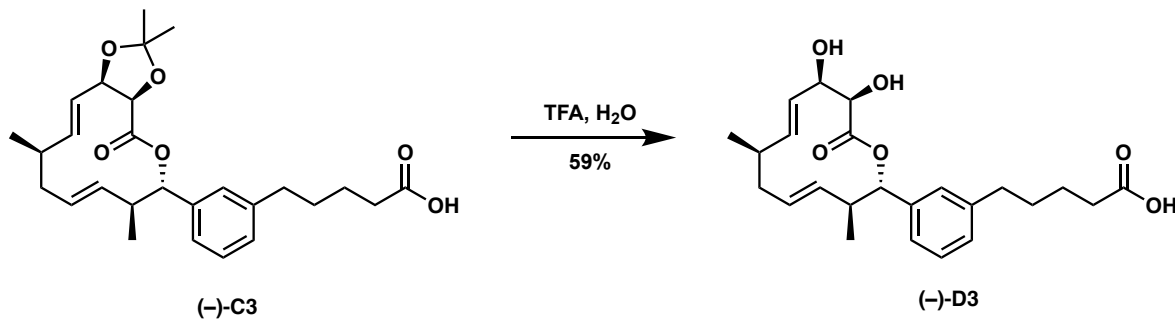
3-((2*S*,3*S*,4*E*,7*R*,8*E*,10*R*,11*R*)-10,11-Dihydroxy-3,7-dimethyl-12-oxooxacyclododeca-4,8-dien-2-yl)benzoic acid ((-)-D1) To a solution of (-)-C1 (6.0 mg, 0.015 mmol) in H₂O (0.08 mL) at room temperature was added TFA (0.08 mL), and the reaction vessel was sparged with argon. The reaction was allowed to stir for 48 hours. The solvent was removed and the residue was co-evaporated with ethanol twice to remove residual water. If necessary, nonpolar impurities may be removed by taking up the product in acetonitrile, washing 5 x 1mL pentane, and reducing the acetonitrile fraction. In this manner, 4.4 mg (79%) of the product was obtained as an off-white residue.

¹H NMR (500 MHz, CDCl₃) δ 8.08 (s, 1H), 8.04 (d, *J* = 7.7 Hz, 1H), 7.58 (d, *J* = 7.5 Hz, 1H), 7.46 (t, *J* = 7.5 Hz, 1H), 5.45 – 5.31 (m, 4H), 5.03 (dd, *J* = 14.9, 9.6 Hz, 1H), 4.49 (s, 1H), 4.16 – 4.11 (m, 1H), 2.68 – 2.57 (m, 1H), 2.24 (d, *J* = 12.6 Hz, 2H), 1.77 (q, *J* = 12.2 Hz, 1H), 1.09 (d, *J* = 6.4 Hz, 3H), 0.72 (d, *J* = 6.7 Hz, 3H); **¹³C NMR** (126 MHz, CDCl₃) δ 172.11, 170.57, 139.68, 135.35, 133.69, 133.46, 131.81, 130.41, 129.78, 129.32, 128.89, 126.45, 81.00, 74.10, 73.82, 43.48, 40.91, 38.36, 21.40, 17.55; **IR** (neat): 3409, 2957, 2926, 2871, 1721, 692, 1609, 1591, 1453, 1411, 1375, 1192, 1109, 1080, 1019, 967, 909, 861, 839, 800, 757, 730, 697, 667, 656 cm⁻¹; **[α]²⁵_D** -139 (c = 0.50 in CHCl₃); **HRMS** (ES⁺): Found 383.1503 (+3.2 ppm), C₂₀H₂₄O₆Na (M+Na⁺) requires 383.1471



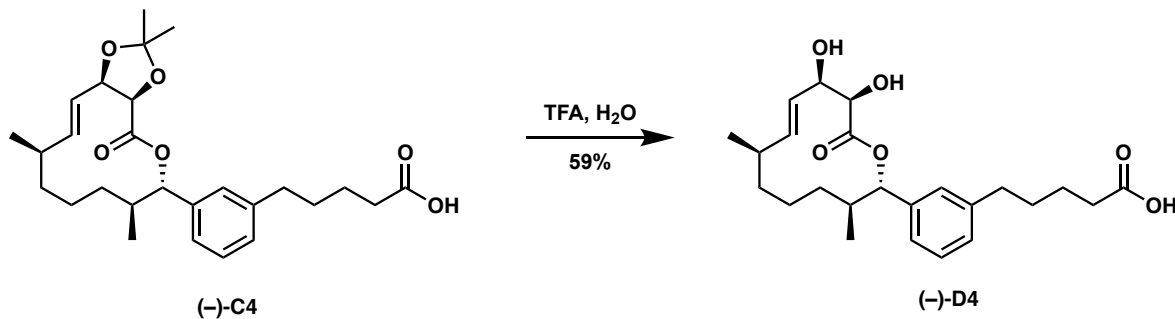
3-((2*S*,3*S*,7*R*,10*R*,*E*)-10,11-dihydroxy-3,7-dimethyl-12-oxooxacyclododec-8-en-2-yl)benzoic acid ((-)-D2) To a solution of (-)-C2 (11.8 mg, 0.029 mmol) in H₂O (1.45 mL) at room temperature was added TFA (1.45 mL), and the reaction vessel was sparged with argon. The reaction was allowed to stir for 48 hours. The solvent was removed and the residue was co-evaporated with ethanol twice to remove residual water. Crude product was purified via preparative TLC (1:1 hexanes in ethyl acetate with 1% acetic acid) to yield 6.1 mg (58%). If necessary, nonpolar impurities may be removed by taking up the product in acetonitrile, washing 5 x 1mL pentane, and reducing the acetonitrile fraction.

¹H NMR (500 MHz, CDCl₃) δ 8.04 (t, *J* = 24.3 Hz, 1H), 7.56 (d, *J* = 25.4 Hz, 1H), 7.43 (s, 1H), 5.61 (d, *J* = 15.2 Hz, 1H), 5.50 (s, 1H), 5.33 (d, *J* = 10.7 Hz, 1H), 4.52 (s, 1H), 4.23 (s, 1H), 3.34 (s, 1H), 2.38 (s, 1H), 2.24 (s, 1H), 2.00 (s, 1H), 1.29 (d, *J* = 46.8 Hz, 3H), 1.09 (s, 1H), 1.00 (s, 1H), 0.92 (s, 1H), 0.72 (s, 1H), 0.66 (s, 1H); [α]_D²⁵ -33 (c = 0.0023 in CHCl₃); **¹³C NMR** (126 MHz, CDCl₃) δ 171.88, 169.23, 140.53, 134.38, 133.14, 130.08, 128.99, 128.78, 128.65, 125.41, 80.17, 77.60, 73.65, 72.86, 36.68, 35.70, 34.41, 28.48, 21.75, 15.40; **IR** (neat): 3335, 2955, 2922, 2853, 1719, 1454, 1377, 1260, 1195, 1084, 1018, 978, 952 cm⁻¹; [α]_D²⁵ -33 (c = 0.0023 in CHCl₃); **HRMS** (ES⁺): Found 385.1629 (+ 0.2 ppm), C₂₀H₂₅O₆Na (M+Na⁺) requires 385.1627.



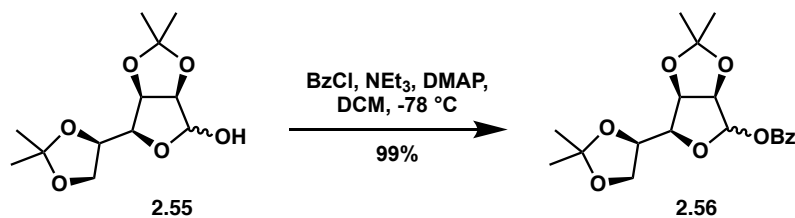
5-(3-((2*S*,3*S*,4*E*,7*R*,8*E*,10*R*,11*R*)-10,11-dihydroxy-3,7-dimethyl-12-oxooxacyclododeca-4,8-dien-2-yl)phenyl)pentanoic acid (-)-D3 To a solution of (-)-C3 (35 mg, 0.077 mmol) in H₂O (0.40 mL) at room temperature was added TFA (0.40 mL), and the reaction vessel was sparged with argon. The reaction was allowed to stir for 48 hours. The solvent was removed and the residue was co-evaporated with ethanol twice to remove residual water. The crude product was purified by preparatory TLC (1:1 hexanes in ethyl acetate with 1% acetic acid). If necessary, nonpolar impurities may be removed by taking up the product in acetonitrile, washing 5 x 1mL pentane, and reducing the acetonitrile fraction. In this manner, 18.8 mg (59%) of the product was obtained as an off-white residue.

¹H NMR (500 MHz, CDCl₃) δ 7.26 – 7.22 (m, 1H), 7.16 – 7.12 (m, 2H), 7.10 (d, *J* = 7.6 Hz, 1H), 5.39 (d, *J* = 4.6 Hz, 2H), 5.34 – 5.29 (m, 2H), 5.06 – 4.99 (m, 1H), 4.46 (s, 1H), 4.13 (s, 1H), 2.70 – 2.50 (m, 3H), 2.33 (t, *J* = 6.9 Hz, 2H), 2.22 (d, *J* = 13.6 Hz, 2H), 1.76 (dd, *J* = 24.2, 12.1 Hz, 2H), 1.66 (ddd, *J* = 23.0, 15.9, 8.3 Hz, 5H), 1.27 (d, *J* = 15.7 Hz, 6H), 1.08 (d, *J* = 6.5 Hz, 3H), 0.72 (d, *J* = 6.8 Hz, 3H); **¹³C NMR** (101 MHz, CDCl₃) δ 177.33, 172.22, 142.62, 139.09, 135.50, 134.47, 131.54, 128.99, 128.73, 128.03, 126.70, 125.63, 81.87, 74.23, 73.95, 43.59, 41.15, 38.58, 35.68, 33.78, 30.76, 30.06, 24.43, 21.64, 17.90; **IR** (neat): 3434, 2923, 2851, 1707, 1453, 1410, 1193, 1081, 966 cm⁻¹; **[α]²⁵_D** -28 (c = 0.0028 in CHCl₃); **HRMS** (ES⁺): Found 439.2102 C₂₄H₃₂O₆Na (M+Na⁺) requires 439.2097



5-(3-((2S,3S,7R,10R,11R,E)-10,11-dihydroxy-3,7-dimethyl-12-oxooxacyclododec-8-en-2-yl)phenyl)penanoic acid (-)-D4 To a solution of (-)-C4 (5 mg, 0.011 mmol) in H₂O (0.60 mL) at room temperature was added TFA (0.60 mL), and the reaction vessel was sparged with argon. The reaction was allowed to stir for 48 hours. The solvent was removed and the residue was co-evaporated with ethanol twice to remove residual water. The crude product was purified by preparatory TLC (1:1 hexanes in ethyl acetate with 1% acetic acid). If necessary, nonpolar impurities may be removed by taking up the product in acetonitrile, washing 5 x 1mL pentane, and reducing the acetonitrile fraction. In this manner, 4.6 mg (59%) of the product was obtained as an off-white residue.

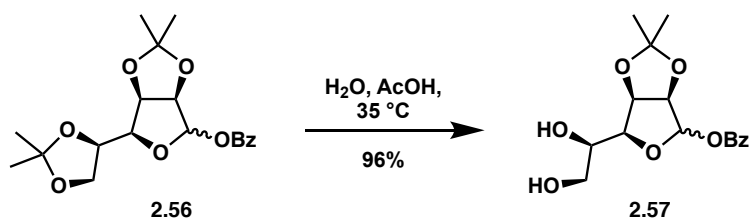
¹H NMR (400 MHz, CDCl₃) δ 7.14 (t, *J* = 7.5 Hz, 1H), 7.02 (dd, *J* = 12.4, 7.7 Hz, 3H), 5.57 – 5.38 (m, 2H), 5.19 (d, *J* = 11.4 Hz, 1H), 4.45 (dt, *J* = 4.1, 2.1 Hz, 1H), 4.17 (d, *J* = 3.6 Hz, 1H), 2.63 – 2.47 (m, 2H), 2.31 (ddd, *J* = 16.5, 11.6, 4.6 Hz, 1H), 2.24 (t, *J* = 7.0 Hz, 2H), 2.19 – 2.09 (m, 1H), 1.93 (td, *J* = 14.5, 9.4 Hz, 1H), 1.57 (ddd, *J* = 23.2, 15.5, 8.6 Hz, 4H), 1.40 – 1.14 (m, 7H), 1.02 (d, *J* = 9.0 Hz, 2H), 0.94 (d, *J* = 6.6 Hz, 3H), 0.61 (d, *J* = 7.0 Hz, 3H); **¹³C NMR** (101 MHz, CDCl₃) δ 177.12, 172.22, 142.46, 140.12, 134.71, 128.83, 128.57, 127.77, 125.79, 125.51, 99.99, 99.86, 81.19, 73.95, 73.14, 36.86, 36.02, 35.62, 34.84, 33.77, 30.62, 28.92, 24.35, 22.11, 19.07, 15.86; **IR** (neat): 3392, 2923, 2852, 2361, 2341, 1735, 1456, 1376, 1241, 1199, 1088 cm⁻¹; **[α]_D²⁵** -410 (c = 0.002 in CHCl₃; **HRMS** (ES⁺): Found 419.2408 (- 2.6 ppm), C₂₄H₃₅O₆ (M+H⁺) requires 419.2434



(3*aR*,6*S*,6*aR*)-6-((*R*)-2,2-Dimethyl-1,3-dioxolan-4-yl)-2,2-dimethyltetrahydro-

furo[3,4-*d*][1,3]dioxol-4-yl benzoate (3.56) A flame dried round bottom flask was charged with **2.55** (41.9 g, 160 mmol) and dry dichloromethane (1000 mL). The solution was cooled to -78°C , whereupon triethylamine (56 mL, 400 mmol) was added, followed by DMAP (2.0 g, 16 mmol), and freshly distilled benzoyl chloride (28.0 mL, 241 mmol). The reaction was allowed to stir overnight while warming to room temperature. Upon completion, the reaction was added to an equal volume of water at 0°C and the layers were separated. The aqueous layer was extracted with dichloromethane (2x 300 mL), and the organic layer was washed with 0.5M HCl (3 x 300 mL), H_2O (2 x 300 mL), NaHCO_3 (3 x 300 mL), and brine (400 mL). The organic fractions were then combined and dried over MgSO_4 , filtered, and reduced, yielding a white solid (58.35 g, 99%). Experimental data matched that previously described.^{86, 123}

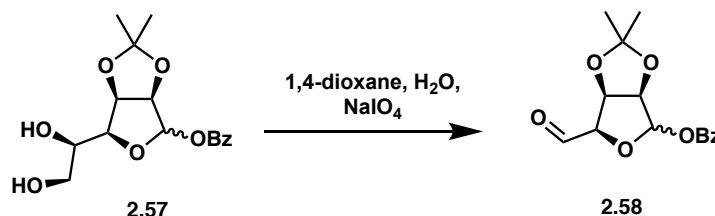
$^1\text{H NMR}$ (500 MHz, CDCl_3) δ 8.04 – 7.97 (m, 2H), 7.61 – 7.53 (m, 1H), 7.47 – 7.39 (m, 2H), 6.50 (s, 1H), 4.90 – 4.80 (m, 2H), 4.43 (q, $J = 7.2$ Hz, 1H), 4.29 – 4.20 (m, 2H), 3.76 (t, $J = 7.8$ Hz, 1H), 1.51 (s, 3H), 1.46 (s, 3H), 1.39 (s, 3H), 1.32 (s, 3H); **$^{13}\text{C NMR}$** (101 MHz, CDCl_3) δ 164.95, 133.54, 129.94, 129.70, 128.56, 113.70, 110.11, 101.87, 85.55, 84.91, 79.66, 75.66, 66.07, 26.90, 26.14, 25.48, 24.93



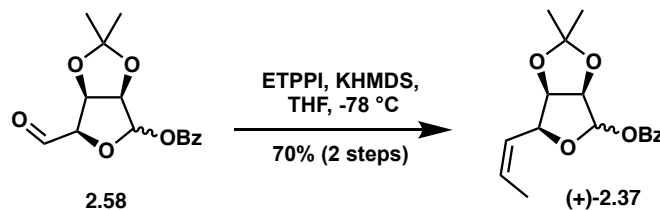
(3aR,6S,6aR)-6-((R)-1,2-Dihydroxyethyl)-2,2-dimethyltetrahydrofuro[3,4-d]

[1,3]dioxol-4-yl benzoate (2.57) A flame dried round bottom flask was charged with **2.56** (10.0 g, 27.4 mmol), H₂O (17 mL), and acetic acid (150 mL). The slurry was heated to 35°C and allowed to stir overnight. The now clear solution was reduced, co-evaporated with toluene (40 mL), reduced, and recrystallized from hot ethanol, yielding white crystals (8.57 g, 96%). Experimental data matched that previously described.^{86, 123}

¹H NMR (500 MHz, CDCl₃) δ 8.08 – 7.94 (m, 2H), 7.64 – 7.55 (m, 1H), 7.52 – 7.41 (m, 2H), 6.43 (s, 1H), 4.95 – 4.88 (m, 2H), 4.30 – 4.24 (m, 1H), 4.19 – 4.09 (m, 1H), 3.89 – 3.69 (m, 2H), 2.84 (s, 1H), 2.21 (s, 1H), 1.52 (s, 3H), 1.35 (s, 3H); **¹³C NMR** (101 MHz, CDCl₃) δ 165.18, 133.68, 129.93, 129.49, 128.60, 113.56, 101.08, 85.74, 82.56, 79.56, 70.86, 63.15, 26.13, 24.79



(3aR,6R,6aR)-6-Formyl-2,2-dimethyltetrahydrofuro[3,4-d][1,3]dioxol-4-yl benzoate (2.58) A round bottom flask was charged with **2.57** (3.07 g, 9.47 mmol), 1,4-dioxane (100 mL), and water (100 mL). Sodium metaperiodate (4.05 g, 18.9 mmol) was added and the reaction was allowed to stir for ~90 minutes. The mixture was then filtered over celite, rinsed with ethyl acetate (3 x 100 mL), and added to a separatory funnel. The aqueous layer was extracted with ethyl acetate (3 x 100 mL) and the organic layers were combined, washed with brine (200 mL), dried over MgSO₄, filtered, and reduced. The resulting viscous oil was then co-eluted with toluene and once again reduced, yielding the intermediate aldehyde as a cloudy oil which was used for the next reaction without further purification.

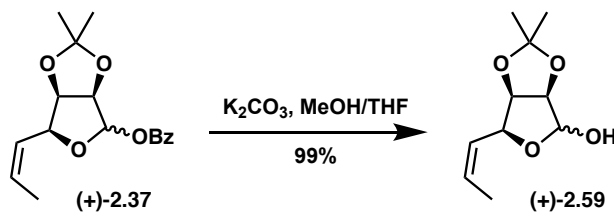


(3*aR*,6*S*,6*aR*)-2,2-Dimethyl-6-((*Z*)-prop-1-en-1-yl)tetrahydrofuro[3,4-*d*][1,3]dioxol-4-yl

benzoate ((+)-2.37) A flame dried round bottom flask was charged with freshly prepared ethyltriphenylphosphonium iodide⁸ (4.59 g, 11.0 mmol) and tetrahydrofuran (82 mL), forming an insoluble white suspension. A solution of 1.0 M KHMDS (10.9 mL) was added, immediately forming an orange solution. The ylide solution was allowed to stir 90 minutes, and was then cooled to -78 °C, whereupon a solution of **2.58** (assuming quantitative yield) in THF (60 mL) was added to the ylide. The reaction was then allowed to stir overnight, warming to room temperature. Upon completion, the reaction was quenched with saturated ammonium chloride (100 mL). The layers were separated and the aqueous layer was extracted with ethyl acetate (3 x 150 mL). The organic layers were combined and washed with brine (200 mL), dried over MgSO₄, filtered, and reduced. Purification via column chromatography (7:3 hexanes/ EtOAc) afforded the product olefin (1.96 g, 70% two steps) as a white crystalline solid. Experimental data matched that previously described.^{86, 123}

¹H NMR (400 MHz, CDCl₃) δ 8.06 – 8.01 (m, 2H), 7.62 – 7.56 (m, 1H), 7.48 – 7.43 (m, 2H), 6.41 (s, 1H), 5.88 – 5.79 (m, 1H), 5.70 – 5.62 (m, 1H), 5.00 (dd, *J* = 8.2, 3.7 Hz, 1H), 4.90 (d, *J* = 5.7 Hz, 1H), 4.82 (dd, *J* = 5.8, 3.7 Hz, 1H), 1.74 (dd, *J* = 7.0, 1.7 Hz, 3H), 1.54 (s, 3H), 1.36 (s, 3H);

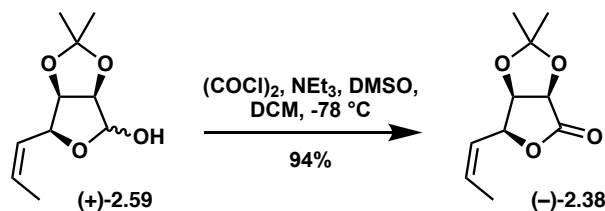
¹³C NMR (101 MHz, CDCl₃) δ 165.22, 157.74, 133.49, 129.87, 128.56, 123.94, 113.25, 101.53, 99.77, 85.65, 81.06, 77.88, 26.26, 25.07, 14.03



(3*aR*,6*S*,6*aR*)-2,2-Dimethyl-6-((*Z*)-prop-1-en-1-yl)tetrahydrofuro[3,4-*d*][1,3]dioxol-4-ol ((+)-

2.59) A flame dried round bottom flask was charged with ((+)-**2.37** (4.77 g, 15.6 mmol), tetrahydrofuran (44 mL), and methanol (44 mL). K_2CO_3 (2.59 g, 18.8 mmol) was then added to the flask and the reaction was allowed to stir 3 h, at which point the starting material was completely consumed by TLC (if starting material remained, the reaction was allowed to continue stirring until which time TLC shows complete conversion to product). The mixture was then filtered, reduced, and purified by column chromatography (3:1-1:2 hexanes/ EtOAc) to afford the lactol (3.11 g, 99%) as a clear oil. Experimental data matched that previously described.^{86, 123}

$^1\text{H NMR}$ (400 MHz, CDCl_3) δ 5.87 – 5.77 (m, 1H), 5.68 – 5.59 (m, 1H), 5.41 (d, $J = 2.2$ Hz, 1H), 5.00 (dd, $J = 8.6, 3.7$ Hz, 1H), 4.71 (dd, $J = 5.8, 3.7$ Hz, 1H), 4.65 (d, $J = 5.8$ Hz, 1H), 2.42 (d, $J = 2.4$ Hz, 1H), 1.75 (dd, $J = 7.0, 1.8$ Hz, 3H), 1.48 (s, 3H), 1.33 (s, 3H); $^{13}\text{C NMR}$ (126 MHz, CDCl_3) δ 129.84, 124.40, 112.66, 101.14, 85.99, 81.44, 75.58, 26.24, 24.96, 13.92

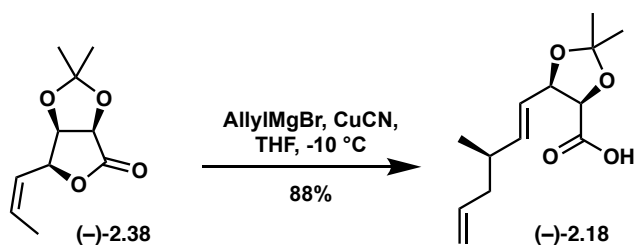


(3*aR*,6*S*,6*aR*)-2,2-Dimethyl-6-((*Z*)-prop-1-en-1-yl)dihydrofuro[3,4-*d*]

[1,3]dioxol-4(3*aH*)-one ((-)-2.38) A flame dried round bottom flask was charged with oxalyl chloride (0.11 mL, 1.3 mmol) and dry dichloromethane (6.5 mL). The stirring solution was cooled to -78°C and DMSO (0.37 mL, 5.2 mmol) was added. The solution was maintained at this

temperature for 1 hour and 20 minutes at which time a solution of ((+)-**2.59**) (126 mg, 0.63 mmol) in dry dichloromethane (1.7 mL + 2x 0.4 mL washes) was added via canula at -78 °C. The reaction was maintained at this temperature for 2 hours and 30 minutes, then triethylamine (0.50 mL, 3.6 mmol) was added. The reaction was allowed to stir in the presence of the cooling bath for 2 hours, then at room temperature for an additional 1 hour. The reaction was then poured into a separatory funnel and washed with 0.5M HCl (2x 10 mL), saturated sodium bicarbonate (2x 10 mL), and brine. The organic fraction was dried over sodium sulfate, filtered and concentrated. Elution through a short plug of silica gel with dichloromethane (~50 mL) and concentration of the eluate afforded the product lactone as a white solid (117 mg, 94%), which may be used without further purification. Experimental data matched that previously described.^{86, 123}

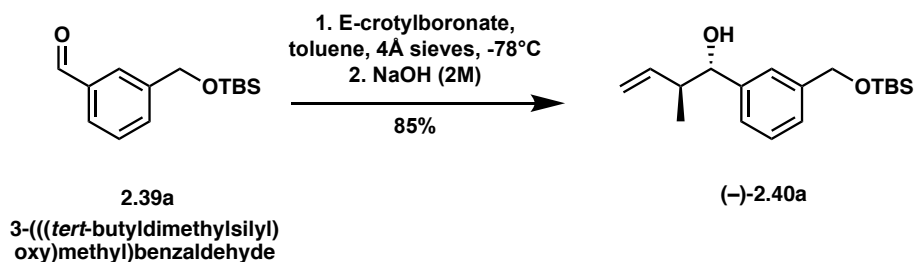
¹H NMR (500 MHz, CDCl₃) δ 6.00 – 5.92 (m, 1H), 5.72 – 5.65 (m, 1H), 5.28 (ddd, *J* = 8.8, 3.6, 1.2 Hz, 1H), 4.83 (d, *J* = 5.3 Hz, 1H), 4.77 (dd, *J* = 5.3, 3.6 Hz, 1H), 1.79 (dd, *J* = 7.1, 1.8 Hz, 3H), 1.50 (s, 3H), 1.40 (s, 3H); ¹³C NMR (101 MHz, CDCl₃) δ 174.26, 132.57, 122.31, 114.15, 77.85, 76.35, 74.64, 65.65, 26.91, 25.97, 13.87



(4*R*,5*R*)-2,2-Dimethyl-5-((*R,E*)-3-methylhexa-1,5-dien-1-yl)-1,3-dioxolane-4-carboxylic acid
((-)-2.18) A flame dried round bottom flask (previously rinsed in a base bath and oven dried) was charged with copper (I) cyanide (1.13 g, 12.61 mmol) and dry THF (630 mL). The slurry was cooled to -10 °C in an ice-salt water bath and freshly prepared allylmagnesium bromide (0.61M, 16.6 mL, 10.13 mmol) was added very slowly. The solution was stirred at -10 °C for 30 minutes

prior to dropwise addition of a solution of ((-)-**2.38**) (1.00 g, 5.04 mmol) in THF (10 mL). The reaction was maintained at this temperature for ~ 10 minutes, then allowed to warm to room temperature and stirred an additional 3 hours at which point the starting material has been consumed (by TLC). The reaction was quenched by addition of a 9:1 solution of saturated aqueous ammonium chloride and 1-M ammonium hydroxide (630 mL total volume). The solution was stirred ~ 1 hour until it reached a deep blue color. The reaction was then poured into a separatory funnel and the aqueous layer was separated and acidified to ~ pH 2 with 1-M HCl. The acidified aqueous layer was extracted with diethyl ether (5x 50 mL). The combined organic layer was washed with saturated aqueous ammonium chloride (2x 50mL) and brine, dried over sodium sulfate, filtered, and concentrated. Purification via column chromatography (9:1 DCM/MeOH) provided the acid as a pale yellow oil (1.07 g, 88%). Experimental data matched that previously described.^{86, 123}

¹H NMR (500 MHz, CDCl₃) δ 5.84 (dd, *J* = 15.4, 7.1 Hz, 1H), 5.78 – 5.68 (m, 1H), 5.40 – 5.33 (m, 1H), 5.03 – 4.97 (m, 2H), 4.84 (t, *J* = 7.6 Hz, 1H), 4.64 (d, *J* = 7.5 Hz, 1H), 2.31 – 2.24 (m, 1H), 2.15 – 2.09 (m, 1H), 2.06 – 1.98 (m, 1H), 1.63 (s, 3H), 1.42 (s, 3H), 0.98 (d, *J* = 6.7 Hz, 3H);
¹³C NMR (126 MHz, CDCl₃) δ 173.78, 142.58, 136.64, 122.04, 116.33, 111.27, 78.80, 76.91, 40.85, 36.10, 27.05, 25.41, 19.53

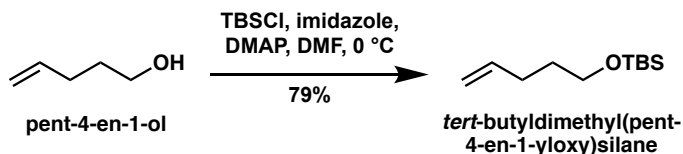


(1*S*,2*S*)-1-(3-(((*tert*-Butyldimethylsilyl)oxy)methyl)phenyl)-2-methylbut-3-en-1-ol ((-)-2.40a**)**

A flask was charged with a stir bar and powdered 4Å mol sieves (250 mg) and was then flame

dried. A solution of *E*-crotylboronate in toluene (prepared *via* known procedure) (1.29M, 8.5 mL) was added, followed by additional toluene (19 mL). The solution was cooled to -78°C . **2.39a** (922 mg, 3.68 mmol) was then added as a solution in toluene (9 mL + 2 mL wash) slowly *via* syringe pump over ~20 minutes. The reaction was stirred for 3 hours at this temperature. NaOH was then added (2M (aq), 14 mL) and the reaction was transferred to a 0°C cooling bath and stirred for 20 minutes. The reaction was then filtered through a pad of celite. The organic layer was separated and the aqueous layer was extracted 4 times with diethyl ether. The combined organic layers are washed with water and brine, dried over sodium sulfate, filtered, and concentrated. The crude product was purified by flash column chromatography (4:1 hexanes/EtOAc) to afford the product alcohol as a clear oil (961 mg, 85%). The product was thus obtained as a single diastereomer as determined by ^1H NMR.

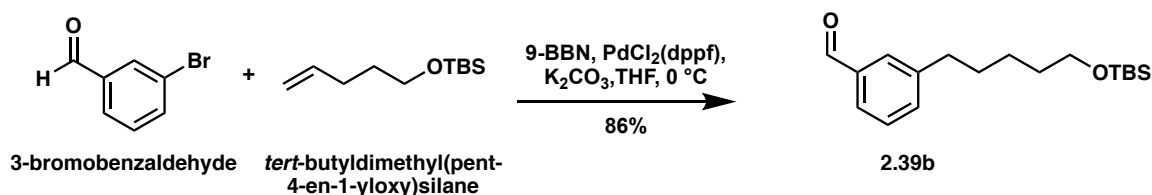
^1H NMR (500 MHz, CDCl_3) δ 7.36 – 7.18 (m, 4H), 5.88 – 5.75 (m, 1H), 5.25 – 5.14 (m, 2H), 4.75 (s, 2H), 4.36 (d, $J = 7.8$ Hz, 1H), 2.52 – 2.42 (m, 1H), 2.12 (s, 1H), 0.94 (s, 9H), 0.87 (d, $J = 6.8$ Hz, 3H), 0.10 (s, 6H); ^{13}C NMR (126 MHz, CDCl_3) δ 142.50, 141.61, 140.84, 128.30, 125.57, 124.67, 116.91, 78.05, 65.10, 46.39, 26.09, 18.56, 16.68, -5.07; IR (neat): 3436, 3078, 3031, 2956, 2928, 2856, 1710, 1639, 1607, 1488, 1472, 1462, 1387, 1360, 1254, 1155, 1097, 1032, 1005, 938, 910, 836, 774, 707, 680, 662 cm^{-1} ; $[\alpha]^{25}_{\text{D}}$ -39 ($c = 1.00$ in CHCl_3); HRMS (ES^+): Found 329.1896 (-1.7 ppm), $\text{C}_{18}\text{H}_{30}\text{O}_2\text{SiNa}$ ($\text{M}+\text{Na}^+$) requires 329.1913



tert-Butyldimethyl(pent-4-en-1-yloxy)silane. Prepared according to known procedures:⁵ A flask was charged with 4-penten-1-ol (2.35 mL, 23.2 mmol) and DMF (23 mL). The solution was cooled

to 0°C, followed by addition of *tert*-butyldimethylsilyl chloride (4.55 g, 30.2 mmol), imidazole (2.06 g, 30.2 mmol), and DMAP (142 mg, 1.16 mmol). The reaction was allowed to slowly warm to room temperature and was stirred for 19 hours. The reaction was quenched by addition of brine and the organic layer was separated. The aqueous layer was extracted 5 times with EtOAc. The combined organic layers were washed with a saturated aqueous ammonium chloride, sodium bicarbonate, water, and brine, dried over sodium sulfate, filtered, and concentrated. The crude product was purified by flash column chromatography (5% EtOAc in hexanes) to afford the product alkene as a clear oil (3.68 g, 79%). *NOTE: The product is a volatile compound. Care should be taken when removing solvent. Refrain from leaving under vacuum for extended periods.* Experimental data matched that previously described.⁵

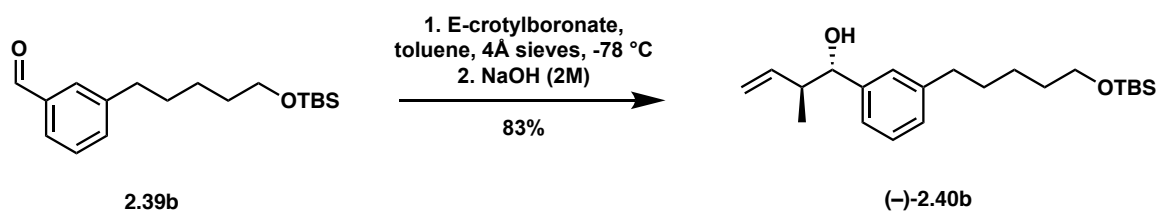
¹H NMR (500 MHz, CDCl₃) δ 5.88 – 5.78 (m, 1H), 5.07 – 4.92 (m, 2H), 3.62 (t, *J* = 6.5 Hz, 2H), 2.13 – 2.07 (m, 2H), 1.65 – 1.58 (m, 2H), 0.89 (s, 9H), 0.05 (s, 6H)



3-(5-((*tert*-Butyldimethylsilyloxy)pentyl) benzaldehyde (2.39b) A 2-neck flask fitted with a reflux condenser and septum was charged with *tert*-butyldimethyl(pent-4-en-1-yloxy)silane (1.25 g, 6.24 mmol) and THF (2.8 mL). The solution was cooled to 0 °C followed by slow addition of 9-BBN (0.5M in THF, 12.5 mL). The reaction was allowed to warm to room temperature in the presence of the cooling bath, and was then stirred a further 19 hours at room temperature. DMF (16 mL), PdCl₂(dppf)-CH₂Cl₂ (69 mg, 0.094 mmol), *meta*-bromobenzaldehyde (0.36 mL, 3.12 mmol) and potassium carbonate (1.55 g, 11.2 mmol) were added. The mixture was heated to 50°C

and stirred a further 24 hours. The reaction was then cooled to room temperature and poured into a separatory funnel containing water (50 mL). Toluene was added (it may be necessary to add additional water for layers to separate) and the organic layer was separated. The aqueous layer was extracted 5 times with toluene (4x 50 mL), and the combined organic layers were washed 4 times with water (4x 25 mL) and one time with brine, dried over sodium sulfate, filtered, and concentrated to afford a viscous brown oil as the crude product. Purification by flash column chromatography (0 to 10% EtOAc in hexanes) afforded the product aldehyde as a clear oil (821 mg, 86%).

$^1\text{H NMR}$ (500 MHz, CDCl_3) δ 10.00 (s, 1H), 7.72 – 7.61 (m, 2H), 7.54 – 7.40 (m, 2H), 3.60 (t, J = 6.5 Hz, 2H), 2.72 – 2.68 (m, 2H), 1.70 – 1.62 (m, 2H), 1.55 – 1.50 (m, 2H), 1.41 – 1.33 (m, 2H), 0.88 (s, 9H), 0.03 (s, 6H); $^{13}\text{C NMR}$ (126 MHz, CDCl_3) δ 192.74, 143.91, 136.66, 134.86, 129.52, 129.05, 127.65, 63.17, 35.76, 32.76, 31.21, 26.09, 25.57, 18.49, -5.14; **IR** (neat): 2928, 2856, 2726, 1702, 1603, 1588, 1471, 1462, 1386, 1360, 1301, 1250, 1142, 1096, 1005, 938, 910, 833, 774, 692, 651 cm^{-1} ; **HRMS** (ES^+): Found 307.2117 (+2.4 ppm), $\text{C}_{18}\text{H}_{30}\text{O}_2\text{Si}$ ($\text{M}+\text{H}^+$) requires 307.2093



(1*S*,2*S*)-1-(3-(5-((*tert*-Butyldimethylsilyloxy)pentyl)phenyl)-2-methylbut-3-en-1-ol ((-)-**2.40b**) Prepared with same procedure as (-)-**2.40a**. **2.39b** (821 mg, 2.68 mmol), E-crotylboronate solution (6.2 mL, 8.0 mmol), toluene (20 mL), and NaOH (2M, 10mL) yielded 810mg (83%) of the product as a clear oil. Purified by column chromatography (10% EtOAc in hexanes).

¹H NMR (500 MHz, CDCl₃) δ 7.26 – 7.22 (m, 1H), 7.15 – 7.12 (m, 2H), 7.11 – 7.08 (m, 1H), 5.86 – 5.76 (m, 1H), 5.23 – 5.15 (m, 2H), 4.33 (dd, *J* = 8.0, 2.0 Hz, 1H), 3.60 (t, *J* = 6.6 Hz, 2H), 2.66 – 2.57 (m, 2H), 2.53 – 2.42 (m, 1H), 1.67 – 1.59 (m, 2H), 1.57 – 1.51 (m, 2H), 1.40 – 1.33 (m, 2H), 0.89 (s, 9H), 0.86 (d, *J* = 6.8 Hz, 3H), 0.04 (s, 6H); **¹³C NMR** (126 MHz, CDCl₃) δ 142.84, 142.48, 140.92, 128.24, 127.86, 126.98, 124.31, 116.79, 78.07, 63.31, 46.37, 36.09, 32.83, 31.47, 25.66, 18.49, 16.71, -5.14; **IR** (neat): 3438, 3080, 3022, 2928, 2856, 1639, 1607, 1471, 1462, 1387, 1361, 1254, 1155, 1098, 1005, 911, 833, 813, 774, 707, 679, 661 cm⁻¹; **[α]²⁵_D** -24.1 (c = 4.20 in CHCl₃); **HRMS** (ES⁺): Found 385.2544 (+0.5 ppm), C₂₂H₃₈O₂SiNa (M+Na⁺) requires 385.2539

Generation 2 Procedures:**Representative Procedure A: Parikh-Doering Oxidation**

A flame dried flask was charged with the monoprotected diol starting material and DCM. Dimethyl sulfoxide and then triethylamine were then added to the reaction mixture. The reaction was then cooled to 0°C. SO₃•pyridine was added and the reaction was allowed to warm to room temperature. After 1 hour of stirring at room temperature reaction was diluted with DCM and then quenched with saturated aqueous solution of ammonium chloride. After separation, the aqueous layer was extracted with ethyl acetate three times. The combined organics were rinsed with brine twice, dried with magnesium sulfate, filtered and then condensed.

Representative Procedure B: Roush Crotylation

A flask was charged with a stir bar and powdered 4Å mol sieves and was then flame dried. A solution of E-crotylboronate in toluene (prepared via known procedure)¹²⁴ was added, followed by additional toluene. The solution was cooled to -78°C. The aldehyde (3a/3b) was then added, as a solution in toluene, slowly via syringe pump over ~20 minutes. The reaction was stirred for 3 hours at this temperature. NaOH was then added and the reaction was transferred to a 0 °C cooling bath and stirred for 20 minutes. The reaction was filtered through a pad of celite. The organic layer was separated and the aqueous layer was extracted with diethyl ether (4 x X mL). The combined organic layers were washed with water and brine, dried over sodium sulfate, filtered, and concentrated. The product was thus obtained as a single diastereomer as determined by ¹HNMR.

Representative Procedure C: EDC Esterification

A flame dried flask was charged with argon, the carboxylic acid starting material and DCM. The reaction was subsequently cooled to 0°C. Once cool, DMAP and EDC were added consecutively. After 10 minutes of stirring, a solution of the alcohol (4a/4b) in DCM was added via syringe pump. The reaction was stirred 24-30 hours depending on completion and then added to a separatory funnel containing equal volume of H₂O. The organic layer was separated and the aqueous layer was extracted with DCM (3 x 15 mL). The combined organic layers were washed with brine, dried over magnesium sulfate, filtered, and concentrated.

Representative Procedure D: Ring-Closing Metathesis

A flask was charged with the alkene starting material (5a/5b) and DCM. Grubbs II generation catalyst was added and the reaction was stirred at room temperature for 24 hours. The solvent was removed. NOTE: In our experience, adding a second equivalent of catalyst ~6 hours after start helps with starting material consumption.

Representative Procedure E: TBS removal

To a solution of protected macrocycle (6a/6b) in THF, was added tetra-butylammonium fluoride (1M in THF). The reaction was stirred for 1 hour. The reaction was quenched with saturated aqueous ammonium chloride and diluted in diethyl ether. The organic layer was separated and the aqueous layer was extracted 4 times with diethyl ether. The combined organic layers were washed with water and brine, dried over sodium sulfate, filtered, and concentrated.

Representative Procedure F: TEMPO Oxidation

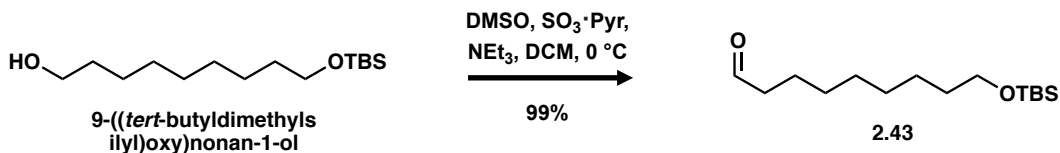
A vial was charged with deprotected macrocycle (7a/7b/10a), acetonitrile, TEMPO, and sodium phosphate buffer (0.67 M, pH 6.7). The reaction was warmed to 35°C and stirred for 30 minutes. Then aqueous solutions of bleach and sodium chlorite were added to the reaction drop wise over 30 minutes. Reaction was stirred at 35°C for 24 hours at which time it was quenched with aqueous thiosulfate solution. The aqueous layer was extracted once with ethyl acetate (first ethyl acetate layer set aside). Then the aqueous layer was acidified to ~pH 4 and extracted 3 times with ethyl acetate. The organics were washed with brine, dried over magnesium sulfate, filtered and concentrated.

Representative Procedure G: Acetonide Deprotection

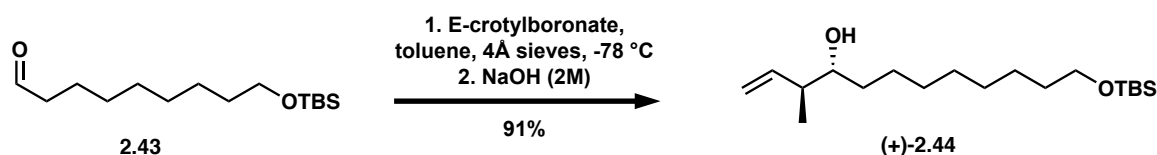
To a solution of carboxylic acid macrocycle (8a/8b) in THF was added HF pyridine and H₂O. The mixture was stirred for 4-6 hours and then quenched with 1 M NaOH. The aqueous layer was acidified to ~pH 4 and then the product was extracted 3 times with ethyl acetate, washed with brine, dried with MgSO₄ and condensed.

Representative Procedure H: Hydrogenation

A vial was charged with deprotected macrocycle (7a), 1:1 Ethyl Acetate:Ethanol and 10% Pd/C. Using a balloon, the vial was purged multiple times with H₂. Full hydrogenation was realized after 4 hours at which point the reaction mixture was poured over celite and condensed.

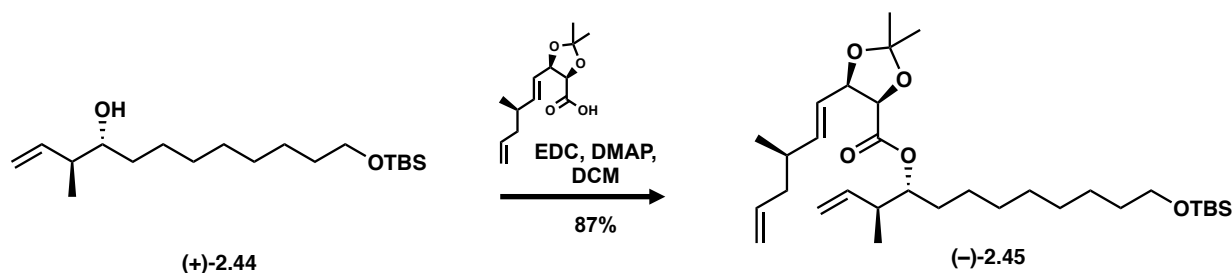


9-((*tert*-butyldimethylsilyl)oxy)nonanal (2.43) was synthesized according to Representative Procedure A: **9-((*tert*-butyldimethylsilyl)oxy)nonan-1-ol** (0.76 g, 2.78 mmol), dimethyl sulfoxide (4.0 mL, 55.55 mmol), sulfur trioxide pyridine complex (3.54 g, 22.22 mmol), triethylamine (3.9 mL, 27.78 mmol) in DCM (28 mL) yielded 0.75 g of **3a** (99% yield). Purified by column chromatography (0 to 10% EtOAc:Hexanes). $R_f = 0.79$ (10% EtOAc:Hexanes). $^1\text{H NMR}$ (500 MHz, CDCl_3) δ 9.76 (t, $J = 1.8$ Hz, 1H), 3.59 (t, $J = 6.6$ Hz, 2H), 2.42 (td, $J = 7.4, 1.9$ Hz, 2H), 1.62 (p, $J = 7.4$ Hz, 2H), 1.54 – 1.47 (m, 2H), 1.33 – 1.26 (m, 9H), 0.89 (s, 9H), 0.04 (s, 6H). $^{13}\text{C NMR}$ (126 MHz, CDCl_3) δ 203.29, 63.66, 44.32, 33.23, 29.74, 29.62, 29.52, 26.39, 26.14, 22.48, 18.79, -4.85. **HRMS (ES⁺)**: Found 273.22469 (0.94 ppm), $\text{C}_{15}\text{H}_{32}\text{O}_2\text{Si}$ ($\text{M}+\text{H}^+$) requires 273.22443. **IR** 2929.02 (C-H), 1724.10 (CHO), 1463.11, 1264.73, 1093.86 cm^{-1} .



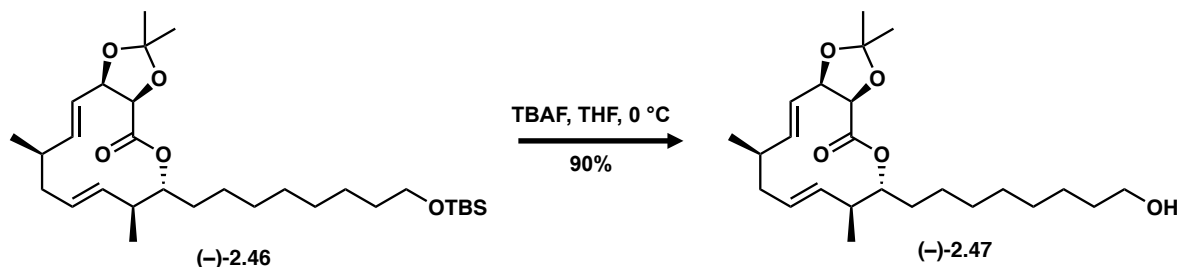
(3*S*,4*R*)-12-((*tert*-butyldimethylsilyl)oxy)-3-methyldodec-1-en-4-ol (+)-2.44 was synthesized according to Representative Procedure B: **2.43** (200 mg, 0.73 mmol), *E*-crotylboronate (4.3 mL, 2.2 mmol), toluene (7 mL), 4Å molecular sieves (49 mg), and 2 M NaOH (2.8 mL) yielded 220 mg of **(+)-2.44** (91% yield). Purified by column chromatography (0 to 15% EtOAc:Hexanes). $R_f = 0.22$ (30% EtOAc:Hexanes). $^1\text{H NMR}$ (500 MHz, CDCl_3) δ 5.75 (ddd, $J = 16.9, 10.7, 8.2$ Hz,

1H), 5.13 (tt, $J = 1.9, 1.1$ Hz, 1H), 5.10 (ddd, $J = 9.9, 1.9, 0.9$ Hz, 1H), 3.59 (t, $J = 6.6$ Hz, 2H), 3.38 (ddd, $J = 8.0, 5.9, 3.3$ Hz, 1H), 2.24 – 2.16 (m, 1H), 1.53 – 1.48 (m, 4H), 1.41 – 1.33 (m, 2H), 1.29 (s, 10H), 1.03 (d, $J = 6.9$ Hz, 3H), 0.89 (s, 9H), 0.04 (s, 6H). ^{13}C NMR (126 MHz, CDCl_3) δ 140.54, 116.40, 74.87, 63.49, 44.29, 34.43, 33.05, 29.84, 29.78, 29.57, 26.16, 25.96, 25.89, 18.55, 16.48, -5.08. **HRMS (ES⁺):** Found 329.28742 (1.17 ppm), $\text{C}_{19}\text{H}_{41}\text{O}_2\text{Si}$ ($\text{M}+\text{H}^+$) requires 329.28311. **IR** 3371.33 (OH), 2927.91, 2855.36 (C-H), 1638.69 (C=C), 1462.52, 1387.75, 1360.65, 1254.35, 1099.04 cm^{-1} . $[\alpha]^{25}_{\text{D}} +0.28$ ($c = 1.0$ in CHCl_3).

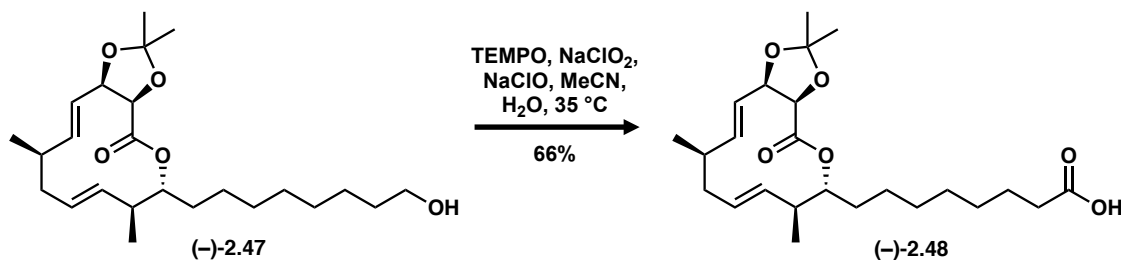


(3*S*,4*R*)-12-((*tert*-butyldimethylsilyl)oxy)-3-methyldodec-1-en-4-yl ((4*R*,5*R*)-2,2-dimethyl-5-((*S*)-3-methylhex-5-en-1-yl)-1,3-dioxolane-4-carboxylate ((-)-2.45) was synthesized according to Representative Procedure C: **(+)-2.44** (155 mg, 0.4716 mmol), acid precursor⁸⁶ (170 mg, 0.7074 mmol), EDC (180 mg, .9432 mmol), 4-(dimethylamino)pyridine (5.8 mg, 0.0472 mmol) in DCM (12 mL) yielded 260 mg of **((-)-2.45)** (87% yield). Purified by column chromatography (0 to 5% EtOAc:Hexanes). $R_f = 0.50$ (10% EtOAc:Hexanes). ^1H NMR (500 MHz, CDCl_3) δ 5.82 (dd, $J = 15.4, 7.1$ Hz, 1H), 5.79 – 5.68 (m, 2H), 5.37 (ddd, $J = 15.4, 8.2, 1.2$ Hz, 1H), 5.07 – 4.97 (m, 4H), 4.89 (dt, $J = 8.5, 4.2$ Hz, 1H), 4.77 – 4.72 (m, 1H), 4.59 (d, $J = 6.9$ Hz, 1H), 3.58 (t, $J = 6.6$ Hz, 2H), 2.43 (dq, $J = 10.7, 6.8$ Hz, 1H), 2.22 (p, $J = 6.9, 6.4$ Hz, 1H), 2.17 – 2.09 (m, 1H), 2.02 – 1.94 (m, 1H), 1.62 (s, 3H), 1.52 – 1.45 (m, 4H), 1.40 (s, 3H), 1.26 (s, 12H), 0.99 (d, $J = 6.9$ Hz, 3H), 0.97 (d, $J = 6.7$ Hz, 3H), 0.89 (s, 9H), 0.04 (s, 6H). ^{13}C NMR (126 MHz, CDCl_3) δ

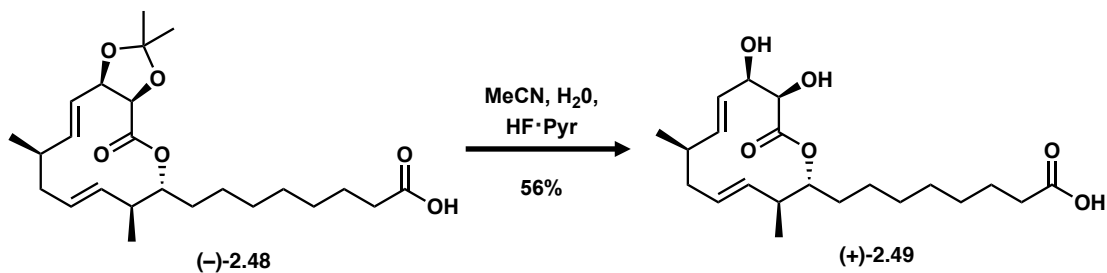
(C=O), 1461.80, 1379.01, 1253.12, 1223.29, 1186.18, 1088.12 cm^{-1} . $[\alpha]^{25}_{\text{D}}$ -13.4 ($c = 1.0$ in CHCl_3).



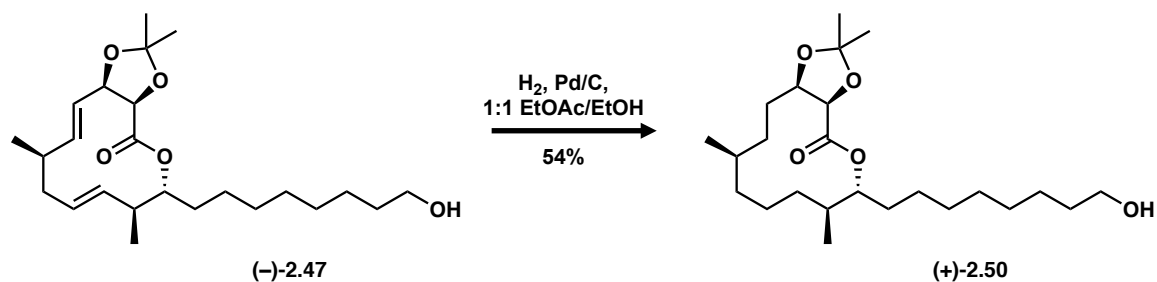
(3aR,6R,7S,8E,11R,12E,13aR)-6-(8-hydroxyoctyl)-2,2,7,11-tetramethyl-3a,6,7,10,11,13a-hexahydro-4H-[1,3]dioxolo[4,5-c][1]oxacyclododecin-4-one ((-)-2.47) was synthesized according to Representative Procedure E: **((-)-2.46)** (50.0 mg, 0.0960 mmol), tetrabutylammonium fluoride solution (1 M, 0.28 ml, 0.2794 mmol) in THF (1 ml) yielded 34.3 mg (90% yield). Purified by column chromatography (30% EtOAc:Hexanes). $R_f = 0.39$ (30% EtOAc:Hexanes). $^1\text{H NMR}$ (400 MHz, CDCl_3) δ 5.74 (dd, $J = 15.7, 7.1$ Hz, 1H), 5.25 (dd, $J = 15.8, 6.8$ Hz, 1H), 5.09 (dd, $J = 6.3, 3.0$ Hz, 2H), 4.83 – 4.70 (m, 2H), 4.52 (d, $J = 6.6$ Hz, 1H), 3.63 (t, $J = 6.6$ Hz, 2H), 2.19 (ddd, $J = 15.1, 9.5, 3.0$ Hz, 3H), 1.94 (tdd, $J = 13.9, 8.2, 4.1$ Hz, 1H), 1.70 (s, 3H), 1.65 – 1.59 (m, 1H), 1.55 (p, $J = 6.7$ Hz, 3H), 1.41 (s, 3H), 1.32 – 1.22 (m, 12H), 1.05 (d, $J = 6.7$ Hz, 3H), 0.96 (d, $J = 6.8$ Hz, 3H). $^{13}\text{C NMR}$ (100 MHz, CDCl_3) δ 170.37, 138.68, 135.11, 129.92, 123.48, 111.05, 78.71, 78.53, 78.40, 63.05, 42.43, 38.82, 36.05, 32.82, 32.48, 29.53, 29.40, 29.35, 26.89, 25.96, 25.73, 24.90, 21.24, 18.18. **HRMS (ES⁺):** Found 431.27696 (0.38 ppm), $\text{C}_{24}\text{H}_{40}\text{O}_5$ ($\text{M}+\text{Na}^+$) requires 431.27680. **IR** 3430.00 (OH), 2928.10, 2855.58 (C-H), 1753.69, 1745.55, 1726.59 (C=O), 1188.55, 1086.13 cm^{-1} . $[\alpha]^{25}_{\text{D}}$ -9.3 ($c = 1.0$ in CHCl_3).



8-((3a*R*,6*R*,7*S*,8*E*,11*R*,12*E*,13a*R*)-2,2,7,11-tetramethyl-4-oxo-3a,6,7,10,11,13a-hexahydro-4*H*-[1,3]dioxolo[4,5-*c*][1]oxacyclododecin-6-yl)octanoic acid ((-)-2.48) was synthesized according to Representative Procedure F: ((-)-2.47) (34.5 mg, 0.0844 mmol), TEMPO (1.0 mg, 0.0059 mmol), sodium chlorite (19 mg, 0.1688 mmol) in 0.25 mL H₂O, bleach (8.25% sodium hypochlorite) (0.01 ml) in 0.25 ml H₂O, sodium phosphate buffer (0.67 M, pH 6.7, 0.31 ml) in CH₃CN (0.4 ml) yielded 23.4 mg of ((-)-2.48) (66% yield). Purified by column chromatography (0 to 50% EtOAc [with 0.01% acetic acid]:hexanes). $R_f = 0.12$ (50% EtOAc:Hexanes). $^1\text{H NMR}$ (500 MHz, CDCl₃) 5.73 (dd, $J = 15.7, 7.2$ Hz, 1H), 5.24 (dd, $J = 15.6, 6.9$ Hz, 1H), 5.11 – 5.07 (m, 2H), 4.80 – 4.72 (m, 2H), 4.53 (d, $J = 6.7$ Hz, 1H), 2.33 (t, $J = 7.4$ Hz, 2H), 2.22 – 2.15 (m, 3H), 1.96 – 1.89 (m, 1H), 1.69 (s, 3H), 1.61 (td, $J = 13.3, 5.9$ Hz, 4H), 1.41 (s, 3H), 1.29 – 1.24 (m, 8H), 1.05 (d, $J = 6.7$ Hz, 3H), 0.96 (d, $J = 6.7$ Hz, 3H). $^{13}\text{C NMR}$ (126 MHz, CDCl₃) δ 179.37, 170.37, 138.75, 135.14, 129.97, 123.53, 111.14, 78.76, 78.56, 78.43, 42.43, 38.88, 36.11, 34.07, 32.48, 29.37, 29.03, 28.94, 26.93, 26.00, 24.84, 24.71, 21.27, 18.20. **HRMS (APCI):** Found 421.26005 (0.49 ppm), C₂₄H₃₈O₆ (M-H⁺) requires 421.25956. **IR** 2927.92, 2855.92 (C-H), 1747.04, 1708.65 (C=O), 1457.04, 1379.41, 1188.81, 1086.56 cm⁻¹. $[\alpha]^{25}_D -10.2$ ($c = 1.0$ in CHCl₃).

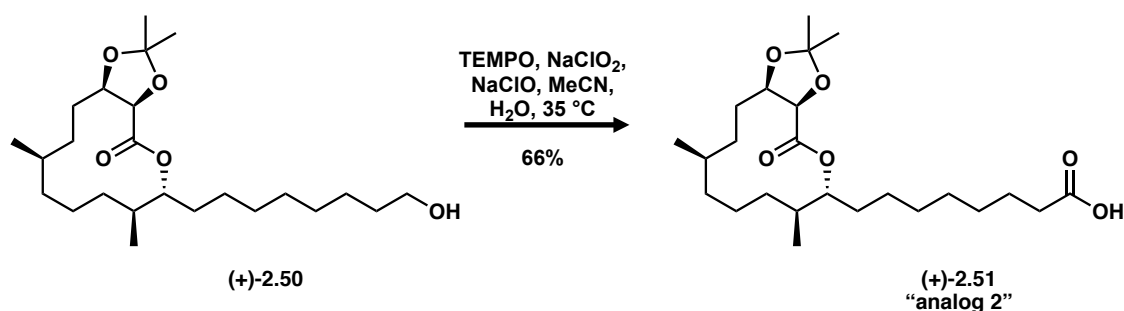


8-((2*R*,3*S*,4*E*,7*R*,8*E*,10*R*,11*R*)-10,11-dihydroxy-3,7-dimethyl-12-oxooxacyclododeca-4,8-dien-2-yl)octanoic acid (+)-2.49 was synthesized according to Representative Procedure G: ((-)-2.48) (10 mg, 0.0237 mmol), HF·pyridine (0.34 ml), H₂O (0.01 mL) in CH₃CN (5 mL) yielded 5 mg of (+)-2.49 (56% yield). Purified by column chromatography (0 to 50% EtOAc [with 0.01% acetic acid]:hexanes). *R_f* = 0.38 (10% MeOH:DCM). ¹H NMR (400 MHz, CDCl₃) δ 5.35 – 5.24 (m, 2H), 5.14 (ddd, *J* = 14.8, 10.9, 3.8 Hz, 1H), 4.90 (dd, *J* = 15.0, 9.5 Hz, 1H), 4.73 (ddd, *J* = 10.7, 7.7, 2.9 Hz, 1H), 4.42 (s, 1H), 4.13 (d, *J* = 3.2 Hz, 1H), 2.34 (t, *J* = 7.3 Hz, 2H), 2.23 (td, *J* = 10.1, 6.8 Hz, 1H), 2.19 – 2.12 (m, 2H), 1.68 – 1.60 (m, 4H), 1.31 (s, 5H), 1.25 (s, 4H), 1.04 (d, *J* = 6.5 Hz, 3H), 0.95 (d, *J* = 6.8 Hz, 3H). ¹³C NMR (151 MHz, CDCl₃) δ 177.67, 172.80, 135.67, 134.74, 130.27, 126.41, 78.57, 73.55, 73.41, 41.99, 40.93, 38.10, 33.78, 31.83, 28.92, 28.67, 28.46, 24.59, 24.01, 21.29, 18.02. **HRMS (APCI):** Found 381.22826 (0.33 ppm), C₂₁H₃₄O₆ (M-H⁺) requires 381.22826. **IR** 3422.41 (O-H), 2924.83, 2852.86 (C-H), 1717.21 (C=O), 1456.95, 1196.87, 1077.90 cm⁻¹. [α]_D²⁵ +16.9 (c = 0.33 in CHCl₃).



(3aR,6R,7S,11R,13aR)-6-(8-hydroxyoctyl)-2,2,7,11-tetramethyldecahydro-4H-

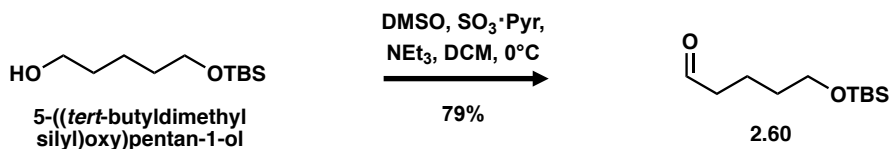
[1,3]dioxolo[4,5-c][1]oxacyclododecin-4-one ((+)-2.50) was synthesized according to Representative Procedure H: **(-)-2.47** (32 mg, 0.0908 mmol), Pd/C 10% (14 mg, 15 mol % catalyst load) in 1:1 EtOAc:EtOH (4.5 mL) yielded 17.2 mg of **(+)-2.50** (54% yield). Purified by column chromatography (0 to 20% EtOAc:hexanes). $R_f = 0.40$ (20% EtOAc:Hexanes). $^1\text{H NMR}$ (500 MHz, CDCl_3) δ 4.78 (ddd, $J = 10.0, 6.3, 3.4$ Hz, 1H), 4.56 (d, $J = 6.1$ Hz, 1H), 4.36 (ddd, $J = 9.7, 6.1, 3.2$ Hz, 1H), 3.63 (t, $J = 6.7$ Hz, 2H), 1.83 (dp, $J = 10.7, 3.7$ Hz, 1H), 1.76 (ddd, $J = 10.4, 5.1, 2.4$ Hz, 1H), 1.70 (tt, $J = 10.1, 4.3$ Hz, 3H), 1.63 (s, 3H), 1.60 – 1.52 (m, 4H), 1.48 (ddt, $J = 6.2, 3.7, 2.1$ Hz, 3H), 1.38 (s, 3H), 1.31 – 1.25 (m, 11H), 1.19 – 1.14 (m, 2H), 1.03 (ddd, $J = 11.0, 9.0, 4.8$ Hz, 1H), 0.89 (dd, $J = 8.6, 6.9$ Hz, 6H). $^{13}\text{C NMR}$ (151 MHz, CDCl_3) δ 170.09, 110.01, 79.15, 78.18, 63.17, 36.06, 33.65, 32.89, 32.42, 31.70, 29.85, 29.72, 29.51, 29.41, 28.00, 27.36, 26.03, 25.78, 25.13, 25.11, 24.12, 21.96, 20.88, 16.96. **HRMS (ES⁺):** Found 413.32615 (0.68 ppm), $\text{C}_{24}\text{H}_{44}\text{O}_5$ (M-H⁺) requires 413.32615. **IR** 3369.45 (OH), 2928.27, 2856.35 (C-H), 1746.00 (C=O), 1379.54, 1184.56, 1077.92 cm^{-1} . $[\alpha]^{25}_{\text{D}} +38.9$ (c = 1.0 in CHCl_3).



8-((3aR,6R,7S,11R,13aR)-2,2,7,11-tetramethyl-4-oxodecahydro-4H-[1,3]dioxolo[4,5-c][1]oxacyclododecin-6-yl)octanoic acid ((+)-2.51; analog 2) was synthesized according to

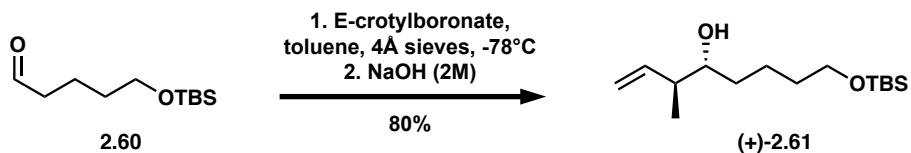
Representative Procedure G: **(+)-2.50** (15 mg, 0.0363 mmol), TEMPO (4.5 mg, 0.0029 mmol), sodium chlorite (8 mg, 0.0842 mmol) in 0.5 mL H_2O , bleach (8.25% sodium hypochlorite) (0.01

ml) in 0.5 ml H₂O, sodium phosphate buffer (0.67 M, pH 6.7, 0.2 ml) in CH₃CN (0.2 ml) yielded 10.6 mg of **(+)-2.51** (66% yield). Purified by column chromatography (0 to 50% EtOAc [with 0.01% acetic acid]:hexanes). *R_f* = 0.67 (50% EtOAc:Hexanes with acetic acid). ¹H NMR (600 MHz, CDCl₃) δ 4.78 (ddd, *J* = 10.1, 6.3, 3.4 Hz, 1H), 4.58 (d, *J* = 6.1 Hz, 1H), 4.37 (ddd, *J* = 9.7, 6.1, 3.2 Hz, 1H), 2.34 (t, *J* = 7.4 Hz, 2H), 1.84 (dddd, *J* = 14.0, 10.5, 6.9, 3.3 Hz, 1H), 1.75 (dd, *J* = 9.6, 5.2 Hz, 1H), 1.69 (ddd, *J* = 14.4, 9.3, 3.9 Hz, 3H), 1.64 (s, 3H), 1.47 (ddt, *J* = 16.2, 12.8, 4.3 Hz, 3H), 1.32 – 1.27 (m, 8H), 1.25 (s, 4H), 1.17 (dp, *J* = 11.4, 4.4 Hz, 3H), 1.04 (ddd, *J* = 13.9, 9.1, 4.7 Hz, 1H), 0.89 (dd, *J* = 9.7, 6.8 Hz, 6H). ¹³C NMR (151 MHz, CDCl₃) δ 178.29, 171.70, 109.96, 79.05, 78.10, 33.78, 33.50, 32.24, 31.44, 29.72, 29.26, 28.68, 27.83, 27.20, 27.13, 25.89, 24.93, 24.57, 23.80, 20.73, 20.00, 19.19, 19.12, 16.83. HRMS (ES⁺): Found 449.28747 (0.24 ppm), C₂₄H₄₂O₆ (M+Na⁺) requires 449.28736. IR 2929.50, 2857.77 (C-H), 1746.37, 1709.13 (C=O), 1461.66, 1379.86, 1245.98, 1184.66, 1079.39 cm⁻¹. [α]_D²⁵ +24.16 (c = 1.0 in CHCl₃)

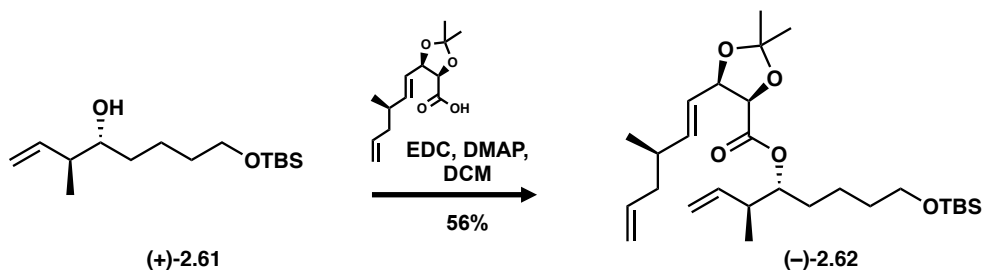


5-((*tert*-butyldimethylsilyl)oxy)pentanal (2.60) was synthesized according to Representative Procedure A: **5-((*tert*-butyldimethylsilyl)oxy)pentan-1-ol** (1.43 g, 6.55 mmol), dimethyl sulfoxide (9.3 mL, 131.05 mmol), sulfur trioxide pyridine complex (8.34 g, 52.54 mmol), triethylamine (9.1 mL, 65.52 mmol) in DCM 16 mL yielded 1.12 g of **2.60** (79% yield). Purified by column chromatography (0 to 10% EtOAc:Hexanes). *R_f* = 0.85 (30% EtOAc:Hexanes). ¹H NMR (300 MHz, CDCl₃) δ 9.77 (s, 1H), 3.62 (t, *J* = 6.1 Hz, 2H), 2.46 (td, *J* = 7.2, 1.8 Hz, 2H), 1.76 – 1.64 (m, 2H), 1.56 (td, *J* = 3.6, 0.9 Hz, 2H), 0.89 (s, 9H), 0.05 (s, 6H). ¹³C NMR (126 MHz,

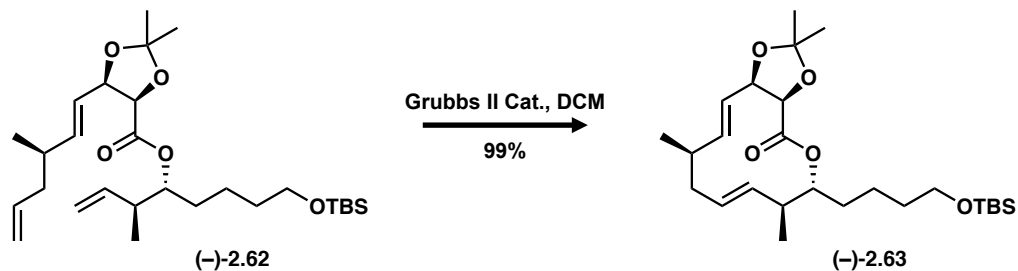
CDCl₃) δ 202.65, 62.57, 43.61, 32.10, 25.92, 25.92, 18.62, -5.35. **HRMS (APCI⁺):** Found 217.16195 (0.54 ppm), C₁₁H₂₄O₂Si (M+H⁺) requires 217.16183. **IR** 2955.24, 2925.59, 2854.81, 2361.05, 2336.28, 2174.39, 2157.11 (C-H), 1740.05 (CHO) cm⁻¹.



(3*S*,4*R*)-8-((*tert*-butyldimethylsilyl)oxy)-3-methyloct-1-en-4-ol ((+)-2.61) was synthesized according to Representative Procedure B: **2.60** (449 mg, 2.07 mmol), E-crotylboronate (13.5 mL, 6.22 mmol), toluene 19.6 mL), 4Å molecular sieves (139 mg), and 2 M NaOH (4.8 mL) yielded 454 mg of (+)-**2.61** (80% yield). Purified by column chromatography (0 to 15% EtOAc:Hexanes). **R_f** = 0.15 (10% EtOAc:Hexanes). **¹H NMR** (400 MHz, CDCl₃) δ 5.75 (ddd, *J* = 16.7, 10.8, 8.2 Hz, 1H), 5.13 (t, *J* = 0.9 Hz, 1H), 5.09 (ddd, *J* = 8.8, 1.9, 0.9 Hz, 1H), 3.62 (t, *J* = 6.1 Hz, 2H), 3.39 (tt, *J* = 6.0, 2.7 Hz, 1H), 2.25 – 2.15 (m, 1H), 1.59 (s, 1H), 1.56 – 1.50 (m, 4H), 1.42 – 1.36 (m, 2H), 1.03 (d, *J* = 6.8 Hz, 3H), 0.89 (s, 9H), 0.05 (s, 6H). **¹³C NMR** (100 MHz, CDCl₃) δ 140.47, 116.41, 74.78, 63.34, 44.27, 34.14, 32.97, 26.14, 26.13, 22.21, 16.44, -5.11. **HRMS (APCI⁺):** Found 273.22471 (1.01 ppm), C₁₅H₃₂O₂Si (M+H⁺) requires 273.22471. **IR** 3339.7 (OH), 2928.94, 2857.09 (alkane), 1639.31 (C=C) 1471.80, 1462.53, 1387.66, 1360.77, 1253.72, 1253.72, 1095.78 cm⁻¹. [α]_D²⁵ +1.0 (c = 1.0 in CHCl₃).

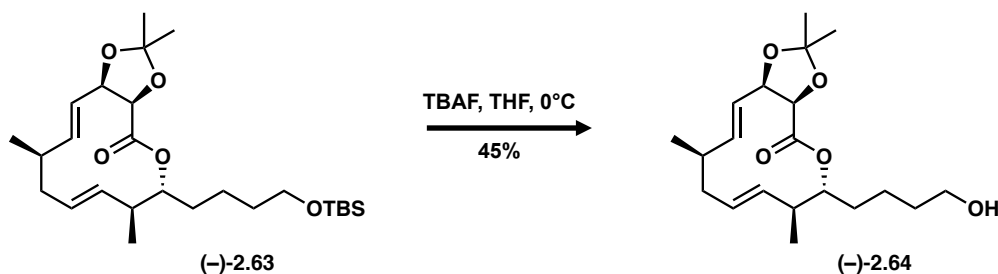


(3*S*,4*R*)-8-((*tert*-butyldimethylsilyl)oxy)-3-methyloct-1-en-4-yl (4*R*,5*R*)-2,2-dimethyl-5-((*R*,*E*)-3-methylhexa-1,5-dien-1-yl)-1,3-dioxolane-4-carboxylate ((-)-2.62) was synthesized according to Representative Procedure C: (+)-2.61 (49.7 mg, 0.1825 mmol), acid precursor⁸⁶ (70 mg, 0.2910 mmol), EDC (70 mg, .3652 mmol), 4-(dimethylamino)pyridine (2.2 mg, 0.0183 mmol) in DCM (5.5 mL) yielded 48.2 mg of ((-)-2.62) (56% yield). Purified by column chromatography (0 to 5% EtOAc:Hexanes). R_f = 0.26 (5% EtOAc:Hexanes). ¹H NMR (400 MHz, CDCl₃) δ (dd, J = 15.4, 7.0 Hz, 1H), 5.78 – 5.67 (m, 2H), 5.37 (ddd, J = 15.4, 8.2, 1.2 Hz, 1H), 5.08 – 4.97 (m, 4H), 4.89 (dt, J = 8.2, 4.6 Hz, 1H), 4.75 (t, J = 7.6 Hz, 1H), 4.59 (d, J = 6.9 Hz, 1H), 3.57 (t, J = 6.5 Hz, 2H), 2.49 – 2.39 (m, 1H), 2.22 (dt, J = 13.7, 6.8 Hz, 1H), 2.13 (dt, J = 12.7, 6.3 Hz, 1H), 1.98 (dt, J = 13.9, 7.5 Hz, 1H), 1.62 (s, 3H), 1.50 (tdd, J = 9.2, 6.8, 4.2 Hz, 4H), 1.39 (s, 3H), 1.25 (s, 2H), 0.98 (dd, J = 10.4, 6.8 Hz, 6H), 0.88 (s, 9H), 0.03 (s, 6H). ¹³C NMR (100 MHz, CDCl₃) δ 169.63, 142.79, 139.11, 136.63, 122.44, 116.37, 115.92, 110.83, 79.27, 78.32, 78.08, 63.00, 40.91, 40.84, 36.21, 32.76, 30.58, 27.21, 26.11, 25.88, 22.00, 19.25, 15.64, -5.13. HRMS (ES⁺): Found 517.33233 (0.69 ppm), C₂₈H₅₀O₅Si (M+Na⁺) requires 517.33197. IR 2928.72, 2857.23, 2361.20 (C-H), 1753.23, 1730.08 (C=O), 1640.84 (C=C), 1461.17, 1379.90, 1254.07, 1218.53, 1164.32, 1090.62 cm⁻¹. $[\alpha]_D^{25}$ -23.2 (c = 1.0 in CHCl₃).



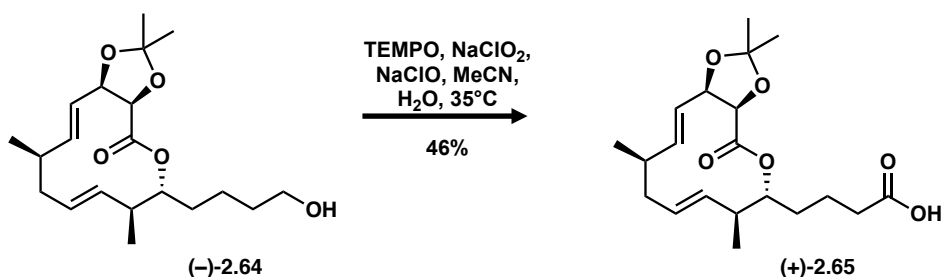
(3*aR*,6*R*,7*S*,8*E*,11*R*,12*E*,13*aR*)-6-(4-((*tert*-butyldimethylsilyl)oxy)butyl)-2,2,7,11-tetramethyl-3*a*,6,7,10,11,13*a*-hexahydro-4*H*-[1,3]dioxolo[4,5-*c*][1]oxacyclododecin-4-one ((-

(-)-2.63) was synthesized according to Representative Procedure D: **((-)-2.62)** (24 mg, 0.0485 mmol), Grubbs II Generation Catalyst (2.0 mg, 0.0024 mmol) in DCM (8 mL) yielded 23 mg of **((-)-2.63)** (99% yield). Purified by column chromatography (0 to 5% EtOAc:Hexanes). $R_f = 0.30$ (5% EtOAc:Hexanes). $^1\text{H NMR}$ (400 MHz, CDCl_3) δ 5.73 (dd, $J = 15.6, 7.2$ Hz, 1H), 5.25 (dd, $J = 15.6, 6.9$ Hz, 1H), 5.09 (dd, $J = 6.3, 3.0$ Hz, 2H), 4.83 – 4.76 (m, 1H), 4.73 (t, $J = 6.8$ Hz, 1H), 4.51 (d, $J = 6.7$ Hz, 1H), 3.57 (t, $J = 6.6$ Hz, 2H), 2.27 – 2.14 (m, 3H), 2.00 – 1.87 (m, 1H), 1.69 (s, 3H), 1.58 (d, $J = 4.1$ Hz, 1H), 1.54 – 1.45 (m, 3H), 1.40 (s, 3H), 1.38 – 1.28 (m, 2H), 1.05 (d, $J = 6.7$ Hz, 3H), 0.96 (d, $J = 6.7$ Hz, 3H), 0.88 (s, 9H), 0.03 (s, 6H). $^{13}\text{C NMR}$ (100 MHz, CDCl_3) δ 170.40, 138.76, 135.12, 129.99, 123.57, 111.08, 78.76, 78.47, 63.08, 42.36, 38.85, 36.08, 32.91, 32.33, 29.86, 26.95, 26.12, 26.01, 26.01, 21.28, 18.18, -5.12. **HRMS (ES⁺)**: Found 489.30075 (0.16 ppm), $\text{C}_{26}\text{H}_{46}\text{O}_5\text{Si}$ ($\text{M}+\text{Na}^+$) requires 489.30067. **IR** 2954.92, 2928.17, 2856.27 (C-H), 1764.72, 1754.03, 1745.24 (C=O), 1468.20, 1461.69, 1451.70, 1408.58, 1254.79, 1090.48 cm^{-1} . $[\alpha]^{25}_{\text{D}} -5.5$ ($c = 0.84$ in CHCl_3).



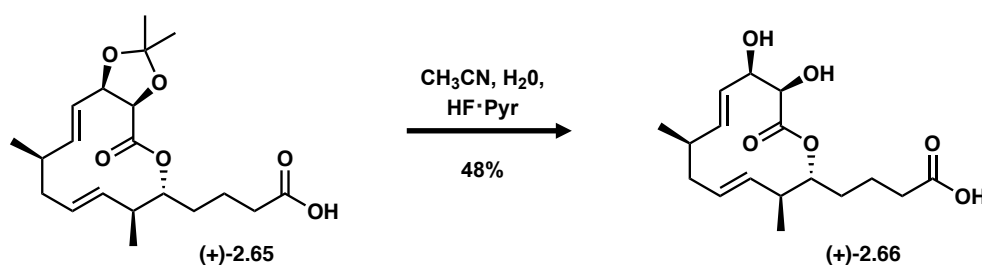
(3aR,6R,7S,8E,11R,12E,13aR)-6-(4-hydroxybutyl)-2,2,7,11-tetramethyl-3a,6,7,10,11,13a-hexahydro-4H-[1,3]dioxolo[4,5-c][1]oxacyclododecin-4-one **((-)-2.64)** was synthesized according to Representative Procedure E: **((-)-2.63)** (292 mg, 0.6259 mmol), tetrabutylammonium fluoride solution (1 M, 1.90 ml, 1.90 mmol) in THF (6.2 ml) yielded 100 mg of **((-)-2.64)** (45% yield). Purified by column chromatography (0 to 30% EtOAc:Hexanes). $R_f = 0.22$ (30%

EtOAc:Hexanes). $^1\text{H NMR}$ (500 MHz, CDCl_3) δ 5.74 (dd, $J = 15.7, 7.3$ Hz, 1H), 5.25 (dd, $J = 15.7, 6.9$ Hz, 1H), 5.10 (dd, $J = 6.2, 2.8$ Hz, 2H), 4.84 – 4.77 (m, 1H), 4.74 (t, $J = 6.8$ Hz, 1H), 4.53 (d, $J = 6.7$ Hz, 1H), 3.62 (t, $J = 6.1$ Hz, 2H), 2.25 – 2.15 (m, 3H), 1.99 – 1.88 (m, 1H), 1.69 (s, 3H), 1.53 (ddt, $J = 20.3, 11.0, 4.0$ Hz, 4H), 1.41 (s, 3H), 1.25 (s, 2H), 1.05 (d, $J = 6.7$ Hz, 3H), 0.97 (d, $J = 6.5$ Hz, 3H). $^{13}\text{C NMR}$ (126 MHz, CDCl_3) δ 170.32, 138.63, 134.86, 129.93, 123.36, 110.98, 78.60, 78.30, 78.17, 62.66, 42.25, 38.69, 35.94, 32.59, 32.17, 26.78, 25.84, 21.16, 21.11, 18.04. **HRMS (ES⁺):** Found 375.21418 (-0.04 ppm), $\text{C}_{20}\text{H}_{32}\text{O}_5$ ($\text{M}+\text{Na}^+$) requires 375.21420. **IR** 3434.86 (OH), 2926.61, 2870.69 (C-H), 1746.37, 1729.85 (C=O), 1379.80, 1191.19, 1085.98 cm^{-1} . $[\alpha]_{\text{D}}^{25}$ -5.9 ($c = 0.37$ in CHCl_3).



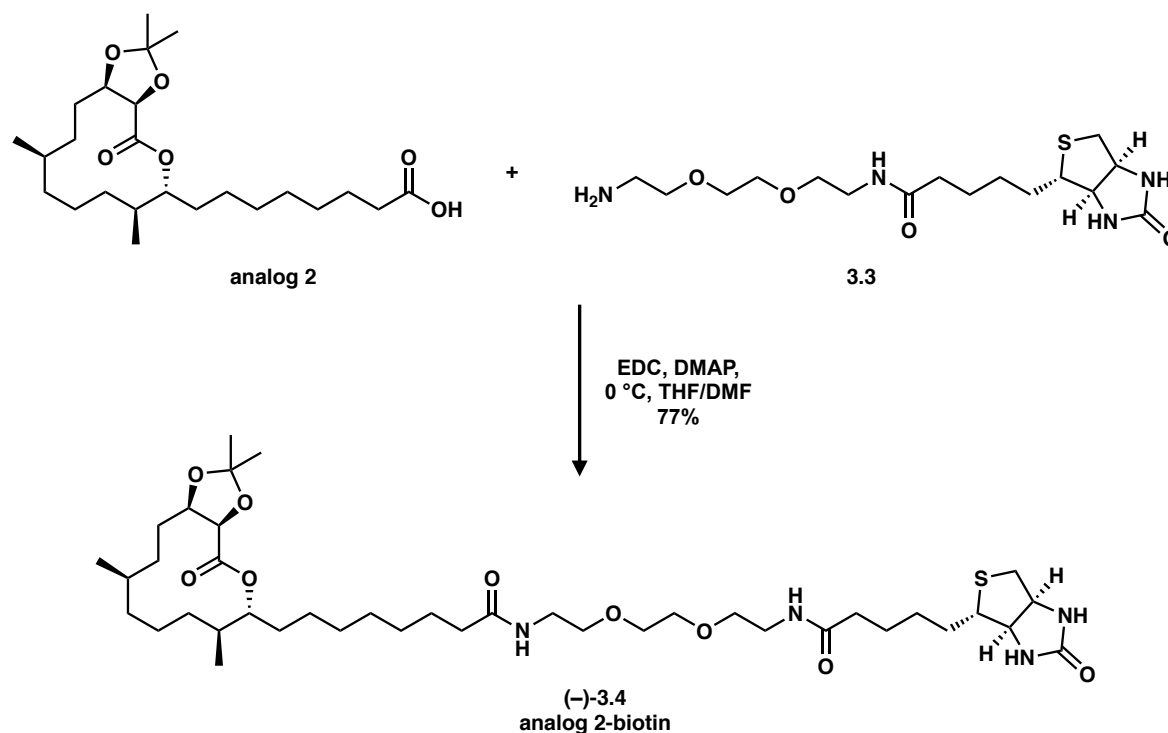
4-((3aR,6R,7S,8E,11R,12E,13aR)-2,2,7,11-tetramethyl-4-oxo-3a,6,7,10,11,13a-hexahydro-4H-[1,3]dioxolo[4,5-c][1]oxacyclododecin-6-yl)butanoic acid ((+)-2.65) was synthesized according to Representative Procedure F: ((-)-2.64) (5.5 mg, 0.0156 mmol), TEMPO (2.0 mg, 0.013 mmol), sodium chlorite (2.8 mg, 0.0312 mmol) in 0.25 mL H_2O , bleach (8.25% sodium hypochlorite) (0.01 ml) in 0.25 ml H_2O , sodium phosphate buffer (0.67 M, pH 6.7, 0.10 ml) in CH_3CN (0.1 ml) yielded 2.6 mg of ((+)-2.65) (46% yield). Purified by column chromatography (0 to 20% EtOAc [with 0.01% acetic acid]:hexanes). $R_f = 0.28$ (50% EtOAc:Hexanes). $^1\text{H NMR}$ (600 MHz, CDCl_3) δ 5.73 (dd, $J = 15.7, 6.9$ Hz, 1H), 5.25 (dd, $J = 15.7, 6.9$ Hz, 1H), 5.10 (td, $J = 6.1, 5.6, 2.2$ Hz, 2H), 4.81 (ddd, $J = 10.1, 7.6, 2.2$ Hz, 1H), 4.76 – 4.72 (m, 1H), 4.54 (d, $J = 6.6$

Hz, 1H), 2.35 (tt, $J = 16.2, 9.3$ Hz, 2H), 2.27 – 2.20 (m, 2H), 1.97 – 1.90 (m, 1H), 1.69 (s, 3H), 1.65 – 1.54 (m, 3H), 1.41 (s, 3H), 1.25 (s, 4H), 1.05 (d, $J = 6.7$ Hz, 3H), 0.97 (d, $J = 6.8$ Hz, 3H). ^{13}C NMR (600 MHz, CDCl_3) δ 186.80, 172.75, 142.79, 138.83, 134.86, 130.25, 123.52, 78.77, 78.43, 42.08, 38.83, 36.09, 33.57, 31.69, 29.85, 26.93, 26.00, 21.24, 18.10. **HRMS (ES⁺):** Found 389.19355 (0.23 ppm), $\text{C}_{20}\text{H}_{30}\text{O}_6$ ($\text{M}+\text{Na}^+$) requires 389.19355. **IR** 3439.80 (COOH) 2953.79, 2925.32 (C-H), 1734.08, 1712.38 cm^{-1} . $[\alpha]^{25}_{\text{D}} + 12.9$ ($c = 0.39$ in CHCl_3).



4-((2*R*,3*S*,4*E*,7*R*,8*E*,10*R*,11*R*)-10,11-dihydroxy-3,7-dimethyl-12-oxooxacyclododeca-4,8-dien-2-yl)butanoic acid (+)-2.66 was synthesized according to Representative Procedure G: ((+)-**2.65**) (12 mg, 0.0327 mmol), HF·pyridine (0.5 ml), H_2O (0.01 mL) in CH_3CN (4 mL) yielded 5.1 mg of (+)-**2.66** (48% yield). Purified by column chromatography (0 to 50% EtOAc [with 0.01% acetic acid]:hexanes). $R_f = 0.19$ (5% MeOH:DCM). ^1H NMR (600 MHz, CDCl_3) δ 5.31 (dt, $J = 30.8, 9.5$ Hz, 3H), 5.15 (ddd, $J = 14.8, 11.0, 3.5$ Hz, 2H), 4.90 (dd, $J = 14.7, 9.9$ Hz, 1H), 4.78 – 4.71 (m, 1H), 4.43 (s, 1H), 4.13 (s, 1H), 2.37 (s, 2H), 2.25 (ddd, $J = 31.2, 15.7, 7.3$ Hz, 2H), 2.07 – 1.98 (m, 1H), 1.83 – 1.72 (m, 2H), 1.25 (s, 5H), 1.05 (d, $J = 6.4$ Hz, 3H), 0.96 (d, $J = 6.7$ Hz, 3H). ^{13}C NMR (600 MHz, CDCl_3) δ 172.81, 166.98, 135.62, 134.44, 130.57, 126.43, 77.95, 73.74, 73.43, 56.13, 41.54, 40.90, 38.15, 32.08, 29.85, 21.31, 17.86, 1.17. **HRMS (ES⁻):** Found 325.16600 (1.04 ppm), $\text{C}_{17}\text{H}_{26}\text{O}_6$ ($\text{M}-\text{H}^+$) requires 325.16566. **IR** 3450.00 (OH), 2953.95, 2925.94,

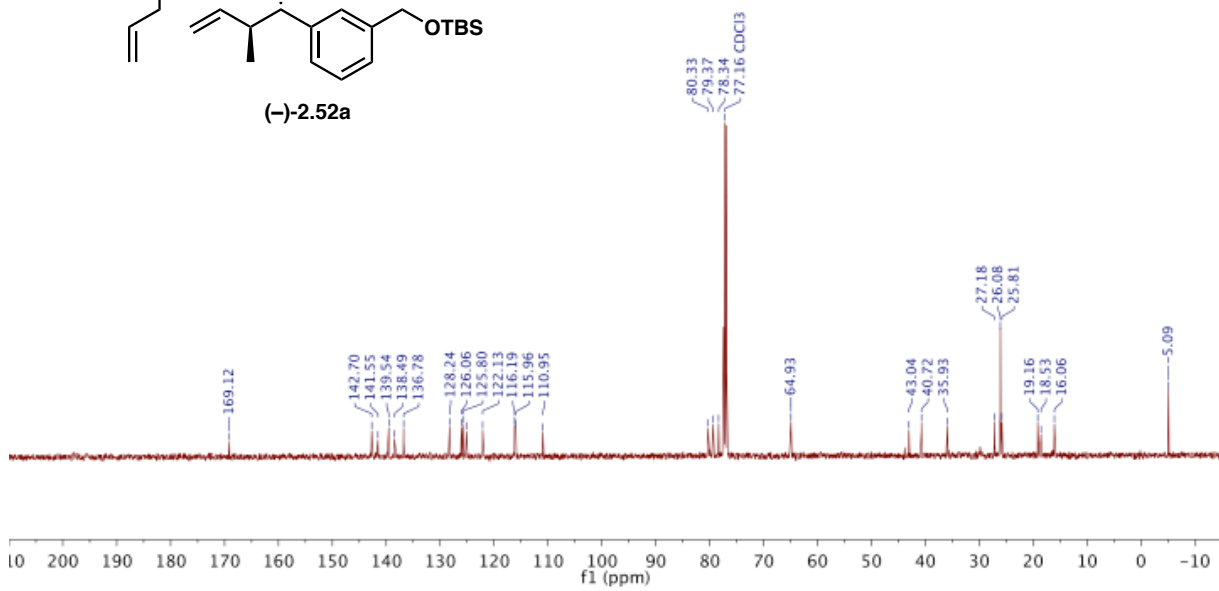
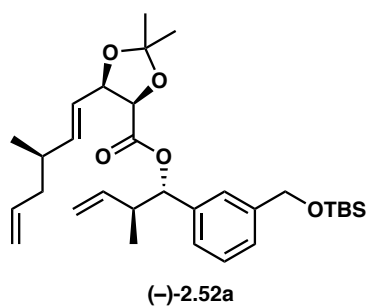
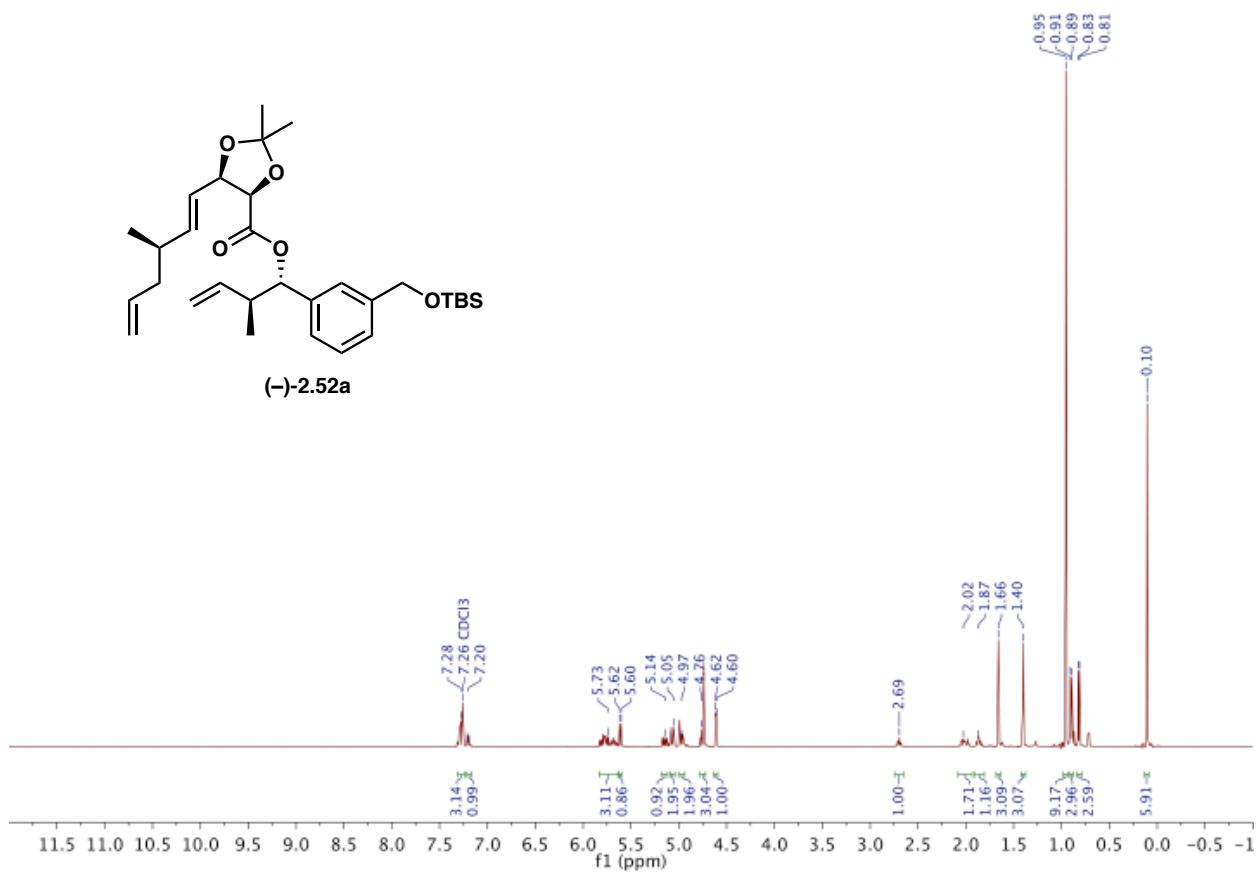
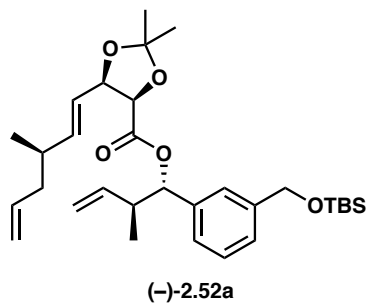
173.31, 170.13, 109.99, 93.74, 92.66, 82.84, 79.09, 78.16, 77.41, 77.36, 77.16, 76.91, 69.53, 36.86, 36.06, 34.37, 33.64, 32.69, 32.38, 32.32, 29.28, 29.26, 27.98, 27.39, 26.05, 25.73, 24.12, 20.89, 16.95, 13.39. **HRMS (ES⁺):** Found 546.39024 (0.19 ppm), C₃₁H₅₁N₃O₅ (M+H⁺) requires 546.39015. **IR** 3750.37 (N-H), 2927.07 (C-H), 1746.37, 2361.42, 2336.50 (C≡C) 1733.98 (C=O), 1540.05 (N=N) cm⁻¹. [α]_D²⁵ -16.67 (*c* = 0.18 in CHCl₃).

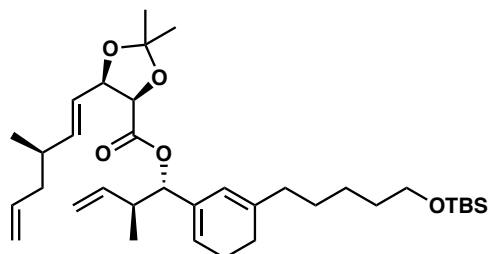


N-(2-(2-(2-(5-((3*aR*,4*S*,6*aS*)-2-oxohexahydro-1*H*-thieno[3,4-*d*]imidazol-4-yl)pentanamido)ethoxy)ethoxy)ethyl)-8-((3*aR*,6*R*,7*S*,11*R*,13*aR*)-2,2,7,11-tetramethyl-4-oxodecahydro-4*H*-[1,3]dioxolo[4,5-*c*][1]oxacyclododecin-6-yl)octanamide ((-)-3.4) was synthesized using amidation conditions. A flame dried vial was charged with argon, **analog 2** (5 mg, 0.01172 mmol) and DCM (0.2 mL). The reaction was subsequently cooled to 0°C, then DMAP (0.1 mg, 0.00078 mmol) and EDC (3.0 mg, 0.0156 mmol) were added consecutively. After the reaction stirred for 10 minutes, a solution of the *N*-(2-(2-(2-aminoethoxy)ethoxy)ethyl)-5-((3*aR*,4*S*,6*aS*)-2-oxohexahydro-1*H*-thieno[3,4-*d*]imidazol-4-yl)pentanamide (**3.3**), dissolved in

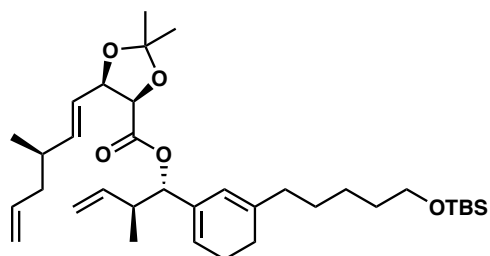
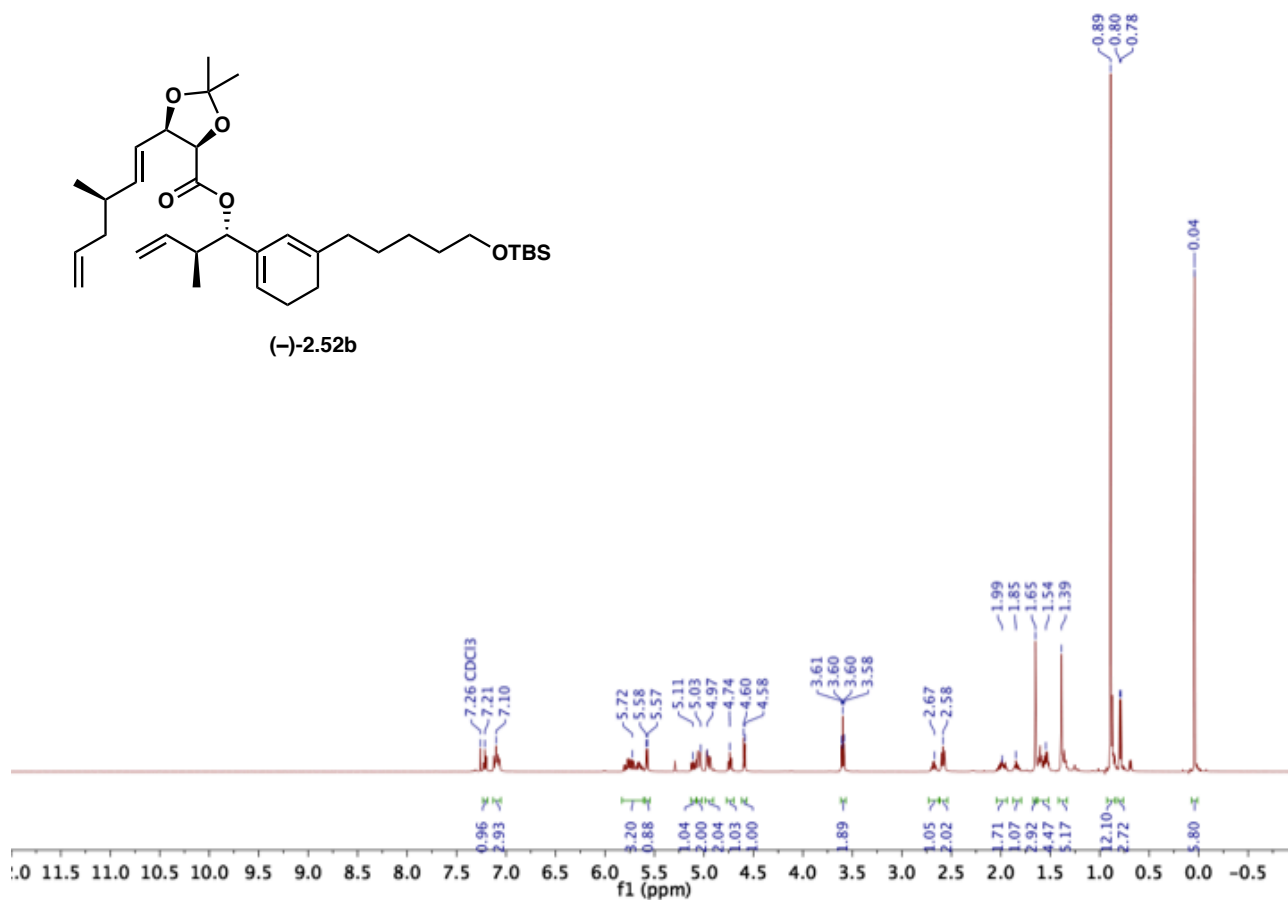
DCM (0.2 mL) was added dropwise. The reaction was stirred 24 hours and then added to a separatory funnel containing H₂O and DCM. The organic layer was separated, and the aqueous layer was extracted with DCM (3 x 5 mL). The combined organic layers were washed with brine, dried over MgSO₄, filtered and concentrated. Purified by column chromatography (10% MeOH (with 0.01 % acetic acid):DCM). $R_f = 0.23$ (10% MeOH (with 0.01 % acetic acid):DCM). **¹H NMR** (500 MHz, CDCl₃) δ 6.44 – 6.39 (m, 1H), 6.31 (d, $J = 5.6$ Hz, 1H), 6.08 (s, 1H), 5.22 (s, 1H), 4.77 (ddd, $J = 10.0, 6.4, 3.4$ Hz, 1H), 4.56 (d, $J = 6.1$ Hz, 1H), 4.51 (dd, $J = 7.8, 5.0$ Hz, 1H), 4.37 (ddd, $J = 9.6, 6.1, 3.2$ Hz, 1H), 4.32 (ddd, $J = 8.0, 4.7, 1.4$ Hz, 1H), 3.62 (s, 1H), 3.57 (ddd, $J = 4.8, 3.5, 2.0$ Hz, 3H), 3.53 – 3.37 (m, 3H), 3.16 (td, $J = 7.3, 4.5$ Hz, 1H), 2.92 (dd, $J = 12.8, 4.9$ Hz, 1H), 2.74 (d, $J = 12.8$ Hz, 1H), 2.23 (t, $J = 7.3$ Hz, 2H), 2.20 – 2.15 (t, 2H), 1.84 (dddd, $J = 14.0, 10.5, 7.0, 3.2$ Hz, 0H), 1.77 – 1.64 (m, 3H), 1.62 (s, 2H), 1.45 (p, $J = 7.6$ Hz, 2H), 1.38 (s, 2H), 1.32 – 1.23 (m, 11H), 1.17 (dd, $J = 9.0, 5.8$ Hz, 0H), 1.11 – 1.01 (m, 0H), 0.89 (t, $J = 7.3$ Hz, 4H). **¹³C NMR** (126 MHz, CDCl₃) δ 173.95, 173.54, 170.41, 164.03, 110.25, 79.41, 77.67, 77.63, 77.41, 77.16, 70.51, 70.45, 70.24, 62.17, 60.56, 57.31, 55.65, 40.90, 39.53, 37.04, 36.31, 33.91, 32.70, 30.10, 29.97, 29.66, 28.42, 28.26, 27.64, 26.30, 26.10, 25.78, 25.44, 24.46, 21.14, 17.21. **HRMS (ES⁺):** Found 805.47405 (1.44 ppm), C₃₆H₆₆N₁₀O₇²³N³²S (M+Na⁺) requires 805.47557. **IR** 3291.88 (N-H), 2928.16, 2859.65 (C-H), 1745.14, 1703.14 (C=O), 1080.09 (C-O-C) cm⁻¹. **$[\alpha]^{25}_D$** -2.44 ($c = 0.62$ in CHCl₃).

86. Hallside, M. S.; Brzozowski, R. S.; Wuest, W. M.; Phillips, A. J., A concise synthesis of carolacton. *Org Lett* **2014**, *16* (4), 1148-51.
123. Solinski, A. E.; Koval, A. B.; Brzozowski, R. S.; Morrison, K. R.; Fraboni, A. J.; Carson, C. E.; Eshraghi, A. R.; Zhou, G.; Quivey, R. G., Jr.; Voelz, V. A.; Buttaro, B. A.; Wuest, W. M., Diverted Total Synthesis of Carolacton-Inspired Analogs Yields Three Distinct Phenotypes in *Streptococcus mutans* Biofilms. *J Am Chem Soc* **2017**, *139* (21), 7188-7191.
124. Sun, H.; Roush, W. R.; Candito, D. A.; Blanchot, M.; Lautens, M., SYNTHESIS OF (S,S)-DIISOPROPYL TARTRATE (E)-CROTYLBORONATE AND ITS REACTION WITH ALDEHYDES: (2R,3R,4R)-1,2-DIDEOXY-2-ETHENYL-4,5-O-(1-METHYLETHYLIDENE)-XYLITOL. *Org Synth.* **2011**, *88*, 181-196.

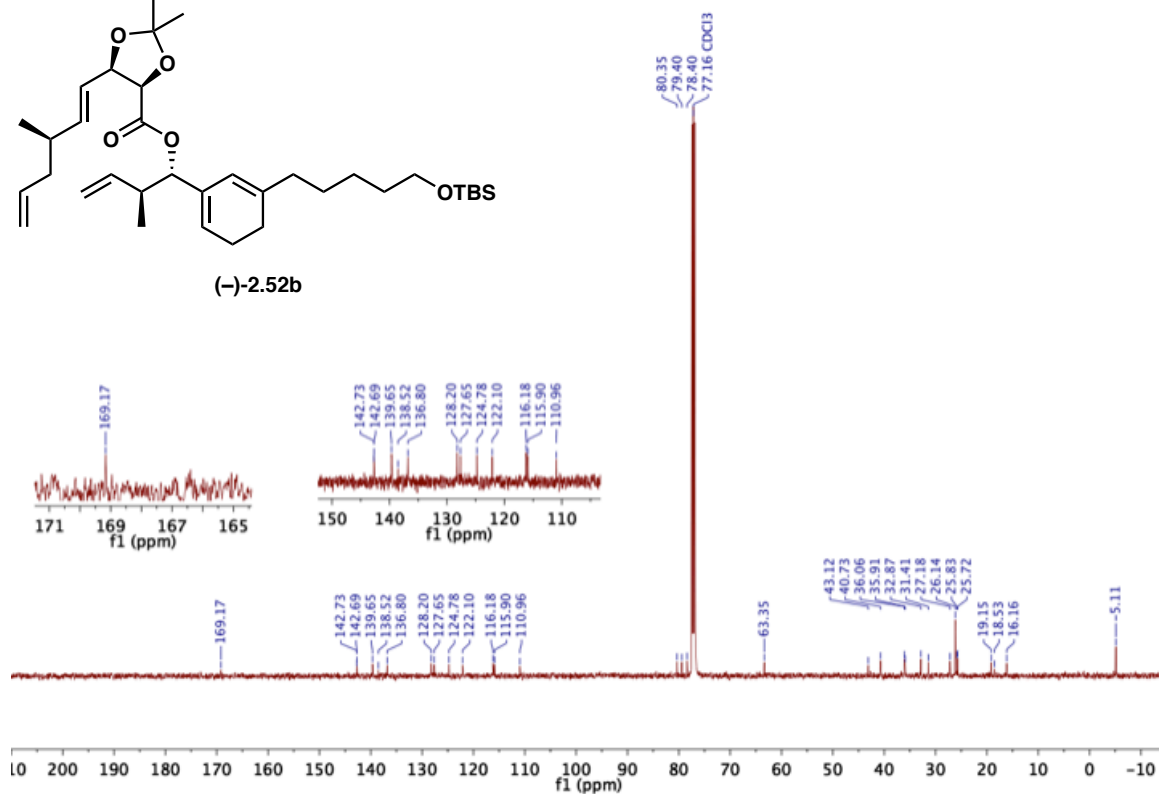


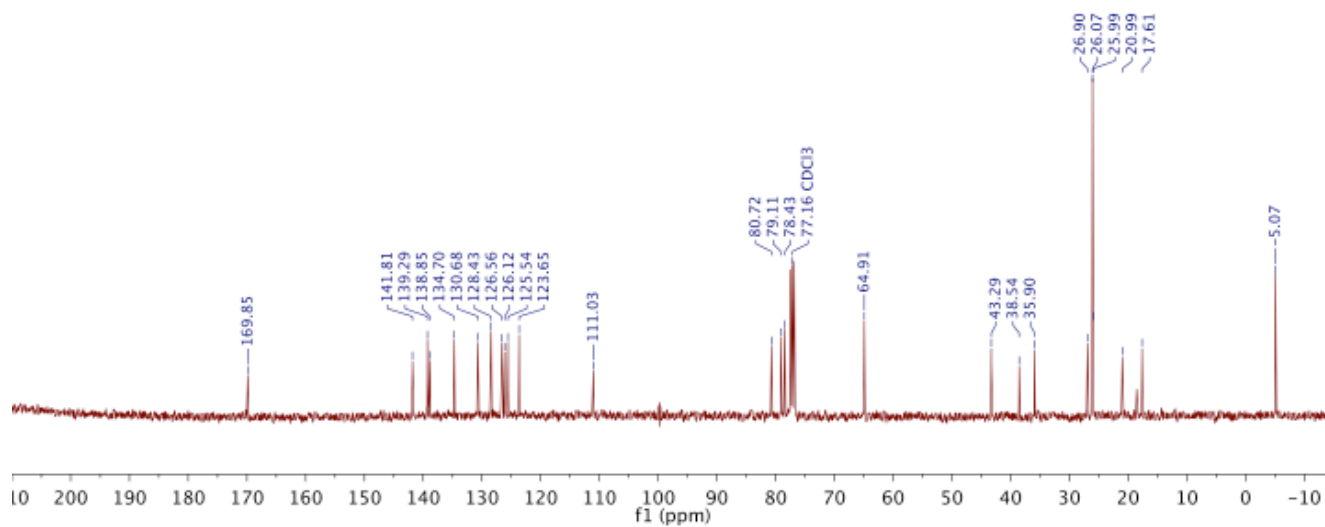
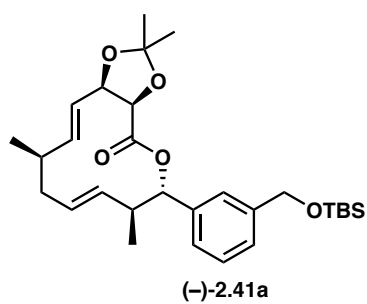
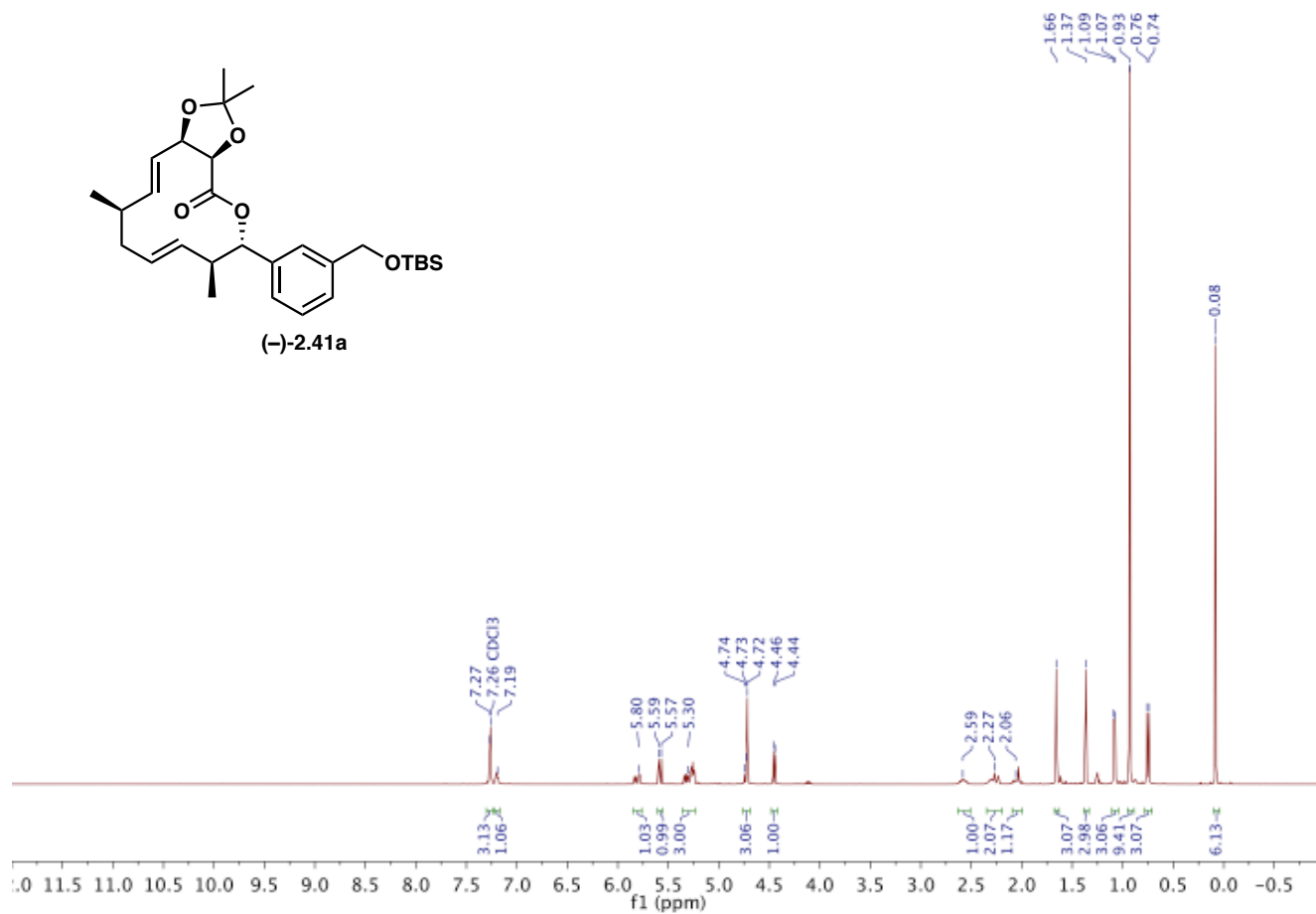
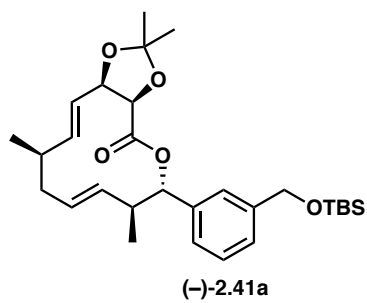


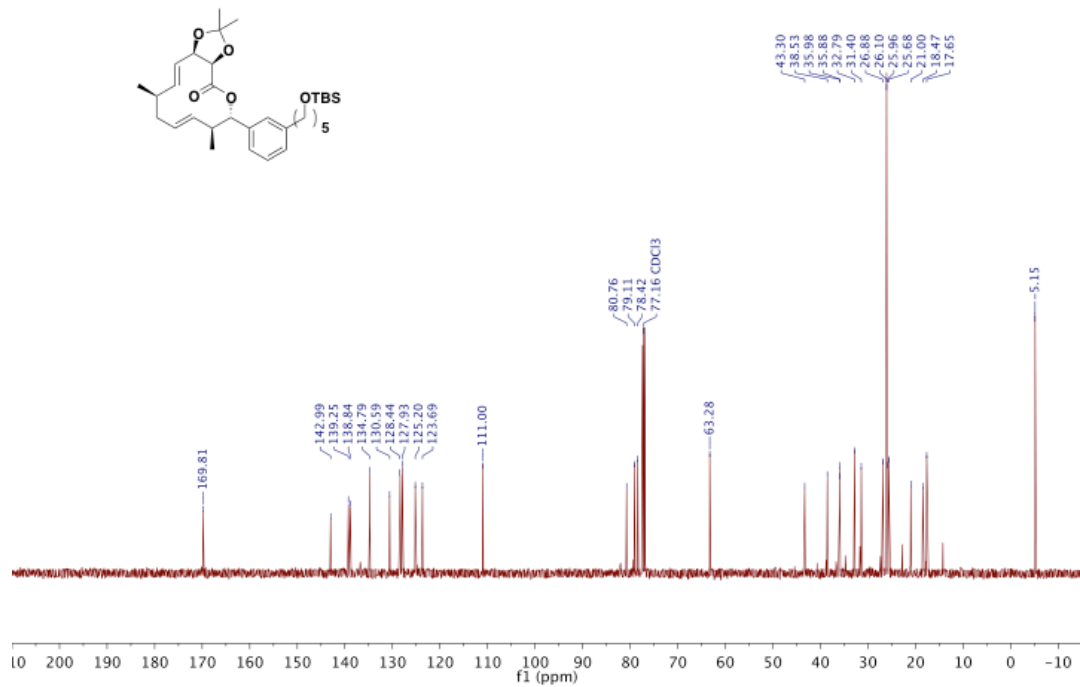
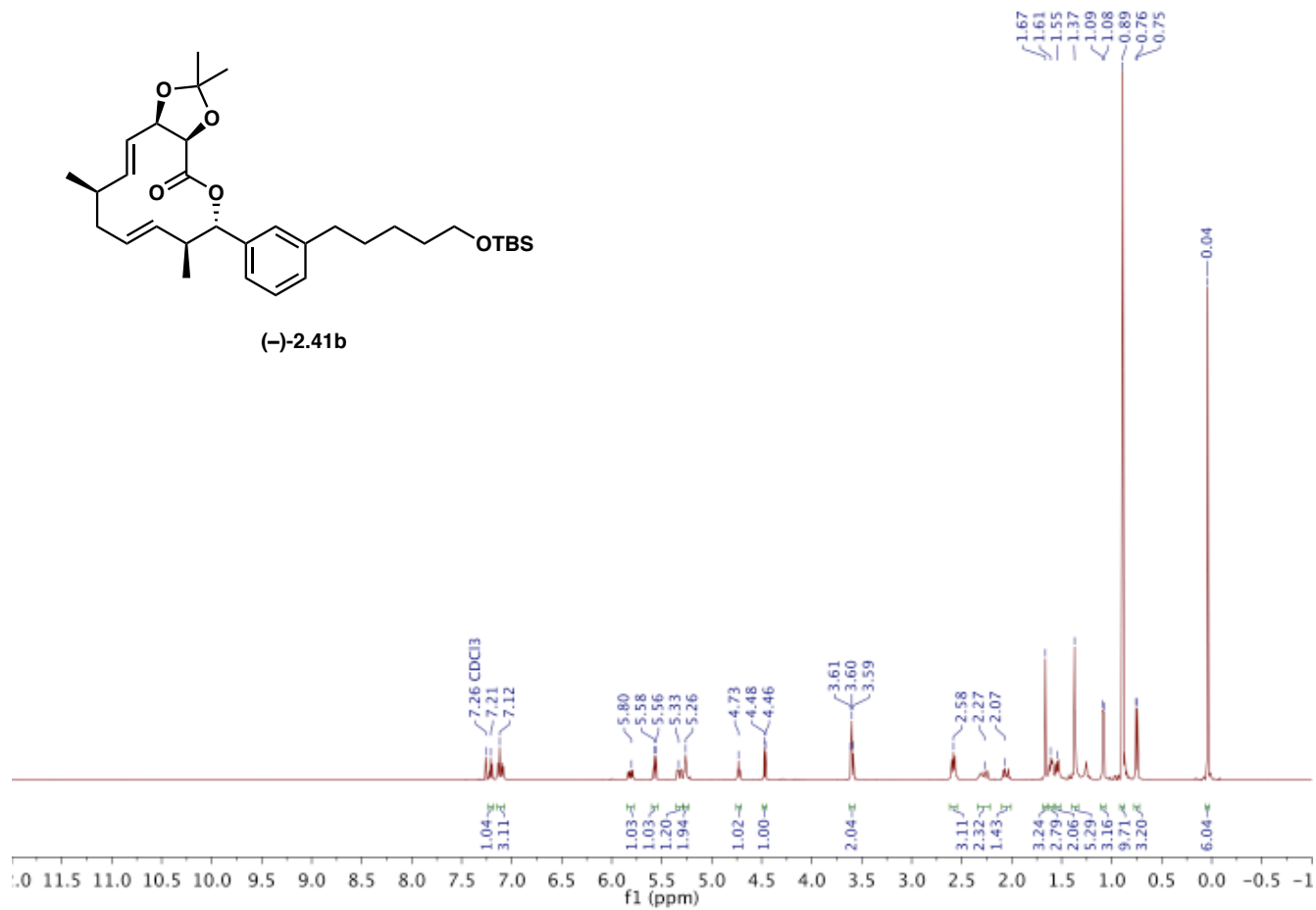
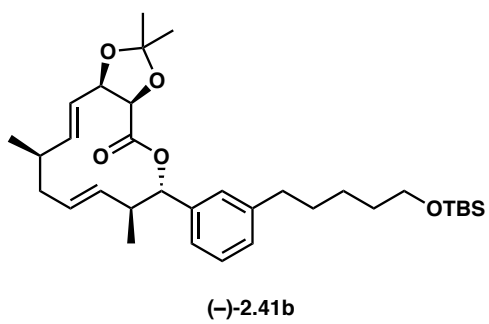
(-)-2.52b

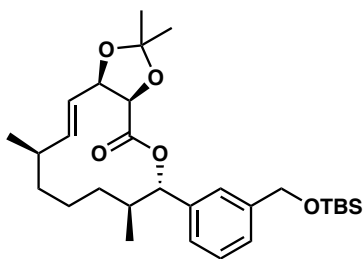


(-)-2.52b

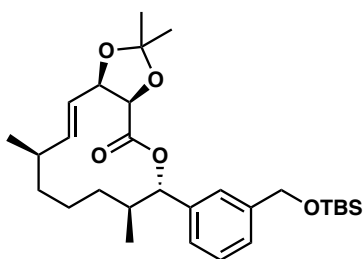
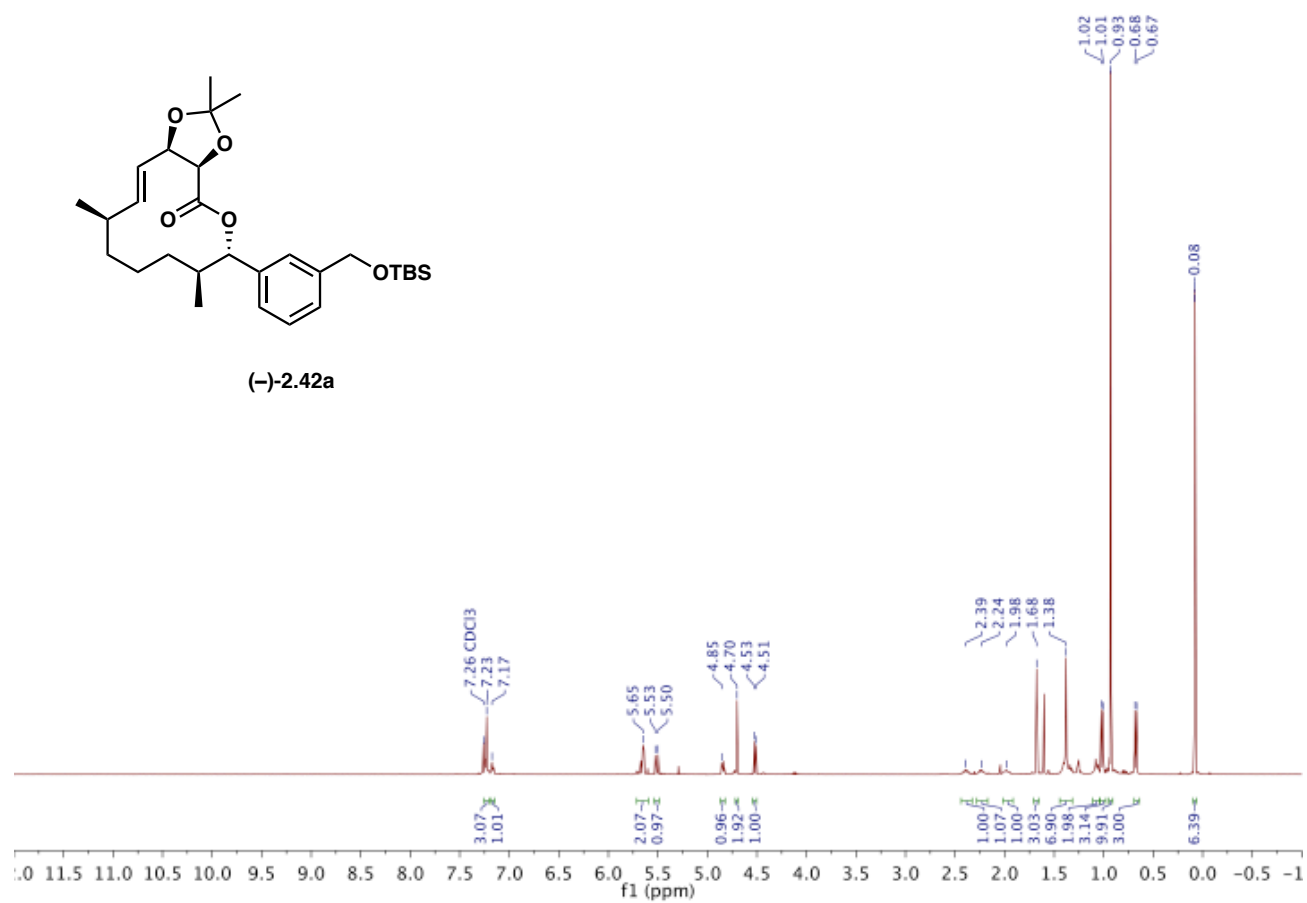




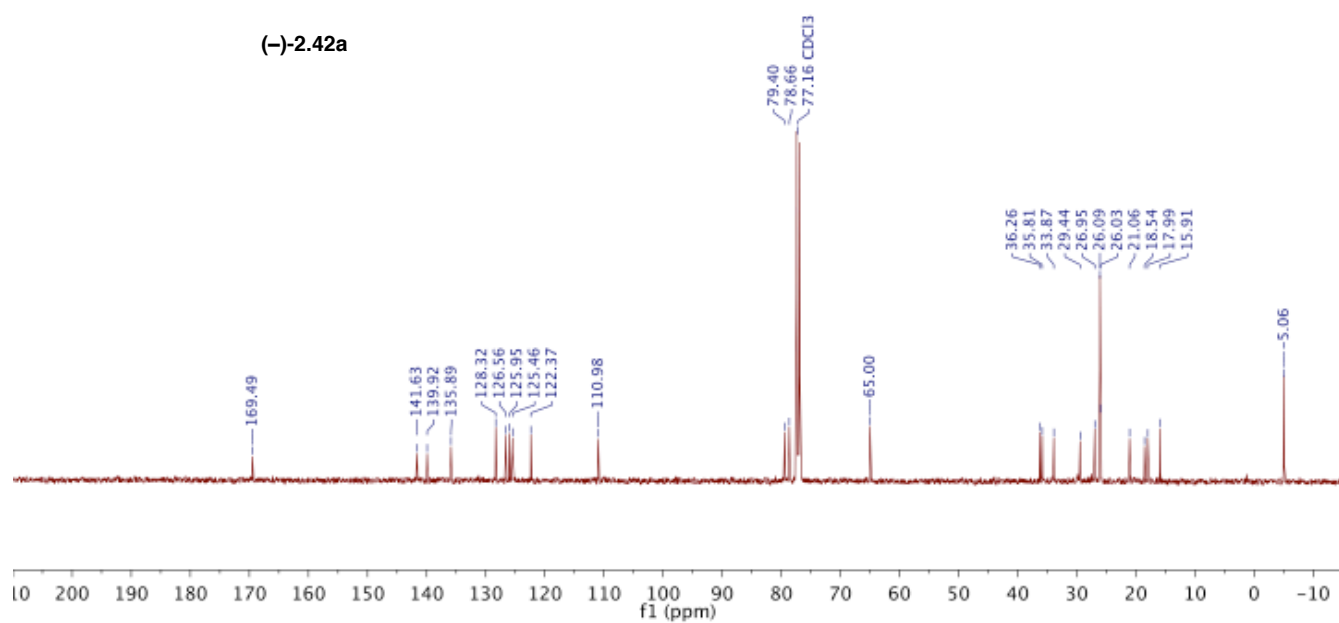


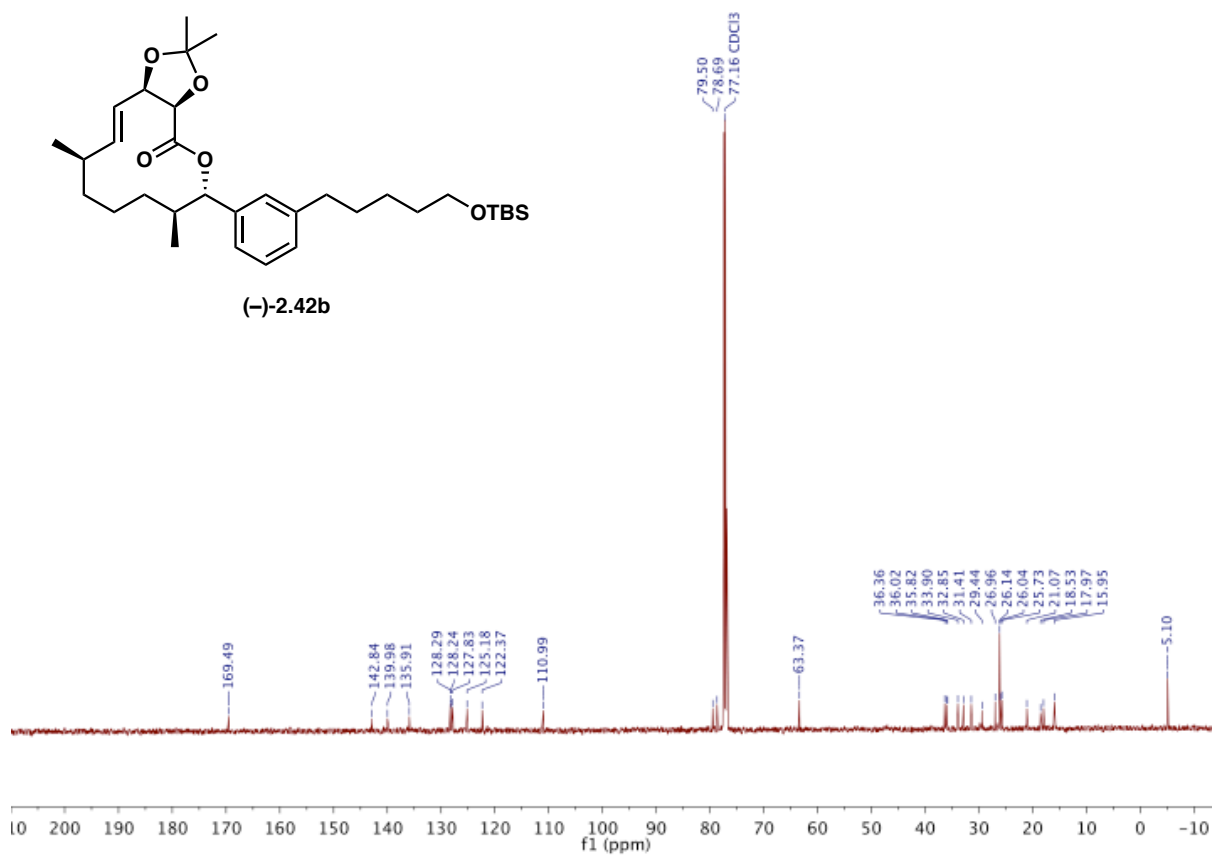
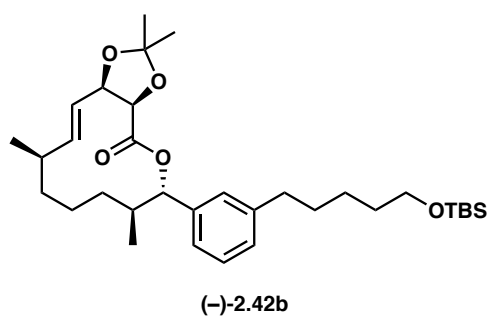
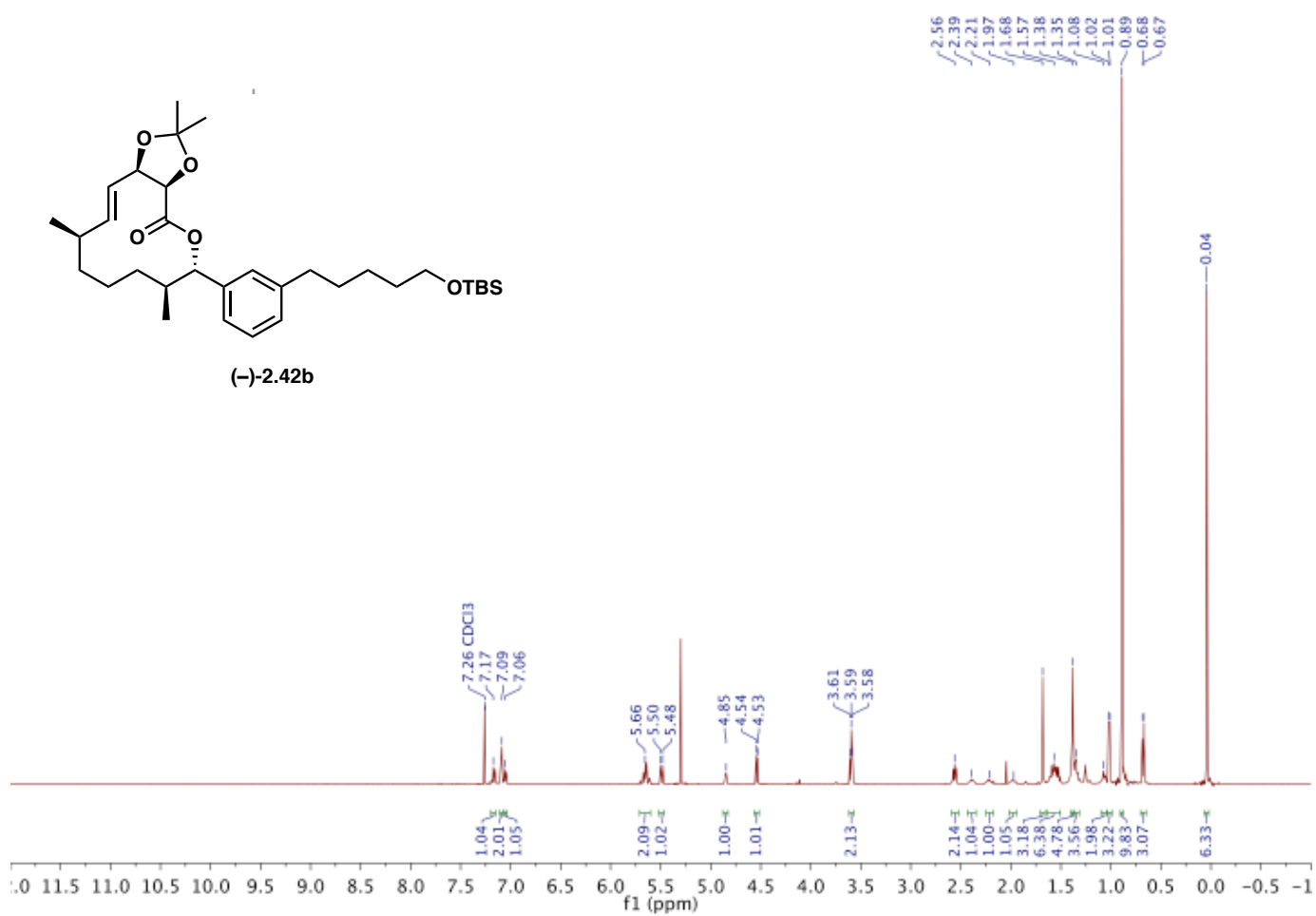
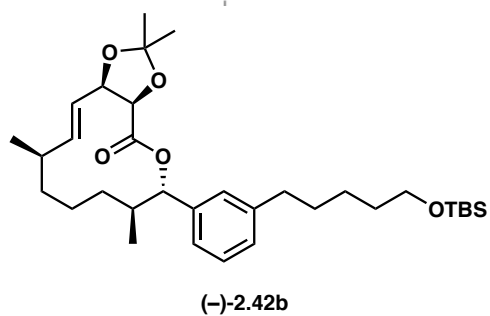


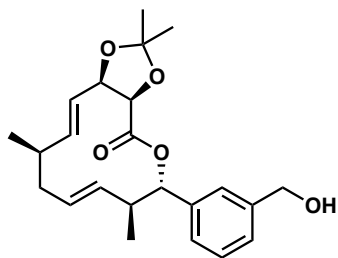
(-)-2.42a



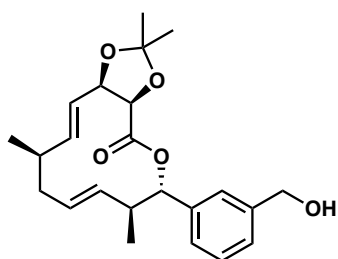
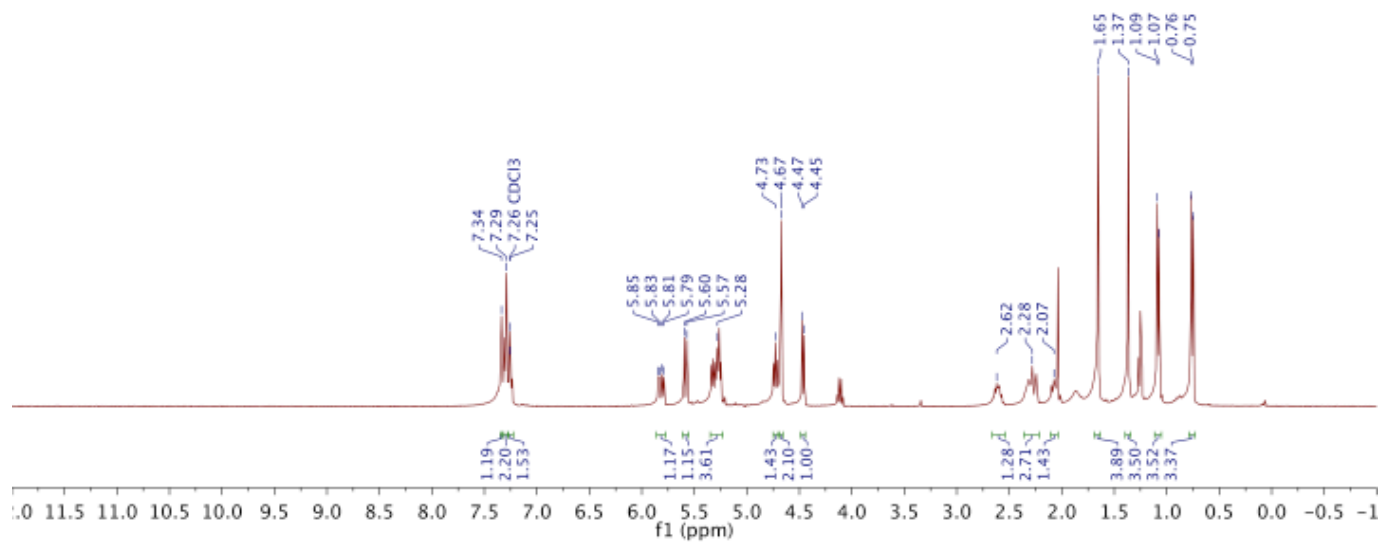
(-)-2.42a



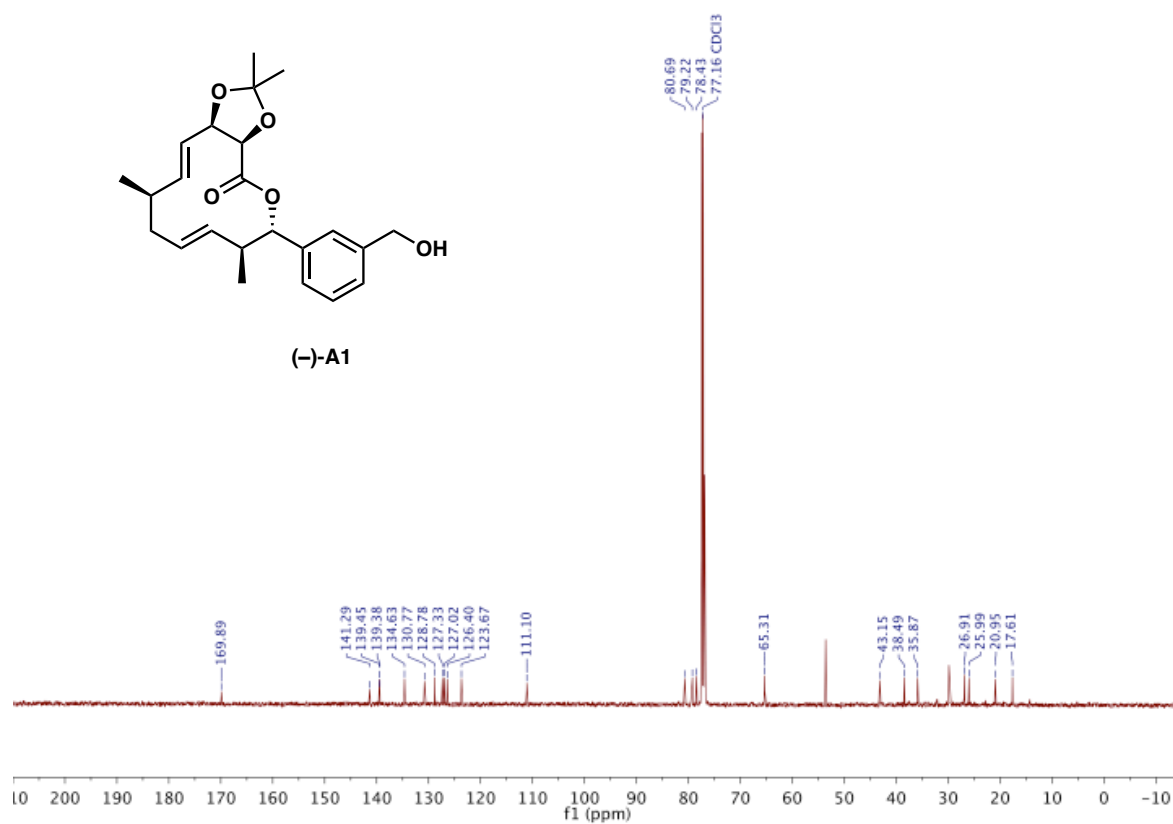


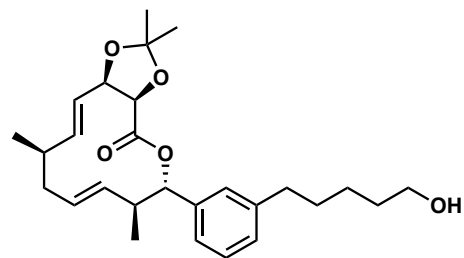


(-)-A1

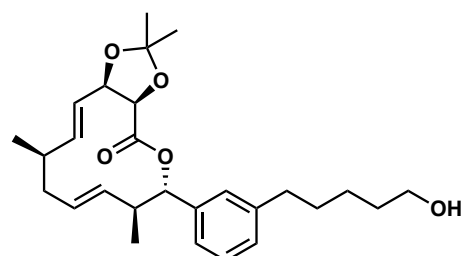
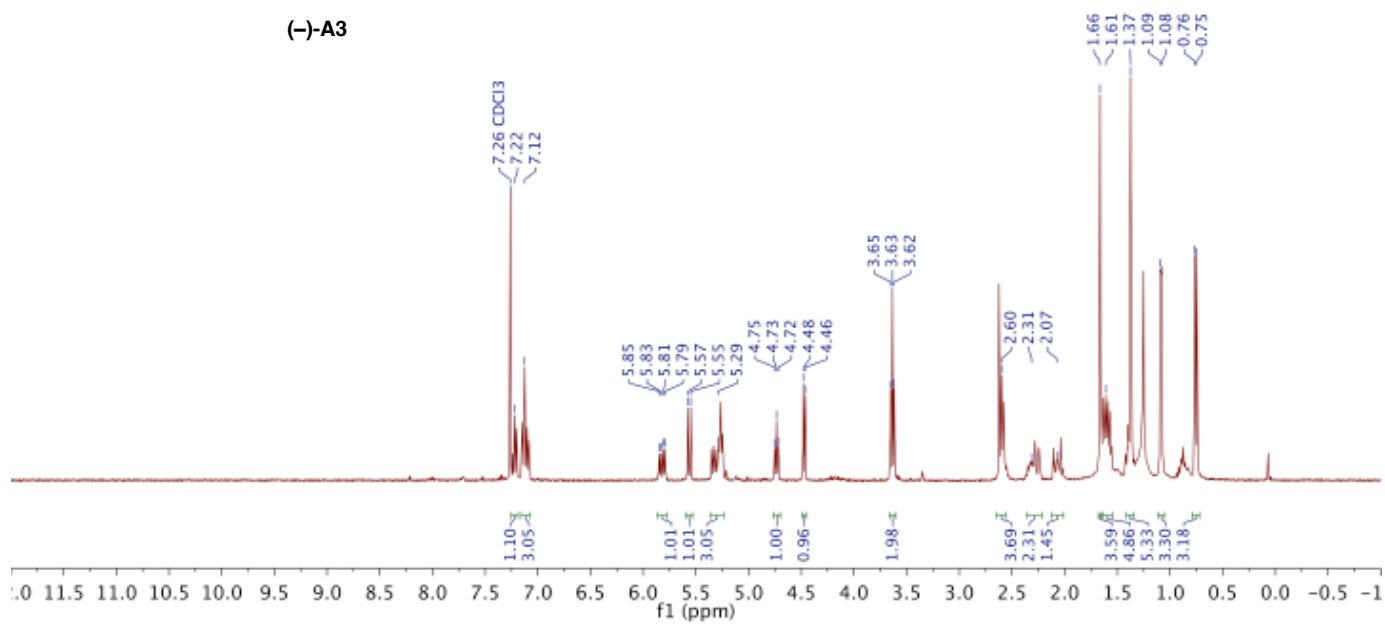


(-)-A1

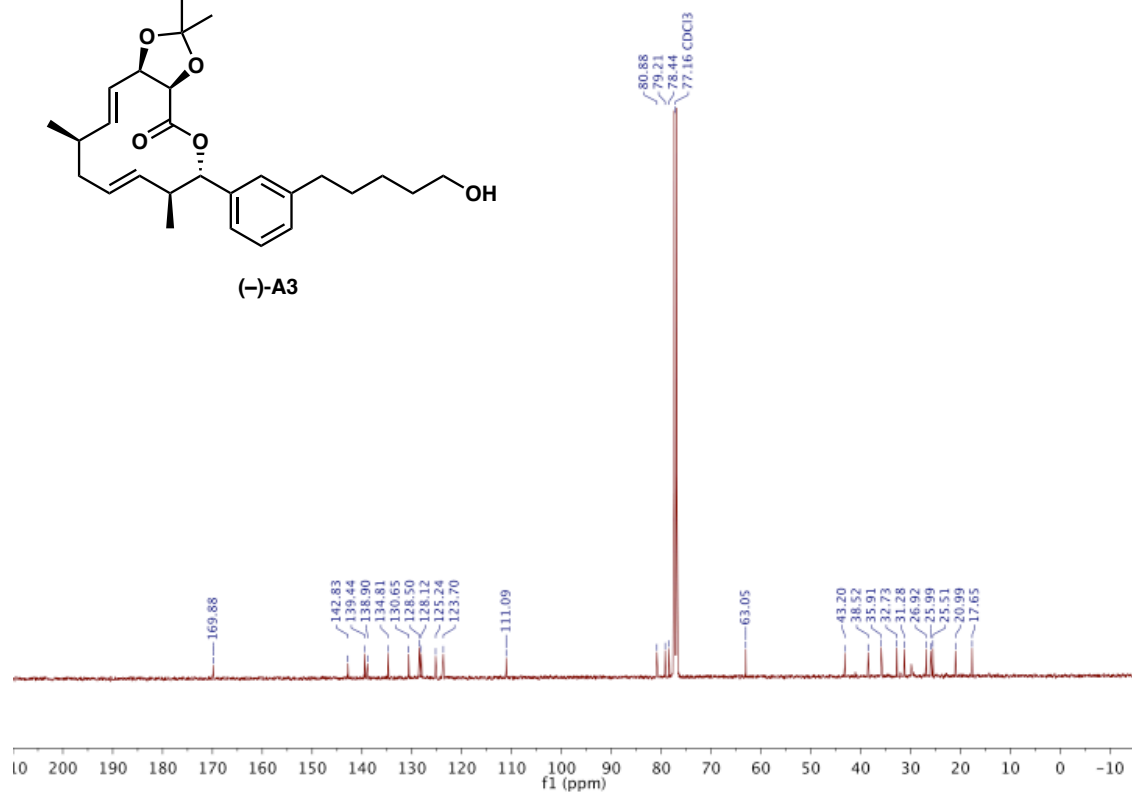


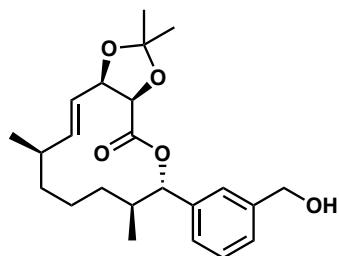


(-)-A3

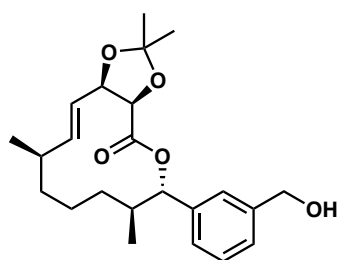
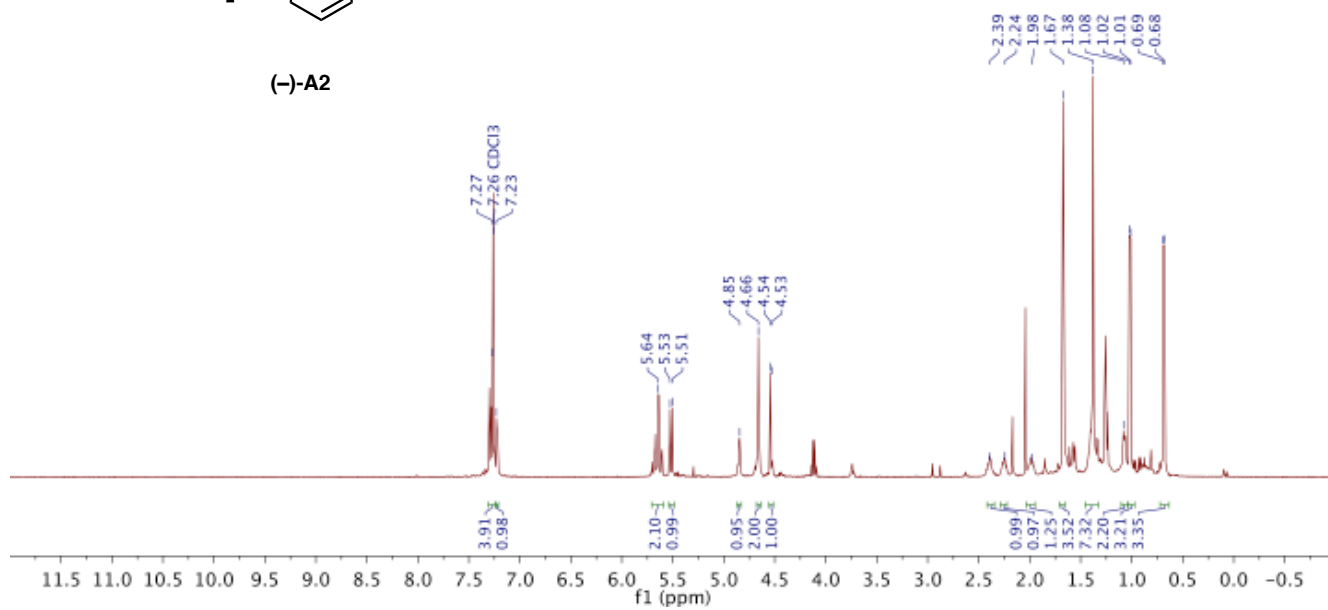


(-)-A3

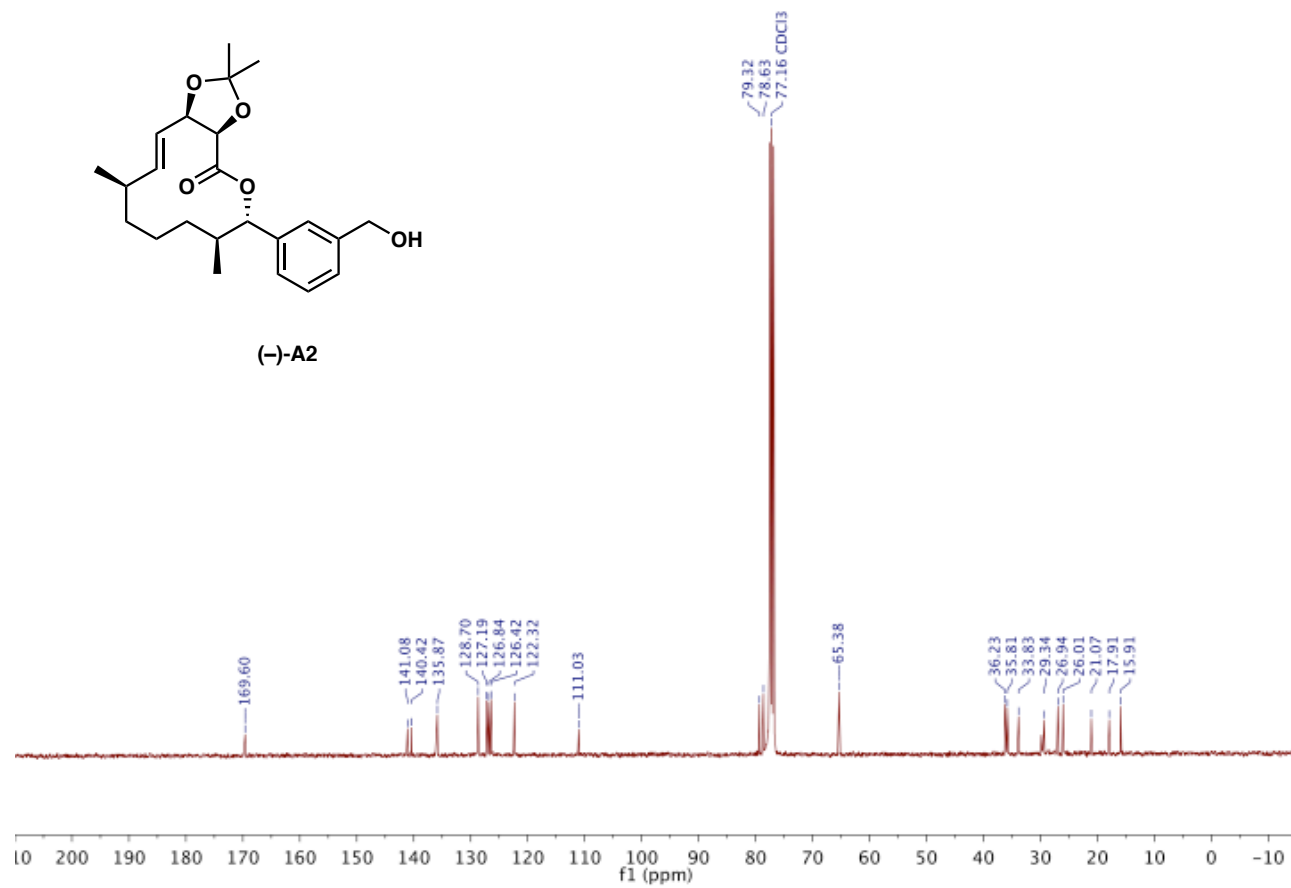


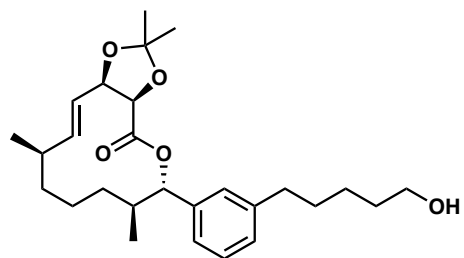


(-)-A2

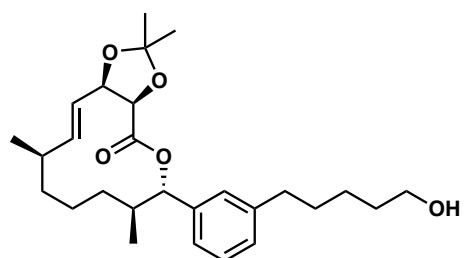
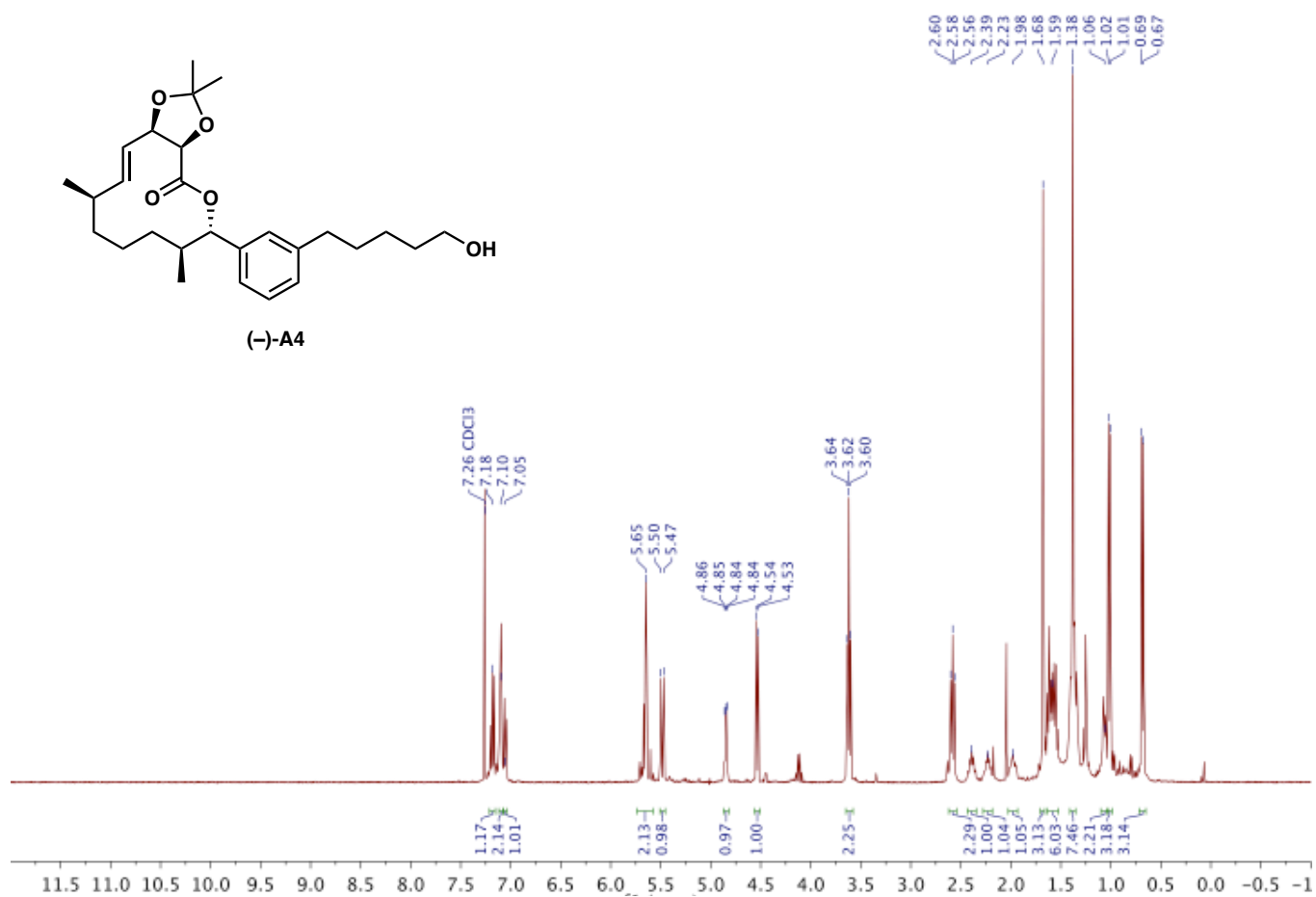


(-)-A2

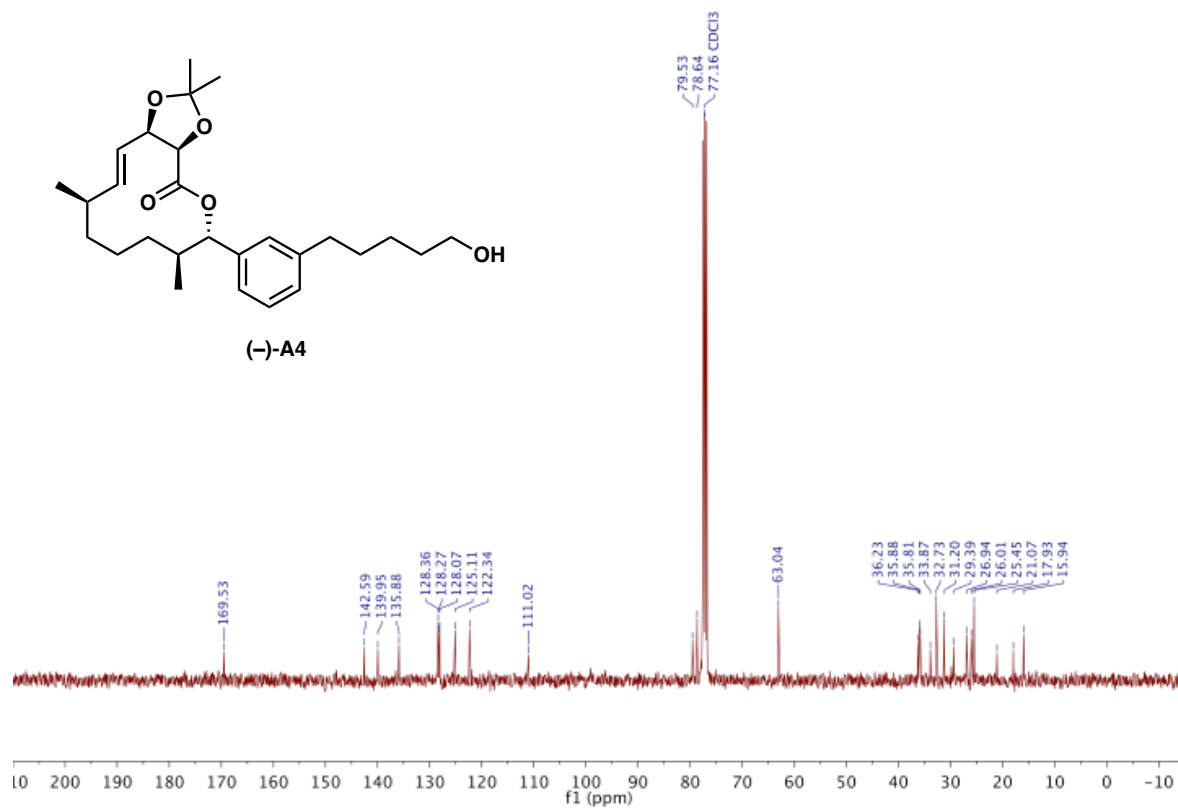


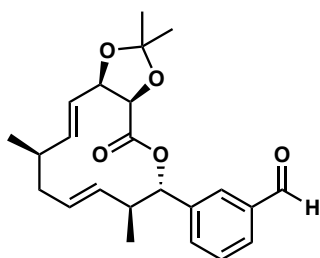


(-)-A4

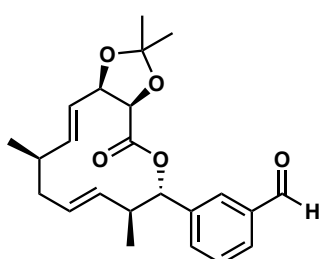
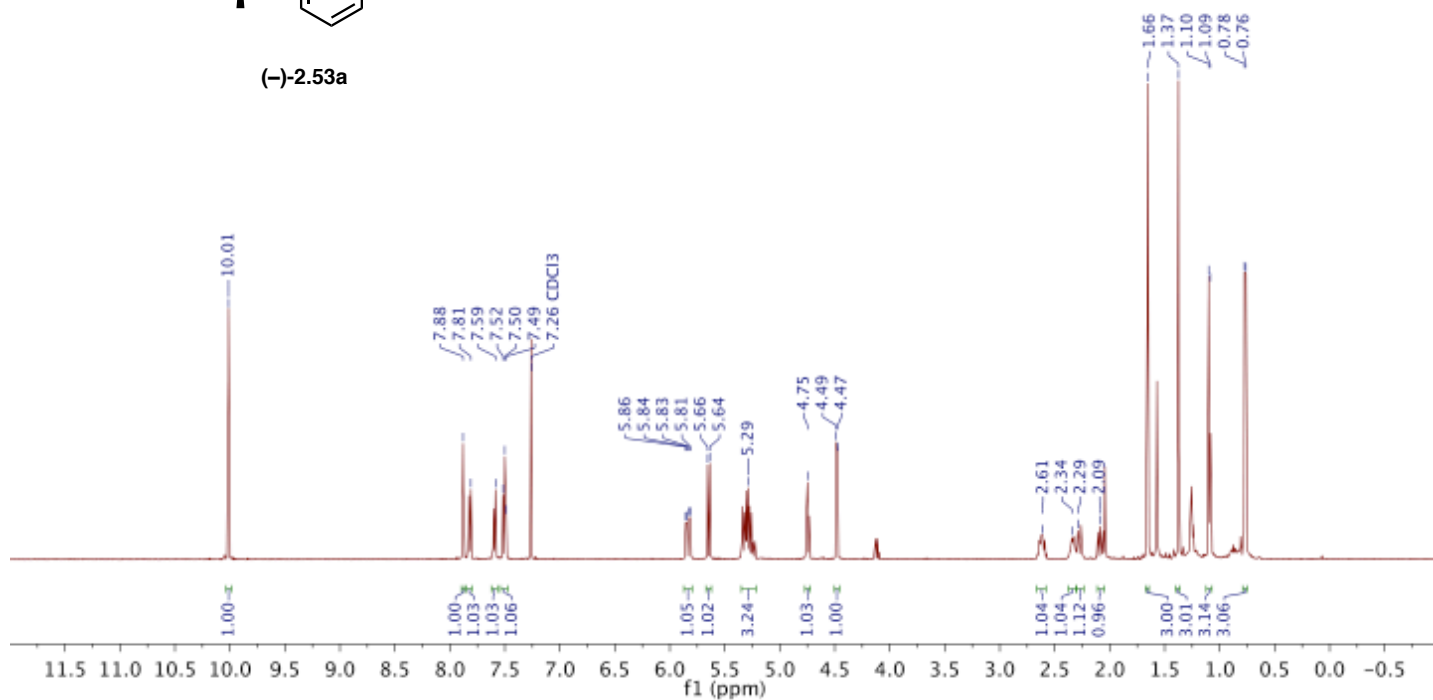


(-)-A4

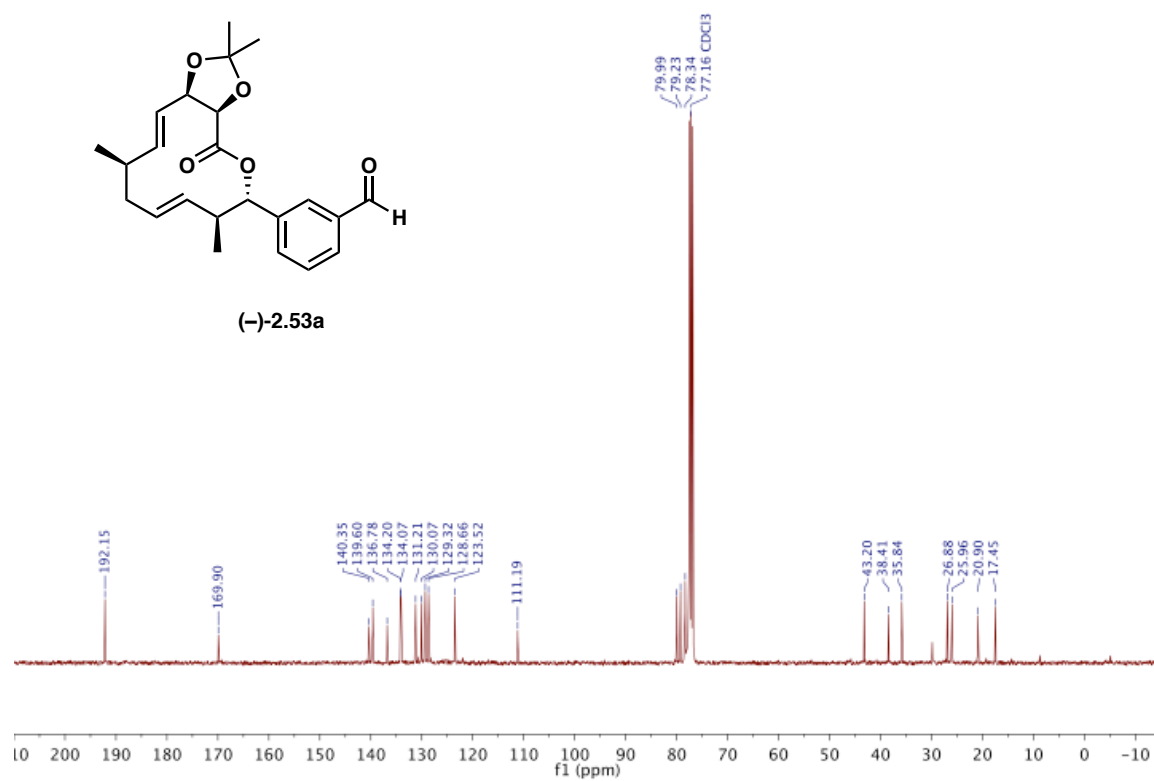


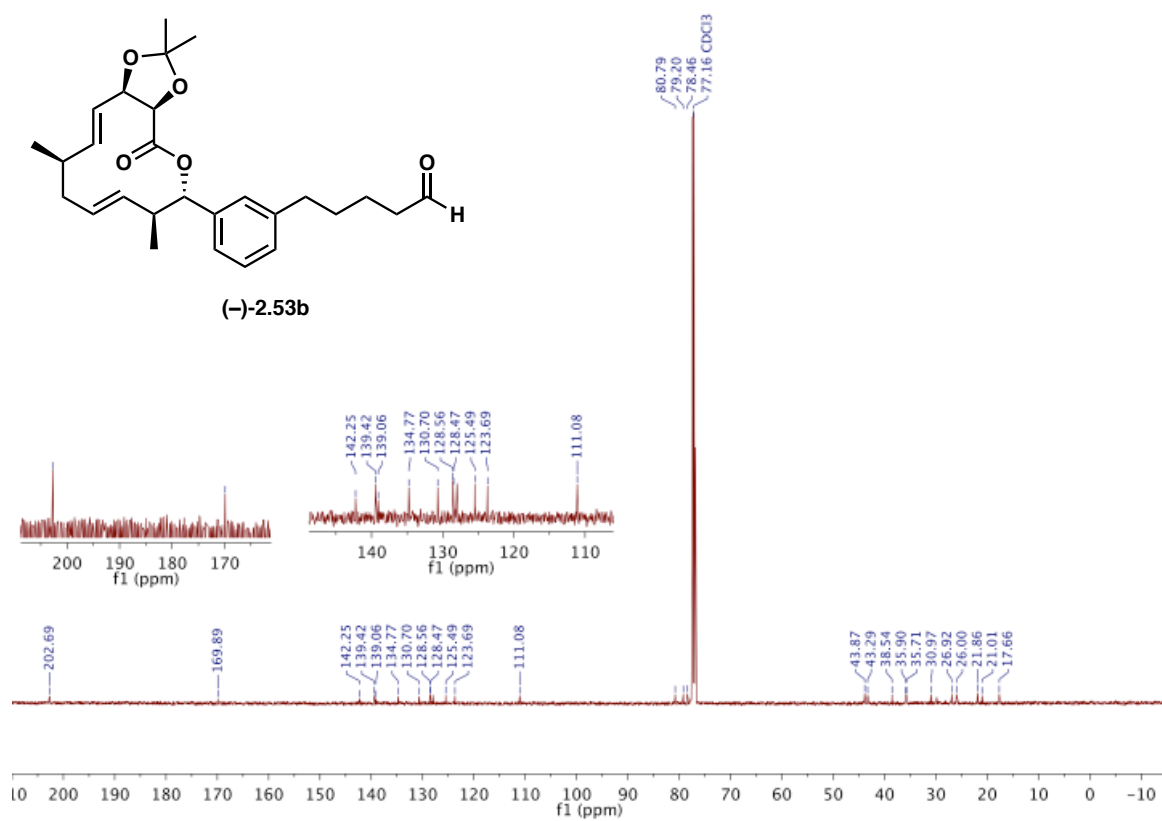
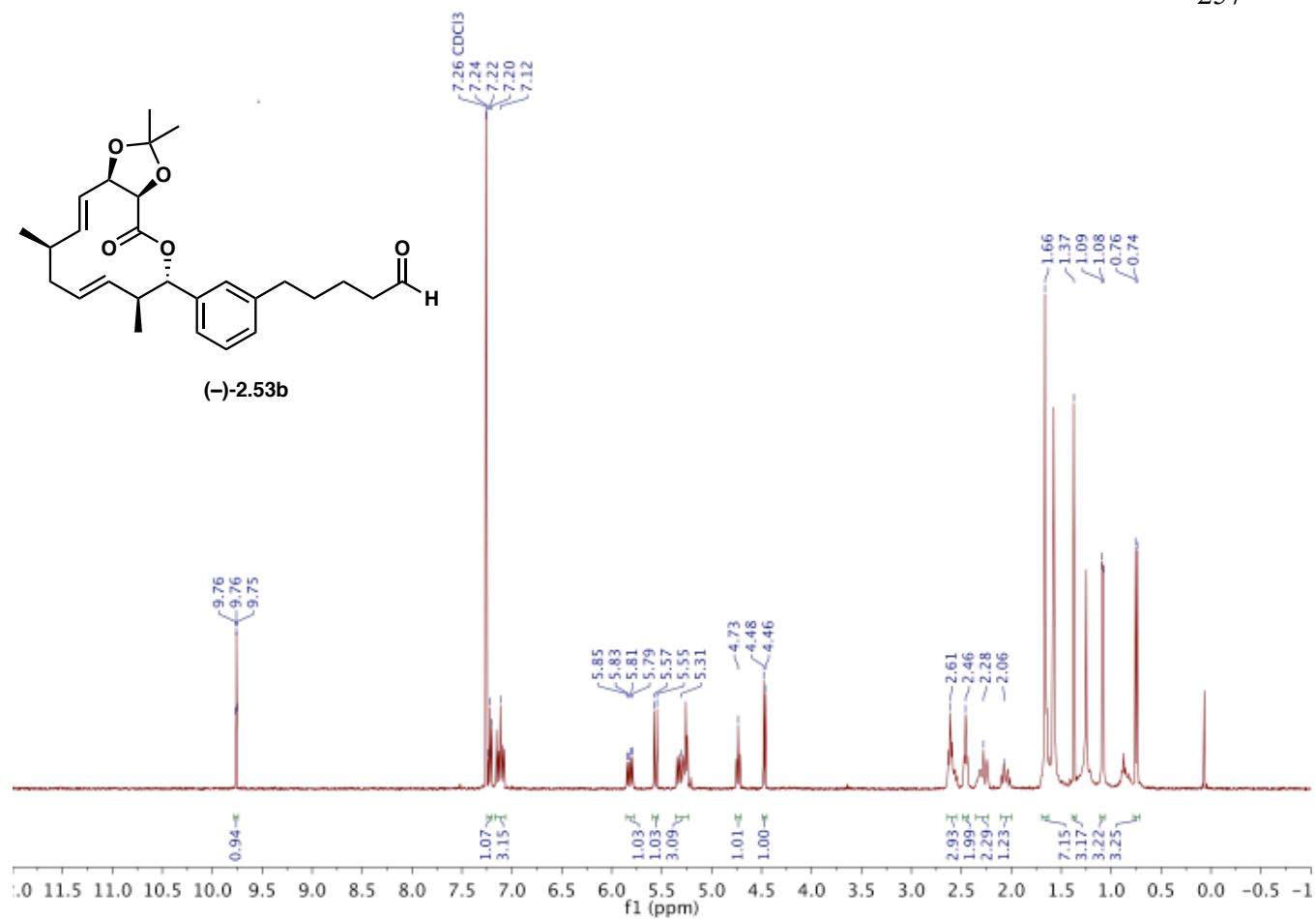


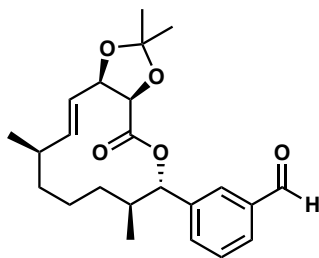
(-)-2.53a



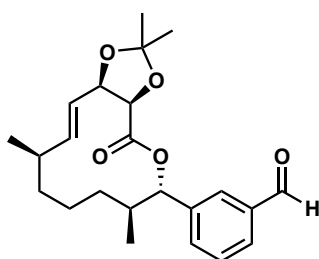
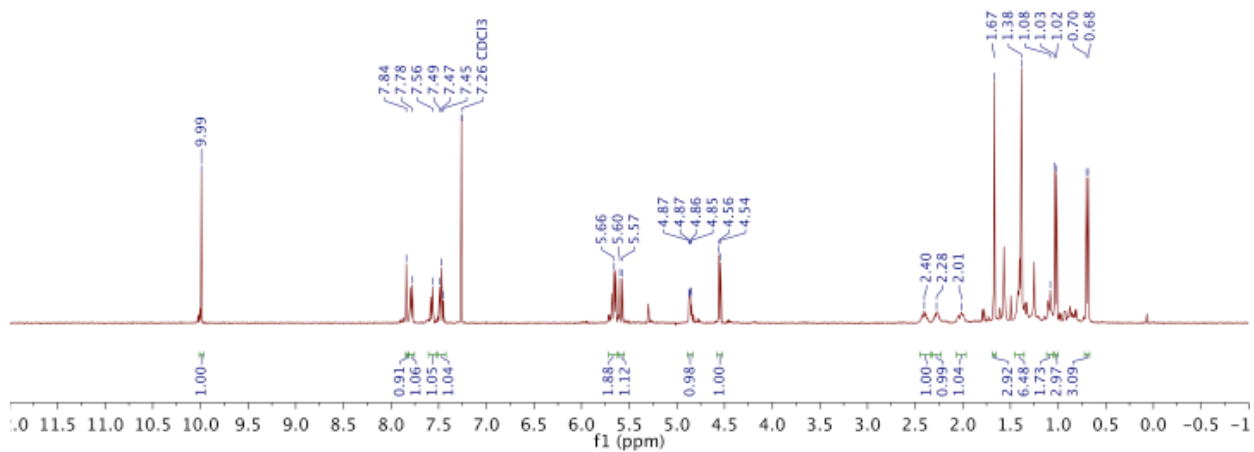
(-)-2.53a



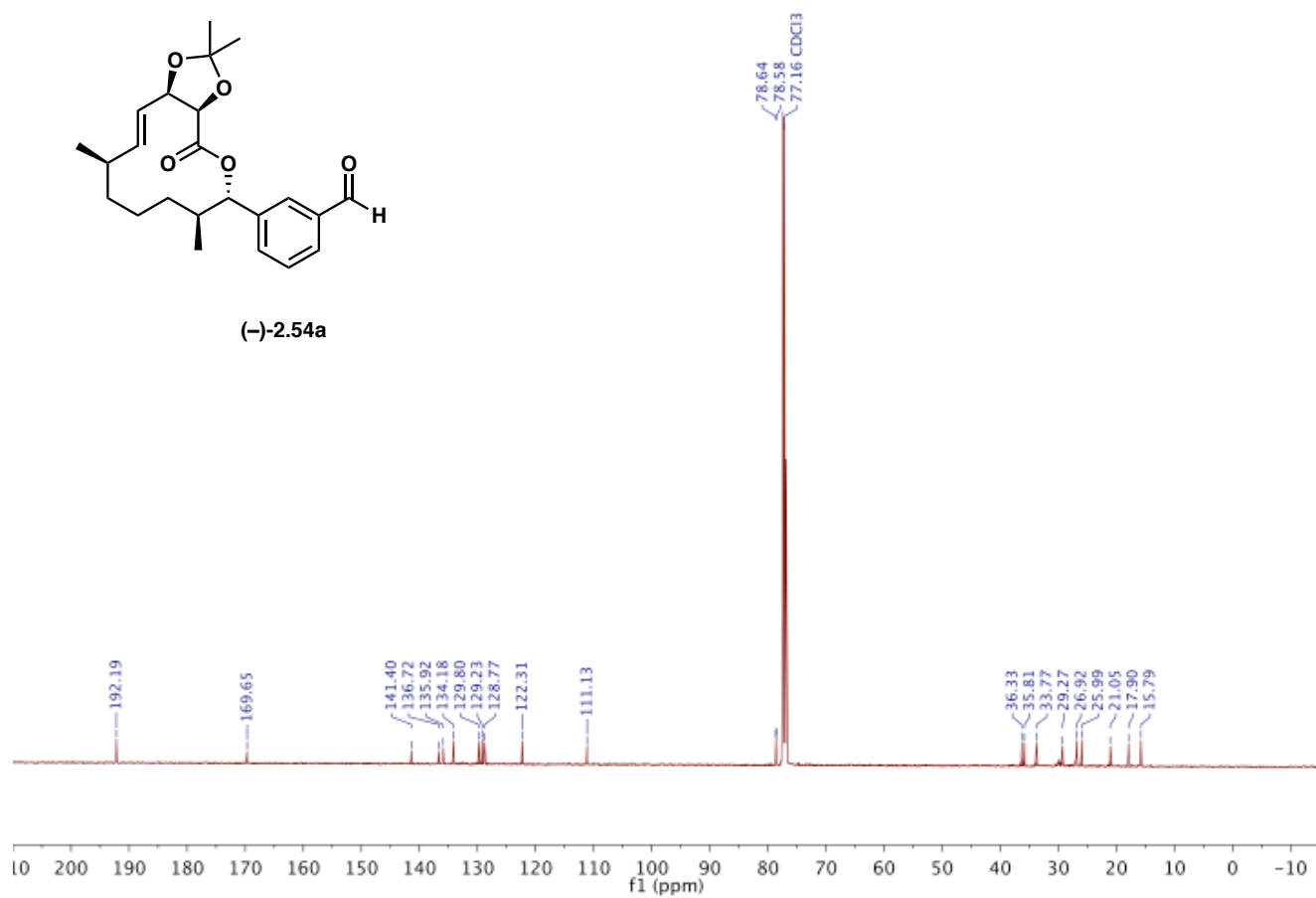


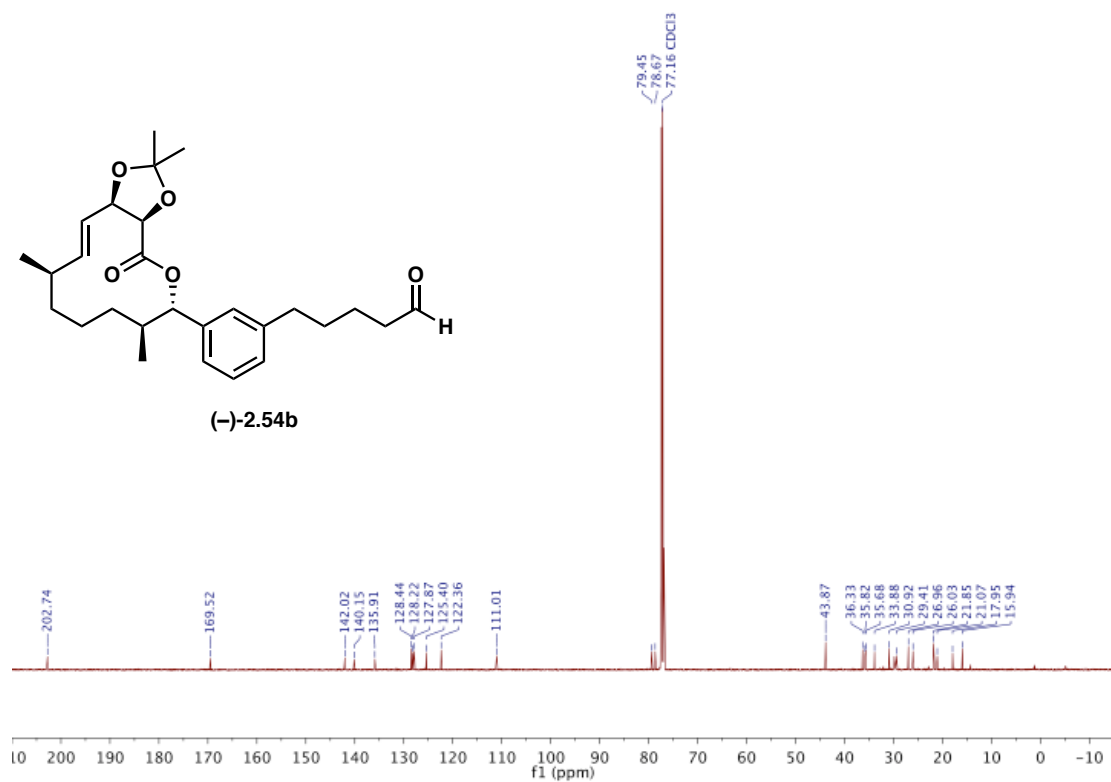
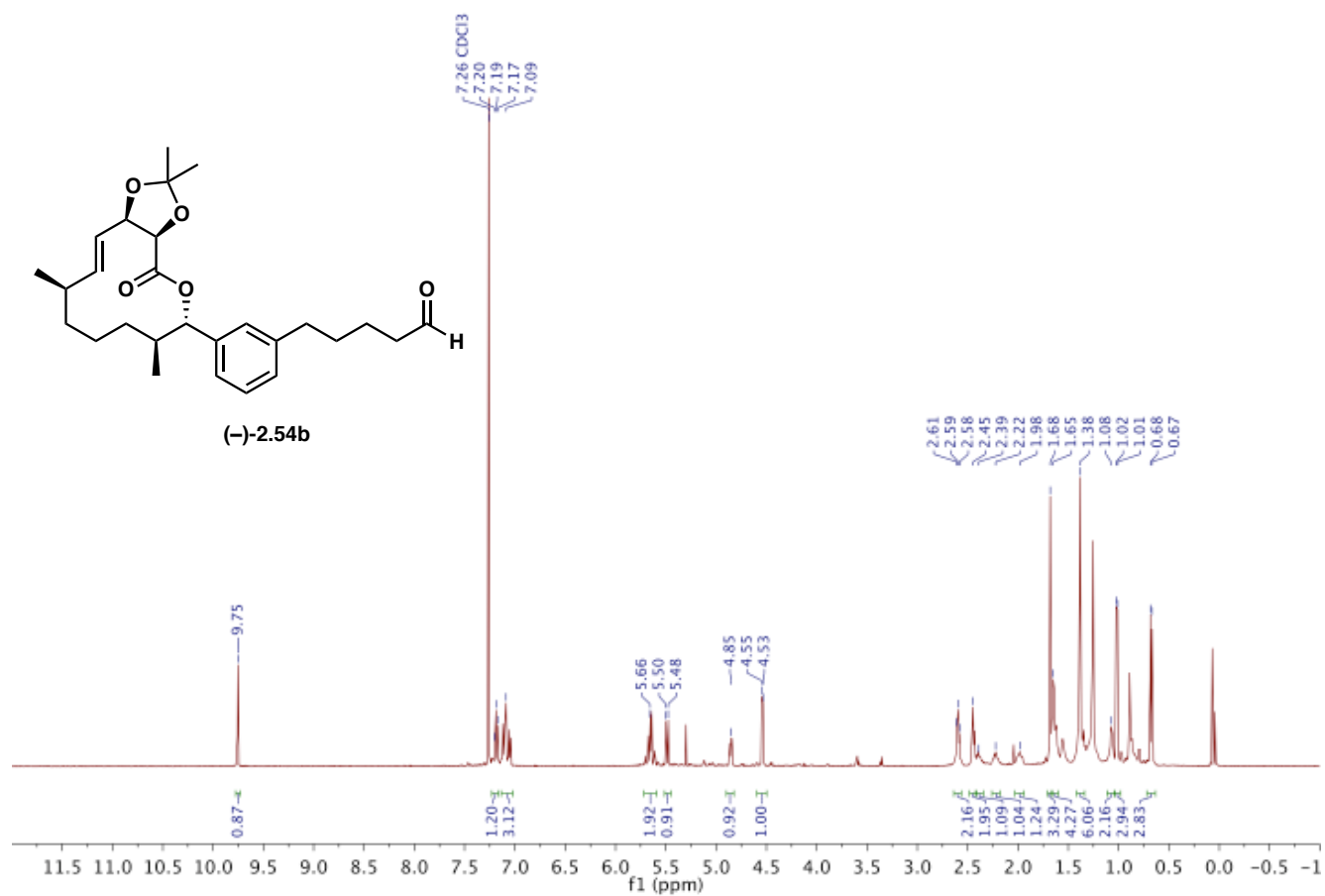


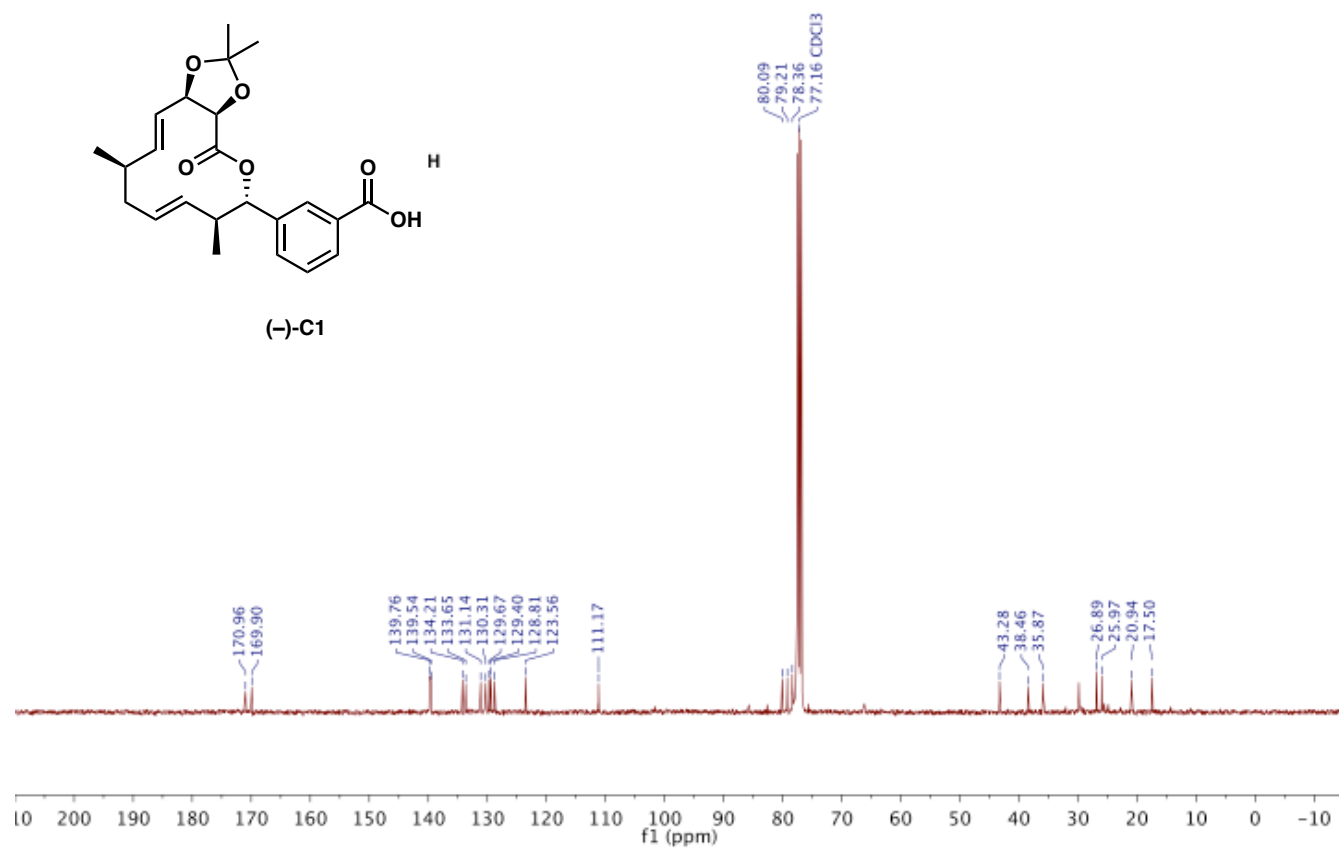
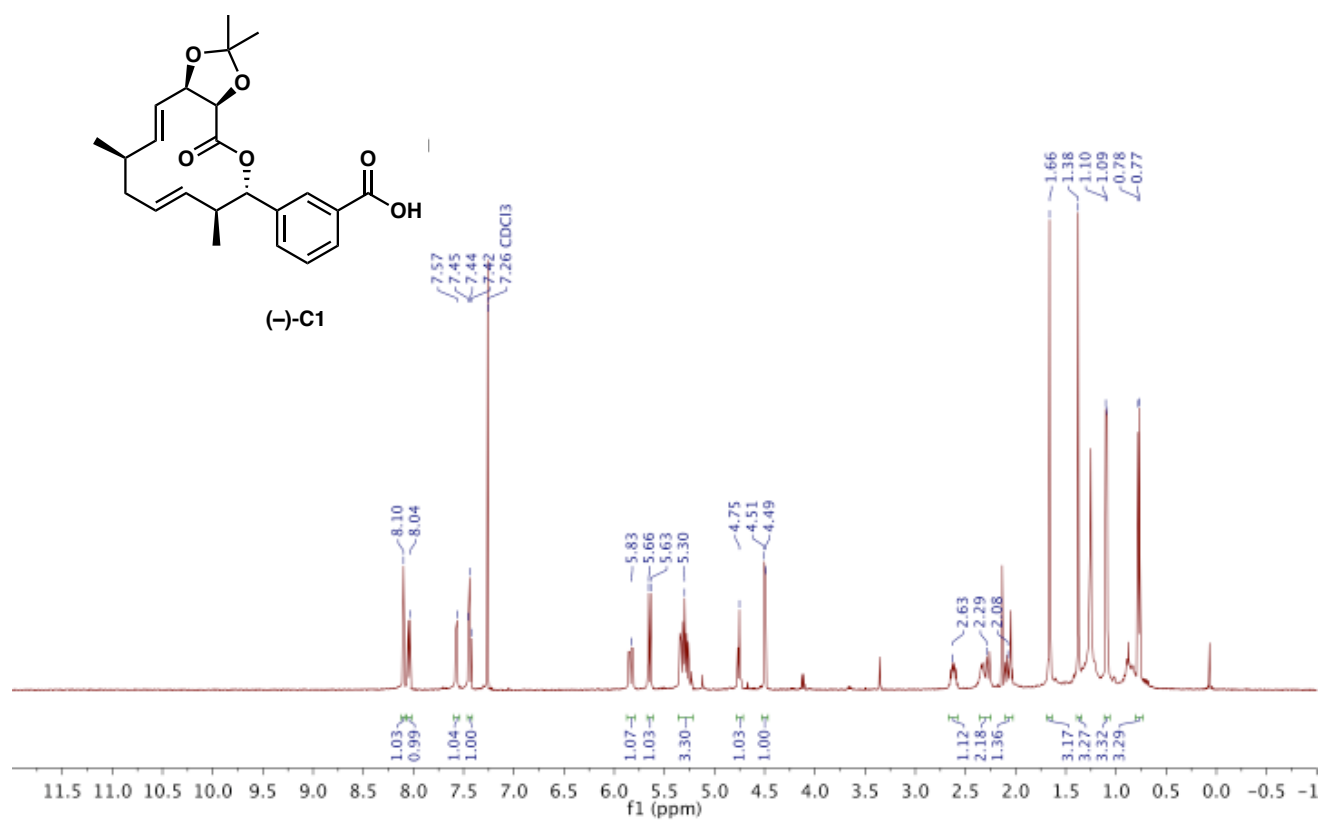
(-)-2.54a

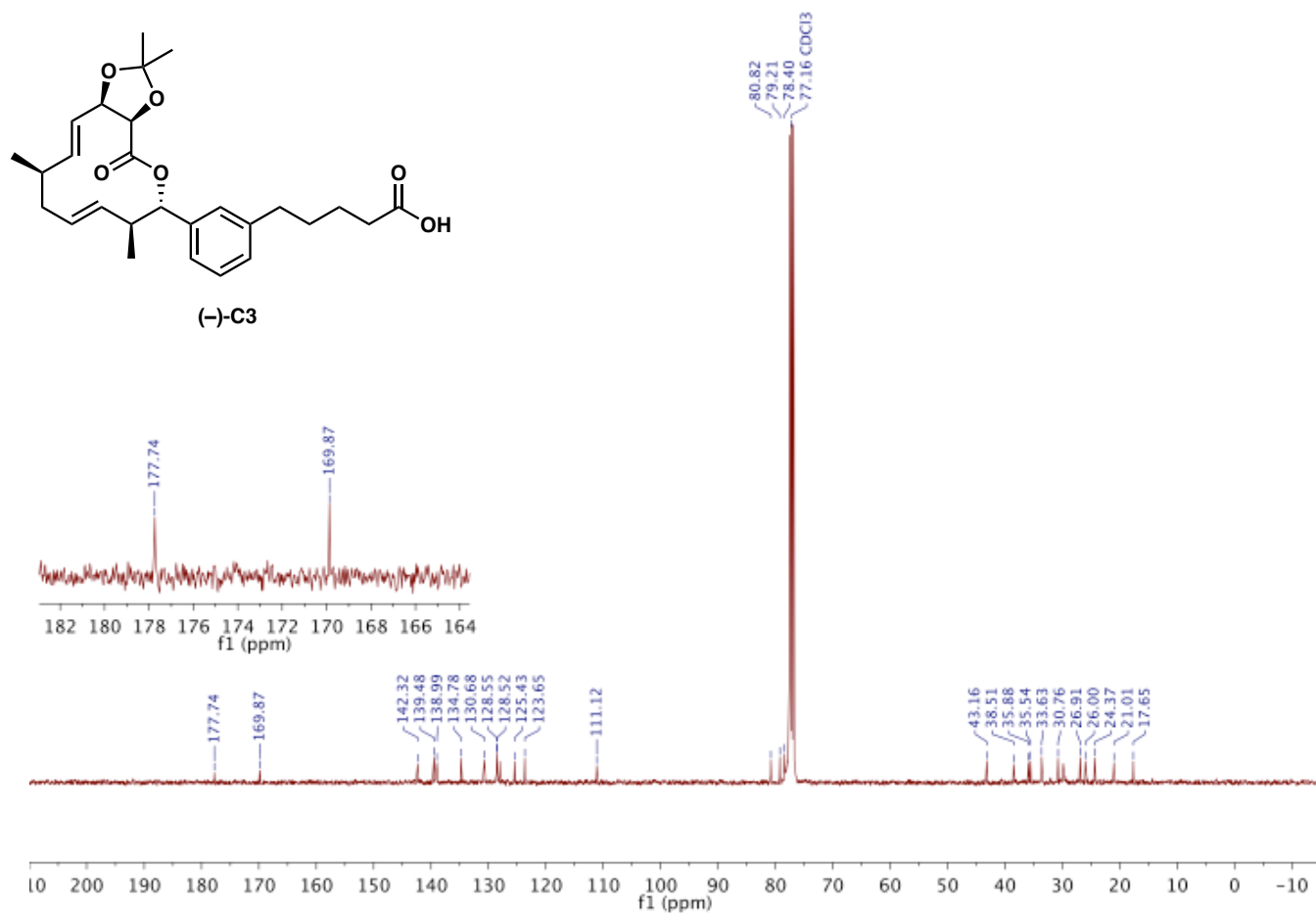
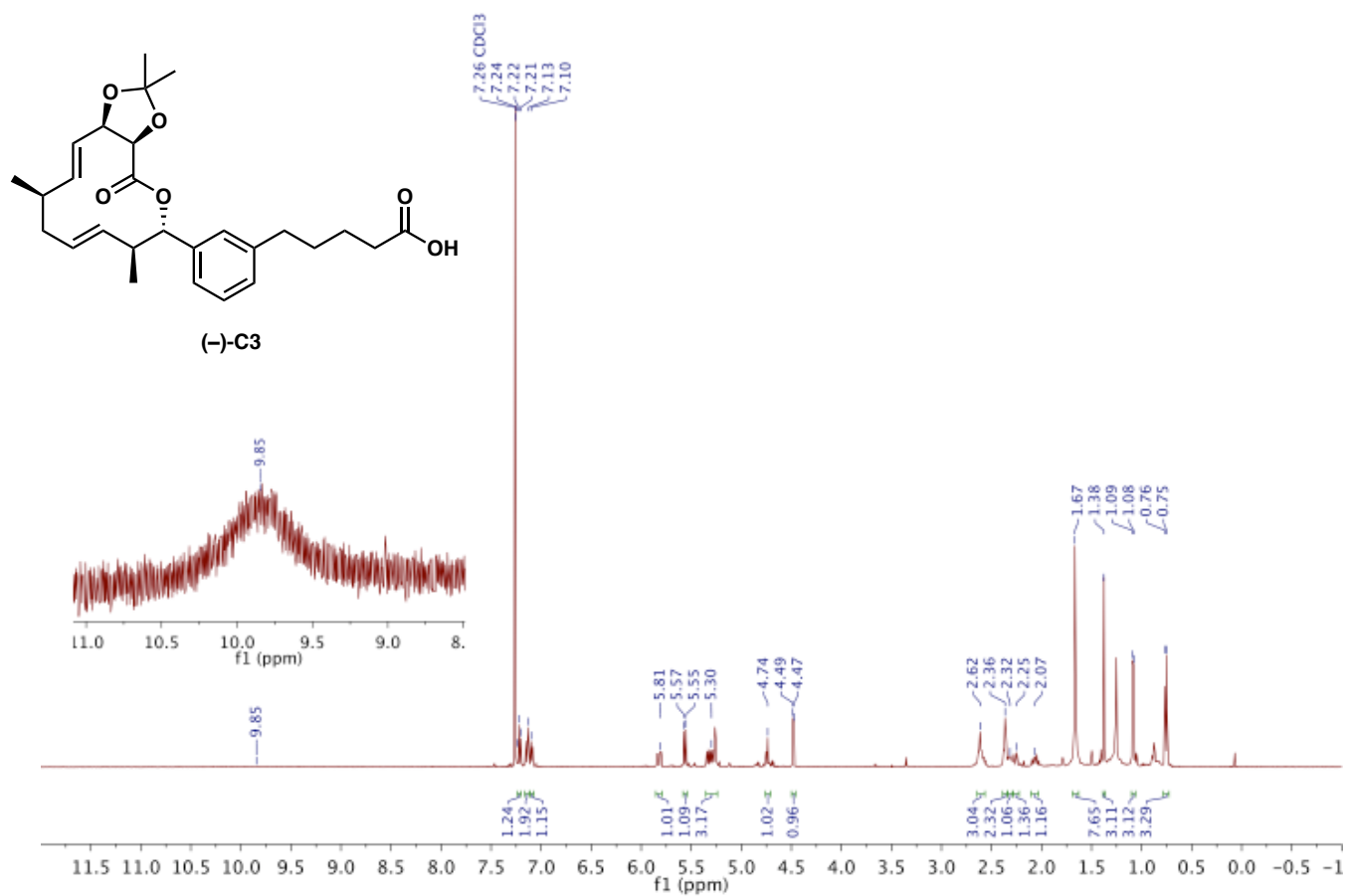


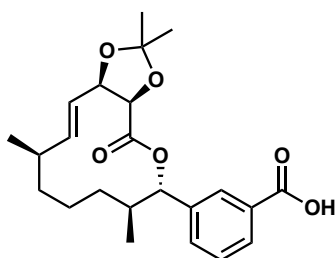
(-)-2.54a



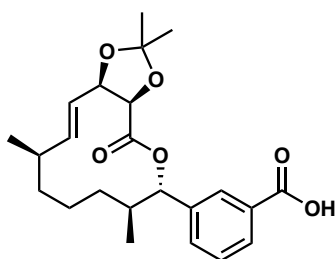
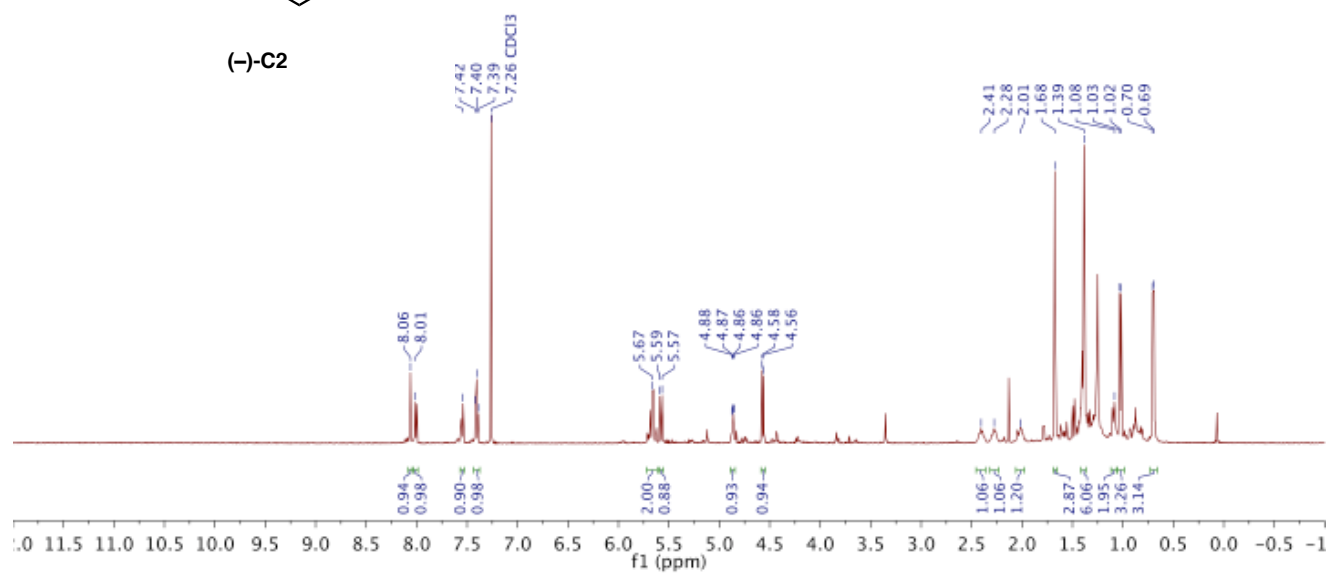




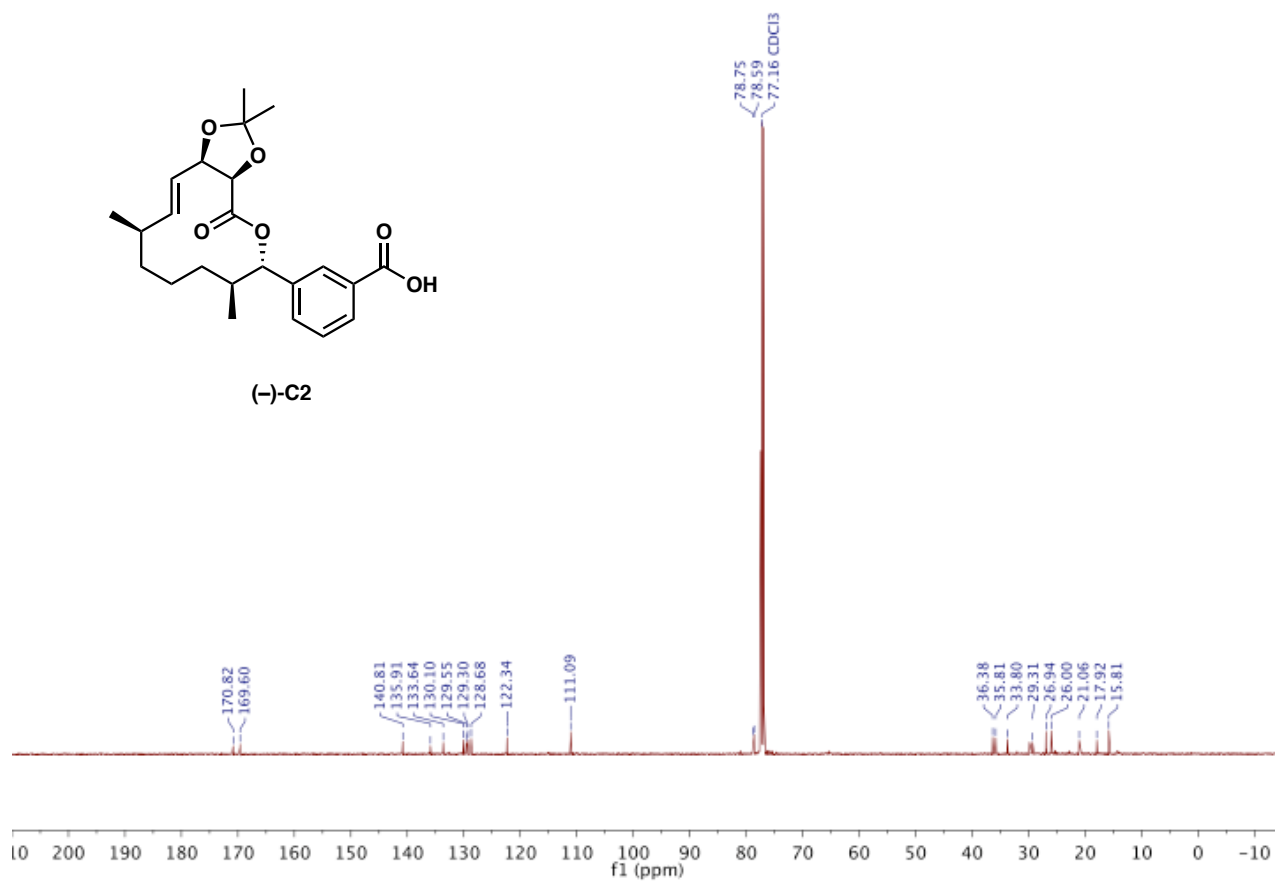


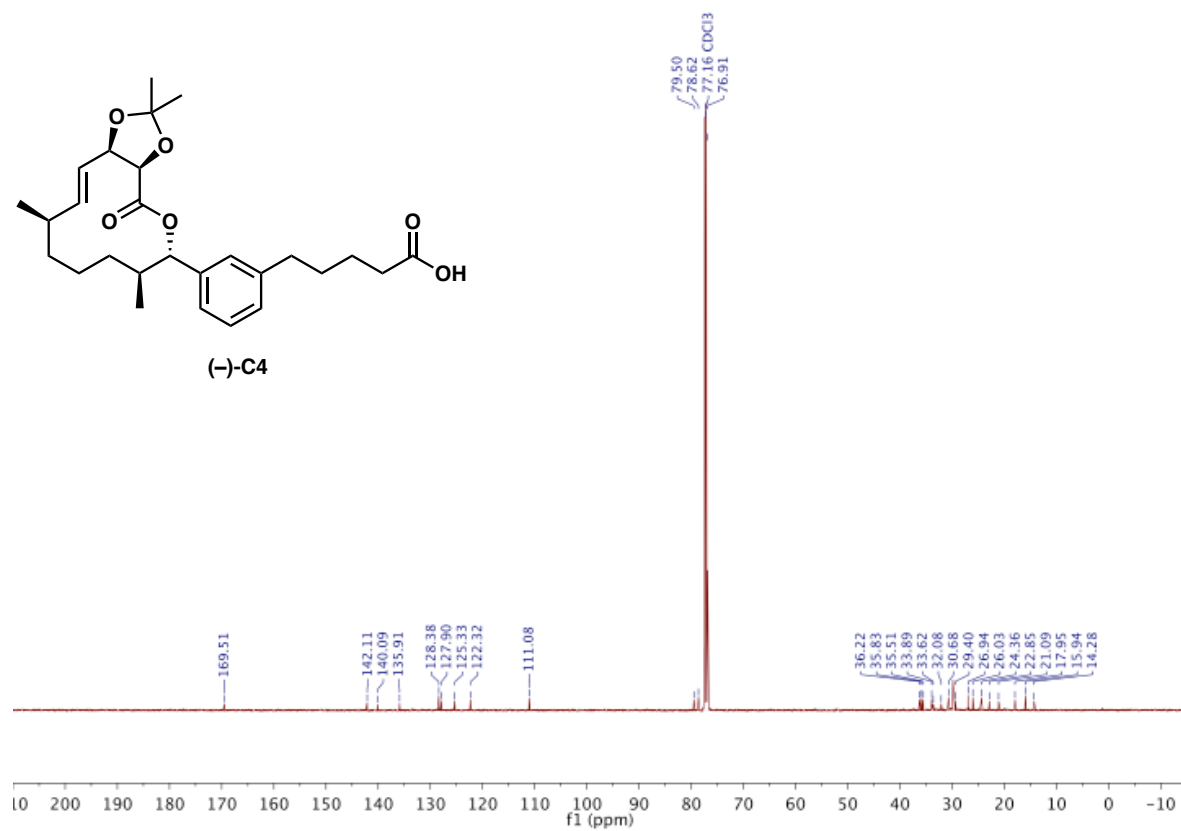
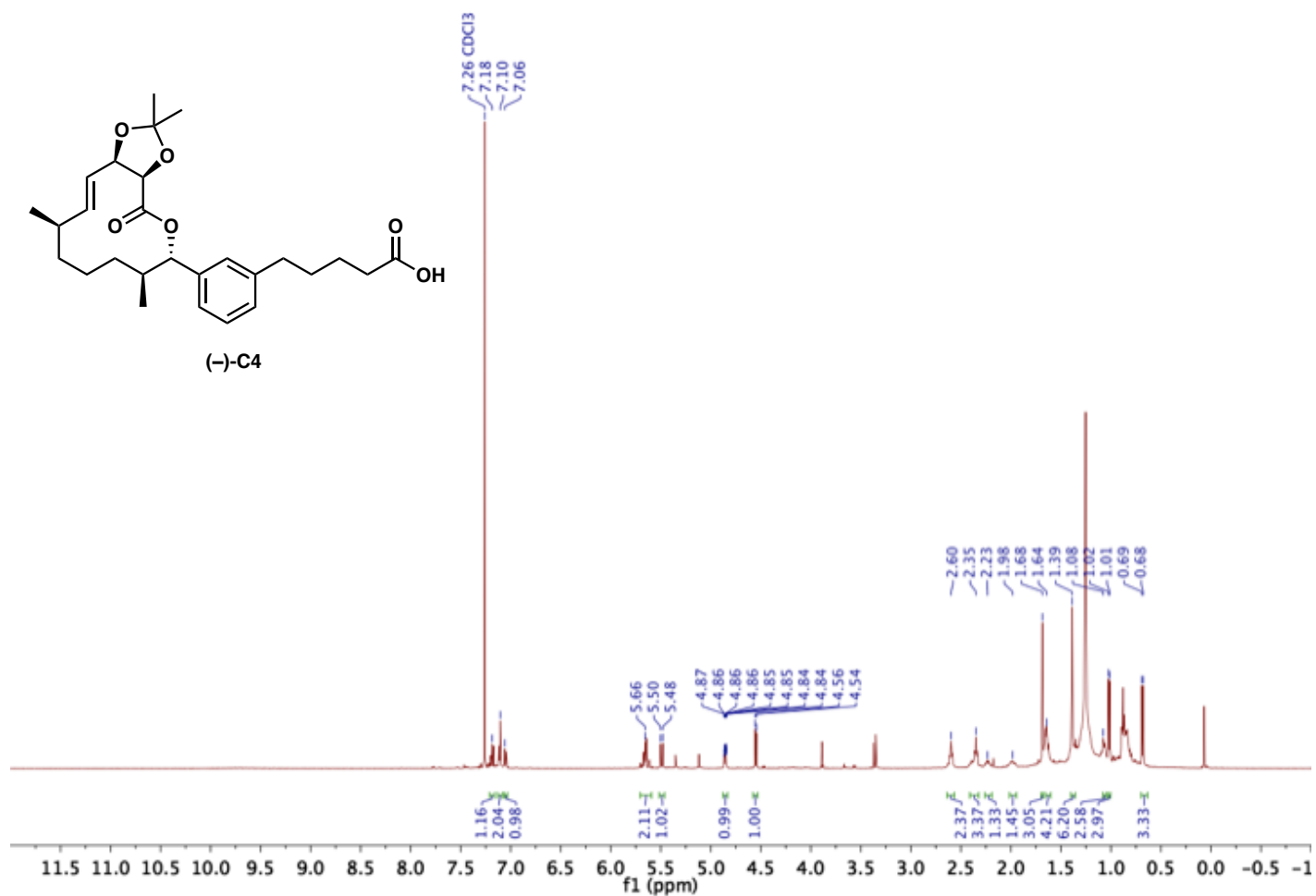


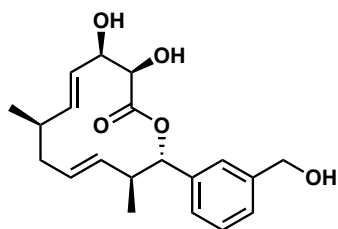
(-)-C2



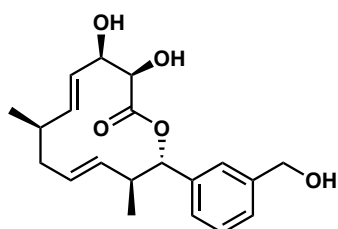
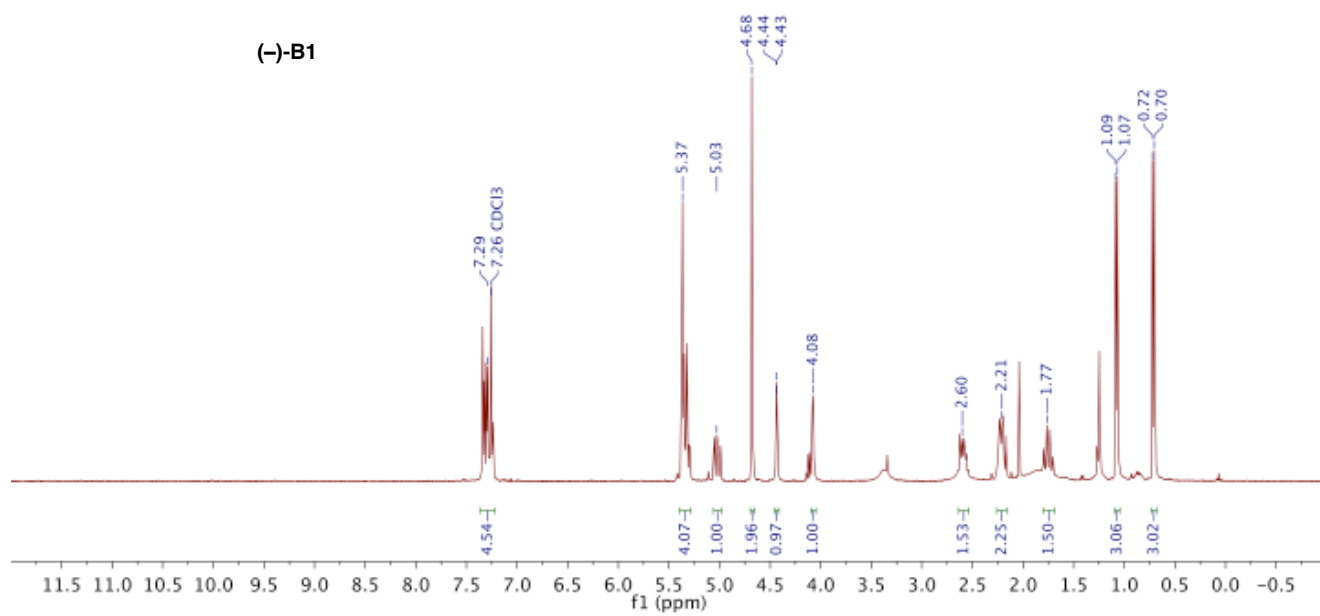
(-)-C2



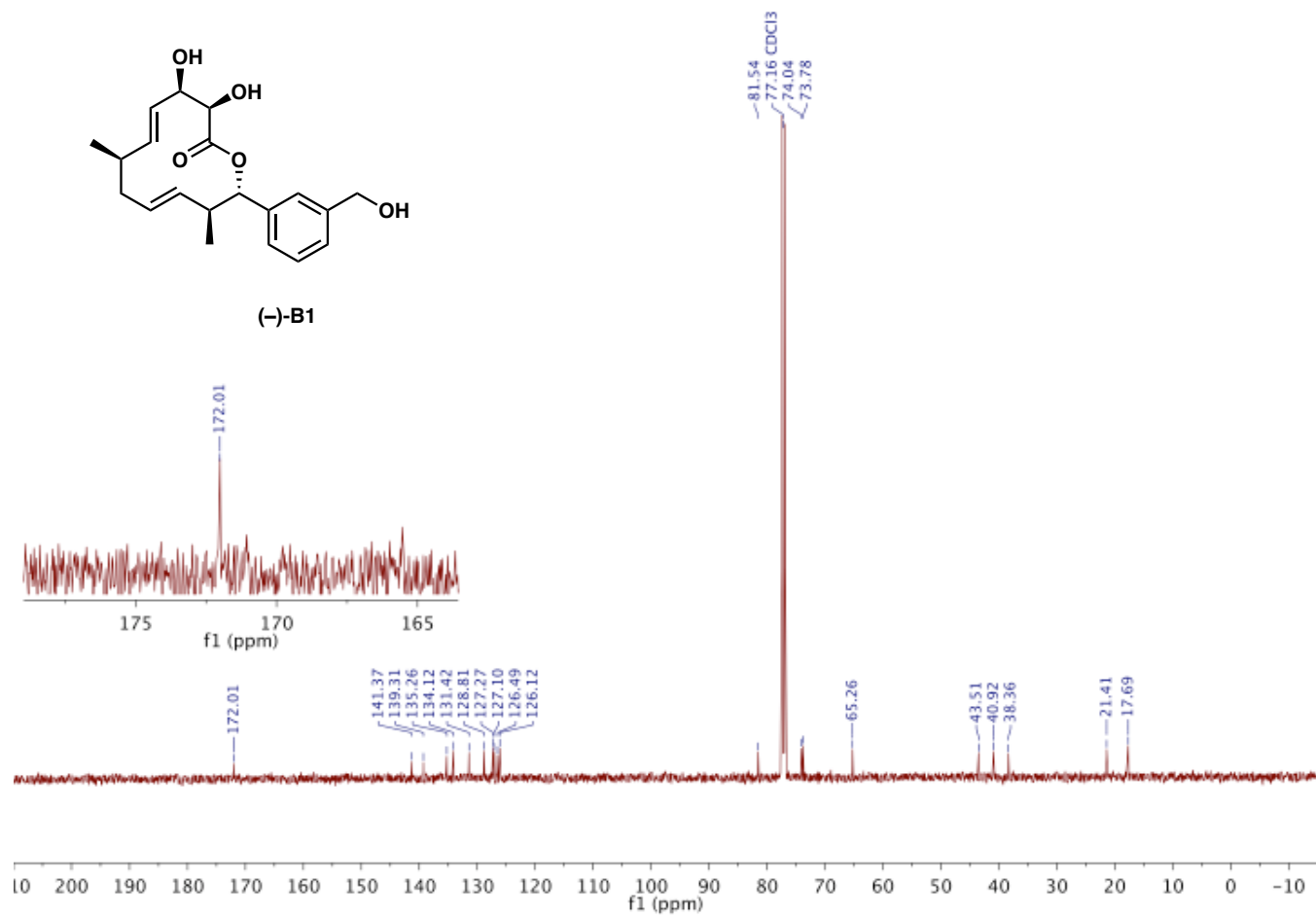


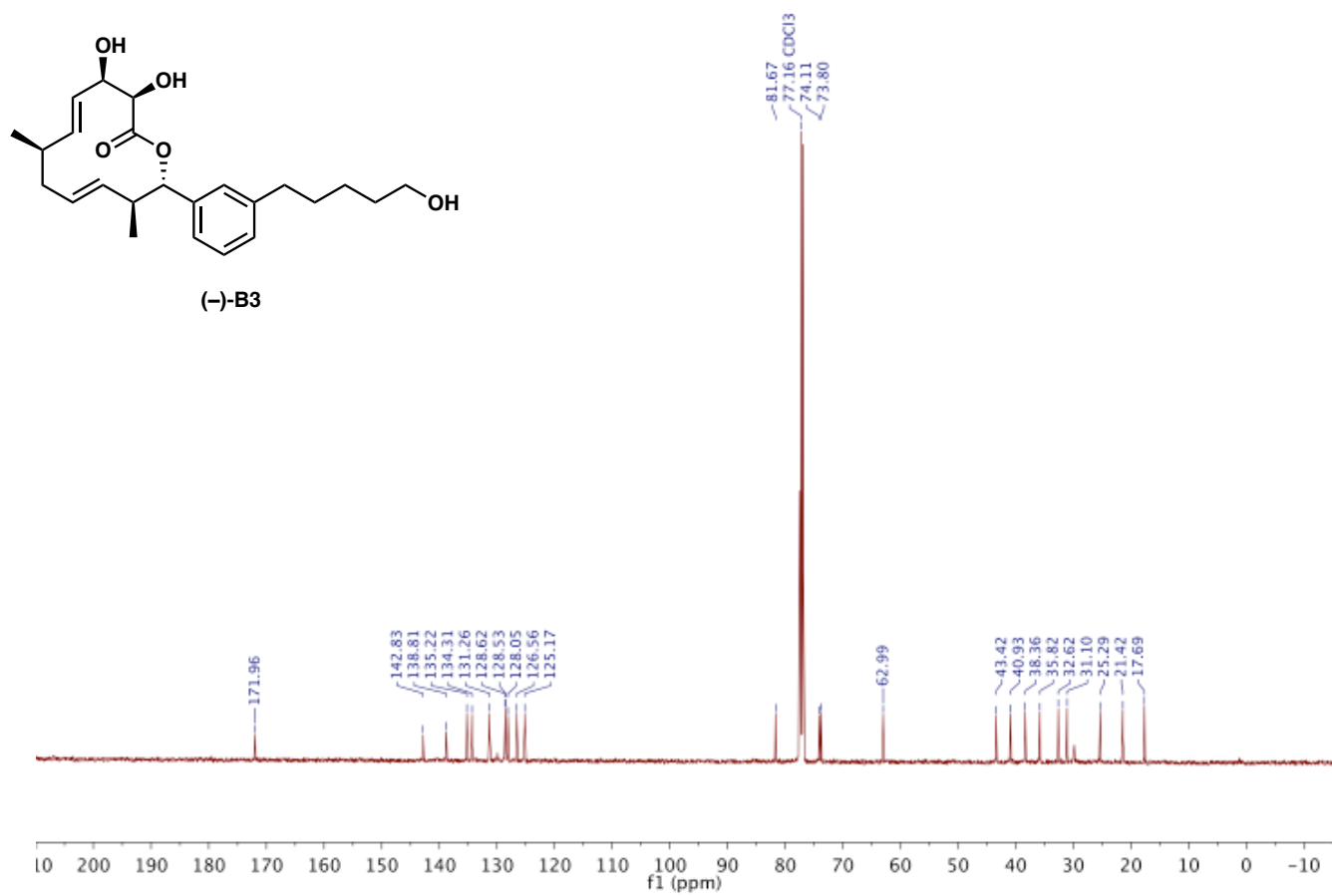
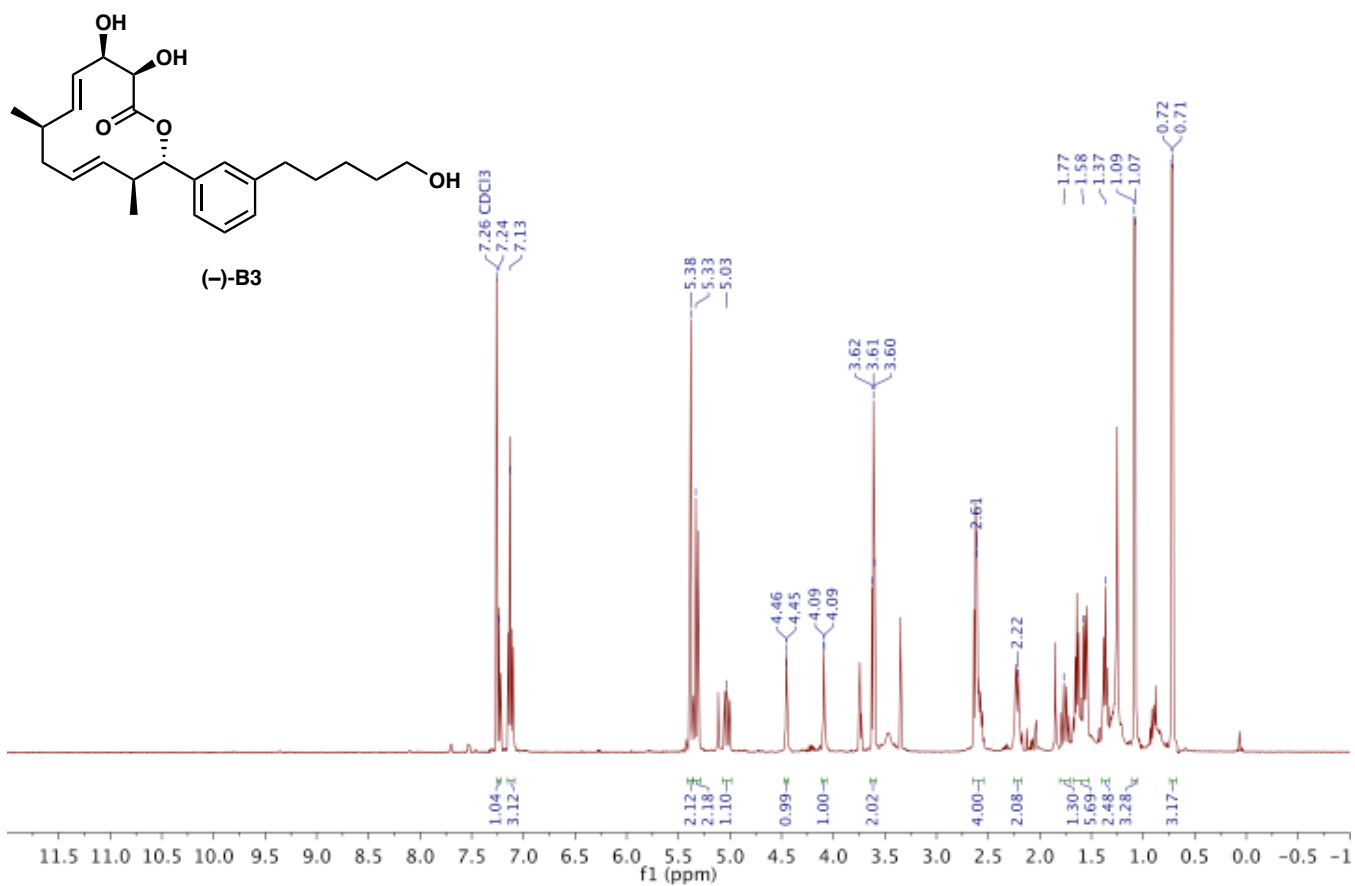


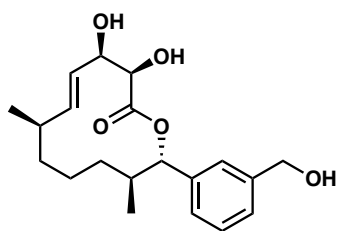
(-)-B1



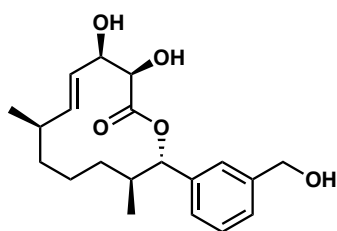
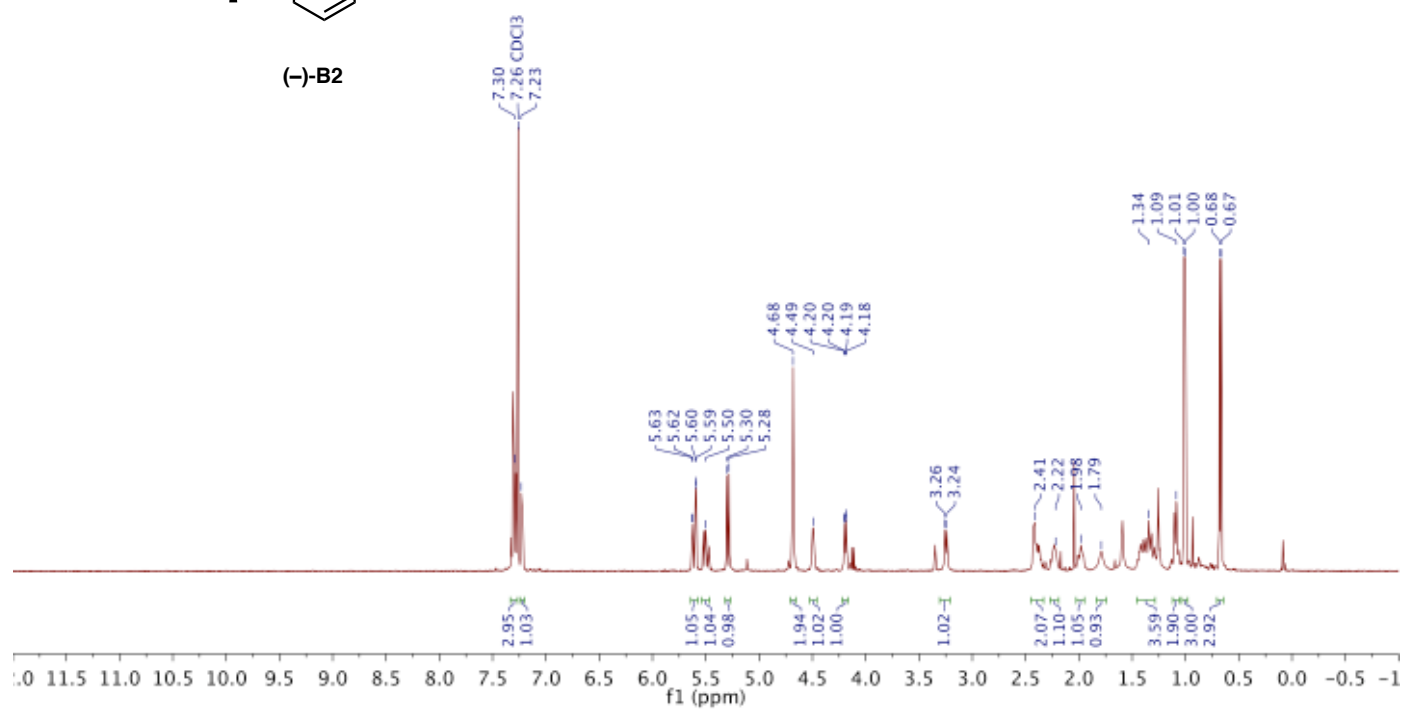
(-)-B1



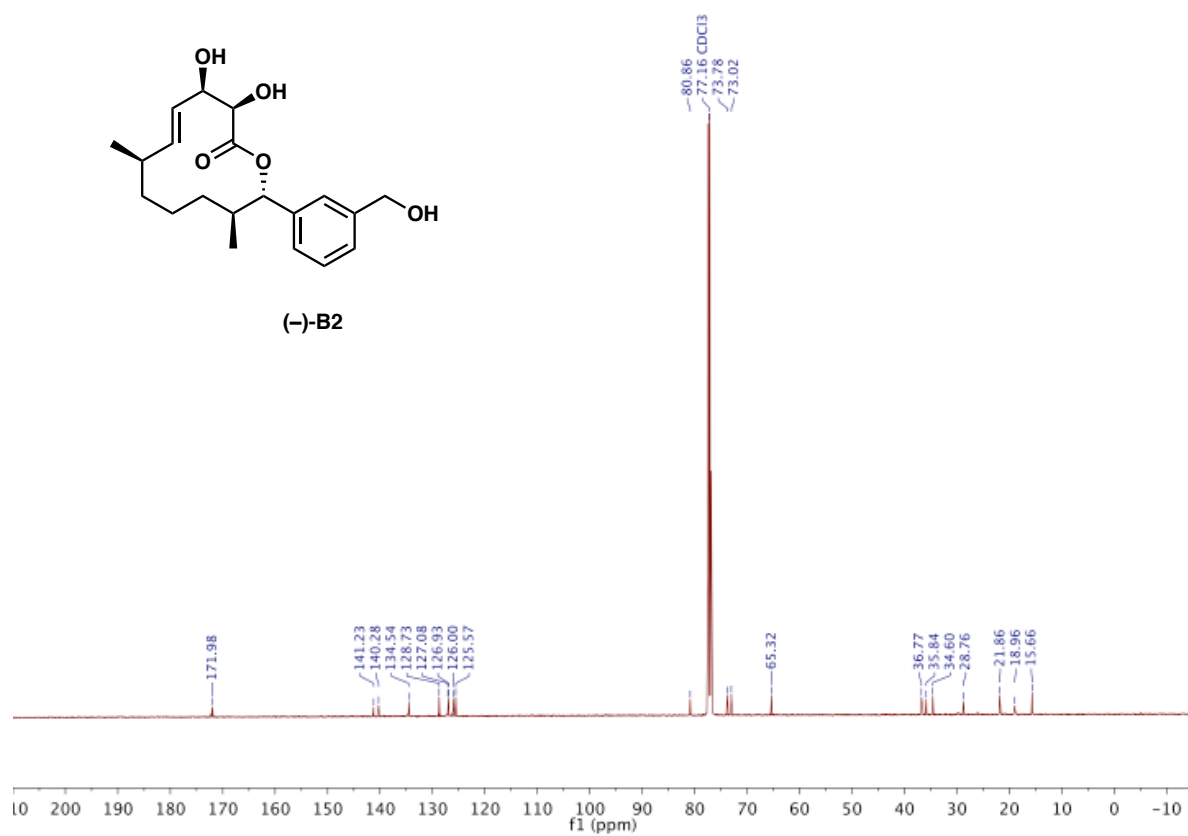


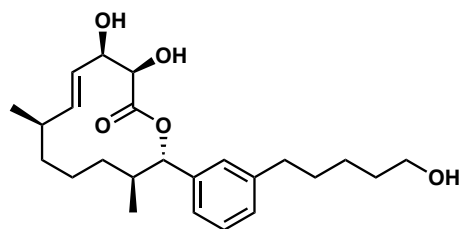


(-)-B2

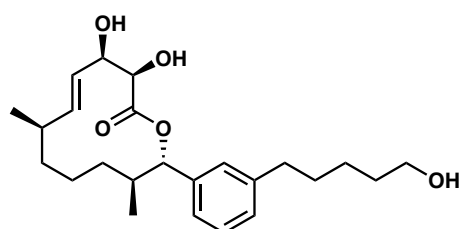
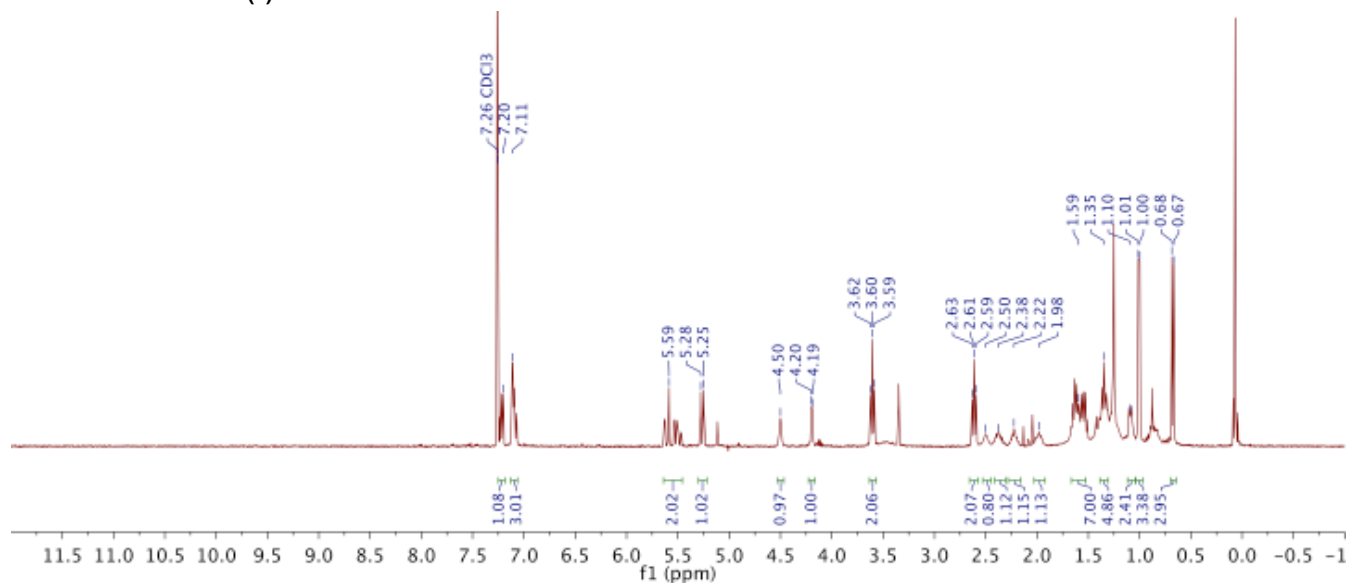


(-)-B2

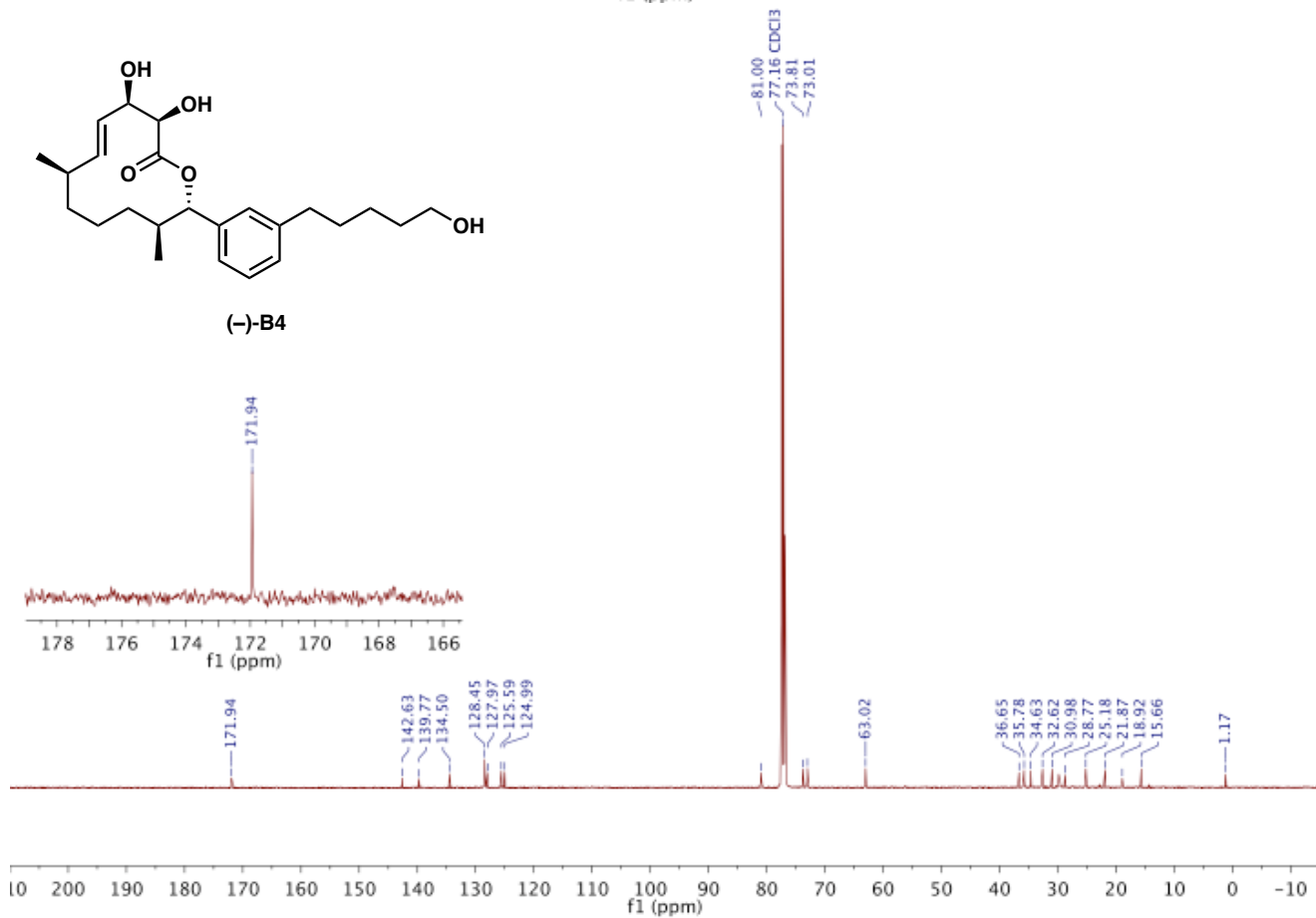


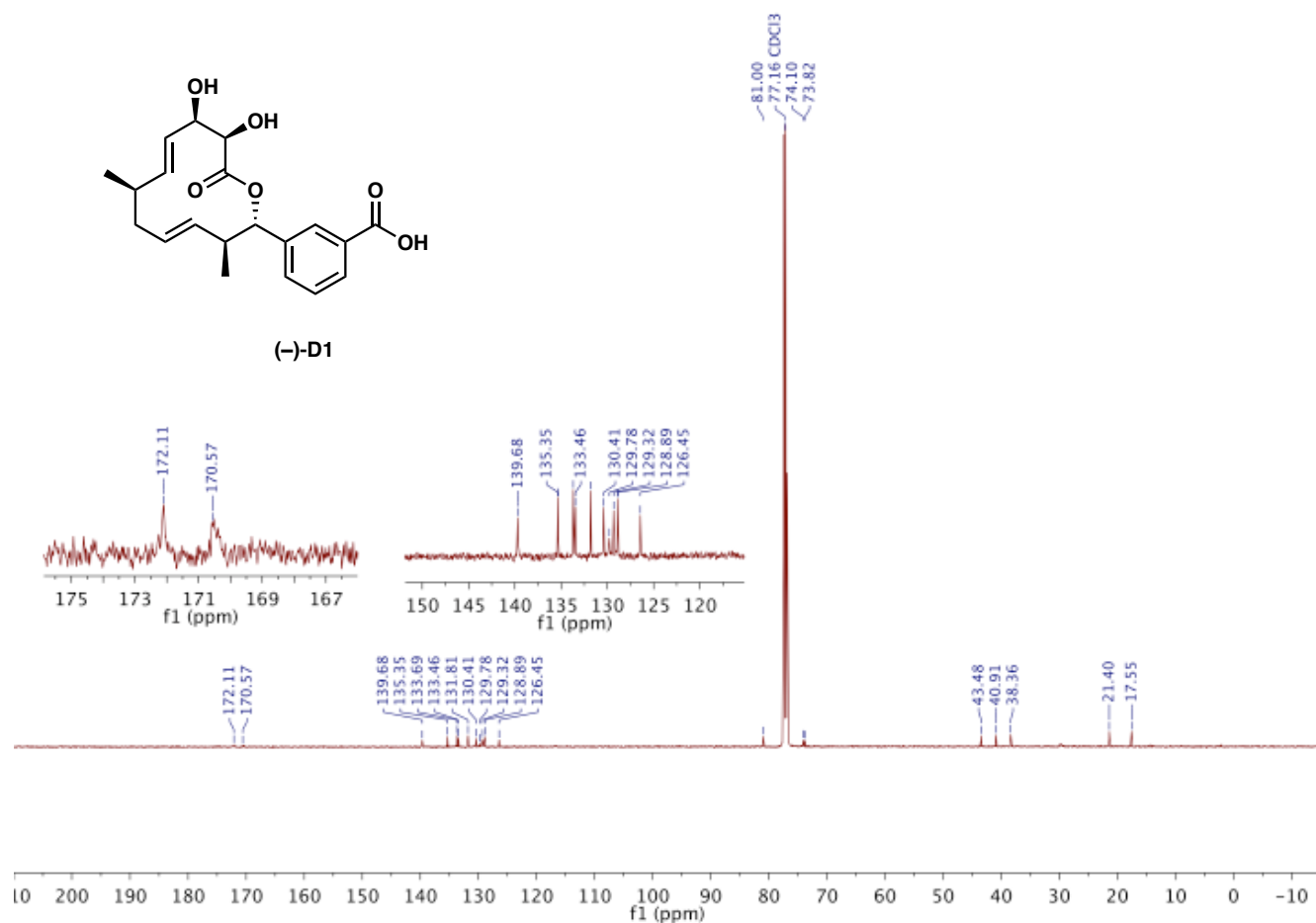
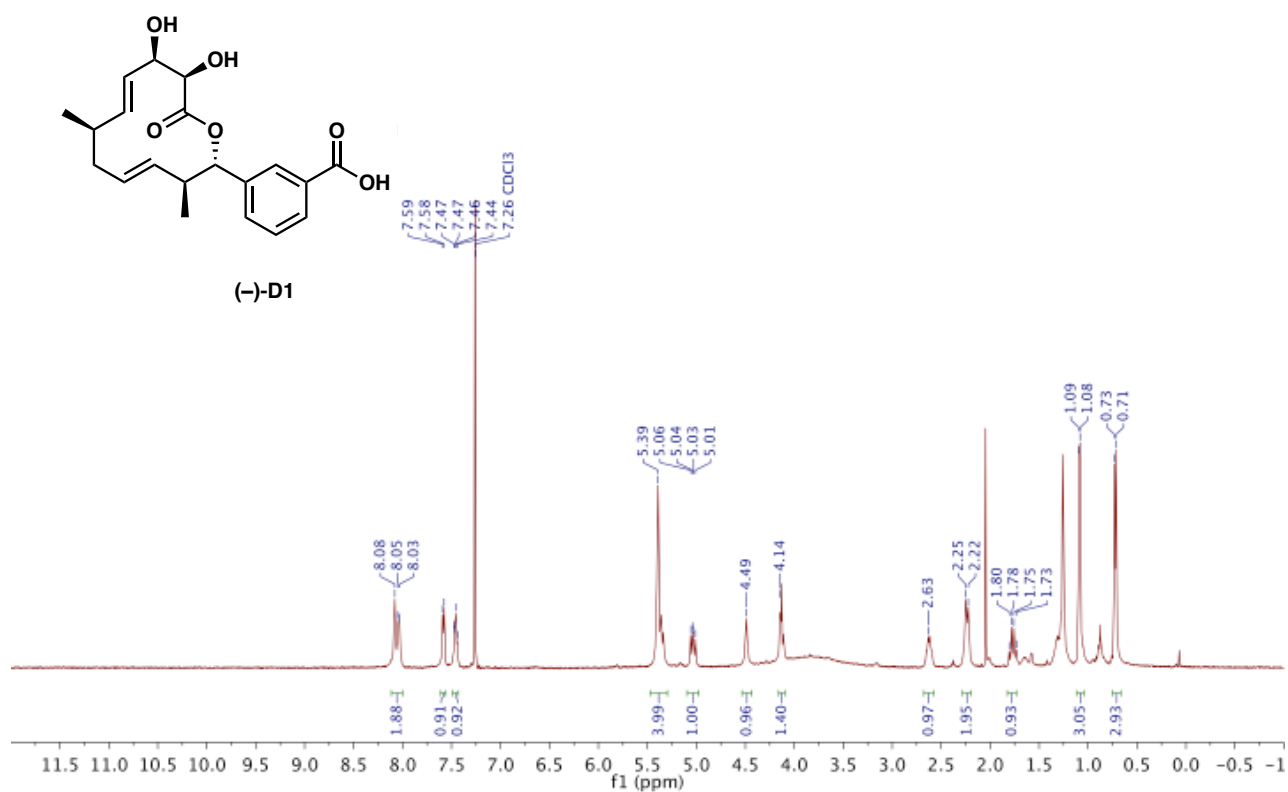


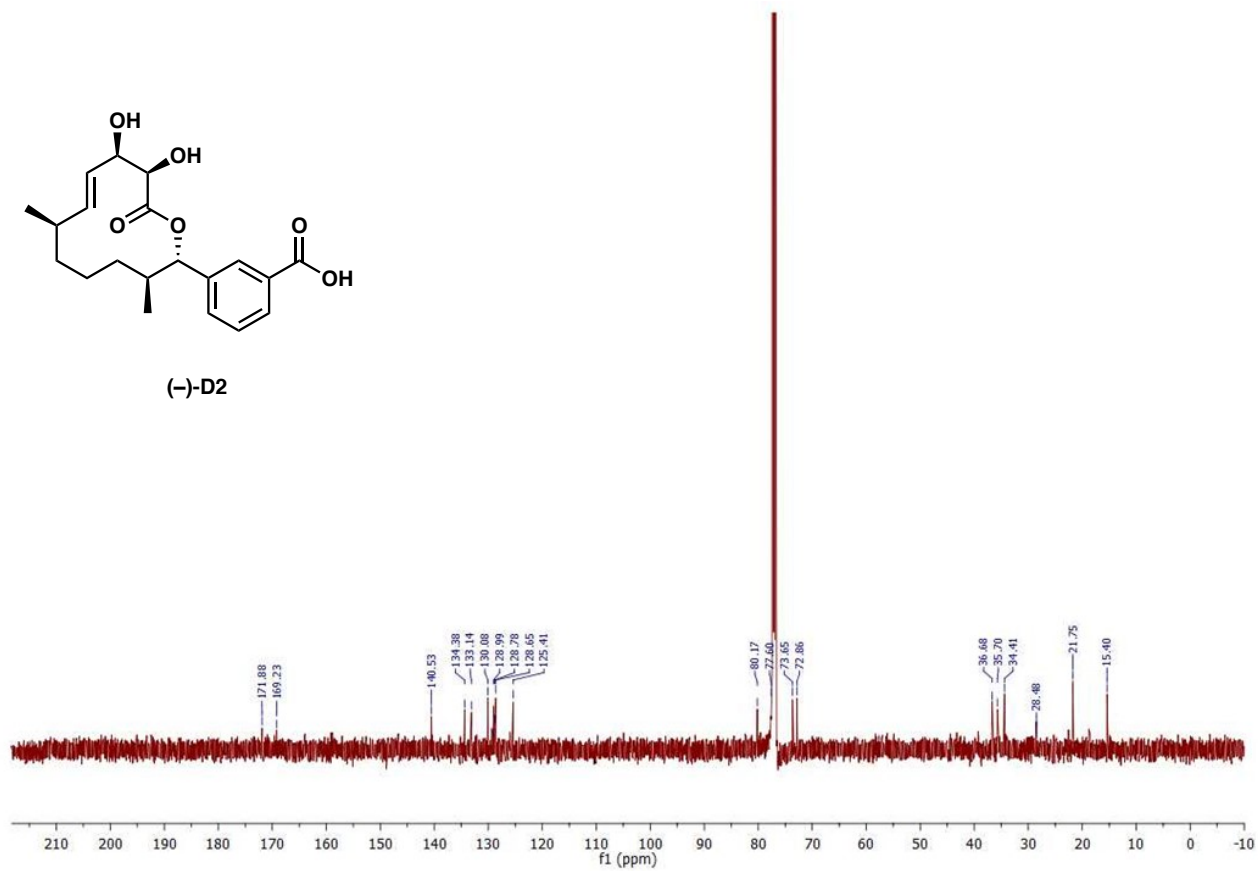
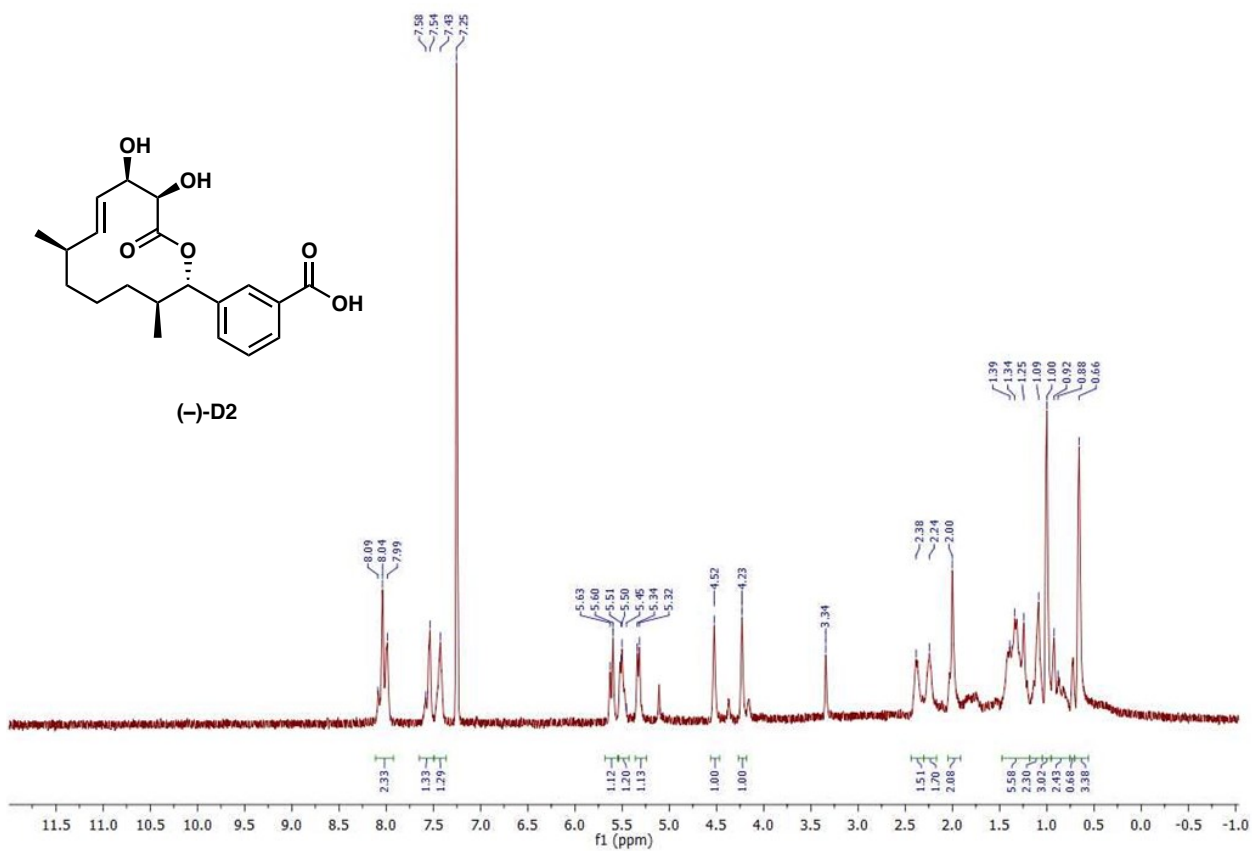
(-)-B4

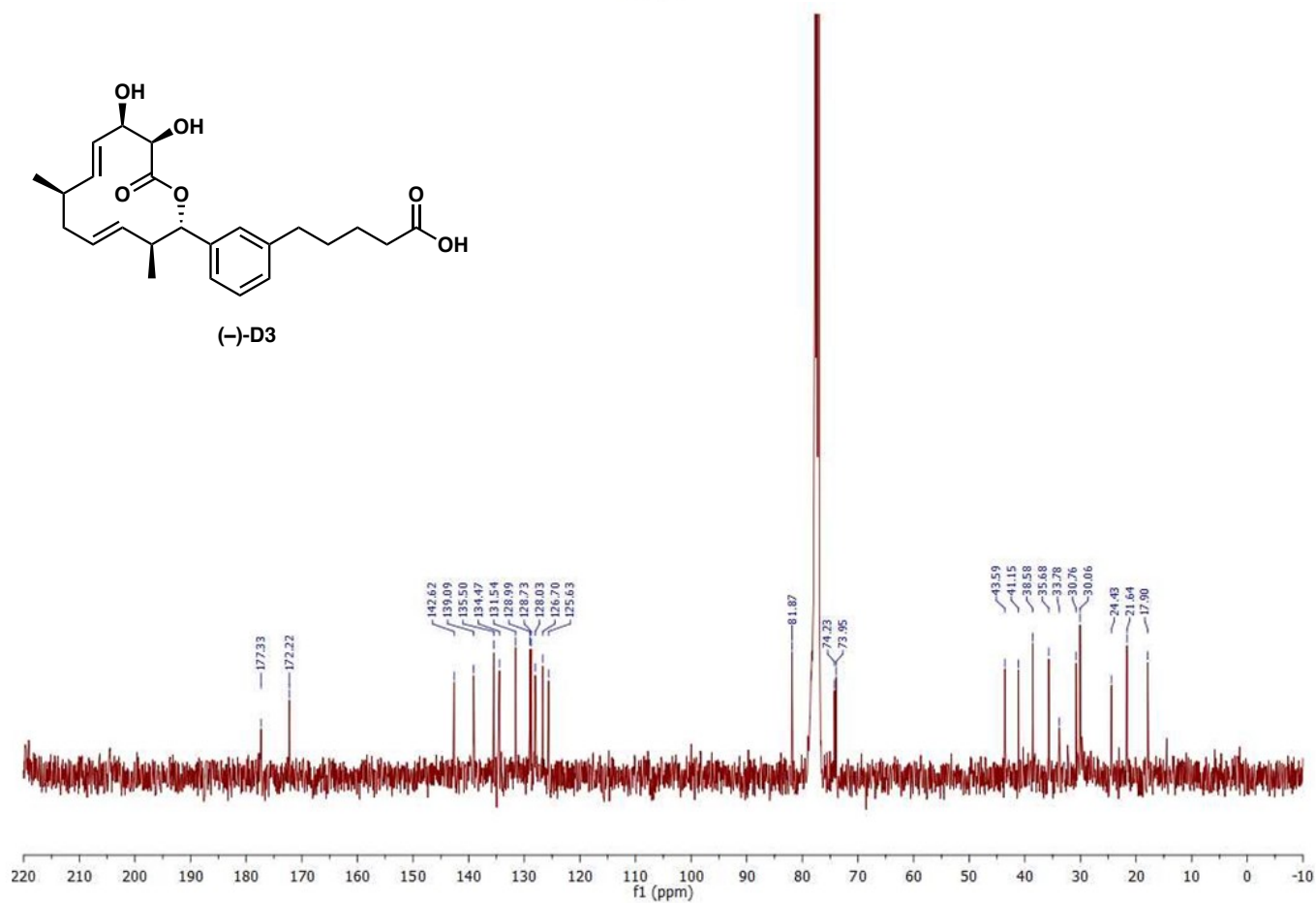
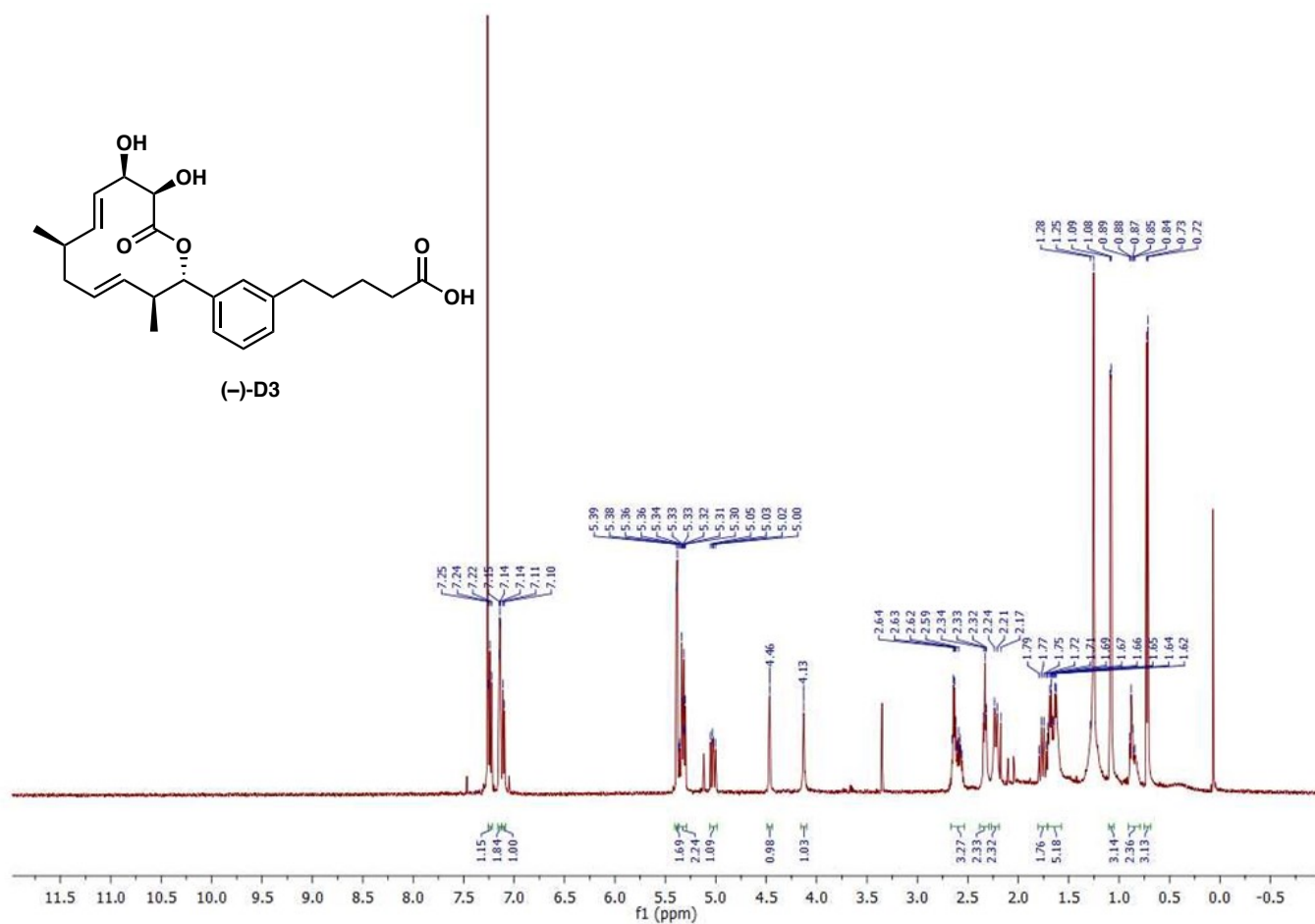


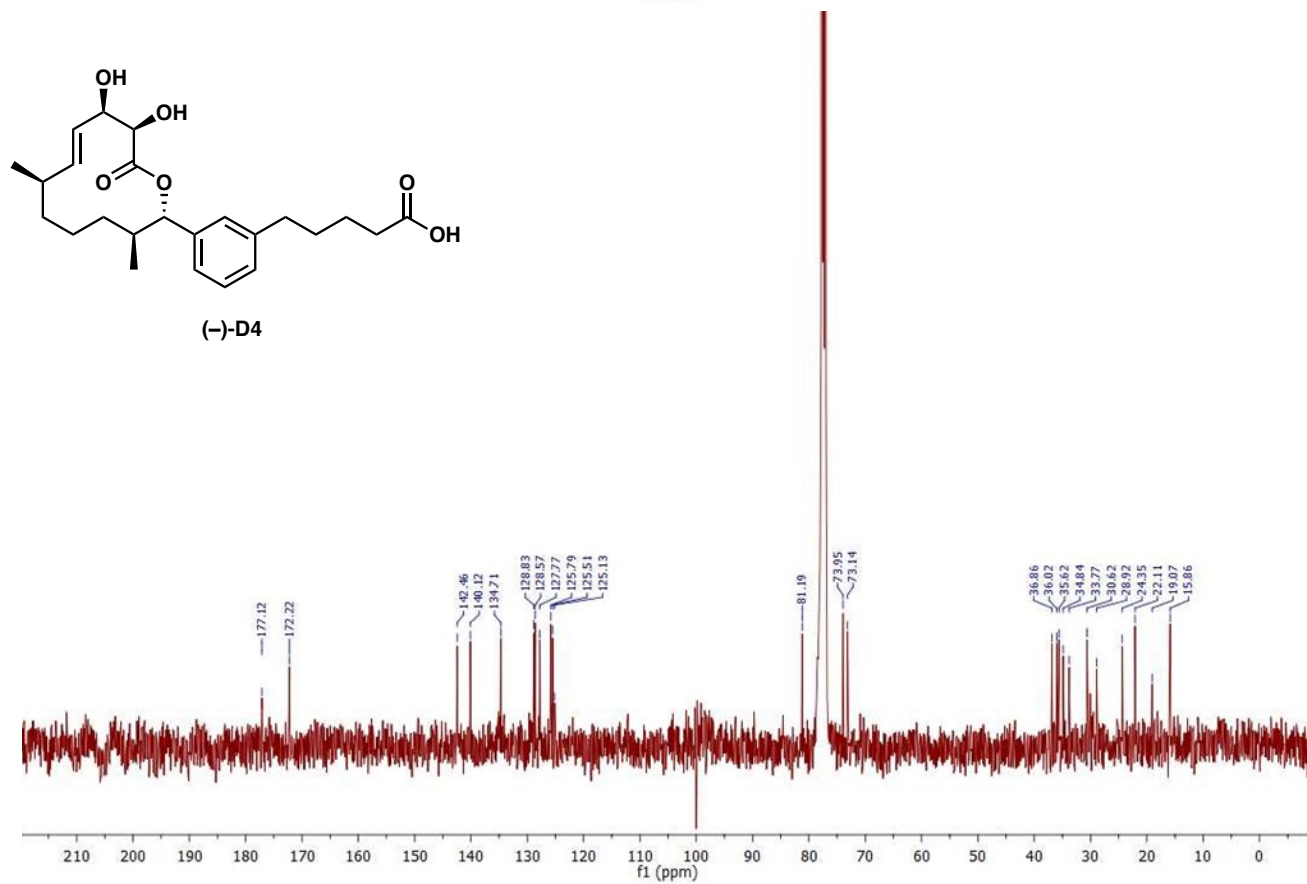
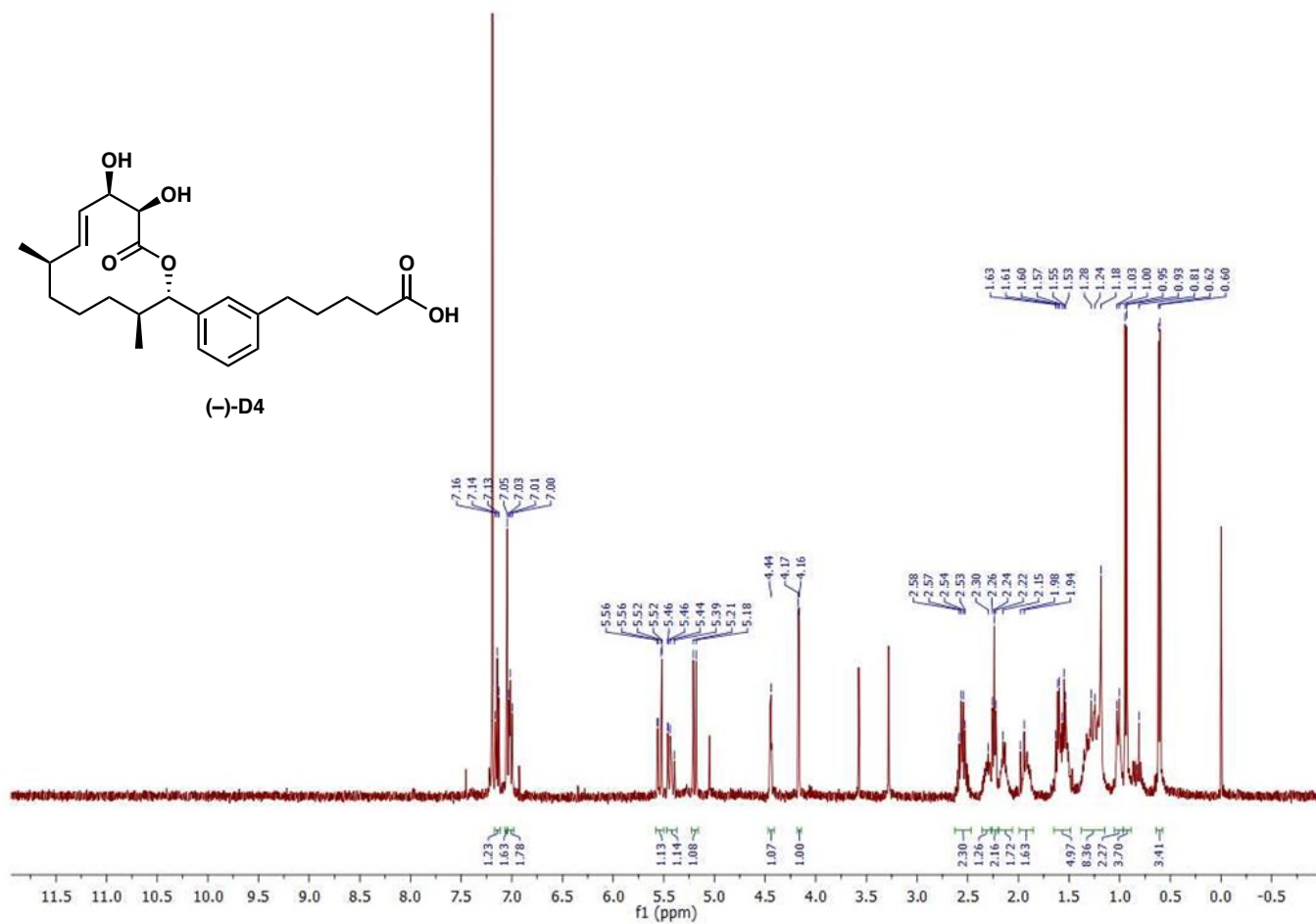
(-)-B4

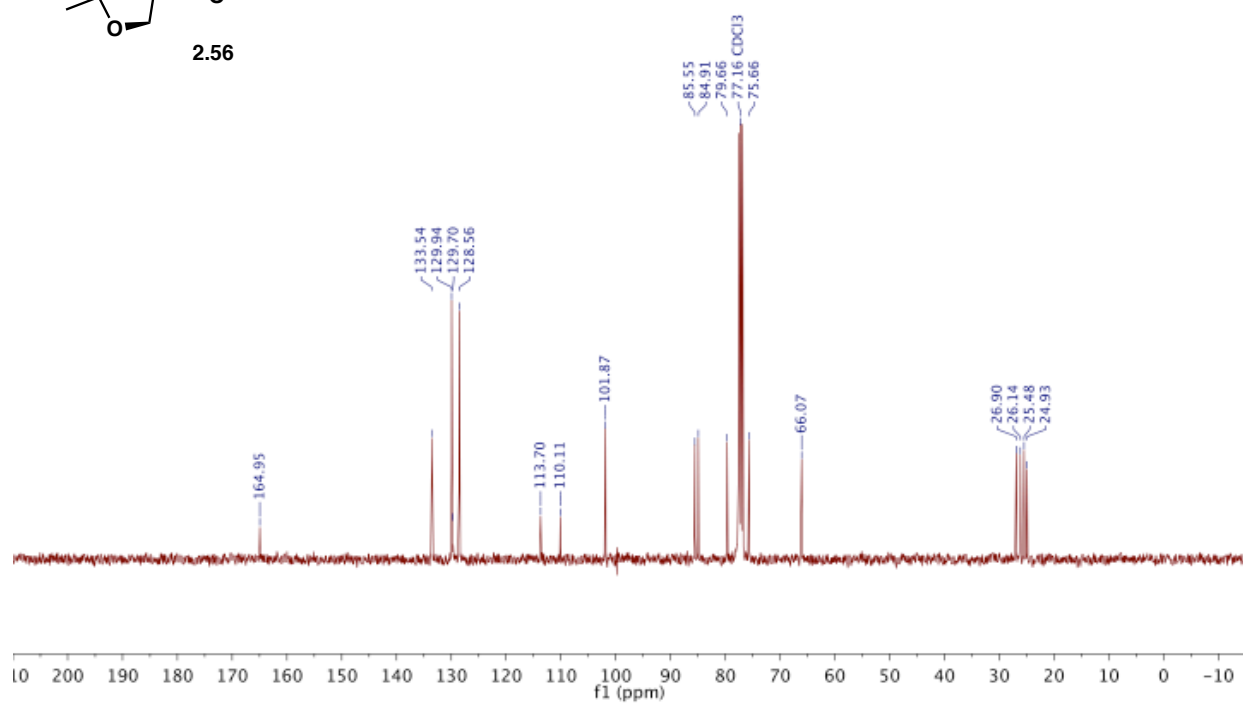
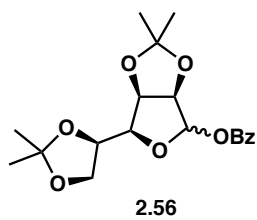
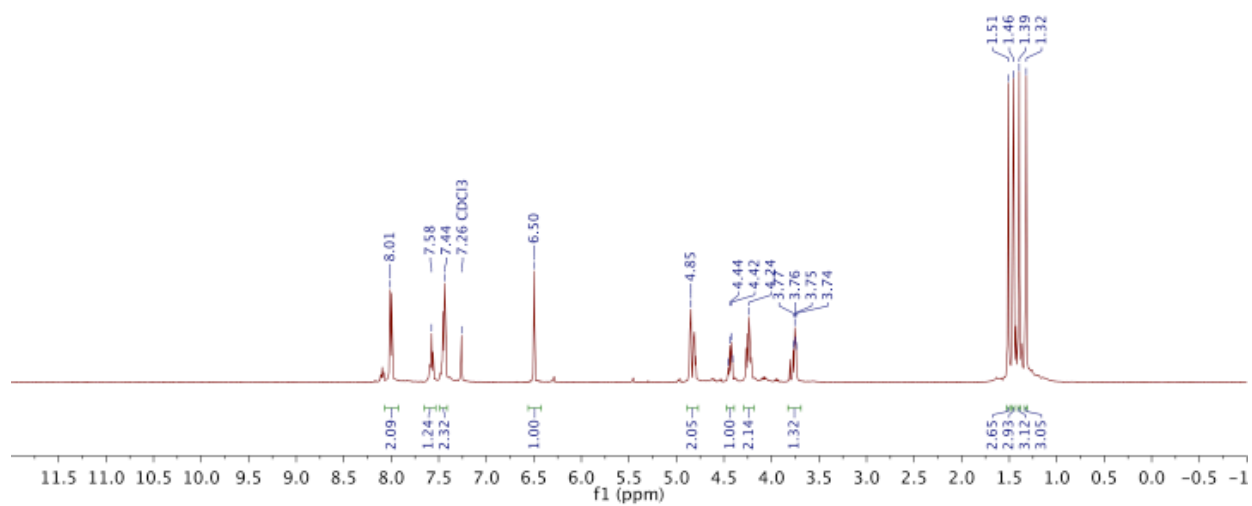
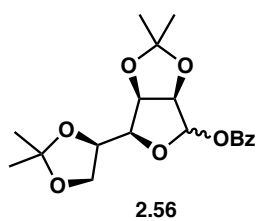


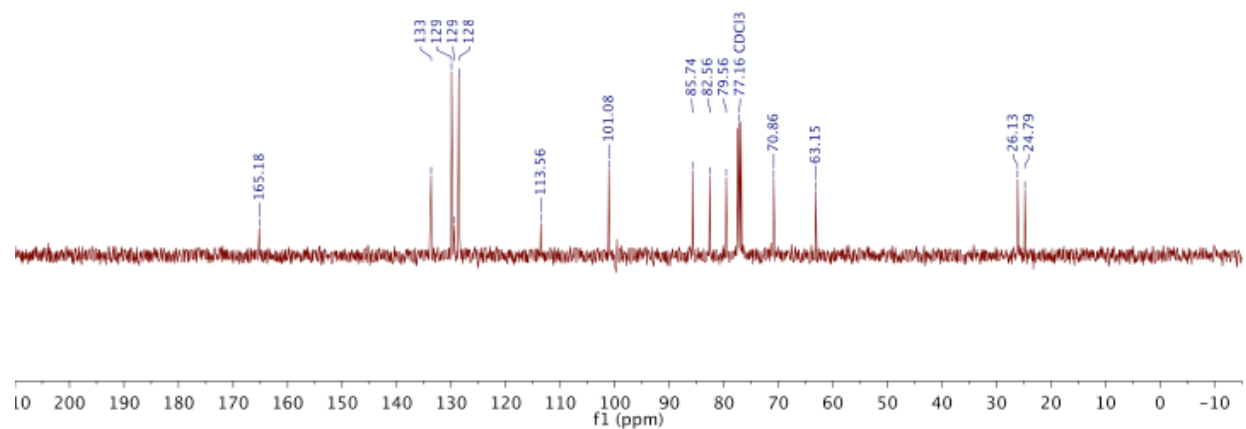
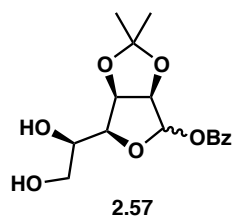
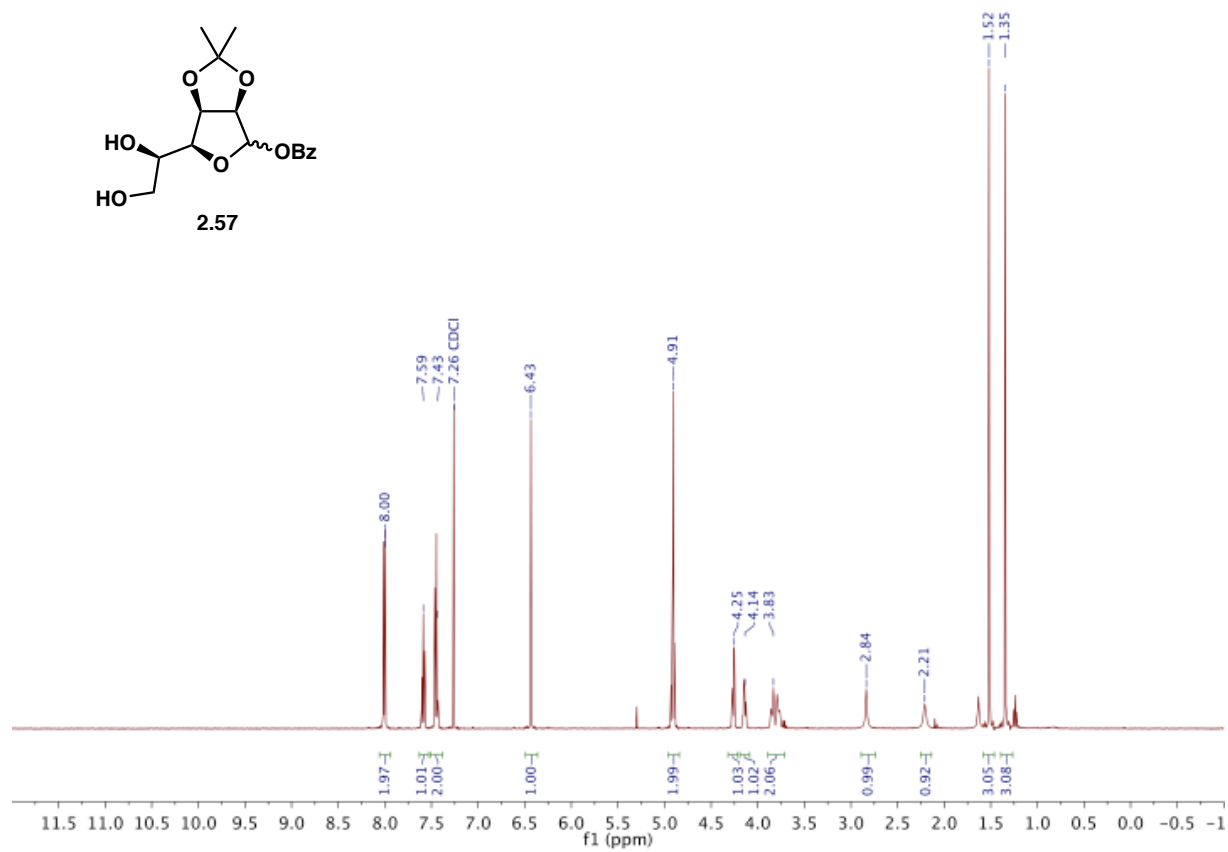
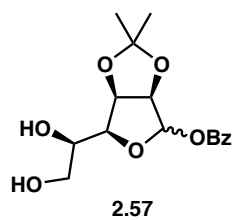


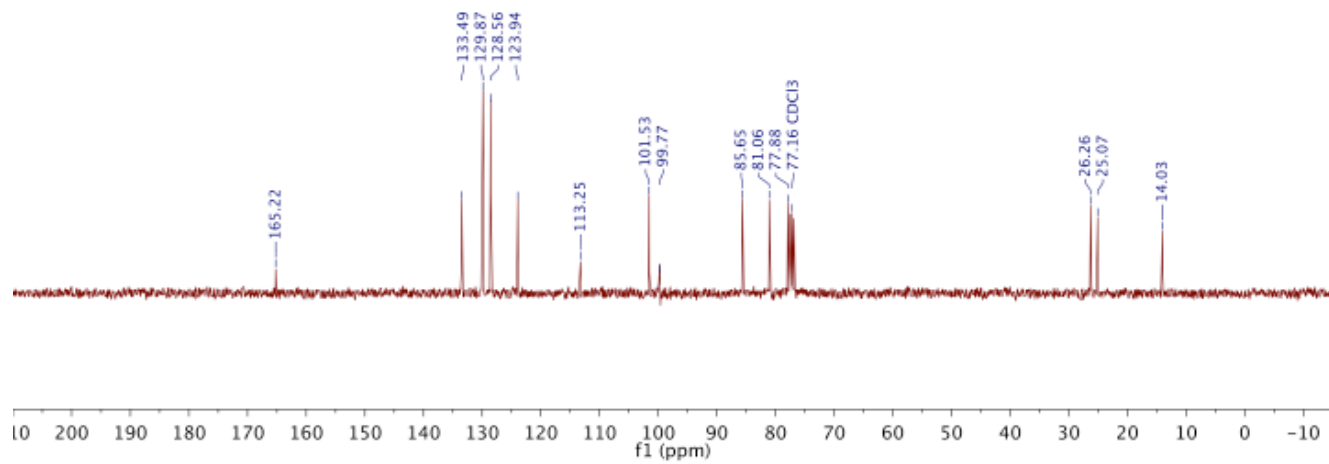
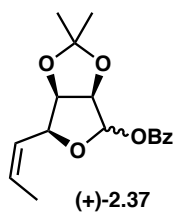
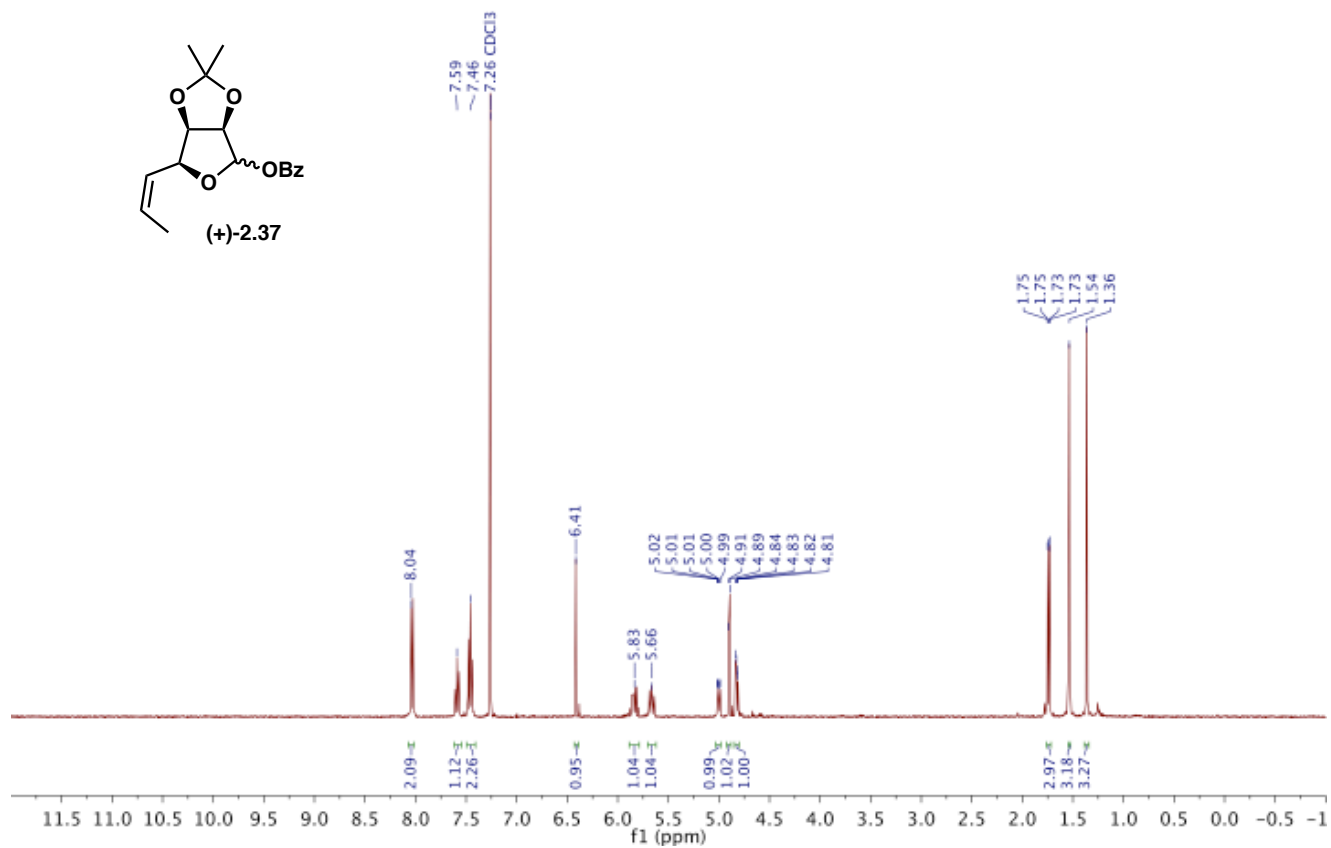
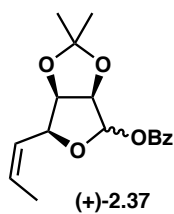


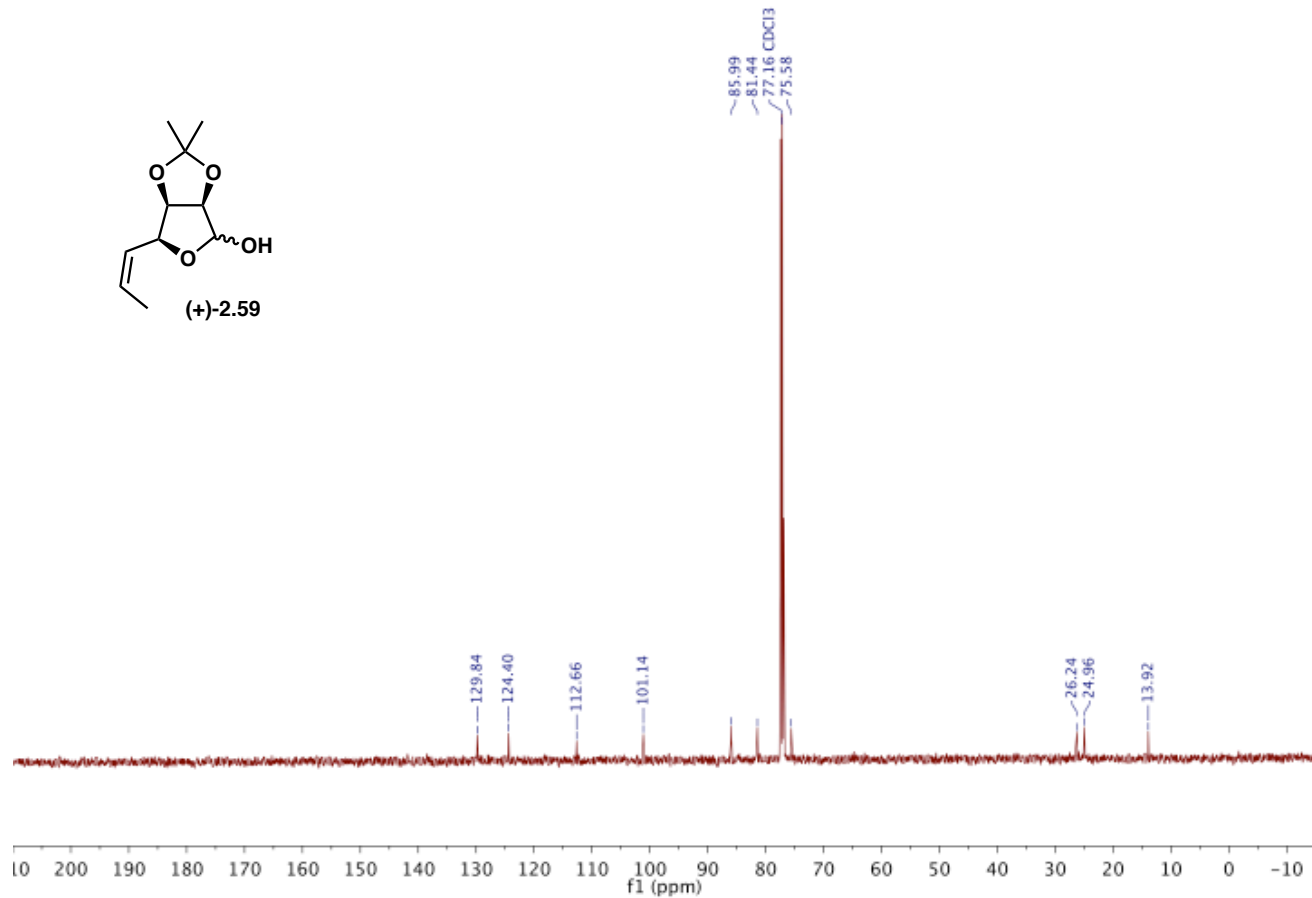
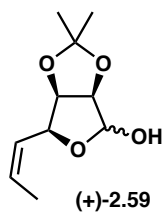
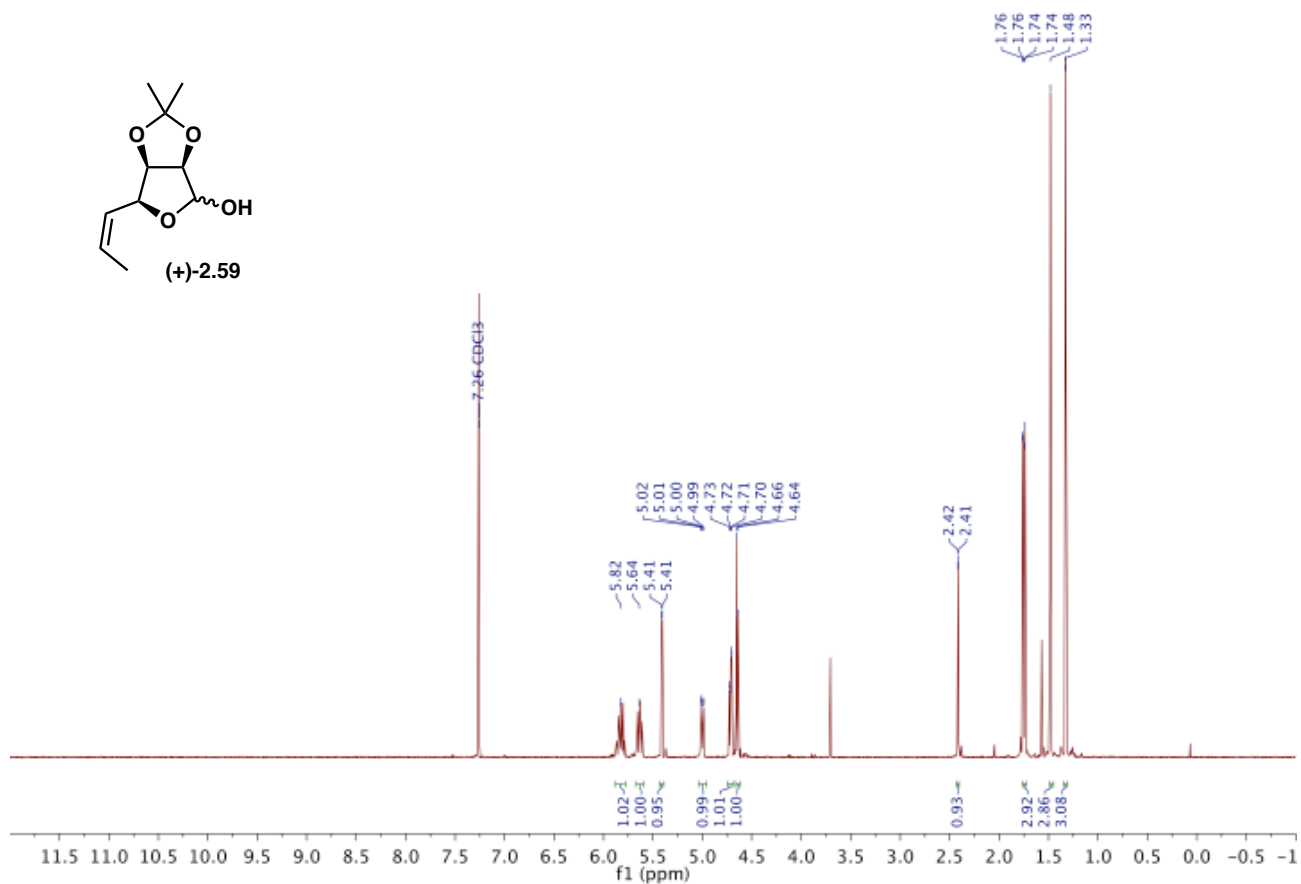
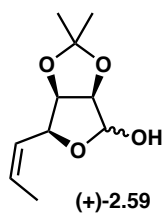


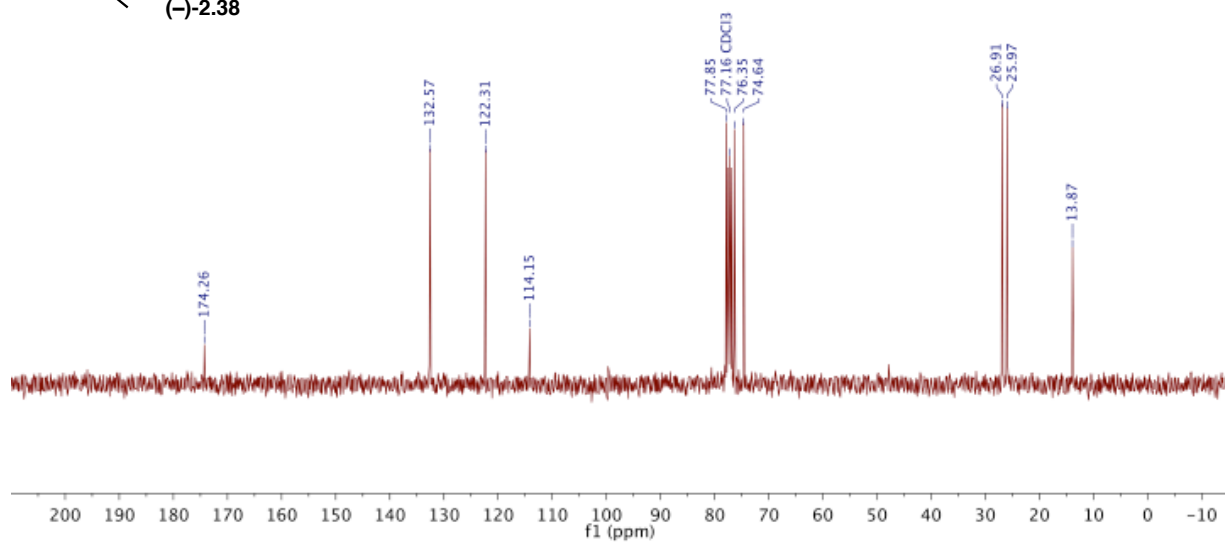
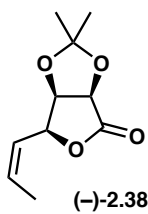
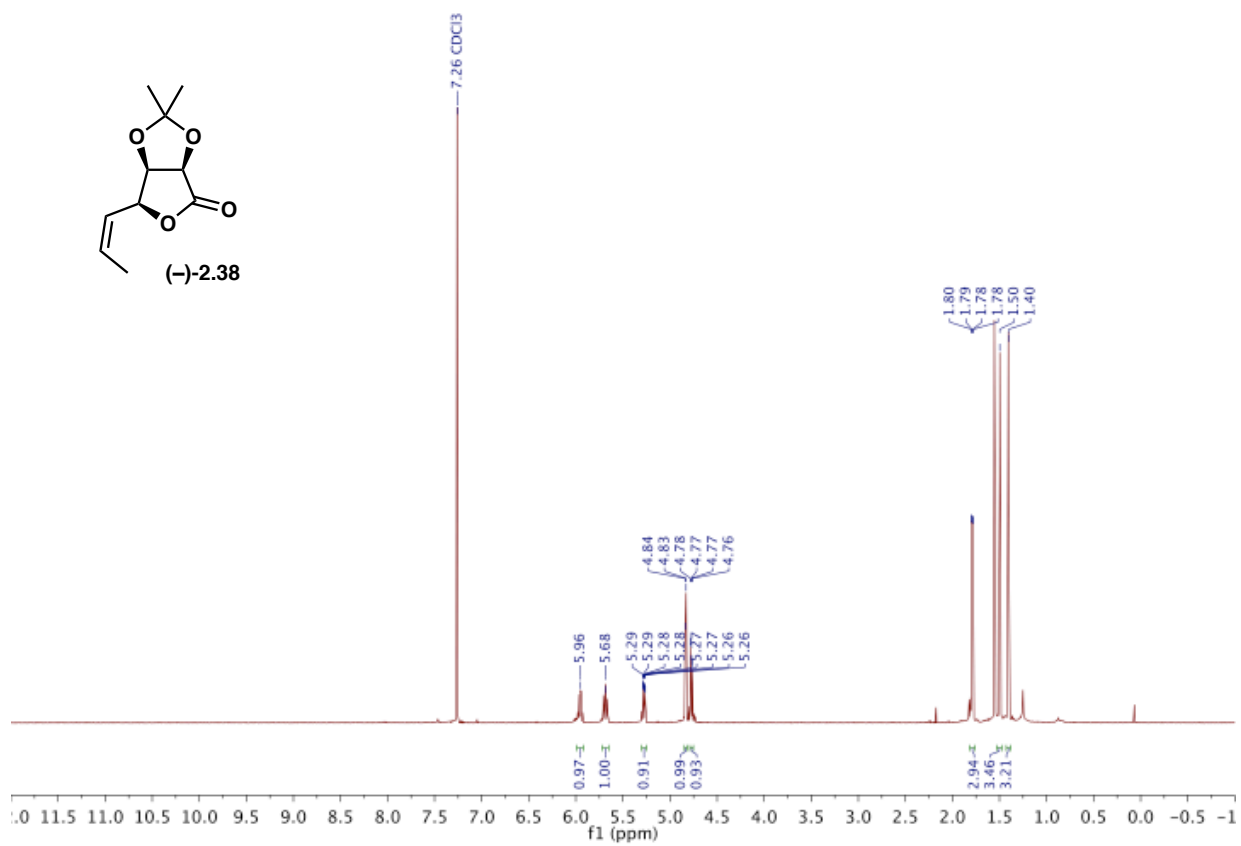
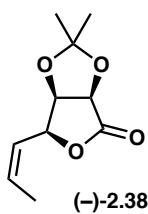


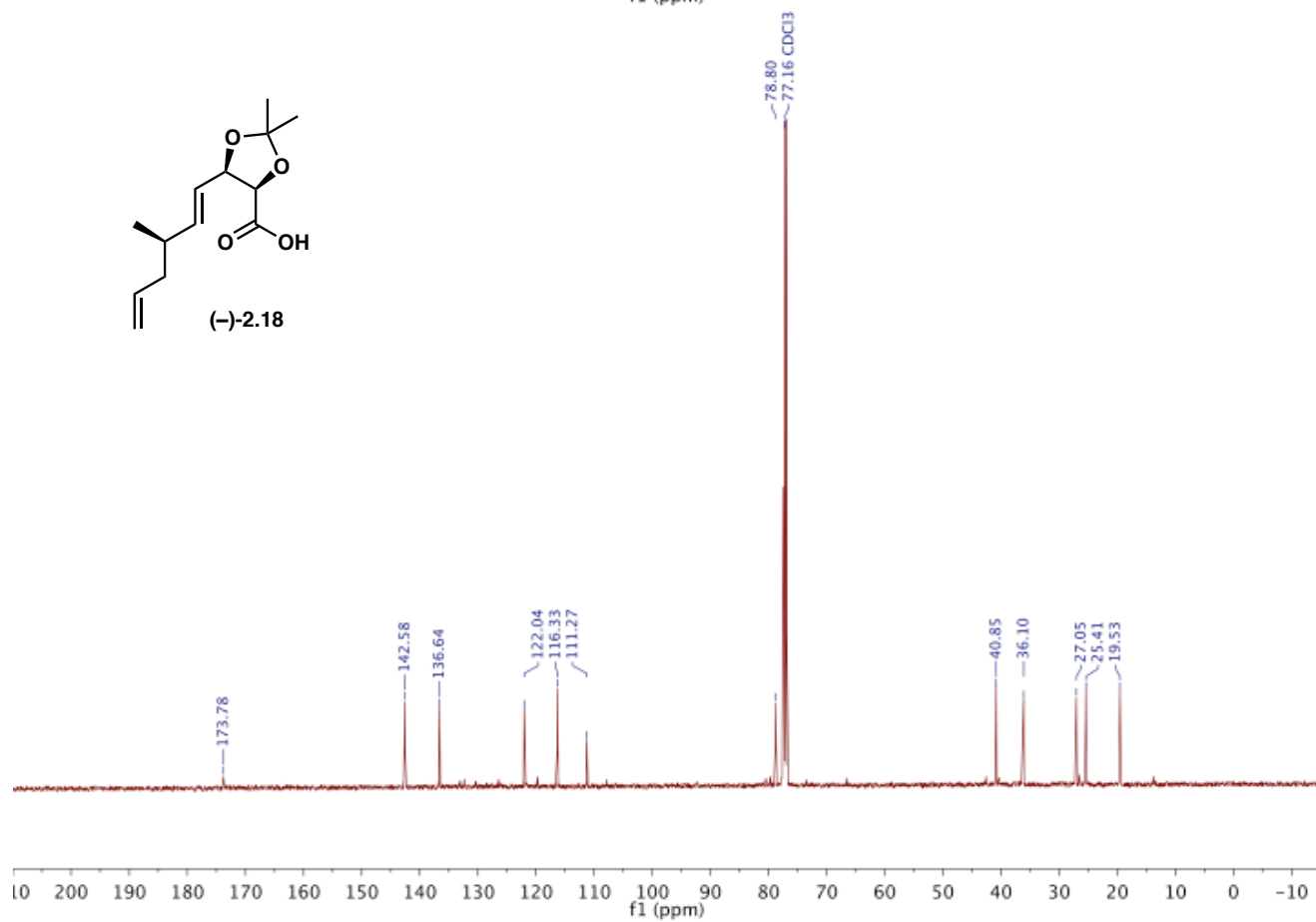
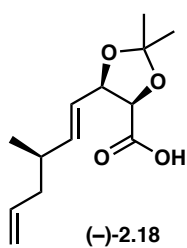
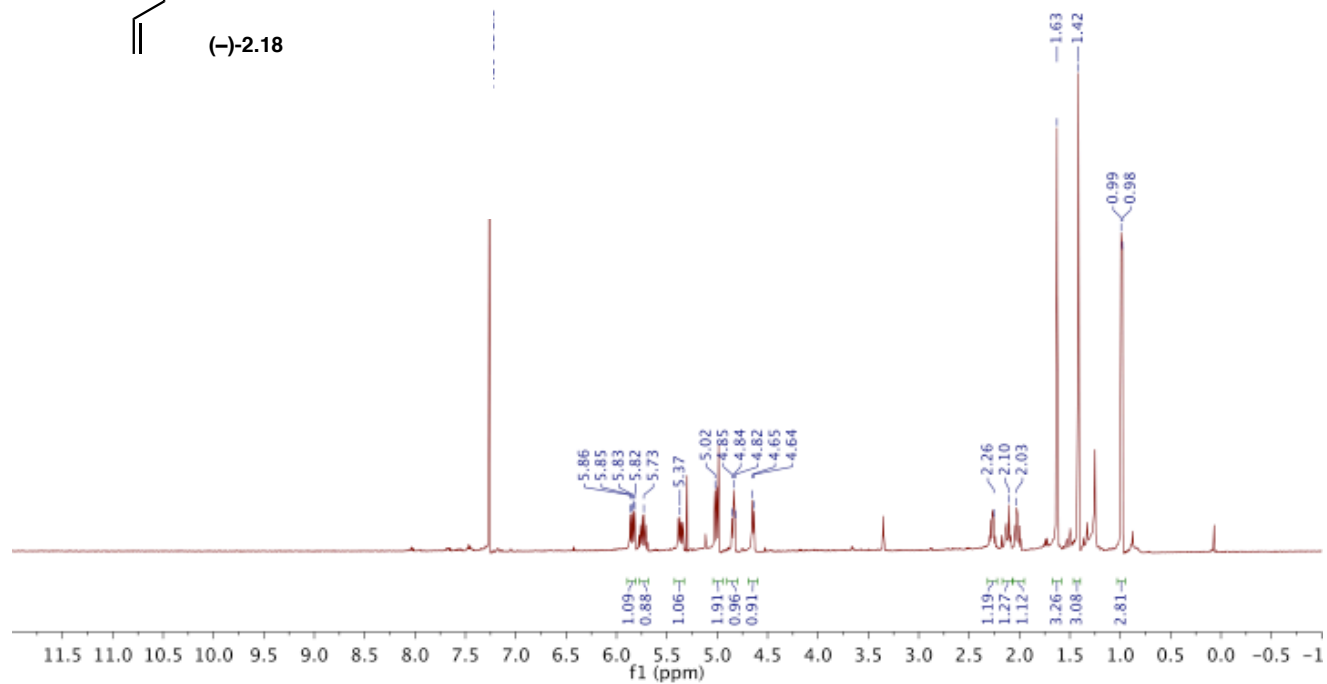
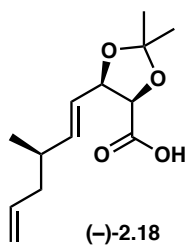


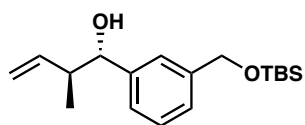




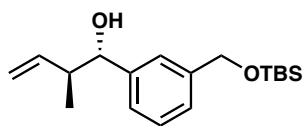
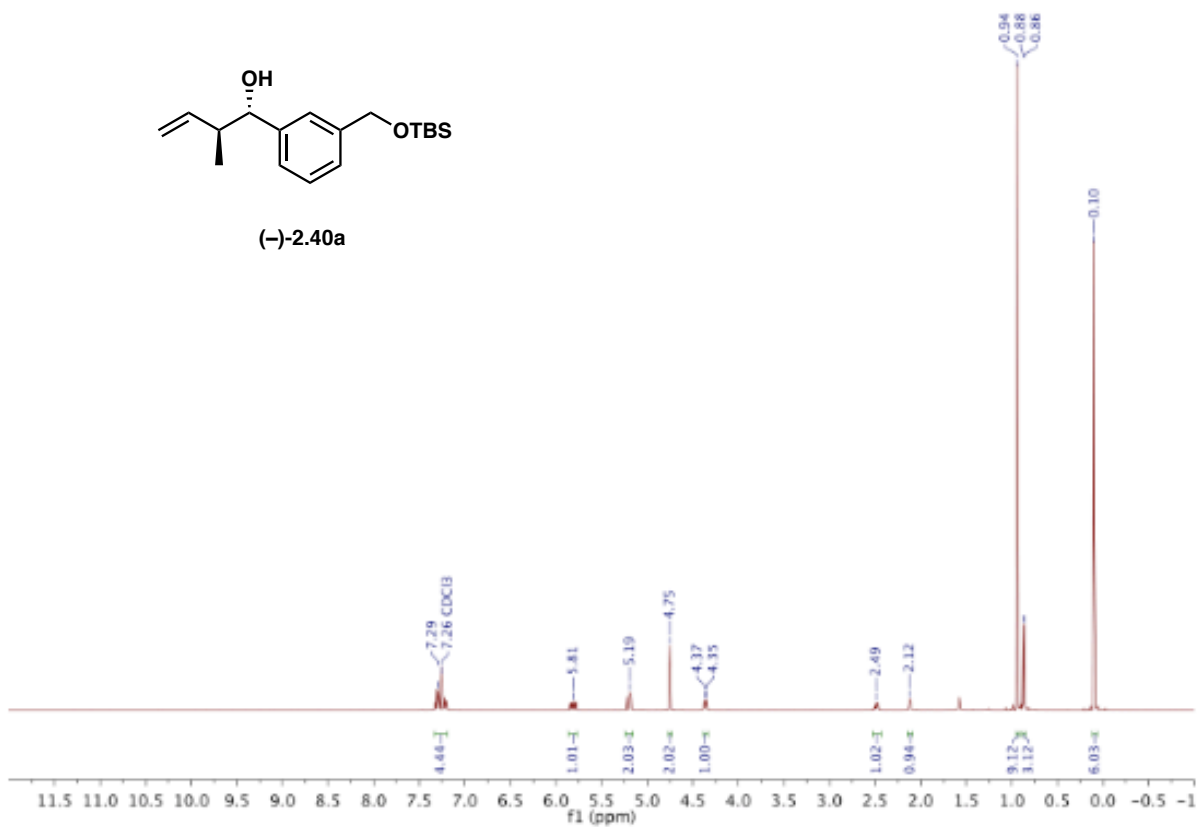




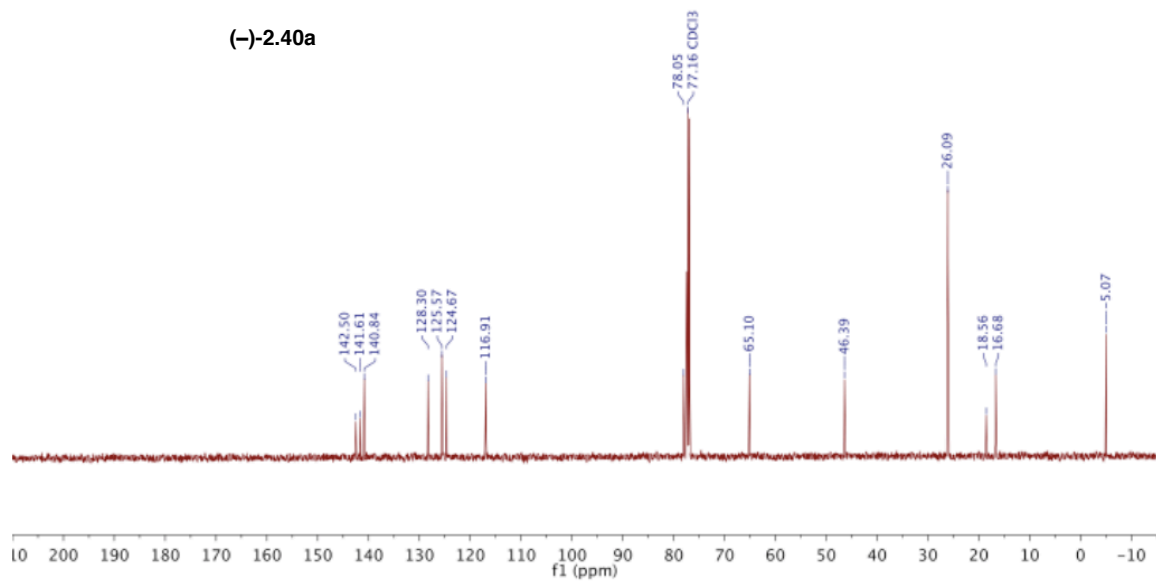


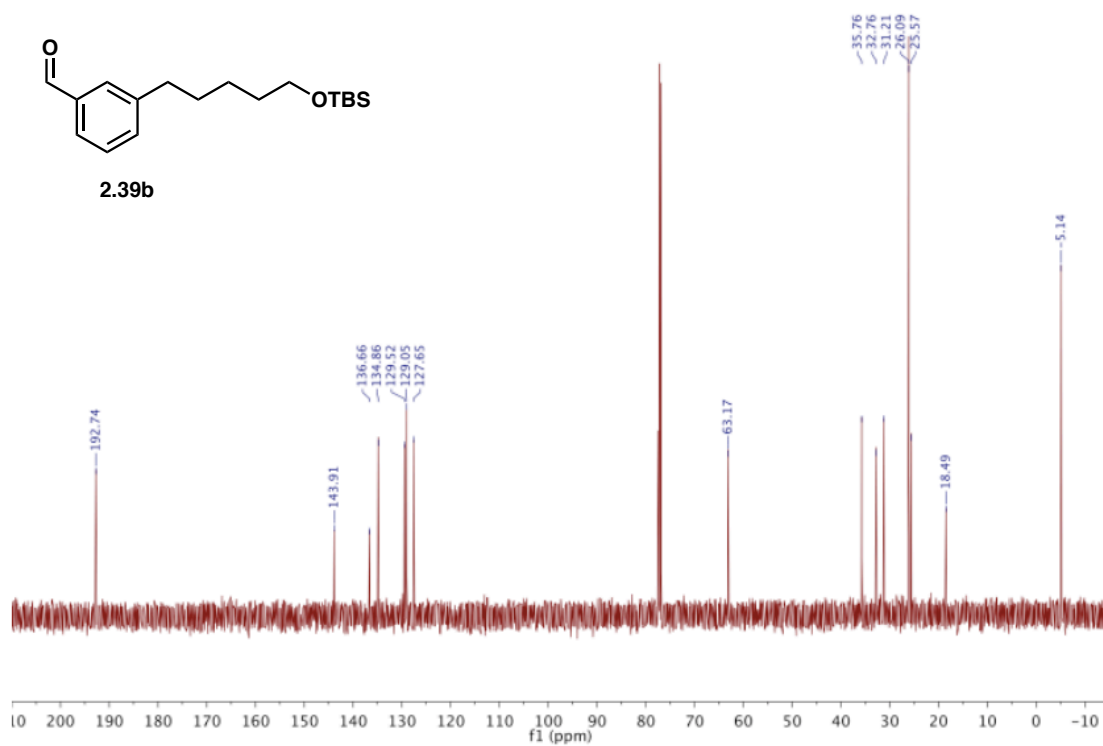
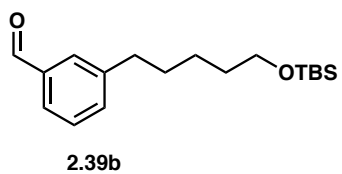
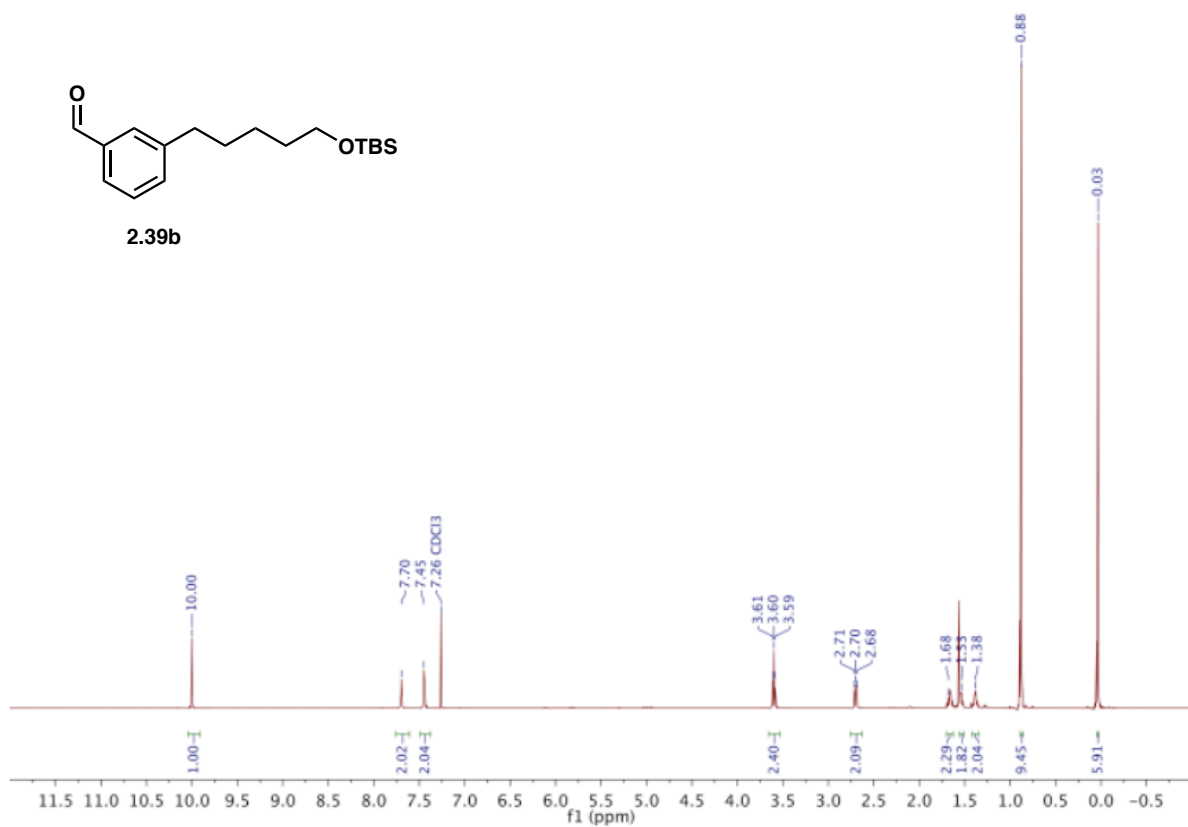
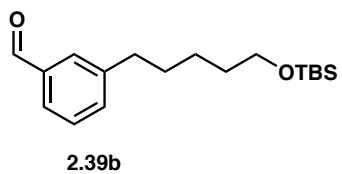


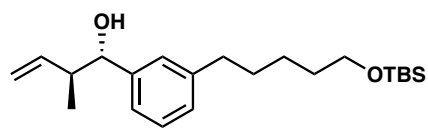
(-)-2.40a



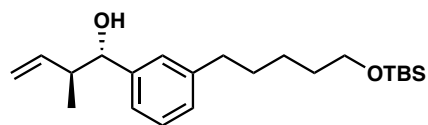
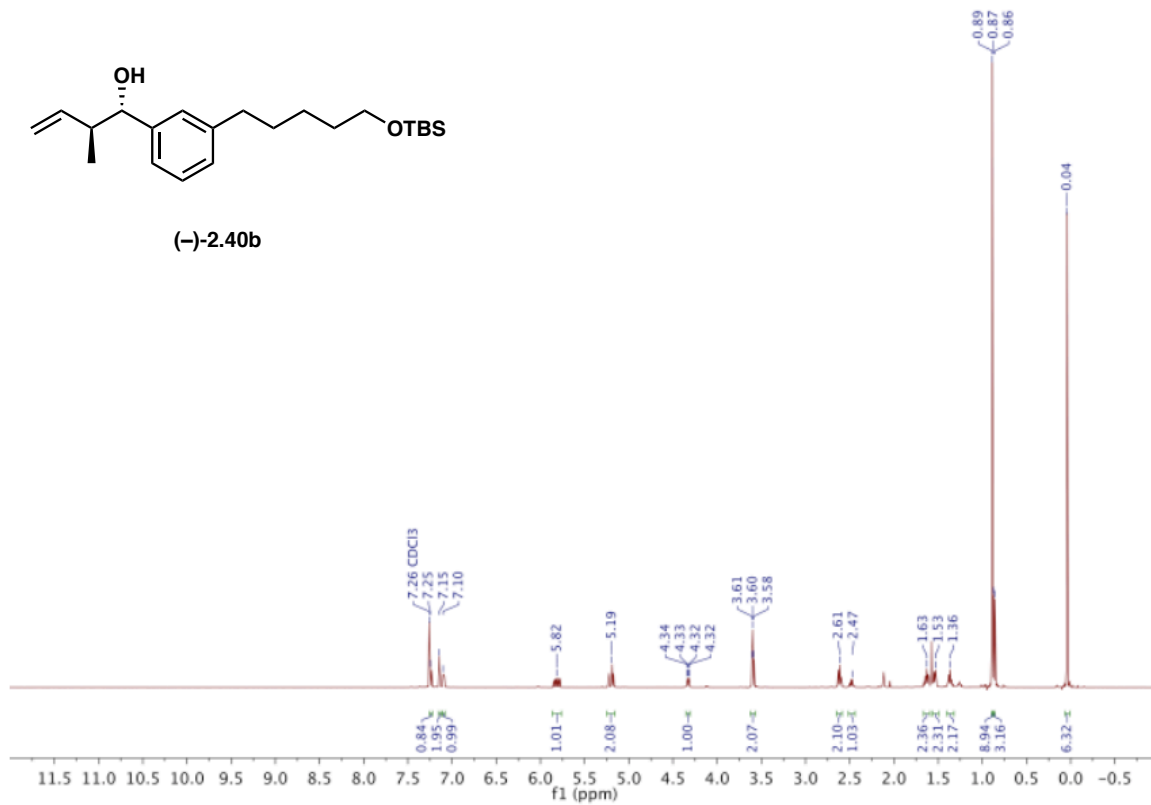
(-)-2.40a







(-)-2.40b



(-)-2.40b

